Donor-Substituted Cyclopentadienyl Ligands in Rare-Earth Metal-Based Isoprene Polymerization

Dissertation

der Mathematisch-Naturwissenschaftlichen Fakultät
der Eberhard Karls Universität Tübingen
zur Erlangung des Grades eines
Doktors der Naturwissenschaften
(Dr. rer. nat.)

vorgelegt von
Dipl.-Chem. Lars Norman Jende
aus Werneck

Tübingen
2015

Gedruckt mit Genehmigung der Mathematisch-Naturwissenschaftlichen Fakultät der Eberhard Karls Universität Tübingen.

Tag der mündlichen Qualifikation:	13.03.2015
Dekan:	Prof. Dr. Wolfgang Rosenstiel
1. Berichterstatter:	Prof. Dr. Reiner Anwander
2. Berichterstatter:	Prof. Dr. Martin E. Maier

In Memoriam

Eike Kuschka

28.10.1980 — 11.02.2012

„Wahre Freundschaft kennt keine Trennung“

Raffael, Tjalle, Domenico, Jörg, Lars

Preface

The work has been carried out during the period June 2009 to September 2014 under the supervision of Prof. Dr. Reiner Anwander at the University of Tübingen, Germany.

This thesis begins with a survey of the evolution of ´single-site´ Ziegler-Natta polymerization catalysts with primary focus on structure-reactivity/selectivity issues and the development of new organometallic catalysts for coordinative polymerization of conjugated 1,3-dienes. Special emphasis is put on donor-functionalized cyclopentadienyls as ancillary ligands of rare-earth metal complexes and their implication for the stereoregulation in isoprene polymerization. Following the introduction, a summary of the main results and scientific papers will be given.

From January to March 2012, I was fortunate to work with Prof. Dr. Kazushi Mashima at Osaka University, Osaka, Japan, on a collaborative project on Iodine-catalyzed diene redox chemistry of divalent rare-earth metals.

Acknowledgements

First of all, I am particularly grateful to my supervisor Prof. Dr. Reiner Anwander for accepting me into his group. I am especially thankful for directing and supporting me with your expertise to develop this research topic and giving me the opportunity to publish, contribute to conferences, and in particular for the chance to gain experiences in Japan. Beyond that, I also appreciate the free hand I was given to bring my ideas to fruition and your patience over all this time.

A special thanks goes to Prof. Dr. Kazushi Mashima, not only for the invitation to join his group at the Osaka University, his personal interest in my research project,but also for making my stay a pleasure. I will never forget his support in a personally difficult time. I would also like to thank Dr. Hiroshi Kaneko and Keshi Yamamoto for their support in- and outside of the laboratory. Especially the Sumo tournament, the dinner at the King Crab restaurant and the Karaoke nights are only some of my unforgettable experiences.

I thank Dr. Cäcilia Maichle-Mössmer and Prof. Dr. Karl W. Törnroos for the comprehensive crystallographic work, Wolfgang Bock for conducting the elemental analysis, and Daniela Kauling for performing the differential scanning calorimetry (DSC). I also thank Karl-Heinz Ableitner and Elke Niquet for their work, keeping the laboratory running.

I also would like to thank Dr. Bernd Schäfer and Dr. Bernd Tartsch from the Malvern Instruments GmbH for their support and giving me a fundamental understanding of the size exclusion chromatograph (SEC) and its calibration.

I am especially grateful to Dr. H. Martin Dietrich for his assistance in the early days and sharing his extensive knowledge in rare-earth metal chemistry with me. Together with Christoph O. Hollfelder, the discussions about difficulties in our polymerization reactions kept it “living” and inspired my work.

Out of office, I will remember activities with my colleagues Damir Barisic supporting the VfB and Christoph Stuhl having beer adH. To all my further colleagues of the Anwander group, André Bienfait, Martin Bonath, Dr. Nicole Dettenrieder, Jochen Friedrich, Dr. Sonja König, Andreas Krenzer, Dr. Yucang Liang, Leilei Luo, Dorothea Schädle, David Schneider, Andrea Sonström, Tatiana Spallek, Renita Thim, Benjamin Wolf and Ning Yuan, you are all great people generating nice atmosphere in the lab and I am proud I have a story to tell about each of you. Unforgettable are also the times with Dr. Shima Hamidi and Dr. Daniel Werner from the Australian Junk/Deacon group, Big-Head and Beer-Boot are just two subjects to mention.

Thanks go to my parents Sabine and Siegfried for their financial support in my academic education and particularly to my granny Thea, for her lovable and incomparable attitude.

I will always be grateful for my siblings Inga, Jörg, and Britta as you are the ones I can always trust, always build on and I will always preserve. Especially, I wish to thank Dr. Inga Jende, for incentivizing and motivating me as well as for the proof-reading of my thesis and improving my writing skills.

Contents

Preface i

Acknowledgements ii

Contents iv

Abbrevations vi

List of Publications vii

Personal Contribution to Collaborative Publications viii

Summary x

Zusammenfassung xi

Donor-Substituted Cyclopentadienyl Ligands in Rare-Earth Metal-Based Isoprene Polymerization 1

1 Introduction 2

1.1 Ziegler-Natta Catalysis 3

1.2 Single-Site Catalysts (SSC) 4

1.3 Organolanthanide Catalysts 9

1.4 1,3-Diene Polymerization 11

1.5 Constrained Geometry Catalysts (CGC) 13

1.6 Modification of Donor-Functionalized Cyclopentadienyls 15

1.7 Synthesis of Functionalized Cyclopentadienes 16

1.8 Mechanistic Aspects 18

1.8.1 α-Olefin Polymerization 18

1.8.2 1,3-Diene Polymerization 20

1.8.3 DFT Calculations 22

1.8.4 Isoprene Analysis 30

2 Cp^{Do} Rare-Earth Metal Complexes as Pre-Catalysts in Polymerization Reactions 33

2.1 Homo- and Co-Polymerization of Isoprene 33

2.2 Non-Isoprene Polymerization 40

Summary of Main Results 45

1 Synthesis of N-Donor Substituted Cp-Ligands 46

2 Rare-Earth Metal Complexes Bearing Nitrogen Functionalized Cyclopentadienyl Ligands 47

3 Isoprene Polymerization 57
3.1 Polymer Analysis 59
Concluding Remarks 61
D References 63
E Unpublished Results 71
I. Thermal C–H Bond Activation and Ether-Induced Aluminate/Cluster Seperation of $Cp^{Q}Y(AlMe_4)_2$ 72
II. Half-Sandwich Rare-Earth Metal Bis(tetramethyl-aluminate), Bismethyl, and Methylidene Complexes 79
III. Mixed Rare-Earth Metal Chloride/Methylidene Complexes 89
IV. Mixed Formamidinate/Aluminate Half-Sandwich Rare-Earth Metal Complexes 101
F Publications 107

Abbrevations

Ar	aryl
Av.	average
*i*Bu	*iso*-butyl
*t*Bu	*tertiary*-butyl
Cp	cyclopentadienyl
Cp*	1,2,3,4,5-tetramethylcyclopentadienyl
Cp^R	substituted cyclopentadienyl
Cp^{NMe2}	dimethylaminoethyl-functionalized Cp
Cp^{AMe2}	dimethylanilinyl-functionalized Cp
DFT	density functional theory
DME	1,2-dimethoxyethane
Do	donor atom or molecule
DRIFT	diffuse reflectance infrared Fourier transform
EA	elemental analysis
Et	ethyl
exc	excess
FTIR	Fourier transform infrared
h	Hour(s)
HMSC	heteronuclear single quantum coherence
HMQC	heteronuclear multiple quantum coherence
Hz	Hertz
IP	isoprene
^nJ	coupling constant over n bonds
Ln	rare-earth metals (Sc, Y, La-Lu)
M	metal
M_n	number average molar mass
M_w	weight average molar mass
MAO	methylaluminoxane
Me	methyl
min	minute(s)
MMA	methyl methacrylate
NMR	nuclear magnetic resonance
PBD	polybutadiene
PDI	polydispersity index
Ph	phenyl
PIP	polyisoprene
PMMA	poly(methyl-methacrylate)
*i*Pr	*iso*-Propyl
ppm	parts per million
R	organic substituent
ref.	reference
rt	ambient (room) temperature
SEC	size exclusion chromatography
THF	tetrahydrofuran
X	halide
Z	linker between Cp and Do

List of Publications

This thesis is based on the following scientific papers. In the text they will be referred to by their roman numerals.

Paper I L. N. Jende, C. Maichle-Mössmer, R. Anwander:
"***Rare-Earth Metal Alkylaluminates supported by N-Donor Functionalized Cyclopentadienyl Ligands: Synthesis, Structural Characterization, and Performance in Isoprene Polymerization***"
Chem. Eur. J. **2013**, *19*, 16321-16333

Paper II L. N. Jende, C. Maichle-Mössmer, C. Schädle, R. Anwander:
"***Yttrium Half-Sandwich Complexes Bearing the 2-(N,N-Dimethylaminoethyl)tetramethylcyclopentadienyl Ligand***"
J. Organomet. Chem. **2013**, *744*, 74-81

Paper III L. N. Jende, C. O. Hollfelder, C. Maichle-Mössmer, R. Anwander:
"***Rare-Earth Metal Allyl Complexes Supported by the [2-(N,N-Dimethylaminoethyl)]-tetramethyl-cyclopentadienyl Ligand: Structural Characterization, Reactivity, and Isoprene Polymerization***"
Organometallics **2015**, *34*, 32-41

Paper IV S. Hamidi, L. N. Jende, H. M. Dietrich, C. Maichle-Mössmer, K. W. Törnroos, G. B. Deacon, P. C. Junk, R. Anwander:
"***C–H Bond Activation and Isoprene Polymerization by Rare-Earth Metal Tetramethylaluminate Complexes Bearing Formamidinato N-Ancillary Ligands***",
Organometallics **2013**, *32*, 1209-1223

Paper V S. Hamidi, L. N. Jende, H. M. Dietrich, D. Werner, C. Maichle-Mössmer, K. W. Törnroos, G. B. Deacon, P. C. Junk, R. Anwander:
"***Organoaluminum and -gallium Formamidinate Complexes",***
Eur. J. Inorg. Chem. **2013**, 2460-2466

Paper VI N. Dettenrieder, C. O. Hollfelder, L. N. Jende, C. Maichle-Mössmer, R. Anwander:
"***Half-Sandwich Rare-Earth Metal Methylaluminate Complexes Bearing Peripheral Boryl Ligands*** "
Organometallics **2014**, *7*, 1528-1531

Personal Contribution to Collaborative Publications

Paper I: 3 authors; candidate 1st author

The experimental work, analyses (except single crystal structure analyses, which were acquired by Dr. C. Maichle-Mössmer), and writing were planned and conducted by the candidate. Analyses include one and two dimensional NMR spectroscopic methods, DRIFT spectroscopy, and molecular weight determination via size-exclusion chromatography of the polymers.

Paper II: 4 authors; candidate 1st author

The experimental work, analyses (except single crystal structure analyses, which were acquired by Dr. C. Maichle-Mössmer and Dr. C. Schädle), and writing were planned and conducted by the candidate. Analyses include one and two dimensional NMR spectroscopic methods and DRIFT spectroscopy.

Paper III: 4 authors; candidate 1st author

The experimental work, analyses (except single crystal structure analyses, which were acquired by Dr. Maichle-Mössmer), and writing were planned and conducted by the candidate. Analyses include one and two dimensional NMR spectroscopic methods, DRIFT spectroscopy, and molecular weight determination via size-exclusion chromatography of the polymers. C. O. Hollfelder contributed to the polymerization experiments and the graphical comparison of the polyisoprene microstructures.

Paper IV: 8 authors; candidate 2nd author (co-author)

The publication was a collaborative work with Prof. G. B. Deacon and Prof. P. Junk and their coworker Dr. S. Hamidi. The syntheses and analyses of the complexes (except single crystal structure analyses, which were acquired by Dr. Maichle-Mössmer and Prof. Dr. K. W. Törnroos) were done by Dr. S. Hamidi, Dr. H. M. Dietrich and the candidate, the writing of the first part was mainly done by Dr. S. Hamidi. Polymerizations of isoprene including full microstructure analyses and writing of the corresponding chapter (part two) as well as the graphical representations of the reactions (Chemdraw) and molecular structures (ORTEP, Tables) were contributed by the candidate.

Paper V: 9 authors; candidate 4th author

The publication was a collaborative work with Prof. G. B. Deacon and Prof. P. Junk and their coworkers Dr. S. Hamidi and Dr. D. Werner. The syntheses and analyses of the complexes (except single crystal structure analyses, which were acquired by Dr. Maichle-Mössmer and Prof. Dr. K. W. Törnroos) were done by Dr. S. Hamidi, Dr. H. M. Dietrich, Dr. D. Werner and the candidate. Writing of the publication was mainly done by Dr. S. Hamidi.

Paper VI: 5 authors; candidate 3rd author

The scientific work, analyses (except single crystal structure analyses, which were acquired by Dr. C. Maichle-Mössmer), and writing were planned and conducted by Dr. N. Dettenrieder. Polymerizations of isoprene including data acquisition and investigations on the active species were carried out by C. O. Hollfelder and the candidate.

Unpublished results: 4 manuscripts

The experimental work, analyses, and writing were planned and conducted by the candidate. Single crystal diffraction analyses were acquired by Dr. C. Maichle-Mössmer (**Manuscripts I-IV**) and Prof. Dr. K. W. Törnroos (**Manuscript IV**). Experiments regarding to chloro/methylidene cluster complexes (**Manuscript IV**) were inspired by the work of Dr. H. M. Dietrich, who also contributed to the interpretation of the results.

Summary

The objective of this thesis was to synthesize half-sandwich rare-earth metal bis(hydrocarbyl) complexes for isoprene polymerization, bearing a donor-sidearm substituted cyclopentadienyl as mono-anionic ancillary ligand to mimic a constrained geometry configuration. In a first approach the protonolysis reactions of dimethylaminoethyl- and dimethylanilinyl- substituted cyclopentadienyls HCp^{NMe2} and HCp^{AMe2} with homoleptic $[Ln(AlMe_4)_3]$ precursors were investigated. At ambient temperature, only the anilinyl-substituted ligand formed the desired $[Cp^{AMe2}Ln(AlMe_4)_2]$ complexes. Instead, the flexible ethyl bridge of the HCp^{NMe2} ligand led to donor-induced cleavage of one aluminate moiety generating $[Cp^{NMe2\rightarrow AlMe3}Ln(AlMe_4)_2]$. Removal of the nitrogen bonded $AlMe_3$ with ether directly initiated C–H bond activation of one aminomethyl group yielding $[\{Cp^{NMe}(\mu\text{-}CH_2)AlMe_3\}Ln(AlMe_4)_2]$. The dependence of the C–H bond activation on temperature and rare-earth metal center was further investigated with the corresponding anilinyl complexes and a mechanism could be proposed.

To avoid the inadvertent activation, alternative synthesis strategies with focus on precoordination of the Cp^{NMe2} ligand in a $\eta^5{:}\kappa^1$ fashion to the rare-earth metal center were tested. From the *extended silylamide route*, the intermediate bis(dimethylsilylamide) complex $[Cp^{NMe2}Y\{N(SiHMe_2)_2\}]$ and the Si–H activated complex $[Cp^{NMe2}Y\{\eta^2\text{-}SiMe_2(NSiHMe_2)_2\}(thf)]$ were isolated. Salt-metathesis reaction, starting from $LnCl_3(thf)_x$ with the lithiated ligand $LiCp^{NMe2}$ and subsequent reaction with MeLi yielded $[Cp^{NMe2}YMe_2(MeLi)]_2$ and $[Cp^{NMe2}LuMe_2]_2$ as structurally characterized precursors. However, treatment with $AlMe_3$ led to coordination switch of the donor-sidearm from the rare-earth metal to the aluminum center in all cases.

Additionally, the Cp^{NMe2} ligand was utilized to form half-sandwich bis(allyl) complexes $[Cp^{NMe2}Ln(\eta^3\text{-}C_3H_5)_2]$ in a two-step salt-metathesis reaction, implying $LnCl_3(thf)_x$, $LiCp^{NMe2}$ and the Grignard reagent C_3H_5MgCl, but in case of the larger neodymium only the dimeric monoallyl-chlorido complex $[Cp^{NMe2}Ln(\eta^3\text{-}C_3H_5)(\mu\text{-}Cl)]_2$ could be isolated.

The presented aluminate and allyl complexes were tested in isoprene polymerization under various conditions. The resulting polymers were structurally characterized by ^1H, ^{13}C, and partially ^1H–^{13}C HSQC NMR spectroscopy. The molecular weights and the molecular weight distributions were determined by size-exclusion chromatography (SEC) against polystyrene standards. The influence of the donor-sidearm was investigated by comparison with non-functionalized half-sandwich complexes $[Cp^*Ln(AlMe_4)_2]$.

Zusammenfassung

Ziel der vorliegenden Arbeit war die Synthese von Halbsandwich-Bis(hydrocarbyl)-Komplexen der Seltenerdmetalle mit donor-funktionalisierten Cyclopentadienylliganden sowie deren Untersuchungen hinsichtlich ihrer Eignung als Prä-Katalysator für die Polymerisation von Isopren.
Im ersten Ansatz wurde die protonolytische Reaktion von dimethylaminoethyl- und dimethylanilinyl-substituiertem Cyclopentadienyl HCp^{NMe2} und HCp^{AMe2} mit homoleptischen Tetrametylaluminaten $[Ln(AlMe_4)_3]$ (Ln = Y, La, Nd) untersucht. Bei Raumtemperatur konnten nur gewünschte Produkte des anilinyl-substituierten Liganden in Form von $[Cp^{AMe2}Ln(AlMe_4)_2]$ generiert werden. Die flexible Ethylbrücke des Cp^{NMe2} Liganden hingegen verursachte die Koordination des Sticktoffatoms an ein $AlMe_3$ Molekül $[Cp^{NMe2\rightarrow AlMe3}Ln(AlMe_4)_2]$. Die Abtrennung des Trimethylaluminiums mittels Diethylether führte zu einer C–H-Bindungs-Aktivierung einer Aminomethylgruppe $[\{Cp^{NMe}(\mu\text{-}CH_2)AlMe_3\}Ln(AlMe_4)_2]$. Die Temperaturabhängigkeit dieser Aktivierung konnte im Folgenden auch an dem anilinyl-substituierten Komplex nachgewiesen werden, was auf einen zugrunde liegenden Mechanismus hinweist. Auf Grund dessen fokussierten alternative Synthesestrategien auf eine $\eta^5{:}\kappa^1$ Prä-Koordination der Liganden an den Seltenerdmetallzentren. Aus Salzmetathesen des lithiierten Liganden $LiCp^{NMe2}$ mit den entsprechenden Metallchloriden wurden zunächst die Halbsandwich-Bischlorid-Komplexe generiert. Die weitere Umsetzung mit $[LiN(SiHMe_2)_2]$ führte zu dem Komplex $[Cp^{NMe2}Y\{N(SiHMe_2)_2\}]$, sowie der Si–H bindungsaktivierten Spezies $[Cp^{NMe2}Y\{\eta^2\text{-}SiMe_2(NSiHMe_2)_2\}(thf)]$. Wurde im zweiten Schritt hingegen MeLi verwendet, konnten die Komplexe $[Cp^{NMe2}YMe_2(MeLi)]_2$ und $[Cp^{NMe2}LuMe_2]_2$ isoliert werden. Bei Zugabe von $AlMe_3$ wurde jedoch, sowohl bei den Amid- als auch den Methyl-Komplexen, die erneute Koordination des Stickstoffes an das Trimethylaluminium beobachtet. Des Weiteren konnten durch Salzmetathese-Reaktionen auch die Allylkomplexe $[Cp^{NMe2}Ln(\eta^3\text{-}C_3H_5)_2]$ (Ln = Y, Ho, Lu) und $[Cp^{NMe2}Nd(\mu\text{-}Cl)(\eta^3\text{-}C_3H_5)]_2$ hergestellt werden.

Nach Kationisierung mit entsprechenden perfluorierten Arylboraten erwiesen sich die dargestellten Halbsandwich-Seltenerdmetall-Aluminat- und Allyl-Komplexe als aktive Katalysatoren für die Isoprenpolymerisation. Die erhaltenen Polymere wurden durch ^1H, ^{13}C, und teils ^1H–^{13}C HSQC NMR Spektroskopie strukturell untersucht. Die Molekulargewichte und die Molekulargewichtsverteilungen wurden mit Hilfe der Gel-Permeations-Chromatografie (GPC/SEC) ermittelt. Der Einfluss des donor-funktionalisierten

Seitenarms wurde durch den Vergleich mit den Polymerisationsergebnissen von unsubstituierten Halbsandwichkomplexen [Cp*Ln($AlMe_4$)$_2$] bestimmt.

Donor-Substituted Cyclopentadienyl Ligands in Rare-Earth Metal-Based Isoprene Polymerization

1 Introduction

In the last century, synthetic polymers became one of the most common construction materials in our daily life. The potential to modify their application-specific properties concerning rigidity, density, thermal stability, and processability, led to a large quantity of polymers and a wide range of applications. Natural polymers including tar, horns, cellulose, silk and tree saps have been employed since ancient times, but their chemical modification, such as the vulcanization of rubber by HANCOCK[1] and GOODYEAR[2], began only in the nineteenth century. The first commercially produced synthetic polymers were the phenol-formaldehyde resin "Bakelite" developed by BAEKELAND in 1907,[3] the polyisoprene "Buna" patented by HOFMANN in 1909,[4] and polyvinylchloride introduced by KLATTE IN 1912,[5] but the molecular nature of these polymers was not understood. A major breakthrough was the proposition of STAUDINGER in 1922,[6] that polymers are long chains consisting of a large number of individual small molecules linked together by covalent bonds, a work for which he was awarded the Noble Prize in 1953. In the following years, several new polymers were invented and patented, but the most significant discovery was probably the polymerization of α-olefins. In 1937, FAWCETT and GIBSON at the Imperial Chemical Industries (ICI) patented the radical polymerization of ethylene under harsh conditions (500-3000 bar, 100-300 °C) initiated by traces of oxygen.[7] The resulting polyethylene exhibited a reduced melting temperature and lower density than the lateron fabricated linear crystalline polyethylene (HDPE, *high density polyethylene*) due to branching via chain transfer reactions and was therefore called LDPE (*low density polyethylene*) (Table 1).

Table 1: Properties of the three most common polyethylene grades.

	LDPE	**LLDPE**	**HDPE**
			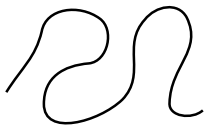
density [g/cm^3]	0.910-0.925	0.910-0.940	0.941-0.965
melting point	90-110 °C	50-125 °C	130-145 °C
crystallinity	40-50%	10-50%	60-80%
elasticity modulus	~200	100-600	~1000

1.1 Ziegler-Natta Catalysis

With the discovery of a new two component catalysis system based on a transition metal compound (halide, alkoxide, alkyl or aryl), preferentially involving group 4 metal, activated by an organoaluminum compound by ZIEGLER at the Max Planck Institute for Coal Research in 1953, the polymer industries changed remarkably and opened a new field in academic research.[8-9] In this regard it is worth mentioning that in the same year, HOGAN and BANKS at Phillips Petroleum Co. reported the polymerization of ethylene employing chromium oxide on silica material to produce HDPE under mild conditions (30-35 bar, 200°C).[10] However, the high linearity of the produced HDPE through ZIEGLER´s metalorganic mixed catalyst was verified by IR spectroscopy and the ethylene polymerization could be performed at atmospheric pressure and room temperature. In fact, the discovery was made accidentally, when an autoclave employed for C-C coupling reactions of ethylene at triethylaluminum following the "Aufbaureaktion"[11] was contaminated with colloidal nickel. Further investigations, including most of the transition metals, revealed the predominance of the group 4 metals and the system $TiCl_4/AlR_3$ was optimized (Scheme 1).

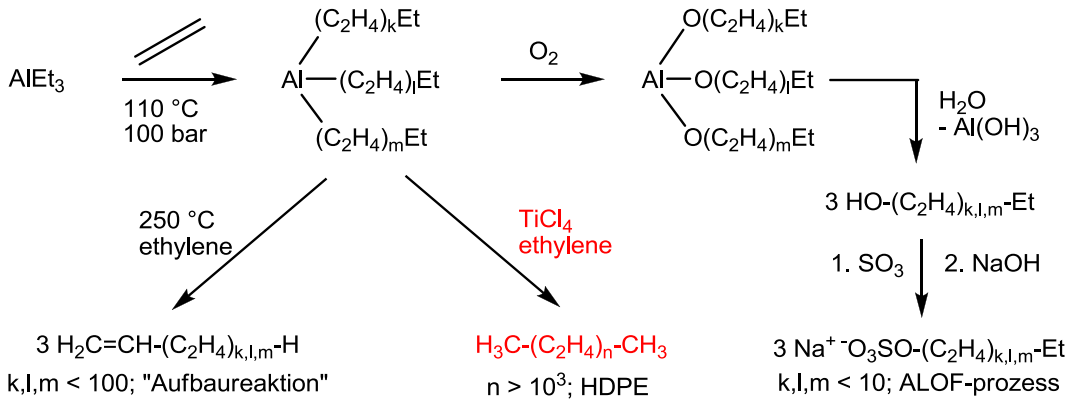

Scheme 1: Fundamental work of Karl Ziegler, based on organo-aluminum compounds.

NATTA, already inspired by the "Aufbaureaktion" in 1952, swiftly adopted the new findings in his investigations of the polymerization of propylene, higher α-olefins, and 1,3-conjugated dienes with Ziegler´s catalysts.[12] Only one year later, he discovered the different stereoregularities of the produced polypropylene through testing their different physical characteristics, such as solubility, melting point, crystallinity and mechanical properties (Figure 1).[13] Comprehensive studies were published in the following years including analysis of several polymers via nuclear magnetic resonance, infrared spectroscopy, and X-ray diffraction.[14]

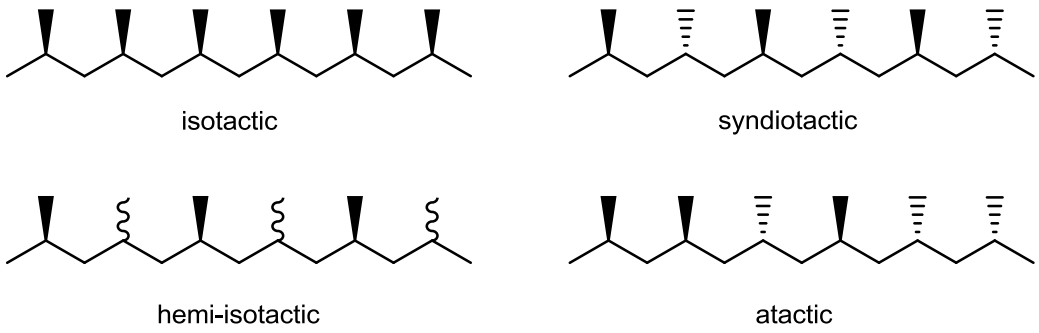

Figure 1. Tacticity of polypropylene.

These findings demonstrated that polymeric products with very different physical properties can be obtained from the same monomer by influencing the catalytic process. This was the beginning of the next generation research in polyolefin industries, focusing on new and well defined structures of single-site catalysts and their capacity to produce tailor-made polymers.

1.2 Single-Site Catalysts (SSC)

Conventional ZIEGLER–NATTA catalysts, as mentioned above, are widely used in the industrial production of polymers, but mostly generate polymer mixtures with varying microstructures and broad molecular weight distributions. The reason for this inhomogeneity is the insolubility of the heterogeneous catalyst, promoting aggregation and formation of multisided active centers. The first step towards catalytic active species more appropriate for mechanistic studies was made by NATTA ET AL.,[15] and BRESLOW and NEWBURG[16]. In 1957, they discovered the soluble bis(cyclopentadienyl)titanium dichloride [Cp_2TiCl_2] as a promising new catalyst when activated with alkyl aluminum chloride [AlR_2Cl]. However, low activity and decomposition to an inactive species rendered it unattractive for further investigations. In 1980, SINN and KAMINSKY discovered methylaluminumoxane (MAO) as a highly effective activator.[17] With this finding, the work on metallocene complexes based on group 4 metals became revitalized. Especially the zirconium metal complexes were intensively studied, due to their thermal stability, and systematic substitution of the π-bonded ligand, thus generating the first stereoselective Ziegler-Natta catalyst system, for the production of isotactic polypropylene (Figure 1). In the following decade, many research groups including BRINZINGER, KAMINSKY, MÜHLHAUPT, and WAYMOUNTH became interested in the field of these homogeneous catalysts. Hence, a reference to highly recommended review articles is provided at this point.[18-20]

Even though the first success in structure-reactivity relationship was achieved, mechanistic insights into monomer coordination, activation, and polymerization as well as termination were difficult to achieve, due to the poorly characterized MAO co-catalyst. However, a very important discovery was made, MAO always contained a significant ratio of trimethylaluminum (10-15%), which was proven to react as an alkylation reagent.[21] This finding directed the focus on new metallocene alkyl complexes and their cationic species. Another breakthrough was made, when JORDAN ET AL. isolated and fully characterized a cationic metallocene alkyl compound, received by methyl abstraction of [Cp_2ZrMe_2] (**1**) (Scheme 2).[22] In addition, the same group showed that the weakly coordinating anion $[BPh_4]^-$ did not prevent the catalytic activity, and the compound was active in olefin polymerization in the absence of any further co-catalyst. This was consistent with a polymerization mechanism proposed by COSSEE[23] and ARLMAN[24], which predicted a coordinatively unsaturated cationic alkyl complex $[L_xMR(Do)_y]^+$ as the active species (vide infra).

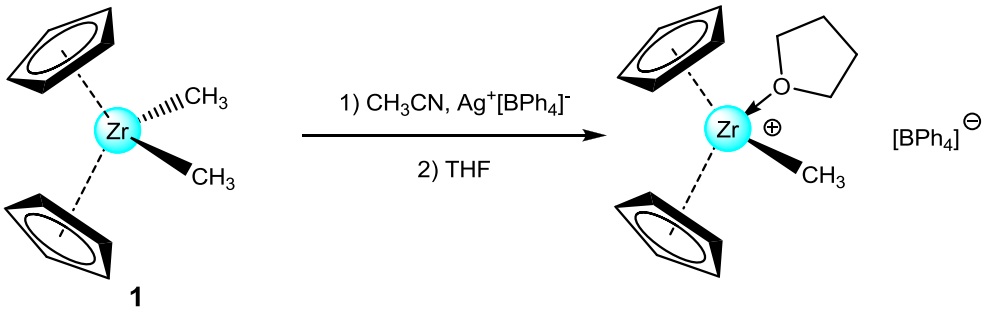

Scheme 2: Cationization of dimethyl zirconocene generates an active catalyst for ethylene polymerization.[22]

With the aim of gaining more knowledge about the cationic species and influence of weakly coordinating anions, new organo-borane and –borate reagents were developed as efficient co-catalysts. The formation of the cationic complex differed from the alkyl abstraction, most common are the reaction with trityl-borate [Ph_3C][$B(C_6F_5)_4$] (**A**), protonolysis of one alkyl ligand via bulky ammonium reagents [$RNMe_2H$][$B(C_6F_5)_4$] (**B**) or ligand transfer to the neutral organoboron reagent [$B(C_6F_5)$] (**C**) (Scheme 3). The thermodynamic and geometric nature of the weakly bonded ion-pair has significant influence on the catalytic activity and was intensively studied by MARKS and co-workers.[25-27] A review article concerning structure-activity relationships of various co-catalysts for olefin polymerization was presented in 2000.[28]

$Cp_2MR_2 + [Ph_3C][B(C_6F_5)_4]$ (**A**) ⟶ $[Cp_2MR]^+[B(C_6F_5)_4]^- + [Ph_3CR]$

$Cp_2MR_2 + [RNMe_2H][B(C_6F_5)_4]$ (**B**) ⟶ $[Cp_2MR]^+[B(C_6F_5)_4]^- + HR + RNMe_2$

$Cp_2MR_2 + [B(C_6F_5)_3]$ (**C**) ⟶ $[Cp_2MR]^+[RB(C_6F_5)_3]^-$

Scheme 3: Perfluorated organo-borate and -borane reagents as co-catalysts.

A correlation between the weakness of the coordination of anions with delocalized borate structure towards zircocene dimethyl complexes L_2ZrMe_2 and the activity in propylene polymerization was also presented by the group of BOCHMANN. The introduction of cyanoborates revealed anions with reduced nucleophilicity and resulted in enhanced catalytic activities (Figure 2).[29] Furthermore, it is known that the use of aluminum alkyl species as co-activator can significantly influence the catalytic system, whereas the reaction of boron-C_6F_5 compounds with organoaluminum reagents is not fully understood.[30] Some aspects concerning $[C_6F_5]^- \rightarrow [R]^-$ (R = Me, ^{i}Bu) ligand exchange between boron and aluminum species as well as the following coordination of the resulting anionic species were reported recently.[30] Solid-state structural analysis of the activated species features information about the charge–separated character, but single crystal growth is often hindered by the formation of oily products, especially in case of rare-earth metal complexes. Basic achievements are given in the review article by CHEN and MARKS.[28] An interesting crystal structure of an activated rare-earth metal half-sandwich aluminate complex was presented by the group of ANWANDER.[31] The activation of $[(C_5Me_5)La(AlMe_4)_2]$ with one equivalent of Lewis acidic $B(C_6F_5)_3$ instantly and quantitatively yielded the ion pair $[\{[(C_5Me_5)La\{(\mu\text{-}Me)_2AlMe(C_6F_5)\}][Me_2Al(C_6F_5)_2]\}_2]$ as the product of very fast sequential CH_3/C_6F_5 exchange processes (Scheme 4). The isolated compound was further shown to act as a single-component catalyst in isoprene polymerization.

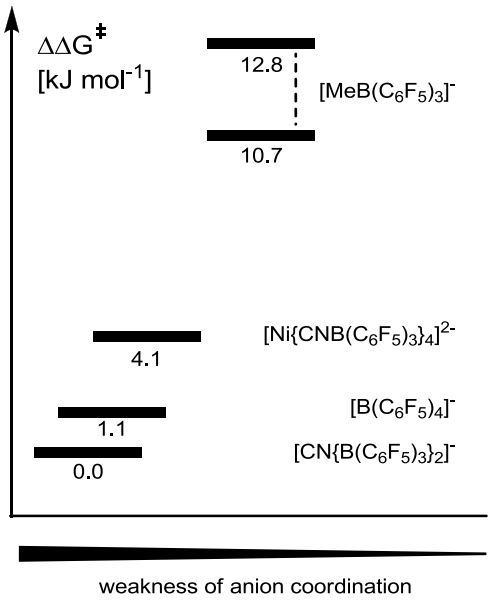

Figure 2: Differences in activation barriers for propen polymerization with $Me_2Si(Ind)_2ZrMe_2$.[29]

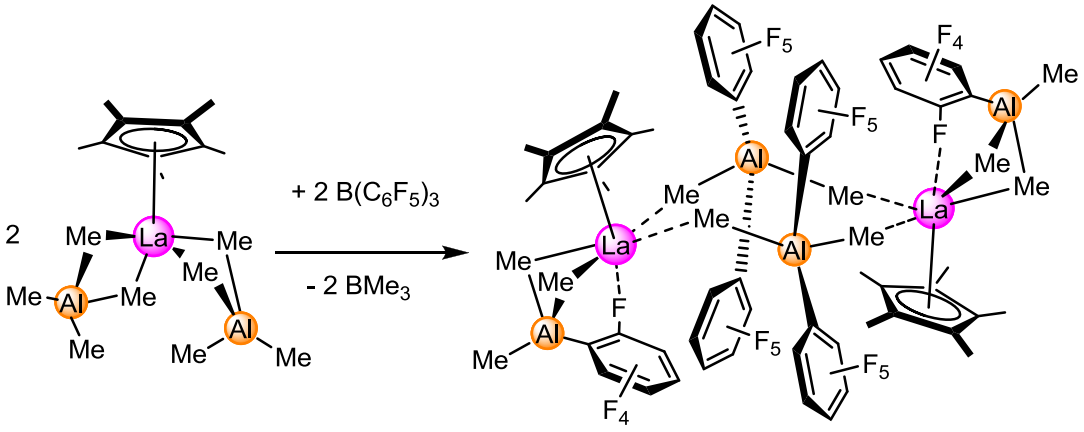

Scheme 4: Single-component catalyst formed by activation of [Cp*La($AlMe_4$)$_2$] with $B(C_6F_5)_3$.[31]

During the studies of polymerization reactions with a variety of olefins, it became clear, that the catalytic activity depends on the tendency to coordinate with the weak LEWIS base olefin molecule at the vacant site of the metal center. Heavier α-olefins were sterically hindered by the cyclopentadienyls of the metallocenes. A useful tool, to increase the open coordination sphere at the metal center, was the connection of the two Cp ligands with a small linker. The first *ansa*-metallocene tested in the polymerization of ethylene was the 1,1-methylenetitanocene dichloride [$CH_2(C_5H_4)_2TiCl_2$] reported by KATZ and ACTON,[32] and was structurally characterized by the group of BRINTZINGER (Figure 3).[33] Unfortunately, no significant difference to [Cp_2TiCl_2] could be observed. Nevertheless, BRINTZINGER continued his research in the field of chiral bridged metallocenes and could enlighten the structure-selectivity relationship of single-site catalysts in stereoselective α-olefin polymerization.[34] Together with EWEN and KAMINSKY, he demonstrated that *meso ansa*-metallocenes gave *atactic*, while the *racemic* ones produced *isotactic* polypropylene.[35-36]

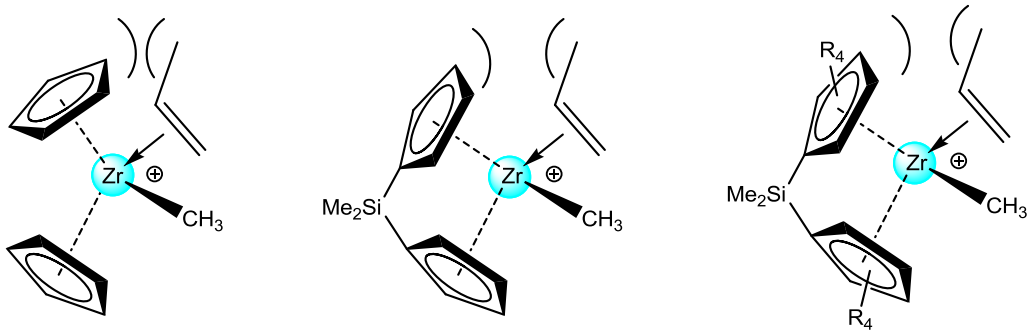

Figure 3: Steric hindrance guides monomer coordination at *ansa*-metallocene catalysts.

The resulting polymer microstructure depends on the regioselectivity and enantiofacial selectivity as well as the stereospecificity of the monomer insertion. Thereby, two different modes are possible, either the last monomer of the growing chain influences the insertion of the next one in a “chain end controlled” manner or the catalysts geometry directs the orientation of the incoming monomer in an “enantiomorphic site control” mechanism. The *ansa*-metallocene catalysts for olefin polymerization are classified in five symmetry categories, referred to as “Ewen´s symmetry rules” (Figure 4).

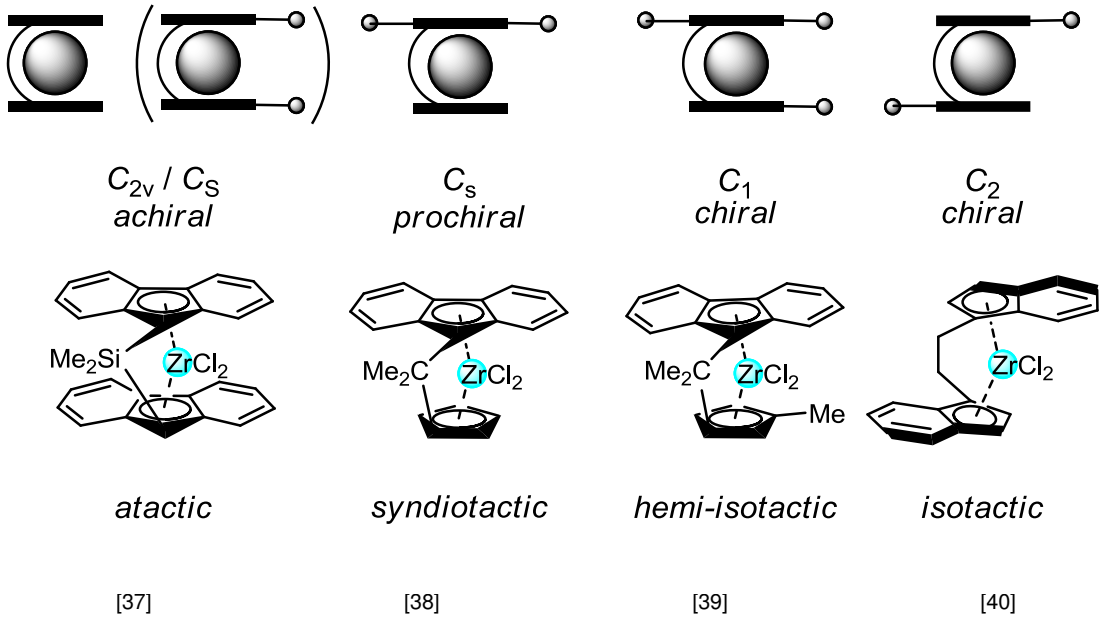

Figure 4: Symmetry of selected metallocene catalysts for stereo-specific propylene polymerization.

When the metallocene is achiral (C_{2v}, C_S), a special coordination mode of the incoming monomer is not preferred, thus an *atactic* microstructure is achieved. In contrast, (pro-)chirality of the catalyst leads to specific tacticity of the resulting polymer. In particular, the two alternating potential vacant sites in C_S-symmetric catalysts lead to *syndiotacticity*, while the vacant sites in C_2-symmetry are homotopic resulting in *isotactic* polymers. In case of the C_1-symmetric metallocenes only one site has significant effect on the stereoregulation, producing *hemi-isotactic* polyolefines.

1.3 Organolanthanide Catalysts

The rare-earth metals compromise the group 3 metals Sc, Y, and La, as well as the fourteen 4*f* electron shell elements Ce, Pr, Nd, Pm, Sm, Eu, Gd, Tb, Dy, Ho, Er, Tm and Yb, also known as the lanthanides. Their predominant oxidation state is Ln^{III}, but in case of Ce organometallic compounds in the tetravalent Ln^{IV} spezies have been synthesized, while the divalent Ln^{II} oxidation state is easily accessible for Sm, Eu, Tm, and Yb. The 4*f* valence orbitals of the lanthanides can be seen as an inner shell, shielded by the 5*s* and 5*p* orbitals being part of the inner xenon core and even if the internal structure is very intricate, this results in two very striking features. First, poor overlap with ligand orbitals lead to predominant ionic character of the organo-metal bond in lanthanide complexes and in contrast to *d*-block transition metals a wide range of coordination numbers from 6 to 12 is accessible. Furthermore, the 18 valence electron rule and donor/acceptor interaction cannot be applied. Secondly, due to the weak shielding of the 4*f* electrons a gradual decrease in the ionic radii with increasing effective nuclear charge from lanthanum to lutetium is observed (Figure 5).

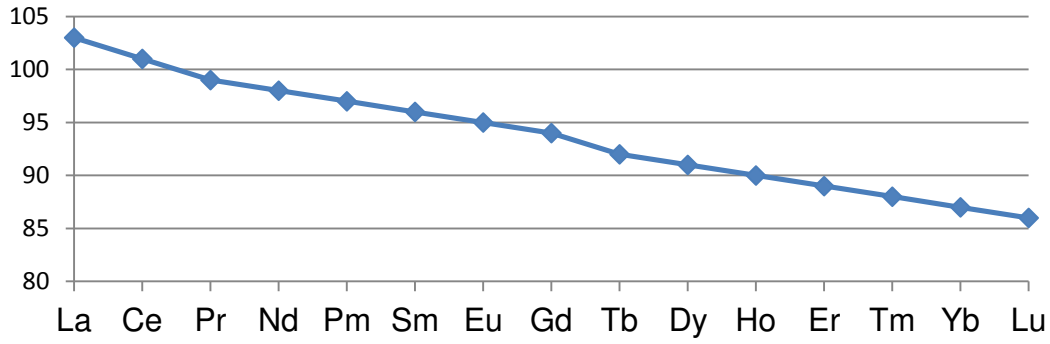

Figure 5: Lanthanide contraction from lanthanum (57) to lutetium (71).[41]

These characteristics lead to significant differences in the organometallic chemistry of the rare-earth elements compared to the d-block transition metals. The accessibility, stability, and reactivity of lanthanide complexes are mainly influenced by electronic and steric saturation and can specifically fine-tuned by the bulkiness of the ligands and the choice of the metal center. Additional donor coordination or solvent complexation is often observed when the metal environment is sterically unsaturated and ionic ate complex formation can occur during salt metathesis reactions, usually causing a decrease in reactivity. To counteract the undesirable reactions, subtle synthetic pathways have been elaborated and complexes of metallocene, half-sandwich and post-metallocene type represent a large number of rare-earth metal based catalysts.

In 1965, lanthanide-based polymerization systems for 1,3-dienes were already patented,[42-43] but it took another thirteen years before BALLARD ET AL.[44] described the first isolated organolanthanide complexes active in ethylene polymerization. The neutral metallocene alkyl and aluminate complexes $[(C_5H_4R)_2LnMe]_2$ and $[(C_5H_4R)_2LnMe_2AlMe_2]$ are isoelectronic compared to the cationic complexes of group 4 metals and showed moderate activity at 70-105 °C without the addition of any further co-catalyst (Figure 6).

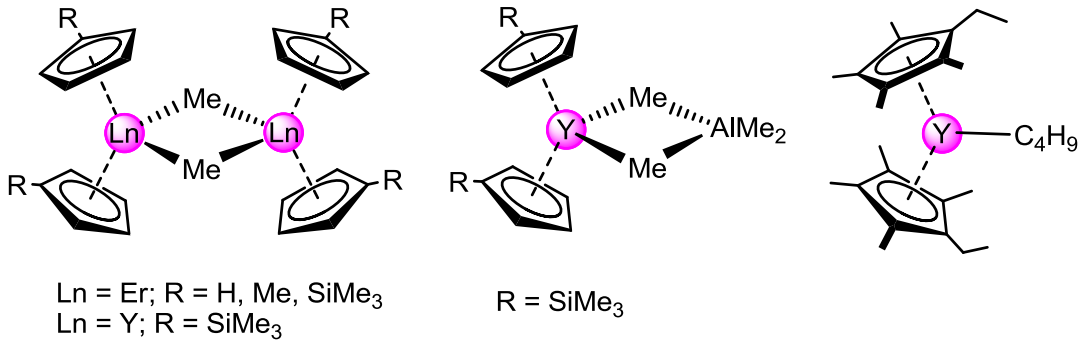

Figure 6: First isolated lanthanide metallocene complexes active in ethylene polymerization.[44]

Encouraged by this findings, WATSON investigated the polymerization activity of the methyl complexes $[(C_5Me_5)_2LnMe]_2$ of the heavier lanthanide elements ytterbium and lutetium, chosen because of their smaller ionic radii, and hence more related to those of the transition metals (Scheme 5).[45-47] Due to its diamagnetism, the lutetium complex enabled mechanistic investigations via NMR spectroscopy and the insertion of propylene into the metal-methyl bond was verified. In 1985, MARKS and co-workers reported a comprehensive study on lanthanide metallocene hydrocarbyl and hydride complexes as catalysts in ethylene polymerization in a series of three publications.[48-50] They found, that the catalytic activity decreased with the ion radii of the lanthanide metal across the series lanthanum to lutetium and that the hydride complexes outperfomed the alkyl counterparts.[49] The change from bis(pentamethylclyclopentadienyl) to $[Me_2Si]$ ansa-bridged lanthanide hydride complexes $[Me_2Si(C_5Me_4)_2LnH]$ generated a tenfold higher activity, as a result of their wider open ligand sphere.[50]

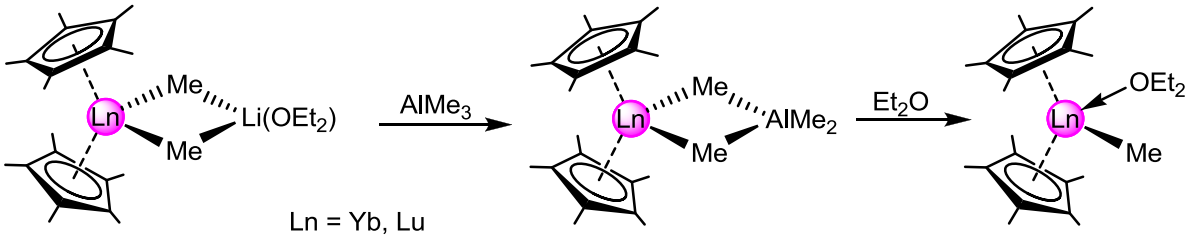

Scheme 5: First synthesis of lanthanide metallocene complexes active in propylene polymerization.[51]

1.4 1,3-Diene Polymerization

Some of the most important polymers produced by plants are natural rubber (NR, caoutchouc or *cis*-polyisoprene; >99% *cis* content, M_n = 2 x 10^6 $gmol^{-1}$) from the rubber tree *hevea brasiliensis*, which is used for numerous latex applications, and the all-*trans* isomer Gutta–percha (>99% *trans*) produced by *Palaquium gutta* and several other evergreen trees of East Asia. Considering the limited supply of these natural products and increasing demand on high performance synthetic rubbers, the development of catalyst systems producing highly stereoregulated polymers has grown in importance. The first synthetic rubber was produced by BOUCHARDAT in 1879, when he heated a mixture of isoprene with hydrochlorid acid, but the quality was low and the isoprene was extracted from natural rubber.[52-53] Searching for low cost alternatives, it was HOFMANN in 1909 who patented the first sodium metal initiated 1,3-diene polymerization of 2,4-dimethylbutadiene at the Bayer Werke.[4] One year later, the Russian chemist LEBEDEV reported the polymerization of 1,3-butadiene, obtaining a product much more similar to natural rubber in physical properties and application-specific processability.[54] His further work, summarized in his book *Research in polymerization of diethylene hydrocarbons*, laid the foundation of industrial large-scale production, which experienced an intense growth during World War II. Although the 1,3-conjugated dienes could later be co-polymerized with styrene (BunaS)[55] and acrylnitrile (NBR)[56], to enhance their characteristics, via anionic and radical mechanisms, the molecular weight distributions were broad and their stereoregularity poor. Beside the *cis*-1,4 and *trans*-1,4 configuration found in the natural rubbers, 1,2 (polybutadiene) and 3,4 (polyisoprene) carbon-carbon bond formations where found in synthesized polymers, which further show *iso*-, *syndio*-, or *atactic*- regularities of the vinyl groups similar to *α*-polyolefins (Figure 7).[57]

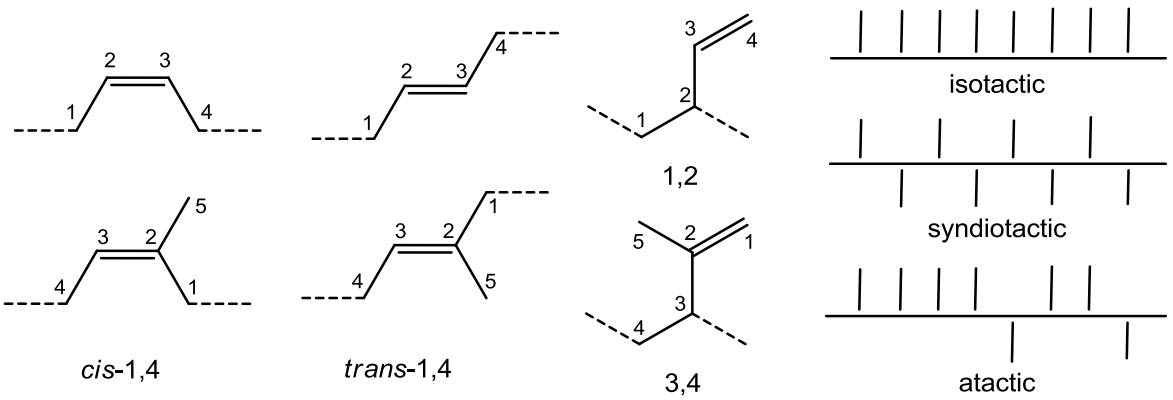

Figure 7: Possible stereoisomers of polybutadiene and isoprene.

The major breakthrough in the stereoregulated polymerization of 1,3-dienes came with the development of the transition-metal ([Cr][58], [Ti][59], [V][60-62], [Ln][63]) based Ziegler-Natta catalysts in the mid 1950s.[64] Today, mainly two systems are commercially used, as they exhibit advantages in preparation, thermal stability, economics, and handling compared to metallocene catalysts. The heterogeneous binary systems consist of metal-halides and organoaluminum compounds as alkylation agent and the homogeneous ternary systems are based on various metal precursors (ML_x, L = alkyl/aryl oxide, carboxylate, phosphate, allyl, amide) combined with alkyl- (AlR_3, MgR_2) and halide- (R_2AlX, X = halogen) sources. The versatility of those catalyst systems regarding their stereoregulation in the polymerization of 1,3-dienes depends on the chosen transition metal, the coordinated ligands, the kind of activator, and the substitution of the 1,3-diene monomer. Historical developments and selective catalytic systems are given in the *Encyclopedia of Polymer Science and Technology* by KERNS[65] and in *Principles of Coordination Polymerization* by KURAN.[66] As neodymium demonstrates the most striking features in 1,3-diene polymerization of the rare-earth elements, a comprehensive overview highlighting binary and ternary systems of conventional and modified (Nd)-based Ziegler-Natta catalysts, is given by FRIEBE[67] and FISCHBACH.[68] In 2010, Zhang et al. reviewed the progress in rare-earth metal-based 1,3-diene polymerization in the decade from 1999 to 2009.[69] Special emphasis was put on the evolution of homogeneous single-site catalysts, the correlation between the molecular structure and their catalytic performance and the proposed generation of the activated species.

1.5 Constrained Geometry Catalysts (CGC)

From the early days of single-site catalysts, the above mentioned metallocene and *ansa*-metallocene complexes predominated the field in organolanthanide chemistry and their application in catalytic processes. On the one hand, the ligand framework with its η^5-coordinating cyclopentadienyls, exhibits excellent steric saturation and thermal stability, on the other hand it generates a well defined reaction site, hence allowing investigations in structure-reactivity relationships and fine-tuning of the vacant site. In contrast to the group 4 metals, metallocene complexes of the rare-earth elements do not permit formation of a catalytically active species via alkyl abstracting cationization, since no σ-metal-carbon bond for the monomer insertion remains. Corresponding half-sandwich complexes of [$CpLnR_2$] type involve considerable synthetic difficulties as a result of the reduced steric shielding of the electron deficient rare-earth metal center. An important progress was the invention of the chelating amido-cyclopentadienyl ligand by BERCAW and SHAPIRO in the late 1980´s, creating a well-controlled reaction site, offering systematical investigations in structure depending reactivity (Figure 8).[70-72]

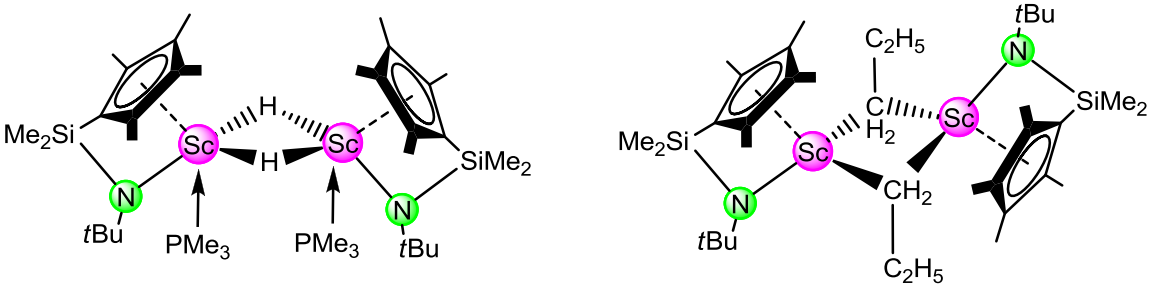

Figure 8: Scandium hydride and propyl complexes with constrained geometry.[72]

The term “constrained geometry catalyst” (CGC) was introduced shortly afterwards when the DOW CHEMICAL[73] and the EXXON CHEMICAL[74] companies independently developed analogous complexes of group 4 metals, which have become some of the industrially most important single-site olefin polymerization catalysts.[75] The eight electron donating amido-cyclopentadienyl (**2**) ligands can be conceived as a hybrid between a six-electron diamido ligand (**1**) and the more common *ansa*-bis(cyclopentadienyl) ligand (**3**) donating ten electrons (Figure 9). A comprehensive overview of rare-earth metal-based CGC´s, detailing steric and electronic effects, configuration geometries, variation of the active ligands as well as application in catalysis reactions was given by OKUDA in 2003.[76]

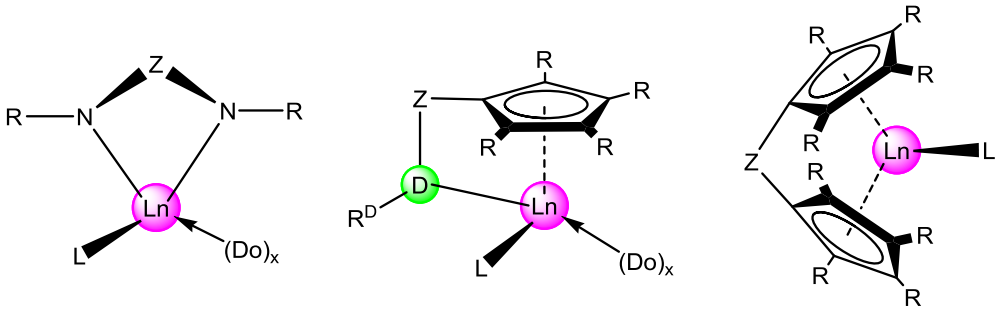

6 e⁻ donor
L_2X_2-type
1

8 e⁻ donor
L_3X_2-type
2

10 e⁻ donor
L_4X_2-type
3

Figure 9: Variable amount of electrons donated by dianionic ancillary ligands.[76]

As a rule, these complexes display no activity in 1,3-diene polymerization, requiring a metal–carbon or –hydride bond for the monomer insertion after cationization. The most investigated catalysts therefore are half-sandwich rare-earth metal complexes of the $[(Cp^R)Ln^{III}(Do)_xR_2]$-type, bearing the six-electron donating cyclopentadienyl ligand and σ-bonded alkyl groups, but electronic and steric unsaturation often led to incorporation of neutral donor ligands (**4**, Figure 10).

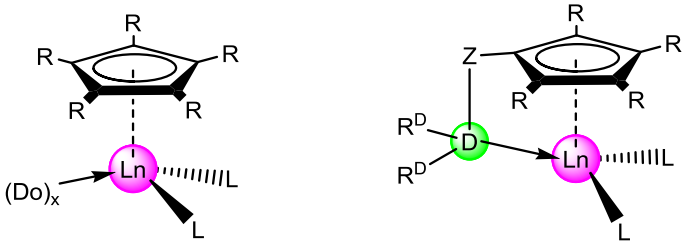

5 e⁻ donor
L_2X_1-type
4

7 e⁻ donor
L_3X_1-type
5

Figure 10: Electronic and steric modification of mono-anionic cyclopentadienyl ligands.[76]

Avoiding unintended coordination, the introduction of a neutral donor-sidearm functionality at the cyclopentadienyls, indenyls, and fluorenyls as monoanionic ancillary ligands can mimic “constrained geometry” configuration, creating “solvent free” and highly stable pre-catalysts for 1,3-diene polymerization. Additionally, the functionalization allows independent variations, accomplishing well-defined reaction sites.

1.6 Modification of Donor-Functionalized Cyclopentadienyls

The properties of the above described single-site complexes are directly dependent on the ligand environment. The choice of ligands, in regard to their size, basicity and functionalization, has a strong influence on the stability of the binding towards the metal center. Ligand variations present an opportunity to explore the structure-reactivity relationship of the final complex in catalytic reactions.

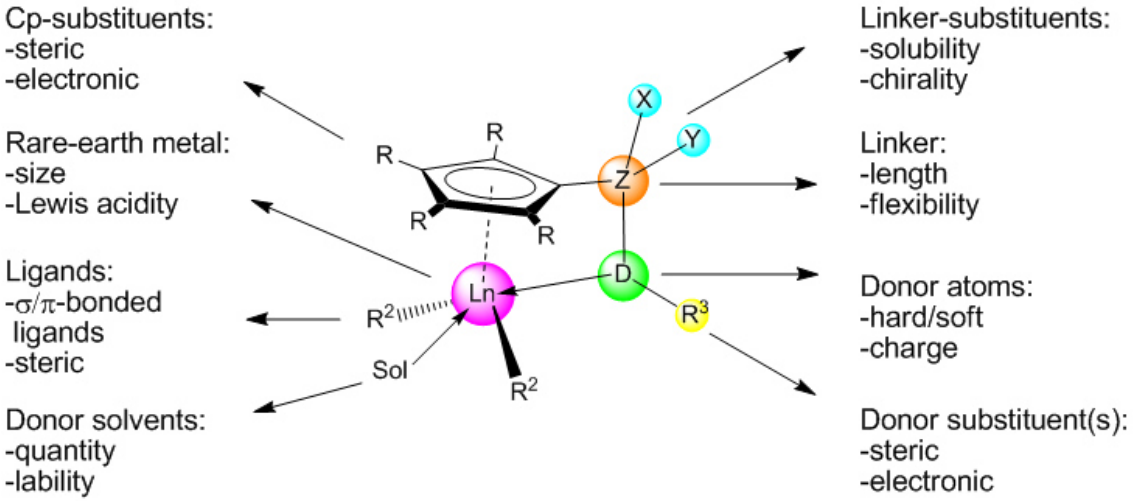

Figure 11: Versatile possibilities in modification of constrained geometry catalysts.

Possible variations at the cyclopentadienyl fragments of the rare-earth metal complexes are shown in Figure 11 on the left hand side. Beside the significant influence of the choice of the metal center **Ln** itself, modifications at the "spectator ligand", also described as ancillary ligand, which does not directly participate in the reactions, and the "actor ligands", which play a prominent role in insertion, exchange and activation sequences are tuned to optimize the desired activity.

Changes at the Cp^R ligand mainly influence the steric and electronic properties of the single-site complexes and also affect their solubility in aliphatic or aromatic hydrocarbonyl solvents. While initially only un- or methyl-substituted cyclopentadienyls of $[C_5H_{(5-X)}R_X]$ type were of major interest, variation of the substituents like **R** = $SiMe_3$, *t*Bu, Ph, have been intensively explored in the last decades.[77] Furthermore, other η^5 coordinating ligands like indenyl and fluorenyl were tested, but in some cases a change of the hapticity to η^3 and η^1 via "ring-slippage" was observed. Similar behavior occurred when heterocyclic 6-electron donating fragments like pyrrolyl,[78] boratabenzene,[79-80] and phospholide[81] were used.

The alteration of the “actor ligands” $\mathbf{R_2}$ for catalytically active half-sandwich and constrained-geometry complexes of the rare-earth metals is predominantly based on the halides, amides, alkyls and aryls, while the latter are preferred due to their superior cationization accessibility with borane and borate activation reagents.

In addition, the constrained-geometry complexes feature several modification possibilities, due to the supplementary donor-sidearm, which can generate chirality when attached to a single or unsymmetrical substituted cyclopentadienyl or bearing a stereogenic center (**X**, **Y**) in the linker **Z** or at the donoratom **D**. One of the most common linker fragments is -SiR_2-, because of its relatively simple incorporation and thermal, as well as chemical, stability. The bite angle of the ligand can be varied by the length of the bridge to form five- or six-membered metallocycles and significantly affects the open reactive site. More rigid spacers are received when double-bonds like –CH=CH-, -P=N-, and aromatic rings are used which also influence the electronic effects of the chelating ligand. As atoms for coordination towards the relatively hard LEWIS acidic rare-earth elements, the hard donors nitrogen and oxygen are commonly used but also sulfur and phosphorous are reported in literature (Chapter 2). For the polymerization of 1,3-conjugated dienes these atoms are neutral 2-electron donators via their lone electron pair, while in α-olefin polymerization often di-anionic ligands are presented (Figure 9). Very recently carbenes and olefines were also tested as potential electron donors in the CGC synthesis (Chapter 2).

1.7 Synthesis of Functionalized Cyclopentadienes

Beside the functionalization of Cp ligands, which are already bound towards a metal center *via* intramolecular coupling reactions, five synthesis routes dominate the literature (Scheme 6, **A**-**E**).

The most common route follows the salt-metathesis reaction of alkali-metalated cyclopentadienyl AMCp (AM = Li, Na, K) with ω-halogenids of the sidearm (Scheme 6, **A**). This route is limited by unsubstituted cyclopentadienyl C_5H_5 due to formation of an isomer mixture with geminal disubstitution and the requirement of stable ω-halides. Alternatively, the nucleophilic reaction at the cyclopropane ring of spiro[2.4]hepta-4.6-diene allows substituents in 4-7 positions to form bulkier cyclopentadienes, but requires stable, nucleophilic anions of the donor-functionalized sidearm (Scheme 6, **B**). Very similar, the conversion of fulvene with nucleophilic anions leads to the desired substituted cyclopentadienyl derivatives (Scheme 6, **C**). However, substituted fulvenes are only accessible from the corresponding ketones.

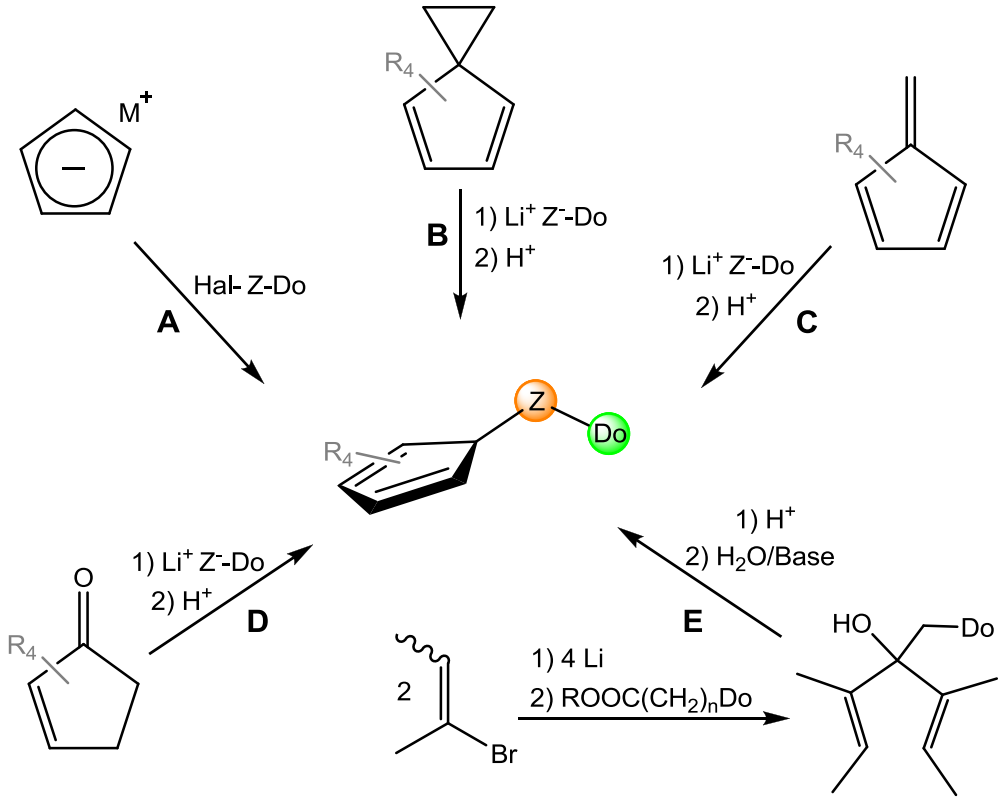

Scheme 6: Synthesis approaches for donor substituted cyclopentadienes.

Therefore, the synthesis of donor-functionalized tetramethylcyclopentadienyls is commonly based on one of the following two strategies. If the desired sidearm can be easily transformed into a stable nucleophilic anion as already required for route **B** and **C**, it can react with 2,3,4,5-tetramethylcyclopent-2-en-1-on to form the 1-functionalized cyclopent-2-en-1-olat. Acidic workup will then lead to the second double bond under water elimination (Scheme 6, **D**). In contrast to the previous strategies, involving functionalization of cyclopentadiene, the last synthesis route begins from two C_2 and one C_1 units to build the ring in a "bottom-up" reaction (Scheme 6, **E**). The dicondensation of appropriately substituted esters with 2-but-2-enyllithium yields the corresponding 4-functionalized 3,5-dimethylhepta-2,5-dien-4-ol and the following acid catalyzed ring closing reaction of NAZAROV type leads to the expected cyclopentadiens.[82-83]

1.8 Mechanistic Aspects

As previously mentioned, the understanding of the basic reaction mechanisms responsible for the regio- and stereoselective growth of polymer chains at heterogeneous ZIEGLER-NATTA catalysts, have been a challenging task since their discovery. A fundamental review, written by PINO and MÜLHAUPT in 1980, ends with the sentence:[18] "In spite of the great amount of research in the field of stereospecific polymerization that has been performed in the 25 years since its discovery, it appears that this subject will remain of paramount importance for the development of chemistry and of polymer science for a long time in the future." With the evolution of the metallocene single-site catalysts, tremendous developments have been made in the mechanistic comprehensions of key steps in α-olefin polymerization processes, involving the formation of the active species, chain propagation and termination sequences, but also the polymerization of many other monomers, like methyl methacrylate (MMA) and 1,3-diene as well as a large variety of co-polymerizations were disclosed.

1.8.1 α-Olefin Polymerization

Not only in compliance with the historical development but also in regard to the lateron described 1,2- and 3,4-polymerization of 1,3-dienes some mechanistic aspects of the widely explored α-olefin polymerization will be summarized. The fundamental requirement of ZIEGLER-NATTA type catalysts is a LEWIS acidic transition metal with a vacant coordination site and a *cis*-positioned metal hydrogen or carbon bond into which the monomer can insert. In the heterogeneous systems, only a few of the transition metal atoms are actually catalytically active, limited to the alkylated atoms on the surface as shown in Scheme 7.

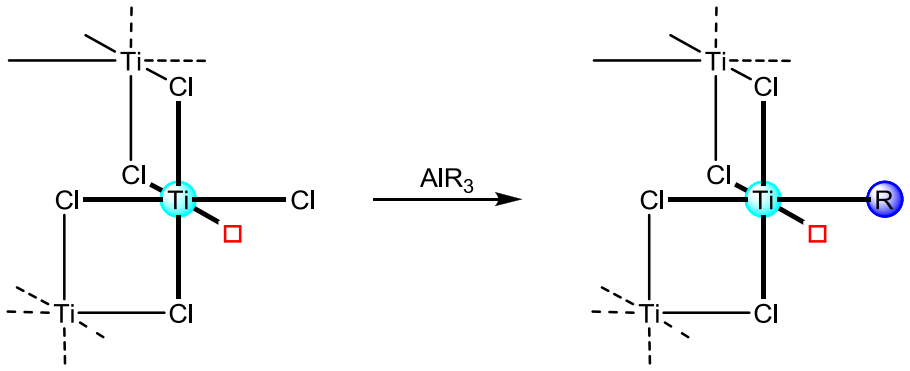

Scheme 7: Alkylation of the penta-coordinated titanium ions on the surface of α-$TiCl_3$.

In the general accepted mechanism for heterogeneous catalysts as postulated by COSSEE and ARLMAN,[23-24] the initial step is the π-coordination of the olefin, followed by formation of a four member intermediate and subsequent *cis*-insertion into the metal-carbon bond (Scheme 8).

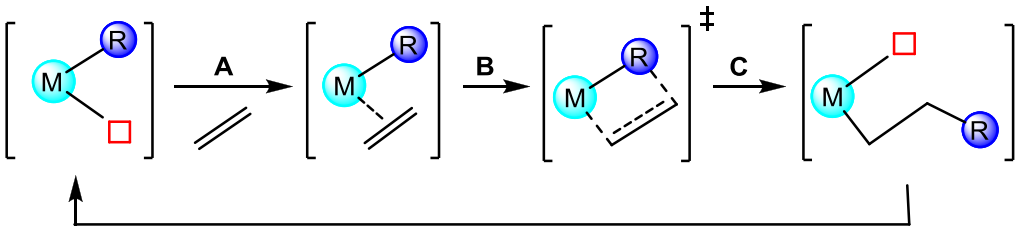

Scheme 8: COSSEE-ARLMAN mechanism for α-olefin polymerization. [23-24]

The transition state of the insertion has been widely discussed because experimental identifictions of the highly reactive intermediates are very limited. A stereoregulative effect might be reversible α-hydrogen elimination under formation of a hydride carbene species. [84] The following [2+2] addition of the olefin would lead to a metallacyclobutane and the propagation sequence ends via reductive elimination (Scheme 9, Path B). Investigations by BROOKHART and co-workers showed that the C–H bond is never fully broken, but α-agostic interaction with the metal center occurs (Scheme 9, Path A).[85-86] A detailed analysis of the possible mechanism was reported by GRUBBS and COATS.[87]

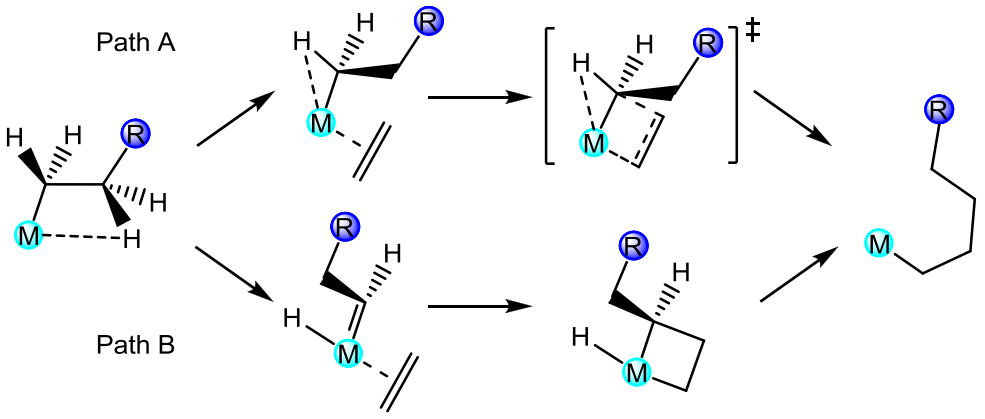

Scheme 9: Possible pathways for the *cis*-insertion of the olefin by Grubbs and Coats.[87]

The first examinations of regioselectivity were carried out already in the 1950s by end group determination of the produced polymers, where terminal methyl or methylene groups were detected for the [1,2] insertion, as shown in Scheme 10. In case of the larger vanadium metal based heterogeneous catalysts, the sterically more demanding [2,1] insertion was observed.[35, 88]

With the emergence of well defined single-site catalysts and the elaboration of stereo-controlled polymerization of propylene and higher α-olefins, mechanistic investigations of the coordination of the monomer and propagation of the polymer chain became feasible (see 1.2). Further, IR and NMR spectroscopy as well as powder X-ray diffraction of the resulting polymers became important tools for identifying stereoselective catalysts.[18]

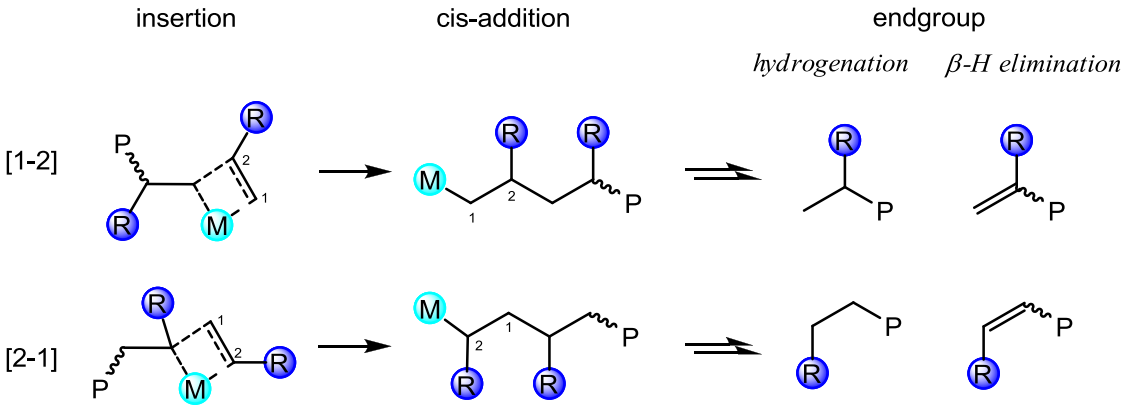

Scheme 10: [1,2] & [2,1] insertion analyzed by endgroup determination via NMR spectroscopy.

Additionally, combination of experimental data and quantum mechanical and molecular mechanics (QM/MM) studies could allocate the regioselective [1,2] insertion of propene for selected metallocene catalysts. In 2002, BORELLI ET AL. investigated the (co-)polymerization of propene and ethane by titanium and zirconium based metallocenes and evaluated the possible dormant character of secondary alkyls towards propene.[89] As described previously, the stereocontrol of olefin polymerization highly depends on the structure of the catalyst.[19]

1.8.2 1,3-Diene Polymerization

The mechanistic aspects of 1,3-diene polymerization, as already introduced in chapter 1.4, is far more complicated than the one of monoalkenes. Thereby, the 1,2- or 3,4-insertion of butadiene and isoprene, respectively, can follow afore mentioned COSSEE and ARLMAN mechanism.

However, the structure-reactivity relationship of the catalytic reaction mechanism for the 1,3-diene polymerization is controversially discussed. In the early stage, the coordination mode of the monomer was the essential step for the stereoregulation. While the monodentate η^2 coordination leads to *trans*-1,4 polymer, the formation of *cis*-1,4 polymers requires the bidentate η^4 coordination of the diene. With the discovery of allyl-transition complexes as promising pre-catalysts for diene polymerization by PORRI[90] and WILKE[91] in the mid 1960´s, this organometallic species moved into the focus and the allyl-insertion mechanism was proven by ^{1}H NMR spectroscopy.[92] Further studies

on transition-metal allyl complexes lead to the chain-end controlled mechanism, whereby the last coordinated monomer unit of the growing polymer is critical for the stereoregulation.[93-94] Mechanistic studies dealing with rare-earth metal allyl complexes as catalysts for 1,3-dienes were reported by TAUBE ET AL more recently.[95]

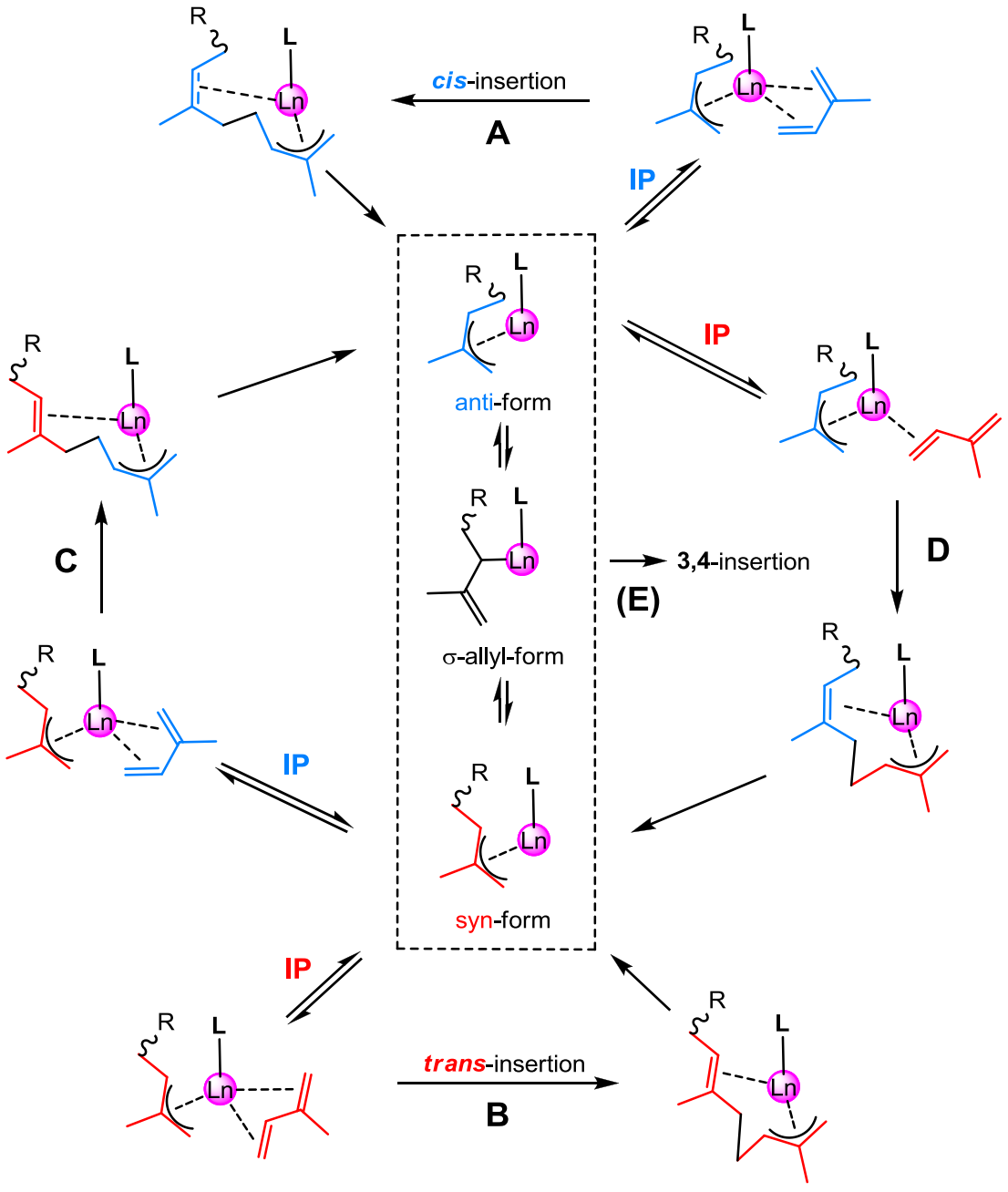

Scheme 11: Proposed mechanism for the isoprene insertion into the π-allyl metal complex.[105]

The pathway of the direct allyl-insertion mechanism, in respect to the *syn*- and *anti*-conformation of the allylic species initiating the *trans* and *cis* stereochemistry of the polymer, is summarized in Scheme 11. It is worth mentioning, that the first insertion of a 1,3-diene into a metal-carbon or –hydride

bond will lead to the active π-bonded allyl species and therefore the following scenario is universal for anionic coordination polymerization of 1,3-dienes at any active cationic rare-earth metal pre-catalyst.

Independent of the coordination mode of the inserting monomer, the *anti*-η^3 intermediate will form a *cis* unit as shown for pathways **A** and **D** (blue), while the *syn*-η^3 bonded allylic intermediate results in a *trans* unit (**B** and **C**, red). The pre-conformation of the inserted diene certainly affects the coordination of the newly generated allyl species. The η^4-*cis* or η^2-*cis* coordination (blue) favors the *anti*-, whereas the corresponding *trans* coordination (red) favors the *syn*-π-allylic intermediate. Hence, the most straightforward pathways to highly stereoregulated 1,4-polymers are those, where the *anti-cis* or the *syn-trans* correlation is supported by a convenient pre-coordination of the monomer (**A** and **B**). But even when the insertion of the next monomer leads to a change of the allylic conformation (**C** and **D**), highly *cis* or *trans* regulation can be obtained through *syn-anti* isomerization via σ-π-rearrangement. Otherwise, this rearrangement can hamper selectivity if none of the coordination is remarkably favored. Furthermore, the σ-bonded allyl intermediate can interact as an α-olefine catalyst leading to 3,4 polymerization of isoprene (Scheme 12).

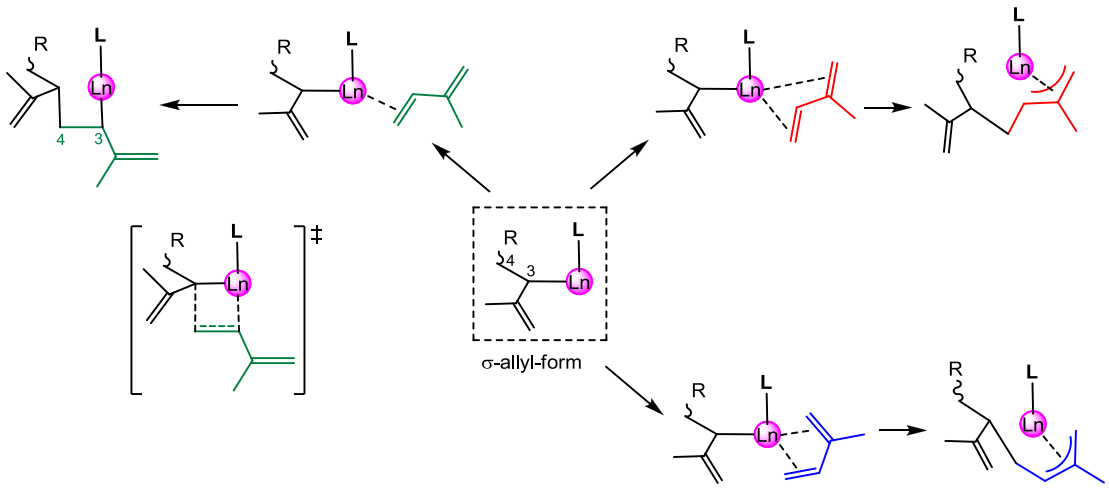

Scheme 12: Isoprene insertion into the σ-allyl species leading to 3,4-units in the polymer.

1.8.3 DFT Calculations

In the last decades, computational approaches have been becoming increasingly important to provide insights into mechanistic aspects of transition metal based polymerization reactions. Thereby, the most investigated catalyst

systems for polymerization of conjugated 1,3-dienes are either titanium or nickel based, and fundamental research results were published by TOBISCH.[96-105] A good overview is given in the introduction of a review article dealing with early and late transition metals.[106] However, reports of theoretical investigations in case of rare-earth metal based homo-diene and diene-olefin co-polymerizations remain scare (vide infra).

1.8.3.1 *Cis*-1,4-diene insertion

In 2009, the ternary catalytic system [Cp*Sc(BH_4)$_2$(thf)]/[Ph_3C][B(C_5F_5)$_4$]/Al(^{i}Bu)$_3$ was reported to polymerize isoprene highly selective (*cis*-1,4 PIP >97%) and was also shown to afford purely syndiotactic polystyrene.[107] One year later, BONNET and MARON published theoretical investigations, which provided insight into the mechanistic aspects of the isoprene polymerization.[108] Therefore, the active catalyst species was modeled as [Cp*ScEt]$^+$ and butadiene insertion was calculated instead of isoprene. However, the first diene insertion into the [Sc]-Et bond could only be realized by a *trans*-1,4 pre-coordination of the monomer, resulting in the formation of the [Cp*Sc(η^3-*syn*-(C_6H_{11})]$^+$ allylic species. The second and third monomer insertions were then calculated with either η^4-*cis*-1,4 or η^4-*trans*-1,4 coordination of the monomer, the energetic profiles are illustrated in Figure 12.

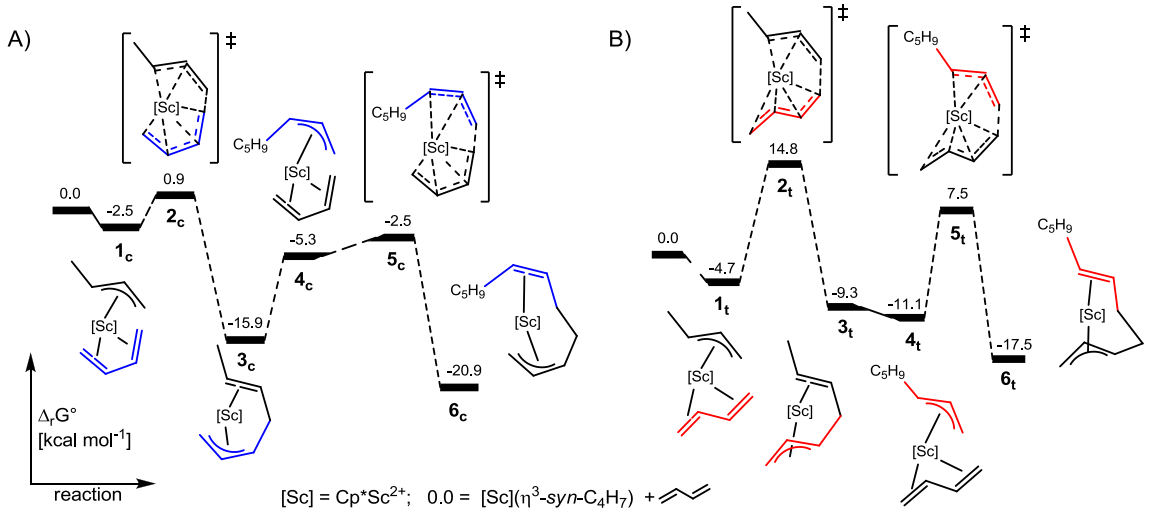

Figure 12: Free energy profile for A) *cis*-1,4- and B) *trans*-1,4-butadiene polymerization.[108]

In summary, *thermodynamically*, the *cis*-1,4 insertions for the products **3$_c$** and **6$_c$** (15.9 and 5.0 kcal mol^{-1}) are slightly favored over the *trans*-1,4 insertions for the products **3$_t$** and **6$_t$** (9.3 and 8.2 kcal mol^{-1}). However, *kinetically*, the *cis*-1,4 insertion showed much lower activation barriers for the transition states (TS) **2$_c$** and **5$_c$** than the *trans*-1,4 insertions for TS **2$_t$** and **5$_t$** (3.2 and 13.4 vs. 19.5 and 18.6 kcal mol^{-1}).Overall, the preferred *cis*-1,4 insertion is further facilitated by

the low steric hindrance in conjunction with the high acidity of the small rare-earth metal center of the cationic $[Cp^*ScR]^+$ complex. The calculated transition states further indicate, that an incoming η^4-butadiene inserts directly in the π-allyl system without a σ-π-rearrangement, preventing any 3,4-insertion of the monomer.

Possible scenarios of isoprene polymerization catalyzed by cationized half-sandwich scandium alkyl complexes supported by DFT calculations have also been reported by LI ET AL. in 2009. For the highly *cis*-1,4 selective polymerization (up to 95%), the intermediates of isoprene coordination and insertion at the least sterically crowded $[CpSc(CH_2SiMe_3)(thf)]^+$ were optimized. Thereby, the first coordination takes place in a η^2-3,4-*trans* mode. After insertion of a second isoprene molecule the η^3-*anti*-allyl intermediate of the growing polymer chain was calculated as *thermodynamically* favored, and thus afford the *cis*-1,4 poly-isoprene sequence. It is not further described that the η^2-3,4-*trans* coordination of the third isoprene molecule prefers a η^3-*anti*-allyl coordination of the growing chain and no transition state intermediates were calculated, disregarding activation barriers from *kinetic* aspects of the C–C coupling reaction. However, it is mentioned, that small steric hindrance around the metal center should shift the *syn-anti* equilibrium to the *thermodynamic* intermediate.

1.8.3.2 *Trans*-1,4-diene insertion

Based on the catalytically active system $[Cp^*La(BH_4)_2(thf)_{2.5}]$/EtMg^{n}Bu published in 2009,[109] theoretical investigations in homo- and co-polymerization of isoprene (calculated as butadiene) and ethylene were carried out by BONNET and MARON ET AL. in 2010.[110] The use of lithium *n*-butyl-tri-*n*-octyl-aluminate as alkylating reagent led to $[Cp^*La(BH_4)R]$ (R= *n*-butyl or *n*-octyl) as the initiating species. With focus on the homo-polymerization of the diene, the energetic profiles regarding *cis*-1,4 and *trans*-1,4 insertion are shown in Figure 13 adapted from the publication. In agreement with the experimental results, the *trans*-1,4 insertion was calculated to be *thermodynamically* and *kinetically* favored by 7.0 kcal mol^{-1} (B, $\mathbf{10_t}$) over the *cis*-1,4 insertion (endergonic 6.2 kcal mol^{-1}, $\mathbf{10_c}$).

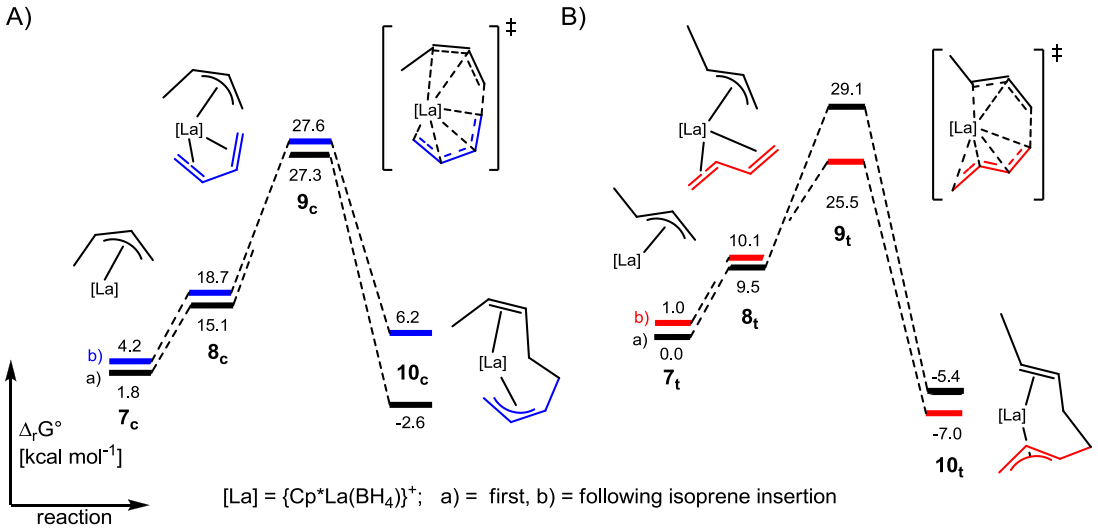

Figure 13: Free energy profile for *trans*-1,4 (A) and *cis*-1,4 (B) butadiene polymerization.[110]

1.8.3.3 3,4-Diene insertion

Unfortunately, no comprehensive computational studies have been undertaken for 3,4-insertion of butadiene or isoprene in case of rare-earth metal based catalysts concerning the *allyl*-insertion mechanism. However, in 2005, the silylene-linked cyclopentadienyl-phosphido rare-earth metal complexes $[(C_5Me_4)SiMe_2P(Cy)Ln(CH_2SiMe_3)]_2$ (Ln = Y, Lu; Cy = cyclohexyl) were reported to polymerize isoprene in isospecific 3,4 tacticity, when activated with $[Ph_3C][B(C_5F_5)_4]$ as co-catalyst.[111] It was also shown by DFT calculation, that the remaining alkyl group, CH_2SiMe_3, prefers a bridging mode between the two yttrium metal centers. Further calculations on the insertion of isoprene, and for comparison ethylene, into the metal-carbon bond were published one year later, whereas only the CH_2SiMe_3 ligand was modeled as CH_2SiH_3 and the methyl groups of the cyclopentadienyl were neglected (Figure 14 A and B).[112] The main difference was observed for the η^2-*trans*-3,4 coordination either on the vacant site (A, $\mathbf{1_v}$) or in exchange of the alkyl ligand (B, $\mathbf{1_v^I}$) of the less sterically crowded yttrium metal center. The isoprene insertion in case of A would lead to a four-center transition state $\mathbf{2_v}$, while the pathway B comes along a five-membered intermediate $\mathbf{2_v^I}$. The latter is kinetically favored by a lower free-energy barrier of 22.9 kcal mol^{-1} than the first (37.6 kcal mol^{-1}). The methylene carbon C4 of the inserted isoprene is in the rare-earth metal bridging position at the end of the sequences in both cases ($\mathbf{3_v}$).

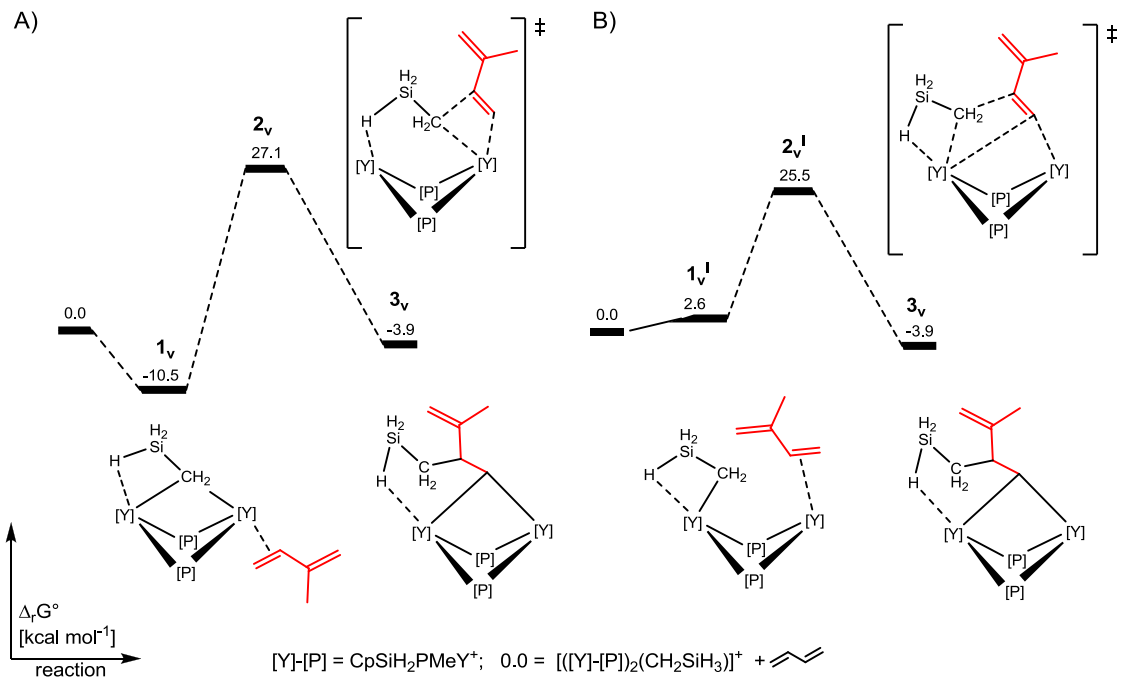

Figure 14: Computed energy profiles for 3,4 isoprene insertion into the metal-alkyl bond via A) a conventional four-center transition state and B) the kinetically preferred five-center transition state.[111]

Furthermore, the agostic interaction at the second yttrium metal center was proposed to be replaced by *π*-coordination of the unreacted doublebond by additional isoprene uptake (Figure 15). This pre-coordination of the growing polymer chain is responsible for the high stereoselectivity of the catalyst.

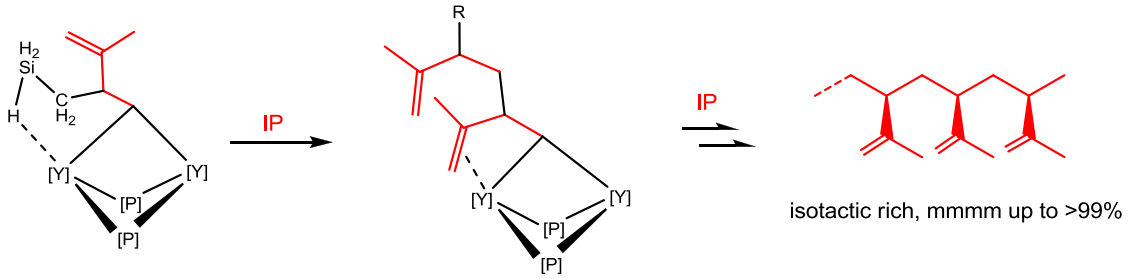

Figure 15: *π*-Coordination of the growing 3,4-PIP chain lead to high stereoregulation. [111]

Additionally, DFT calculations on various scandium half-sandwich complexes which are also discussed in chapter 2.1 have to be mentioned. Interestingly, an initial η^2-*trans* 3,4-coordination was observed in all cases, independent of the catalysts stereoselectivity.[77] The subsequent isoprene insertion was suggested to induce the formation of either a η^3-*π*-allyl or a η^3-*σ*-allyl species.

1.8.3.4 *Trans*- vs *Cis*-Diene insertion

In 2014, LUO ET AL. calculated the energy profiles for the isoprene polymerization with the half-sandwich rare-earth metal bis(tetramethyl)aluminate complexes [Cp*Ln($AlMe_4$)$_2$] (Ln = Y, La),[113] developed by the group of ANWANDER.[31, 114-115] In the first step, the structure of the initial active species for the lanthanum complex was modeled with main focus on the coordination mode of the aluminate moiety. From the four possible species [La](μ-Me)$_3$AlMe (**A**), [La](μ-Me)$_2$AlMe$_2$ (**B**), [La](Me)(μ-Me)AlMe$_2$ (**C**) and [La](μ-Me)AlMe$_3$ (**D**) ([La] = Cp*La^{2+}) species **C** was demonstrated as the energetically favored one, but in contact with the borate anion [B(C_6F_5)$_4$]$^-$ species **A** and **B** became more stable (Figure 16). Additionally, the energies for the separation of the ion pairs via coordination of the isoprene monomer were calculated and led to the conclusion, that species **B** is the initial species.

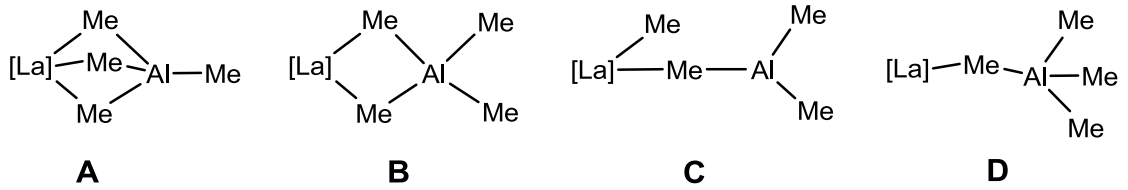

Figure 16: Possible coordination of the [$AlMe_4$] moiety at the lanthanum metal center for the cationic complex ([La] = {C_5Me_5La}$^{2+}$).[113]

The coordination of one molecule *trans*-isoprene in a η^4-fashion led to the adduct complex **Coo$^{B}_{t}$** (in the following **Coo** = complex, **Ts** = transition state, **P** = product; superscript = species; subscript = *trans*/*cis* (**t**/**c**) and *syn*/*anti* (**s**/**a**)) with a small raise in energy from 6.1 kcal mol^{-1} (Figure 17). The direct insertion into the metal methyl (Me^1) bond via the transition state **Ts$^{B}_{t}$** with an energy barrier of 34.6 kcal mol^{-1} and led to the slightly exergonic (-1.4 kcal mol^{-1}) product **P$^{B}_{t}$**, where the remaining $AlMe_3$ is (μ-Me)$_2$ bonded as spectator ligand (Figure 17, black energy levels). However, it was calculated, that **Coo$^{B}_{t}$** could favorably isomerize to **Coo$^{C}_{t}$** by an energy barrier of 22.2 kcal mol^{-1} (**Ts$^{B}_{t}$**), which correlates with the insertion into initial species **C**. The insertion of the monomer into the terminal Me^1 group is then kinetically favored by the lower energy barrier of 27.2 kcal mol^{-1} (**Ts$^{C}_{t}$**) and results exergonic by -11.2 kcal mol^{-1} in the thermodynamically more stable product **P$^{C}_{t}$** (Figure 17, red energy levels). The remaining $AlMe_3$ is calculated to bind via one methyl group to the rare-earth metal center, a coordination mode, which has not been structurally characterized so far.

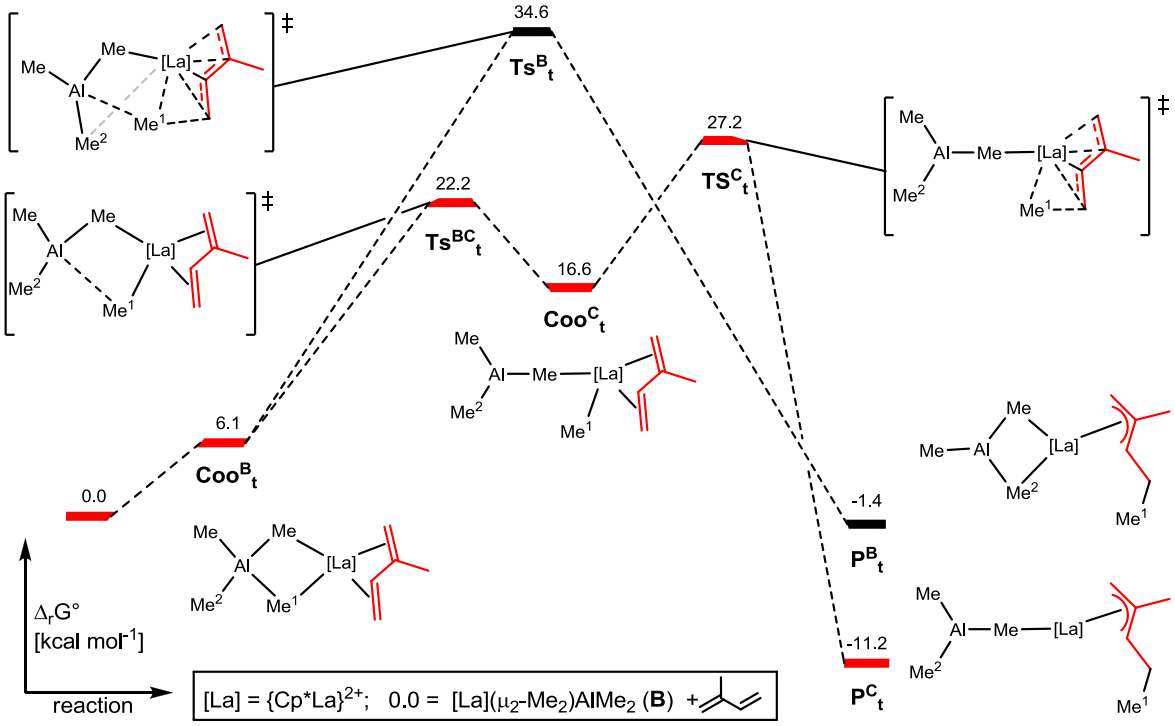

Figure 17: Calculated free energy profiles for the *trans*-1,4 isoprene insertion directly into the μ-Me rare-earth metal bond at $[Cp^*La(\mu\text{-}Me)_2AlMe_2]^+$ (**Ts^B_t**, black), and in the terminal methyl-metal bond at $[Cp^*La(Me)(\mu\text{-}Me)AlMe_2]^+$ (**Ts^C_t**, green). [113]

Furthermore, the second and third insertion of isoprene in the growing polymer chain was calculated. Following the route **P^C_t** → **Coo^C_{st}** → **Ts^C_{st}** → **$P_2{}^C_{st}$** the lowest energies were found for *trans*-isoprene coordination and subsequent insertion into the η^3-*syn* coordinated polymer chain. Thereby the $(\mu\text{-}Me)AlMe_2$ moiety remains terminally bonded to the rare-earth metal center as spectator ligand, influencing the selectivity by its sterical demand (Figure 18).

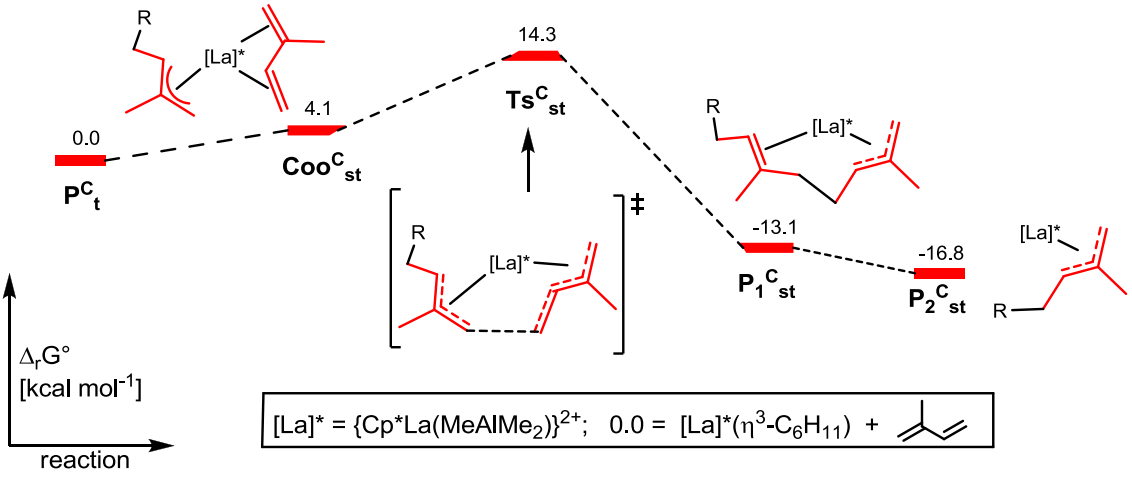

Figure 18: Computed energy profiles for *trans*-1,4 isoprene polymerization at $[Cp^*La(syn\text{-}C_5H_8R)(\mu\text{-}Me)AlMe_2]^+$. [113]

Any inclusion of the aluminum metal center in the polymerization process generated higher energy barriers or even led to dormant species, when the polymer chain engages a bridging position between the rare-earth and aluminum metal center.

In contrast to the lanthanum half-sandwich complex [Cp*La($AlMe_4$)$_2$], the yttrium analogues showed moderate *cis*-1,4 selectivity in isoprene polymerization.[114] To identify the responsible effect, the investigator also calculated the isoprene insertion for [Cp*Y(Me)(μ-Me)$AlMe_2$], but surprisingly, the *trans*-1,4 product was slightly favored. Considering *syn* and *anti* coordination of the first isoprene unit, chain propagation at [Cp*Y(η^3-C_6H_{11})(μ-Me)$AlMe_2$]$^+$ was also calculated to prefer *syn-trans* insertion by a lower energy barrier (22.0 kcal mol-1) and more stable product (Figure 19A, **i** red energy levels). These results were inconsistent with the experimental results, and the author investigated different decomposition pathways to find the abstraction of $AlMe_3$ as possible process generating less steric hindrance at the metal center. The calculated selectivity of isoprene insertion shifted towards *cis*-1,4 with the lowest energy barriers for the *anti-cis* correlation (Figure 19A, **ii** blue energy levels). The calculated intermediates and the transition state are shown in Figure 19B.

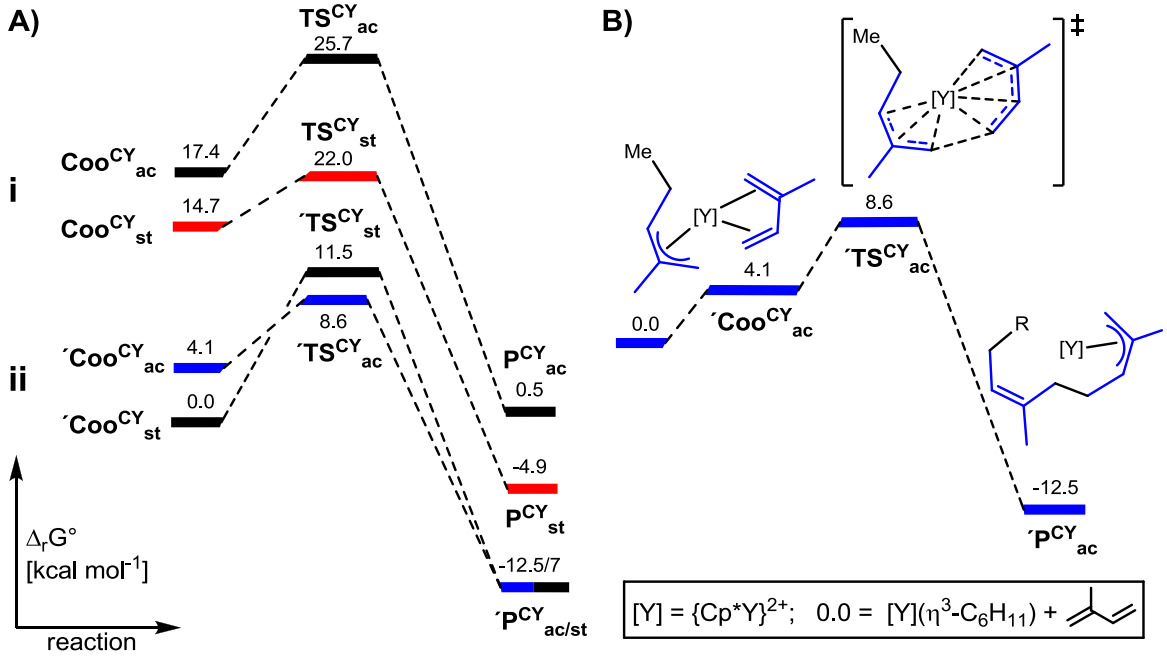

Figure 19: Calculated free energy profiles for the isoprene insertion at [Cp*Y(η^3-C_6H_{11})(μ-Me)$AlMe_2$]$^+$ (**A**, **i**), and [Cp*Y(η^3-C_6H_{11})]$^+$ (**A**, **ii**). Transition state and formation of the *anti* allylic product are shown in Figure **B**. [113]

1.8.4 Isoprene Analysis

IR spectroscopy

Already in 1949, SAUNDERS ET AL. identified *cis*- and *trans*-1,4-units in the natural rubbers by infrared spectroscopy making use of the different vibrational assignments (Table 2).[116] A short gradual development of this field is given in the introduction of a report by NALLASAMY and MOHAN, dealing with Raman and infrared spectroscopy of *cis*-polyisoprene.[117] However, a method of calculating the microstructure content of polyisoprene by FTIR through comparison of the intensity of corresponding peaks with NMR spectroscopic data was published only recently.[118]

Table 2: Absorption peaks of the FTIR spectrum of polyisoprene. [116]

[cm^{-1}]	Attribution	[cm^{-1}]	Attribution
1663	C=C stretching vibration of 1,4-unit	910	Out-of-plane bending vibration of CH_2 in the –CH=CH_2 (1,2-unit)
1644	C=C stretching vibration of 3,4- or 1,2-unit	888	Out-of-plane bending vibration of CH_2 in the –C=CH_2 (3,4-unit)
1383	Scissoring vibration of CH_3 in trans-1,4-unit	843	Out-of-plane bending vibration of C–H in the –CH=CH– group of trans-1,4-unit
1375	Scissoring vibration of CH_3 in cis-1,4-, 3,4- and 1,2-units	837	Out-of-plane bending vibration of C–H in the –CH=CH– group of cis-1,4-unit

Only the peaks at 910, 888, and 843 cm^{-1} are suitable for qualitative calculations of the composition of the microstructure as they exhibit moderate intensities, little interfering factors of other peaks and can clearly be integrated. Nevertheless, IR analysis has its advantages as it is uncomplicated in probe preparation and a much faster method than ^{13}C NMR spectroscopy.

NMR spectroscopy

The most useful tool in organic polymer analysis is the high-resolution nuclear magnetic resonance spectroscopy allowing the study of the stereochemical configuration of polymer chains. First investigations into microstructure determination of polyisoprenes by proton NMR spectroscopy were made by GOLUB ET AL. to verify the content of 3,4-units in natural rubber, based on small absorption peaks found in IR spectra, which could be excluded.[119] Till now, the

ratio between 1,4 and 3,4-polyisoprene units can be calculated by the equation of the integrals between the area from 5.4 to 4.9 ppm, corresponding to the 1,4-polyisoprene vinylic protons, and the signals in the range of 4.8–4.6 ppm, from those of the 3,4-units, respectively. However, since separation between *cis*- and *trans*-1,4 microstructures remained difficult, DUCH and GRANT, examined the natural polyisoprene rubbers (all-*cis*) and gutta percha (all-*trans*) by ^{13}C NMR spectroscopy and assignments for all resonance peaks have been given in 1970 (Figures 20 and 21).[120] The chemical shifts do not change significantly when the polyisoprene contains a mixture of *cis*- and *trans*-1,4-units and well separated resonances ease interpretation (Table 3).

Table 3: Assignments of peaks in the NMR spectra of *trans*(T), *cis*(C) and 3,4(V) polyisoprene.

Position	^{13}C	Position	^{13}C
T_5	16.0	T_3	124.3
T_4	26.8	T_2	135.0
T_1	39.8	C_3	125.0
C_5	23.4	C_2	135.2
C_4	26.4	V_1	111.9-112.8
C_1	32.2	V_2	146.5-148.8
V_5	17.9-18.2		^{1}H
V_4	35.2-39.9	T_3/C_3	4.9-5.6
V_3	42.0-42.4	V_1	4.6-4.8

To date, not all detected signals could be clearly assigned, but various studies dealing with shifts in ^{13}C NMR spectra for the most commonly observed sequences compile a fundamental library. A table of chemical shifts can be found in a study on sequence distribution of 3,4-polyisoprene,[121] and more recently, microstructure analysis of polyisoprene produced by cationic polymerization.[122] The challenge in analyzing synthesized polyisoprenes by ^{13}C NMR spectroscopy, is the inclusion of 3,4-units, as they a) show at least five additional peaks for

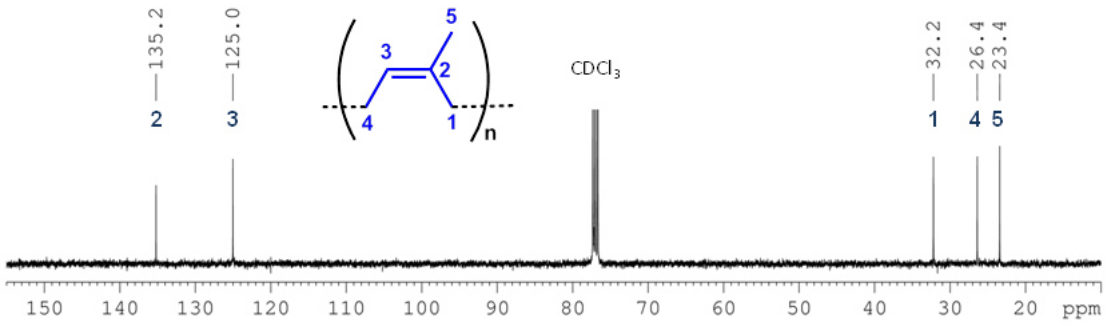

Figure 20: ^{13}C NMR spectrum of highly *cis*-1,4 polyisoprene in $CDCl_3$ (20 °C).

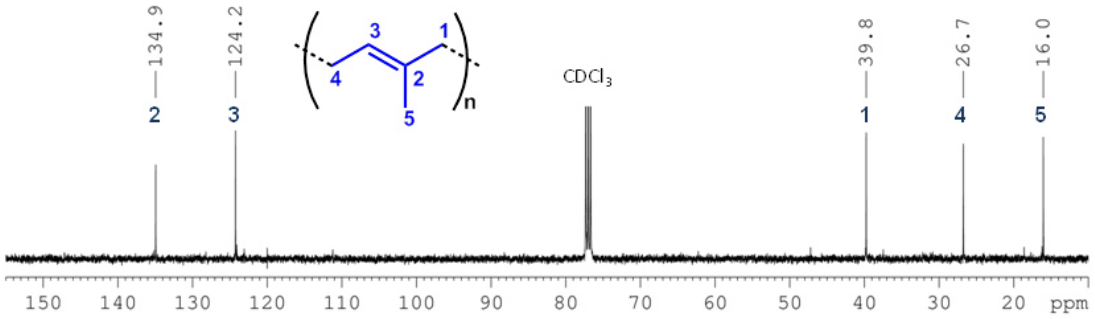

Figure 21: ^{13}C NMR spectrum of highly *trans*-1,4 polyisoprene in $CDCl_3$ (20 °C).

one periodic unit, b) have significant effect on the chemical shifts of the adjacent isoprene units c) can possibly insert in 3,4 and 4,3 orientation and d) have various tacticities when connected to block sequences (*isotactic*, *syndiotactic*, *atactic* see chapter 1.2), which generate different peaks for individual triads to pentads and also effect the shifts of the 1,4-units. A ^{13}NMR spectrum of highly *atactic* 3,4-polyisoprene is shown in Figure 22. The shift of the C_2 carbon gives information about the stereoregulation content from high meso (mmmm, *isotactic*) to high racemic (rrrr, *syndiotactic*) triads and pentads.[123-124]

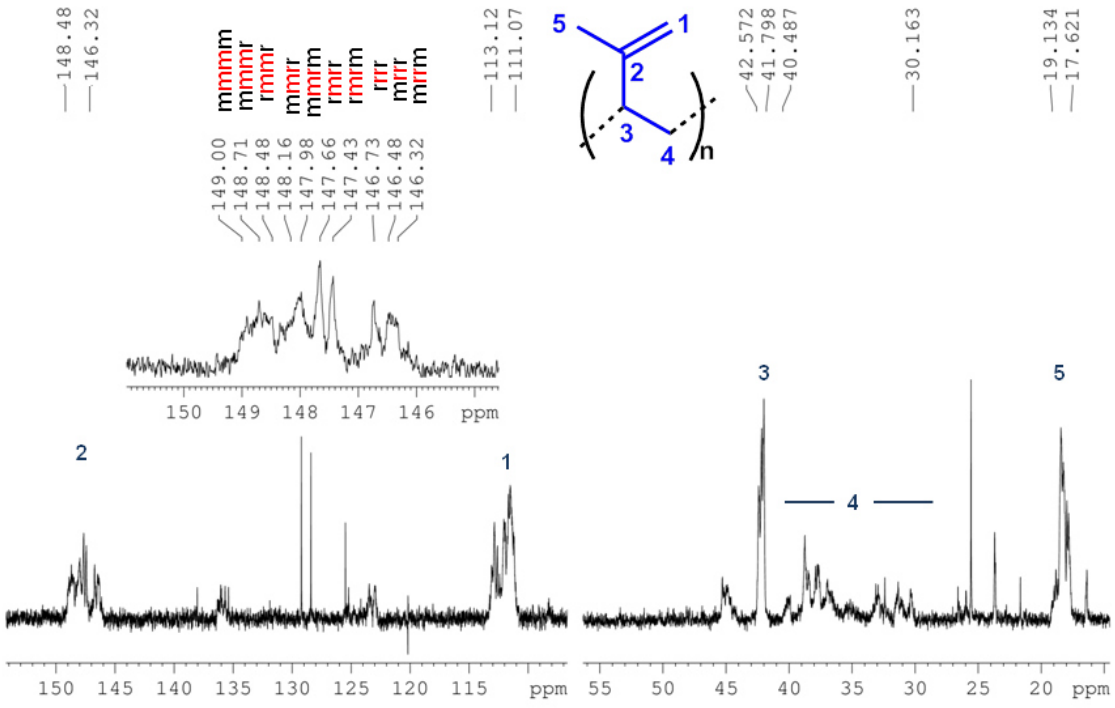

Figure 22: ^{13}C NMR spectrum of *atactic* 3,4-polyisoprene in $CDCl_3$ (20 °C).[123-124]

2 Cp^{Do} Rare-Earth Metal Complexes as Pre-Catalysts in Polymerization Reactions

2.1 Homo- and Co-Polymerization of Isoprene

The first constrained geometric complexes of rare-earth metals utilized in 1,3-diene polymerization were published in 2007 by WANG ET AL. in an attempt to synthesize donor free bis(alkyl) complexes (Scheme 13).[125] To avoid ligand redistribution, formation of salt or solvent adducts or dimerization of the highly unsaturated and reactive half-sandwich bis(alkyl) complexes bearing the η^1 σ-bonded CH_2SiMe_3 ligands, a N-heterocyclic carbene (NHC) was attached to indenyl in order to form (Ind-NHC) and introduced as a rigid chelating spectator ligand. The synthesized indenyl-imidazolium bromide (IndH-NHC-H)Br could be deprotonated under release of TMS and LiBr by $LiCH_2SiMe_3$ to form the neutral intermediate IndH-NHC, which was then reacted in a subsequent protonolysis reaction with $Ln(CH_2SiMe_3)_3(thf)_2$ to yield the desired bis(alkyl) complex **1** (Y = 62%).

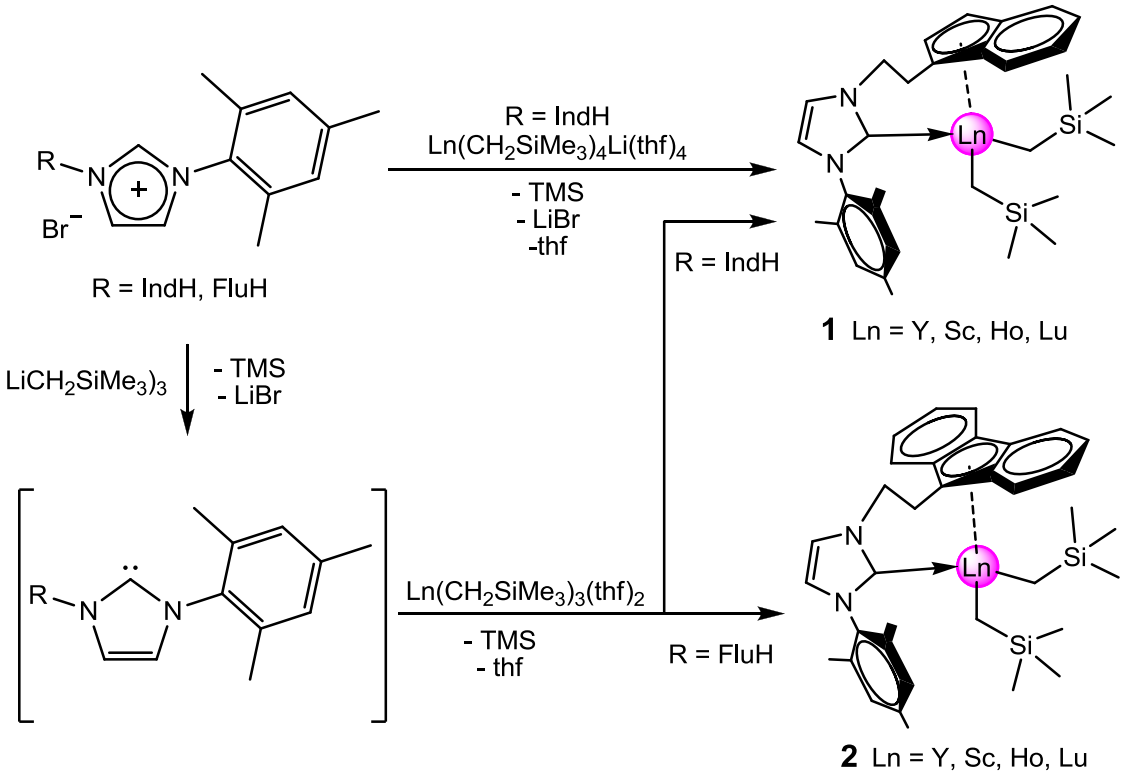

Scheme 13: Synthesis of NHC-substituted half-sandwich rare-earth metal complexes.[124-125]

Otherwise, the bromide salt was reacted directly with the tetra(alkyl)yttrium lithium salt $Ln(CH_2SiMe_3)_4Li(thf)_4$, which can be explained as a double deprotonation process, to give (Ind-NHC)$Ln(CH_2SiMe_3)_2$ **1** (Y = 38%). One year later, in 2008, WANG ET AL. also published the fluorenyl variant of the NHC

coordinated rare-earth metal bis(alkyl) complexes **2** following the sequential protonolysis protocol.[124] Complexes **1** and **2** showed no or low activity in isoprene polymerization when activated with $[Ph_3C][B(C_6F_5)_4]$ to generate the cationic species. In contrast, addition of 10 equivalents of Al*i*Bu$_3$, gave a ternary system in 1:1:10 ratio, which afforded high yields of 3,4-polyisoprene (up to 99%) for the steric bulkier fluorenyl-modified NHC ligand (**2**) (Table 4, run 1 and 2). A correlation between selectivity and effective ionic radii of the rare-earth metals following Lu > Ho ~ Y was observed. Interestingly, both complexes of the smallest metal ion scandium were inactive. This was in disagreement with previous studies, where Sc^{III} featured the superior central metal in α-olefin and 3,4-selective isoprene polymerization and was explained by the steric shielding of the larger ancillary ligands.

Based on the unique polymerization performance for various monomers by diverse scandium half-sandwich bis(alkyl) complexes, which have also been investigated in the reaction with borate compounds to form the active cationic species, LI ET AL. published a comprehensive study on scandium complexes including CGC´s with donating heteroatoms in 2009.[77] The paper focused on the homo-polymerization of isoprene and co-polymerization of isoprene with ethylene. To this end, the half-sandwich complexes $(Cp^R)Sc(CH_2SiMe_3)_2(thf)$, ($Cp^R$ = C_5H_5, C_5MeH_4, C_5Me_5, $C_5Me_4SiMe_3$, $C_5H_3(SiMe_3)_2$, $C_5Me_4SiMe_3$, $C_5Me_4SiMe_3$) **3** were synthesized (Scheme 14) and compared with the heteroatom-containing side arm substituted mono(cyclopentadienyl)scandium complexes $(C_5Me_4R)Sc(CH_2SiMe_3)_2$ (**4**: R = C_6H_4OMe, **5**: $CH_2CH_2PPh_2$; Scheme 15).

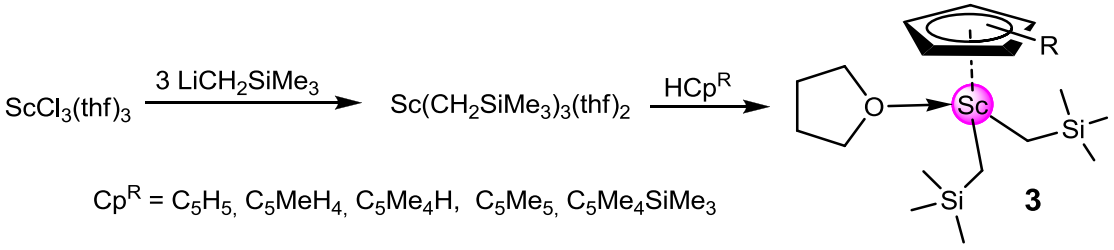

Scheme 14: Synthesis of $[Cp^RSc(CH_2SiMe_3)_2]$ complexes. [77]

The homopolymerization of isoprene with complexes **3**-**5** disclosed a direct correlation of steric bulk of the substituted cyclopentadienyl and stereoregulation of the polymer. The microstructure in the polyisoprene shifted from the least bulky C_5H_5 to the highest crowded $C_5Me_4SiMe_3$ from a *cis*-1,4 (95%) to 3,4 (65%) content, respectively (Table 4, run 3 and 4). Interestingly, the ether functionalized one (**4**) preferred *trans*-1,4-polyisoprene (79%)

formation, whereas the phosphine side arm coordinated complex (**5**) showed high *cis*-1,4 (90%) selectivity (Table 4, run 5 and 6).

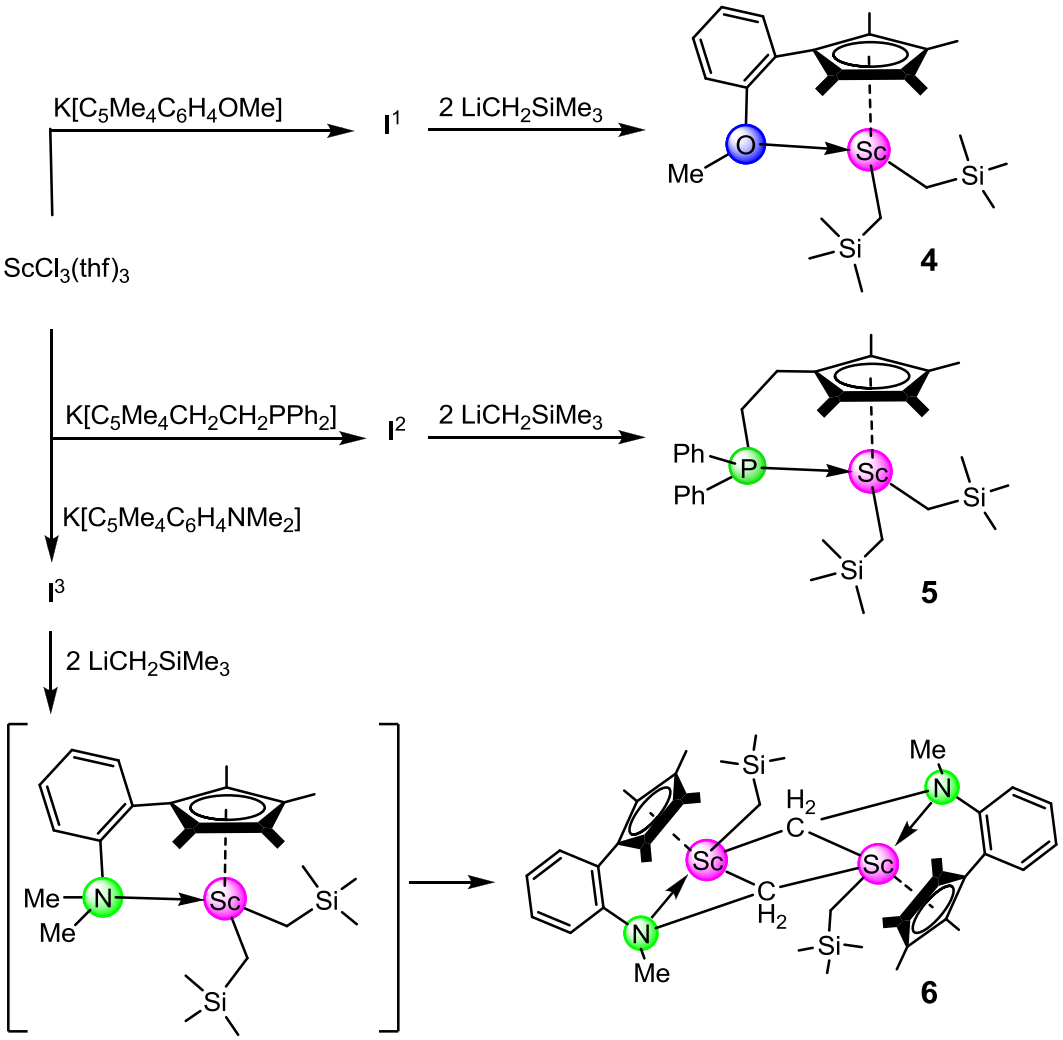

Scheme 15: Synthesis of donor substituted half-sandwich rare-earth metal complexes. [77]

Investigations of the copolymerization of isoprene with ethylene specified the influence of the steric hindrance of the ligands. Upon cationization with the borate salt $[Ph_3C][B(C_6F_5)_4]$ (**A**) the smaller ancillary ligands in complex **3** (Cp^R = C_5H_5) produced copolymers with high *cis*-1,4 polyisoprene content (80-90% IP, 85-90% *cis*). With higher substituted cyclopentadienyls, **3** showed a main content of 3,4-polyisoprene (> 55%) instead but co-polymerized in an alternating fashion. For both complexes bearing a donor-substituted cyclopentadienyl ligand, high 3,4 selectivity was observed (**4** = 81%, **5** = 68-81%) and aalternated co-polymer was determined by NMR-spectroscopy. A possible mechanism was presented, suggesting a η^3-σ-ally species as the first intermediate after insertion of one η^2-*trans* 3,4-coordinated isoprene molecule based on DFT calculations.

In 2010, CUI ET AL. published the synthesis and characterization of a series of novel linked-half-sandwich rare-earth bis(allyl) complexes and demonstrated their excellent performance in catalytic polymerization of 1,3-diene and styrene following cationization with organoborate activators with or without the addition of trialkylaluminum (Scheme 16).[126-129] In particular, a comprehensive study in isoprene polymerization of the *N*,*N*-dimethylanilinyl substituted half-sandwich rare-earth complexes [(C_5Me_4–C_6H_4-*o*-NMe_2)Ln(η^3-C_3H_5)$_2$] (**8**, Ln = Y, Nd, Gd, Dy) was published in 2010.[127] The activation of the gadolinium complex bearing the ligand in a constrained-geometry conformation with [$PhNMe_2H$][$B(C_6F_5)_4$] in addition of 10 eqiv. $AlMe_3$ presented the first rare-earth metal bis(allyl) mediated system that polymerized isoprene in a living fashion. The resulting polymer showed a very narrow molecular weight distribution of 1.11 and moderate *cis*-1,4 selectivity of 82.9%, which rose to 98.2% when Al^iBu_3 was used (Table 4, run 8). It was also shown, that the organoaluminium compound acted as a chain-transfer agent depending on its molar ratio, allowing up to 8 growing polymer chains, per gadolinium metal center, resulting in an 800% catalytic efficiency.

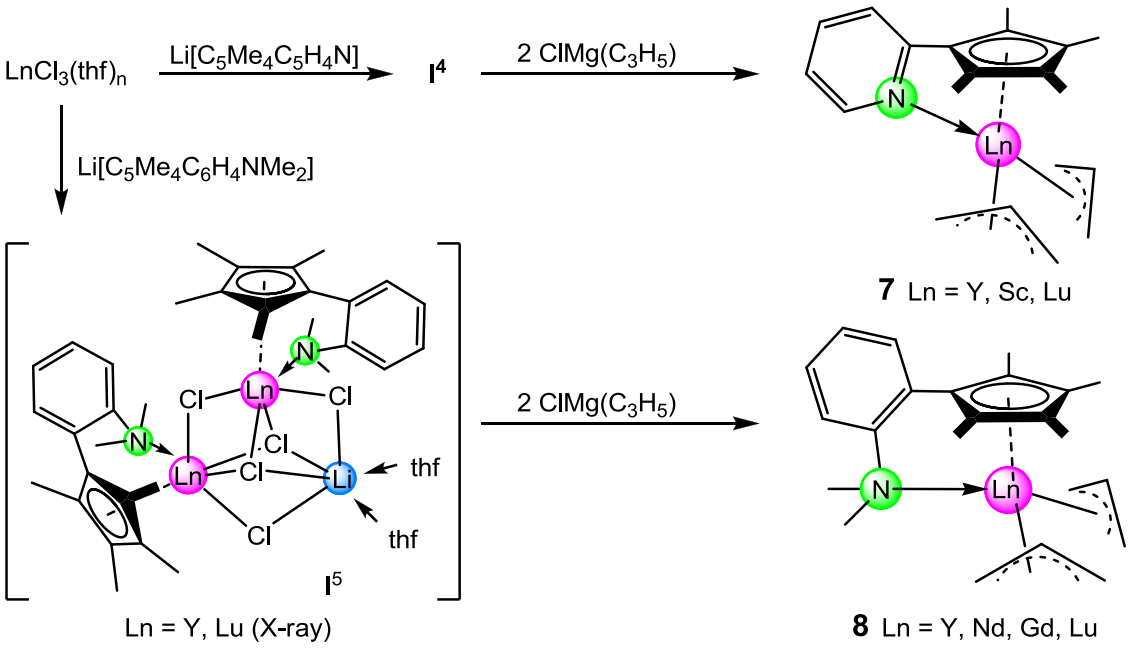

Scheme 16: Synthesis of N-donor substituted half-sandwich bis(allyl) complexes.[127,128]

In the same year, the group of CUI reported the bis(allyl) lutetium complex [(C_5Me_4–C_6H_4N)Lu(η^3-C_3H_5)$_2$] (**7**) supported by a pyridyl substituted cyclopentadienyl as an excellent catalyst in highly *cis*-1,4-selective (99%) butadiene and purely syndiotactic (rrrr > 99%) styrene polymerization when activated with the tritylborate agent [Ph_3C][$B(C_6F_5)_4$] (**A**).[128] In further

investigations, they showed that this cationic lutetium catalyst could also be used for terpolymerization of styrene with butadiene and isoprene with outstanding control over the region and stereoregularity as well as the composition of the resulting polymers.[129]

At the end of 2010, ANWANDER ET AL. reported the first rare-earth metal bis(tetramethylaluminate) complexes supported by a quinolyl substituted cyclopentadienyl ligand.[130] The complexes of the middle and large size metal ions yttrium and lanthanum (**9**) where synthesized in a protonolysis reaction utilizing the protonated ligand and homoleptic tris(tetramethylaluminate) rare-earth metal complexes (Scheme 17). Interestingly, the hard N-donor functionality did not interfere with the formation of the half-sandwich complex through donor-induced cleavage of the trimethylaluminum. Both complexes were tested in isoprene polymerization upon activation with the borate salts **A** and **B** as well as the neutral boron compound **C**, showing high *trans*-1,4 selectivity (up to 93.1%) and narrow molecular weight distributions (Table 4, run 9).

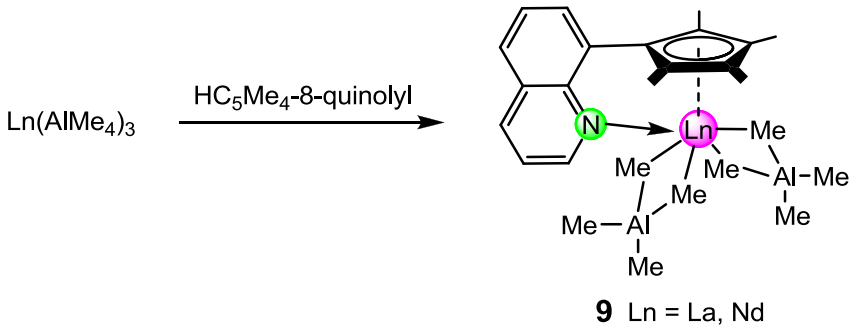

9 Ln = La, Nd

Scheme 17: Synthesis of N-donor substituted half-sandwich bis(tetramethylaluminate) complexes.[130]

A new class of cyclopentadienyliden-phosphorane ligands (CpPC) to generate rare-earth metal based constrained geometry catalysts were invented by HILLERSHEIM and SUNDMAYER in 2013.[131] Based on earlier investigations in deprotonation reactions forming litihium[132] and zirconium[133] posphonium diylide complexes, alkane elimination reaction with homoleptic tris(trimethylsilylmethyl) rare-earth metal complexes lead to the corresponding [(CpPC)Ln(CH_2SiMe_3)$_2$] complexes (Scheme 18). The cyclopentadienyl ring was either tetrametyl- (**10**, **11**) or singly *tert*-butyl- (**12**, **13**) substituted, whereby the phosphor bridge was modified with methyl or phenyl groups. Interestingly, a dimerization under a second elimination of tetramethylsilane was only observed when the ligand with the PPh_2 moiety was used. The complexes were tested in the polymerization of isoprene, utilizing the activating borate salt **B** under

addition of 11.6 equiv triisobutylaluminum. Only complexes **10** and **13** produced polyisoprene in high yields with stereoregulation strongly depending on the cation size, preferring higher *cis*-1,4 content (up to 82.2%) for the smallest scandium metal center (Table 4, run 10 and 11).

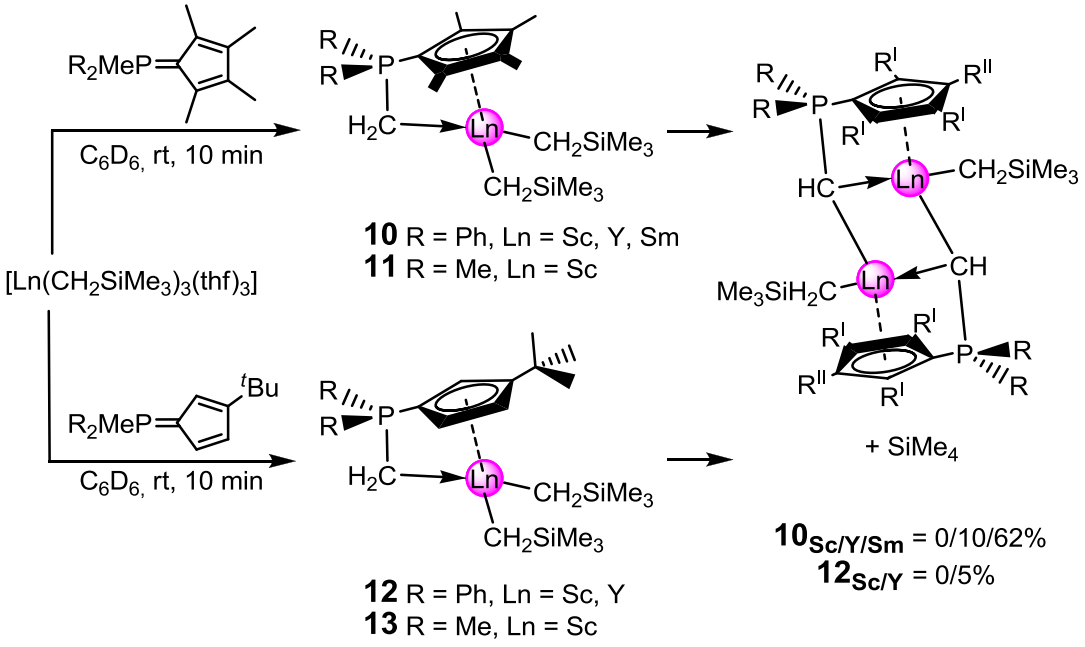

Scheme 18: Synthesis of rare-earth metal cyclopentadienyliden-phosphorane complexes.[131]

Table 4. Selected examples of isoprene polymerization at 25° C.

entry[a]	complex	precatalyst	cocatalyst[b]	time (min)	yield (%)	*cis*-1,4[c]	*trans*-1,4[c]	3,4	T_m[d] (°C)	M_n[e] (×10⁴)	M_w/M_n[e]	further monomer	Ref.
1	**1**$_{Y}$	(IndNHC)Y(CH_2SiMe_3)$_2$	**A**/Al^{i}Bu$_3$	360	50	n.d.	n.d.	89.4	23	2.0	1.36	–	[125]
2	**2**$_{Lu}$	(FluNHC)Lu(CH_2SiMe_3)$_2$	**A**/Al^{i}Bu$_3$	360	100	n.d.	n.d.	99.0	45	4.1	1.05	–	[125]
3	**3**$_{Sc}$	(C_5H_5)Sc(CH_2SiMe_3)$_2$(thf)	**A**/-	5	100	95	-	5	-57	12.0	2.39	IP-Et	[77]
4[f]	**3**$_{Sc}$	($C_5Me_4SiMe_3$)Sc(CH_2SiMe_3)$_2$(thf)	**A**/-	180	100	20	15	65	-18	7.7	1.07	IP-Et	[77]
5[f]	**4**$_{Sc}$	(Cp^{OMe})Sc(CH_2SiMe_3)$_2$	**C**/-	120	100	10	79	11	-65	6.9	1.08	IP-Et	[77]
6[f]	**5**$_{Sc}$	(Cp^{PPh2})Sc(CH_2SiMe_3)$_2$	**A**/-	120	100	90	0	10	-59	7.3	1.12	IP-Et	[77]
7	**7**$_{Lu}$	(Cp^{Py})Lu(C_3H_5)$_2$	**A**/-	30	100	80.3	7.0	12.7	-51	9.0	1.05	St, BD, IP-St-BD	[129]
8	**8**$_{Gd}$	(Cp^{ANMe2})Gd(C_3H_5)$_2$	**B**/Al^{i}Bu$_3$	60	100	98.2	n.d.	n.d.	n.d.	5.0	1.36	BD, IP-BD	[127]
9[f]	**9**$_{La}$	(Cp^{Q})La($AlMe_4$)$_2$	**B**/-	24	100	2.1	93.1	4.9	n.d.	15.9	1.28	–	[130]
10[g]	**10**$_{Sc}$	(Cp^{Me4}CP^{Ph2})Sc(CH_2SiMe_3)$_2$	**B**/Al^{i}Bu$_3$	24h	96	80.5	-	19.5	-51	>60.0	n.d.	–	[131]
11[g]	**13**$_{Sc}$	(Cp^{tBu}CP^{Me2})Sc(CH_2SiMe_3)$_2$	**B**/Al^{i}Bu$_3$	24h	100	82.2	-	17.8	-53	n.d.	n.d.	–	[131]

[a]Conditions: 0.02 mmol precatalyst, [Ln]/[cocat]/AlR_3 = 1:1:10, solvent toluene, ethylene 1bar; [b]Cocatalyst: **A** = [Ph_3C][$B(C_6F_5)_4$], **B** = [$PhNMe_2H$][$B(C_6F_5)_4$], **C** = $B(C_6F_5)_3$; [c]Determined by ^1H and ^{13}C NMR spectroscopy in $CDCl_3$. [d]Determined by DSC. [e]Determined by means of size-exclusion chromatography (SEC) against polystyrene standards; [f]in hexane at 40° C; [g]in C_6H_5Cl.

2.2 Non-Isoprene Polymerization

Ethylene

The NHC-substituted indenyl and fluorenyl half-sandwich bis(alkyl) complexes **1** and **2** have also been shown to be active in the co-polymerization of ethylene with norbornene when activated in situ with Al^{i}Bu$_3$ and [Ph$_3$C][B(C$_6$F$_5$)$_4$], however, the homo-polymerization revealed only moderate activity (10^5 g mol$_{(Sc)}^{-1}$ h^{-1} atm^{-1}).[134] Furthermore, the co-polymerization of ethylene with isoprene with the ether- and phosphine-functionalized cyclopentadienyl scandium half-sandwich complexes **4** and **5** has been discussed above, but no pure ethylene polymerization was presented.[77] As isolobal analogue of the well established dianionic CpSiN-type ligands JIAN ET AL. reported rare-earth metal bis(alkyl) complexes bearing monoanionic phosphazene-functionalized cyclopentadienyl derivatives (complexes **10**-**17**, Figure 23).[135]

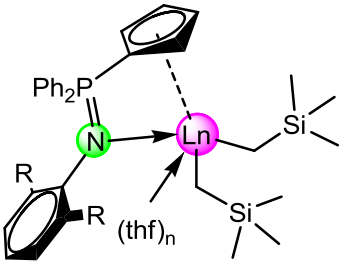

10 R = Me, n = 0, Ln = Sc
11 R = ^{i}Pr, n = 0, Ln = Sc;
n = 1, Ln = Y, Nd, Sm, Nd

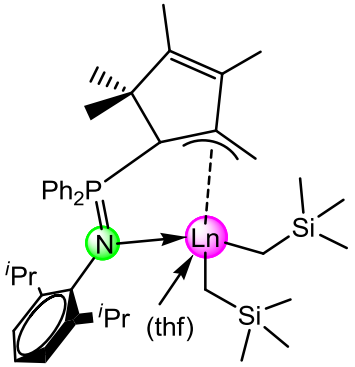

12 Ln = Y, Lu

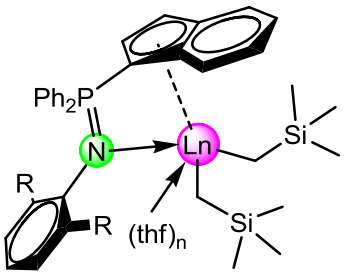

13 R = Me, n = 0, Ln = Sc;
n = 1, Ln = Y, Lu
14 R = Et, n = 0, Ln = Sc
15 R = ^{i}Pr, n = 0, Ln = Sc;
n = 1, Ln = Y, Lu

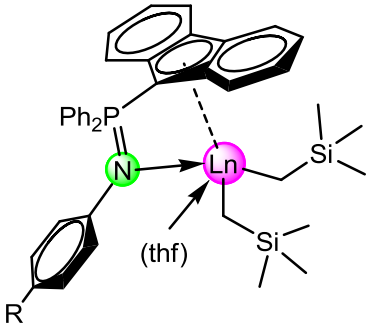

16 R = H, Ln = Sc
17 R = Me, Ln = Sc, Lu

Figure 23: Rare-earth metal complexes bearing phosphacene-modified ancillary ligands.[135]

All complexes were tested in ethylene polymerization upon activation with Al^{i}Bu$_3$ and [Ph$_3$C][B(C$_6$F$_5$)$_4$], but only the scandium derived ones showed high activity (Table 5). This can be attributed to the lack of THF coordination and the more LEWIS acidic nature of the metal ion. Thereby, the sterics and electronics of the

ligands influenced the activity of the scandium complexes; in particular, it follows the trend of the cyclopentadienyl derivate = **11** (^{i}Pr) > **10** (Me), Ind = **17** (Me) > **16** (H) and Flu = **13** (Me) > **15** (^{i}Pr) > **14** (Et).

Styrene

In 2012, JIAN ET AL. extended their investigations of the bis(allyl) complexes **7** and **8** (Scheme 12) as catalysts for the polymerization of styrene and compared their activity with the new bis(hydrocarbyl) rare-earth metal complexes **18** and **19**, bearing N-donor functionalized fluorenyl ligands (Figure 24).[126] Without addition of Al^{i}Bu$_3$ only the bis(allyl) complexes **7** showed moderate to high activity, depending on the metal center, whereby the larger yttrium ion produced polystyrene with less stereoregularity in lower yield (Table 5, run 1-3). It was mentioned, that use of chlorobenzene as a solvent led to full conversion but the selectivity decreased dramatically. Complexes **8** in contrast were inactive and the larger bite angle of the anilinyl- against the pyridinyl-functionalization was suggested to hamper the monomer insertion of the bulk styrene monomer. The modified fluorenyl half-sandwich complexes **18** and **19** only became active in styrene polymerization, when the ternary system under addition of Al^{i}Bu$_3$ was used. However, the activity and selectivity was low and again, the disadvantages of the yttrium complexes were verified (Table 6, run 4-7).

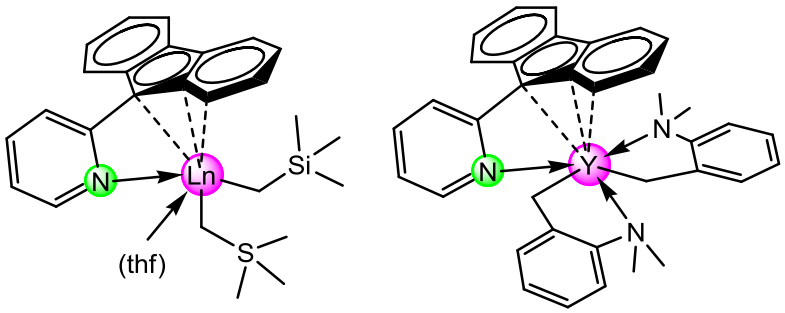

18 Ln = Y, Sc, lu **19**

Figure 24: Rare-earth metal complexes bearing pyridinyl-functionalized fluorenyl ligands.[126]

After LUO ET AL. have shown the activity of half-sandwich scandium bis(alkyl) complexes [(CpMe$_4$SiMe$_3$)Sc(CH$_2$SiMe$_3$)$_2$] in styrene polymerization in 2004,[136] their investigation of corresponding bis(amido) complexes [(CpMe$_4$R^I)Sc(N{SiRMe$_2$}$_2$)$_2$] displayed the first active amide complexes in styrene polymerization.[137] Very recently, the study was extended to a new series of rare-earth metal bis(amide) and bis(allyl) complexes supported by a

pyrrolidinyl-functionalized cyclopentadienyl ligand.[138] The donor-sidearm does not coordinate to the metal center in case of the scandium complexes **20** and **21**, but the ligand coordinates in a κ^1:η^5 fashion at the larger yttrium and lutetium metal ions in complexes **22** and **23** (Figure 25).

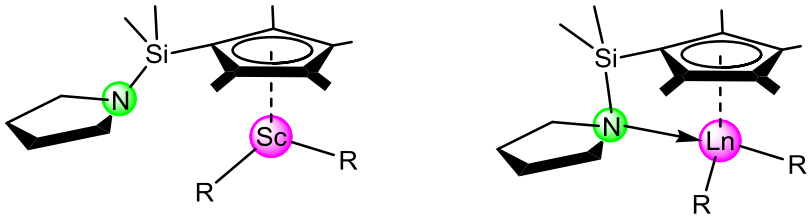

20 R = (C_3H_5)
21 R = $N(SiHMe_2)_2$

22 R = (C_3H_5)
23 R = $N(SiHMe_2)_2$
Ln = Y, Lu

Figure 25: Pyrrolidinyl-functionalized cyclopentadienyl-supported rare-earth metal complexes.[138]

The scandium complex **20** showed high activity producing >99% syndiotactic polystyrene upon activation with co-catalyst $[Ph_3C][B(C_6F_5)_4]$, either with or without addition of Al^iBu_3 (Table 6, runs 8 and 10), while the bis(amide) complex **21** was only active in the presents of trialkylaluminum (Table 5, run 12). In case of complexes **22** and **23** only the yttrium complex was moderately active, suggesting steric hindrance for the monomer insertion at the lutetium metal ion due to the chelating donor-coordination (Table 6, runs 9 and 13).

Table 5. Selected examples of ethylene polymerization at 50 °C.

entry[a]	complex	precatalyst	cocatalyst[b]	yield (g)	productivity[c]	activity[d]	T_m (°C)[e]	M_n[d] (×10³)[f]	M_w/M_n[f]	Ref
1	**10**	$CpPN^{Me}$ $Sc(CH_2SiMe_3)_2$	**B/Al^{i}Bu$_3$**	0.27	14	162	126	10.6	5.34	[135]
2	**11**	$CpPN^{iPr}$ $Sc(CH_2SiMe_3)_2$	**B/Al^{i}Bu$_3$**	0.65	33	228	126	5.0	1.69	[135]
3	**13**	$IndPN^{Me}$ $Sc(CH_2SiMe_3)_2$	**B/Al^{i}Bu$_3$**	0.60	30	360	132	6.7	1.97	[135]
4	**14**	$IndPN^{Et}$ $Sc(CH_2SiMe_3)_2$	**B/Al^{i}Bu$_3$**	0.20	10	120	133	4.2	2.34	[135]
5	**15**	$IndPN^{iPr}$ $Sc(CH_2SiMe_3)_2$	**B/Al^{i}Bu$_3$**	0.44	22	264	132	5.8	2.65	[135]
6	**16**	$FluPN^{H}$ $Sc(CH_2SiMe_3)_2$	**B/Al^{i}Bu$_3$**	0.18	9	108	123	3.3	1.58	[135]
7	**17**	$FluPN^{Me}$ $Sc(CH_2SiMe_3)_2$	**B/Al^{i}Bu$_3$**	0.36	18	216	125	14.1	2.07	[135]

[a]Conditions: 0.02 mmol precatalyst, [Ln]/AlR_3/[cocat] = 1:10:1, solvent toluene (50 mL), ethylene 1bar; [b]Cocatalyst: **A** = $[Ph_3C][B(C_6F_5)_4]$, **B** = $[PhNMe_2H][B(C_6F_5)_4]$; [c]Given in kg of PE (mol_{Ln} bar)$^{-1}$; [d]Given in kg of PE (mol_{Ln} h bar)$^{-1}$ [e]Determined by DSC. [f]Determined by means of size-exclusion chromatography (SEC) against polystyrene standards;

Table 6. Selected examples of styrene polymerization at 20 °C.

entry[a]	complex	precatalyst	cocatalyst[b]	time (min)	yield (g)	activity[c]	T_m (°C)[d]	sPS[e] (%)	M_n[d] (×10³)[f]	M_w/M_n[f]	Ref
1	**7**	$(Cp^{Py})Y(C_3H_5)_2$	**B**	50	20	13	266	88	4.6	2.50	[126]
2	**7**	$(Cp^{Py})Sc(C_3H_5)_2$	**B**	1	>99	3120	271	>99	14.4	1.40	[126]
3	**7**	$(Cp^{Py})Lu(C_3H_5)_2$	**B**	1	>99	3120	270	>99	9.7	1.94	[126]
4	**18**	$(Flu^{Py})Y(CH_2SiMe_3)_2$	**B/Al^{i}Bu$_3$**	360	5	0.4	n.d.	n.d.	n.d.	n.d.	[126]
5	**18**	$(Flu^{Py})Sc(CH_2SiMe_3)_2$	**B/Al^{i}Bu$_3$**	360	48	4	260	85	1.5	1.84	[126]
6	**18**	$(Flu^{Py})Lu(CH_2SiMe_3)_2$	**B/Al^{i}Bu$_3$**	360	19	1.6	256	81	1.0	2.23	[126]
7	**19**	$(Flu^{Py})Y(CH_2C_6H_4\text{-}o\text{-}NMe_2)_2$	**B/Al^{i}Bu$_3$**	360	13	1.0	251	76	1.1	1.92	[126]
8	**20**	$(Cp^{SiPy})Sc(C_3H_5)_2$	**B**	120	>99	–	269	>99	10.9	1.86	[138]
9	**22**	$(Cp^{SiPy})Y(C_3H_5)_2$	**B**	120	28	–	267	>99	9.7	1.93	[138]
10	**20**	$(Cp^{SiPy})Sc(C_3H_5)_2$	**B/Al^{i}Bu$_3$**	20	>99	–	271	>99	14.5	2.15	[138]
11	**22**	$(Cp^{SiPy})Y(C_3H_5)_2$	**B/Al^{i}Bu$_3$**	120	trace	–	–	–	–	–	[138]
12	**21**	$(Cp^{SiPy})Sc(N\{SiHMe_2\}_2)_2$	**B/Al^{i}Bu$_3$**	120	80	–	270	>99	11.6	2.15	[138]
13	**23**	$(Cp^{SiPy})Y(N\{SiHMe_2\}_2)_2$	**B/Al^{i}Bu$_3$**	120	31	–	266	>99	8.2	2.27	[138]

[a]Conditions: 0.01 mmol precatalyst, [Ln]/AlR_3/[cocat] = 1:10:1, toluene/monomer = 5:1 (v/v); [b]Cocatalyst: **A** = $[Ph_3C][B(C_6F_5)_4]$, **B** = $[PhNMe_2H][B(C_6F_5)_4]$; [c]Given in kg of St (mol_{Ln} h bar)$^{-1}$ [d]Determined by DSC. [e]Determined by means of size-exclusion chromatography (SEC) against polystyrene standards;

Polar Monomer

The first borohydride lanthanide complexes active in methyl methacrylate (MMA) polymerization were published in 2005 by BONNET ET AL. bearing amino-amide ligands, but their selectivity was poor even at low temperature (68% rr at -78° C).[139] In 2010, JIAN ET AL. reported the first rare-earth metal borohydride complexes **25** stabilized by a rigid dimethyl-anilinyl functionalized cyclopendienyl ligand (Figure 26, left).[140] Performance in MMA polymerization was investigated under various conditions depending on the presence of co-catalyst (Mg{^{n}Bu}$_2$ or ^{n}BuLi), temperature, and solvent. The main focus is generally on the larger rare-earth metals as they are known to afford efficient MMA polymerization catalysts, but interestingly, the smaller scandium complex was more active and exhibited higher stereocontrol than its samarium counterpart. The highest catalytic activity was achieved with ^{n}BuLi as co-catalyst in THF, producing 1116 kg of PMMA mol^{-1} h^{-1} with a syndio-selectivity of 75%.

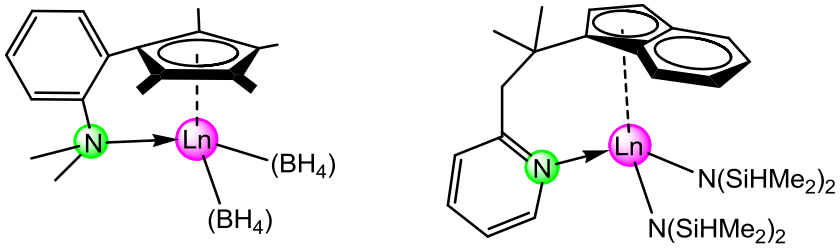

25 Ln = Sc, Sm **26** Ln = La, Sm, Er, Lu

Figure 26: N-donor functionalized half-sandwich rare-earth metal complexes for polar monomer polymerization.[139,140]

In 2013, WANG ET AL. presented rare-earth metal bis(silylamide) complexes **26** bearing a pyridyl-functionalized indenyl ligand active in the living ring-opening polymerization of lactides (Figure 26, right).[141] Lactide polymerization is insofar of interest, as the polylactide promises to be a valuable alternative to petroleum-based polymers with environmentally friendly properties through its production from renewable resources and biodegradability.[142] The lanthanum complex showed the highest activity and in the presents of 2 equivalents of benzyl alcohol livingness was observed. Additionally, end-group analysis of the polymers revealed that the polymerization proceeds *via* the coordination-insertion mechanism.

Summary of Main Results

1 Synthesis of N-Donor Substituted Cp-Ligands

Within the scope of this thesis, three nitrogen-donor substituted tetramethylcyclopentadienyl ligands were synthesized, featuring the 1-(2-*N*,*N*-dimethylaminoethyl)- (HCp^{NMe2}), the 1-(2-*N*,*N*-dimethylaminophenyl)- (HCp^{AMe2}), and the 8-quinolyl- (HCp^{Q}) functionalization. According to the synthesis strategy **E** (Chapter 1.7), HCp^{NMe2} was synthesized following the procedure reported by JUTZI, starting with the dicondensation of ethyl 3-dimethylaminopropionate with 2-but-2-enyllithium (Scheme S1).[143] Crucially, after acid catalyzed ring closing reaction, purification of the product was only achievable by "Kugelrohr" distillation at reduced pressure. The syntheses of HCp^{AMe2} and HCp^{Q} were given by ENDERS, and follow strategy **D** (Chapter A1.7), involving the reaction of the lithiated donor functionality with tetramethylcyclopentenone (Scheme S1).[144-145] Again, the "Kugelrohr" distillation could be demonstrated as the method of choice to receive the pure ligands as oily products.

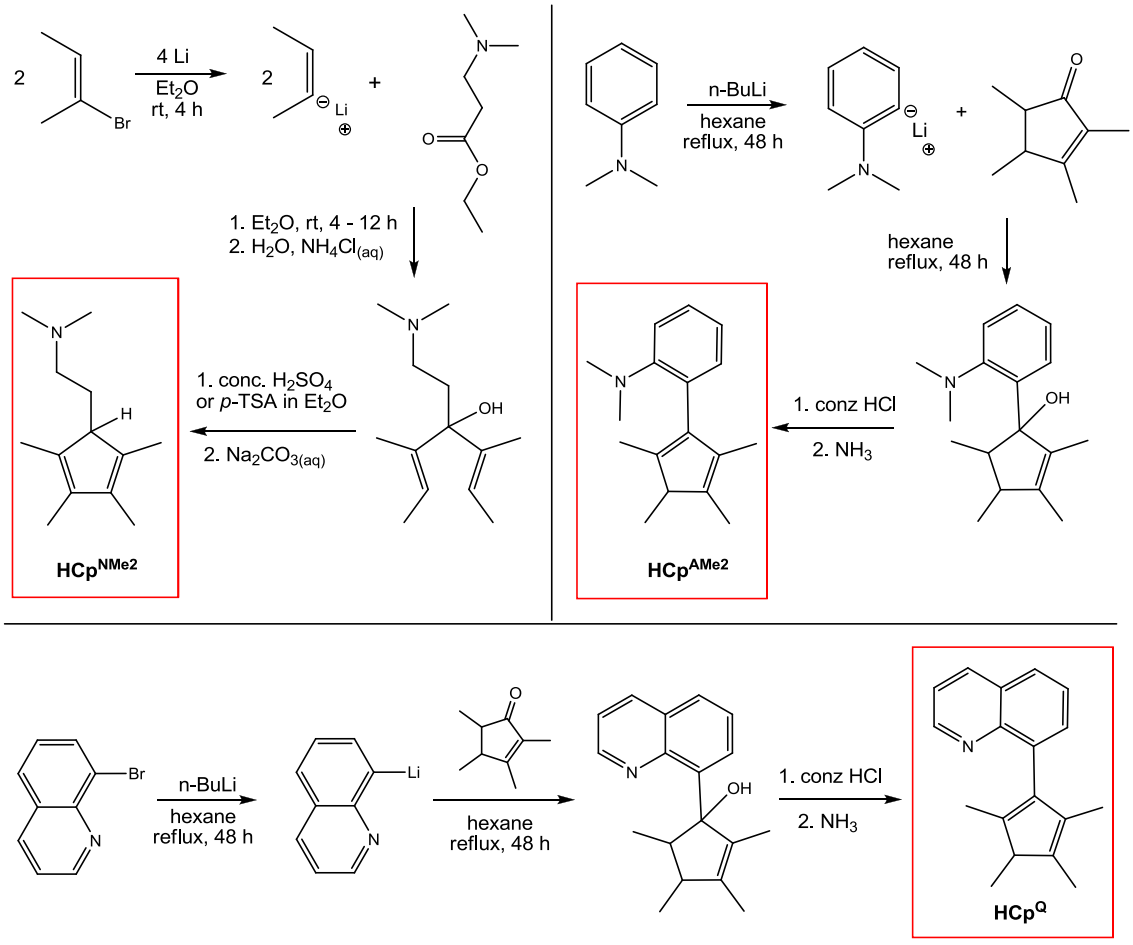

Scheme S1. Synthesis of N-donor functionalized cyclopendienyl ligands.

2 Rare-Earth Metal Complexes Bearing Nitrogen Functionalized Cyclopentadienyl Ligands

Half-sandwich rare-earth metal bisalkyl complexes and their cationic species have revealed tremendous catalytic potential in polymerization reactions, but the choice of applicable hydrocarbyl ligands is crucial concerning steric and electronic saturation affecting stability and activity. The use of bulky neopentyl-type ligands and silyl-substituted derivatives [CH_2SiMe_3], [$CH(SiMe_3)_2$], and [$C(SiMe_3)_3$] results in relatively stable complexes as a rule displaying decreased catalytic reactivity. After the development of homoleptic rare-earth metal tris(tetramethylaluminate) complexes [$Ln(AlMe_4)_3$] by EVANS ET AL in 1995,[146] the group of ANWANDER investigated the application of these thermally robust "alkyls in disguise" as precursors for rare-earth metal half-metallocene complexes.[147-148] Methane elimination with one equivalent of substituted HCp^R yielded the bis(aluminate) complexes [$Cp^RLn(AlMe_4)_2$] (Cp^R = C_5Me_5, C_5Me_4H, 1,3-$(Me_3Si)_2C_5H_3$, $C_5H_4SiMe_3$, 1,2,3-$(Me_3C)_3C_5H_2$), which showed good-to-excellent catalytic activities and high *trans*-1,4 selectivity in isoprene polymerization upon cationization with organoborate co-catalysts.[31, 114-115] In 2010, the half-sandwich bis(tetramethylaluminate) library was extended to the quinolyl-substituted complex [$Cp^QLn(AlMe_4)_2$], synthesized via the respective protonolysis protocol, in which the rigid quinolyl donor function did not interfere with the tetramethylaluminate moieties (*vide supra*).[130] In contrast, no identifiable product could be obtained when applying the same protocol with cyclopentadienyl HCp^{NMe2} bearing the flexible ethyl linked amino donor, presumably due to multiple C–H bond activations. However, reaction at –35 °C yielded [($C_5Me_4CH_2CH_2NMe_2${$AlMe_3$})$Ln(AlMe_4)_2$] (**I**) as the main product for yttrium, lanthanum and neodymium (Figure S1, **Paper I**). We hypothesized that in the first step, a donor-induced cleavage of one tetramethylaluminate moiety, under formation of a proligand trimetylaluminum adduct along with a transient rare-earth metal methyl complex occurred (Scheme S2). These highly reactive Ln–CH_3 species are proposed to

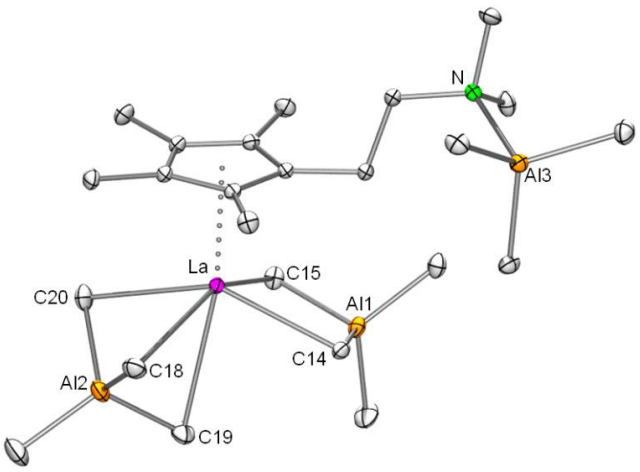

Figure S1 Solid-state structure of complex $\mathbf{I}_{La}$.

deprotonate the cyclopentadiene, giving complexes **I**. In case of the smaller rare-earth metal lutetium the protonolysis reaction sequence is much less active, as already observed for the non-functionalized pentamethylcyclopentadiene.

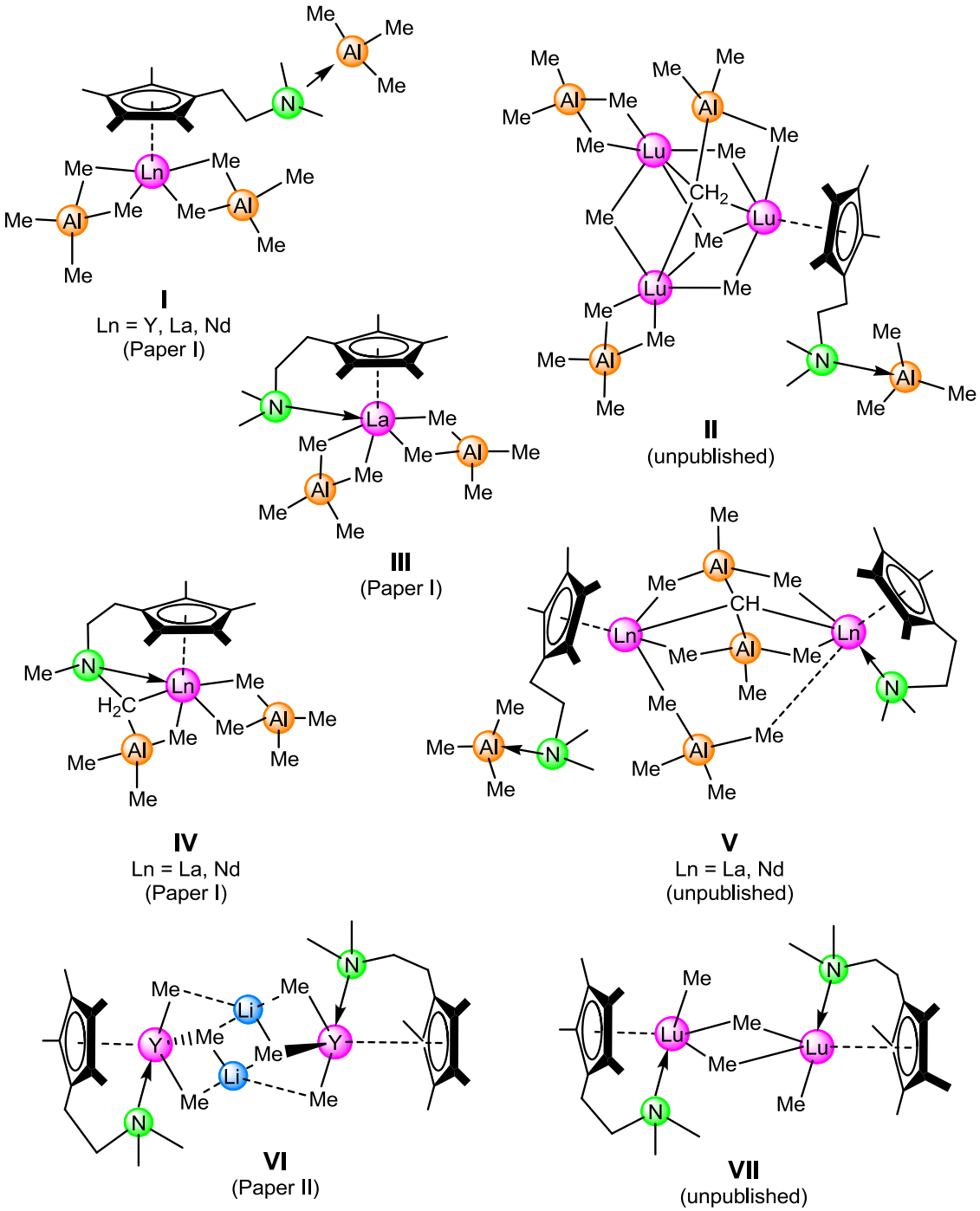

Chart S1. Structurally characterized bisalkyl comlexes bearing the Cp^{NMe2} ligand.

Even after three days at ambient tempera-ture, no formation of complex **I** was observed. This hypo-thesis is further reinforced by the generation of complex **V** as an isolated by-product of the alternative salt-metathesis reaction of the homoleptic lanthanum and neodymium tetramethylaluminates with the lithium salt of the ancillary ligand, which was supposed to suppress the additional $AlMe_3$ coordination of the sidearm due to the separation of $LiAlMe_4$. In the dimeric complex **V**, both rare-earth metal centers are coordinated by the cyclopentadienyl rings of the Cp^{NMe2} ligands, while only one is additionally coordinated by the donor functionality (Figure S2). The amino-sidearm of the other ligand attaches to trimethylaluminum instead. The metal centers are bridged by an $[AlMe_4]$ moiety, coordinating in a η^1 fashion towards both, while additional agostic interactions to the less coordinated may be discussed. Also, the two metals are linked via a trimethylaluminum stabilized methin $[(AlMe_3)_2(\mu_4\text{-}CH)]$ moiety (C1) in a butterfly arrangement. A similar motif was found by DIETRICH in our group in 2006.[149]

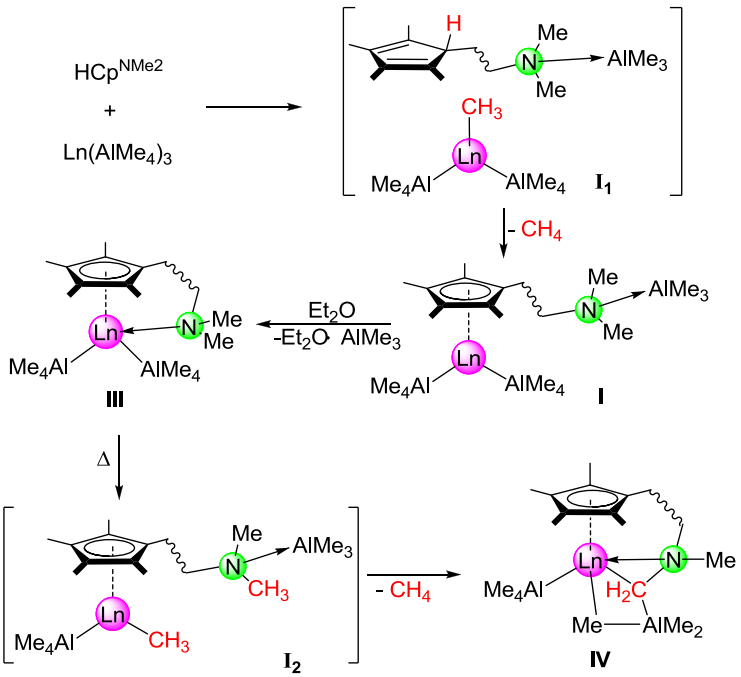

Scheme S2. Hypothesized C-H bond activation via intramolecular donor-cleavage.

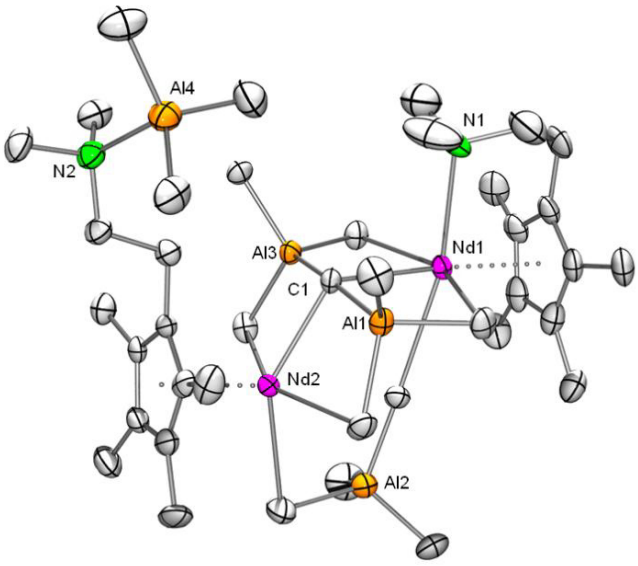

Figure S2 Solid-state structure of complex $\mathbf{V_{Nd}}$

Back then, it was proposed that partial ether-induced donor-cleavage of [Cp*Y(AlMe$_4$)$_2$] to form [Cp*YMe$_2$]$_3$ led to the tetranuclear complex [Cp*$_2$Y$_2${(AlMe$_3$)$_2$(μ_4-CH)}(μ_2-Me)]$_2$. Apparently, the open coordination site available in case of the sterical less demanding Cp* ligand in comparison to the chelating Cp^{NMe2} cyclopentadienyl at the one metal atom is compensated by the dimerization via two bridging methyl groups (Scheme S3). In order to promote the chelating coordination of the donor-substituted cyclopentadienyl at the bis(tetramethylaluminate) rare-earth metal half-sandwich complexes **I**, the distracting trimethylaluminum was removed through the addition of one equivalent of diethyl ether. Spontaneous gas evolution was observed at ambient temperature and only the C–H bond activated complex **IV** could be isolated for the lanthanum and the neodymium complexes (Figure S3, **Paper I**). The inadvertent activation could be suppressed in case of the lanthanum complex when the reaction was carried out at –35 °C, and a single crystal of the corresponding complex [Cp^{NMe2}La(AlMe$_4$)$_2$] (**III**) was structurally analyzed (**Paper I**). However, when the reaction solution was permitted to warm to ambient temperature, the C-H bond activation at the amino group occurred, confirming its temperature dependency.

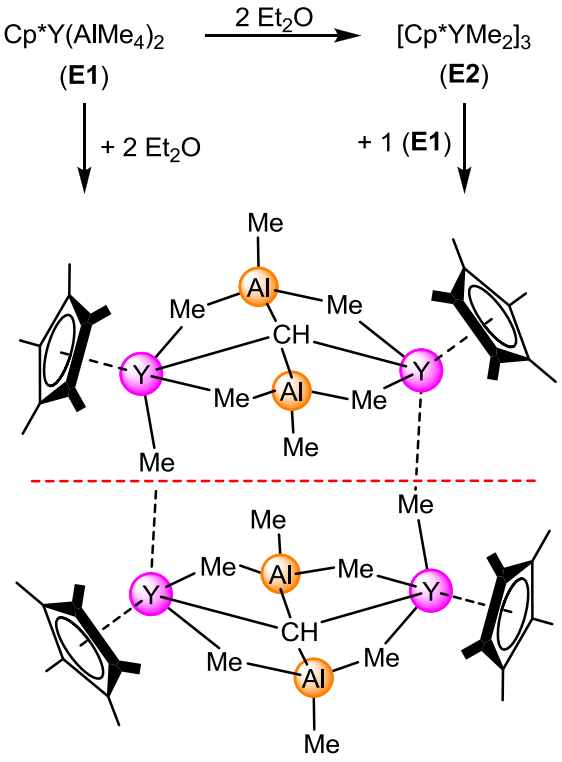

Scheme S3. Previously observed C–H bond activation on [Cp*Ln(AlMe$_4$)$_2$].[149]

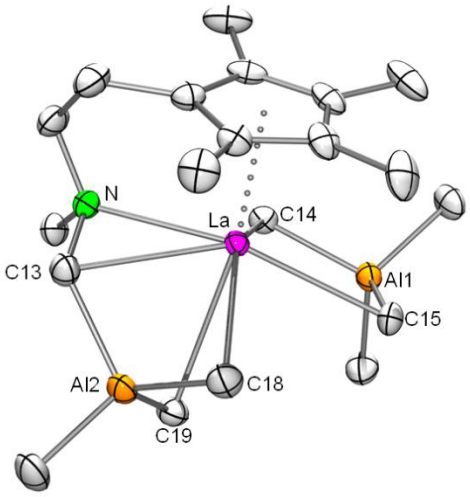

Figure S3 Solid-state structure of complex **IV$_{La}$** (**Paper I**).

The influence of the metal size, showing a higher degree of activation for the smaller rare-earth metal centers, became more obvious with the introduction of the anilinyl-functionalized cyclopentadienyl ligand HCp^{AMe2} (**Paper I**). The protonolysis reaction at –35 °C with homoleptic tris(tetramethyl-aluminate) complexes of lanthanum and neodymium yielded the non-activated complexes $[Cp^{AMe2}Ln(AlMe_4)_2]$ (Figure S4, **XV**), which undergo C-H bond activation at elevated temperature under formation of $[(C_5Me_4C_6H_4NMe\{\mu\text{-}CH_2\}AlMe_3)Ln(AlMe_4)]$ (**XVI**) comparable with complexes **IV**. In contrast, the smaller yttrium metal center already gave the aminomethyl-activated complex at low temperature. The performances of the stable complexes **I**, **IV**, **XV** and **XVI** as pre-catalysts in isoprene polymerization were investigated (vide infra, **Paper I**).

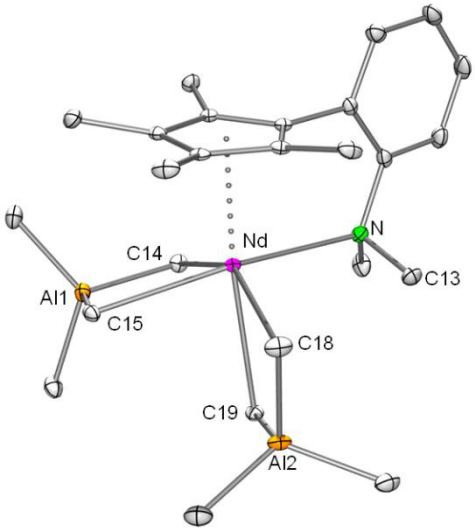

Figure S4. Solid-state structure of complex $\mathbf{XV_{Nd}}$ (**Paper I**).

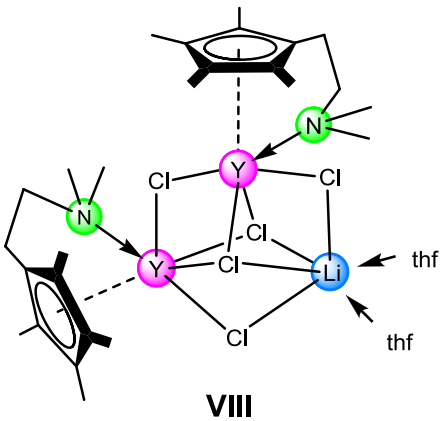

VIII
(Paper II)

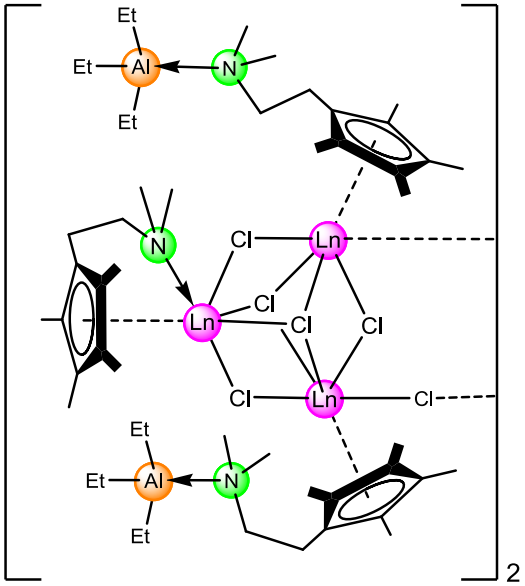

IX
Ln = Y, Ho
(Paper III)

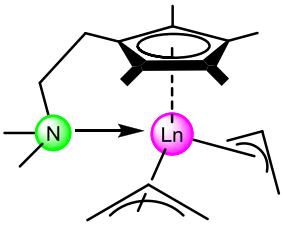

X
Ln = Y, Ho, Lu
(Paper III)

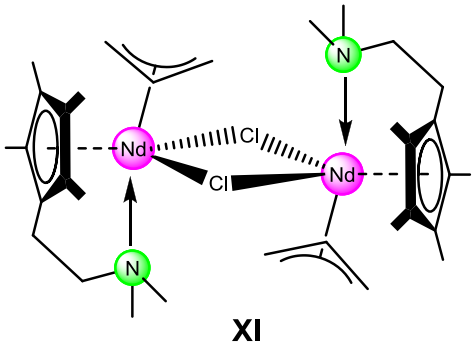

XI
(Paper III)

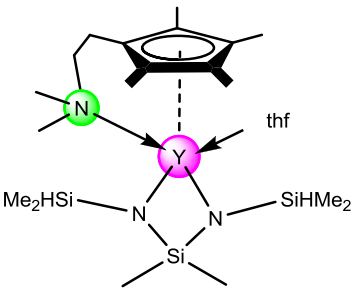

XII
(Paper II)

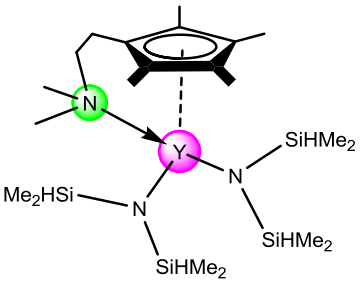

XIII
(Paper II)

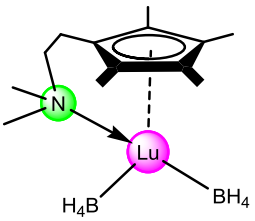

XIV
(unpublished)

Chart S2. Structurally characterized chloride, allyl, amide and borohydride complexes bearing the Cp^{NMe2} ligand.

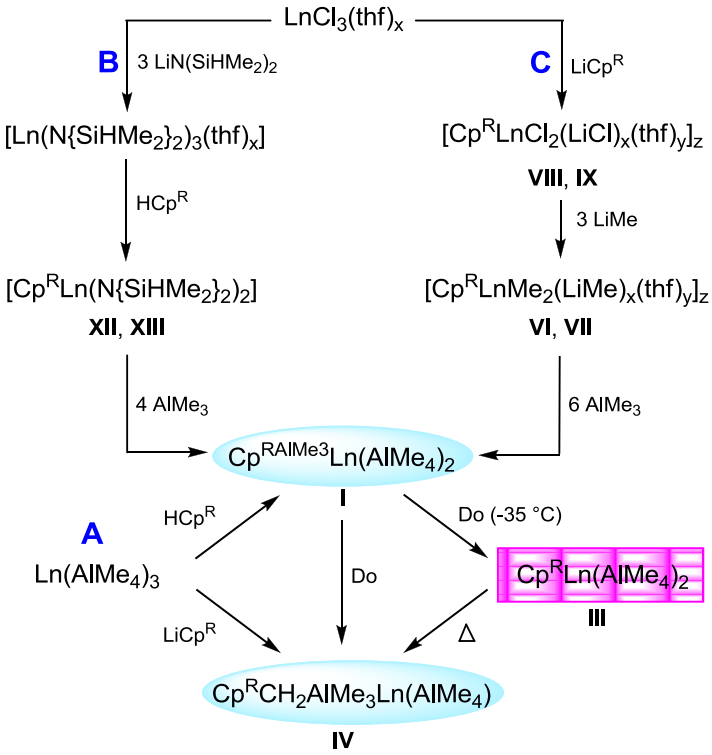

Scheme S4. Synthesis approaches for $[Cp^{R}Ln(AlMe_4)_2]$.

To date, rare-earth metal tetramethylaluminate complexes have been synthesized by alkylation of a number of Ln(III) precursors, like alkylamide $[Ln(NMe_2)_3(LiCl)_3]$, silylamide $[Ln(N\{SiHMe_2\}_2)_3(thf)_2]$, alkoxide $[Ln(OR)_3]_4$, aryloxide $[Ln(OAr^{R})_3]_2$, and silyloxide $[Ln(OSiR'_2R'')_3]_2$ complexes. Synthesis of the corresponding half-sandwich bis(aluminate) complexes via protonolysis or salt-metathesis protocol are well established (Scheme S4, A), but in order to prevent inadvertent activation by the highly reactive $[AlMe_4]$ moieties, two further reaction sequences have been investigated. One known as the *extended silylamide route* refers to the bis(dimethylsilyl)amide derivates,[150] while the other elaborates salt metathesis reactions to form half-sandwich bis-chloride and -methyl complexes (Scheme S4, B and C). From reaction path C, the key precursor $[Cp^{NMe2}YCl_2]_2[LiCl(thf)_2]$ (**VIII**) was isolated and structurally analyzed (**Paper II**). The *ate* complex **VIII** displays the same trinuclear core as $[Cp^{AMe2}YCl_2]_2[LiCl(thf)_2]$ reported by CUI ET AL. in 2010.[140] Subsequent reaction with an excess of methyllithium in toluene led to the dimeric *ate* complex $[Cp^{NMe2}YMe_2(MeLi)]_2$ (**VI**) in case of yttrium. Complex **VI** represents a rare case in which the lithium atoms are bound to four carbon atoms in a tetrahedral geometry without any donor coordination (**Paper II**). When the smaller rare-earth

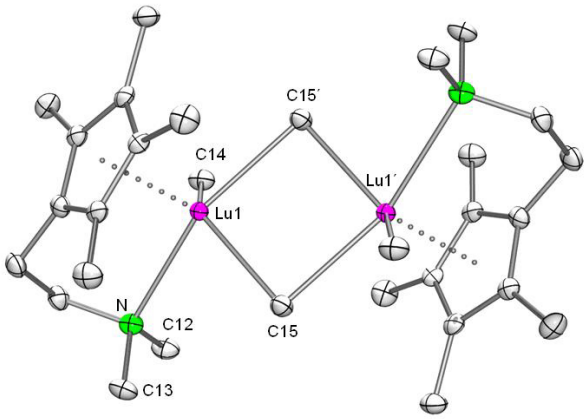

Figure S5. X-ray structure of complex $\mathbf{VII_{Lu}}$

metal center lutetium was used instead, the dimeric bismethyl complex $[Cp^{NMe2}LuMe_2]_2$ (**VII**) was obtained devoid of any salt incorporation (Figure S5). The two metal centers are bridged by two methyl groups forming a tetragon with angels of 90.92° at the carbon and 89.08° at the lutetium atoms. The Cp^{NMe2} ligands coordinate η^5:κ^1 towards each metal center which bear additionally one terminal methyl group. A similar structural geometry was reported for the half-sandwich scandium dimethyl complex $[(C_5Me_4SiMe_3)ScMe_2]_2$.[151] Both complexes are stable at ambient temperature and the lack of C–H bond activation of the highly reactive methyl groups might be a result of either the absence of any aluminum compound or the less crowded ligand sphere around the metal center.

Interestingly, in case of the acid-base reaction of $[Y(N\{SiHMe_2\}_2)_3(thf)_2]$ with HCp^{NMe2} at elevated temperature (Scheme S4, B), additional Si-H bond activation occurred and a dianionic bisamindo ligand was formed under elimination of dimethylsilane, which was unambiguously proven by ^1H-^1H COSY NMR spectroscopy (**Paper II**). Additionally coordinated THF molecules saturate the metal centers in $[Cp^{NMe2}Y(SiMe_2\{NSiHMe_2\}_2)(thf)]$ (Figure S6, **XII**). In contrast, the desired half-sandwich yttrium bis(silylamide) complex $[Cp^{NMe2}Y(N\{SiHMe_2\}_2)_2]$ (Figure S6, **XIII**) could be synthesized via salt metathesis reaction following reaction path B (Scheme S4). Additional monoagostic Y–SiH interactions of each amide ligand result in an asymmetric coordination and prevent further donor solvent coordinations. Both amido complexes as well as the bismethyl *ate* complex have been verified as potential precursors for the synthesis of the half-sandwich yttrium bis(tetramethylaluminate) complex **I** in NMR scale reactions, when treated with excess of trimethylaluminum.

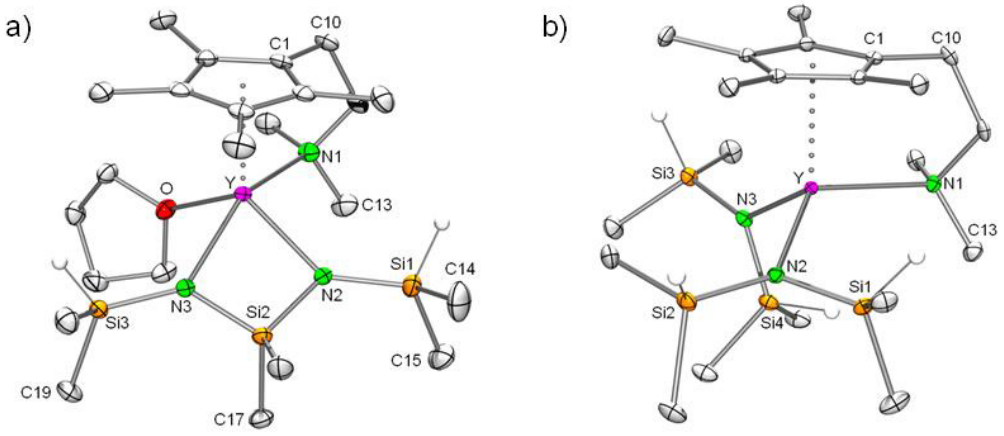

Figure S6. Solid-state structure of complexes a) **XII** and b) **XIII** (**paper III**)

The most striking feature of the presented tetramethylaluminate ligands, also referred as “alkyls in disguise”, is their ability to stabilize the otherwise highly reactive rare-earth metal methyl groups under formation of donor-solvent and *ate* complex free species due to their variable η^1, η^2 or η^3 coordination modes. Similar advantages can be achieved by the use of allyl ligands where the η^3 coordination shields the LEWIS acidic metal center, while the $\eta^3 \rightarrow \eta^1$ bonding mode switches lead to the reactive metal σ carbon bond. According to the synthesis of anilinyl- and pyridinyl-functionalized half-sandwich rare-earth metal bis(allyl) complexes reported by CUI ET AL in 2010 (vide supra),[128, 152] the amino-ethyl supported cyclopentadienyl was introduced in a two step, one pot salt metathesis reaction of the lithiated ligand with the rare-earth metal chloride followed by the GRIGNARD reagent allylmagnesium chloride. The obtained complexes $[Cp^{NMe2}Ln(C_3H_5)_2]$ (**X**, Ln = Y, Ho, Lu) were tested as precursors in isoprene polymerization under various conditions (Figure S7, **Paper III**). In case of the larger rare-earth metal neodymium, only the partially alkylated mono(allyl) mono(chloride) half-sandwich complex $[Cp^{NMe2}Nd(C_3H_5)(\mu\text{-Cl})]_2$ could be achieved (Figure S8, **Paper III**). Furthermore, [allyl]→[aluminate] and [allyl]→[chloride] exchange reactions with $AlMe_3$ and Et_2AlCl were investigated, revealing the partial formation of yttrium bis(aluminate) complex **I** by NMR studies in the first case. From the reaction with the chlorination reagent, single crystals of holmium and yttrium bis(chloride) were obtained and analyzed by X-ray diffraction method, disclosing hexameric cluster complexes $[\{(Cp^{NMe2AlEt3})_2(Cp^{NMe2})\text{-}Ln_3Cl_5\}(\mu\text{-Cl})]_2$ (**IX**, Chart S2).

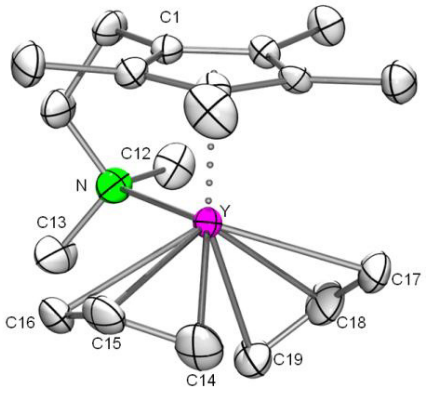

Figure S7. Solid-state structure of complex $\mathbf{X_Y}$ (**paper III**)

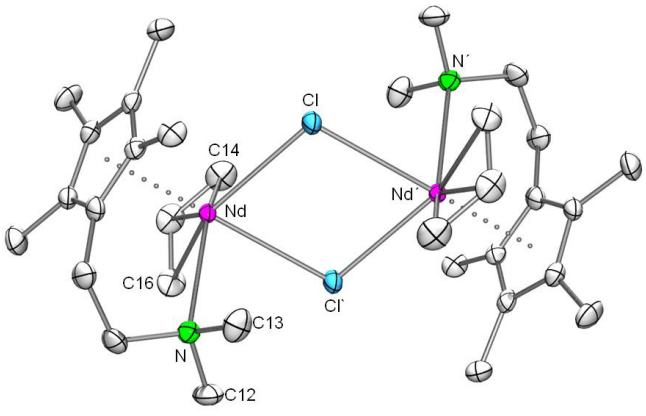

Figure S8. Solid-state structure of complex $\mathbf{XI_{Nd}}$ (**paper III**)

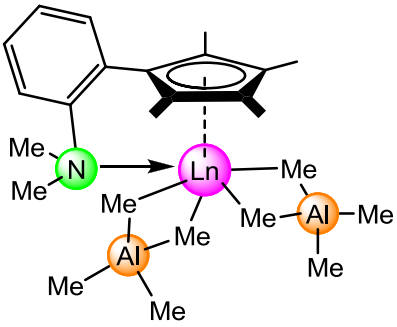

XV
Ln = Nd, La
(Paper I)

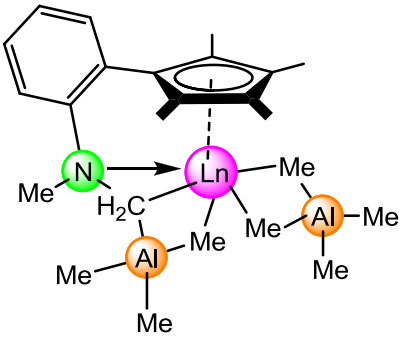

XVI
Ln = Y, La, Nd
(Paper I)

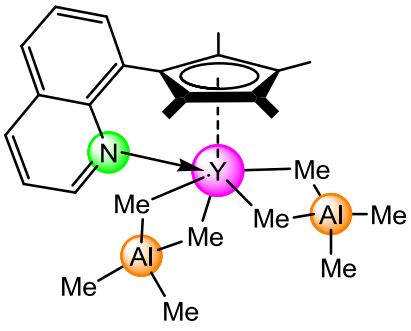

XVII
(unpublished)

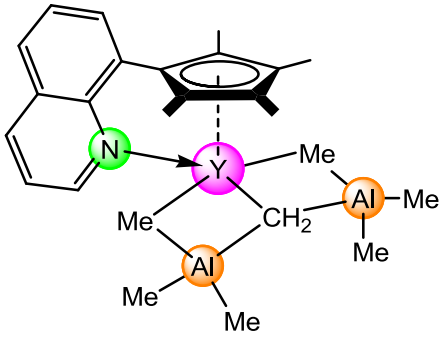

XVIII
Ln = Y, La, Nd
(unpublished)

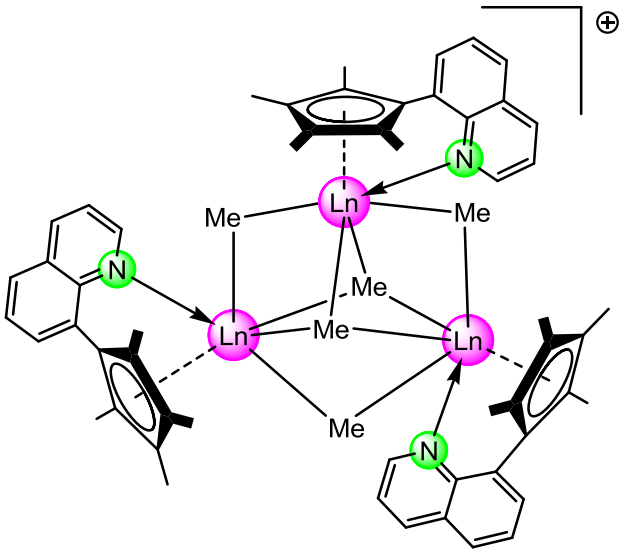

XIX
(unpublished)

Chart S2. Structurally characterized complexes bearing the Cp^{AMe2} and Cp^{Q} ligands

3 Isoprene Polymerization

With increasing demands of tailor-made polymers possessing distinct properties, insights into structure-reactivity relationships of catalysts concerning adjustable microstructures of polymer chains is a major topic in macromolecular science. Tremendous efforts in 1,3-diene polymerization are made due to the steadily growing rubber consumption, mainly caused by tire fabrication. Therefore, highly *cis*-1,4-regulated polybutadiene is blended with further elastomers to form high-performance rubbers. The isoprene counterpart represents the synthetic alternative (SR) to natural rubber (NR), which is extracted from evergreen trees in Asia, but cannot longer cover the needs. Furthermore, the *trans*-1,4-polyisoprene exhibits benefits as a component in tread rubbers and shape-memory elastomers due to its crystallinity and blending rubber with the 3,4-regulated polyisoprene can raise wet-skid resistance while the rolling resistance can be lowered.

As described in chapter 1.8.1, the enanthiomorphic site-control mechanism of *α*-olefin polymerization is well explored, while the explanation of the structure-reactivity relation in 1,3-diene polymerization remains challenging, dealing with the additional chain-end mechanism. Up to date, it is difficult to predict a catalysts performance and every new catalyst provides a contribution to generate a more comprehensive understanding. Hence, the rare-earth metal bis(tetramethylaluminate) complexes supported by nitrogen-donor functionalized cyclopentadienyl ligands (**I**, **IV**, **XV** and **XVI**) were examined as pre-catalysts in isoprene polymerization under various conditions (**Paper I**). The results presented in Table S1 refer to standard procedures, where the complexes were activated with borate salt $[C_6H_5NMe_2H][B(C_6F_5)_4]$ (**B**) in toluene at 40 °C followed by the addition of isoprene. Beside the size effect of the rare-earth metal cation generating higher *trans*-1,4-regulation for the larger metal centers (run 1 vs. 4 vs. 7) confirming earlier achievements on $[Cp^*Ln(AlMe_4)_2]$ (**Cp***) (runs 8-10),[31] the absence of any *cis*-1,4 units in the polymer chains produced by the lanthanum and neodymium complexes is to emphasize. The *π*-*σ*-rearrangement described in chapter 1.8.2 allows 3,4-insertion into the growing polymer, but the additional coordination of the nitrogen functionalized sidearm might sterically hinder the generation of the *anti*-allylic coordination of the polymer chain and hence suppress the formation of *cis*-1,4 polyisoprene motifs.

Tabel S1: Selected isoprene polymerization by bis(tetramethylaluminate) complexes

Run	No.	Metal	Isoprene insertion		M_n ($\times 10^5$)	M_w/M_n	Paper/
			trans/cis-1,4	3,4			Ref.
1	**XVI**	**Y**	27.3/58.1	14.6	1.4	1.72	**I**
2	**IV**	**Nd**	83.3/–	16.7	1.0	1.09	**I**
3	**XV**	**Nd**	87.3/–	12.7	1.6	1.19	**I**
4	**XVI**	**Nd**	84.1/–	15.9	0.8	1.23	**I**
5	**IV**	**La**	92.0/–	8.0	1.0	1.09	**I**
6	**XV**	**La**	91.6/–	8.4	2.5	1.13	**I**
7	**XVI**	**La**	92.1/–	7.9	0.7	1.07	**I**
8	**Cp***	**Y**	28.7/43.5	27.8	0.6	1.59	[31]
9	**Cp***	**Nd**	79.9/6.9	13.2	0.4	1.16	[31]
10	**Cp***	**La**	87.5/2.9	9.6	0.7	1.23	[31]

Metal allyl complexes are of particular interest, as the *π*-allylic bonded species of the growing polymer chain is generally considered as the transition-state model in diene-polymerization (see chapter 1.8). Therefore, the performances of the rare-earth allyl complexes **X** and **XI**, bearing the amino-functionalized cyclopentadienyl ligand were investigated (**Paper III**). Selected examples are summarized in Table S2 referring to standard procedures ($[C_6H_5NMe_2H][B(C_6F_5)_4]$/toluene/ 40° C). Due to the similar ionic radii, the complexes of yttrium and holmium produced almost identical polymers, and only the results for $[Cp^{NMe2}Y(C_3H_5)_2]$ are presented. Upon activation with $[PhNMe_2H][B(C_6F_5)_4]$ only, mainly 3,4-selective isoprene polyisoprene was obtained (run 11). In the presence of 10 equiv of AlR_3, dramatic shifts toward 1,4-selectivity were observed. The addition of an excess of Al^iBu_3 led to mainly *cis*-1,4-regulated polyisoprene, while the use of $AlMe_3$ produced polymers with a dominant *trans*-1,4-microstructure (run 12 and 13). The decrease of the molecular weight of the polymer to 1.5×10^4 g mol^{-1} suggests [Ln] → [Al] chain transfer reaction of the growing polymer as reported for the catalytic system $[Cp^{AMe2}Ln(C_3H_5)_2]/Al^iBu_3/[PhNMe_2H][B(C_6F_5)_4]$ previously (see 2.1).[152] In contrast, catalytic systems based on the smaller rare-earth metal lutetium were far less selective and only affected by the addition of $AlMe_3$, resulting in decreased counts of *cis*-1,4 microstructure in the produced polymer (runs 14-16). The dimeric neodymium complex **XI** showed no activity, when a [Ln]:[co-cat] ratio of 1:1 was applied, indicating the loss of both allyl moieties. When complex **XI** was activated with one equivalent of $[PhNMe_2H][B(C_6F_5)_4]$, polyisoprene with dominant 3,4-microstructure was produced.

Tabel S2: Selected isoprene polymerization by bis(allyl) and monoallyl-chloride complexes

Run	No.	Metal	AlR_3 10 equiv.	*trans/cis*	3,4	M_n (×10^4)	M_w/M_n	Paper/ Ref.
11	**X**	**Y**	-	-/14.7	85.3	6.1	1.06	**III**
12	**X**	**Y**	$AlMe_3$	71.9/-	28.3	5.1	1.05	**III**
13	**X**	**Y**	Al^iBu_3	-/74.1	25.9	1.5	1.19	**III**
14	**X**	**Lu**	-	30.8/31.6	37.6	2.6	1.04	**III**
15	**X**	**Lu**	$AlMe_3$	50.8/4.4	44.8	3.3	1.39	**III**
16	**X**	**Lu**	Al^iBu_3	24.6/39.5	33.9	1.0	1.72	**III**
17	**XI**	**Nd**	-	30.4/5.8	63.8	4.7	1.11	**III**
18	**XI**	**Nd**	$AlMe_3$	85.4/-	14.6	4.3	1.06	**III**
19	**XI**	**Nd**	Al^iBu_3	9.9/5.3	84.8	1.2	1.29	**III**

Similar behavior was observed by applying the binuclear complexes $[(C_5Me_4)SiMe_2P(Cy)Ln(CH_2SiMe_3)]_2$ (Ln = Y, Lu; Cy = cyclohexyl) bearing a chelating phosphido-substituted cyclopentadienyl. Upon activation with one half equivalent per metal center, the first isospecific 3,4-polymerization (100% 3,4; *mmmm* > 99%) of isoprene with rare-earth metal complexes was achieved (see 1.8.3.3).[111]

3.1 Polymer Analysis

NMR Spectroscopy

As mentioned earlier, natural rubber occurs as highly pure *cis*-1,4- or *trans*-1,4-polyisoprene while synthesized rubbers often contain a mixture of both and can involve two further kinds of possible microstructures, namely 3,4-, and 1,2-units in its molecular chain. Even in low percentages, these have significant impact on the polymers properties. Especially, glass-transition temperature, curing rate, elasticity and hardness, but also tearing strength and processability are affected and disclose “new” polymers as “tailor-made” construction materials. Thereby, most reports on synthetic rubber NMR analysis deal with the incorporation of 3,4-units in high *cis*-1,4-polyisoprene.[154-156]

The catalytic system based on the monoallyl-chloride neodymium complex **XI** activated with co-catalyst **B** in the presence of 10 equivalents of $AlMe_3$ produced predominatly *trans*-1,4 polyisoprene with a content of 14.6% 3,4-units as determined by ^{1}H NMR spectroscopy (Table S2, run 18). In the ^{13}C NMR spectrum, the integral ratio of the peaks at 18.6, 47.2, 111.2 and 147.7 fits to the presence of single isolated 3,4-units (**V**) incorporated into the *trans*-1,4 polymer (**T**) chain as shown in Figure S12. To verify the ^{13}C NMR signals at

31.1 and 32.1 ppm, a two-dimensional $^{1}H–^{13}C$ HSQC NMR spectrum was recorded and the peaks assigned to the $\mathbf{T_4^I}$ and $\mathbf{V_4}$ carbons (**Paper III**). This type of polyisoprene microstructure and its corresponding NMR data have not been described in detail to date. Further investigations into the physiochemical properties might be reasonable as such polymers might open interesting avenues for selective functionalization of the free vinylic groups.

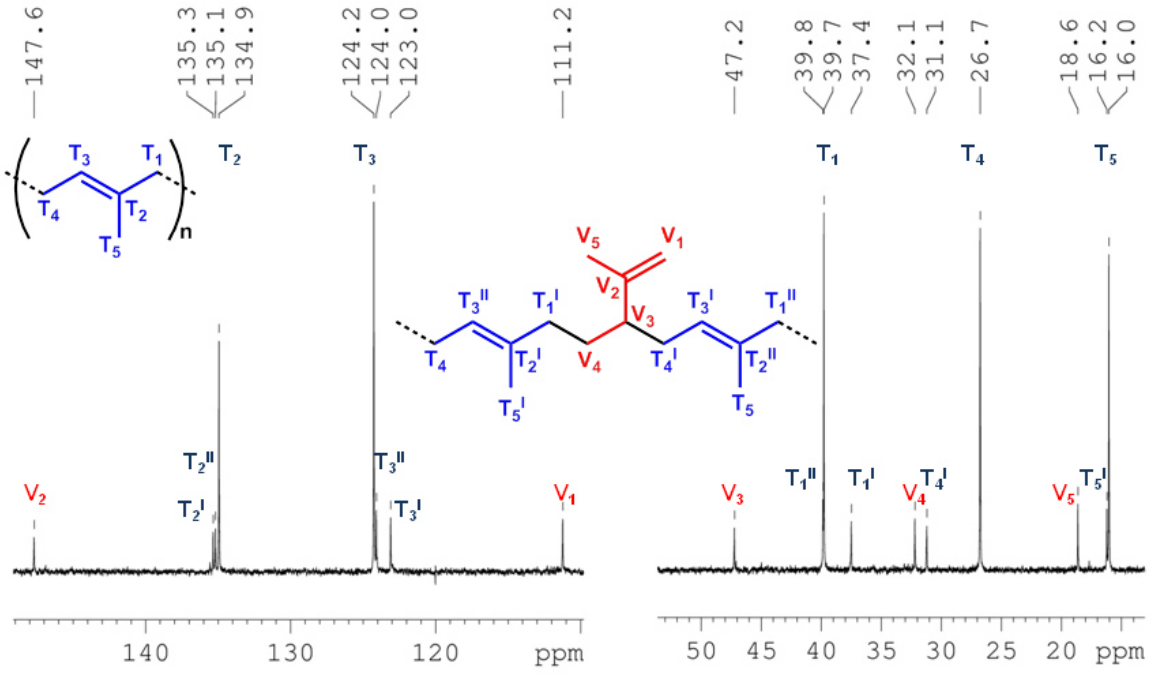

Figure S11. Olefinic and aliphatic regions of the ^{13}C NMR spectra of PIP form $\mathbf{XI_{Nd}}$/$AlMe_3$/**B** (run 18).

Concluding Remarks

A series of rare-earth metal half-sandwich complexes bearing nitrogen-donor functionalized cyclopentadienyl ligands have been synthesized. Beside the desired formation of [$Cp^{Do}LnR_2$]-type complexes (Cp^{Do} = $C_5Me_4CH_2CH_2NMe_2$ {Cp^{NMe2}}, $C_5Me_4C_6H_4NMe_2$ {Cp^{AMe2}}, $C_5Me_4C_{10}H_6NMe_2$ {Cp^{Q}}; R = $AlMe_4$, C_3H_5, Me, $N\{SiHMe_2\}_2$, BH_4), a variety of side-products from unpredictable C–H and Si–H bond activations as well as *ate*-complex formation were isolated. Comprehensive analysis provides important insights into the reactivity and structural properties of these compounds, paving the way for further synthesis strategies. For instance, the observed highly selective C–H bond activation is governed by the mobility/rigidity of the donor linker (Cp^{NMe2} > Cp^{AMe2}), the metal size/Lewis acidity (Y^{III} > La^{III}), and the reaction temperature.

Special emphasis was put on the performance of aluminate and allyl complexes ([($C_5Me_4C_2H_4NMe\{\mu\text{-}CH_2\}AlMe_3$)$Ln(AlMe_4)_2$], [($C_5Me_4C_6H_4NMe\{\mu\text{-}CH_2\}AlMe_3$) $Ln(AlMe_4)_2$], [$Cp^{AMe2}Ln(AlMe_4)_2$], [$Cp^{NMe2}Ln(C_3H_5)_2$] and [$Cp^{NMe2}Nd(C_3H_5)(\mu\text{-}Cl)]_2$) in isoprene polymerization under various conditions, related to solvent, temperature and activator. All of the aluminate half-sandwich complexes displayed excellent activity upon the addition of fluorinated organoboron reagents as co-catalysts. The high *trans*-1,4 selectivity (up to 96%) increased with increasing size of the rare-earth metal center. Importantly, the additional coordination of the amino moieties prevented the formation of *cis*-1,4 contents in the produced polymer for the lanthanum and neodymium complexes. Furthermore, very narrow molecular weight distributions (Mw/Mn<1.1) were achieved upon activation with [$PhNMe_2H$][$B(C_6F_5)_4$] in toluene.

The yttrium and holmium bis(allyl) complexes showed only moderate activity for mainly 3,4-selective (up to 79%) isoprene polymerization upon activation with the boron co-catalyst alone, but the performance increased dramatically and shifts towards either *trans*-1,4- ($AlMe_3$) or *cis*-1,4-selectivity (Al^iBu_3) when trialkylaluminum was added. NMR spectroscopic studies of the mixture including $AlMe_3$ revealed rapid [allyl]→[aluminate] exchange (allyl/methyl scrambling) under loss of the constrained geometry conformation. High *trans*-1,4 polyisoprene containing 14% 3,4-units was obtained from the catalyst system [$Cp^{NMe2}Nd(C_3H_5)(\mu\text{-}Cl)]_2$/[$PhNMe_2H$][$B(C_6F_5)_4$]/$AlMe_3$. Comprehensive NMR spectroscopic analyses of the polymer demonstrated the presence of single isolated 3,4-units incorporated into the *trans*-1,4-polymer chain. Such polymers might open interesting avenues for selective functionalization of the free vinylic groups.

D References

[1] T. Hancock, *English patent 9952* **1843**.

[2] C. Goodyear, *US patent 3.633* **1844**.

[3] L. H. Baekeland, *J. Ind. Eng. Chem.* **1909**, *1*, 149-161.

[4] F. Hofmann, K. Delbrück, *German Patent 250.690 to Farbenfabriken Bayer* **1909**.

[5] F. Klatte, *Deutsche Reichs Patent no. 281687* **1912**.

[6] H. Staudinger, J. Fritschi, *Helv. Chim. Acta* **1922**, *5*, 785-806.

[7] E. W. Fawcett, R. O. Gibson, Perrin, J. G. Patton, E. W. Williams, *British patent 471.590* **1937**.

[8] K. Ziegler, *Belg. patent 533362* **1955**, (German priority, Nov. 16, 1953).

[9] K. Ziegler, E. Holzkamp, H. Breil, H. Martin, *Angew. Chem.* **1955**, *67*, 426-426.

[10] J. P. Hogan, R. L. Banks, *US patent 2825721* **1955**.

[11] K. Ziegler, *Angew. Chem.* **1952**, *64*, 323-329.

[12] G. Natta, P. Pino, P. Corradini, F. Danusso, E. Mantica, G. Mazzanti, G. Moraglio, *J. Am. Chem. Soc.* **1955**, *77*, 1708-1710.

[13] G. Natta, P. Pino, G. Mazzanti, *Gazz. Chim. Ital* **1957**, *87*, 528.

[14] G. Natta, P. Pino, G. Mazzanti, *US patent 3715344* **1973**, (Italian priority June, 1954).

[15] G. Natta, P. Pino, G. Mazzanti, R. Lanzo, *Chim. Ind. (Milan)* **1957**, *39*, 1032-1033.

[16] D. S. Breslow, N. R. Newburg, *J. Am. Chem. Soc.* **1957**, *79*, 5072-5073.

[17] H. Sinn, W. Kaminsky, in *Adv. Organomet. Chem., Vol. Volume 18* (Eds.: F. G. A. Stone, W. Robert), Academic Press, **1980**, pp. 99-149.

[18] P. Pino, R. Mülhaupt, *Angew. Chem. Int. Ed.* **1980**, *19*, 857-875.

[19] H. H. Brintzinger, D. Fischer, R. Mülhaupt, B. Rieger, R. M. Waymouth, *Angew. Chem. Int. Ed.* **1995**, *34*, 1143-1170.

[20] G. W. Coates, P. D. Hustad, S. Reinartz, *Angew. Chem.* **2002**, *114*, 2340-2361.

[21] J. C. W. Chien, B.-P. Wang, *J. Polym. Sci., Part A: Polym. Chem.* **1988**, *26*, 3089-3102.

[22] R. F. Jordan, C. S. Bajgur, R. Willett, B. Scott, *J. Am. Chem. Soc.* **1986**, *108*, 7410-7411.

[23] P. Cossee, *J. Catal.* **1964**, *3*, 80-88.

[24] E. J. Arlman, *J. Catal.* **1964**, *3*, 89-98.

[25] X. Yang, C. Stern, T. J. Marks, *Organometallics* **1991**, *10*, 840-842.

[26] X. Yang, C. L. Stern, T. J. Marks, *J. Am. Chem. Soc.* **1991**, *113*, 3623-3625.

[27] X. Yang, C. L. Stern, T. J. Marks, *J. Am. Chem. Soc.* **1994**, *116*, 10015-10031.

[28] E. Y.-X. Chen, T. J. Marks, *Chem. Rev.* **2000**, *100*, 1391-1434.

[29] J. Zhou, S. J. Lancaster, D. A. Walker, S. Beck, M. Thornton-Pett, M. Bochmann, *J. Am. Chem. Soc.* **2000**, *123*, 223-237.

[30] D. Mathis, E. P. A. Couzijn, P. Chen, *Organometallics* **2011**, *30*, 3834-3843.

[31] M. Zimmermann, K. W. Törnroos, R. Anwander, *Angew. Chem. Int. Ed.* **2008**, *47*, 775-778.

[32] J. T. Katz, N. Acton, *Tetrahedron Lett.* **1970**, *11*, 2497-2499.

[33] J. A. Smith, J. von Seyerl, G. Huttner, H. H. Brintzinger, *J. Organomet. Chem.* **1979**, *173*, 175-185.

[34] F. R. W. P. Wild, L. Zsolnai, G. Huttner, H. H. Brintzinger, *J. Organomet. Chem.* **1982**, *232*, 233-247.

[35] J. A. Ewen, *J. Am. Chem. Soc.* **1984**, *106*, 6355-6364.

[36] W. Kaminsky, K. Külper, H. H. Brintzinger, F. R. W. P. Wild, *Angew. Chem.* **1985**, *97*, 507-508.

[37] L. Resconi, R. L. Jones, A. L. Rheingold, G. P. A. Yap, *Organometallics* **1996**, *15*, 998-1005.

[38] A. Razavi, V. Bellia, Y. De Brauwer, K. Hortmann, L. Peters, S. Sirole, S. Van Belle, U. Thewalt, *Macromol. Chem. Phys.* **2004**, *205*, 347-356.

[39] S. A. Miller, J. E. Bercaw, *Organometallics* **2002**, *21*, 934-945.

[40] W. Spaleck, F. Kueber, A. Winter, J. Rohrmann, B. Bachmann, M. Antberg, V. Dolle, E. F. Paulus, *Organometallics* **1994**, *13*, 954-963.

[41] Y. Q. Jia, *J. Solid State Chem.* **1991**, *95*, 184-187.

[42] W. C. von Dohlen, T. P. Wilson, E. G. Caflisch, BE 644.291 **1964**, p. (to Union Carbide Co.).

[43] W. C. von Dohlen, T. P. Wilson, E. G. Caflisch, US 3.297.667 **1967** p. (to Union Carbide Co.).

[44] D. G. H. Ballard, A. Courtis, J. Holton, J. McMeeking, R. Pearce, *J. Chem. Soc., Chem. Commun.* **1978**, 994-995.

[45] P. L. Watson, *J. Am. Chem. Soc.* **1982**, *104*, 337-339.

[46] P. L. Watson, *J. Am. Chem. Soc.* **1983**, *105*, 6491-6493.

[47] P. L. Watson, G. W. Parshall, *Acc. Chem. Res.* **1985**, *18*, 51-56.

[48] G. Jeske, H. Lauke, H. Mauermann, H. Schumann, T. J. Marks, *J. Am. Chem. Soc.* **1985**, *107*, 8111-8118.

[49] G. Jeske, H. Lauke, H. Mauermann, P. N. Swepston, H. Schumann, T. J. Marks, *J. Am. Chem. Soc.* **1985**, *107*, 8091-8103.

[50] G. Jeske, L. E. Schock, P. N. Swepston, H. Schumann, T. J. Marks, *J. Am. Chem. Soc.* **1985**, *107*, 8103-8110.

[51] P. L. Watson, *J. Chem. Soc., Chem. Commun.* **1980**, 652-653.

[52] G. Bouchardat, **1909**.

[53] C. Harries, *Justus Liebigs Ann. Chem.* **1911**, *383*, 157-227.

[54] S. V. Lebedev, *J. Russ. Phys. Chem. soc.* **1910**, *42*, 949-961.

[55] W. Boch, E. Tschunker, *DE 573568C (Mar 16, 1933),* , (to I. G. Farbenindustrie).

[56] E. Konrad, E. Tschunkur, *DE 658172 C* **1938**, (to I. G. Farbenindustrie).

[57] J. L. Binder, *Ind. Eng. Chem.* **1954**, *46*, 1727-1730.

[58] G. P. Natta, L.; Zanini, G.; Palvarini, A. , *Chim. Ind. (Milan)* **1959**, 1165-1169.

[59] G. P. Natta, L.; Mazzei, A.; Morero, D. , *Chim. Ind. (Milan)* **1959**, *41*, 398-404.

[60] G. P. Natta, L.; Zanini, G.; Fiore, L. , *Chim. Ind. (Milan)* **1959**, *41*, 526-533.

[61] G. P. Natta, L.; Mazzei, A. , *Chim. Ind. (Milan)* **1959**, *41*, 116-122.

[62] G. P. Natta, L.; Corradini, P.; Morero, D. , *Chim. Ind. (Milan)* **1958**, *40*, 362-371.

[63] Z. G. Shen, Z. Y.; Zhong, Z. Q.;OUYang, J., *Sci Sin (engl. transl.)* **1964**, *13*, 13339.

[64] S. E. Horne, J. P. Kiehl, J. J. Shipman, V. L. Folt, C. F. Gibbs, E. A. Willson, E. B. Newton, M. A. Reinhart, *Ind. Eng. Chem.* **1956**, *48*, 784-791.

[65] M. Kerns, S. Henning, M. Rachita, in *Encyclopedia of Polymer Science and Technology*, John Wiley & Sons, Inc., **2002**.

[66] W. Kuran, in *Principles of Coordination Polymerisation*, John Wiley & Sons, Ltd, **2002**, pp. 275-329.

[67] L. Friebe, O. Nuyken, W. Obrecht, in *Neodymium Based Ziegler Catalysts – Fundamental Chemistry, Vol. 204* (Ed.: O. Nuyken), Springer Berlin Heidelberg, **2006**, pp. 1-154.

[68] A. Fischbach, R. Anwander, in *Neodymium Based Ziegler Catalysts – Fundamental Chemistry, Vol. 204* (Ed.: O. Nuyken), Springer Berlin Heidelberg, **2006**, pp. 155-281.

[69] Z. Zhang, D. Cui, B. Wang, B. Liu, Y. Yang, in *Molecular Catalysis of Rare-Earth Elements, Vol. 137* (Ed.: P. W. Roesky), Springer Berlin Heidelberg, **2010**, pp. 49-108.

[70] P. J. Shapiro, E. Bunel, W. P. Schaefer, J. E. Bercaw, *Organometallics* **1990**, *9*, 867-869.

[71] W. E. Piers, P. J. Shapiro, E. E. Bunel, J. E. Bercaw, *Synlett* **1990**, 74-84.

[72] P. J. Shapiro, W. P. Schaefer, J. A. Labinger, J. E. Bercaw, W. D. Cotter, *J. Am. Chem. Soc.* **1994**, *116*, 4623-4640.

[73] J. C. Stevens, F. J. Timmers, G. W. Rosen, G. W. Knight, S. Y. Lai, *(Dow Chemical Co.), Eur. Pat. Appl.,* **1991**, EP 0 416 815 A412 (filed August 430, 1990).

[74] J. A. Canich, *(Exxon Chemical Co.), Eur. Pat. Appl.* **1991**, EP 0 420 436 A421, (filed September 410, 1990).

[75] A. L. McKnight, R. M. Waymouth, *Chem. Rev.* **1998**, *98*, 2587-2598.

[76] J. Okuda, *Dalton Trans.* **2003**, 2367-2378.

[77] X. Li, M. Nishiura, L. Hu, K. Mori, Z. Hou, *J. Am. Chem. Soc.* **2009**, *131*, 13870-13882.

[78] M. Nishiura, T. Mashiko, Z. Hou, *Chem. Commun.* **2008**, 2019-2021.

[79] X. Wang, W. Peng, P. Cui, X. Leng, W. Xia, Y. Chen, *Organometallics* **2013**, *32*, 6166-6169.

[80] Y. Yuan, Y. Chen, G. Li, W. Xia, *Organometallics* **2010**, *29*, 3722-3728.

[81] E. Le Roux, F. Nief, F. Jaroschik, K. W. Tornroos, R. Anwander, *Dalton Trans.* **2007**, 4866-4870.

[82] P. H. Campbell, N. W. K. Chiu, K. Deugau, I. J. Miller, T. S. Sorensen, *J. Am. Chem. Soc.* **1969**, *91*, 6404-6410.

[83] R. S. Threlkel, J. E. Bercaw, *J. Organomet. Chem.* **1977**, *136*, 1-5.

[84] K. J. Ivin, J. J. Rooney, C. D. Stewart, M. L. H. Green, R. Mahtab, *J. Chem. Soc., Chem. Commun.* **1978**, 604-606.

[85] M. Brookhart, M. L. H. Green, *J. Organomet. Chem.* **1983**, *250*, 395-408.

[86] G. F. Schmidt, M. Brookhart, *J. Am. Chem. Soc.* **1985**, *107*, 1443-1444.

[87] R. H. Grubbs, G. W. Coates, *Acc. Chem. Res.* **1996**, *29*, 85-93.

[88] A. Zambelli, G. Allegra, *Macromol.* **1980**, *13*, 42-49.

[89] M. Borrelli, V. Busico, R. Cipullo, S. Ronca, P. H. M. Budzelaar, *Macromol.* **2002**, *35*, 2835-2844.

[90] L. Porri, G. Natta, M. C. Gallazzi, *J. Polym. Sci., Part C* **1967**, *16*, 2525-2537.

[91] G. Wilke, B. Bogdanović, P. Hardt, P. Heimbach, W. Keim, M. Kröner, W. Oberkirch, K. Tanaka, E. Steinrücke, D. Walter, H. Zimmermann, *Angew. Chem. Int. Ed.* **1966**, *5*, 151-164.

[92] R. Warin, P. Teyssié, P. Bourdaudurq, F. Dawans, *J. Polym. Sci.: Polym. Letters Ed.* **1973**, *11*, 177-183.

[93] B. A. Dolgoplosk, S. I. Beilin, Y. V. Korshak, K. L. Makovetsky, E. I. Tinyakova, *J. Polym. Sci.: Polym. Chem. Ed.* **1973**, *11*, 2569-2590.

[94] V. A. Vasiliev, N. A. Kalinicheva, V. A. Kormer, M. I. Lobach, V. I. Klepikova, *J. Polym. Sci.: Polym. Chem. Ed.* **1973**, *11*, 2489-2499.

[95] R. Taube, H. Windisch, S. Maiwald, *Macromol. Symp.* **1995**, *89*, 393-409.

[96] S. Tobisch, *Can. J. Chem.* **2009**, *87*, 1392-1405.

[97] S. Tobisch, *Chem. –Eur. J.* **2003**, *9*, 1217-1232.

[98] S. Tobisch, *Organometallics* **2003**, *22*, 2729-2740.

[99] S. Tobisch, *Macromol.* **2003**, *36*, 6235-6244.

[100] S. Tobisch, *Chem. –Eur. J.* **2002**, *8*, 4756-4766.

[101] S. Tobisch, *Acc. Chem. Res.* **2002**, *35*, 96-104.

[102] S. Tobisch, R. Taube, *Chem. Eur. J.* **2001**, *7*, 3681-3695.

[103] S. Tobisch, R. Taube, *Organometallics* **1999**, *18*, 5204-5218.

[104] S. Tobisch, H. Bögel, R. Taube, *Organometallics* **1998**, *17*, 1177-1196.

[105] S. Tobisch, H. Bögel, R. Taube, *Organometallics* **1996**, *15*, 3563-3571.

[106] S. Tobisch, *J. Mol. Struc.* **2006**, *771*, 171-179.

[107] F. Bonnet, C. Da Costa Violante, P. Roussel, A. Mortreux, M. Visseaux, *Chem. Commun.* **2009**, 3380-3382.

[108] L. Perrin, F. Bonnet, M. Visseaux, L. Maron, *Chem. Commun.* **2010**, *46*, 2965-2967.

[109] A. Valente, P. Zinck, A. Mortreux, M. Visseaux, *Macromol. Rapid Commun.* **2009**, *30*, 528-531.

[110] L. Perrin, F. Bonnet, T. Chenal, M. Visseaux, L. Maron, *Chem. –Eur. J.* **2010**, *16*, 11376-11385.

[111] L. Zhang, Y. Luo, Z. Hou, *J. Am. Chem. Soc.* **2005**, *127*, 14562-14563.

[112] Y. Luo, Z. Hou, *Organometallics* **2006**, *25*, 6162-6165.

[113] X. Kang, Y. Luo, G. Zhou, X. Wang, X. Yu, Z. Hou, J. Qu, *Macromol.* **2014**, *47*, 4596-4606.

[114] M. Zimmermann, K. W. Törnroos, H. Sitzmann, R. Anwander, *Chem. Eur. J.* **2008**, *14*, 7266-7277.

[115] M. Zimmermann, J. Volbeda, K. W. Törnroos, R. Anwander, *C. R. Chim.* **2010**, *13*, 651-660.

[116] R. A. Saunders, D. C. Smith, *J. Appl. Phys.* **1949**, *20*, 953-965.

[117] P. Nallasamy, S. Mohan, *Arab. J. Sci. Eng.* **2004**, *29*, 17-26.

[118] D. Chen, H. Shao, W. Yao, B. Huang, *Intern. J. Polym. Sci.* **2013**, 5.

[119] M. A. Golub, S. A. Fuqua, N. S. Bhacca, *J. Am. Chem. Soc.* **1962**, *84*, 4981-4982.

[120] M. W. Duch, D. M. Grant, *Macromol.* **1970**, *3*, 165-174.

[121] D. Xie, Q. Sun, *Chin. J. Polym. Sci.* **1987**, *5*, 114-119.

[122] V. A. Rozentsvet, A. S. Khachaturov, V. P. Ivanova, *Polym. Sci. Ser. A* **2009**, *51*, 870-876.

[123] B. Liu, L. Li, G. Sun, J. Liu, M. Wang, S. Li, D. Cui, *Macromol.* **2014**, *47*, 4971-4978.

[124] B. Wang, D. Cui, K. Lv, *Macromol.* **2008**, *41*, 1983-1988.

[125] B. Wang, D. Wang, D. Cui, W. Gao, T. Tang, X. Chen, X. Jing, *Organometallics* **2007**, *26*, 3167-3172.

[126] Z. Jian, D. Cui, Z. Hou, *Chem. –Eur. J.* **2012**, *18*, 2674-2684.

[127] Z. Jian, D. Cui, Z. Hou, X. Li, *Chem. Commun.* **2010**, *46*, 3022-3024.

[128] Z. Jian, S. Tang, D. Cui, *Chem. –Eur. J.* **2010**, *16*, 14007-14015.

[129] Z. Jian, S. Tang, D. Cui, *Macromol.* **2011**, *44*, 7675-7681.

[130] R. Litlabø, M. Enders, K. W. Törnroos, R. Anwander, *Organometallics* **2010**, *29*, 2588-2595.

[131] N. Hillersheim, J. Sundermeyer, *DE 102012213694A1* **2013**, (02.08.2012).

[132] C. Lichtenberg, N. S. Hillesheim, M. Elfferding, B. Oelkers, J. Sundermeyer, *Organometallics* **2012**, *31*, 4259-4266.

[133] F. G. Schröder, C. Lichtenberg, M. Elfferding, J. Sundermeyer, *Organometallics* **2013**, *32*, 5082-5091.

[134] B. Wang, T. Tang, Y. Li, D. Cui, *Dalton Trans.* **2009**, 8963-8969.

[135] Z. Jian, A. R. Petrov, N. K. Hangaly, S. Li, W. Rong, Z. Mou, K. A. Rufanov, K. Harms, J. Sundermeyer, D. Cui, *Organometallics* **2012**, *31*, 4267-4282.

[136] Y. Luo, J. Baldamus, Z. Hou, *J. Am. Chem. Soc.* **2004**, *126*, 13910-13911.

[137] Y. Luo, X. Feng, Y. Wang, S. Fan, J. Chen, Y. Lei, H. Liang, *Organometallics* **2011**, *30*, 3270-3274.

[138] Y. Luo, S. Chi, J. Chen, *New Journal of Chemistry* **2013**, *37*, 2675-2682.

[139] F. Bonnet, A. C. Hillier, A. Collins, S. R. Dubberley, P. Mountford, *Dalton Trans.* **2005**, 421-423.

[140] Z. Jian, W. Zhao, X. Liu, X. Chen, T. Tang, D. Cui, *Dalton Trans.* **2010**, *39*, 6871-6876.

[141] Y. Wang, Y. Lei, S. Chi, Y. Luo, *Dalton Trans.* **2013**, *42*, 1862-1871.

[142] G. Swift, *Acc. Chem. Res.* **1993**, *26*, 105-110.

[143] P. Jutzi, J. Dahlhaus, *Synthesis* **1993**, *7*, 684-686.

[144] M. Enders, G. Ludwig, H. Pritzkow, *Organometallics* **2001**, *20*, 827-833.

[145] M. Enders, R. Rudolph, H. Pritzkow, *Chem. Ber.* **1996**, *129*, 459-463.

[146] W. J. Evans, R. Anwander, J. W. Ziller, *Organometallics* **1995**, *14*, 1107-1109.

[147] G. Occhipinti, C. Meermann, H. M. Dietrich, R. Litlabø, F. Auras, K. W. Törnroos, C. Maichle-Mössmer, V. R. Jensen, R. Anwander, *J. Am. Chem. Soc.* **2011**, *133*, 6323-6337.

[148] M. Zimmermann, N. Å. Frøystein, A. Fischbach, P. Sirsch, H. M. Dietrich, K. W. Törnroos, E. Herdtweck, R. Anwander, *Chem. –Eur. J.* **2007**, *13*, 8784-8800.

[149] H. M. Dietrich, H. Grove, K. W. Törnroos, R. Anwander, *J. Am. Chem. Soc.* **2006**, *128*, 1458-1459.

[150] R. Anwander, O. Runte, J. Eppinger, G. Gerstberger, E. Herdtweck, M. Spiegler, *J. Chem. Soc., Dalton Trans.* **1998**, 847-858.

[151] D. Robert, T. P. Spaniol, J. Okuda, *Eur. J. Inorg. Chem.* **2008**, 2801-2809.

[152] Z. Jian, D. Cui, Z. Hou, X. Li, *Chem. Commun.* **2010**, *46*, 3022-3024.

[153] R. Litlabø, M. Zimmermann, K. Saliu, J. Takats, K. W. Törnroos, R. Anwander, *Angew. Chem. Int. Ed.* **2008**, *47*, 9560-9564.

[154] N. Makhiyanov, *Polym. Sci. Ser. A* **2014**, *56*, 241-255.

[155] N. Makhiyanov, I. G. Akhmetov, A. M. Vagizov, *Polym. Sci. Ser. A* **2012**, *54*, 942-949.

[156] Z. W. Qiu, X. Chen, B. Sun, Z. Zhou, F. Wang, *J. Macromol. Sci.: Part A - Chem.* **1988**, *25*, 127-141.

E Unpublished Results

I. Thermal C–H Bond Activation and Ether-Induced Aluminate/Cluster Seperation of $Cp^{Q}Y(AlMe_4)_2$

Encouraged by the findings of the thermally adjustable C–H bond activation of rare-earth metal methyl groups via intramolecular donor-cleavage of tetramethylaluminates, further investigations were made on the quinolyl-cyclopentadienyl supported rear-earth metal bis(aluminate) complexes $[Cp^{Q}Ln(AlMe_4)_2]$ (Ln = Y, La, Nd) (Figure 1).[1] According to NMR spectroscopy, heating the lanthanum and neodymium complexes in deuterated benzene did not lead to activation, instead decomposition was observed above the critical temperature of 90 °C. In contrast, thermal treatment of the yttrium complex $[Cp^{Q}Y(AlMe_4)_2]$ in a C_6D_6 solution at 120° C over a period of five days led to selective C–H bond activation of one methyl group along with release of methane (Scheme 1). Such activation was not observed with any donor-free complexes, indicating a thermally induced disruption of the hemi-labile yttrium nitrogen donor-bond followed by an intramolecular aluminate cleavage. The resulting complex $[(Cp^{Q})Y(\mu\text{-}CH_2)\{(\mu\text{-}Me)Al(Me)_2\}_2]$ **XVIII$_Y$** features an yttrium bonded methylidene, stabilized by two trimethylaluminum molecules, thus forming a butterfly-shaped Tebbe-like moiety (Figure 2).

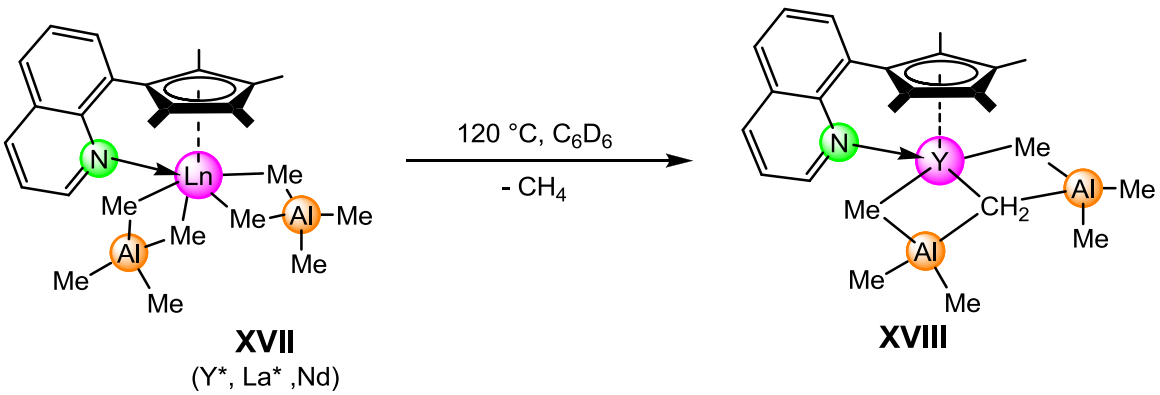

XVII
(Y*, La* ,Nd)

XVIII

Scheme 1. Thermal induced C–H bond activation of quinolinyl functionalized half-sandwich complexes $[Cp^{Q}Y(AlMe_4)_2]$.

Similar structural motifs have been found in rare-earth metal complexes $[(PNP)Sc(\mu_3\text{-}CH_2)\{(\mu\text{-}Me)AlMe_2\}_2]$ (PNP = N{2-P(CHMe$_2$)$_2$-4-methylphenyl}$_2$),[2] $[(Tp^{tBu,Me})La(\mu_3\text{-}CH_2)\{(\mu\text{-}Me)Al(Me)_2\}_2]$ ($Tp^{tBu,Me}$ = hydrotris(pyrazolyl)borate),[3] $[(TMTAC)La(\mu_3\text{-}CH_2)\{(\mu\text{-}Me)AlMe_2\}_2\{(\mu\text{-}Me)_2AlMe_2\}]$ (TMTAC = 1,3,5-trimethyl-1,3,5-triazacyclo-hexane),[4] and $[(TiPTAC)Y(\mu_3\text{-}CH_2)\{(\mu\text{-}Me)AlMe_2\}_2\{(\mu\text{-}$

Me)AlMe$_3$}] (TiPTAC = 1,3,5-triisopropyl-1,3,5-triazacyclohexane).[5] The complex was further fully characterized, but the resonances of the methylidene protons and its carbon atom could not be clearly assigned (Figure 4). As previously observed for similar complexes,[2-5] the signals are overlapped by the AlMe$_3$ methyl groups and even low-temperature NMR spectroscopy did not resolve the problem. With the aim of generating aluminum-free methylidene species, ether-induced aluminate cleavage of complex **XVII$_Y$** was performed at low temperature (Scheme 2).

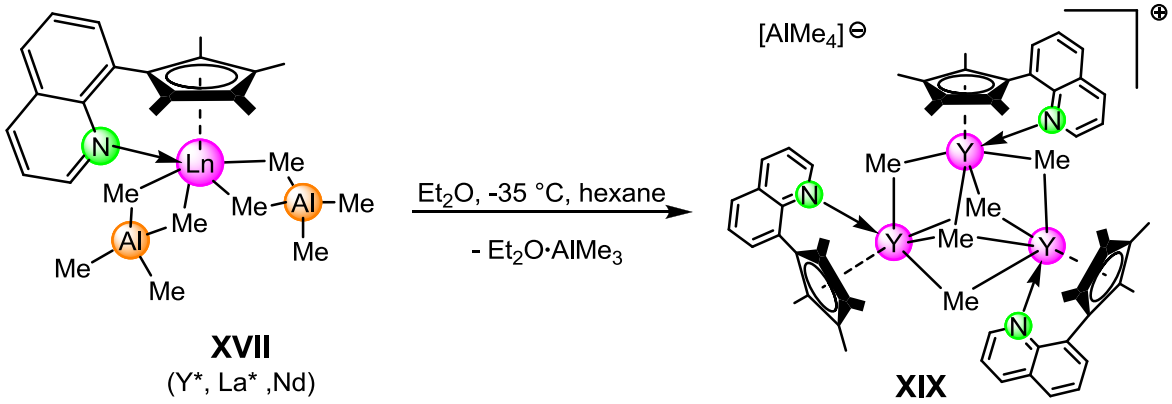

Scheme 2. Donor-induced aluminate cleavage of quinolinyl-functionalized half-sandwich complexes [Cp^{Q}Ln(AlMe$_4$)$_2$].

However, C–H bond activation did not occure bur a trimeric cationic methyl complex [(Cp^{Q}Y{μ_2-Me})$_3$(μ_3-Me)$_2$][AlMe$_4$] **XIX** with a separated tetramethylaluminate anion was obtained (Figure 3). This kind of ion separated aluminate species is quite rare and has previously been published for dimethyl complexes [L$_x$LnMe$_2$][AlMe$_4$] with different neutral donor ligands (L = triazacyclohexyl, x = 2. Ln = Y; L = THF, x = 5, Ln = Y, Ho, Sm).[5-6] The complex is quite stable even in ethereal solvents and C–H bond activation did not take place even when heated to 80 °C. The ^{1}H NMR spectrum recorded at ambient temperature is shown in Figure 5. The signals for the Cp^Q ligand appear in the expected range. Interestingly, beside the 18 protons of the aluminate moiety at 0.17 ppm and the 9 protons for the μ_2-bridging methyl groups at -0.69 ppm, two signals with integration of 3 appear at 0.77 and -0.51 ppm for the μ_3-bridging methyl groups. This indicates a rigid conformation of the Cp^Q ligands in solution as found in the solid-state structure, where the cyclopentadienyl centroids are all in *cis* and the nitrogen donor atoms are all in *trans* position to the C1 carbon atom, while the conformation to the C2 methyl group is the other way round.

Synthesis of [(Cp^Q)Nd($AlMe_4$)$_2$] ($XVII_{Nd}$). Following the procedure published previously for the yttrium and lanthanum complexes,[1] in a glovebox HCp^Q (125 mg, 0.50 mmol) was suspended in 3 mL of hexane and added dropwise to a stirred solution of [Nd($AlMe_4$)$_3$] (204.6 mg, 0.50 mmol) in 2 mL of hexane. Instant gas formation was observed, and the blue mixture gradually turned more and more brownish. The reaction mixture was stirred another 2 h at ambient temperature and then dried under vacuum to yield $XVII_{Nd}$ as a powdery yellow solid. Crystallization from a toluene/hexane solution at –35 °C afforded green crystals suitable for X-ray diffraction analysis. IR (cm^{-1}): 3029 w, 2991 s, 2885 s, 2815 w, 2735 w, 1507 w, 1431 w, 1186 s, 840 m, 791 w, 766 m, 691 s, 593 s, 569 s, 540 w; elemental analysis calcd (%) for $C_{26}H_{42}Al_2NNd$ (566.82): C 55.09, H 7.47, N 2.47; found: C 54.99, H 7.07, N 2.19.

Synthesis of [(Cp^Q)Y(μ_3-CH_2){(μ_2-Me)$AlMe_2$}$_2$] (XVIII). Complex $XVII_Y$ (214 mg, 0.4 mmol) was transferred into a *J. Young* NMR tube using C_6D_6 and heated up to 120 °C. After 5 days, evaporation of the solvent in vacuo yields the crude product as slightly yellow powder in quantitative yield. Single crystals suitable for X-ray diffraction analysis were obtained from crystallization from toluol/hexane solution at –35 °C. ^{1}H NMR (400 MHz, C_6D_6, 25 °C): δ = 8.08 (dd, 1 H, $^3J_{H\text{-}H}$ = 4.79 Hz and 1.58 Hz, Q*H*), 7.32 (dd, 1 H, $^3J_{H\text{-}H}$ = 8.25 Hz and 1.58 Hz, Q*H*), 7.27 (dd, 1 H, $^3J_{H\text{-}H}$ = 5.87 Hz and 2.48 Hz, Q*H*), 7.13-7.08 (m, 2 H, Q*H*), 6.42 (dd, 1 H, $^3J_{H\text{-}H}$ = 8.25 Hz and 4.79 Hz, Q*H*), 2.26 (s, 6 H, 2,5-$C_5(CH_3)_5$), 1.85 (s, 6 H, 3,4-$C_5(CH_3)_5$), –0.21 (s br, 18 H, $Al(CH_3)_3$). ^{13}C(dept135) NMR (100 MHz, C_6D_6, 25 °C): δ = 149.3, 139.8, 133.7, 127.9, 127.0, 121.1 (quinolinyl *C*-H), 11.9, 11.5 ($C_5(CH_3)_5$), -1.47 ($Al(CH_3)_3$); elemental analysis calcd (%) for $C_{25}H_{38}Al_2NNd$ (566.82): C 60.61, H 7.74, N 2.83; found: C 60.79, H 8.22, N 2.93.

Synthesis of [{(Cp^Q)Y(μ_2-CH_3)}$_3$(μ_3-CH_3)$_2$][$AlMe_4$] (XIX). In a glovebox, complex $XVII_Y$ (153 mg, 0.30 mmol) was dissolved in 5 mL hexane. Diethyl ether (2 equiv) was added with vigorous stirring. Instantly, the formation of a yellow precipitate was observed. After 5 min, the precipitate was separated by centrifugation and washed three times with hexane. Drying in vacuo and crystallization from toluene/hexane solution yielded **XIX** (93 mg, 0.80 mmol, 79%) as yellow crystals. Due to the low solubility of complex **XIX** in benzene, useful solution ^{13}C NMR spectra could not be obtained but selected carbon shifts could be assigned by 2D HSQC NMR spectroscopy. ^{1}H NMR (400 MHz, C_6D_6, 25 °C): δ = 9.08 (d, 3H, $^3J_{H\text{-}H}$ = 4.07 Hz, Q*H*), 8.11 (dd, 3H, $^4J_{H\text{-}H}$ = 8.25 Hz, $^3J_{H\text{-}H}$ = 4.82 Hz, Q*H*), 7.60 (d, 3H, $^3J_{H\text{-}H}$ = 1.91 Hz, Q*H*), 7.33 (m, 3H, Q*H*), 7.31 (m, 6H, Q*H*), 2.15 (s, 18H, 3,4-$C_5(CH_3)_5$), 1.74 (s, 18H, 2,5-

$C_5(CH_3)_5$), 0.77 (br, 3H, μ_3-CH_3), 0.18/ (s, 12H, $Al(CH_3)_4$), –0.51 (br, 3H, μ_3-CH_3), –0.69 (br, 9H, μ_2-$CH3$) ppm. ^{13}C (^1H–^{13}C HSQC) NMR (100 MHz, C_6D_6, 25 °C): δ = 153.3 (Q*C*H), 140.3 (Q*C*H), 131.3 (Q*C*H), 127.9 (Q*C*H), 126.8 (Q*C*H), 33.3 (μ_2-CH_3), 30.7 (μ_3-CH_3), 12.3 (μ_3-CH_3), 12.0, ($C_5(CH_3)_4$), 11.9 ($C_5(CH_3)_4$), n.d. ($Al(CH_3)_4$); elemental analysis calcd (%) for $C_{63}H_{81}AlN_3Y_3$ (1174.04): C 64.45, H 6.59, N 3.58; found: C 65.22, H 7.35, N 3.34.

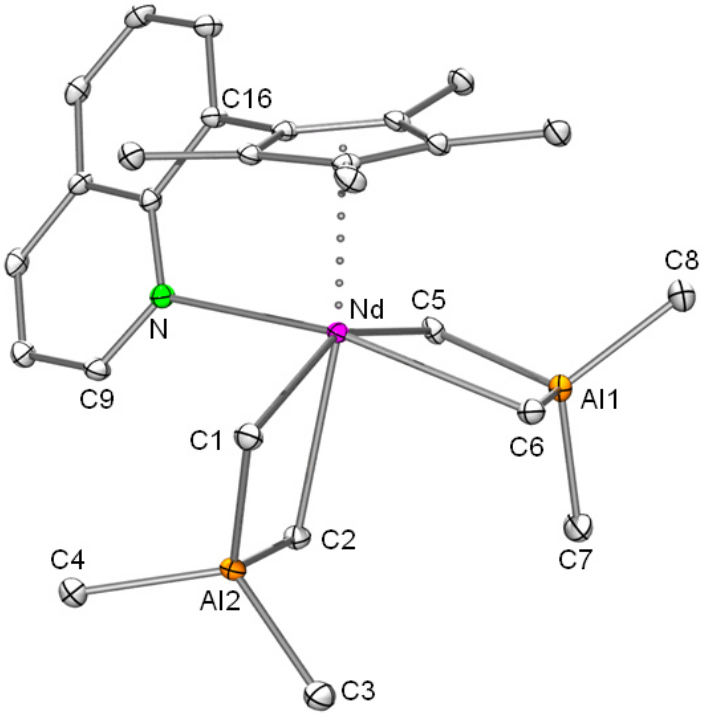

Figure 1. ORTEP view of the molecular structure of [(Cp^{Q})Nd($AlMe_4$)$_2$] (**XVII$_{Nd}$**). Atomic displacement parameters are set at the 50% probability level. Hydrogen atoms omitted for clarity. As complex **XXII$_{Nd}$** crystallize with two independent molecules per unit cell, selected bond lengths (Å) and angles (°) are reffered to the independent parameters as X/X^I: Nd–Cp = 2.647(3)-2.820(3)/2.647(3)-2.819(3), Nd–C1 = 2.704(5)/2.690(4), Nd–C2 = 2.813(4)/2.822(4), Nd–C5 = 2.690(5)/2.682(4), Nd–C6 = 2.678(5)/2.671(5), Nd–N = 2.648(3)/2.636(3), C1–Nd–C2 = 76.1(1)/75.7(1), C5–Nd–C6 = 79.2(1)/79.7(1), N–Nd–C1 = 97.2(1)/97.2(1), N–Nd–C2 = 80.8(1)/81.4(1), N–Nd–C5 = 89.3(1)/88.7(1), N–Nd–C6 = 163.8(1)/163.5(1), C1–Nd–C5 = 152.8(1)/152.9(1).

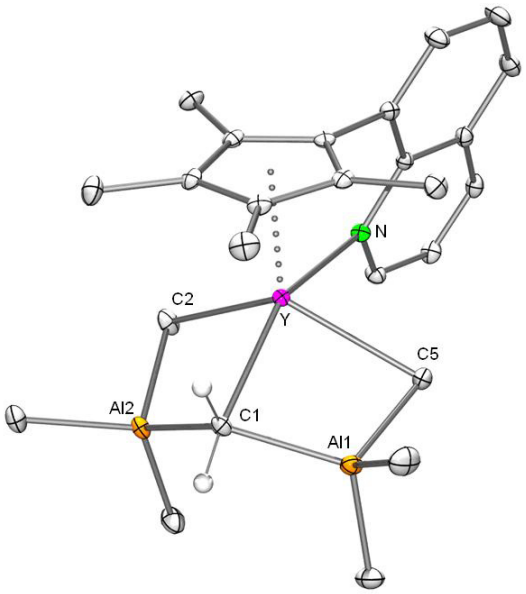

Figure 2. ORTEP view of the molecular structure of **XVIII**. Atomic displacement parameters are set at the 50% probability level. Hydrogen atoms omitted for clarity. Selected bond lengths (Å) and angles (°) for complex **XVIII**: Y–N = 2.5127(14), Y–C1 = 2.4150(17), Y–C2 = 2.533(2), Y–C5 = 2.527(2), Y–Cp = 2.5775(16)-2.6587(16), C1–Y–C2 = 85.02(6), C1–Y–C5 = 84.35(6), C2–Y–C5 = 125.17(6), C1–Y–N = 150.93(5), Al1–C1–Al2 = 132.7

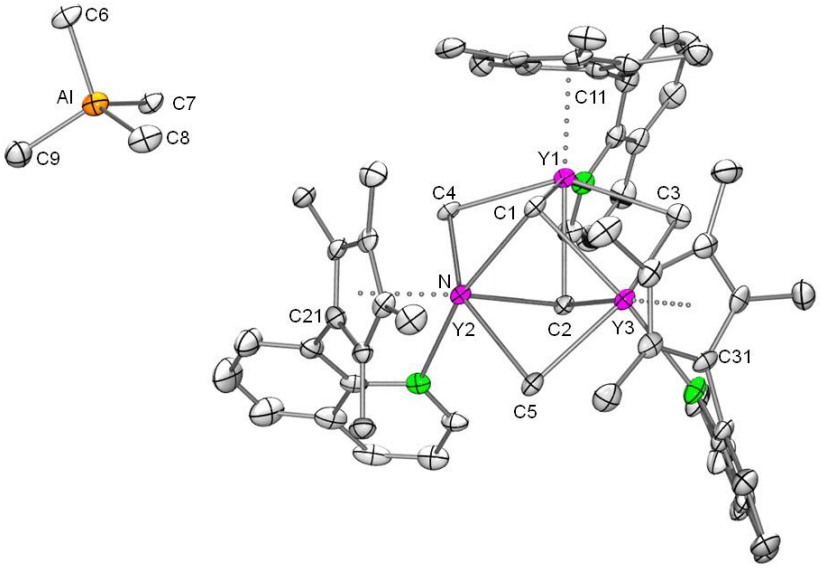

Figure 3. ORTEP view of the molecular structure of **XIX**. Atomic displacement parameters are set at the 50% probability level. Hydrogen atoms omitted for clarity. Y1–Cp = 2.611(6)-2.738(6), Y2–Cp = 2.584(6)-2.740(7), Y3–Cp = 2.584(7)-2.751(6), Y1/Y2/Y3–C1 = 2.626(6)/2.336(6)/2.620(6), Y1/Y2/Y3–C2 = 2.653(6)/2.636(7)/2.661(6), Y1/Y3–C3 = 2.544(6)/2.549(7), Y1/Y2–C4 = 2.563(6)/2.531(6), Y2/Y3–C5 = 2.552(5)/2.528(6), Y1–N1 = 2.590(5), Y2–N2 = 2.603(5), Y3–N3 = 2.594(5), C1–Y1/Y2/Y3–C2= 82.2(2)/82.4/82.2(2), (μ_3-CH_3)–Y1/Y2/Y3–(μ_3-CH_3) = 146.6(2)/148.3(2)/147.2(2), C1–Y1/Y2/Y3–N = 164.5(2)/164.7(2)/163.9(2)

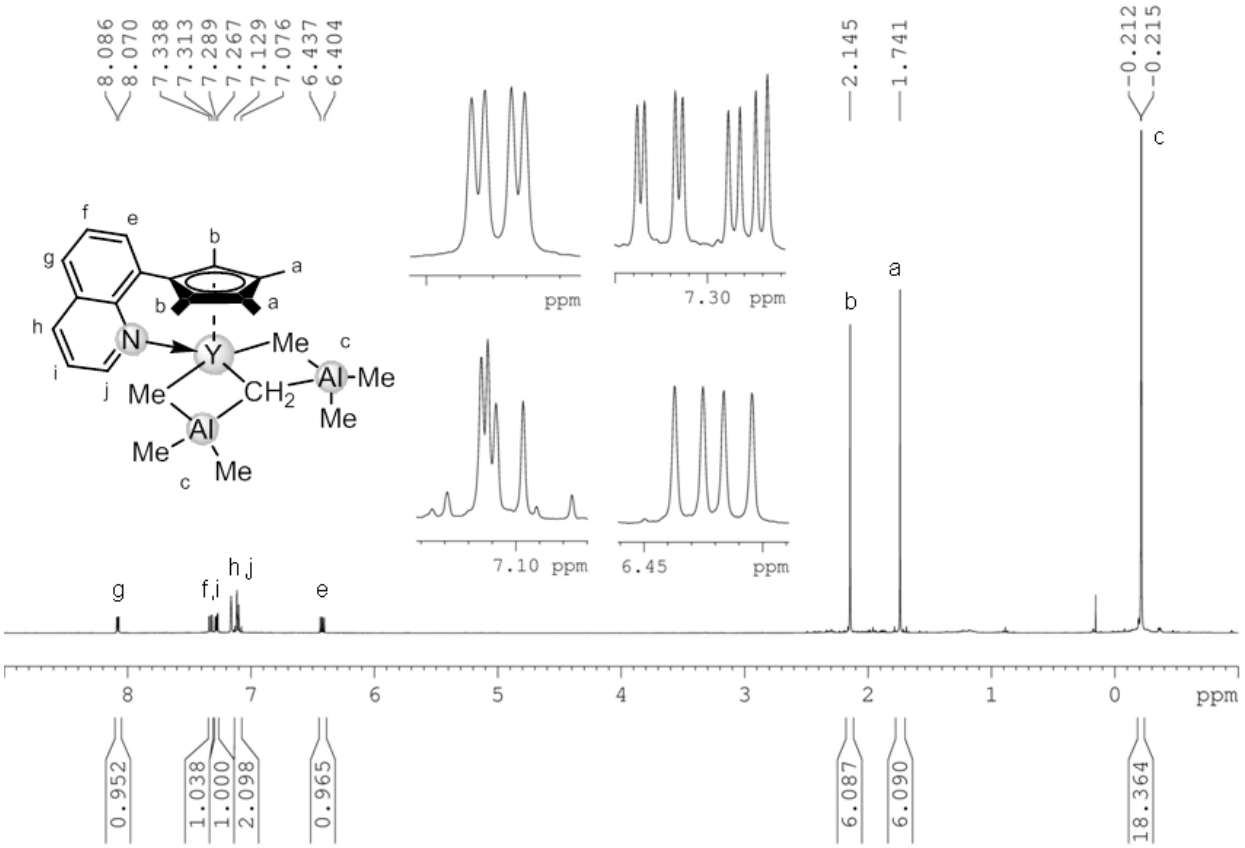

Figure 4: ^{1}H NMR spectrum (C_6D_6, 25 °C) of complex **XVIII**.

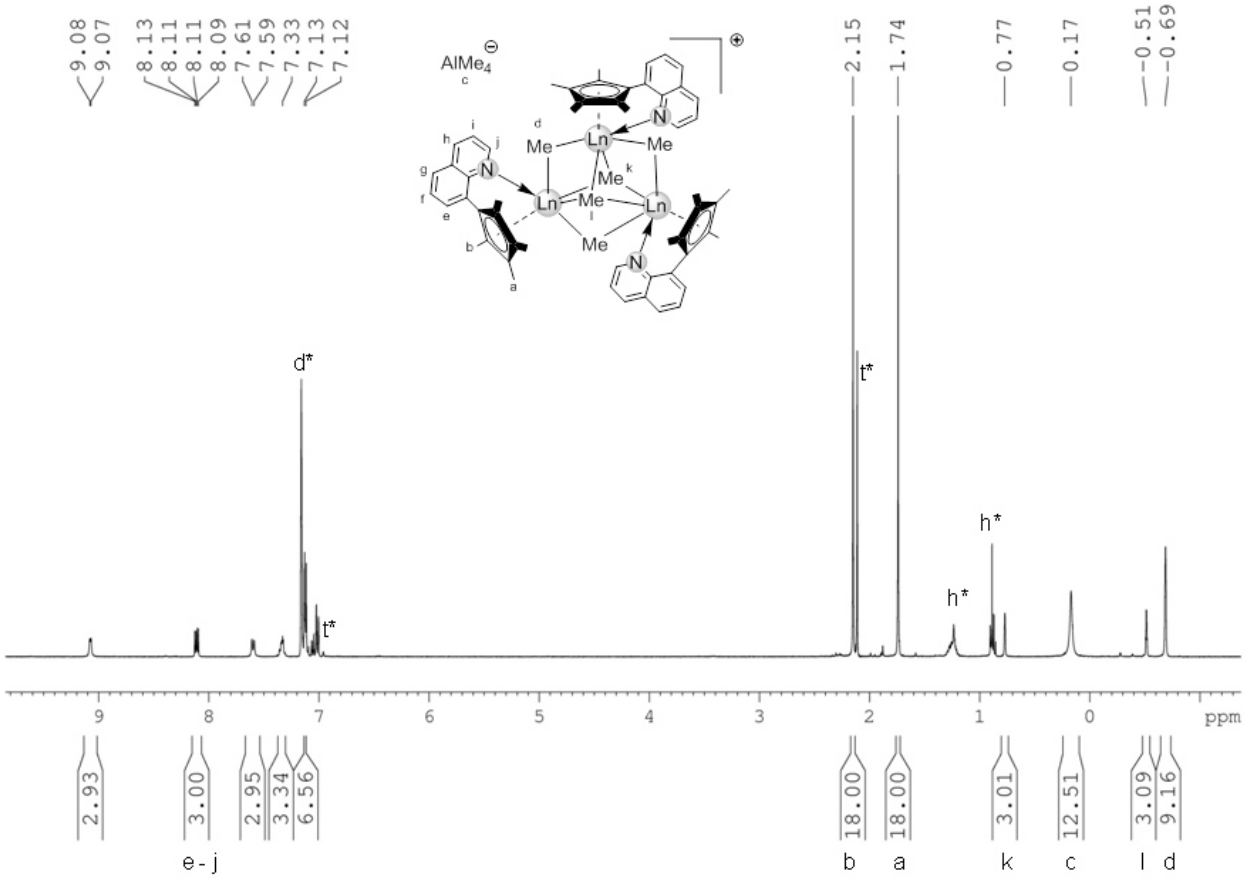

Figure 5: ^{1}H NMR spectrum (C_6D_6, 25 °C) of complex **XIX**.

[1] R. Litlabø, M. Enders, K. W. Tȍrnroos, R. Anwander, *Organometallics* **2010**, *29*, 2588-2595.
[2] J. Scott, H. Fan, B. F. Wicker, A. R. Fout, M.-H. Baik, D. J. Mindiola, *J. Am. Chem. Soc.* **2008**, *130*, 14438-14439.
[3] R. Litlabø, M. Zimmermann, K. Saliu, J. Takats, K. W. Törnroos, R. Anwander, *Angew. Chem.Int. Ed.* **2008**, *47*, 9560-9564.
[4] A. Venugopal, I. Kamps, D. Bojer, R. J. F. Berger, A. Mix, A. Willner, B. Neumann, H.-G. Stammler, N. W. Mitzel, *Dalton Trans.* **2009**, 5755-5765.
[5] D. Bojer, A. Venugopal, A. Mix, B. Neumann, H.-G. Stammler, N. W. Mitzel, *Chem. – Eur. J.* **2011**, *17*, 6248-6255.
[6] A. Nieland, A. Mix, B. Neumann, H.-G. Stammler, N. W. Mitzel, *Eur. J. Inorg. Chem.* **2014**, 51-57.

II. Half-Sandwich Rare-Earth Metal Bis(tetramethyl-aluminate), Bismethyl, and Methylidene Complexes

Abstract: A new synthesis strategy for the generation of homoleptic lutetium tris(tetramethylaluminate) complex [Lu($AlMe_4$)$_3$] as well as optimized reaction conditions for the subsequent protonolysis reaction with pentamethylcyclopentadiene to form the corresponding half-sandwich complex [Cp*Lu($AlMe_4$)$_2$] are presented. As for its yttrium analogon, upon treatment with ether solvents (THF or diethyl ether) the formation of the trimetallic composition [Cp*$LuMe_2$]$_3$ has been postulated previously. We have now succeeded in obtaining single crystals of the lutetium complex which were fully characterized. Furthermore, thermally induced C–H bond activation of the half-sandwich bis(hydrocarbyl) complex led to a new tetrameric methylidene complex [Cp*Ln(CH)]$_4$ under methane elimination only in case of lutetium, which was fully characterized and verified by X-ray structure analysis. In contrast, upon treatment with THF, the yttrium complex [Cp*YMe_2]$_3$ forms the mixed methyl/methyliden species [Cp*$_3$Y$_3$(μ_2-Me)$_3$(μ_3-Me)(μ_3-CH_2)(THF)$_2$], while the lutetium bismethyl complex did not engage into CH_3 degradation.

Results: Homoleptic tris(tetramethylaluminate) complexes [Ln($AlMe_4$)$_3$][1] found entry into organolanthanide synthesis, as their availability for the entire Ln^{3+} size-range, except scandium, without ate complex formation, make these “metal alkyls in disguise” versatile synthesis precursors for the generation of a variety of heterobimetallic Ln/Al complexes.[2] However, the established straightforward synthesis via the dimethylamido ate complexes [Ln(NMe_2)$_3$($LiCl$)$_3$] and subsequent $AlMe_3$-mediated [NMe_2]→[$AlMe_4$] exchange in hexane gave compounds in high yields only for the larger rare-earth metal ions (Scheme 1, route A). [2] In case of lutetium, purification requires additional sublimation and only 15% yield of the desired product could be obtained.[3] These drawbacks of the precursor synthesis result in a lack of corresponding lutetium complexes and investigations into the chemical behavior of the smallest rare-earth metal are far behind those of the analogous complexes of the earlier lanthanides.

The new synthesis approach is based on the trianionic hexamethylate complexes [$LnMe_6${Li(Do)$_x$}$_3$] (Do = tmeda, dme, THF, diethyl ether) reported by Schumann et al.,[4] which in case of the smallest rare-earth metal lutetium can directly react with excess of $AlMe_3$ to produce the homoleptic aluminate complex [Lu($AlMe_4$)$_3$] (**1$_{Lu}$**) (Scheme 1, route B). The side-products $LiAlMe_4$ and donor coordinated $AlMe_3$ can easily be removed via filtration and evaporation, respectively. The absence of ate-complex formation is due to the high steric

saturation of the metal center by the tetramethylaluminate moieties, which show additional agostic or coordinative interactions only for the larger rare-earth metal ions.[2] Even though the hexamethylate and tetramethylaluminate complexes are simultaneously presented in several publications,[5] the synthesis of the latter starting from the first has not been reported so far. The generation of the half-sandwich complex [Cp*Lu($AlMe_4$)$_2$] (**2$_{Lu}$**) was slightly modified (Scheme 1, route B), as the previously reported method only resulted in low yield and an excess of pentamethylcyclopentadiene (HCp*) was required.[6] Changing the reaction conditions from ambient to an elevated temperature of 60°C and replacement of hexane by benzene reduced the time for quantitatively conversion to 4 h as determined by NMR-scale reactions. Initial investigations of [Cp*Lu($AlMe_4$)$_2$] as pre-catalyst in isoprene polymerization were presented by our group recently and full experimental data are presented in Table 1.[7] Furthermore, we have described the high-yield synthesis of the half-sandwich dimethyl complexes [Cp*LnMe_2]$_3$ (**XX**) of yttrium and lutetium,[3, 6, 8] utilizing the donor-solvent induced alkylaluminate cleavage (Scheme 1).[9] Thereby, only the single-crystal structure of the yttrium complex could be presented so far. Now, we obtained X-ray diffraction data from the lutetium complex and the molecular structure is shown in Figure 1. Complex **XX$_{Lu}$** is soluble in hot benzene (not exceeding 60 °C) and crystallizes in the hexagonal space group $P6_3$ when cooled to ambient temperature. Beside the application as suitable precursor for various half-sandwich complexes (e.g., [Cp*Ln($GaMe_4$)$_2$],[10] [Cp*Y(N{$SiMe_3$}$_2$)(μ_2-H)]$_2$,[11] [Cp*Ln($AlMe_3$-{B(NDippCH)$_2$})$_2$],[7] [Cp*Ln($AlMe_4$)(Dipp-Form)]), rare-earth dimethyl complexes of [**L**LnMe_2]$_n$–type often engage in distinct C–H bond activation. Single methane elimination generates mixed methyl/methylidene complexes [**L**$_3$Ln$_3$(μ_2-Me)$_3$(μ_3-Me)(μ_3-CH_2)] (**L** = $C_5Me_4SiMe_3$, Ln = Tm, Lu;[12] PhC(NC_6H_3*i*Pr_2-2,6)$_2$, Ln = Sc, Lu;[13] $NSiMe_3C_6H_3$*i*Pr_2-2,6/thf, Ln = Y, Ho, Lu[14]), which are capable of either methylene transfer to ketones and imines or deprotonation of amines, phosphines, thioles, and alkines. Very recently, the group of Hou reported a new class of complexes consisting only of the simple "Cp´LnCH_2" (Cp´= $C_5Me_4SiMe_3$) methylidene units, arranged in a tetrameric cubane-like Ln$_4$(CH_2)$_4$ core-structure (Ln = Tm, Lu).[12] Herein, we present the similar cluster complex [Cp*Lu(CH_2)]$_4$ (**XXI**), obtained quantitatively by thermal C–H bond activation of the trimeric hexamethyl complex in deuterated benzene (Scheme 1). Complex **XXI** crystallized from the solution in the triclinic space group $P\bar{1}$ when cooled to ambient temperature. The molecular structure is shown in Figure 2. This highly selective C–H bond activation could not be observed for the yttrium analogon, which revealed multiple undefined activations, also involving the ancillary

cyclopentadienyl ligand; hence no product could be isolated. However, when complex **XX$_Y$** was treated with THF, methane elimination was observed and the mono-methylidene species [Cp*$_3$Y$_3$(μ_2-Me)$_3$(μ_3-Me)(μ_3-CH$_2$)(THF)$_2$] **XXII** was reproducibly obtained (Figure 3). Interestingly, only two of the three yttrium atoms bear weakly coordinated THF solvent molecules which exhibit long Y–O bond distances of 2.624(4) and 2.577(4) Å. In case of lutetium, no elimination reaction was monitored in THF-d$_8$. These findings demonstrate that the type of C–H bond activation depends significantly on the ionic radius of the rare-earth metal.

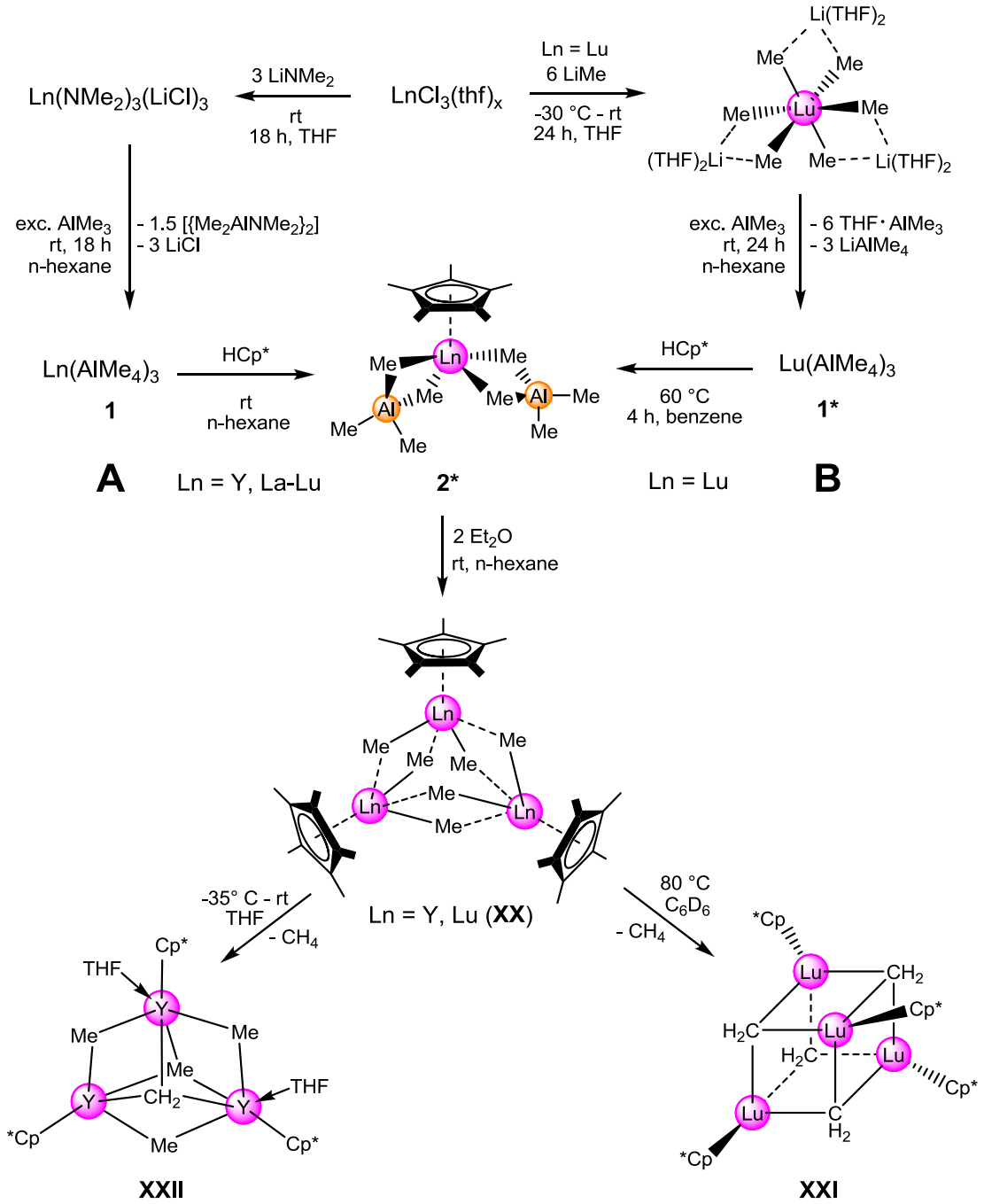

Scheme 1 Synthesis of rare-earth metal half-sandwich methyl and methylidene complexes.

Synthesis of $Lu(AlMe_4)_3$ (1*): In a 100 mL Schlenk flask, $LuCl_3(thf)_3$ (4.97 g, 10.0 mmol) was dissolved in THF (30 mL) and methyllithium (1.32 g, 60.0 mmol) was added under vigorous stirring. After 24 h, the solvent was evaporated under vacuum, the residue redissolved in toluene (10 mL), and the LiCl was removed via centrifugation and filtration. Toluene was removed and the crude $LuMe_3(MeLi)_3(thf)_x$ was suspended in hexane (15 mL). Trimethylaluminum (6.48 g, 90.0 mmol, 9 equiv.) was added, the reaction mixture stirred for 24 h, and $LiAlMe_4$ was separated via filtration. The homoleptic lutetium tris(tetramethylaluminate) crystallized from a saturated hexane solution at –35 °C (2.55 g, 5.84 mmol, 58%). ^{1}H NMR (400 MHz, C_6D_6, 25 °C): δ = –0.19 (s, 36 H, AlCH_3) ppm. ^{13}C NMR (100 MHz, C_6D_6, 25 °C): δ = 3.7 ppm; elemental analysis calcd (%) for $C_{12}H_{36}Al_3Lu$ (436.33): C 33.03, H 8.32; found: C 33.08, H 8.61.

Synthesis of $(C_5Me_5)Lu(AlMe_4)_2$ (2*). Complex **1*** (131 mg, 0.30 mmol) was dissolved in deuterated benzene (2 mL) and 1,2,3,4,5-pentamethycyclopentadiene (45 mg, 0.33 mmol) was added and the reaction mixture was stirred overnight at 60 °C. After evaporation of the solvent, complex **2*** was crystallized from hexane solution at –35 °C (136 mg, 0.28 mmol, 94%). ^{1}H NMR (400 MHz, C_6D_6, 25 °C): δ = 1.76 (s, 15 H, CpCH_3), –0.17 (s, 24 H, AlCH_3). ^{13}C NMR (100 MHz, C_6D_6, 25 °C): δ = 120.7 ($C_5(CH_3)_5$), 11.6 (Cp(CH_3)$_5$), 1.1 (Al(CH_3)$_4$). Elemental analysis calcd (%) for $C_{18}H_{39}Al_2Lu$ (484.43): C 44.63, H 8.11; found: C 44.32, H 8.47.

Synthesis of $[(C_5Me_5)Lu(\mu\text{-}Me)_2]_3$ (XX). Following the procedure published previously,[8] complex **2*** (484 mg, 1.00 mmol) was dissolved in hexane (5 mL) and diethyl ether (148 mg, 2.00 mmol) was added under vigorous stirring. The white precipitate was separated via centrifugation and washed three times with hexane. Drying in vacuo yielded **XX** (315 mg, 93%) as white powder. Single crystals were obtained through re-crystallization from a hot (60 °C) benzene solution at ambient temperature. ^{1}H NMR (400 MHz, C_6D_6, 25 °C): δ = 2.00 (s, 45 H, CH_3Cp), 0.05 (s, 18 H, LuCH_3). ^{13}C NMR (100 MHz, C_6D_6, 25 °C): δ = 117.4 ($C_5(CH_3)_4$), 36.1 (CH_3), 11.5 (Cp(CH_3)$_5$). IR (cm^{-1}): 3016 m, 2989 m, 2974 m, 2921 s, 2821 m, 2735 w, 1477 m, 1462 m, 1439 m, 1384 w, 1301 w, 1256 w, 1223 m, 1201 m, 1185 s, 1142 w, 1064 w, 1047 w, 1015 w, 964 m. 858 m. 808 w, 703 s, 665 m, 573 m; elemental analysis calcd (%) for $C_{36}H_{63}Lu_3$ (1020.78): C 42.36, H 6.22; found: C 42.81, H 6.57.

Synthesis of $[(C_5Me_5)Lu(\mu_3\text{-}CH_2)]_4$ (XXI). Complex **XX** (102 mg, 0.10 mmol) was transferred into a *J. Young* NMR tube using C_6D_6 and heated up to 80 °C in steps of 10 °C. After two days at 80 °C, the integration of the signals in the ^{1}H

NMR spectrum stayed constant and additional ^{1}H-^{13}C HSQC, ^{1}H-^{13}C HMBC and ^{1}H-^{1}H COSY NMR spectra were recorded to identify the product, which was obtained in quantitative yields. Single crystals suitable for X-ray structure analysis were obtained from the solution when cooled to ambient temperature. ^{1}H NMR (400 MHz, C_6D_6, 25 °C): δ = 2.17 (s, 60 H, CH_3Cp), 1.65 (s, 8 H, LuCH_2). ^{13}C NMR (100 MHz, C_6D_6, 25 °C): δ = 117.5 (C_5Me_5), 113.5 (LuCH$_2$), 11.0 (Cp(CH$_3$)$_5$). IR (cm^{-1}): 2907 s, 2857 s, 2791 m, 2726 m, 1652 w, 1558 w, 1539 w, 1521 w, 1506 w, 1487 w, 1436 m, 1375 m, 1263 w, 1061 w, 1022 m, 797 w, 642 m, 546 m; elemental analysis calcd (%) for $C_{44}H_{68}Lu_4$ (1296.88): C 40.75, H 5.28; found: C 40.51, H 5.28.

Synthesis of [Cp*$_3$Y$_3$(μ_2-Me)$_3$(μ_3-Me)(μ_3-CH$_2$)(THF)$_2$] (XXII).

Route A: Complex **XX$_Y$** was dissolved in THF, whereby instant gas formation was observed. The clear solution was layered with toluene and stored at –35° C. Single crystals of complex **XXII** suitable for X-ray diffraction analysis were obtained within 2 days.

Route B: Complex **XX$_Y$** was transferred into a *J. Young* NMR tube using cold THF-d_8 (–35° C). Gas formation was observed within 10 minutes when warmed to ambient temperature. Single crystals of complex **XXII** suitable for X-ray diffraction analysis grow from the THF solution within 1 day.

^{1}H NMR (400 MHz, C_6D_6, 25 °C): δ = 3.58 (br, 4 H, THF), 1.92 (s, 45 H, CH_3Cp), 1.73 (br, 4 H, THF), –0.31 (q, 2 H, μ_3-CH_2), –0.53 (vbr, 3 H, μ_3-CH_3). –0.89 (br, 9 H, μ_2-CH_3). ^{13}C NMR (100 MHz, C_6D_6, 25 °C): δ = 120.0 (μ_3-CH$_3$), 113.0 (C_5Me_5), 95.6 (μ_3-CH$_2$), 64.5 (THF), 24.7 (μ_2-CH$_3$), 22.5 (THF), 9.3 (Cp(CH$_3$)$_5$). IR (cm^{-1}): 2958 s, 2896 s, 2855 s, 2754 m, 2722 m, 2241 m, 2184 w, 2160 w, 2138 w, 2125 w, 2105 w, 2088 w, 1492 w, 1440 m, 1374 m, 1249 w, 1176 m, 1110 m, 1059 w, 1006 s, 994 s, 961 w, 824 s, 748 s, 590 m, 548 m, 512 m; elemental analysis calcd (%) for $C_{43}H_{75}O_2Y_3$ (890.77): C 57.98, H 8.49; calcd (%) for **XX$_Y$**–(THF)$_2$, $C_{35}H_{59}Y_3$ (746.56): C 56.31, H 7.97; found: C 56.37, H 7.74.

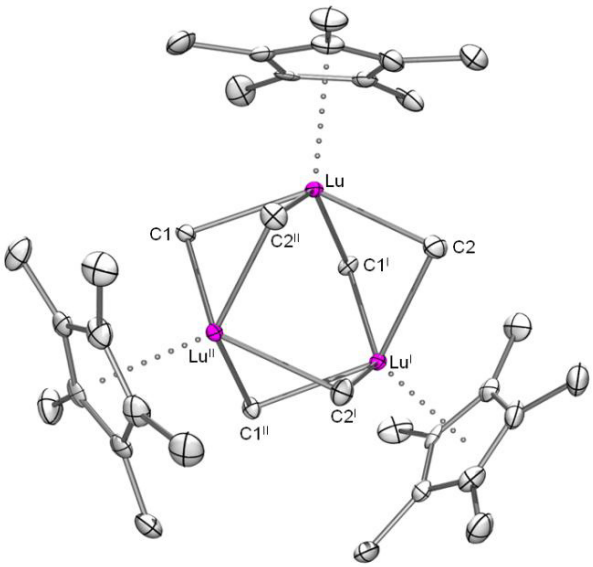

Figure 1. ORTEP view of the molecular structure of $[Cp^*LuMe_2]_3$ (**XX**). Atomic displacement parameters are set at the 50% probability level. Hydrogen atoms are omitted for clarity. Selected bond lengths (Å) and angles (°) for **XX**: Lu–Cp = 2.5988(1)-2.6795(1), Lu–Cp_{cent} = 2.338, Lu–C1 = 2.4650(1), Lu–$C1^I$ = 2.4650(1), Lu–C2 = 2.517(6), Lu–$C2^{II}$ = 2.553(1), C1-Lu–C2 = 135.32, C1-Lu–$C1^I$ = 86.70, C1-Lu–$C2^{II}$ = 80.49, C2-Lu–$C1^I$ = 81.24, C2-Lu–$C2^{II}$ = 78.08, $C1^I$-Lu–$C2^{II}$ = 134.50.

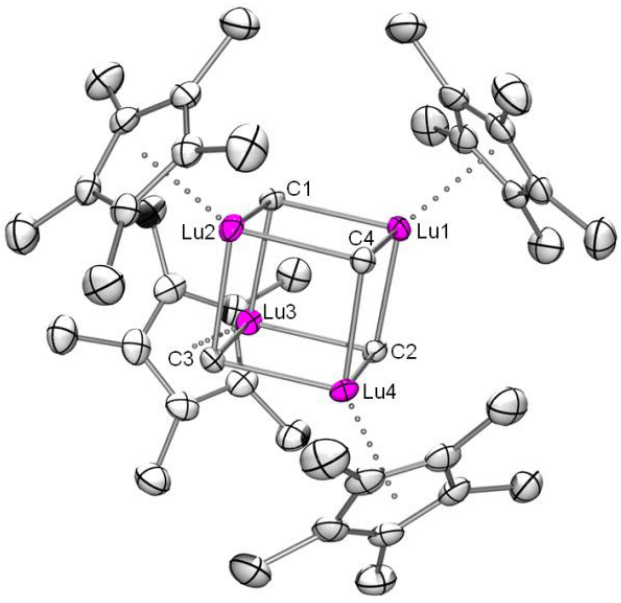

Figure 2. ORTEP view of the molecular structure of $[Cp^*LuCH_2]_4$ (**XXI**). Atomic displacement parameters are set at the 50% probability level. Hydrogen atoms are omitted for clarity. Selected bond lengths (Å) and angles (°) for **XXI**: Lu1–Cp = 2.570(5)-2.587(5), Lu2–Cp = 2.577(4)-2.588(4), Lu3–Cp = 2.568(5)-2.582(5), Lu4–Cp = 2.572(4)-2.579(4), Lu1–C1/C2/C4 = 2.390(4)/2.372(4)/2.341(4), Lu2–C1/C3/C4 = 2.333(4)/2.396(4)/2.371(4), Lu3–C1/C2/C3 = 2.355(4)/2.393(4)/2.346(4), Lu4–C2/C3/C4 = 2.346(4)/2.377(4)/2.376(4), C–Lu–C = 88.22(14)-91.77(14).

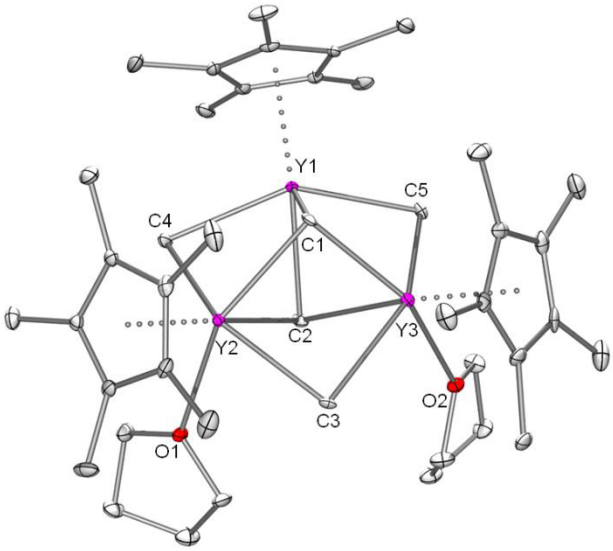

Figure 3. ORTEP view of the molecular structure of [Cp*$_3$ Y$_3$(μ_2-Me)$_3$(μ_3-Me)(μ_2-CH$_2$)(THF)$_2$] (**XXII**). Atomic displacement parameters are set at the 50% probability level. Hydrogen atoms are omitted for clarity. Selected bond lengths (Å) and angles (°) for **XXII**: Y1–Cp = 2.701(6)-2.716(6), Y2–Cp = 2.683(6)-2.710(7), Y3–Cp = 2.686(7)-2.722(6), Y1/Y2/Y3–C1 = 2.296(7)/2.483(6)/2.453(6), Y1/Y2/Y3–C2 = 2.598(6)/2.755(7)/2.778(6), Y1/Y2–C4 = 2.593(7)/2.566(6), Y1/Y3–C5 = 2.551(7)/2.553(6), Y2/Y3–C3 = 2.545(6)/2.588(7), Y2–O1 = 2.624(4), Y3–O2 = 2.577(4), C1–Y1/Y2/Y3–C2= 85.5(2)/78.8/78.8(2), (μ_3-CH$_3$)–Y1/Y2/Y3–(μ_3-CH$_3$) = 144.1(2)/147.8(2)/146.(2), C1–Y2/Y3–O = 151.(2)/151.9(2), C2–Y2/Y3–O = 74.0(2)/73.1(2).

Table 1. Selected examples of isoprene polymerization at 40 °C.

entry[a]	precatalyst	cocatalyst[b]	t	solvent	yield	*cis*[c]	*trans*[c]	3,4[c]	M_n[d] (x 10^5)	M_w/M_n[d]
1	Cp*Lu(AlMe$_4$)$_2$	**A**	15	toluene	>99	73.9	19.7	6.4	10.0	1.49
2[e]	Cp*Lu(AlMe$_4$)$_2$	**A**	15	toluene	>99	69.9	11.6	18.5	3.7	1.74
3[f]	Cp*Lu(AlMe$_4$)$_2$	**A**	15	toluene	>99	64.9	29.6	5.5	8.9	1.66
4	Cp*Lu(AlMe$_4$)$_2$	**B**	15	toluene	>99	70.3	20.3	9.4	9.5	1.45
5[e]	Cp*Lu(AlMe$_4$)$_2$	**B**	15	toluene	>99	65.2	14.5	20.3	5.1	1.60
6[f]	Cp*Lu(AlMe$_4$)$_2$	**B**	15	toluene	>99	74.3	17.8	7.9	10.7	1.39
7[g]	Cp*Lu(AlMe$_4$)$_2$	**B**	60	toluene	>99	22.4	17.3	60.3	4.4	1.25
8	Cp*Lu(AlMe$_4$)$_2$	**C**	30	toluene	26	74.6	20.7	4.7	11.0	1.39
9[e]	Cp*Lu(AlMe$_4$)$_2$	**C**	15	toluene	74	85.3	9.7	5.0	10.7	1.49
10[f]	Cp*Lu(AlMe$_4$)$_2$	**C**	30	toluene	46	78.0	17.1	4.9	14.4	1.41
11	Cp*Lu(AlMe$_4$)$_2$	**A**	60	hexane	90	24.4	53.3	22.3	5.6	1.20
12	Cp*Lu(AlMe$_4$)$_2$	**B**	60	hexane	93	21.8	56.0	22.2	5.2	1.33
13	Cp*Lu(AlMe$_4$)$_2$	**C**	180	hexane	15	66.5	29.5	4.0	8.6	1.74

[a]Conditions: 0.02 mmol precatalyst, [Ln]/[cocat] = 1:1, 8 mL solvent, 20 mmol isoprene. [b]Co-catalyst: **A** = [Ph$_3$C][B(C$_6$F$_5$)$_4$], **B** = [PhNMe$_2$H][B(C$_6$F$_5$)$_4$] **C** = B(C$_6$F$_5$)$_3$; [c]Determined by ^{1}H and ^{13}C NMR spectroscopy in CDCl$_3$. [d]Determined by means of size-exclusion chromatography (SEC) against polystyrene standards. [e][Ln]/[cocat] = 1:2. [f]The co-catalyst was added to a mixture of complex **1** and isoprene. [g]The mixture of **1** and **B** was cooled to –35 °C before addition of isoprene and allowed to warm to room temperature during polymerization.

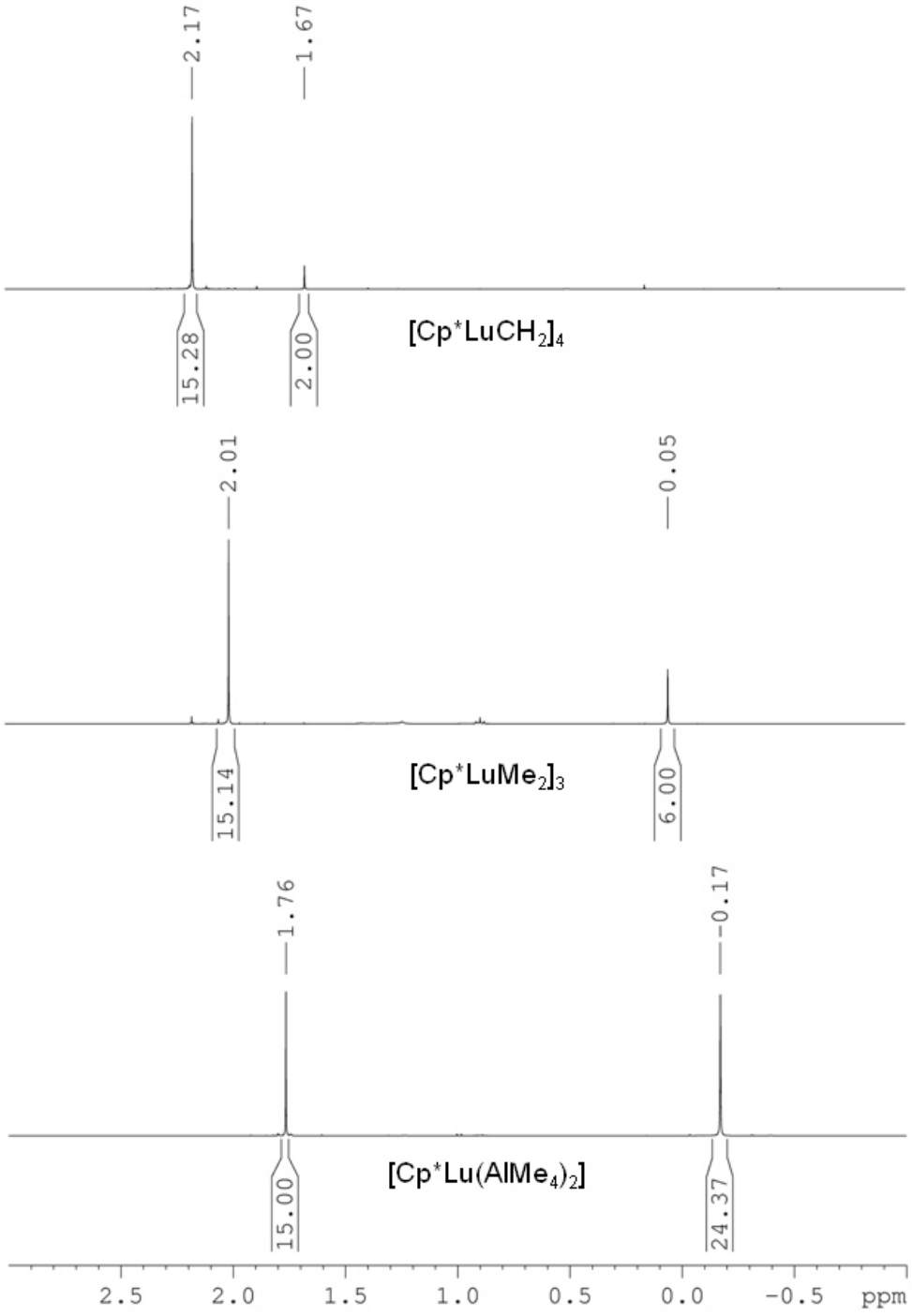

Figure 4: ^{1}H NMR spectra (C_6D_6, 25 °C) of complexes **2*** (bottom), **XX** (middle) and **XXI** (top).

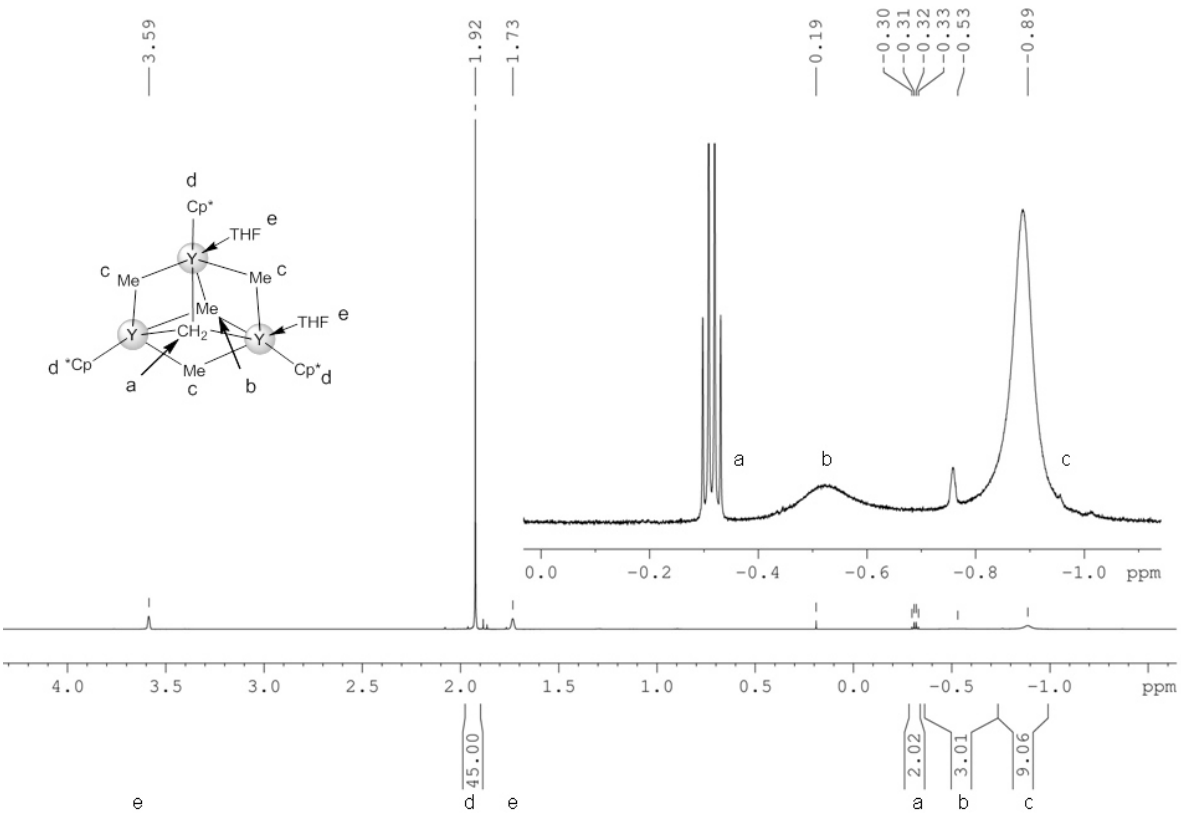

Figure 5: ^{1}H NMR spectra (THF-d_8, 25 °C) of complex $[Cp^*_3Y_3(\mu_2\text{-Me})_3(\mu_3\text{-Me})(\mu_3\text{-CH}_2)(THF)_2]$ (**XXII**).

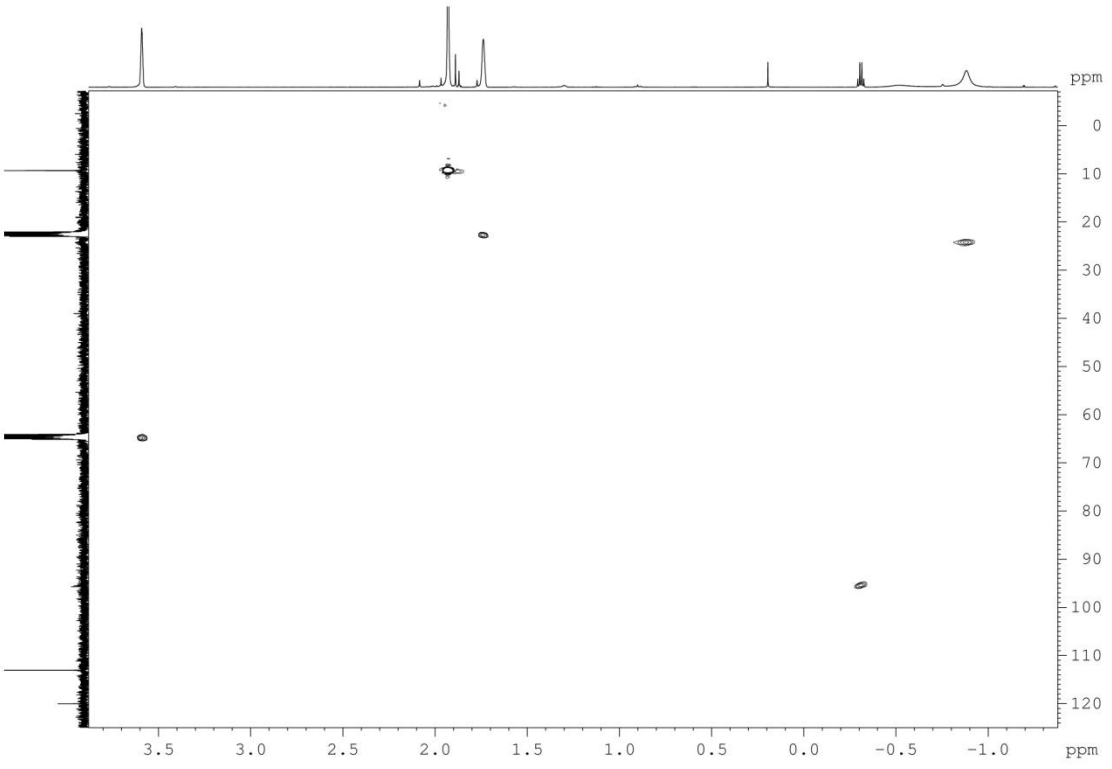

Figure 6: ^{1}H–^{13}C HSQC NMR spectra (THF-d_8, 25 °C) of complex $[Cp^*_3Y_3(\mu_2\text{-Me})_3(\mu_3\text{-Me})(\mu_3\text{-CH}_2)(THF)_2]$ (**XXII**).

[1] W. J. Evans, R. Anwander, J. W. Ziller, *Organometallics* **1995**, *14*, 1107.
[2] M. Zimmermann, N. Å. Frøystein, A. Fischbach, P. Sirsch, H. M. Dietrich, K. W. Törnroos, E. Herdtweck, R. Anwander, *Chem. – Eur. J.* **2007**, *13*, 8784.
[3] H. M. Dietrich, G. Raudaschl-Sieber, R. Anwander, *Angew. Chem. Int. Ed.* **2005**, *44*, 5303.
[4] (a) H. Schumann, J. Mueller, N. Bruncks, H. Lauke, J. Pickardt, H. Schwarz, K. Eckart, *Organometallics* **1984**, *3*, 69; (b) H. Schumann, J. Müller, *Angew. Chem. Int. Ed.* **1978**, *17*, 276; (c) H. Schumann, J. Pickardt, N. Bruncks, *Angew. Chem. Int. Ed.* **1981**, *20*, 120.
[5] M. U. Kramer, D. Robert, S. Arndt, P. M. Zeimentz, T. P. Spaniol, A. Yahia, L. Maron, O. Eisenstein, J. Okuda, *Inorg. Chem.* **2008**, *47*, 9265.
[6] H. M. Dietrich, C. Zapilko, E. Herdtweck, R. Anwander, *Organometallics* **2005**, *24*, 5767.
[7] N. Dettenrieder, C. O. Hollfelder, L. N. Jende, C. Maichle-Mössmer, R. Anwander, *Organometallics* **2014**, *33*, 1528.
[8] H. M. Dietrich, H. Grove, K. W. Törnroos, R. Anwander, *J. Am. Chem. Soc.* **2006**, *128*, 1458.
[9] J. Holton, M. F. Lappert, D. G. H. Ballard, R. Pearce, J. L. Atwood, W. E. Hunter, *J. Chem. Soc., Dalton Trans.* **1979**, 54.
[10] H. M. Dietrich, K. W. Törnroos, E. Herdtweck, R. Anwander, *Organometallics* **2009**, *28*, 6739.
[11] C. Schädle, R. Anwander, *Eur. J. Inorg. Chem.* **2013**, *2013*, 3302.
[12] W.-X. Zhang, Z. Wang, M. Nishiura, Z. Xi, Z. Hou, *J. Am. Chem. Soc.* **2011**, *133*, 5712.
[13] J. Hong, L. Zhang, X. Yu, M. Li, Z. Zhang, P. Zheng, M. Nishiura, Z. Hou, X. Zhou, *Chem. – Eur. J.* **2011**, *17*, 2130.
[14] M. Zimmermann, D. Rauschmaier, K. Eichele, K. W. Tornroos, R. Anwander, *Chem. Comm.* **2010**, *46*, 5346.

III. Mixed Rare-Earth Metal Chloride/Methylidene Complexes

Abstract: The formation and reactivity of mixed chloride/methylidene cluster complexes of the large to mid-size rare-earth metals have been investigated. The slow decomposition of $[Cp^*LnCl_x(AlMe_4)_y]_z$ in THF/toluene yielded not only the desired trinuclear complex $[Cp^*_3Ln_3(\mu_2\text{-}Cl)_3(\mu_3\text{-}Cl)(\mu_2\text{-}CH_2)(THF)_3]$ (Ln = Y, La, Nd, Ho) but also species with remaining μ_2-Me groups were detected, which along with the low solubility of the complexes, significantly hampered any reaction pathway analysis of the methylidene group transfer. Additionally, a new ion-pair separated species of the holmium metal methylidene complex $[Cp^*_3Ho_3(\mu_2\text{-}Cl)_3(\mu_3\text{-}Cl)_2(THF)_3][Cp^*_4Ho_4(\mu_2\text{-}Cl)_6(\mu_3\text{-}Cl)(\mu_4\text{-}CH_2)]$ is presented. Preliminary studies of the reactivity of the methylidene complexes towards ketones aiming a Tebbe-reagent like methylidene transfer could be verified, however, the expected oxo-clusters from clean CH_2^{2-}/O^{2-} group interchange were not isolated. Instead, hexameric cluster complexes $[\{Cp^*_3Ln_3(\mu_2\text{-}Cl)_3(\mu_3\text{-}Cl)(\mu_2\text{-}OH)\}\{\mu_2\text{-}Cl\}]_2$ containing hydroxides were consistently isolated as single crystals and characterized by X-ray diffraction analysis. Furthermore, a unique intermediate $[Cp^*_3Ho_3(\mu_2\text{-}Cl)_3(\mu_3\text{-}Cl_2)(O\{CH_3\}C_6H_8)(THF)_2]$ from the reaction of the holmium metal complex with cyclohexanone was structurally characterized, containing a tertiary alcoholat coordination formed by a nucleophilic attack of a methyl group at the carbonyl carbon atom. As the origin of the additional protons neither for the methyl group nor for the hydroxide formation can undoubtedly be clarified, additional discussions of the NMR spectra of the diamagnetic complexes are presented.

Results: In 2006 we presented the first rare-earth metal methylidene complexes $[Cp^*_3Ln_3(\mu_2\text{-}Cl)_3(\mu_3\text{-}Cl)(\mu_2\text{-}CH_2)(THF)_3]$ (Ln = Y, La).[1] Treatment of the half-sandwich complexes $[Cp^*Ln(AlMe_4)_2]$ with $AlMe_2Cl$ in toluene solution yielded mixed aluminato/chloro complexes $[(Cp^*Ln)_xCl_y(AlMe_4)_z]$ (Ln = Y {x = y = z = 2}; La {x = 6, y = 8, z = 4} Scheme 1,**i**),[2] which underwent donor-induced aluminate cleavage and C–H bond activation upon the addition of THF at ambient temperature to form the trinuclear methylidene species in both cases (Scheme 1, **ii**). It can be assumed, that the aluminate cleavage initially forms $[Cp^*Y(Cl)(Me)]_n$ and $[Cp^*_3La_3(Cl)_4(Me)_2]_n$ and the steric saturation by additional THF coordination promotes methane elimination. Besides the fact that the exact stoichiometry of Ln:Cl = 3:4 is only given in the latter complex, solubility and cluster rearrangement in solution hindered the analysis of the reaction pathway (Figure 1).

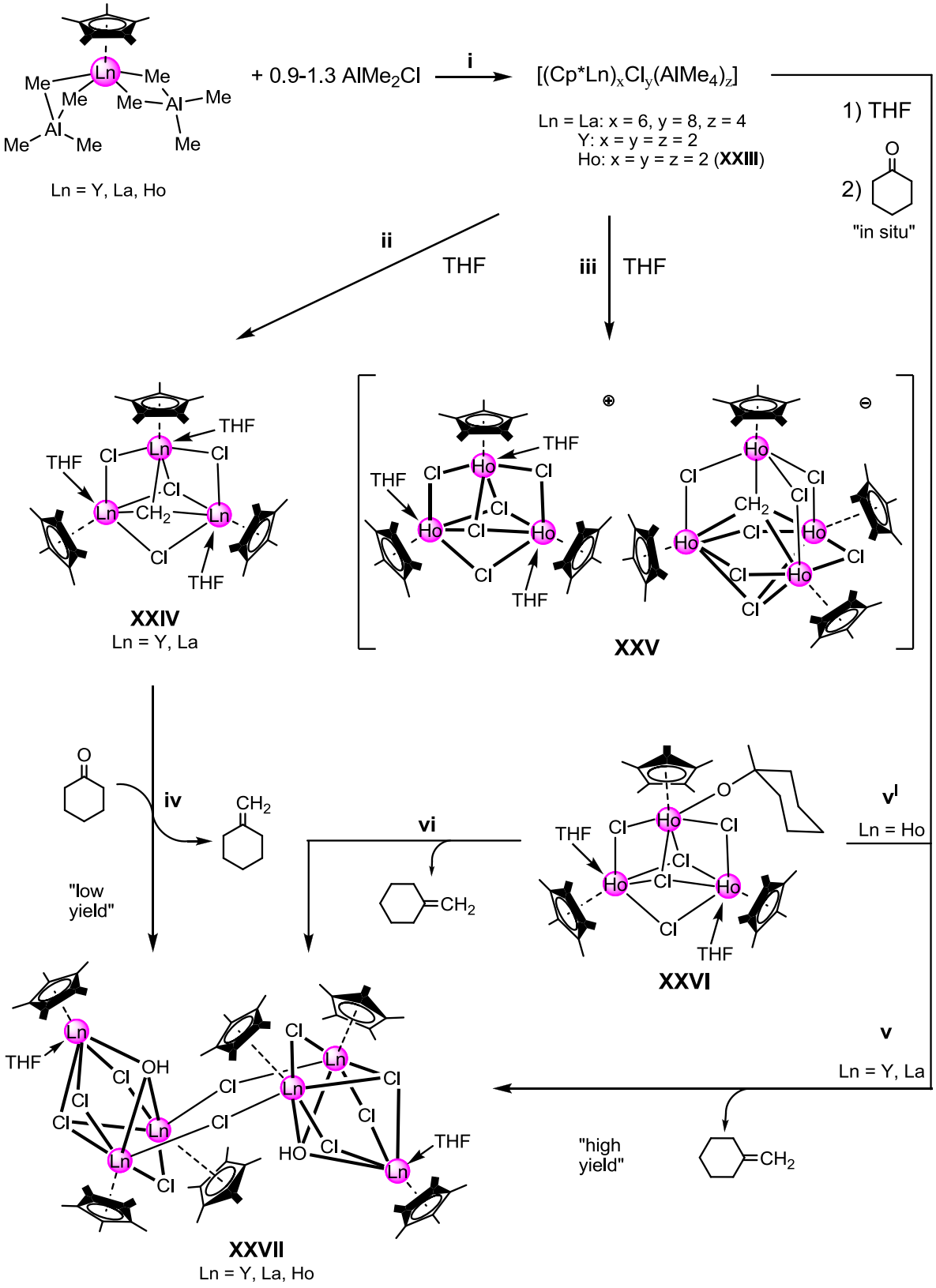

Scheme 1. Synthesis of half-sandwich rare-earth metal mixed chloride/methylidene complexes and their reactivity towards cyclohexanone.

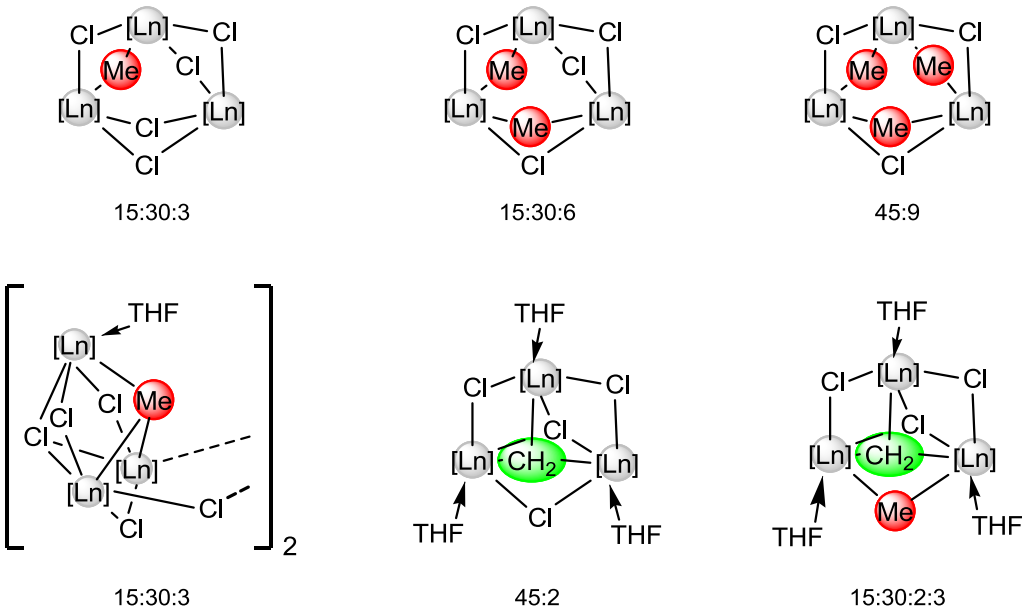

Figure 1. Rare-earth metal cluster complexes ([Ln] = C_5Me_5Ln) with different Cl/CH_3 ratios (top) and resulting donor adducts with partial C–H activation after THF addition (bottom). Ratios of proton integrals in the ^{1}H NMR spectra are given below.

In case of the holmium half-sandwich bis(tetramethylaluminate) complex, the chlorination reaction yielded [Cp*Ho(μ_2-Cl)($AlMe_4$)]$_2$ (**XXIII**) which crystallizes isostructural to the yttrium complex (Figure 2). However, treatment with THF in toluene generates a new, ion separated, methylidene species [$Cp^*_3Ho_3$(μ_2-Cl)$_3$(μ_3-Cl)$_2$($THF)_3$][$Cp^*_4Ho_4$(μ_2-Cl)$_6$(μ_3-Cl)(μ_4-CH_2)] (**XXV**, Scheme 1 **iii**). The cation has a similar core structure as the previously reported methylidene complexes, but the positive charge originates from the replacement of the CH_2^{2-} group by a chloride atom. The anion also includes the methylidene complex core, but instead of THF coordination, the three holmium atoms are μ_2-Cl canopied by a {Cp*$HoCl_3$}$^-$ moiety, where the holmium is further coordinated to the CH_2^{2-} group (Figure 3).

Reaction of the methylidene complexes show Tebbe reagent like CH_2^{2-}/O^{2-} interchange with ketones in NMR scale reactions, but corresponding oxo complexes under retention of the trimeric cluster entity could not be obtained in single crystalline form. Instead, hexameric cluster complexes [{$Cp^*_3Ln_3$(μ_2-Cl)$_3$(μ_3-Cl)(μ_2-OH)}{μ_2-Cl}]$_2$ **XXIV** (Ln = Y, La, Ho) were crystallized from the reaction solution in low yields (Scheme 1, **iv**). Since the crystallographic data of the yttrium and holmium complexes were of low quality (allowing the assignment of a connectivity structure only), ORTEP drawing of the lanthanum structure **XXIV** is shown in Figure 5. All complexes share the same core structure, which can be best described as two distorted hexagonal bipyramides [Ln_3Cl_5] linked by two chlorido ligands. Similar cluster arrangements [**L**Ln_3X_5{μ_2-

X}]$_2$ were found previously for the earlier (“larger”) lanthanides in the presence of small anions (X) like halo, cyano, borohydro, and hydroxy, which favorably act as bridging ligands.[3-7]

The origin of the proton leading to the hydroxy group could not be fully clarified, but displacement of single chloride atoms by methyl groups in the methylidene complex of yttrium was observed by reduced amount of chlorination reagent in its synthesis and verified by NMR spectroscopy as well as X-ray diffraction analysis. This can be assumed as a result from the stoichiometric Ln:Cl:Me ratios in the precursors, as illustrated in Figure 1. An ORTEP drawing of the molecular structure of [Cp*$_3$Y$_3$(μ_2-Cl)$_3$(μ_3-Cl)(μ_3-CH$_2$)(THF)$_3$] with one μ_2-bridging position showing Cl/CH$_3$ group exchange is shown in Figure 6. Furthermore, the corresponding ^{1}H NMR spectra of the yttrium complex at -10° C in THF-d$_8$ is shown in Figure 6. One set of a singulet at 2.01 ppm for the Cp* ligand and a quartet at –0.34 ppm with a coupling constants of $^2J_{Y\text{-}H}$ = 4.4 Hz with the integration ratio of 45:2 represents the desired mono-alkylidene cluster. Additionally, signals for Cp* ligands can be found at 2.00 and 1.99 ppm in a ratio of 15:30 and a doublet of triplet at –0.37 ppm ($^2J_{Y\text{-}H}$ = 5.4/2.2 Hz) as well as a triplet at –0.82 ppm ($^2J_{Y\text{-}H}$ = 2.5Hz) in the ratio of 2:3 representing one methylidene and one methyl group, respectively.

To avoid the poor solubility of the mixed chloride/methylidene complexes, the reaction with cyclohexanone was also carried out shortly after the donor induced aluminate cleavage of the half-sandwich rare-earth metal chloride/aluminate precursors. This directly led to the hydroxy complexes **XXVI** in higher yields suggesting that the C–H bond activation and resulting methylidene species is not the decisive step, it is rather the methyl transfer reaction followed by C–H bond activation leading to the OH$^-$ group (Scheme 1, **v**). The isolation of complex [Cp*$_3$Ho$_3$(μ_2-Cl)$_3$(μ_3-Cl$_2$)(O{CH$_3$}C$_6$H$_{10}$)(THF)$_2$] (**XXVI**) as an intermediate species further indicates a methyl rather than a methylidene transfer (Scheme 1, **v^I**). The molecular structure is shown in Figure 5. A similar insertion reaction of a carbonylic compound into a Ln–CH$_3$ bond has been reported for the reaction of polymeric trimethylyttrium [YMe$_3$]$_n$ with flourenone generating [Y(OC$_{14}$H$_{11}$)$_2$(μ-OC$_{14}$H$_{11}$)]$_2$(9-fluorenone),[8] and for mono- and dicationic yttrium-methyl complexes [YMe$_x$(thf)$_{6-x}$][(BPh$_4$)$_{3-x}$] (x = 1 or 2) leading to the alkoxy complexes [Y(OCMePh$_2$)$_x$(thf)$_{6-x}$][(BPh$_4$)$_{3-x}$] (x = 1 or 2) upon treatment with benzophenone.[9] When complex **XXVI** was re-dissolved in THF under moderate heating, the formation of the hexameric hydroxy complex **XXVII** under the release of methylenecyclohexane was observed (Scheme 1, **vi**).

Synthesis of [Cp*Ho(μ_2-Cl)(AlMe$_4$)]$_2$ (XXIII$_{Ho}$). As described for the yttrium analogon,[2] 474 mg (1.00 mmol) [Cp*Ho(AlMe$_4$)$_2$] was dissolved in 10 ml of hexane. Then 1 mL of 1M AlMe$_2$Cl/hexane solution (1.0 eq) was added at –35° C without stirring and the solution was warmed to ambient temperature. After 3 d crystals of **XXIII$_{Ho}$** were separated from the solution (321 mg, 76%). IR (Nujol): 2968 m, 2934 m, 2900 s, 2857 m, 1451 m, 1433 m, 1025 m, 1009 s, 860 s, 484 m cm^{-1}. Elemental analysis calcd (%) for $C_{43}H_{71}Cl_4Ho_3O_3$ (845.46): C 39.78, H 6.44; found: C 39.94, H 6.57.

Synthesis of [Cp*$_3$Y$_3$(μ_2-Cl)$_3$(μ_3-Cl)(μ_2-CH$_2$)(THF)$_3$] (XXIV$_Y$) As described previously,[1] 400 mg (1.00 mmol) [Cp*Y(AlMe$_4$)$_2$] were dissolved in 10 ml of hexane. Then 1 mL of 1M AlMe$_2$Cl/hexane solution (1.0 eq) was added at –35° C without stirring and warmed to ambient temperature. After 3 h crystallization of [Cp*Y(AlMe$_4$)(μ-Cl)]$_2$ occurred. After 4 d, the crystals were separated from the solution, covered with 2 ml of toluene and dissolved immediately with additional 2 ml of THF. The clear solution gave product **XXIV$_Y$** as clear crystals within 4 d (165 mg, 47%). IR (Nujol): 1307 m, 1170 m, 1022 vs, 919 m, 875 br vs, 723 s, 669 s, 651 s, 434 m cm^{-1}.

^{1}H NMR (500 MHz, THF-*d8*, –10 °C): δ = [3.62 (THF), 1.77 (THF)],
species_1
(45:2H): 2.01 (s, 45H, C*H*$_3$(Cp*)),–0.34 (q, 2H, $J_{Y\text{-}H}$ = 4.4 Hz, Y$_3$C*H*$_2$);
species_2
(15:30:2:3): 2.00 (s, 30H, C*H*$_3$(Cp*)), 1.99 (s, 10 H, C*H*$_3$(Cp*)), -0.37 (dt, 2H, $J_{Y\text{-}H}$ = 5.4 Hz, $J_{Y\text{-}H}$ = 2.2 Hz, YC*H*$_2$), –0.82 (t, 3H, $^2J_{Y\text{-}H}$ = 2.5 Hz, Y$_3$C*H*$_3$);
species_3
(30:3H): 1.98 (s, 0.9H, C*H*$_3$(Cp*)),–0.93 (s, 0.09H Y$_3$C*H*2);

^{13}C NMR (100 MHz, THF-*d8*, –10 °C): δ = [64.6 (THF), 22.5 (THF)],
species_1
(45:2H): 115.2 (Cp*), 9.6*2* (C$_5${*C*H$_3$}$_5$); [HSQC: 88.5/–0.34 μ_3-*C*H$_2$]
species_2
(15:30:2:3): 114.1 (Cp*), 9.6*6* (C$_5${*C*H$_3$}$_5$); [HSQC: 88.5/–0.37 μ_3-*C*H$_2$]
species_3
(30:3H): 114.9 (Cp*), 9.5*7* (C$_5${*C*H$_3$}$_5$); [HSQC: 23.2/–0.82 μ_2-*C*H$_3$]
Elemental analysis calcd (%) for $C_{43}H_{71}Cl_4O_3Y_3$ (1044.55): C 49.44, H 6.85; found: C 51.25, H 6.30.

Synthesis of $[Cp^*_3La_3(\mu_2\text{-}Cl)_3(\mu_3\text{-}Cl)(\mu_2\text{-}CH_2)(THF)_3]$ ($\mathbf{XXIV_{La}}$) As described previously,[1] 448 mg (1.00 mmol) [Cp*La($AlMe_4$)$_2$] were dissolved in 10 ml hexane and 1.3 mL of a 1M $AlMe_2Cl$/hexane solution (1.3 eq) was added at -35° C without stirring. Crystallization of $[Cp^*_6La_6\{(\mu\text{-}Me)_3AlMe\}_4(\mu\text{-}Cl)_6(\mu_3\text{-}Cl)_2]$ was observed within 10 min at ambient temperature. After 3 d the crystals were separated from the solution and dried in vacuum. The crystals were layered with 2 mL of toluene and 2 ml THF were added. The reaction mixture turned into a clear solution within 20 min. The solution was filtered and kept at ambient temperature for 3 d while it became yellow within 1 d. Cooling the mixture to –35 °C resulted in the formation of the product $\mathbf{XXIV_{La}}$ in form of transparent crystals (143 mg, 36% overall yield). IR (Nujol): 1305 m, 1169 m, 1063 w, 1026 s, 967 w, 917 w, 877 br s, 723 w cm^{-1}. ^{1}H NMR (400 MHz, THF-*d8*, 25 °C): δ = 3.61 (m, 12H, THF), 2.05 (s, 45H, CH_3(Cp*)), 1.77 (m, 12H, THF) ppm, –0.96 (s, 1H, 0.5(μ_2-CH_2). ^{13}C NMR (100 MHz, THF-*d8*, 25 °C): δ = 120.8 ($C_5\{CH_3\}_5$), 12.2 ($C_5\{CH_3\}_5$) ppm. Elemental analysis calcd (%) for $C_{43}H_{71}Cl_4La_3O_3$ (1194.55): C 43.23, H 5.99; found: C 43.71, H 5.97.

Synthesis of $[Cp^*_3Ho_3(\mu_2\text{-}Cl)_3(\mu_3\text{-}Cl)(\mu_2\text{-}CH_2)(THF)_3]$ ($\mathbf{XXIV_{Ho}}$). At ambient temperature, crystals of [Cp*Ho($AlMe_4$)(μ-Cl)]$_2$ ($\mathbf{XXIII_{Ho}}$) were layered with 2 mL of toluene and 2 ml THF were added. The reaction mixture turned into a clear pink solution within 20 min. After 1 d, cooling the solution to –35 °C led to the crystallization of $\mathbf{XXIV_{Ho}}$ as pink crystals. IR (Nujol): 1308 m, 1171 m, 1022 vs, 921 m, 876 br vs, 723 s, 671 s, 651 s, 436 m cm^{-1}. Elemental analysis calcd (%) for $C_{43}H_{71}Cl_4Ho_3O_3$ (1272.63): C 40.58, H 5.62; found: C 41.12, H 5.37.

Synthesis of $[Cp^*_3Ho_3(\mu_2\text{-}Cl)_3(\mu_3\text{-}Cl)_2(THF)_3][Cp^*_4Ho_4(\mu_2\text{-}Cl)_6(\mu_3\text{-}Cl)(\mu_4\text{-}CH_2)]$ (XXV). [Cp*Ho($AlMe_4$)(μ-Cl)]$_2$ (422 mg, 0.5 mmol) was dissolved in THF (2 mL) and toluene (2 mL) was added. After 6 h pink crystals appear and the solution was cooled to –35 °C. After 3 d the crystals were separated to yield 120 mg (28%) of complex **XXV.** IR (DRIFT): 2968 m, 2936 m, 2901 s, 2857 m, 1451 m, 1436 m, 10379 m, 1009 s, 859 s, 485 m cm^{-1}.Elemental analysis calcd (%) for $C_{83}H_{131}Cl_{12}Ho_7O_3$ (2756.87): C 36.16, H 4.79; found: C 36.88, H 5.03.

Synthesis of $[Cp^*_3Ho_3(\mu_2\text{-}Cl)_3(\mu_3\text{-}Cl_2)(O\{CH_3\}C_6H_{10})(THF)_2]$ (XXVI). The dimeric tetramethylaluminate/chloro holmium complex [Cp*Ho(μ_2-Cl)($AlMe_4$)]$_2$ ($\mathbf{XXIII_{Ho}}$) was dissolved in THF to generate the methylidene species. An equimolar amount of cyclohexanone and subsequently toluene was added in situ. The solution was stored at –35 °C and after 2 days the crystallization was fully implemented in moderate yields (60%). Elemental analysis calcd (%) for $C_{43}H_{71}Cl_4O_3Ho_3$ (1335.12): C 40.48, H 5.59; found: C 41.45, H 5.49.

General procedure for the synthesis of [{Cp*$_3$Ln$_3$(μ_2-Cl)$_3$(μ_3-Cl)(μ_3-OH)(THF)$_2$}(μ_2-Cl)]$_2$ (XXVII).

Route A: The rare-earth metal methylidene complex [Cp*$_3$Ln$_3$(μ_2-Cl)$_3$(μ_3-Cl)(μ_2-CH$_2$)(THF)$_3$] (Ln = Y, La) and the cyclohexanone were transferred into a *J. Young* NMR tube using THF-d$_8$ and heated up to generate a clear solution. For crystallization, toluene was added to the reaction mixture and cooled to –35 °C. After one week, the hexameric title compound was crystallized in very low yields (<10%).

Route B: The mixed tetramethylaluminate/chloro half-lanthanidocene cluster complexes (**XXIII**) were dissolved in THF to generate the methylidene species. Before any crystallization occured, an equimolar amount of cyclohexanone was added in situ and the solution stored at –35 °C. After one day, toluene was added and the crystallization was fully implemented after 2 days in moderate to good yields (40-70%).

Synthesis of [{Cp*$_3$Y$_3$(μ_2-Cl)$_3$(μ_3-Cl)(μ_3-OH)(THF)$_2$}(μ_2-Cl)]$_2$

Elemental analysis calcd (%) for $C_{76}H_{124}Cl_{10}O_2Y_6$ (2021.76): C 45.15, H 6.18; found: C 46.53, H 7.56.

Synthesis of [{Cp*$_3$La$_3$(μ_2-Cl)$_3$(μ_3-Cl)(μ_3-OH)(THF)$_2$}(μ_2-Cl)]$_2$

Elemental analysis calcd (%) for $C_{76}H_{124}Cl_{10}La_6O_2$ (2321.76): C 39.32, H 5.38; found: C 38.58, H 5.01.

Synthesis of [{Cp*$_3$Ho$_3$(μ_2-Cl)$_3$(μ_3-Cl)(μ_3-OH)(THF)$_2$}(μ_2-Cl)]$_2$

Elemental analysis calcd (%) for $C_{76}H_{124}Cl_{10}Ho_6O_2$ (2477.91): C 36.84, H 5.04; found: C 36.39, H 5.21.

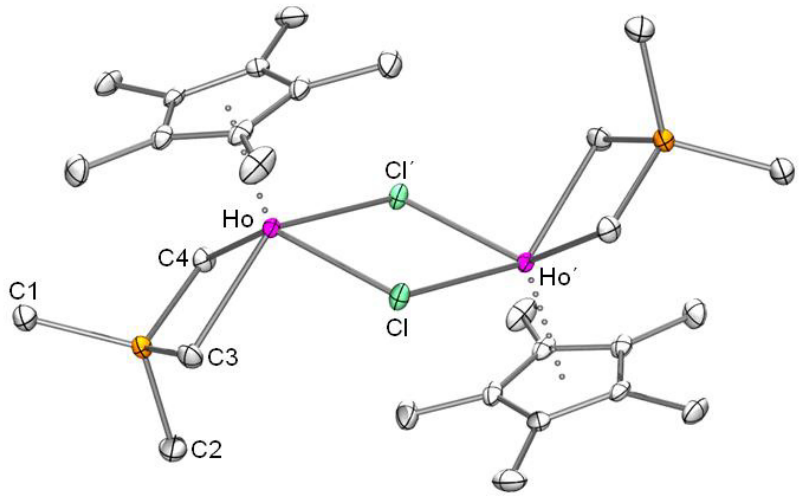

Figure 2. ORTEP view of the molecular structure of $[Cp^{*}Ho(\mu_2\text{-}Cl)(AlMe_4)]_2$ (**XXIII$_{Ho}$**). Atomic displacement parameters are set at the 50% probability level. Hydrogen atoms omitted for clarity.

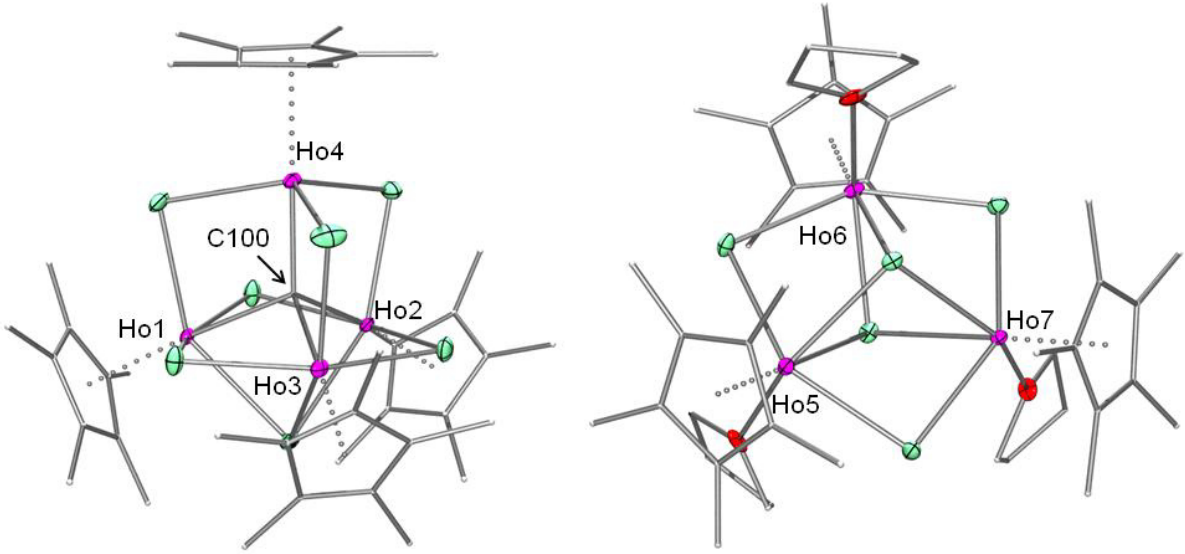

Figure 3. ORTEP view of the molecular structure of $[Cp^{*}_3Ho_3(\mu_2\text{-}Cl)_3(\mu_3\text{-}Cl)_2(THF)_3][Cp^{*}_4Ho_4(\mu_2\text{-}Cl)_6(\mu_3\text{-}Cl)(\mu_4\text{-}CH_2)]$ (**XXV**). Atomic displacement parameters are set at the 50% probability level. Hydrogen atoms are omitted for clarity.

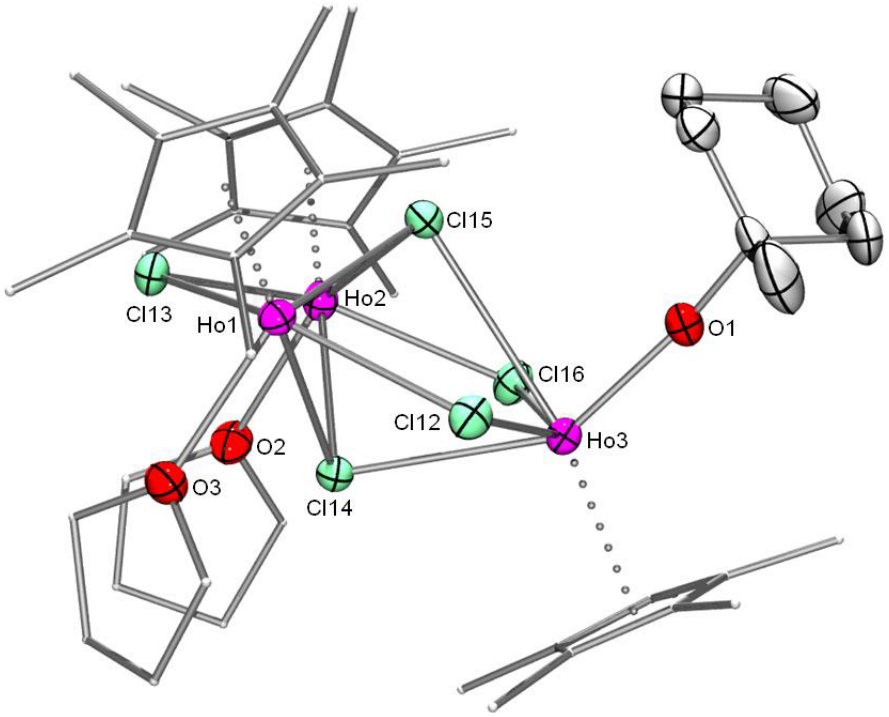

Figure 4. ORTEP view of the molecular structure of $[Cp^{*}_{3}Ho_3(\mu_2\text{-}Cl)_3(\mu_3\text{-}Cl_2)(O\{CH_3\}C_6H_{10})(THF)_2]$ (**XXVI**). Atomic displacement parameters are set at the 50% probability level. Hydrogen atoms omitted for clarity.

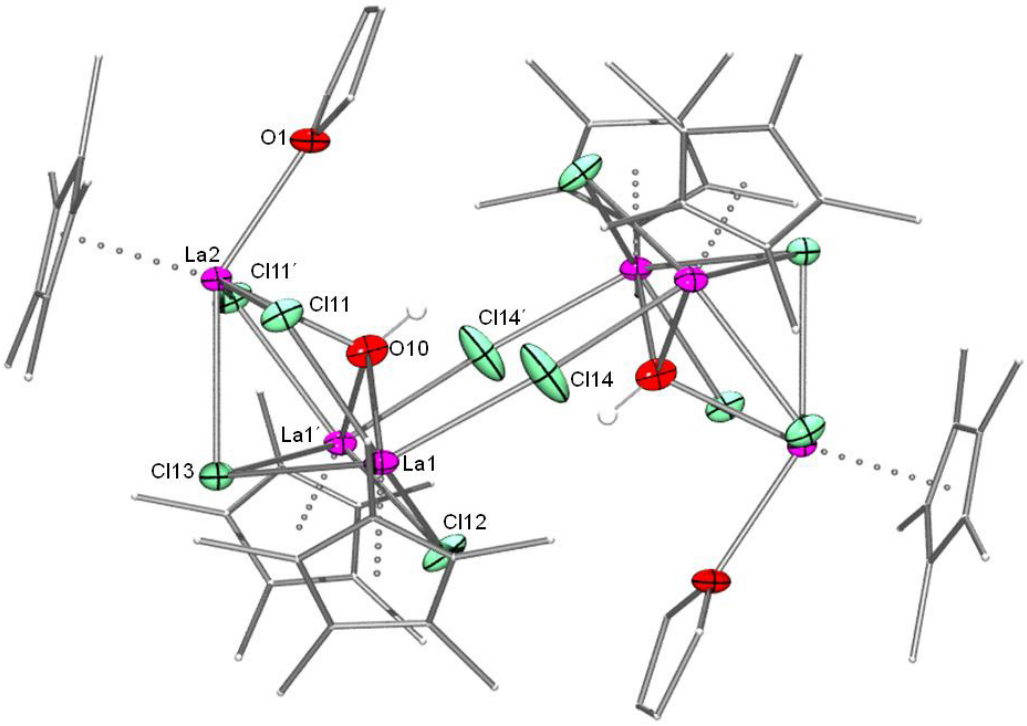

Figure 5. ORTEP view of the molecular structure of $[\{Cp^{*}_{3}Ln_3(\mu_2\text{-}Cl)_3(\mu_3\text{-}Cl)(\mu_2\text{-}OH)\}\{\mu_2\text{-}Cl\}]_2$ representative of isostructural complexes **XXVII**. Atomic displacement parameters are set at the 50% probability level. Hydrogen atoms omitted for clarity.

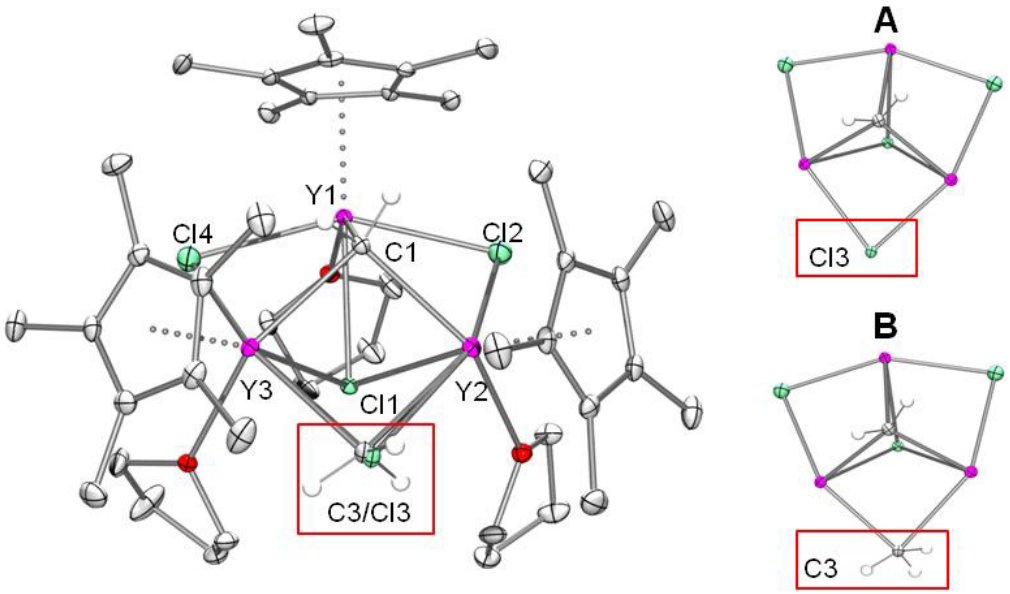

Figure 6. ORTEP view of the molecular structure of $[Cp^{*}_{3}Y_3(\mu_2\text{-}Cl)_x(\mu_2\text{-}CH_3)_y(\mu_3\text{-}Cl)(\mu_3\text{-}CH_2)(THF)_3]$ (x + y = 3; x = 3 {**A**} or 2 {**B**}). Atomic displacement parameters are set at the 50% probability level. Hydrogen atoms omitted for clarity.

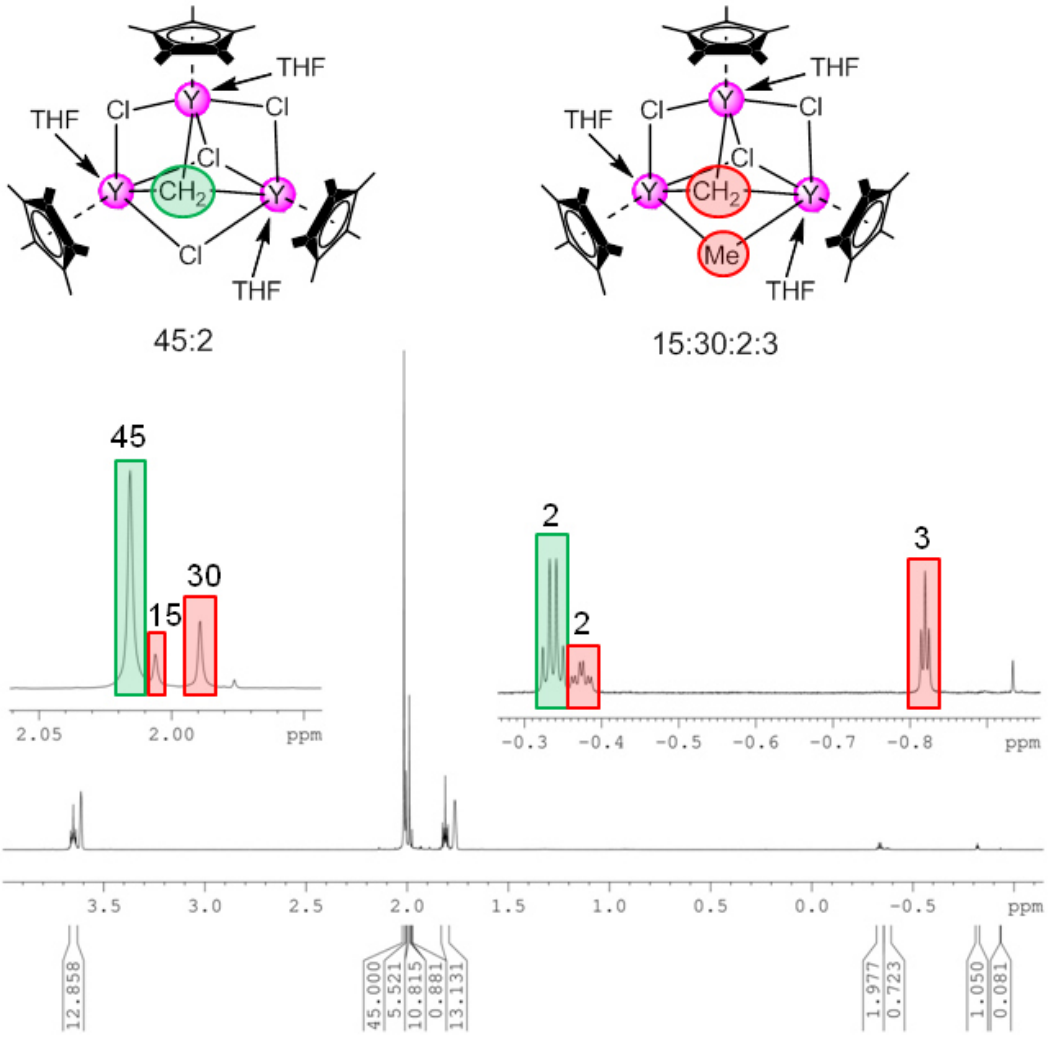

Figure 7. ^{1}H NMR spectrum (500 MHz, THF-d_8, -10° C) of $[Cp^{*}_{3}Y_3(\mu_2\text{-}Cl)_x(\mu_2\text{-}CH_3)_y(\mu_3\text{-}Cl)(\mu_3\text{-}CH_2)(THF)_3]$ (x + y = 3; x = 3 {**A**} or 2 {**B**}).

[1] H. M. Dietrich, K. W. Törnroos, R. Anwander, *J. Am. Chem. Soc.* **2006**, *128*, 9298-9299.
[2] H. M. Dietrich, O. Schuster, K. W. Törnroos, R. Anwander, *Angew. Chem. Int. Ed.* **2006**, *45*, 4858-4863.
[3] W. J. Evans, T. M. Champagne, B. L. Davis, N. T. Allen, G. W. Nyce, M. A. Johnston, Y.-C. Lin, A. Khvostov, J. W. Ziller, *J. Coord. Chem.* **2006**, *59*, 1069-1087.
[4] G. Paolucci, M. Vignola, A. Zanella, V. Bertolasi, E. Polo, S. Sostero, *Eur. J. Inorg.Chem.* **2006**, 4104-4110.
[5] J. Sieler, A. Simon, K. Peters, R. Taube, M. Geitner, *J. Organomet. Chem.* **1989**, *362*, 297-303.
[6] F. Bonnet, M. Visseaux, D. Barbier-Baudry, A. Hafid, E. Vigier, M. M. Kubicki, *Inorg. Chem.* **2004**, *43*, 3682-3690.
[7] E. Barnea, C. Averbuj, M. Kapon, M. Botoshansky, M. S. Eisen, *Eur. J. Inorg. Chem.* **2007**, 4535-4540.
[8] H. M. Dietrich, C. Meermann, K. W. Törnroos, R. Anwander, *Organometallics* **2006**, *25*, 4316-4321.
[9] M. U. Kramer, D. Robert, S. Arndt, P. M. Zeimentz, T. P. Spaniol, A. Yahia, L. Maron, O. Eisenstein, J. Okuda, *Inorg. Chem.* **2008**, *47*, 9265-9278.

IV. Mixed Formamidinate/Aluminate Half-Sandwich Rare-Earth Metal Complexes

1,3-Diazaallyl related ligand systems ([RN=C(R′)NR]$^-$, R′ = H, formamidinate; R′ = alkyl, amidinate; R′ = amine, guanidinate) have found a role as tunable alternatives to the ubiquitous cyclopentdienyl family of ancillary ligands.[1] Though at an early stage, studies in catalytic processes of amidinato/guanidinato rare-earth-metal complexes such as homogeneous polymerizations, have proven to be promising.[2-4] Recently, we reported on rare-earth metal tetramethylaluminate complexes bearing formamidiniato ancillary ligands [Ln(Form)($AlMe_4$)$_2$] (Ln = Y, La; Form (ArNCHNAr) = EtForm (Ar = 2,6-$Et_2C_6H_3$), DippForm (Ar = 2,6-*i*$Pr_2C_6H_3$)), and their performances in isoprene polymerization (**Paper IV**).[5] As the strong N-donors have also a strong affinity for the LEWIS acidic aluminum metal center, the reactivity of the formidinates with MMe_3 (M = Al, Ga) was also investigated. The characterized complexes include the dimethylaluminum formamidinate complex [(DippForm)$AlMe_2$] (**Paper V**).[6] Very recently, we have successfully shown, that the reactions of [Me_2Al{B(NDippCH)$_2$}$_2$]$_2$ (Dipp = 2,6-*i*$Pr_2C_6H_3$)[7] with [Cp*$LnMe_2$]$_3$[8] (Ln = Y, Lu) form the corresponding rare-earth metal half-sandwich complexes with heterosubstituted aluminate ligands (“heteroaluminates”) [Cp*Ln(Me_3Al{B(NDippCH)$_2$}$_2$)$_2$] (**Paper VI**).[9] The bulky carbanion-like boryl ligands were found in the peripheral positions and the performance in isoprene polymerization of these complexes was tested. Herein, we were interested, if the reaction of [Cp*$LnMe_2$]$_3$ with [(DippForm)$AlMe_2$] would also generate half-lantanoidocene heteroaluminate complexes. Interestingly, the reaction led to [Cp*Ln($AlMe_4$)(DippForm)] **XXVIII** under ligand rearrangement, irrespective whether 1 or 2 equivalents of the dimethylaluminum reagent were applied (Scheme 1). Single crystals of complexes **XXVIII** suitable for X-ray diffraction analysis were grown from toluene/hexane at –35 °C and the molecular structure of the lutetium complex is representatively shown in Figure 1. The formamidinato ligand coordinates in a κ^2-fashion to the rare-earth metal center and the released $AlMe_2$ together with the two methyl groups form a tetramethylaluminate moiety. Additionally, the performance in isoprene polymerization was primarily tested. The lutetium complex showed high activity upon cationization with co-catalysts [Ph_3C][$B(C_6F_5)_4$] (**A**) and [$PhNMe_2H$][$B(C_6F_5)_4$] (**B**) but none with $B(C_6F_5)_3$ (**C**) (Table 1, run 1-3). Interestingly, polyisoprene (PIP) with dominant 3,4-units (57% and 58%) was obtained, while in contrast [Cp*Ln($AlMe_4$)$_2$] produces mainly *cis*-1,4-PIP (up to

74%, run 4-6) and [Cp*Ln(Me_3Al{B(NDippCH)$_2$}$_2$)$_2$] generates PIP with predominant *trans*-1,4 units (68%, run 7).

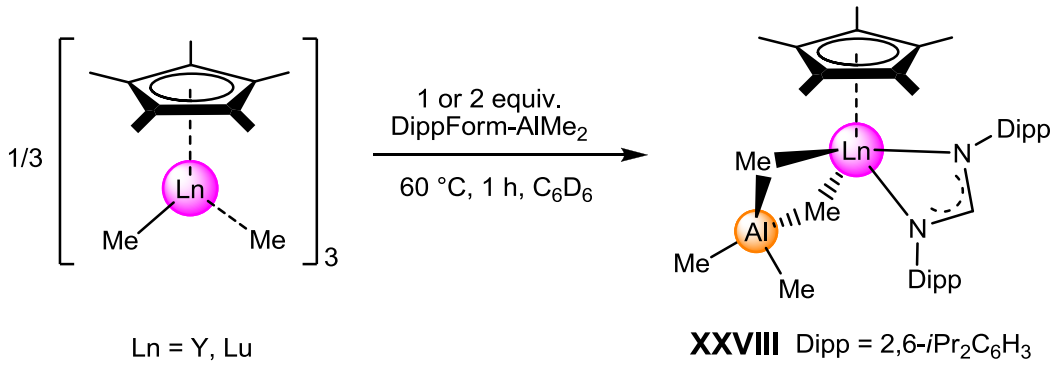

Ln = Y, Lu

XXVIII Dipp = 2,6-*i*Pr$_2$C$_6$H$_3$

Scheme 1. Synthesis of half-sandwich mixed aluminate/formamidinate complexes.

General procedure for the synthesis of [(C_5Me_5)Ln($AlMe_4$)(DippForm)] (XXVIII). The half-sandwich rare-earth metal dimethyl complex [(C_5Me_5)LnMe_2]$_3$ and the organoaluminum formamidinate complex [(*N*,*N*-HC{2,6-*i*Pr$_2$C$_6$H$_3$-N}$_2$)AlMe_2] were transferred to a Teflon sealed *J. Young* NMR tube using C_6D_6 and heated to 60 °C. After one hour, the integration of the proton signals in NMR analysis stayed constant and additional ^{13}C NMR and ^{1}H-^{13}C HSQC spectra were recorded to identify the product, which was obtained in quantitative yields.

Synthesis of [(C_5Me_5)Y($AlMe_4$)(DippForm)] ($XXVIII_Y$). Following the procedure described above, [(C_5Me_5)YMe_2]$_3$ (51 mg, 0.20 mmol) and the organoaluminum formamidinate complex (84 mg, 0.20 mmol) yielded **$XXVIII_Y$** (134 mg, 0.20 mmol, >99%) as a white solid. Crystallization from a toluene/hexane solution at –35 °C afforded colorless crystals suitable for X-ray diffraction analysis. ^{1}H NMR (400 MHz, C_6D_6, 25 °C): 8.24 (d, $^{3}J_{Y\text{-}H}$ = 4.4 Hz, 1 H, NC*H*N), 7.10-7.02 (br, 6 H, Ar-*H*), 3.16 (sept, $^{3}J_{H\text{-}H}$ = 6.7 Hz, 4 H, Ar-C*H*(CH$_3$)$_2$), 1.93 (s, 15 H, C$_5$(C*H*$_3$)$_5$), 1.33 (d, $^{3}J_{H\text{-}H}$ = 6.7 Hz, 12 H, Ar-CH(C*H*$_3$)$_2$), 1.06 (d, $^{3}J_{H\text{-}H}$ = 6.7 Hz, 12 H, Ar-CH(C*H*$_3$)$_2$), –2.4 (d, $^{2}J_{Y\text{-}H}$ = 2.3 Hz, 12 H, Al(C*H*$_3$)$_4$). ^{13}C NMR (100 MHz, C_6D_6, 25 °C): δ = 172.7 (d, $^{2}J_{Y\text{-}C}$ = 3.3 Hz, N*C*HN), 144.0 (d, $^{2}J_{Y\text{-}C}$ = 1.4 Hz, *C*$_6$-N), 142.2 (*C*$_6$-^{i}Pr), 125.0 (*C*$_6$), 123.9 (*C*$_6$), 121.3 (d, $^{1}J_{Y\text{-}C}$ = 1.2 Hz, *C*$_5$(CH$_3$)$_5$), 28.7 (Ar-*C*H(CH$_3$)$_2$), 26.5 (Ar-CH(*C*H$_3$)$_2$), 23.3 (Ar-CH(*C*H$_3$)$_2$), 11.3 (C$_5$(*C*H$_3$)$_5$), 1.3 (Al(*C*H$_3$)$_4$). IR (cm^{-1}): 3067 m, 3016 m, 2957 s, 2924 s, 2893 s, 2866 s, 2728 w, 1652 w, 1595 w, 1521 s, 1461 m, 1435 s, 1381 w, 1358 w, 1336 w, 1317 m, 1282 s, 1231 w, 1200 m, 1181 m, 1114 w, 1098 w, 1023 m, 948 w, 934 w, 798 w, 764 m, 753 w, 719 s, 695 s, 583 m; elemental analysis calcd (%) for $C_{39}H_{60}AlN_2Y$ (672.79): C 69.62, H 8.99, N 4.16; found: C 69.14, H 8.95, N 4.11.

Synthesis of [(C_5Me_5)Lu($AlMe_4$)(DippForm)] ($\mathbf{XXVIII_{Lu}}$). Following the procedure described above, [(C_5Me_5)$LuMe_2$]$_3$ (25 mg, 73 µmol) and the organoaluminum formamidinate complex (31 mg, 74 µmol) yielded $\mathbf{XXVIII_{Lu}}$ (56 mg, 73 µmol, >99%) as a white solid. Crystallization from a toluene/hexane solution at –35 °C afforded colorless crystals suitable for X-ray diffraction analysis. ^{1}H NMR (400 MHz, C_6D_6, 25 °C): 8.29 (s, 1 H, NC*H*N), 7.11-7.02 (br, 6 H, Ar-*H*), 3.19 (sept, $^3J_{H\text{-}H}$ = 6.7 Hz, 4 H, Ar-C*H*(CH_3)$_2$), 1.95 (s, 15 H, C_5(C*H*$_3$)$_5$), 1.33 (d, $^3J_{H\text{-}H}$ = 6.7 Hz, 12 H, Ar-CH(C*H*$_3$)$_2$), 1.05 (d, $^3J_{H\text{-}H}$ = 6.7 Hz, 12 H, Ar-CH(C*H*$_3$)$_2$), –0.06 (s br, 12 H, Al(C*H*$_3$)$_4$). ^{13}C NMR (100 MHz, C_6D_6, 25 °C): δ = 172.1 (N*C*HN), 143.9 (*C*$_6$-N), 142.5 (*C*$_6$-^{i}Pr), 125.2 (*C*$_6$), 124.0 (*C*$_6$), 120.1 (*C*$_5$(CH_3)$_5$), 28.5 (Ar-*C*H(CH_3)$_2$), 26.8 (Ar-CH(*C*H$_3$)$_2$), 23.3 (Ar-CH(*C*H$_3$)$_2$), 11.4 (C_5(*C*H$_3$)$_5$), n.d. (Al(*C*H$_3$)$_4$). IR (cm^{-1}): 3067 m, 3020 m, 2957 s, 2925 s, 2866 s, 2729 w, 1653 w, 1595 w, 1524 s, 1458 m, 1436 s, 1382 w, 1358 w, 1336 w, 1318 m, 1281 s, 1232 w, 1201 m, 1181 m, 1115 w, 1098 w, 1024 m, 949 w, 935 w, 799 w, 764 m, 753 w, 719 s, 697 s, 585 m; elemental analysis calcd (%) for $C_{39}H_{60}AlN_2Lu$ (758.86): C 62.53, H 7.66, N 3.68; found: C 61.73, H 7.97, N 3.69.

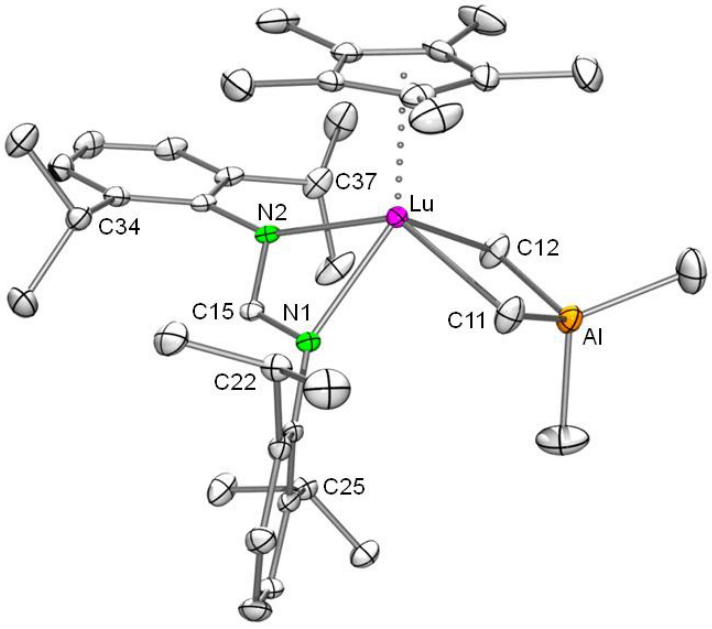

Figure 1. ORTEP view of the molecular structure of [(C_5Me_5)Lu($AlMe_4$)(DippForm)] ($\mathbf{XXVIII_{Lu}}$) representative of isostructural complexes **XXVIII**. Atomic displacement parameters are set at the 50% probability level. Hydrogen atoms omitted for clarity.

Bond length (Å)	Y	Lu	Bond angle (°)	Y	Lu
Ln–C11	2.627(2)	2.598(3)	C11–Ln–C12	82.21(7)	84.11(9)
Ln–C12	2.517(2)	2.448(3)	N1–Ln–N2	57.18(5)	58.31(7)
Ln–N1	2.366(2)	2.314(2)	Cp_{cent}–Ln–C15	127.33	127.67
Ln–N2	2.410(2)	2.366(2)	Cp_{cent}–Ln–Al	118.45	118.71
Ln–Cp_{cent}	2.345	2.296	C15–Ln–Al	114.22	113.61

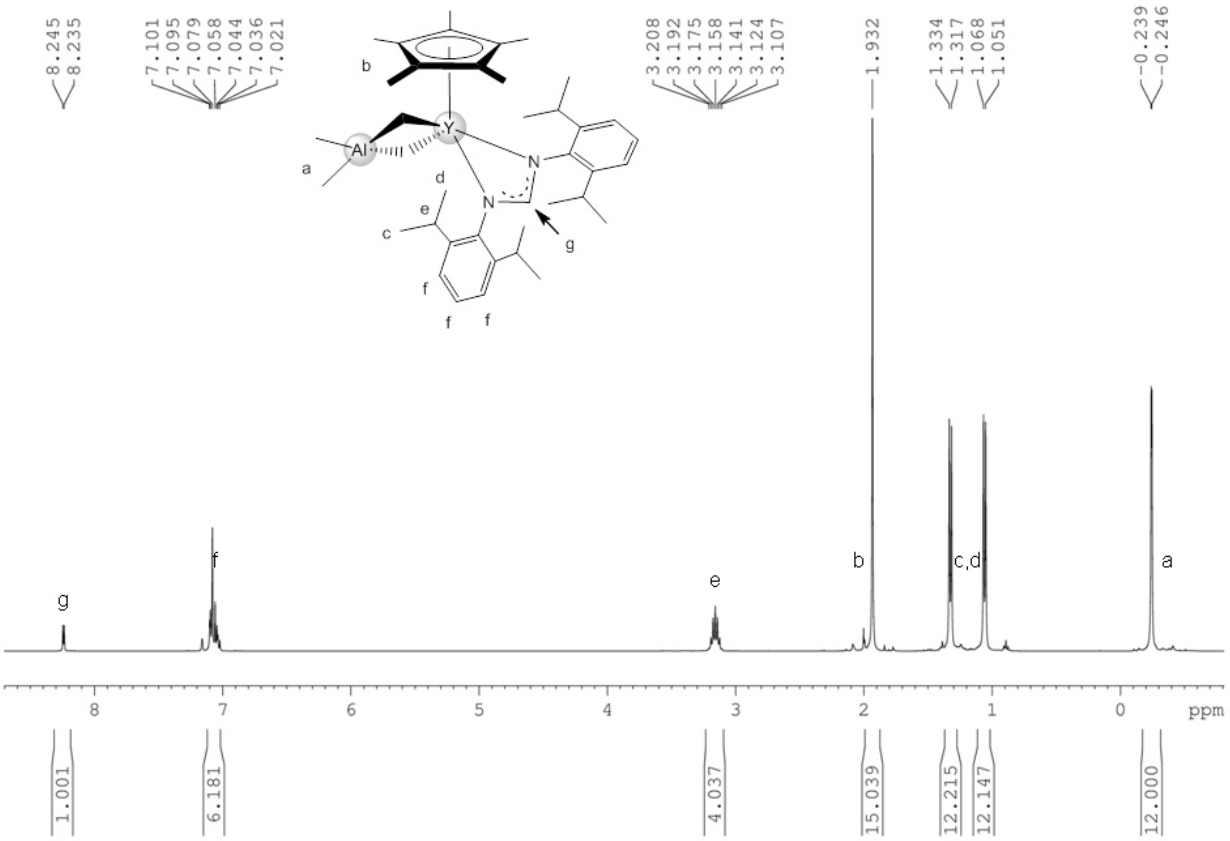

Figure 2: ^{1}H NMR spectrum (C_6D_6, 25 °C) of complex **XXVIII$_Y$**.

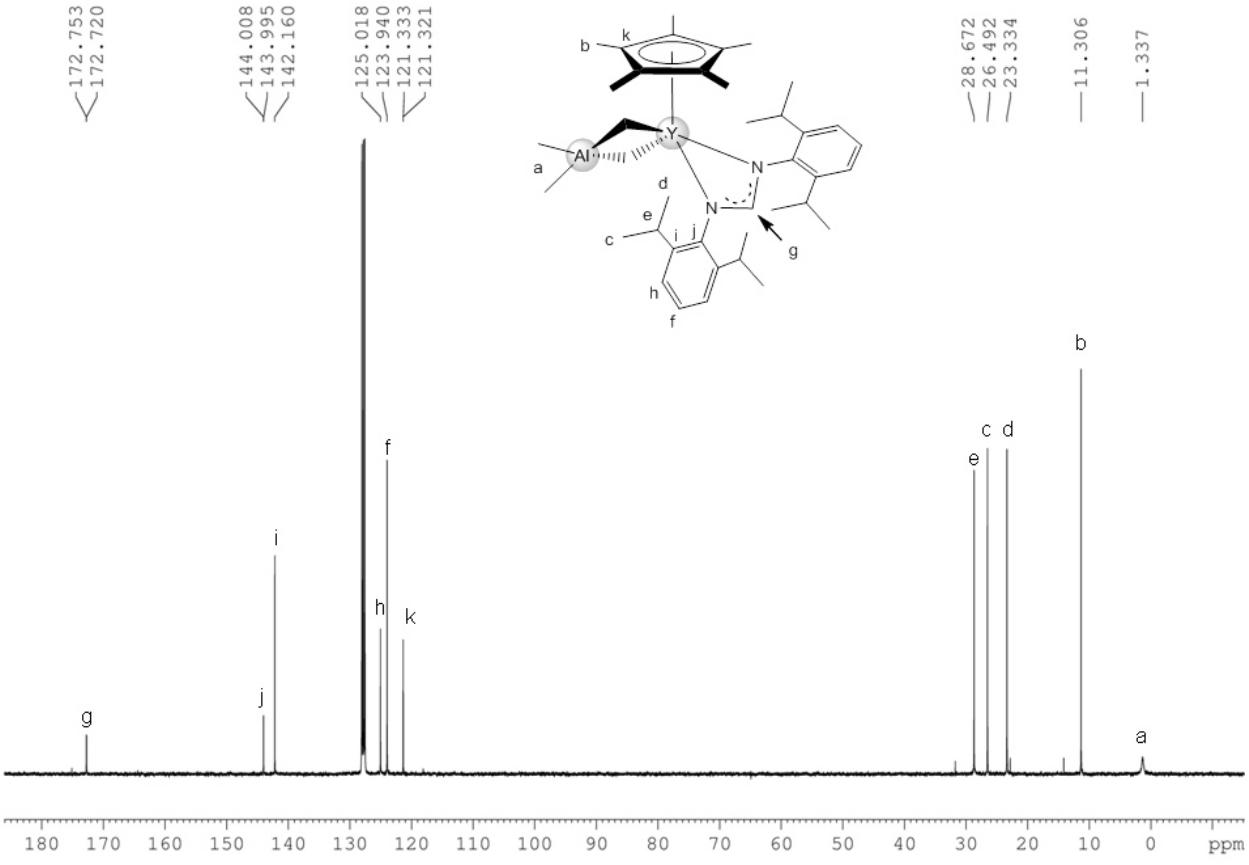

Figure 3: ^{13}C NMR spectrum (C_6D_6, 25 °C) of complex **XXVIII$_Y$**.

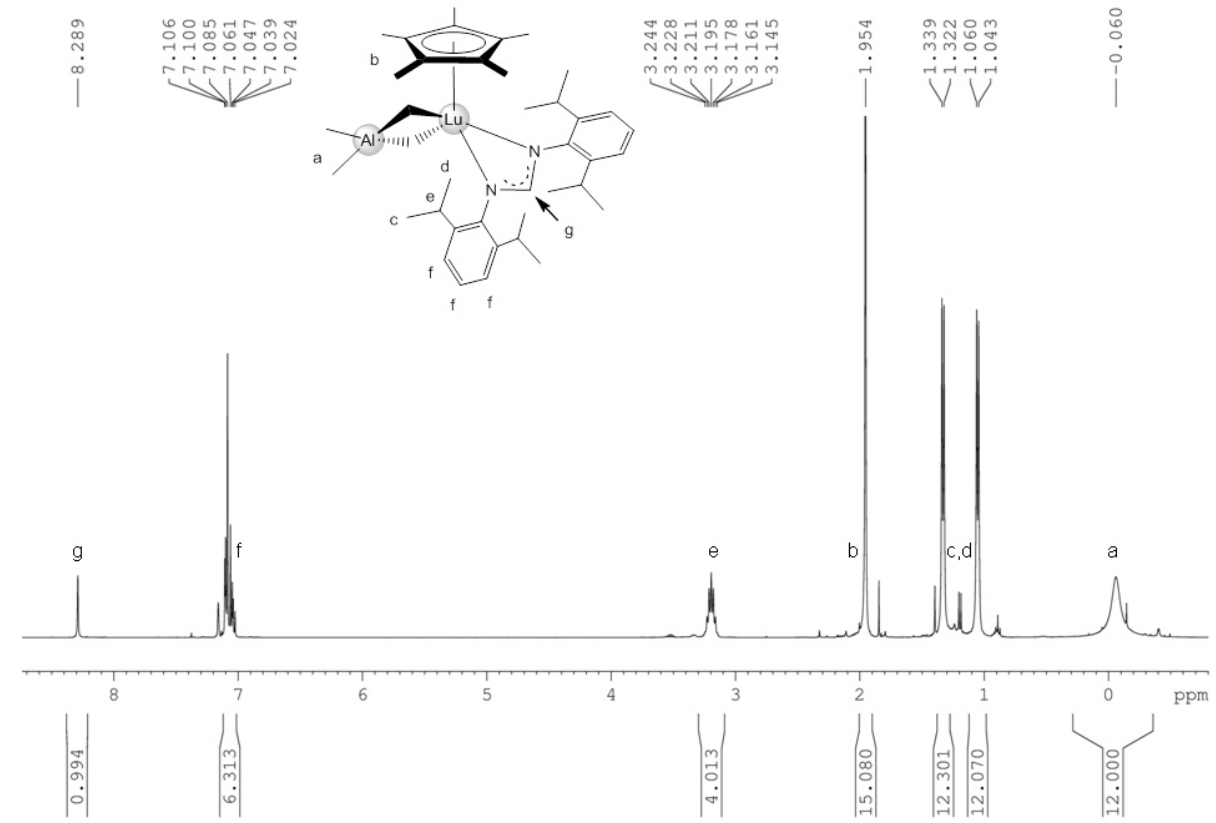

Figure 4: ^{1}H NMR spectrum (C_6D_6, 25 °C) of complex **XXVIII$_{Lu}$**.

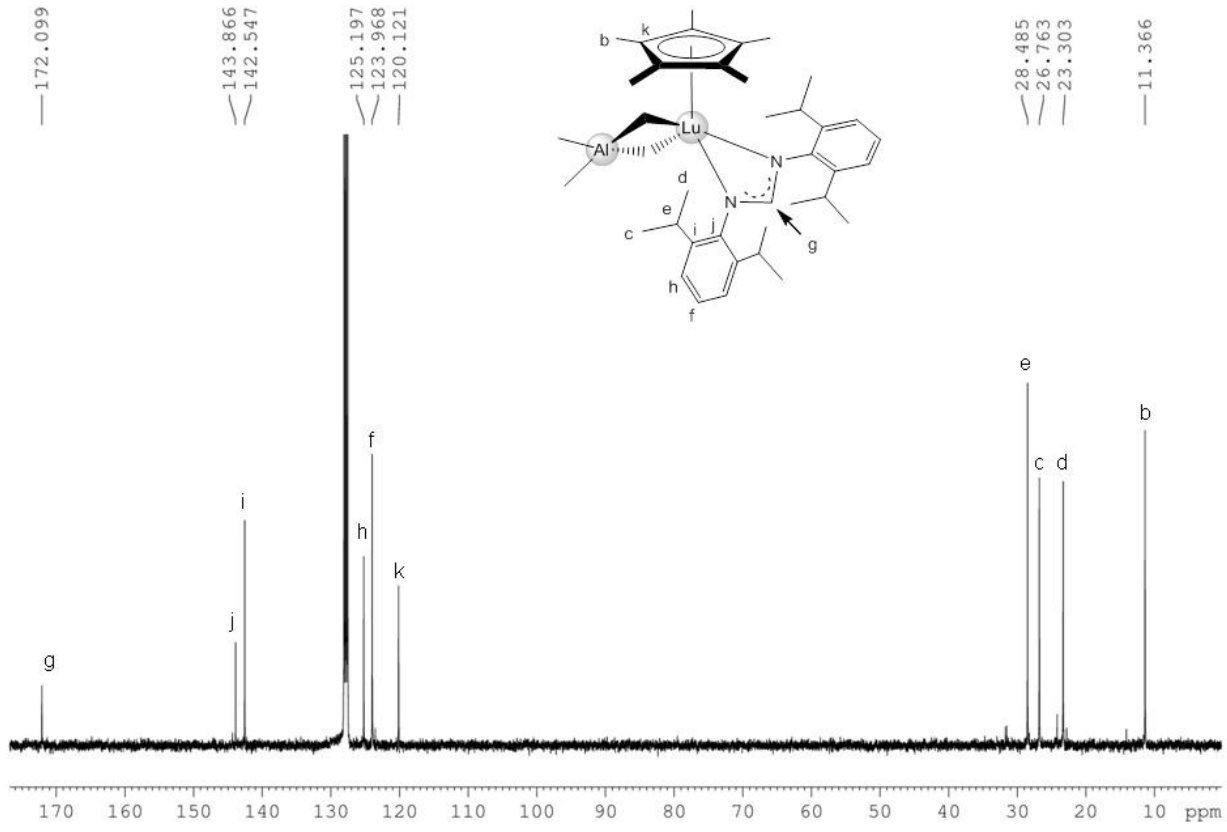

Figure 5: ^{13}C NMR spectrum (C_6D_6, 25 °C) of complex **XXVIII$_{Lu}$**.

Table 1. Selected examples of isoprene polymerization in toluene at 40 °C.

run[a]	catalyst[b]	t (h)	yield	*cis*-	*trans*-	3,4[c]	M_n[d] (x 10^5)	M_w/M_n[d]	ref.
1	**XXVIII$_{Lu}$/A**	12	>99	31.9	9.9	58.2	25.0	1.49	
2	**XXVIII$_{Lu}$/B**	12	>99	32.4	10.1	57.5	30.6	1.47	
3	**XXVIII$_{Lu}$/C**	12	-	-	-	-	-	-	
4[e]	**[Lu^{I}]/A**	0.25	>99	73.9	19.7	6.4	10.0	1.49	
5[e]	**[Lu^{I}]/B**	0.25	>99	70.3	20.3	9.4	9.5	1.45	
6[e]	**[Lu^{I}]/C**	0.5	26	74.6	20.7	4.7	11.0	1.39	[9]
7[f]	**[Lu^{II}]/C**	24	34	21.2	68.4	10.4	3.0	1.97	[9]

[a]Conditions: 0.02 mmol precatalyst, [Ln]/[cocat] = 1:1, 8 mL solvent, 20 mmol isoprene. [b]Co-catalyst: **A** = $[Ph_3C][B(C_6F_5)_4]$, **B** = $[PhNMe_2H][B(C_6F_5)_4]$ **C** = $B(C_6F_5)_3$; [c]Determined by ^1H and ^{13}C NMR spectroscopy in $CDCl_3$; [d]Determined by means of size-exclusion chromatography (SEC) against polystyrene standards; [e][Lu^{I}] = $[Cp^*Lu(AlMe_4)_2]$; [f][Lu^{II}] = $[Cp^*Lu((Me_3Al\{B(NDippCH)_2\}_2)_2]$.

[1] M. L. Cole, G. B. Deacon, C. M. Forsyth, P. C. Junk, K. Konstas, J. Wang, *Chem. – Eur. J.* **2007**, *13*, 8092-8110.

[2] F. T. Edelmann, *Chem. Soc. Rev.* **2009**, *38*, 2253-2268.

[3] F. T. Edelmann, *Chem. Soc. Rev.* **2012**, *41*, 7657-7672.

[4] A. A. Trifonov, *Coord. Chem. Rev.* **2010**, *254*, 1327-1347.

[5] S. Hamidi, L. N. Jende, H. Martin Dietrich, C. Maichle-Mössmer, K. W. Törnroos, G. B. Deacon, P. C. Junk, R. Anwander, *Organometallics* **2013**, *32*, 1209-1223.

[6] S. Hamidi, H. M. Dietrich, D. Werner, L. N. Jende, C. Maichle-Mössmer, K. W. Törnroos, G. B. Deacon, P. C. Junk, R. Anwander, *Eur. J. Inorg. Chem.* **2013**, 2460-2466.

[7] N. Dettenrieder, H. M. Dietrich, C. Schädle, C. Maichle-Mössmer, K. W. Törnroos, R. Anwander, *Ange. Chem. Int. Ed.* **2012**, *51*, 4461-4465.

[8] H. M. Dietrich, H. Grove, K. W. Törnroos, R. Anwander, *J. Am. Chem. Soc.* **2006**, *128*, 1458-1459.

[9] N. Dettenrieder, C. O. Hollfelder, L. N. Jende, C. Maichle-Mössmer, R. Anwander, *Organometallics* **2014**, *33*, 1528-1531.

F Publications

Paper I

JOHN WILEY AND SONS LICENSE
TERMS AND CONDITIONS

Apr 07, 2015

This Agreement between Lars Jende ("You") and John Wiley and Sons ("John Wiley and Sons") consists of your license details and the terms and conditions provided by John Wiley and Sons and Copyright Clearance Center.

License Number	3603711336104
License date	Apr 07, 2015
Licensed Content Publisher	John Wiley and Sons
Licensed Content Publication	Chemistry - A European Journal
Licensed Content Title	Rare-Earth-Metal Alkylaluminates Supported by N-Donor-Functionalized Cyclopentadienyl Ligands: C□H Bond Activation and Performance in Isoprene Polymerization
Licensed Content Author	Lars N. Jende,Cäcilia Maichle-Mössmer,Reiner Anwander
Licensed Content Date	Oct 21, 2013
Pages	13
Type of use	Dissertation/Thesis
Requestor type	Author of this Wiley article
Format	Electronic
Portion	Full article
Will you be translating?	No
Title of your thesis / dissertation	Donor-Substituted Cyclopentadienyl Ligands in Rare-Earth Metal-Based Isoprene Polymerization
Expected completion date	May 2015
Expected size (number of pages)	108
Requestor Location	Lars Jende Eichhaldenstr 23 Tuebingen, Germany 72074 Attn: Lars Jende
Billing Type	Invoice
Billing Address	Lars Jende Eichhaldenstr 23 Tuebingen, Germany 72074 Attn: Lars Jende
Total	0.00 EUR

DOI: 10.1002/chem.201302388

Rare-Earth-Metal Alkylaluminates Supported by N-Donor-Functionalized Cyclopentadienyl Ligands: C–H Bond Activation and Performance in Isoprene Polymerization

Lars N. Jende, Cäcilia Maichle-Mössmer, and Reiner Anwander*[a]

Abstract: Homoleptic tetramethylaluminate complexes $[Ln(AlMe_4)_3]$ (Ln = La, Nd, Y) reacted with HCp^{NMe2} (Cp^{NMe2} = 1-[2-(*N*,*N*-dimethylamino)-ethyl]-2,3,4,5-tetramethyl-cyclopentadienyl) in pentane at −35 °C to yield half-sandwich rare-earth-metal complexes, $[\{C_5Me_4CH_2CH_2NMe_2\text{-}(AlMe_3)\}Ln(AlMe_4)_2]$. Removal of the N-donor-coordinated trimethylaluminum group through donor displacement by using an equimolar amount of Et_2O at ambient temperature only generated the methylene-bridged complexes $[\{C_5Me_4CH_2CH_2NMe(\mu\text{-}CH_2)AlMe_3\}Ln(AlMe_4)]$ with the larger rare-earth-metal ions lanthanum and neodymium. X-ray diffraction analysis revealed the formation of isostructural complexes and the C–H bond activation of one aminomethyl group. The formation of $Ln(\mu\text{-}CH_2)Al$ moieties was further corroborated by ^{13}C and $^{1}H\text{-}^{13}C$ HSQC NMR spectroscopy. In the case of the largest metal center, lanthanum, this C–H bond activation could be suppressed at −35 °C, thereby leading to the isolation of $[(Cp^{NMe2})La(AlMe_4)_2]$, which contains an intramolecularly coordinated amino group. The protonolysis reaction of $[Ln(AlMe_4)_3]$ (Ln = La, Nd) with the anilinyl-substituted cyclopentadiene HCp^{AMe2} (Cp^{AMe2} = 1-[1-(*N*,*N*-dimethylanilinyl)]-2,3,4,5-tetramethylcyclopentadienyl) at −35 °C generated the half-sandwich complexes $[(Cp^{AMe2})Ln(AlMe_4)_2]$. Heating these complexes at 75 °C resulted in the C–H bond activation of one of the anilinium methyl groups and the formation of $[\{C_5Me_4C_6H_4NMe(\mu\text{-}CH_2)AlMe_3\}Ln(AlMe_4)]$ through the elimination of methane. In contrast, the smaller yttrium metal center already gave the aminomethyl-activated complex at −35 °C, which is isostructural to those of lanthanum and neodymium. The performance of complexes $[\{C_5Me_4CH_2CH_2NMe(\mu\text{-}CH_2)AlMe_3\}\text{-}Ln(AlMe_4)]$, $[(Cp^{AMe2})Ln(AlMe_4)_2]$, and $[\{C_5Me_4C_6H_4NMe(\mu\text{-}CH_2)AlMe_3\}\text{-}Ln(AlMe_4)]$ in the polymerization of isoprene was investigated upon activation with $[Ph_3C][B(C_6F_5)_4]$, $[PhNMe_2H][B(C_6F_5)_4]$, and $B(C_6F_5)_3$. The highest stereoselectivities were observed with the lanthanum-based pre-catalysts, thereby producing polyisoprene with *trans*-1,4 contents of up to 95.6 %. Narrow molecular-weight distributions ($M_w/M_n < 1.1$) and complete consumption of the monomer suggested a living-polymerization mechanism.

Keywords: C–H bond activation · isoprene · lanthanides · polymerization · rare-earth metals

Introduction

More than a century ago, in 1909, Fritz Hofmann, a German chemist at Bayer Werke, patented the first synthetic rubber, named "Buna" after its starting materials, butadiene and sodium (ger. Natrium).[1] Thirty years later, caused by the continuously growing demand for economically viable rubber and forced by the rise of World War II, rubber synthesis and process technology were optimized, as exemplified by monomer variation. Even after the war ended, the market for rubber products grew steadily and exceeded the supply of natural rubber (NR). To date, more than 15 million tons of synthetic rubber (SR) are produced per year, which represents over 55 % of the total rubber production.[2] Multicomponent Ziegler-type catalysts, based on rare-earth metals such as neodymium, are commonly used for the highly *cis*-1,4-selective polymerization of 1,3-dienes, although the molecular weights and molecular-weight distributions of the products are broad and the nature of the active species is still under discussion.[3] Over the past two decades, well-defined metal–organic complexes of rare-earth elements have been assessed as single-site catalysts in the anionic coordination polymerization of 1,3-dienes to gain more insight into the polymerization mechanism. Cyclopentadienyl ancillary ligands not only impart kinetic and thermodynamic stability for modeling co-catalyst interactions, but also drastically affect the stereoregular polymerization of 1,3-dienes.[4] We have recently developed a library of rare-earth-metal-based bis(tetramethylaluminate) complexes $[(L)Ln(AlMe_4)_2]$ (L = monoanionic ancillary ligand) to gain a detailed understanding of the effects of the ancillary ligand and the co-catalyst on isoprene polymerization.[5] The first entries in this library were half-sandwich complexes $[(Cp^R)Ln(AlMe_4)_2]$ (Ln = Y, Nd, La, $Cp^R = [C_5Me_5]$; Ln =

[a] L. N. Jende, Dr. C. Maichle-Mössmer, Prof. Dr. R. Anwander
Institut für anorganische Chemie
Universität Tübingen
Auf der Morgenstelle 18, 72076 Tübingen (Germany)
Fax: (+49) 7071-29-2436
E-mail: reiner.anwander@uni-tübingen.de

Supporting information for this article is available on the WWW under http://dx.doi.org/10.1002/chem.201302388.

Nd, La, $Cp^R = [C_5Me_4H]$; Ln = Lu, Y, Sm, Nd, La, $Cp^R = [1,3\text{-}(Me_3Si)_2C_5H_3]$, $[C_5H_4SiMe_3]$; Ln = Sm, Nd, La, $Cp^R = [1,2,3\text{-}(Me_3C)_3C_5H_2]$), which have afforded good-to-excellent catalytic activities with high *trans*-1,4 selectivity upon activation with borate co-catalysts $[Ph_3C][B(C_6F_5)_4]$ or $[PhNMe_2H][B(C_6F_5)_4]$.

Because the steric saturation of the rare-earth-metal centers crucially affects the stereoregular polymerization of 1,3-dienes, it seemed a natural consequence to extensively probe any advanced functionalization of the cyclopentadienyl ligand. On the other hand, the utilization of hard donor functionalities, according to Pearson's hard and soft acids and bases (HSAB) concept, such as neutral amines and monoanionic amides, could be envisaged as a delicate issue, owing to their preferred interaction with widely used organoaluminum co-catalysts. Whilst linked dianionic amido-cyclopentadienyl ligands have been routinely employed for the synthesis of rare-earth-metal-based constrained-geometry catalysts (CGC),[6] thereby successfully promoting α-olefin-polymerization reactions,[7] there have only been a few reported examples of half-sandwich rare-earth-metal–dialkyl complexes with neutral nitrogen donors. In 2003, Hessen and co-workers utilized a cyclopentadienyl-amine–scandium fragment to isolate a rare example of a 1,3-butadiene complex, $[\{C_5H_4(CH_2)_2NMe_2\}Sc(2,3\text{-dimethyl-}1,3\text{-butadiene})]$ (Scheme 1, **A**),[8] which produced a dimeric imide complex upon benzonitrile insertion. Several years later, Otero et al. described heteroscorpionate-supported scandium and yttrium complexes (Scheme 1, **B**)[9] and Hou and co-workers reported the methylene-bridged binuclear complex $[(\{C_5Me_4C_6H_4NMe(\mu\text{-}CH_2)\}Sc(CH_2SiMe_3))_2]$ (Scheme 1, **C**).[4a] More recently, pyridyl-methylene- and phosphazene-functionalized cyclopentadienyl complexes were exploited by Cui and co-workers[10] and Sundermeyer and co-workers[11] for the polymerization of styrene and ethylene (Scheme 1, **D** and **E**), respectively. Anilinyl- (Scheme 1, **C**) and pyridinyl-functionalized cyclopentadienyl ligands were also recently applied to the synthesis of half-sandwich bis(allyl) complexes.[12]

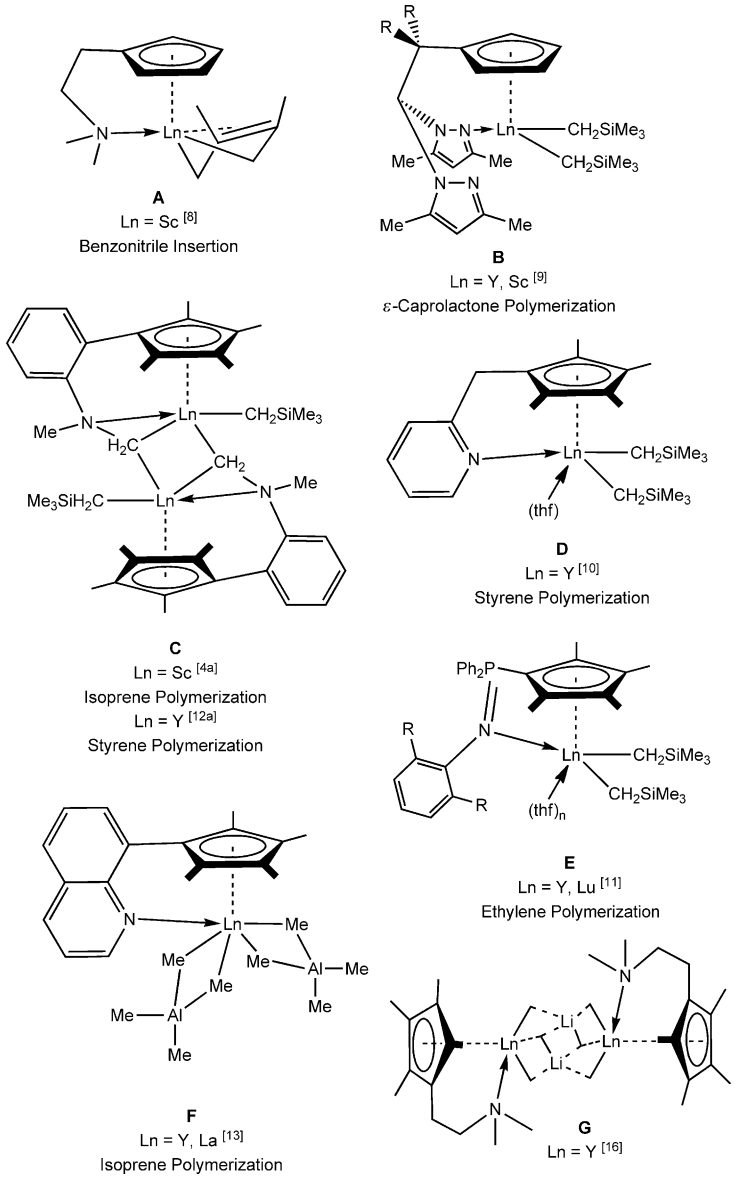

Scheme 1. Examples of N-functionalized half-sandwich rare-earth-metal–bis(alkyl) complexes.

As an extension of our half-sandwich bis(tetramethylaluminate) library, we initially examined the performance of the quinolyl-substituted complexes $[(Cp^Q)Ln(AlMe_4)_2]$ (Cp^Q = 1-(8-quinolyl)-2,3,4,5-tetramethyl-cyclopentadienyl; Scheme 1, **F**).[13] The hard quinolyl donor did not interfere with the formation of rare-earth-metal–bis(tetramethylaluminate) complexes, which displayed good activity in isoprene polymerization. Herein, we report a full account of the feasibility of *N*,*N*-dimethylamino-sidearm-substituted tetramethylcyclopentadienyl ligands, Cp^{NMe2} ($C_5Me_4CH_2CH_2NMe_2$, developed by Jutzi and Dahlhaus)[14] and Cp^{AMe2} ($C_5Me_4C_6H_4NMe_2$, reported by Enders et al.).[15] Apart from their inherent dual reactivity towards homoleptic complexes $[Ln(AlMe_4)_3]$, which contained the distinct

Lewis acidic metal centers Ln^{III} and Al^{III}, the performance of the resulting half-sandwich complexes towards 1,3-diene polymerization has also been investigated. Preliminary work on alternative synthesis procedures involved the formation of $[\{(Cp^{NMe2})YMe_2(MeLi)\}_2]$, which features a rare example of a structurally authenticated half-sandwich dimethyl complex (Scheme 1, **G**).[16]

Results and Discussion

Synthesis: The protonolysis reactions of homoleptic rare-earth-metal–tetramethylaluminate complexes, $[Ln(AlMe_4)_3]$ (Ln = Y, La, Nd),[17] with one equivalent of the N-donor-functionalized cyclopentadiene HCp^{NMe2} (Cp^{NMe2} = 1-[2-(*N*,*N*-dimethylamino)-ethyl]-2,3,4,5-tetramethyl-cyclopentadienyl) in pentane at −35 °C yielded their corresponding rare-earth-metal–bis(tetramethylaluminate) complexes, $[\{C_5Me_4CH_2CH_2NMe_2(AlMe_3)\}Ln(AlMe_4)_2]$ (**1**; Scheme 2i). In contrast to previous reactions with cyclopentadiene proligands that were devoid of any donor functionality, the temporary formation of a precipitate was observed. We hypothesize that, in the first step, the donor-induced cleavage of one tetramethylaluminate moiety occurred, under the formation of a proligand–trimethylaluminum adduct, along with the formation of a transient rare-earth-metal–methyl complex (**I**^{1}, Scheme 3). These highly reactive $Ln-CH_3$ species (**I**^{1}) are proposed to deprotonate the cyclopentadiene group, thereby giving complexes **1**. Accordingly, upon stirring for 15 min, the reaction mixture became completely clear and gas evolution (elimination of methane) was observed. Efforts to remove the trimethylaluminum, coordinated by the proligand, under vacuum or by heating were unsuccessful (see below). The addition of one equivalent of

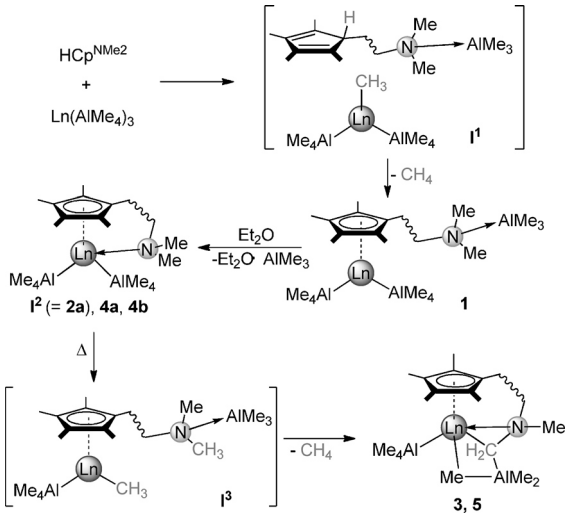

Scheme 3. Proposed C–H bond activation sequence through intramolecular donor-induced aluminate cleavage.

Et_2O to a solution of complexes **1a** (Ln = La) and **1b** (Ln = Nd) at ambient temperature gave instantaneous gas evolution and C–H bond-activated complexes $[\{Cp^{NMe}(\mu\text{-}CH_2)AlMe_3\}Ln(AlMe_4)]$ (Ln = La (**3a**), Nd (**3b**)) could be isolated after removal of the diethyl-ether–trimethylaluminum adduct under vacuum (Scheme 2ii). However, the addition of donor (= solvent) molecules to yttrium complex **1c** under the same conditions led to multiple C–H bond activations and intractable products. The temperature-controlled formation of C–H bond-activated lanthanum and neodymium complexes (**3a** and **3b**, respectively) was confirmed by donor addition to lanthanum complex **1a** at −35 °C. This "low-temperature" reaction afforded complex $[(Cp^{NMe2})La(AlMe_4)_2]$ (**2a**) through the donor-assisted displacement of trimethylaluminum, followed by an intramolecular coordination of the nitrogen donor to the rare-earth-metal center (Scheme 2iii). Intramolecular donor-coordinated complexes **2**, which were only isolable for the largest rare-earth-metal center (lanthanum), were also observed as intermediate species **I**^{2} (Scheme 3). C–H bond activation was only established when complex **2a** was redissolved in toluene and allowed to warm to ambient temperature, thereby forming complex **3a** (Scheme 2iv). Mechanistically, this process would involve a competitive donor-coordination step with an intramolecular donor-induced aluminate cleavage (Scheme 3). The thus-formed highly reac-

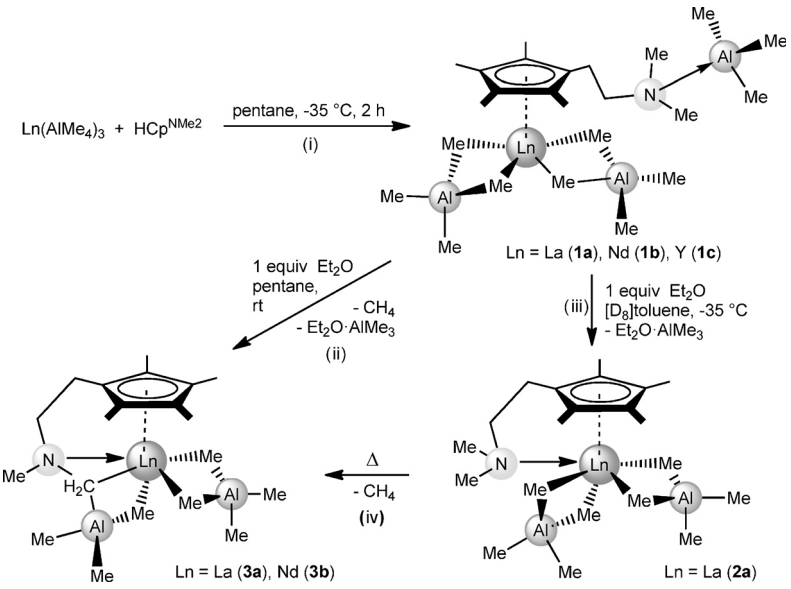

Scheme 2. Synthesis of $[\{Cp^{NMe2(AlMe3)}\}Ln(AlMe_4)_2]$ (**1**), $[(Cp^{NMe2})Ln(AlMe_4)_2]$ (**2**), and $[\{Cp^{NMe}(\mu\text{-}CH_2)AlMe_3\}Ln(AlMe_4)_2]$ (**3**) through a protonolysis procedure and the consecutive donor-induced removal of $AlMe_3$.

tive transient Ln–CH_3 species (**I**[3]) could afford C–H bond-activated and thermally stable complexes **3**. Similar tetramethylaluminate-promoted C–H bond activations have previously been observed in diamido-pyridine-supported yttrium and lutetium complexes that involved the isopropyl groups of the ancillary ligand backbone,[18a] as well as in a lanthanum–formamidinate complex that involved the *o*-methyl group of a mesityl substituent.[18b]

In contrast, the protonolysis of $[Ln(AlMe_4)_3]$ (Ln = La, Nd, Y)[17] with one equivalent of HCp^{AMe2} (Cp^{AMe2} = 1-[1-(*N*,*N*-dimethylanilinyl)]-2,3,4,5-tetramethyl-cyclopentadienyl) in pentane at −35 °C yielded the bis(tetramethyaluminate) complexes $[(Cp^{AMe2})Ln(AlMe_4)_2]$ (**I**[2]; Ln = La (**4a**), Nd (**4b**); Scheme 3) or the C–H bond-activated complex $[\{C_5Me_4C_6H_4NMe(\mu\text{-}CH_2)AlMe_3\}Y(AlMe_4)]$ (**5c**) from the outset (Scheme 4).

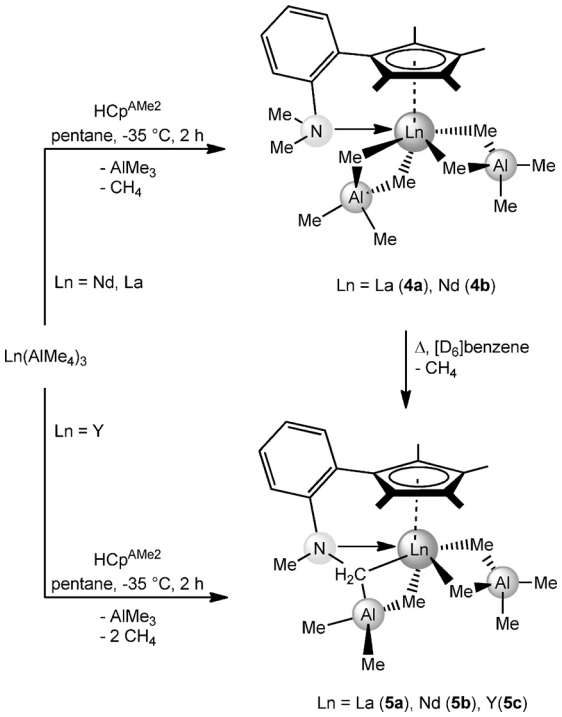

Scheme 4. Synthesis of $[(Cp^{AMe2})Ln(AlMe_4)_2]$ (**4**) and $[\{Cp^{AMe}(\mu\text{-}CH_2)AlMe_3\}Ln(AlMe_4)]$ (**5**) through a protonolysis procedure.

This reaction outcome can be rationalized on the basis of the considerably enhanced rigidity of the Cp^{AMe2} ligand and the smaller radius and higher Lewis acidity of the Y^{III} metal center. Nevertheless, heating the bis(tetramethyaluminate) complexes $[(Cp^{AMe2})Ln(AlMe_4)_2]$ (**4**) in $[D_6]$benzene at 75 °C for 16 h (in an NMR experiment) resulted in the highly selective C–H bond activation of one NCH_3 group, along with methane elimination and the quantitative formation of complexes **5** (Scheme 3). Notably, analogous C–H bond-activation reactions of cyclopentadienyl-linked NMe_2 units have previously been observed,[19] but a dependence on the size of the rare-earth metal or temperature has not been reported. In addition, owing to the use of the sterically less-shielding $\sigma(\eta^1)$-coordinating CH_2SiMe_3 groups, only binuclear mono-alkyl complexes $[(\{C_5Me_4C_6H_4NMe(\mu\text{-}CH_2)\}Ln(CH_2SiMe_3))_2]$ (Ln = Y, Sc) were obtained.[4a,12a]

NMR spectroscopy: Good-quality ^1H and ^{13}C NMR spectra in $[D_6]$benzene could be obtained for all diamagnetic complexes **1**–**5** (Ln = La, Y; see the Supporting Information). Thus, non-activated complexes **1a**, **1c**, and **2a** showed the expected set of signals for the coordinated Cp^{NMe2} ligand.[20] The four methyl groups of the Cp ring appeared as two singlets (**1a**: δ = 1.94, 1.90 ppm; **1c**: δ = 1.92, 1.82 ppm; **2a**: δ = 1.89, 1.79 ppm) and the two aminomethyl groups appeared as a singlet (**1a**: δ = 1.79 ppm, **1c**: δ = 1.71 ppm, **2a**: δ = 1.70 ppm). In complexes **1a** and **1c**, the protons of the ethylene bridge appeared as two multiplets (**1a**: δ = 2.72, 2.11 ppm; **1c**: 2.66, 2.14 ppm), whilst in complex **2**, they appeared as two triplets (δ = 2.12, 2.02 ppm). Beside the signal for the bis(tetramethylaluminate) moiety (**1a**: δ = −0.32 ppm; **1c**: δ = −0.33 ppm; **2a**: δ = −0.27 ppm), the signal of the trimethylaluminum adduct appeared at higher field (**1a**: δ = −0.54 ppm; **1c**: δ = −0.44 ppm). The spectrum for complex **4a** also showed three singlets for the methyl groups at δ = 2.16 (N*Me*$_2$), 1.96, and 1.71 ppm (Cp*Me*$_4$). The signals of the aromatic anilinyl protons were found within the range δ = 6.99–6.66 ppm as four multiplets. At higher field, only one sharp singlet was observed for the $[Al(\mu\text{-}Me)_2Me_2]^-$ moieties (δ = −0.10 ppm), thus indicating a rapid exchange between the terminal and bridging methyl groups in complex **4a**.[17b]

The ambient-temperature ^1H NMR spectra of complexes **3a**, **5a**, and **5c** in $[D_6]$benzene showed unexpected sets of signals. Two narrow ^1H signals with an integral ratio of 12:9 were observed in the high-field region, which could be assigned to one $[AlMe_4]^-$ moiety (**3a**: δ = −0.21 ppm, **5a**: −0.14 ppm, **5c**: δ = −0.21 ppm) and one $AlMe_3$ motif (**3a** δ = −0.41 ppm, **5a**: δ = −0.44 ppm, **5c**: −0.49 ppm), thus indicating fluxional behavior. Interestingly, the typical ^1H-^{89}Y scalar coupling over two bonds for yttrium–aluminate bonding was not observable for complex **5c**.[21] The signals of the aromatic anilinyl protons in complexes **5a** and **5c** were found within the range δ = 7.03–6.85 ppm and δ = 7.07–6.87 ppm, respectively. Instead of the expected set of three singlets for the six methyl groups of the anionic Cp^{NMe2} ligand (2,5M*e*-Cp, 3,4M*e*-Cp, N*Me*$_2$), five distinct resonances were detected within the characteristic range. ^1H-^{13}C HSQC NMR spectroscopy allowed for complete signal assignment and is discussed for complex **3a** herein as a representative example (Figure 1).

C–H bond activation of one aminomethyl group induced the formation of a $Ln(\mu\text{-}CH_2)Al$ moiety, thereby leading to the formation of a stereogenic center at the nitrogen atom. Hence, all of the Cp–Me groups, as well as the protons of the CH_2CH_2 linker (carbon atoms C10 and C11, Figure 2), became magnetically inequivalent, thus showing eight separate resonances. The four methyl groups of the Cp ring appeared within the region δ = 2.00–1.77 ppm in the ^1H NMR spectrum and δ = 12.4–11.0 ppm in the ^{13}C NMR spectrum

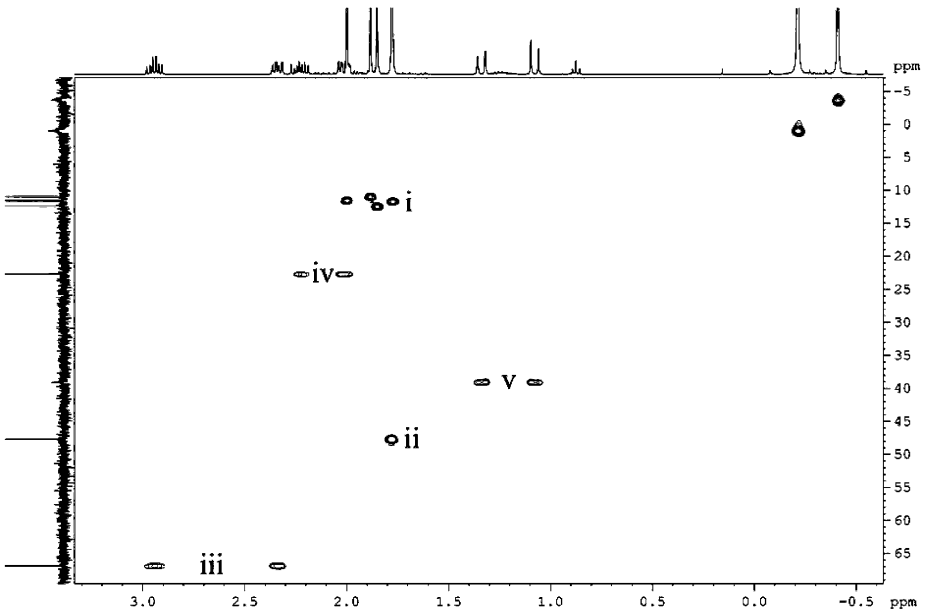

Figure 1. 2D ^{1}H-^{13}C COSY NMR spectrum of [{Cp^{NMe}(μ-CH_2)$AlMe_3$}Ln($AlMe_4$)] (**3a**) in [D_6]benzene at 298 K. The 1D ^{13}C NMR spectrum is shown on the left edge of the contour plot, whilst the ^{1}H NMR spectrum is shown at the top.

(**5a**: $\delta = 2.21$–$1.73/12.3$–10.8 ppm, **5c**: $\delta = 2.05$–$1.64/12.7$–11.4 ppm; Figure 1 i). In addition, complex **3a** showed signals within the regions $\delta = 2.98$–2.91 and 2.37–2.31 ppm, which correlate with the C11 carbon atom ($\delta = 66.8$ ppm, Figure 1 iii), as well as multiplets at $\delta = 2.27$–2.19 and 2.04–1.98 ppm, which correlate with the C10 carbon atom ($\delta =$ 22.7 ppm, Figure 1 iv). The protons of the aminomethyl group appeared at $\delta = 1.78$ ppm and showed a correlation with the ^{13}C NMR signal at $\delta = 47.7$ ppm (**5a**: $\delta = 2.21/45.5$ ppm, **5c**: $\delta = 2.24/47.4$ ppm; Figure 1 ii). The protons of the activated (μ-CH_2) moiety each showed a discrete doublet in the ^{1}H NMR spectrum at $\delta = 1.34$ and 1.08 ppm, respectively, which correlated with the peak at $\delta = 39.1$ ppm in the ^{13}C NMR spectrum (**5a**: $\delta = 1.94$, $1.72/54.8$ ppm; **5c**: $\delta =$ 2.03, $1.83/52.2$ ppm; Figure 1 v).

Solid-state structures: Single crystals of [{$Cp^{NMe2(AlMe3)}$}Ln($AlMe_4$)$_2$] (Ln = La (**1a**), Nd (**1b**), Y (**1c**)) suitable for X-ray crystallographic structure determination were grown from saturated solutions in pentane at −35 °C. Complexes **1a** and **1b**, which contained the larger Ln^{III} ions, crystallized in the monoclinic space groups $P2_1/n$ and $P2_1/c$, respectively, whilst complex **1c**, which contained the smaller yttrium ion, crystallized in the orthorhombic space group $P2_12_12_1$. The coordination mode of the ligands was isostructural in all three complexes and, therefore, the molecular structure of complex **1a** is shown in Figure 2 as a representative example.

The cyclopentadienyl ligand coordinates the rare-earth-metal center in a η^5 mode, whilst the nitrogen atom of the amino group coordinates one trimethylaluminum molecule. Comparable to the half-sandwich rare-earth-metal–bis(aluminate) complexes [(C_5Me_5)Ln($AlMe_4$)$_2$], one of the [$AlMe_4$]$^-$ ligands coordinates in the routinely observed η^2 fashion, thus forming an almost-planar heterobimetallic moiety with inter-planar angles (C14LnC15–C14Al2C15) of 1.75° (**1a**), 3.49° (**1b**), and 8.54° (**1c**), while the second [$AlMe_4$]$^-$ ligand forms an additional close contact with one methyl group (Ln···C19; 3.084(2) (**1a**), 3.053(2) (**1b**), and 3.218(6) Å (**1c**)), accompanied by a bent coordination mode, thereby resulting in interplanar angles (C18LnC19–C18Al2C19) of 64.66° (**1a**), 63.95° (**1b**), and 58.23° (**1c**). Carbon–metal bond lengths are typically affected by the size of the Ln^{III} ion and are in good agreement with those of [(C_5Me_5)La($AlMe_4$)$_2$],[22]

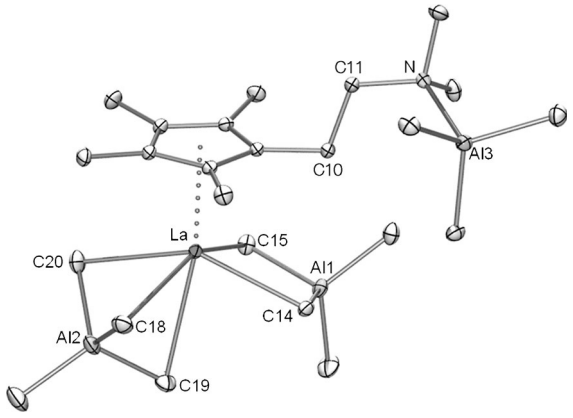

Figure 2. Molecular structure of [{$Cp^{NMe2(AlMe3)}$}La($AlMe_4$)$_2$] (**1a**), representative of isostructural complexes **1**. Atomic displacement parameters are set at the 50% level; hydrogen atoms are omitted for clarity.

[($CpMe_4H$)Nd($AlMe_4$)$_2$],[5d] and [(C_5Me_5)Y($AlMe_4$)$_2$].[23] Selected structural parameters are listed in Table 1.

Complex [(Cp^{NMe2})La($AlMe_4$)$_2$] (**2a**) crystallized from a saturated [D_8]toluene/*n*-hexane mixture at −35 °C in the monoclinic space group $P2_1/c$ (Figure 3). Note: The temperature should not exceed 0 °C during all operations to prevent C–H bond activation.

The rare-earth-metal center is η^2 coordinated by two [$AlMe_4$]$^-$ moieties and the N-donor-functionalized Cp ligand coordinates in a η^5:κ^1 fashion through the Cp ring and the nitrogen atom. This geometry is similar to that of the [(Cp^{AMe2})Ln($AlMe_4$)$_2$] (Ln = La (**4a**), Nd (**4b**)) complexes, which contains the anilinyl-functionalized cyclopentadienyl ligand. Single crystals of complexes **4a** and **4b** were

Table 1. Selected bond lengths and angles in complexes **1**.

	1a (Ln = La)	**1b** (Ln = Nd)	**1c** (Ln = Y)
Bond [Å]			
Ln1−C(Cp)	2.764(1)–2.806(1)	2.706(1)–2.748(1)	2.657(5)–2.628(5)
Ln1−C14	2.691(1)	2.630(2)	2.576(4)
Ln1−C15	2.716(2)	2.650(1)	2.546(6)
Ln1−C18	2.830(2)	2.779(2)	2.686(5)
Ln1−C19	3.084(2)	3.053(2)	3.218(6)
Ln1−C20	2.774(2)	2.748(1)	2.671(5)
N1−Al3	2.063(1)	2.065(2)	2.065(4)
Angle [°]			
C14-Ln1-C15	78.82(4)	82.7(2)	80.62(5)
C18-Ln1-C20	72.40(5)	77.1(2)	73.96(5)
C14-Al1-C15	111.59(6)	109.5(2)	110.51(7)
C18-Al2-C19	105.28(7)	105.3(2)	104.86(8)
C18-Al2-C20	107.20(7)	108.6(2)	108.46(7)
C19-Al2-C20	105.02(8)	105.9(2)	104.78(8)
Interplanar angle [°]			
C14Ln1C15−C14Al1C15	1.75	3.49	8.54
C18Ln1C19−C18Al2C19	64.66	63.95	58.23

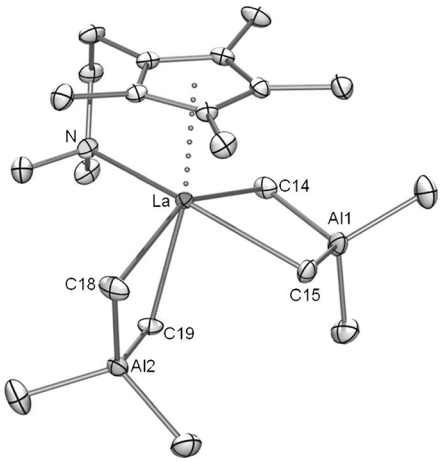

Figure 3. Molecular structure of $(Cp^{NMe2})La(AlMe_4)_2$ (**2**). Atomic displacement parameters are set at the 50% level; hydrogen atoms are omitted for clarity.

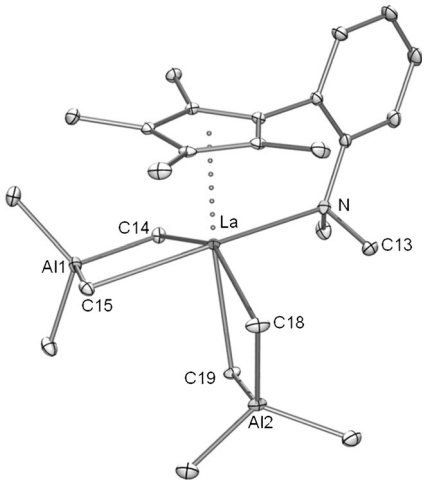

Figure 4. Molecular structure of $[(Cp^{AMe2})La(AlMe_4)_2]$ (**4a**), representative of isostructural complexes **4**. Atomic displacement parameters are set at the 50% level; hydrogen atoms are omitted for clarity.

Table 2. Selected bond lengths and angles in complexes **2** and **4**.

	2 (Ln = La)	**4a** (Ln = La)	**4b** (Ln = Nd)
Bond [Å]			
Ln1−C(Cp)	2.756(2)–2.843(2)	2.732(1)–2.846(1)	2.667(2)–2.788(1)
Ln1−C14	2.788(3)	2.764(1)	2.711 (1)
Ln1−C15	2.729(2)	2.728(1)	2.670(1)
Ln1−C18	2.810(3)	2.798(2)	2.748 (1)
Ln1−C19	2.820(2)	2.883(1)	2.856(1)
Ln1−N1	2.735(2)	2.771(1)	2.745(2)
Angle [°]			
C14-Ln1-N1	82.78(7)	84.03(4)	82.90(7)
C18-Ln1-N1	108.61(7)	105.99(4)	104.78(7)
C19-Ln1-N1	83.58(7)	88.50(4)	86.42(6)
C14-Ln1-C15	76.45(8)	77.31(4)	78.82(8)
C18-Ln1-C19	73.29(8)	73.48(4)	73.97(8)
C14-Al1-C15	111.8(1)	111.95(6)	111.8(1)
C18-Al2-C19	110.9(1)	112.09(6)	111.6(1)
Interplanar angle [°]			
C18Ln1C19−C18Al2C19	11.42	3.22	4.05
C14Ln1C15−C14Al1C15	1.30	5.97	6.87

obtained from a solution in *n*-hexane/toluene at −35 °C in the monoclinic space group $P2_1/c$ (Figure 4).

Selected bond lengths and angles in complexes **2a**, **4a**, and **4b** are listed in Table 2. In contrast to the structural motifs that were observed for the donor-free half-sandwich bis(tetramethylaluminate) complexes, in which one tetramethylaluminate moiety adopts a bent coordination, the additional nitrogen coordination afforded sterically saturated Ln^{III} metal centers, and hence, both $AlMe_4$ moieties adopt a planar arrangement (C14LnC15−C14Al1C15, **2a**: 1.30°, **4a**: 5.97°, **4b**: 6.87°; C18LnC19−C18Al2C19, **2a**: 11.42°, **4a**: 3.22°, **4b**: 4.05°).[5,17b,22–24] A similar impact of the donor on the coordination of the tetramethylaluminate was previously observed for the quinolyl-substituted half-sandwich bis(tetramethylaluminate) complexes of yttrium and lanthanum (Scheme 1, **F**), which features two planar η^2-coordinated $AlMe_4$ moieties (Y = 0.74°/2.7°, La = 0.31°/5.14°, 1.06°/5.42°).[13] Moreover, intermolecular La···P donor interactions, as observed in complex $[\{(\eta^5\text{-}PC_4Me_4)Ln(AlMe_4)_2\}_2]$, were found to counteract any additional weak La···CH_3(aluminate) bonding interactions.[24b] The Ln−C bond lengths were within the expected range and decreased with decreasing size of the Ln^{III} cation ($Ln-C_{(av)}$; **4a**: 2.793 Å, **2a**: 2.787 Å, **4b**: 2.746 Å). Notably, owing to additional donor coordination, the C19 methyl group coordinates in a *trans* manner to the cyclopentadienyl ligand, thereby featuring a Ln−C19 bond that is clearly elongated in complexes $[(Cp^{AMe2})Ln(AlMe_4)_2]$ (**4a**: 2.883(1) Å, **4b**: 2.856(1) Å), but less so for complex $[(Cp^{NMe2})La(AlMe_4)_2]$ (**2**: 2.820(2) Å). A similar electronic effect was observed for the Cp^Q-substituted complexes (2.762 (Y); 2.848, 2.856 Å

(La); Scheme 1).[13] The Ln–N bond lengths (**2a**: 2.735(2) Å, **4a**: 2.771(1) Å, **4b**: 2.745(1) Å) are comparable to those found for neutral N-donor coordination in $[Ln\{C_5H_4(CH_2)_2NMe_2\}_3]$ (La = 2.898 Å, Nd = 2.73/2.70 Å),[25] $[(C_5H_3\{(CH)_2NMe_2\}_2)LaI_2]$ (2.712–2.820 Å),[26] and $[(Cp^O)La(AlMe_4)_2]$ (2.701 Å and 2.683 Å).[13] Owing to the constrained geometry, the cyclopentadienyl ligand is slightly tilted, with the shortest metal–ring-carbon distance for the Ln–C1 bond (**2**: 2.756(2)–2.843(2) Å, **4a**: 2.732(1)–2.846(1) Å, **4b**: 2.667(2)–2.788(1) Å).

Single crystals of complexes $[\{Cp^{NMe}(\mu\text{-}CH_2)AlMe_3\}Ln(AlMe_4)]$ (Ln = La (**3**), Nd (**3b**)) and $[\{Cp^{AMe}(\mu\text{-}CH_2)AlMe_3\}Ln(AlMe_4)]$ (Ln = La (**5a**), Nd (**5b**), Y (**5c**)) suitable for X-ray structural analysis were grown from saturated solutions in pentane at −35 °C. Complexes **3** were isostructural and crystallized in the monoclinic space group $P2_1/c$. The molecular structure of complex **3a** is shown in Figure 5 as a representative example.

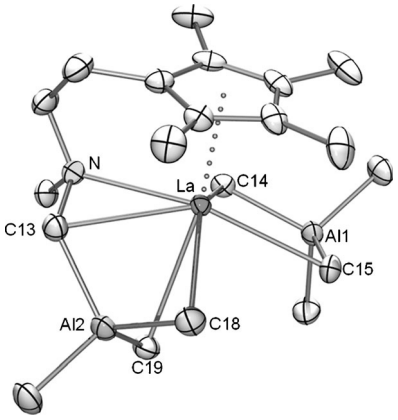

Figure 5. Molecular structure of $[\{Cp^{NMe}(\mu\text{-}CH_2)AlMe_3\}La(AlMe_4)]$ (**3a**), representative of isostructural complexes **3**. Atomic displacement parameters are set at the 50% level; hydrogen atoms are omitted for clarity.

Complex **5a** crystallized in the orthorhombic space group $P2_12_12_1$, whereas complexes **5b** and **5c** crystallized in the monoclinic space groups $P2_1/n$ and $P2_1/c$, respectively. The molecular structure of complex **5a** is shown in Figure 6.

Selected bond lengths and angles for all of the complexes are listed in Table 3. The most-striking feature of the solid-state structures of complexes **3** and **5** is the bridging Ln–(μ-CH_2)–Al(methylene) moiety, which results from C–H bond activation of one of the aminomethyl groups (Figure 5 and Figure 6). Notably, the distances between the activated CH_2 moiety and the metal center were close to those in the $[(\mu\text{-}Me)_2AlMe_2]$ units (**3a**: 2.820 Å, **3b**: 2.764 Å, **5a**: 2.836 Å, **5b**: 2.770 Å, **5c**: 2.753 Å). In contrast, the La–N bond lengths (**3a** : 2.533 Å, **3b**: 2.490 Å, **5a**: 2.578 Å, **5b**: 2.527 Å, **4c**: 2.471 Å) were markedly shorter than those for other neutral nitrogen donors, but slightly elongated compared to the η^2 (N,C) motif in the dimeric complex $[(\{C_5Me_4C_6H_4NMe(\mu\text{-}CH_2)\}Y(CH_2SiMe_3))_2]$ (2.389 Å).[4a,12a] Therefore, the lanthanide center remained sterically unsaturated and the activated aluminate moiety adopts a bent η^2 coordination, with a short Ln···C19 distance (C13LnC18–C13Al2C18; **3a**: 111.1°, **3b**: 111.8°, **5a**: 107.3°, **5b**: 107.9°, **5c**: 108.6°), whilst the intact tetramethylaluminate ligand coordinates in an η^2 fashion (C14LnC15–C14Al1C15; **3a**: 2.66°, **3b**: 3.22°, **5a**: 3.94°, **5b**: 6.52°, **5c**: 7.95°). This result is similar to the structural motifs that are found in donor-free half-sandwich bis(tetramethylaluminate) complexes $[(Cp^R)Ln(AlMe_4)_3]$, such as $[(C_5Me_5)Ln(AlMe_4)_2]$ (118.0° and 2.2°, respectively).[22] The La–Cp metal–ring-carbon bond lengths in complexes **3** fall within a narrow range (**3a**: 2.727(4)–2.781(4) Å, **3b**: 2.668(4)–2.730(5) Å), whereas, in complexes **5**, the Cp plane is tilted, similar to complexes **4**. The average La–CH_3 bond lengths (Ln–$C_{(av)}$; planar: 2.789 Å versus bent: 2.869 Å) are elongated in comparison to bis(tetramethylaluminate) complexes $[(C_5Me_5)La(AlMe_4)_2]$ (2.669 versus 2.798 Å) and $[\{1,2,4\text{-}(Me_3C)_3C_5H_2\}La(AlMe_4)_2]$ (2.705 versus 2.794 Å).[5c,22]

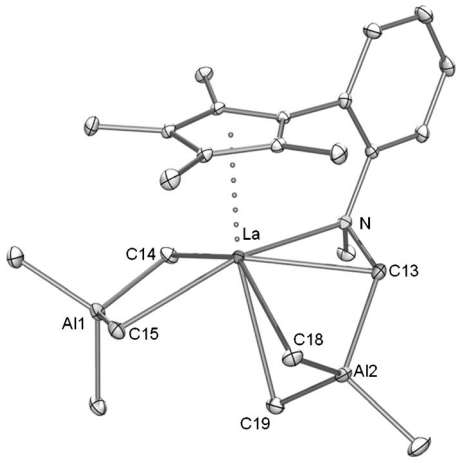

Figure 6. Molecular structure of $[\{Cp^{AMe}(\mu\text{-}CH_2)AlMe_3\}La(AlMe_4)]$ (**5a**), representative of isostructural complexes **5**. Atomic displacement parameters are set at the 50% level; hydrogen atoms are omitted for clarity.

Isoprene polymerization: To extend our recently developed library of rare-earth-metal–bis(tetraalkylaluminate) complexes, the new complexes **3**, **4**, and **5** were examined as pre-catalysts for isoprene polymerization (Table 4). As previously reported for donor-free, half-sandwich rare-earth-metal–bis(tetramethylaluminate) complexes, the activation of complexes **3–5** with one equivalent of fluorinated borate co-catalysts $[Ph_3C][B(C_6F_5)_4]$ (**A**) or $[PhNMe_2H][B(C_6F_5)_4]$ (**B**) led to tight ion pairs,[5] which were highly active in isoprene polymerization. The formation of co-products $Ph_3CMe/AlMe_3$ and $PhNMe_2/AlMe_3/CH_4$ with co-catalysts **A** and **B**, respectively, was clearly indicated by ^1H NMR spectroscopy. Upon activation with the neutral organoboron compound $B(C_6F_5)_3$ (**C**), active catalysts were only formed with complexes **3** and **5**, which polymerized isoprene in lower yields (Table 4, runs 5, 10, 11, and 22). The combination **3b/C** also gave a lower stereoselectivity (Table 4, run 5). High *trans*-1,4 selectivity is mainly governed by the choice of the metal center. In agreement with our previous investigations,[5] the large

Table 3. Selected bond lengths and angles in C–H bond-activated complexes **3** and **5**.

	3a (Ln = La)	**3b** (Ln = Nd)	**5a** (Ln = La)	**5b** (Ln = Nd)	**5c** (Ln = Y)
Bond [Å]					
Ln1–C(Cp)	2.727(4)–2.781(4)	2.668(4)–2.730(5)	2.734(1)–2.804(1)	2.649(2)–2.761(2)	2.564(2)–2.693(2)
Ln1–C13	2.820(4)	2.764(4)	2.836(2)	2.770(2)	2.753(2)
Ln1–C14	2.758(4)	2.704(4)	2.763(2)	2.694(2)	2.628(3)
Ln1–C15	2.819(4)	2.761(5)	2.804(2)	2.718(2)	2.635(3)
Ln1–C18	2.920(6)	2.881(5)	2.964(2)	2.907(2)	2.831(3)
Ln1–C19	3.126(4)	3.104(3)	3.040(2)	3.019(2)	2.976(2)
Ln1–N1	2.533(3)	2.490(4)	2.578(1)	2.527(1)	2.471(2)
Angle [°]					
Al2-C13-Ln1	74.3(1)	74.3(1)	73.52(5)	73.23(5)	72.75(8)
Al2-C13-N1	125.7(3)	125.7(3)	127.1(1)	124.7(1)	122.7(2)
C13-Al2-C18	106.8(2)	107.0(2)	105.31(6)	105.46(7)	105.2(1)
C18-Al2-C19	105.7(2)	105.5(2)	107.63(6)	106.95(8)	107.0(1)
C13-Ln1-C18	70.3(1)	71.6(1)	69.18(4)	70.70(5)	71.42(7)
C13-Ln1-N1	31.9(1)	32.6(1)	32.19(4)	32.71(5)	33.21(7)
C18-Ln1-N1	102.2(1)	104.2(1)	101.32(4)	103.41(5)	104.63(7)
C14-Ln1-N1	89.5(1)	87.5(1)	93.12(4)	85.80(5)	83.15(7)
C11-N1-C13	113.4(3)	113.5(3)	111.7(1)	112.5(1)	111.9(2)
C13-N1-Ln1	84.7(2)	83.8(2)	83.28(8)	82.52(9)	83.7(1)
Interplanar angle [°]					
C18Ln1C19–C18Al2C19	68.93	68.21	72.70	72.1	71.43
C14 Ln1C15–C14 Al1C15	2.66	3.22	3.94	6.52	7.95
C14Ln1C13–C14N1C13	0.18	0.8	3.08	0.59	1.09

lanthanum ion produced polyisoprene with a higher *trans*-1,4 content (up to 95.6%; Table 4, run 11) than the smaller neodymium center (up to 84.1%; Table 4, run 1). For comparison, the *trans*-1,4 content with $[(Cp^{O})La(AlMe_4)_2]$/**B** and $[(Cp^{O})Y(AlMe_4)_2]$/**B** was 93.1% and 88.4%, respectively (Table 4, runs 27 and 28), whilst the *trans*-1,4 content with $[(C_5Me_5)La(AlMe_4)_2]$/**A** and $[(C_5Me_5)Nd(AlMe_4)_2]$/**A** was 87.0% and 69.7%, respectively (Table 4, runs 24 and 25). The catalyst system **5c**/**B**, which contained the smallest metal center (yttrium) gave poor stereoselectivity, with a slightly predominant *cis*-1,4 content (58.1%) in the resulting polyisoprene, similar to that with the previously reported mixture $[(C_5Me_5)Y(AlMe_4)_2]$/**A** (Table 4, run 23

Table 4. Effect of Ln size, Cp substituent, co-catalyst, and solvent on the polymerization of isoprene.

Entry[a]	Pre-catalyst		co-catalyst[b]	Solvent	Yield [%]	Isoprene insertion			M_n[d] ($\times 10^6$)	M_w/M_n[d]
						trans-1,4[c]	*cis*-1,4[c]	3,4[c]		
1	$[\{Cp^{NMe}(\mu\text{-}CH_2)AlMe_3\}Nd(AlMe_4)]$	**3b**	**A**	toluene	>99	84.1	–	15.9	1.1	1.70
2	$[\{Cp^{NMe}(\mu\text{-}CH_2)AlMe_3\}Nd(AlMe_4)]$	**3b**	**A**	*n*-hexane	75	82.4	–	17.6	1.5	1.82
3	$[\{Cp^{NMe}(\mu\text{-}CH_2)AlMe_3\}Nd(AlMe_4)]$	**3b**	**B**	toluene	>99	83.3	–	16.7	1.0	1.09
4	$[\{Cp^{NMe}(\mu\text{-}CH_2)AlMe_3\}Nd(AlMe_4)]$	**3b**	**B**	*n*-hexane	83	82.7	–	17.3	1.8	1.11
5	$[\{Cp^{NMe}(\mu\text{-}CH_2)AlMe_3\}Nd(AlMe_4)]$	**3b**	**C**	toluene	53	53.0	23.1	23.9	0.6	1.94
6	$[\{Cp^{NMe}(\mu\text{-}CH_2)AlMe_3\}La(AlMe_4)]$	**3a**	**A**	toluene	>99	90.8	–	9.2	1.4	1.11
7	$[\{Cp^{NMe}(\mu\text{-}CH_2)AlMe_3\}La(AlMe_4)]$	**3a**	**A**	*n*-hexane	>99	90.2	–	9.8	2.1	1.13
8	$[\{Cp^{NMe}(\mu\text{-}CH_2)AlMe_3\}La(AlMe_4)]$	**3a**	**B**	toluene	>99	92.0	–	8.0	1.0	1.09
9	$[\{Cp^{NMe}(\mu\text{-}CH_2)AlMe_3\}La(AlMe_4)]$	**3a**	**B**	*n*-hexane	>99	90.4	–	9.6	1.8	1.11
10	$[\{Cp^{NMe}(\mu\text{-}CH_2)AlMe_3\}La(AlMe_4)]$	**3a**	**C**	toluene	81	90.6	–	9.4	1.1	1.29
11	$[\{Cp^{NMe}(\mu\text{-}CH_2)AlMe_3\}La(AlMe_4)]$	**3a**	**C**	*n*-hexane	38	95.6	–	4.8	0.6	1.27
12	$[(Cp^{AMe2})Nd(AlMe_4)_2]$	**4b**	**A**	toluene	>99	87.6	–	12.4	2.1	1.26
13	$[(Cp^{AMe2})Nd(AlMe_4)_2]$	**4b**	**B**	toluene	>99	87.3	–	12.7	1.6	1.19
14	$[(Cp^{AMe2})Nd(AlMe_4)_2]$	**4b**	**C**	toluene	8	72.5	16.3	11.2	1.2	1.34
15	$[\{Cp^{AMe}(\mu^2\text{-}CH_2)AlMe_3\}Nd(AlMe_4)]$	**5b**	**A**	toluene	>99	84.5	–	15.5	0.8	1.28
16	$[\{Cp^{AMe}(\mu^2\text{-}CH_2)AlMe_3\}Nd(AlMe_4)]$	**5b**	**B**	toluene	>99	84.1	–	15.9	0.8	1.23
17	$[(Cp^{AMe2})La(AlMe_4)_2]$	**4a**	**A**	toluene	43	92.5	–	7.5	2.4	1.25
18	$[(Cp^{AMe2})La(AlMe_4)_2]$	**4a**	**B**	toluene	>99	91.6	–	8.4	2.5	1.13
19	$[(Cp^{AMe2})La(AlMe_4)_2]$	**4a**	**C**	toluene	–	–	–	–	–	–
20	$[\{Cp^{AMe}(\mu\text{-}CH_2)AlMe_3\}La(AlMe_4)]$	**5a**	**A**	toluene	>99	91.6	–	8.4	0.7	1.08
21	$[\{Cp^{AMe}(\mu\text{-}CH_2)AlMe_3\}La(AlMe_4)]$	**5a**	**B**	toluene	>99	92.1	–	7.9	0.7	1.07
22	$[\{Cp^{AMe}(\mu\text{-}CH_2)AlMe_3\}La(AlMe_4)]$	**5a**	**C**	toluene	58	92.1	–	7.9	0.6	1.21
23	$[\{Cp^{AMe}(\mu\text{-}CH_2)AlMe_3\}Y(AlMe_4)]$	**5c**	**B**	toluene	>99	27.3	58.1	14.6	1.4	1.72
24	$[(C_5Me_5)Nd(AlMe_4)_2]$	**6b**	**A**	toluene	>99	69.7	14.0	16.3	0.3	2.87
25	$[(C_5Me_5)La(AlMe_4)_2]$	**6a**	**A**	toluene	>99	87.0	3.5	9.5	0.7	1.98
26	$[(C_5Me_5)Y(AlMe_4)_2]$	**6c**	**A**	toluene	>99	20.6	60.5	18.9	0.2	8.95
27	$[(Cp^{O})La(AlMe_4)_2]$	**7a**	**B**	*n*-hexane	>99	93.1	2.1	4.9	1.6	1.28
28	$[(Cp^{O})Y(AlMe_4)_2]$	**7c**	**B**	*n*-hexane	>99	88.4	0.6	11.0	0.9	1.07

[a] Conditions: pre-catalyst (0.02 mmol), [Ln]/[co-cat] (1:1), solvent (8 mL), isoprene (20 mmol). [b] Co-catalyst: **A** = $[Ph_3C][B(C_6F_5)_4]$, **B** = $[PhNMe_2H][B(C_6F_5)_4]$ **C** = $B(C_6F_5)_3$. [c] Determined by ^{13}C NMR spectroscopy in $CDCl_3$. [d] Determined by size-exclusion chromatography (SEC) against polystyrene standards.

versus run 26). In contrast to our earlier studies, no significant differences in stereoselectivity were observed on switching from the trityl (**A**) to the anilinium borate (**B**). Even though the formation of the same ion pair is assumed in both activation steps, the methyl-abstraction reaction with borate **A** yields the chemically rather inert Ph_3CMe, whereas the protonolysis reaction with borate **B** forms dimethylaniline ($PhNMe_2$). This latter species could potentially coordinate to the Lewis acidic rare-earth-metal or aluminum centers. This coordination was also presumed to affect the activity and/or stereoselectivity when half-sandwich complexes of the type $[(Cp^R)Ln(AlMe_4)_2]$ ($Cp^R = C_5Me_5$, C_5Me_4H, 1,2,4-$(Me_3C)_3C_5H_2$, 1,3-$(Me_3Si)_2C_5H_3$, $C_5Me_4SiMe_3$)[5,22] were used as pre-catalysts. However, in the case of the donor-functionalized cyclopentadienyl ligands, the coordination of the aniline derivative might be suppressed by the presence of the sterically shielding dianionic $[C_5Me_4(alkyl/aryl)NMe(\mu\text{-}CH_2)]^{2-}$ moiety. Moreover, the chelating binding mode appears to be responsible for the lack of any *cis*-1,4 content within the generated polyisoprene. A similar impact of intramolecular donor coordination on the stereoregularity of the polymer was noted in our study on quinolyl-substituted cyclopentadienyl bis(tetramethylaluminate) rare-earth-metal complexes.[13] In that study, a low cis-1,4 content was rationalized on the basis of the steric encumbrance that a *cis*-η^4 coordinated isoprene would experience by the additional N-donor moiety.

The 3,4-defects that were observed in the mainly *trans*-1,4-regulated polymer chains strongly depend on the size of the Ln^{III} metal center (Nd > La). Our proposed mechanism is based on the assumption that the 3,4-insertion is facilitated by the π–σ allylic rearrangement of the growing polymer chain (Scheme 5).[27] Aside from electronic effects, the σ-

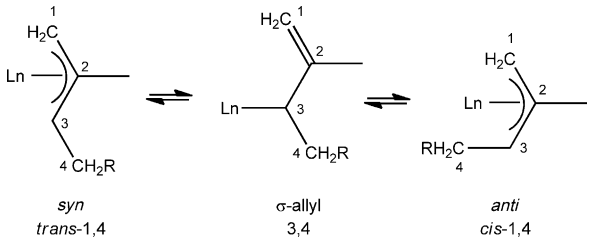

Scheme 5. *anti*/*syn* isomerization through σ/π rearrangement allows for *trans*-1,4-, 3,4-, and *cis*-1,4-insertions of isoprene in the growing polymer chain.

binding mode to the internal C_3 carbon atoms of the allylic species might be preferentially formed at the smaller neodymium center than at the lanthanum center. Furthermore, the π–σ rearrangement allows an *anti*/*syn* isomerization of the growing polymer chain towards the metal center, which might explain the high *cis*-polyisoprene content for the yttrium complex (Scheme 5). Changing the solvent from toluene to *n*-hexane had no strong effect on the stereoselectivity of the reaction, but noticeably increased the average molecular weight of the produced polymers for the initiators that were derived from complexes **3**. Given the similar molecular-weight distributions (M_w/M_n), this result can be explained by the decreased solubility of the active ionic species in aliphatic solvents, thus leading to a lower [cat]/[monomer] ratio (Table 1, runs 1/2, 3/4, 6/7, 8/9). Similar tendencies of narrow M_w/M_n values but considerably higher M_n values of polyisoprene were observed with complexes **4**. Herein, cationization with the borate co-catalyst may lead to the C–H bond activation of one aminomethyl group, as previously reported for a cyclopentadienyl-linked NMe_2 moiety on zirconocene cations and, hence, the formation of a considerable quantity of inactive species.[28] For the initiators that were derived from complexes **5a**/**5b** and borate **B**, the M_n values were within the expected range as implied by the 1:1000 catalyst/isoprene ratio. Narrow polydispersities and complete consumption of the monomer suggested that the isoprene polymerized in a living manner.

Conclusion

Half-sandwich rare-earth-metal–bis(tetramethylaluminate) complexes $[(Cp^{RMe2})Ln(AlMe_4)_2]$, which contains amino-functionalized tetramethylcyclopentadienyl ligands, were accessible in a straightforward manner by using a protonolysis procedure from homoleptic complexes $[Ln(AlMe_4)_3]$ and the corresponding cyclopentadienes. The highly selective C–H bond activation of one aminomethyl group constitutes a prominent consecutive reaction pathway, which is governed by the mobility/rigidity of the donor linker ($CH_2CH_2NMe_2$ > $C_6H_4NMe_2$), the metal size/Lewis acidity ($Y^{III} > La^{III}$), and the reaction temperature. Whilst the intact dimethylamino-functionalized cyclopentadienyl ligand showed the expected η^5:κ^1 coordination in $[(Cp^{RMe2})Ln(AlMe_4)_2]$, the aminomethyl-activated ligands in the $[\{Cp^{RMe}(\mu\text{-}CH_2)AlMe_3\}Ln(AlMe_4)]$ complexes coordinates in an η^5:η^2 (N,C)-fashion. All of the C–H bond-activated linked half-sandwich complexes displayed excellent activity in the polymerization of isoprene upon the addition of fluorinated organoboron reagents as co-catalysts. The high *trans*-1,4 selectivity (up to 95.6%) increased with increasing size of the rare-earth-metal center. Importantly, the additional coordination of the amino moieties prevented the formation of *cis*-1,4 content in the as-produced polymer for the lanthanum and neodymium complexes and very narrow molecular-weight distributions ($M_w/M_n < 1.1$) were achieved upon activation with co-catalyst **B** in toluene.

Experimental Section

General remarks: All of the operations were performed with the rigorous exclusion of air and water, by using standard Schlenk, high-vacuum, and argon-glovebox techniques (MBraun MB 200B; <1 ppm O_2, <1 ppm water). *n*-Hexane, toluene, and THF were purified by using Grubbs columns (MBraun SPS-800, solvent purification system) and stored in a glovebox. [D_6]Benzene and [D_8]toluene were obtained from Aldrich, dried over Na for 24 h, and filtered. $CDCl_3$ and $AlMe_3$ were purchased from

Aldrich and used as received. Isoprene was purchased from Aldrich, dried over trioctylaluminum, and vacuum transferred prior to use. $[Ph_3C][B(C_6F_5)_4]$, $[PhNMe_2H][B(C_6F_5)_4]$, and $B(C_6F_5)_3$ were purchased from Boulder Scientific Company and used without further purification. Homoleptic $[Ln(AlMe_4)_3]$ (Ln = La, Nd, Y) were prepared according to literature procedures.[17] HCp^{NMe2} (Cp^{NMe2} = 1-[2-(*N*,*N*-dimethylamino)-ethyl]-2,3,4,5-tetramethyl-cyclopentadienyl) and HCp^{AMe2} (Cp^{AMe2} = 1-[1-(*N*,*N*-dimethylanilinyl)]-2,3,4,5-tetramethyl-cyclopentadienyl) were synthesized according to literature procedures.[14–15] The solid-state structure of 1-[1-(*N*,*N*-dimethylanilinyl)]-2,3,4,5-tetramethyl-cyclopenten-1-ol, the precursor of HCp^{AMe2}, was determined by X-ray analysis (see the Supporting Information). The NMR spectra of the air- and moisture-sensitive compounds were recorded in NMR tubes that were fitted with J. Young valves at 25 °C on a Bruker AvanceII + 400 (^{1}H: 400.13 Hz, ^{13}C: 100.61 MHz) spectrometer. ^{1}H and ^{13}C shifts were referenced to internal solvent resonances and are reported in parts per million (ppm) relative to TMS. IR spectra were recorded on a NICOLET 6700 FTIR spectrometer by using a DRIFT chamber with dry KBr/sample mixtures and KBr windows; the collected data were transformed by using the Kubelka–Munk refinement. Elemental analysis was performed on an Elementar Vario MICRO cube. The molar masses (M_w and M_n) of the polymers were determined by size-exclusion chromatography (SEC). Sample solutions (1.0 mg polymer per mL THF) were filtered through a 0.45 μm syringe filter prior to injection. SEC was performed with a GPCmax VE 2001 pump (Viscotek) by employing ViscoGEL columns. Signals were detected by using a triple detection array (TDA 305) and calibrated against polystyrene standards ($M_W/M_n < 1.15$). The flow rate was set to 1.0 mL min^{-1}. The microstructure of the polyisoprenes was examined by ^{13}C NMR spectroscopy on an AV400 spectrometer in $CDCl_3$ at ambient temperature.

General procedure for the synthesis of [{η^5-$C_5Me_4C_2H_4NMe_2(AlMe_3)$}Ln($AlMe_4$)$_2$] (1): In a glovebox, HCp^{NMe2} was dissolved in cold (−35 °C) pentane (2 mL) and added dropwise to a stirring solution of $[Ln(AlMe_4)_3]$ in cold (−35 °C) pentane (8 mL). The instantaneous formation of a precipitate was observed. Following completion of the addition, the reaction mixture was stirred for 15 min, during which time the precipitate redissolved. The solvent was removed at −35 °C under vacuum. The title compound was formed as a crystalline solid from the remaining oil within 2 days at ambient temperature. The crude product was washed with cold (−35 °C) pentane, redissolved in pentane at ambient temperature, and recrystallized at −35 °C.

Synthesis of [{η^5-$C_5Me_4C_2H_4NMe_2(AlMe_3)$}La($AlMe_4$)$_2$] (1a): Following the procedure described above, HCp^{NMe2} (97 mg, 0.50 mmol) and $[La(AlMe_4)_3]$ (200 mg, 0.50 mmol) yielded compound **1a** (248 mg, 0.43 mmol, 86 % yield) as colorless crystals. ^{1}H NMR (400 MHz, [D$_6$]benzene, 25 °C): δ = 2.74–2.70 (m, 2H; NCH_2CH$_2$), 2.13–2.10 (m, 2H; CH$_2$CH_2Cp), 1.94 (s, 6H; CH_3Cp), 1.90 (s, 6H; CH_3Cp), 1.79 (s, 6H; NCH_3), −0.32 (s, 24H; Al(CH_3)$_4$), −0.54 ppm (s, 9H; Al(CH_3)$_3$); ^{13}C NMR (100 MHz, [D$_6$]benzene, 25 °C): δ = 125.8, 124.7, 124.4 (Cp), 59.9 (CpCH_2CH$_2$), 44.7 (N(CH_3)$_2$), 22.4 (CH$_2$CH$_2$N), 11.8 (Cp(CH_3)$_4$), 3.0 (Al(CH_3)$_4$), −8.1 ppm (Al(CH_3)$_3$); IR: $\tilde{\nu}$ = 3015 (w), 2922 (s), 2885 (m), 2817 (w), 1475 (m), 1457 (m), 1436 (m), 1185 (m), 1015 (w), 964 (w), 701 (m), 571 cm^{-1} (w); elemental analysis calcd (%) for $C_{24}H_{55}Al_3LaN$ (577.55): C 49.91, H 9.60, N 2.43; found: C 49.76, H 9.58, N 2.53.

Synthesis of [{η^5-$C_5Me_4C_2H_4NMe_2(AlMe_3)$}Nd($AlMe_4$)$_2$] (1b): Following the procedure described above, HCp^{NMe2} (97 mg, 0.50 mmol) and $[Nd(AlMe_4)_3]$ (202 mg, 0.50 mmol) yielded compound **1b** (259 mg, 0.45 mmol, 89 % yield) as blue crystals. ^{1}H NMR (250 MHz, [D$_6$]benzene, 25 °C): δ = 10.95 (s, 12H; CH_3Cp), 8.70 (s, 2H; CH$_2$CH_2Cp), 5.66 (s, 2H; NCH_2CH$_2$), 4.95 (br s, 24H; Al(CH_3)$_4$), 2.77 (s, 6H; NCH_3), −0.69 ppm (s, 9H; Al(CH_3)$_3$); IR: $\tilde{\nu}$ = 3016 (w), 2974 (m), 2921 (s), 2886 (m), 2821 (m), 2736 (w), 1477 (m), 1462 (m), 1439 (m), 1224 (m), 1185 (s), 1015 (m), 964 (m), 858 (w), 703 cm^{-1} (s); elemental analysis calcd (%) for $C_{24}H_{55}Al_3NdN$ (582.88): C 49.45, H 9.51, N 2.40; found: C 49.58, H 9.23, N 2.48.

Synthesis of [{η^5-$C_5Me_4C_2H_4NMe_2(AlMe_3)$}Y($AlMe_4$)$_2$] (1c): Following the procedure described above, HCp^{NMe2} (97 mg, 0.50 mmol) and $[Y(AlMe_4)_3]$ (175 mg, 0.50 mmol) yielded compound **1c** (240 mg, 0.45 mmol, 91 % yield) as colorless crystals. ^{1}H NMR (400 MHz, [D$_6$]benzene, 25 °C): δ = 2.68–2.64 (m, 2H; NCH_2CH$_2$), 2.16–2.12 (m, 2H; CH$_2$CH_2Cp), 1.92 (s, 6H; CH_3Cp), 1.82 (s, 6H; CH_3Cp), 1.71 (s, 6H; NCH_3), −0.33 (d, ^2J(H,Y) = 2.2 Hz, 24H; Al(CH_3)$_4$), −0.44 ppm (s, 9H; Al(CH_3)$_3$); ^{13}C NMR (100 MHz, [D$_6$]benzene, 25 °C): δ = 122.8, 121.8, 121.2 (Cp), 59.1 (CpCH_2CH$_2$), 44.3 (N(CH_3)$_2$), 22.1 (CH$_2$CH$_2$N), 11.8 (Cp(CH_3)$_4$), 0.2 (Al(CH_3)$_4$), −8.5 ppm (Al(CH_3)$_3$); IR: $\tilde{\nu}$ = 3017 (w), 2922 (s), 2887 (m), 2820 (w), 1476 (m), 1457 (m), 1437 m, 1185 (m), 1015 (w), 966 (w), 703 (m), 577 cm^{-1} (w); elemental analysis calcd (%) for $C_{24}H_{55}Al_3NY$ (527.55): C 54.56, H 10.51, N 2.66; found: C 54.49, H 11.30, N 2.58.

Synthesis of [($C_5Me_4C_2H_4NMe_2$)La($AlMe_4$)$_2$] (2a): In a glovebox, [{η^5-$C_5Me_4C_2H_4NMe_2(AlMe_3)$}La($AlMe_4$)$_2$] (**1a**, 60 mg, 0.11 mmol) was placed in an NMR tube that was fitted with a J. Young valve, dissolved in [D$_8$]toluene, and cooled to −35 °C. A solution of Et$_2$O (1 equiv) in [D$_8$]toluene at −35 °C (0.11 mmol, 5,8 μL) was added and the reaction was monitored by ^{1}H NMR spectroscopy at ambient temperature. Single crystals were grown from a concentrated solution in [D$_8$]toluene by adding cold *n*-hexane and cooling to −35 °C. ^{1}H NMR (400 MHz, [D$_8$]toluene, 25 °C): δ = 2.17 (t, ^3J(H,H) = 6.37 Hz, 2H; NCH_2CH$_2$), 2.02 (t, ^3J(H,H) = 6.37 Hz, 2H; CH$_2$CH_2Cp), 1.89 (s, 6H; CH_3Cp), 1.79 (s, 6H; CH_3Cp), 1.70 (s, 6H; NCH_3), −0.27 ppm (s, 24H; Al(CH_3)$_4$).

General procedure for the synthesis of [{$C_5Me_4CH_2CH_2NMe(\mu$-CH_2)$AlMe_3$}Ln($AlMe_4$)$_2$] (3): In a glovebox, [{η^5-$C_5Me_4C_2H_4NMe_2$-($AlMe_3$)}Ln($AlMe_4$)$_2$] (**1**) was dissolved in pentane and cooled to −35 °C. A solution of Et$_2$O (1 equiv) in pentane at −35 °C was added and the reaction mixture was stirred for 30 min whilst warming to ambient temperature. Evaporation of the solvent and the trimethylaluminum ether adduct yielded compound **3** as a crystalline solid. Recrystallization was performed from a saturated solution in *n*-hexane at −35 °C.

Synthesis of [{$C_5Me_4CH_2CH_2NMe(\mu$-CH_2)$AlMe_3$}La($AlMe_4$)$_2$] (3a): Following the procedure described above, employing compound **1a** (200 mg, 0.35 mmol) yielded compound **3a** (151 mg, 0.31 mmol, 89 % yield) as pale yellow crystals. ^{1}H NMR (400 MHz, [D$_6$]benzene, 25 °C): δ = 2.94 (dt, ^3J(H,H) = 6.5 Hz, ^2J(H,H) = 11.5 Hz, 1H; NCH_2CH$_2$), 2.36–2.31 (m, 1H; NCH_2CH$_2$), 2.25–2.19 (m, 1H; CH$_2$CH_2Cp), 2.04–1.98 (m, 1H; CH$_2$CH_2Cp), 2.02 (s, 3H; CH_3Cp), 1.88 (s, 3H; CH_3Cp), 1.85 (s, 3H; CH_3Cp), 1.78 (d, 3H; CH_3N), 1.77 (s, 3H; CH_3Cp), 1.34 (d, 1H; NCH_2Al), 1.08 (d, 1H; NCH_2Al), −0.21 (s, 12H; Al(CH_3)$_4$), −0.41 ppm (s, 9H; Al(CH_3)$_3$); ^{13}C NMR (100 MHz, [D$_6$]benzene, 25 °C): δ = 124.4, 124.0, 122.3, 119.8 (Cp), 66.8 (NCH_2CH$_2$), 47.7 (CH_3N), 39.0 (NCH_2Al), 22.7 (CH$_2$CH_2Cp), 12.4, 11.6, 11.5, 11.0 (Cp(CH_3)$_4$), 1.0 (br; Al(CH_3)$_4$), −3.7 ppm (Al(CH_3)$_3$); IR: $\tilde{\nu}$ = 2954 (s), 2924 (s), 2854 (m), 2726 (w), 2670 (w), 1458 (s, Nujol), 1377 (s, Nujol), 1305 (m), 1189 (s), 1169 (m), 1075 (w), 1024 (m), 964 (w), 766 (w), 720 (m), 714 (m), 581 cm^{-1} (m); elemental calcd (%) for $C_{20}H_{42}Al_2LaN$ (489.42): C 49.08, H 8.65, N 2.86; found: C 49.42, H 8.70, N 2.78.

Synthesis of [{$C_5Me_4CH_2CH_2NMe(\mu$-CH_2)$AlMe_3$}Nd($AlMe_4$)$_2$] (3b): Following the procedure described above, employing compound **1b** (200 mg, 0.34 mmol) yielded compound **3b** (145 mg, 0.29 mmol, 86 % yield) as blue crystals. ^{1}H NMR (400 MHz, [D$_6$]benzene, 25 °C): δ = −9.47 (1H), −4.05 (3H), −1.31 (9H), 8.30 (3H), 9.95 (3H), 10.33–13.38 (br s, 12H) 11.95 (3H), 13.55 (1H), 16.25 (3H), 25.05 (1H), 29.14 (1H), 30.63 (1H), 58.89 ppm (1H); IR: $\tilde{\nu}$ = 2954 (s), 2924 (s), 2854 (m), 2726 (w), 2670 (w), 1460 (s, Nujol), 1377 (s, Nujol), 1305 (m), 1189 (s), 1169 (m), 1075 (w), 1024 (m), 967 (w), 766 (w), 713 (m), 697 (m), 582 cm^{-1} (m); elemental analysis calcd (%) for $C_{20}H_{42}Al_2NdN$ (494.76): C 48.55, H 8.56, N 2.83; found: C 48.13, H 7.83, N 2.83.

General procedure for the synthesis of [($C_5Me_4C_6H_4NMe_2$)Ln($AlMe_4$)$_2$] (4): In a glovebox, HCp^{AMe2} was dissolved in cold (−35 °C) pentane (2 mL) and the mixture was added dropwise to a stirring solution of $[Ln(AlMe_4)_3]$ in cold (−35 °C) pentane (8 mL). Instantaneous gas formation was observed. Following completion of the addition, the reaction mixture was stirred for 2 h whilst warming to ambient temperature. The solution was cooled to −35 °C and the solvent was removed under vacuum. The title compound was washed with cold pentane and recrystallized from the remaining oil within 2 days at room temperature.

Synthesis of [($C_5Me_4C_6H_4NMe_2$)La($AlMe_4$)$_2$] (4a): Following the procedure described above, HCp^{AMe2} (120 mg, 0.50 mmol) and [La($AlMe_4$)$_3$] (200 mg, 0.50 mmol) yielded compound **4a** (196 mg, 0.35 mmol, 71% yield) as the crude product. Recrystallization from toluene/*n*-hexane at −35°C yielded colorless single crystals (138 mg, 0.25 mmol, 50% yield) suitable for X-ray diffraction analysis. ^{1}H NMR (400 MHz, [D$_6$]benzene, 25°C): δ = 6.99–6.95 (dt, ^5J(H,H) = 1.8 Hz, ^3J(H,H) = 7.6 Hz, 1H; C_6H_4), 6.94–6.88 (dt, ^5J(H,H) = = 1.1 Hz, ^3J(H,H) = 7.6 Hz, 1H; C_6H_4), 6.74–6.71 (dd, ^5J(H,H) = = 1.8 Hz, ^3J(H,H) = 7.6 Hz, 1H; C_6H_4), 6.68–6.66 (dd, ^5J-(H,H) = 1.1 Hz, ^3J(H,H) = 8.3 Hz, 1H; C_6H_4), 2.16 (s, 6H; -NCH_3), 1.96 (s, 6H; CH_3Cp), 1.71 (s, 6H; CH_3Cp), −0.10 ppm (s, 24H; Al(CH_3)$_4$); ^{13}C NMR (100 MHz, [D$_6$]benzene, 25°C): δ = 155.3, 133.4, 132.9, 130.3, 128.9, 127.5, 125.4, 124.8, 121.5, 47.6, 12.8, 11.8, −11.5 ppm; IR: $\tilde{\nu}$ = 3059 (m), 2969 (m), 3000 (s), 2915 (m), 2885 (w), 2812 (w), 1506 (m), 1480 (s), 1455 (m), 1193 (m), 1182 (m), 905 (s), 703 (m), 693 (w), 537 cm^{-1} (m); elemental analysis calcd (%) for $C_{25}H_{46}Al_2LaN$ (553.51): C 54.25, H 8.38, N 2.53; found: C 53.58, H 8.32, N 2.50.

Synthesis of [($C_5Me_4C_6H_4NMe_2$)Nd($AlMe_4$)$_2$] (4b): Following the procedure described above, HCp^{AMe2} (120 mg, 0.50 mmol) and [Nd($AlMe_4$)$_3$] (203 mg, 0.50 mmol) yielded compound **4b** (208 mg, 0.37 mmol, 74% yield) as the crude product. Recrystallization from toluene/*n*-hexane at −35°C yielded blue single crystals (115 mg, 0.21 mmol, 41% yield) suitable for X-ray diffraction analysis. IR: $\tilde{\nu}$ = 3059 (m), 3005 (s), 2974 (m), 2914 (w), 2885 (w), 2814 (w), 1506 (m), 1480 (s), 1455 (m), 1194 (m), 1183 (m), 905 (s), 753 (m), 692 (w), 538 cm^{-1} (m); elemental analysis calcd (%) for $C_{25}H_{46}Al_2NdN$ (558.84): C 53.73, H 8.30, N 2.51; found: C 53.79, H 7.74, N 2.60.

Synthesis of [($C_5Me_4C_6H_4NMe$(μ-CH_2)$AlMe_3$)La($AlMe_4$)] (5a): In a glovebox, [(Cp^{AMe2})Ln($AlMe_4$)$_2$] (**4a**, 60 mg, 0.11 mmol) was placed in an NMR tube that was fitted with a J. Young valve and dissolved in C_6D_6. The tube was heated at 75°C for 24 h and the reaction was monitored by ^{1}H NMR spectroscopy to indicate the completion of the C−H bond activation step (quantitative yield). After evaporation of the solvent under vacuum, the solid was dissolved in toluene/*n*-hexane and cooled to −35°C to yield colorless crystals (53 mg, 10 mmol, 91% yield) suitable for X-ray diffraction analysis. ^{1}H NMR (400 MHz, [D$_6$]benzene, 25°C): δ = 7.03–6.99 (dt, ^5J(H,H) = 1.9 Hz, ^3J(H,H) = 7.6 Hz, 1H; C_6H_4), 6.97–6.95 (dt, ^5J(H,H) = 1.2 Hz, ^3J(H,H) = 7.3 Hz, 1H; C_6H_4), 6.94–6.91 (dd, ^5J-(H,H) = 1.9 Hz, ^3J(H,H) = 7.5 Hz, 1H; C_6H_4), 6.87–6.85 (dd, ^5J(H,H) = 1.1 Hz, ^3J(H,H) = 8.2 Hz, 1H; C_6H_4), 2.21 (s, 3H; NCH_3), 2.07 (s, 3H; CH_3Cp), 1.95–1.92 (d, 1H; μ-CH_2), 1.92 (s, 3H; CH_3Cp), 1.76 (s, 3H; CH_3Cp), 1.75–1.70 (d, 1H; μ-CH_2), 1.73 (s, 3H; CH_3Cp), −0.14 (s, 12H; Al(CH_3)$_4$), −0.44 ppm (s, 9H; Al(CH_3)$_3$); ^{13}C NMR (100 MHz, [D$_6$]benzene, 25°C): δ = 159.0, 132.3, 129.6, 128.6, 126.4, 125.2, 124.8, 124.0, 120.7, 120.6 (aromatic Cp and C_6H_4), 54.8 (NCH_2Al), 45.5 (CH_3N), 12.3, 12.1, 11.6, 10.8 (Cp(CH_3)$_4$), 1.24 (br; Al(CH_3)$_4$), −4.1 ppm (Al(CH_3)$_3$); IR: $\tilde{\nu}$ = 2913 (m), 2886 (w), 2826 (w), 2790 (w), 1506 (m), 1446 (s), 1188 (m), 1179 (m), 1027 (m), 692 (m), 574 (m), 507 cm^{-1} (m); elemental analysis calcd (%) for $C_{24}H_{42}Al_2LaN$ (537.47): C 53.63, H 7.88, N 2.61; found: C 54.53, H 7.64, N 2.50.

Synthesis of [{$C_5Me_4C_6H_4NMe$(μ-CH_2)$AlMe_3$}Nd($AlMe_4$)] (5b): In a glovebox, [(Cp^{AMe2})Nd($AlMe_4$)$_2$] (**4b**, 60 mg, 0.11 mmol) was placed in an NMR tube that was fitted with a J. Young valve and dissolved in C_6D_6. The tube was heated at 75°C for 24 h and the reaction was monitored by ^{1}H NMR spectroscopy to indicate the completion of the C−H bond activation step (quantitative). After evaporation of the solvent under vacuum, the solid was dissolved in toluene/*n*-hexane and cooled to −35°C to yield colorless crystals (56 mg, 10 mmol, 96% yield) suitable for X-ray diffraction analysis. IR: $\tilde{\nu}$ = 2907 (m), 2882 (w), 2827 (w), 2793 (w), 1506 (s), 1450 (s), 1185 (m), 1027 (m), 692 (m), 576 (m), 511 cm^{-1} (m); elemental analysis calcd (%) for $C_{25}H_{42}Al_2NdN$ (542.80): C 53.11, H 7.80, N 2.58; found: C 53.34, H 7.64, N 2.39.

Synthesis of [($C_5Me_4C_6H_4NMe$(μ-CH_2)$AlMe_3$)Y($AlMe_4$)] (5c): Following the procedure described for complexes **4a** and **4b**, HCp^{AMe2} (120 mg, 0.50 mmol) and [Y($AlMe_4$)$_3$] (175 mg, 0.50 mmol) yielded a crystalline solid (208 mg, 0.37 mmol, 74% yield) as the crude product. Recrystallization from *n*-hexane at −35°C yielded colorless single crystals (98 mg, 0.20 mmol, 40% yield) suitable for X-ray diffraction. ^{1}H NMR (400 MHz, [D$_6$]benzene, 25°C): δ = 7.07–7.02 (m, 1H; C_6H_4), 6.98–6.94 (m, 2H; C_6H_4), 6.88–6.87 (d, ^3J(H,H) = 8.3 Hz, 1H; C_6H_4), 2.24 (s, 3H; NCH_3), 2.05–2.01 (d, 1H; μ-CH_2), 1.96 (s, 3H; CH_3Cp), 1.87 (s, 3H; CH_3Cp), 1.85–1.81 (d, 1H; μ-CH_2), 1.74 (s, 3H; CH_3Cp), 1.64 (s, 3H; CH_3Cp), −0.22 (s, 12H; Al(CH_3)$_4$), −0.49 ppm (d, ^2J(Y,H) = 1.3 Hz, 9H; Al(CH_3)$_3$); ^{13}C NMR (100 MHz, [D$_6$]benzene, 25°C): δ = 159.3, 132.2, 132.0, 128.7, 127.9, 126.2, 123.9, 122.4, 120.6, 119.8, 118.9 (aromatic Cp and C_6H_4), 52.2 (NCH_2Al), 47.4 (CH_3N), 12.7, 12.5, 12.0, 11.4 (Cp(CH_3)$_4$), −1.7 (br; Al(CH_3)$_4$), −6.4 ppm (Al(CH_3)$_3$); IR: $\tilde{\nu}$ = 2910 (s), 2884 (s), 2827 (m), 2791 (w), 1506 (vs), 1455 (s), 1186 (m), 1024 (w), 691 (w), 571 (m), 516 cm^{-1} (m); elemental analysis calcd (%) for $C_{25}H_{42}Al_2YN$ (487.47): C 59.13, H 8.68, N 2.87; found: C 59.05, H 8.62, N 2.68.

Polymerization of isoprene: A detailed polymerization procedure (Table 2, run 1) is described as a typical example. [Ph_3C][$B(C_6F_5)_4$] (**A**, 18 mg, 0.02 mmol, 1 equiv) was added to a solution of compound **3a** (10 mg, 0.02 mmol) in toluene (8 mL) and the mixture was aged under ambient temperature for 30 min. After the addition of isoprene (1.36 g, 20 mmol), the polymerization reaction was carried out at ambient temperature for 24 h. The reaction was terminated by pouring the polymerization mixture into 2-propanol (200 mL) that contained 2,6-di-*tert*-butyl-4-methylphenol (0.1%, w/w) as a stabilizer and stirred for 12 h. The polymer was washed with 2-propanol and dried under vacuum at ambient temperature to constant weight.

Crystallographic data collection and refinement: Single crystals suitable for X-ray diffraction were selected in a glovebox, covered in Paratone-N (Hampton Research), and mounted onto a glass fiber. The crystal data for complexes **1c**, **3a**, and **3b** were collected on an STOE IPDS II diffractometer by using graphite-monochromated $Mo_{K\alpha}$ radiation (λ = 0.71073 Å) at 173(2) K by performing ω scans at two ϕ positions. Data collections for complexes **1a**, **1b**, **2**, **4a**, **4b**, **5a**, **5b**, and **5c** were performed on a Bruker APEX2 Duo at 100(2) K by using multilayer monochromated $Mo_{K\alpha}$ radiation (λ = 0.71073 Å). The raw data were collected by using the SMART[29] program and integrated and reduced with the SAINT program.[30] Corrections for absorption effects were applied by using SHELXTL[31] and/or SADABS.[32] Structure solutions and refinements were performed by using the SHELXS[33] and SHELXL programs.[34] The structures in this article are represented by using the ORTEP-III program.[35] For further structure-refinement details and crystallographic data, see Table 5 and Table 6. CCDC-937574 (**1a**), CCDC-

Table 5. Crystallographic data for complexes **1** and **2**.

	1a (Ln = La)[d]	**1b** (Ln = Nd)[d]	**1c** (Ln = Y)[e]	**2** (Ln = La)[d]
formula	$C_{24}H_{55}Al_3NLa$	$C_{24}H_{55}Al_3NNd$	$C_{24}H_{55}Al_3NY$	$C_{21}H_{46}Al_2NLa$
M_w	577.54	582.87	527.54	505.46
T [K]	173(2)	173(2)	173(2)	100(2)
crystal system	monoclinic	monoclinic	orthorhombic	monoclinic
space group	$P2_1/n$	$P2_1/c$	$P2_12_12_1$	$P2_1/c$
a [Å]	14.015(2)	13.9848(2)	12.1662(6)	10.1138(5)
b [Å]	14.755(2)	14.7469(2)	13.9987(10)	14.0194(7)
c [Å]	15.391(2)	20.4049(3)	18.2789(9)	20.9034(9)
α [°]	90.00	90.00	90.00	90.00
β [°]	91.449(6)	131.3590(10)	90.00	116.155(2)
γ [°]	90.00	90.00	90.00	90.00
V [Å^3]	3181.7(8)	3158.57(8)	3113.1(3)	2660.4(2)
Z	4	4	4	4
ρ_{calcd} [mg mm^{-3}]	1.206	1.226	1.126	1.262
μ [mm^{-1}]	1.435	1.737	1.968	1.676
$R1$[a]	0.0197	0.0164	0.0703	0.0300
$wR2$[b]	0.0464	0.0379	0.1108	0.0514
GOF (on F^2)[c]	1.076	1.089	1.257	1.049

[a] $R1 = \Sigma(||F_o|-|F_c||)/\Sigma|F_o|$. [b] $wR2 = \{\Sigma[w(F_o^2-F_c^2)^2/\Sigma[w(F_o^2)^2]\}^{1/2}$. [c] GOF = $\{\Sigma[w(F_o^2-F_c^2)^2]/(n-p)\}^{1/2}$. [d] The data were recorded on a Bruker APEX2 DUO CCD diffractometer. [e] The data were recorded on a STOE IPDS II diffractometer.

Table 6. Crystallographic data for complexes **3**, **4**, and **5**.

	3a (Ln = La)[d]	**3b** (Ln = Nd)[d]	**4a** (Ln = La)[e]	**4b** (Ln = Nd)[e]	**5a** (Ln = La)[e]	**5b** (Ln = Nd)[e]	**5c** (Ln = Y)[e]
formula	$C_{20}H_{42}Al_2NLa$	$C_{20}H_{42}Al_2NNd$	$C_{25}H_{46}Al_2NLa$	$C_{25}H_{46}Al_2NNd$	$C_{24}H_{42}Al_2NLa$	$C_{24}H_{42}Al_2NNd$	$C_{24}H_{42}Al_2NY$
M_w	489.42	494.75	553.50	558.84	537.46	542.80	487.46
T [K]	173(2)	173(2)	173(2)	100(2)	100(2)	100(2)	101(2)
crystal system	monoclinic	monoclinic	monoclinic	monoclinic	orthorhombic	monoclinic	monoclinic
space group	$P2_1/c$	$P2_1/c$	$P2_1/c$	$P2_1/c$	$P2_12_12_1$	$P2_1/n$	$P2_1/c$
a [Å]	8.9421(3)	8.9283(4)	11.0879(4)	11.0713(3)	13.184(3)	13.0233(3)	12.9964(5)
b [Å]	29.6872(12)	29.6718(9)	17.6299(6)	17.5299(6)	13.220(3)	12.5193(3)	12.4220(5)
c [Å]	9.7782(4)	9.6658(4)	17.8207(6)	17.7648(5)	15.285(3)	16.2753(3)	18.8555(5)
α [°]	90.00	90.00	90.00	90.00	90.00	90.00	90.00
β [°]	108.206(3)	108.129(3)	125.255(2)	125.0980(10)	90.00	100.6040(10)	122.181(2)
γ [°]	90.00	90.00	90.00	90.00	90.00	90.00	90.00
V [Å^3]	2465.83(16)	2433.54(17)	2844.65(17)	2820.86(15)	2663.9(10)	2608.25(10)	2576.40(16)
Z	4	4	4	4	4	4	4
ρ_{calcd} [mg mm^{-3}]	1.318	1.350	1.292	1.316	1.340	1.382	1.257
μ [mm^{-1}]	1.806	2.208	1.574	1.913	1.679	2.067	2.341
$R1$[a]	0.0458	0.0449	0.0172	0.0271	0.0107	0.0200	0.0617
$wR2$[b]	0.0935	0.0753	0.0428	0.0645	0.0284	0.0426	0.0874
GOF (on F^2)[c]	1.107	1.202	0.916	1.057	1.077	1.065	1.034

[a] $R1 = \Sigma(||F_0|-|F_c||)/\Sigma|F_0|$. [b] $wR2 = \{\Sigma[w(F_0^2-F_c^2)^2/\Sigma[w(F_0^2)^2]\}^{1/2}$. [c] GOF $= \{\Sigma[w(F_0^2-F_c^2)^2]/(n-p)\}^{1/2}$. [d] The data were recorded on an STOE IPDS II diffractometer. [e] The data were recorded on a Bruker APEX2 DUO CCD diffractometer.

937575 (**1b**), CCDC-937576 (**1c**), CCDC-937577 (**2**), CCDC-937578 (**3a**), CCDC-937579 (**3b**), CCDC-937580 (**4a**), CCDC-937581 (**4b**), CCDC-937582 (**5a**), CCDC-937583 (**5b**), CCDC-937584 (**5c**), and CCDC-950316 (1-[1-(*N*,*N*-dimethylanilinyl)]-2,3,4,5-tetramethyl-cyclopenten-1-ol) contain the supplementary crystallographic data for this paper. These data can be obtained free of charge from The Cambridge Crystallographic Data Centre via www.ccdc.cam.ac.uk/data_request/cif.

Acknowledgements

Support from the German Science Foundation is gratefully acknowledged. We thank Daniel Werner for providing technical assistance with the crystallographic data collection for compound 1-[1-(*N*,*N*-dimethylanilinyl)]-2,3,4,5-tetramethyl-cyclopenten-1-ol.

[1] F. Hofmann, K. Delbrück, German Patent 250.690, Farbenfabriken Bayer, **1909**.
[2] International Rubber Study Group (IRSG), http://www.rubberstudy.com.
[3] a) L. Friebe, O. Nuyken, W. Obrecht in *Neodymium Based Ziegler Catalysts – Fundamental Chemistry, Vol. 204* (Ed.: O. Nuyken), Springer, Heidelberg, **2006**, pp. 1–154; b) A. Fischbach, R. Anwander in *Neodymium Based Ziegler Catalysts – Fundamental Chemistry, Vol. 204* (Ed.: O. Nuyken), Springer, Heidelberg, **2006**, pp. 155–281.
[4] a) X. Li, M. Nishiura, L. Hu, K. Mori, Z. Hou, *J. Am. Chem. Soc.* **2009**, *131*, 13870–13882; b) H. Zhang, Y. Luo, Z. Hou, *Macromolecules* **2008**, *41*, 1064–1066; c) L. Zhang, Y. Luo, Z. Hou, *J. Am. Chem. Soc.* **2005**, *127*, 14562–14563.
[5] a) M. Zimmermann, K. W. Törnroos, R. Anwander, *Angew. Chem.* **2008**, *120*, 787–790; *Angew. Chem. Int. Ed.* **2008**, *47*, 775–778; b) M. Zimmermann, K. W. Törnroos, H. Sitzmann, R. Anwander, *Chem. Eur. J.* **2008**, *14*, 7266–7277; c) M. Zimmermann, J. Volbeda, K. W. Törnroos, R. Anwander, *C. R. Chim.* **2010**, *13*, 651–660.
[6] a) W. E. Piers, P. J. Shapiro, E. E. Bunel, J. E. Bercaw, *Synlett* **1990**, *1990*, 74–84; b) P. J. Shapiro, E. Bunel, W. P. Schaefer, J. E. Bercaw, *Organometallics* **1990**, *9*, 867–869.
[7] a) S. Arndt, K. Beckerle, K. C. Hultzsch, P.-J. Sinnema, P. Voth, T. P. Spaniol, J. Okuda, *J. Mol. Catal. A* **2002**, *190*, 215–223; b) H. Braunschweig, F. M. Breitling, *Coord. Chem. Rev.* **2006**, *250*, 2691–2720; c) K. C. Hultzsch, P. Voth, K. Beckerle, T. P. Spaniol, J. Okuda, *Organometallics* **1999**, *18*, 228–243; d) S. Arndt, P. Voth, T. P. Spaniol, J. Okuda, *Organometallics* **2000**, *19*, 4690–4700; e) M. Nishiura, Z. Hou, Y. Wakatsuki, T. Yamaki, T. Miyamoto, *J. Am. Chem. Soc.* **2003**, *125*, 1184–1185.
[8] D. J. Beetstra, A. Meetsma, B. Hessen, J. H. Teuben, *Organometallics* **2003**, *22*, 4372–4374.
[9] A. Otero, J. Fernández-Baeza, A. Antiñolo, A. Lara-Sánchez, E. Martínez-Caballero, J. Tejeda, L. F. Sánchez-Barba, C. Alonso-Moreno, I. López-Solera, *Organometallics* **2008**, *27*, 976–983.
[10] Y. Pan, W. Rong, Z. Jian, D. Cui, *Macromolecules* **2012**, *45*, 1248–1253.
[11] Z. Jian, A. R. Petrov, N. K. Hangaly, S. Li, W. Rong, Z. Mou, K. A. Rufanov, K. Harms, J. Sundermeyer, D. Cui, *Organometallics* **2012**, *31*, 4267–4282.
[12] a) Z. Jian, D. Cui, Z. Hou, *Chem. Eur. J.* **2012**, *18*, 2674–2684; b) Z. Jian, D. Cui, Z. Hou, X. Li, *Chem. Commun.* **2010**, *46*, 3022–3024; c) Z. Jian, S. Tang, D. Cui, *Chem. Eur. J.* **2010**, *16*, 14007–14015.
[13] R. Litlabø, M. Enders, K. W. Törnroos, R. Anwander, *Organometallics* **2010**, *29*, 2588–2595.
[14] P. Jutzi, J. Dahlhaus, *Synthesis* **1993**, *7*, 684–686.
[15] M. Enders, G. Ludwig, H. Pritzkow, *Organometallics* **2001**, *20*, 827–833.
[16] L. N. Jende, C. Maichle-Mössmer, C. Schädle, R. Anwander, *J. Organomet. Chem.* **2013**, 744, 74–81.
[17] a) W. J. Evans, R. Anwander, J. W. Ziller, *Organometallics* **1995**, *14*, 1107–1109; b) M. Zimmermann, N. Å. Frøystein, A. Fischbach, P. Sirsch, H. M. Dietrich, K. W. Törnroos, E. Herdtweck, R. Anwander, *Chem. Eur. J.* **2007**, *13*, 8784–8800.
[18] a) M. Zimmermann, F. Estler, E. Herdtweck, K. W. Törnroos, R. Anwander, *Organometallics* **2007**, *26*, 6029–6041; b) S. Hamidi, L. N. Jende, H. M. Dietrich, C. Maichle-Mössmer, K. W. Törnroos, G. B. Deacon, P. C. Junk, R. Anwander, *Organometallics* **2013**, *32*, 1209–1223.
[19] a) D. P. Krut′ko, M. V. Borzov, R. S. Kirsanov, A. V. Churakov, L. G. Kuz′mina, *J. Organomet. Chem.* **2005**, *690*, 3243–3250; b) D. P. Krut′ko, M. V. Borzov, R. S. Kirsanov, M. Y. Antipin, A. V. Churakov, *J. Organomet. Chem.* **2004**, *689*, 595–604.
[20] P. Jutzi, J. Dahlhaus, M. Bangel, *J. Organomet. Chem.* **1993**, *460*, C13–C15.
[21] W. J. Evans, J. H. Meadows, A. G. Kostka, G. L. Closs, *Organometallics* **1985**, *4*, 324–326.
[22] H. M. Dietrich, C. Zapilko, E. Herdtweck, R. Anwander, *Organometallics* **2005**, *24*, 5767–5771.

[23] H. M. Dietrich, K. W. Törnroos, E. Herdtweck, R. Anwander, *Organometallics* **2009**, *28*, 6739–6749.
[24] a) R. Anwander, M. G. Klimpel, H. M. Dietrich, D. J. Shorokhov, W. Scherer, *Chem. Commun.* **2003**, 1008–1009; b) E. Le Roux, F. Nief, F. Jaroschik, K. W. Tornroos, R. Anwander, *Dalton Trans.* **2007**, 4866–4870.
[25] R. Anwander, W. A. Herrmann, W. Scherer, F. C. Munck, *J. Organomet. Chem.* **1993**, *462*, 163–174.
[26] I. L. Fedushkin, S. Dechert, H. Schumann, *Organometallics* **2000**, *19*, 4066–4076.
[27] M. Terrier, M. Visseaux, T. Chenal, A. Mortreux, *J. Polym. Sci. Part A J. Polym. Sci. Part A: Polym. Chem.* **2007**, *45*, 2400–2409.
[28] J. Pflug, A. Bertuleit, G. Kehr, R. Fröhlich, G. Erker, *Organometallics* **1999**, *18*, 3818–3826.
[29] SMART, v.5.054, Data Collection Software for Bruker AXS CCD, Bruker AXS, Inc., Madison, WI **1999**.
[30] SAINT, v.6.45A, Data Integration Software for Bruker AXS CCD, Bruker AXS, Inc., Madison, WI **2002**.
[31] SHELXTL, v.6.14, Structure Determination Software Suite, Bruker AXS, Inc., Madison, WI **2000**.
[32] G. M. Scheldrick, SADABS, v.2001/1, University of Göttingen, Germany, **2001**.
[33] G. M. Scheldrick, SHELXS-97, Program for Crystal Structure Solution, University of Göttingen, Germany, **1997**.
[34] G. M. Scheldrick, SHELXL-97, Program for Crystal Structure Refinement, University of Göttingen, Germany, **1997**.
[35] L. J. Farrugia, *J. Appl. Crystallogr.* **1997**, *30*, 565.

Received: June 21, 2013
Published online: October 21, 2013

CHEMISTRY
A EUROPEAN JOURNAL

Supporting Information

Rare-Earth-Metal Alkylaluminates Supported by N-Donor-Functionalized Cyclopentadienyl Ligands: C−H Bond Activation and Performance in Isoprene Polymerization

Lars N. Jende, Cäcilia Maichle-Mössmer, and Reiner Anwander*[a]

chem_201302388_sm_miscellaneous_information.pdf

Figure S1: ^{1}H NMR spectrum (C_6D_6, 25 °C) of complex **1a**

Figure S2: 2D ^{1}H-^{13}C HSQC NMR spectrum (C_6D_6, 25 °C) of complex **1a**

Figure S3: ^{1}H NMR spectrum (C_6D_6, 25 °C) of complex **1c**

Figure S4: 2D ^{1}H-^{13}C HSQC NMR spectrum (C_6D_6, 25 °C) of complex **1c**

Figure S5: ^{1}H NMR spectrum (C_7D_8, 25 °C) of complex **2**

Figure S6: ^{1}H NMR spectrum (C_6D_6, 25 °C) of complex **3a**

Figure S7: 2D ^{1}H-^{13}C HSQC NMR spectrum (C_6D_6, 25 °C) of complex **3a**

Figure S8: ^{1}H NMR spectrum (C_6D_6, 25 °C) of complex **4a**

Figure S9: 2D ^{1}H-^{13}C HSQC NMR spectrum (C_6D_6, 25 °C) of complex **4a**

Figure S10: ^{1}H NMR spectrum (C_6D_6, 25 °C) of complex **5a**

Figure S11: 2D ^{1}H-^{13}C HSQC NMR spectrum (C_6D_6, 25 °C) of complex **5a**

Figure S12: ^{1}H NMR spectrum (C_6D_6, 25 °C) of complex **5c**

Figure S13: 2D ^{1}H-^{13}C HSQC NMR spectrum (C_6D_6, 25 °C) of complex **5c**

Figure S14: Molecular structure of [($Cp^{NMe2\{AlMe3\}}$)Nd($AlMe_4$)$_2$] (**1b**)

Figure S15: Molecular structure of [($Cp^{NMe2\{AlMe3\}}$)Y($AlMe_4$)$_2$] (**1c**)

Figure S16: Molecular structure of [(Cp^{NMe}\{μ-CH_2\}$AlMe_3$)Nd($AlMe_4$)] (**3b**)

Figure S17: Molecular structure of [($Cp^{AMe2\{AlMe3\}}$)Nd($AlMe_4$)$_2$] (**4b**)

Figure S18: Molecular structure of [(Cp^{AMe}\{μ-CH_2\}$AlMe_3$)Nd($AlMe_4$)] (**5b**)

Figure S19: Molecular structure of [(Cp^{NMe}\{μ-CH_2\}$AlMe_3$)Y($AlMe_4$)] (**5c**)

Figure S20: Molecular structure of the cyclopentenol intermediate

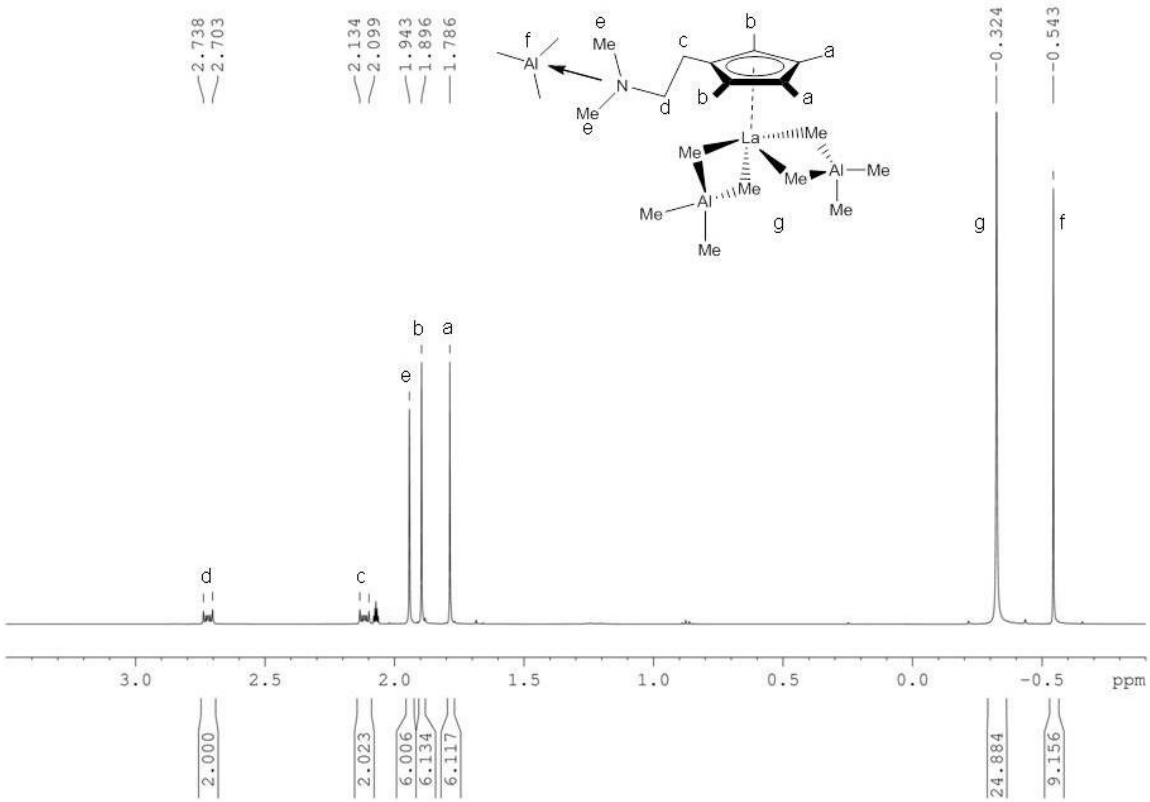

Figure S1: ^{1}H NMR spectrum (C_6D_6, 25 °C) of complex **1a**

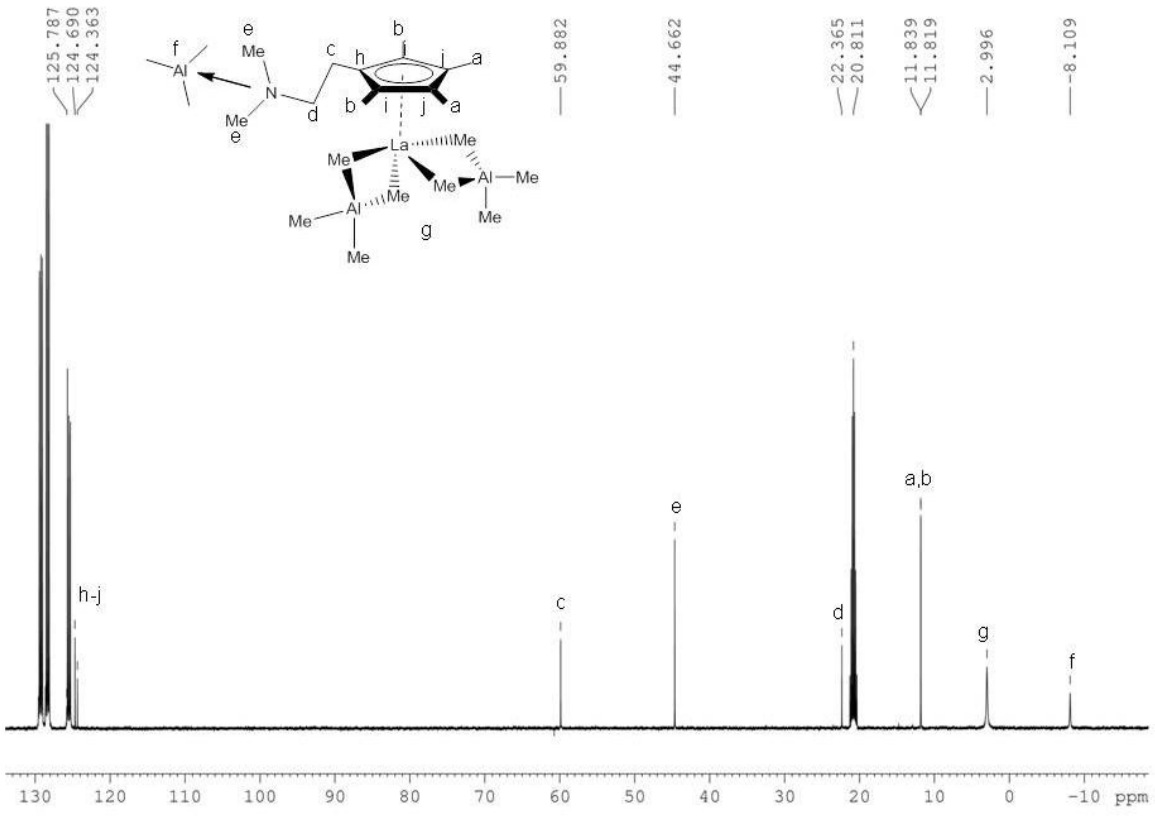

Figure S2: ^{13}C NMR spectrum (C_6D_6, 25 °C) of complex **1a**

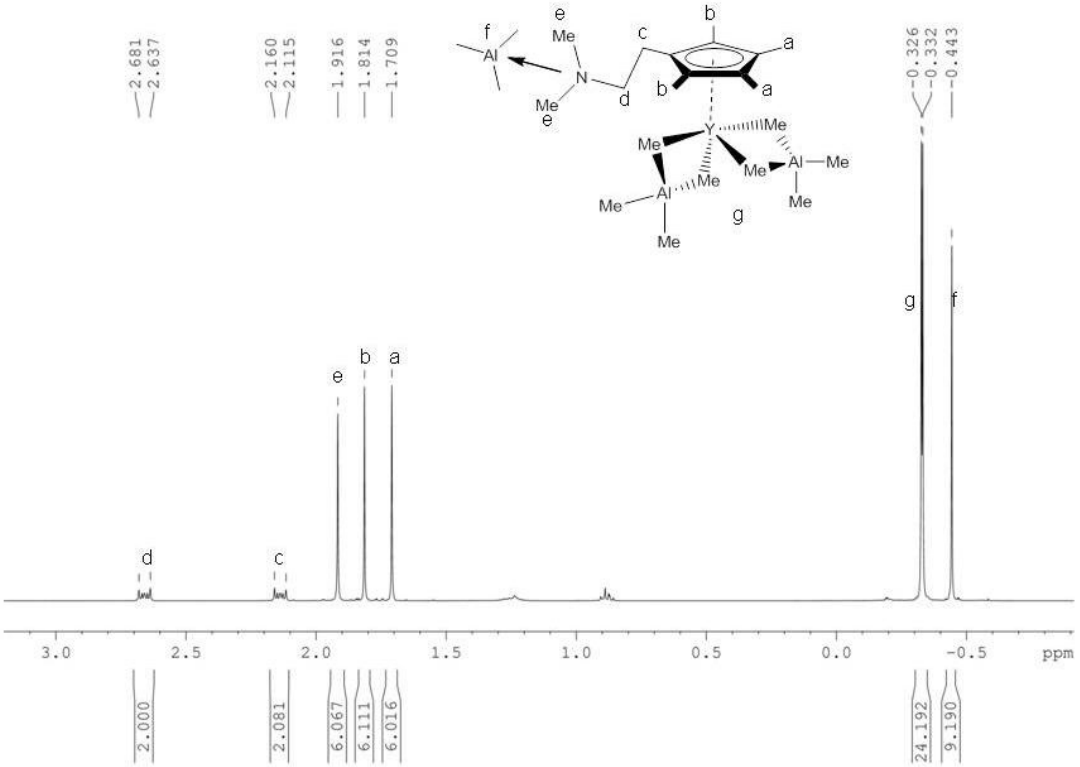

Figure S3: ^{1}H NMR spectrum (C_6D_6, 25 °C) of complex **1c**

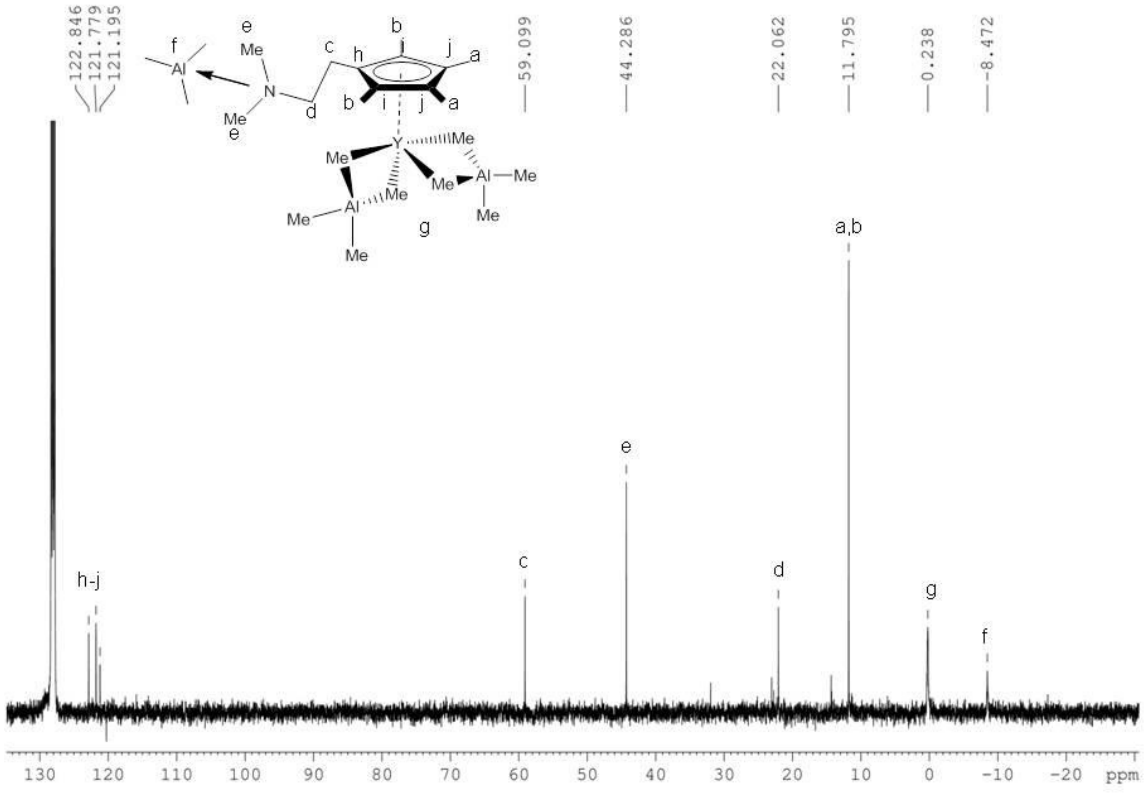

Figure S4: ^{13}C NMR spectrum (C_6D_6, 25 °C) of complex **1c**

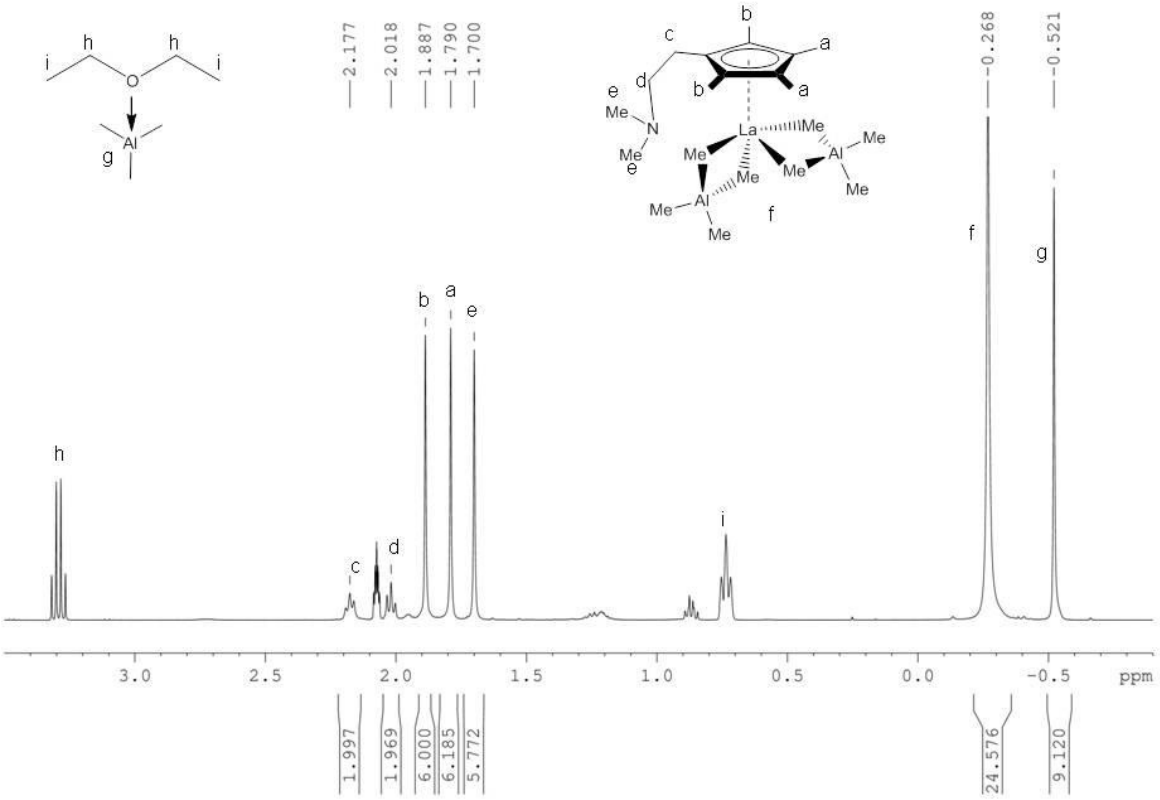

Figure S5: ^{1}H NMR spectrum (C_7D_8, 25 °C) of complex **2**

Note! To prevent C-H activation, donor-assisted displacement of trimethylaluminum from complex **1a** was carried out at -35 °C (see experimental section). The *J. Young* NMR valve was then further cooled until the start of the NMR experiment.

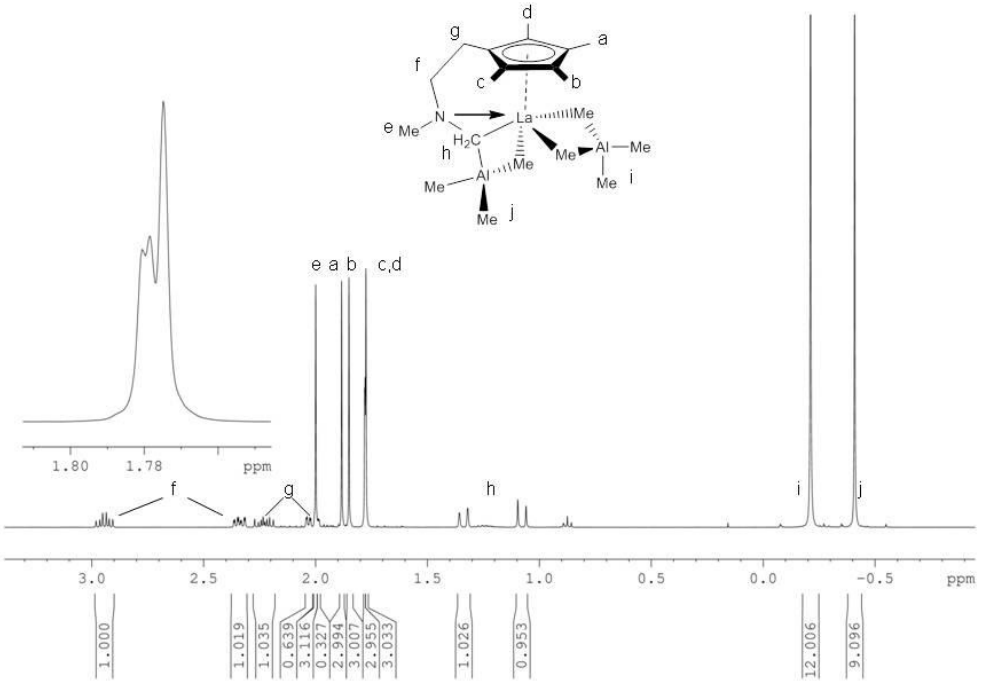

Figure S6: ^{1}H NMR spectrum (C_6D_6, 25 °C) of complex **3a**

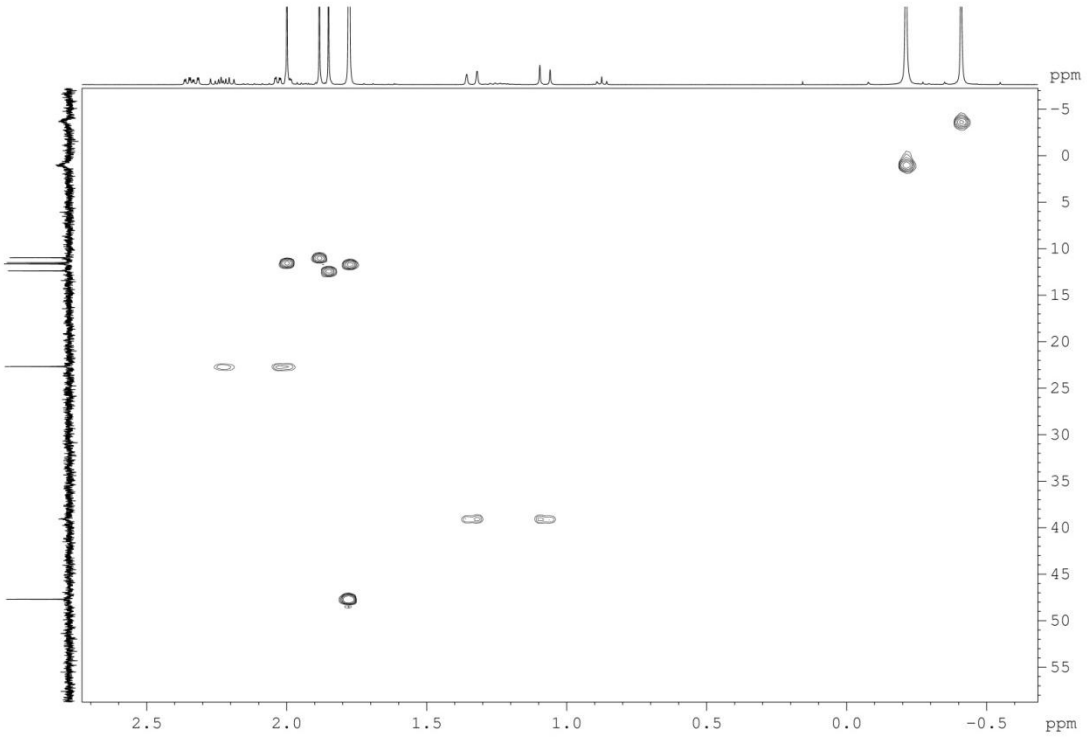

Figure S7: 2D ^{1}H-^{13}C HSQC NMR spectrum (C_6D_6, 25 °C) of complex **3a**

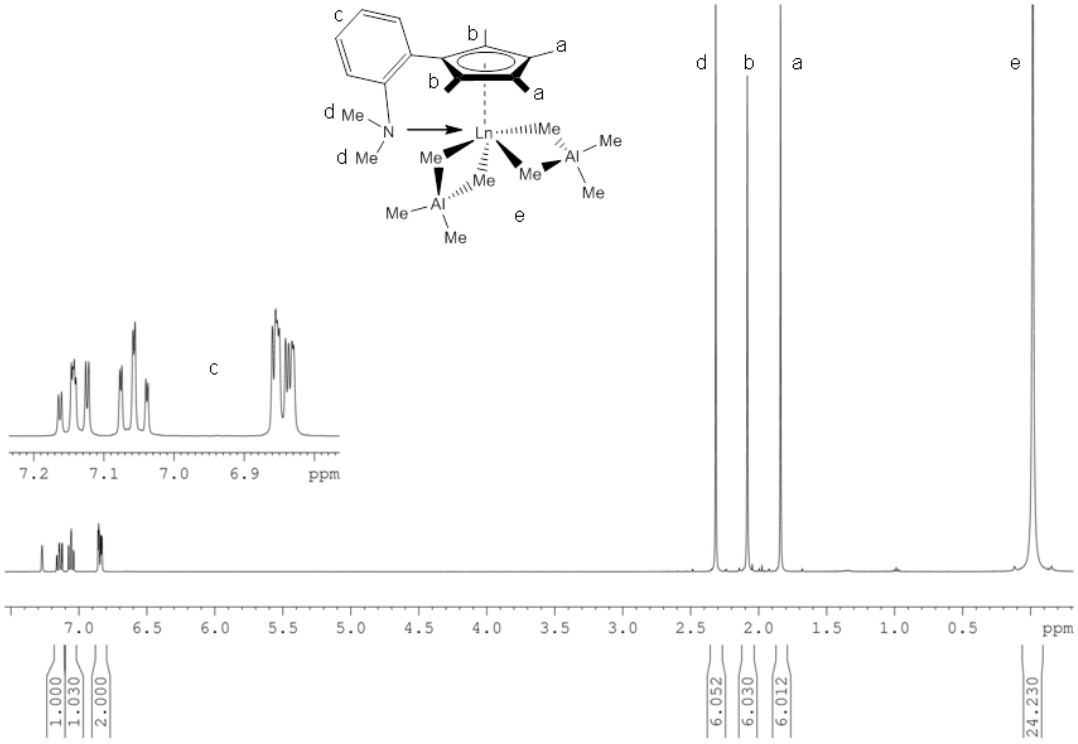

Figure S8: ^{1}H NMR spectrum (C_6D_6, 25 °C) of complex **4a**

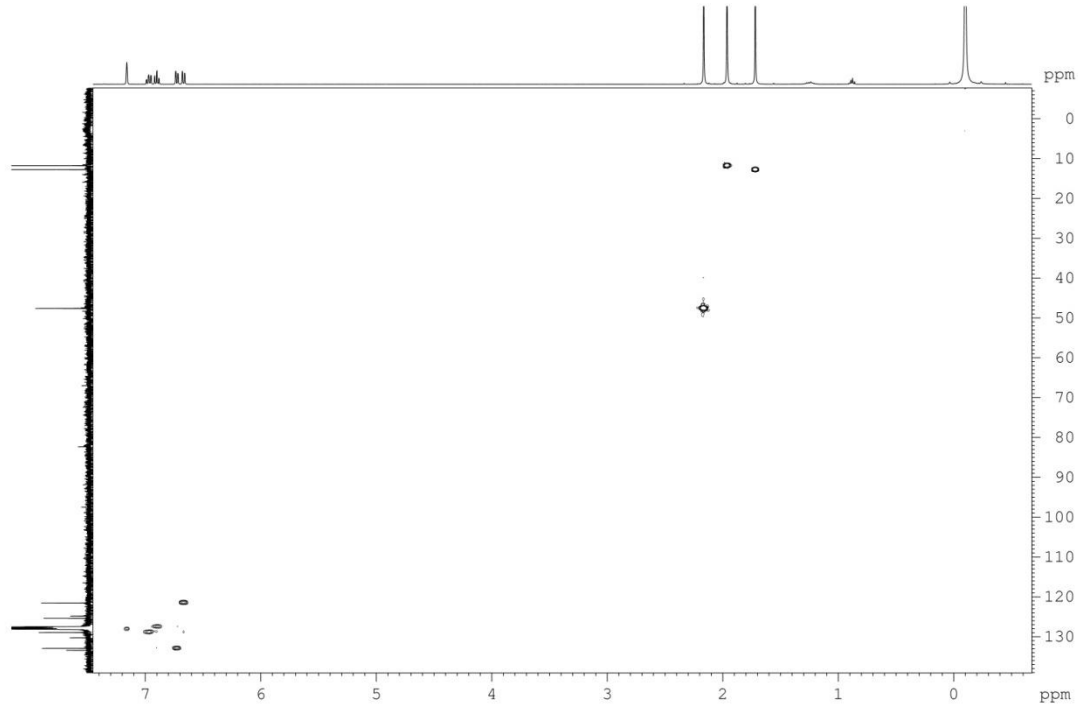

Figure S9: 2D ^{1}H-^{13}C HSQC NMR spectrum (C_6D_6, 25 °C) of complex **4a**

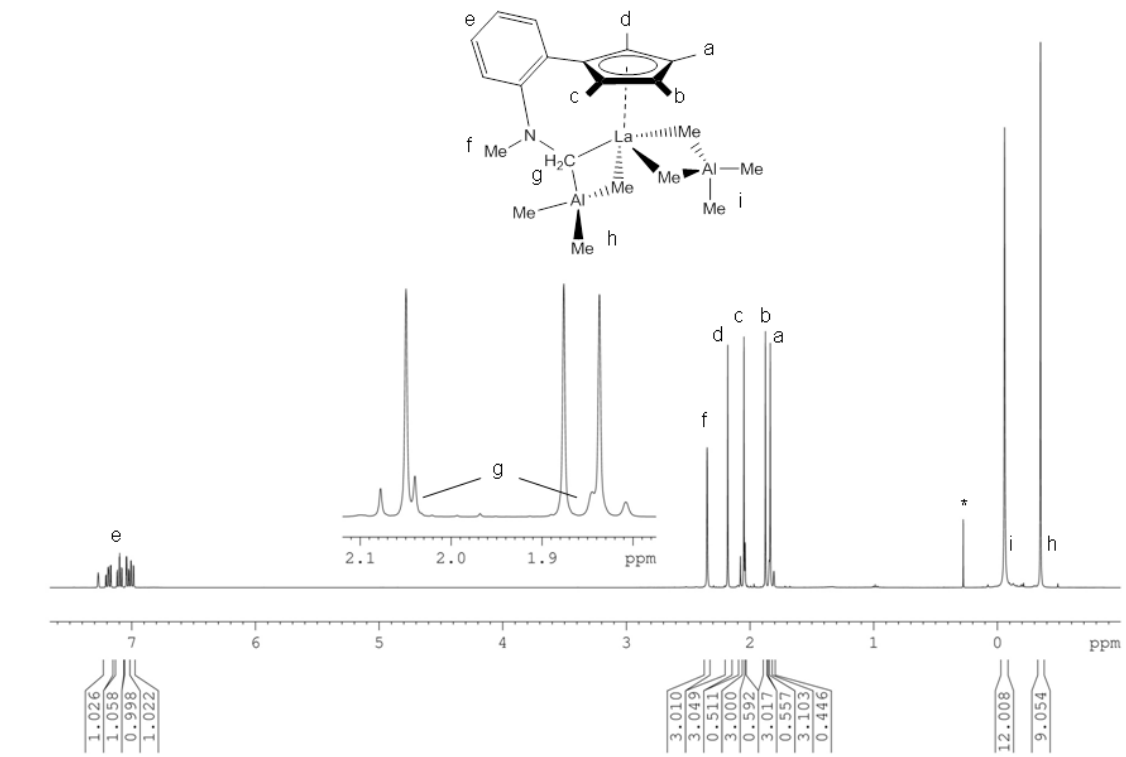

Figure S10: ^{1}H NMR spectrum (C_6D_6, 25 °C) of complex **5a** (* = methane)

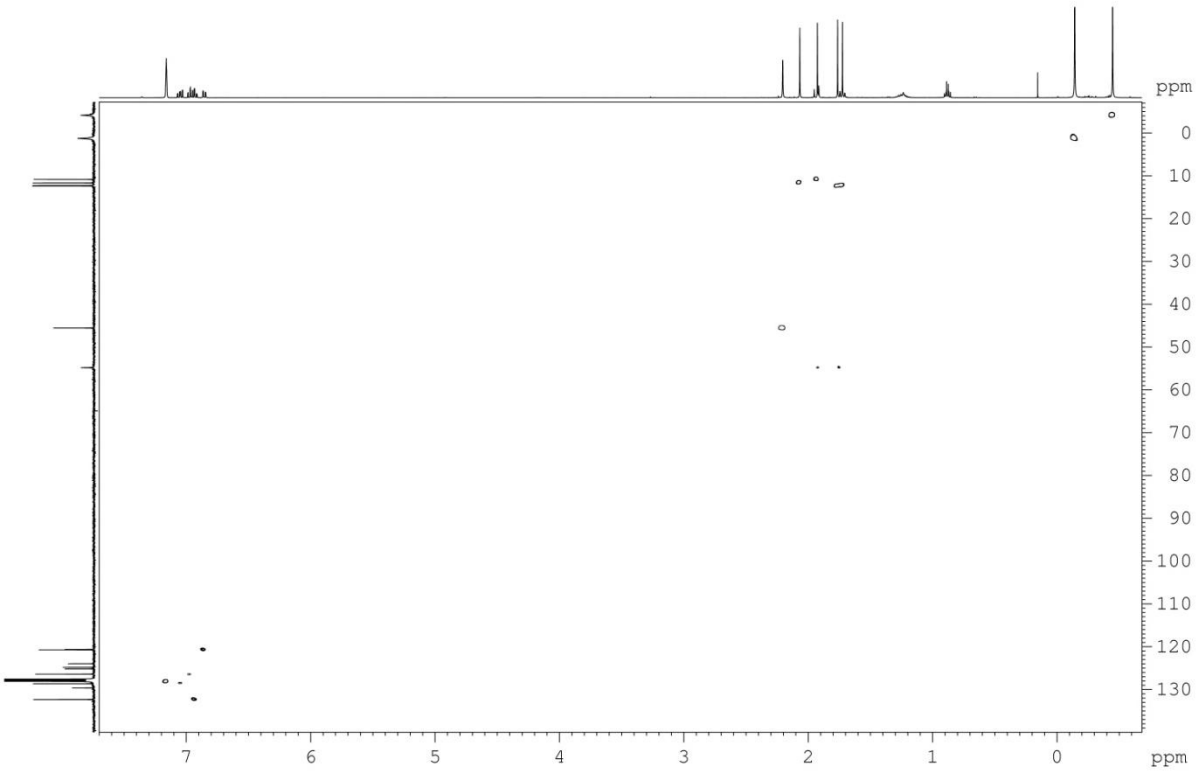

Figure S11: 2D ^{1}H-^{13}C HSQC NMR spectrum (C_6D_6, 25 °C) of complex **5a**

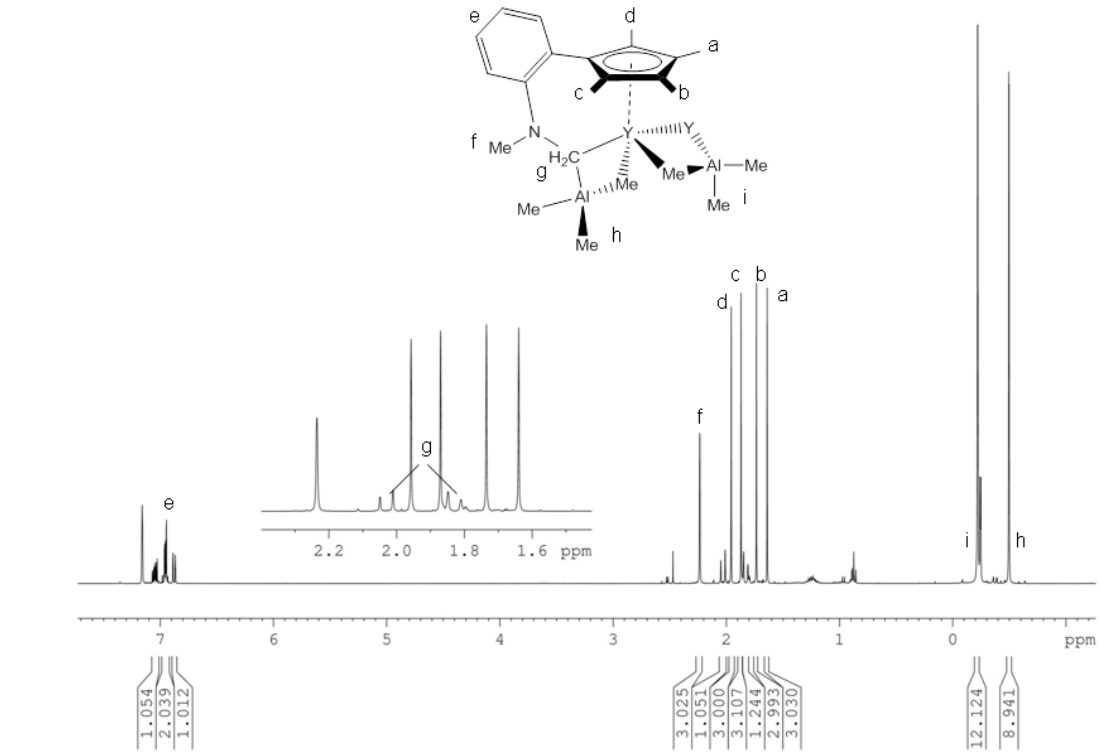

Figure S12: ^{1}H NMR spectrum (C_6D_6, 25°C) of complex **5c**

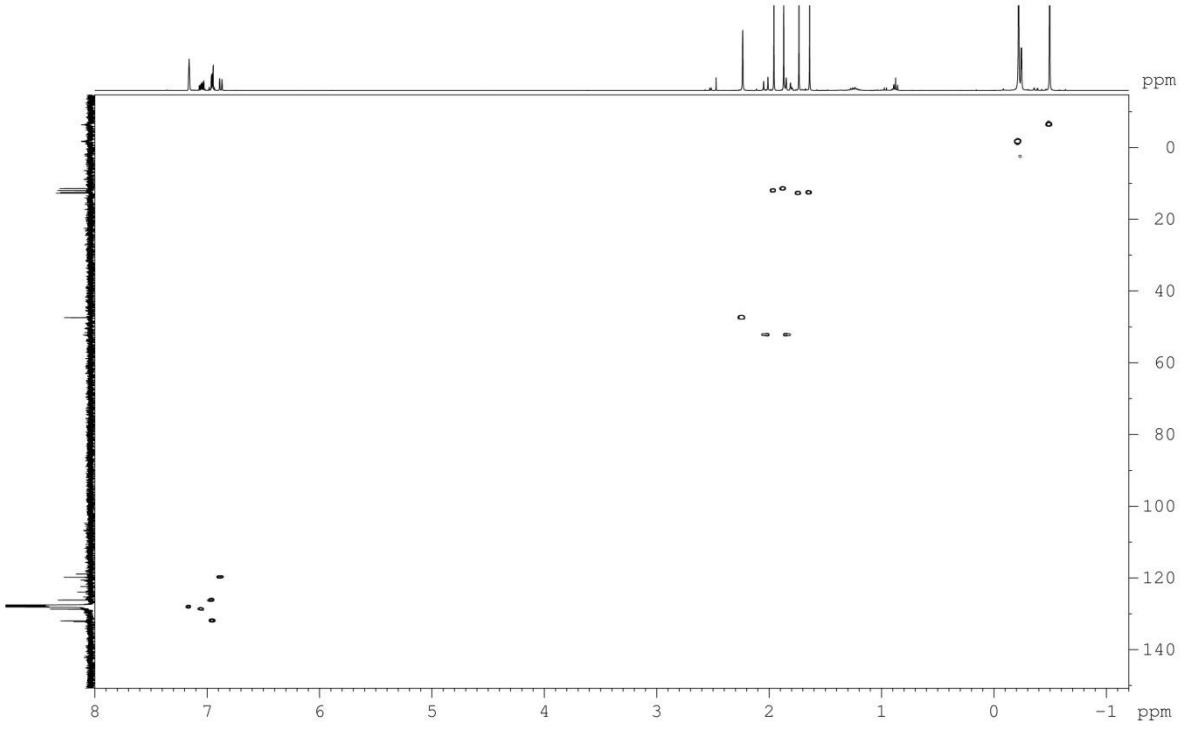

Figure S13: 2D ^{1}H-^{13}C HSQC NMR spectrum (C_6D_6, 25°C) of complex **5c**

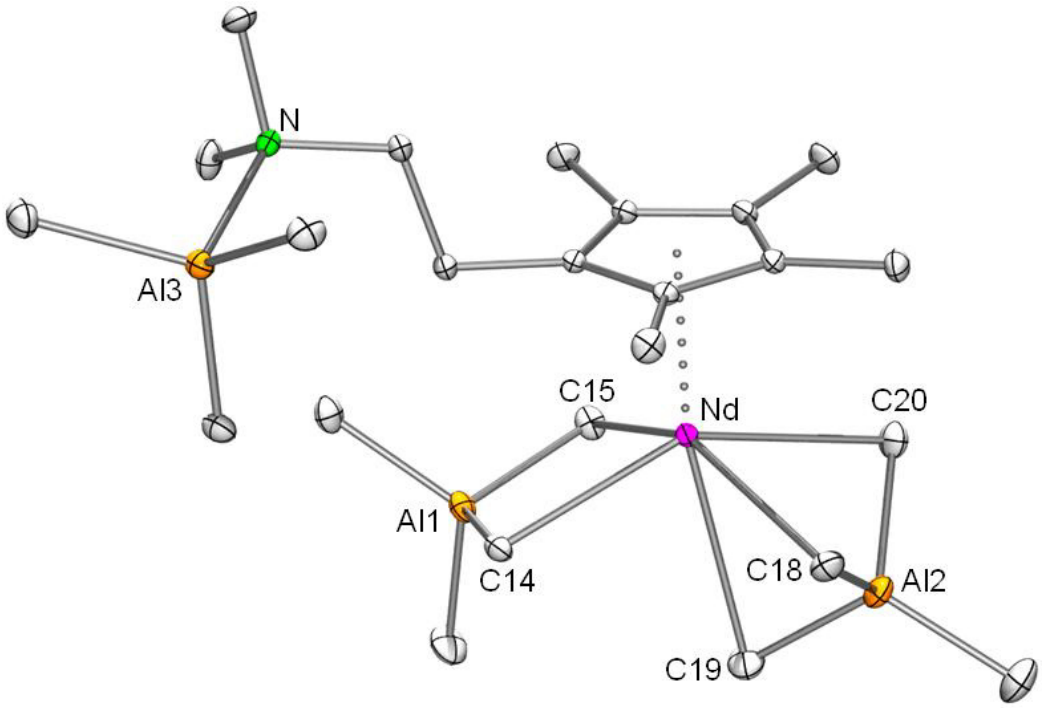

Figure S14: Molecular structure of [($Cp^{NMe2\{AlMe3\}}$)Nd($AlMe_4$)$_2$] (**1b**); atomic displacement parameters are set at the 50% level; hydrogen atoms have been omitted for clarity.

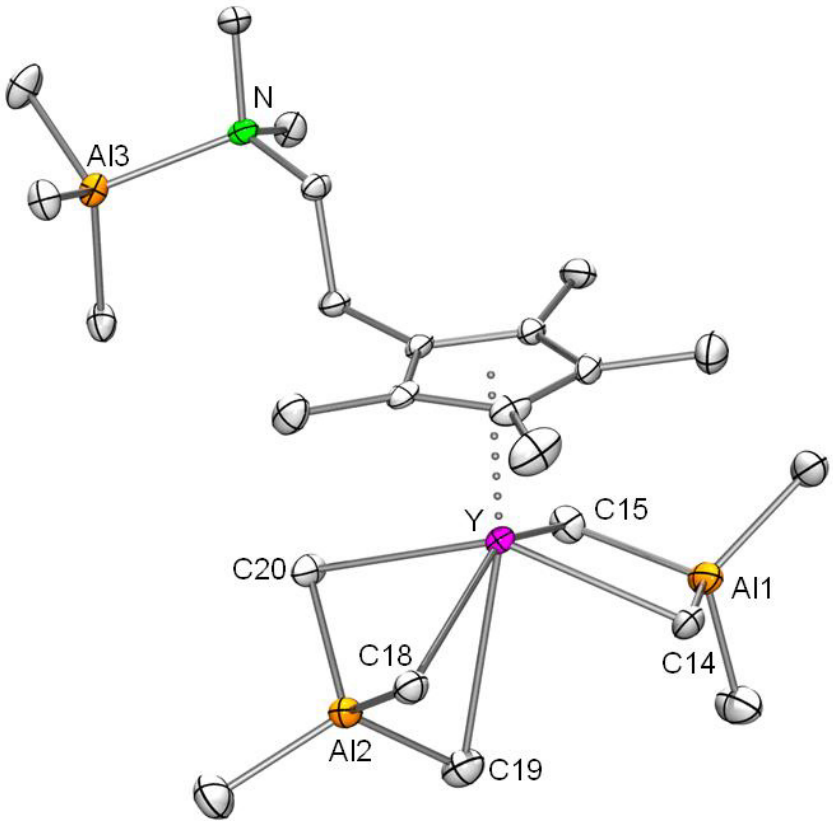

Figure S15: Molecular structure of [($Cp^{NMe2\{AlMe3\}}$)Y($AlMe_4$)$_2$] (**1c**); atomic displacement parameters are set at the 50% level; hydrogen atoms have been omitted for clarity.

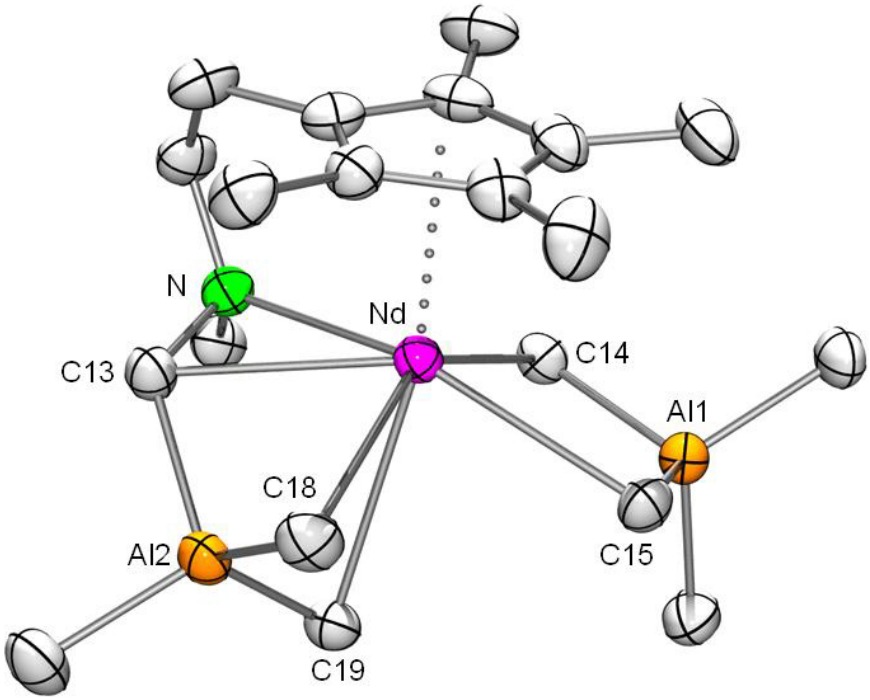

Figure S16: Molecular structure of [(Cp^{NMe}\{μ-CH_2\}$AlMe_3$)Nd($AlMe_4$)] (**3b**); atomic displacement parameters are set at the 50% level; hydrogen atoms have been omitted for clarity.

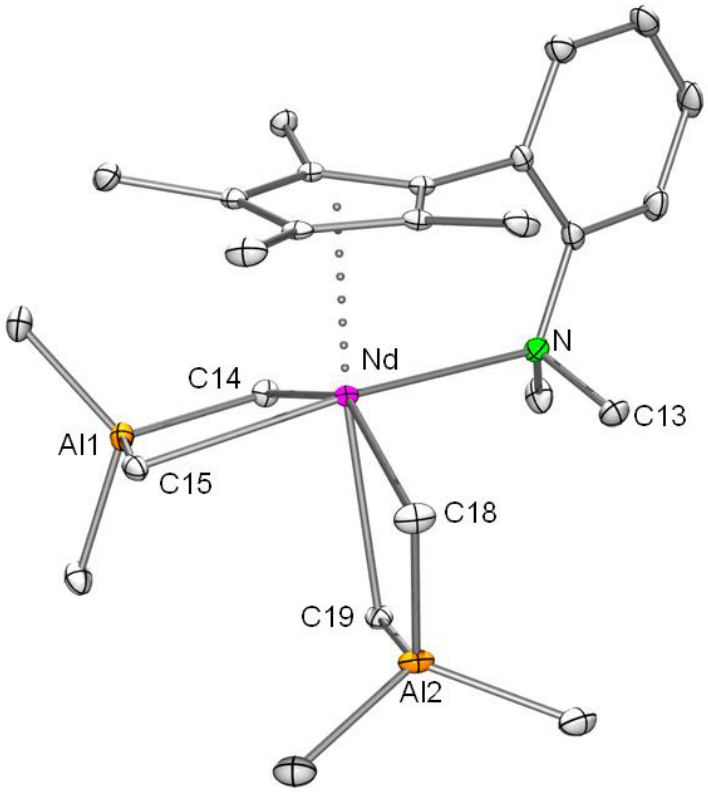

Figure S17: Molecular structure of [(Cp^{AMe2})Nd($AlMe_4$)$_2$] (**4b**); atomic displacement parameters are set at the 50% level; hydrogen atoms have been omitted for clarity.

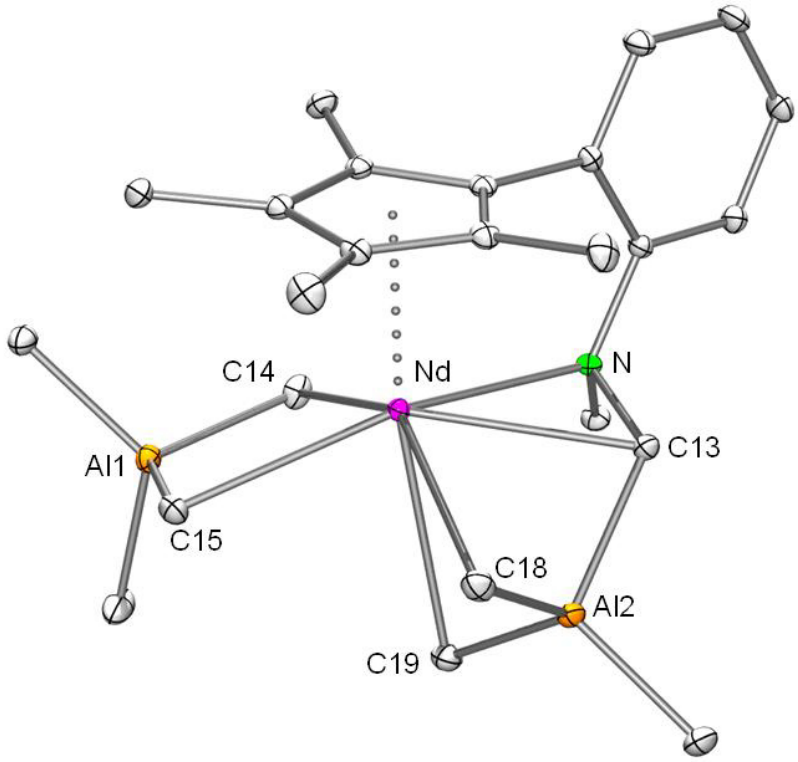

Figure S18: Molecular structure of [(Cp^{AMe}\{μ-CH_2\}$AlMe_3$)Nd($AlMe_4$)] (**5b**); atomic displacement parameters are set at the 50% level; hydrogen atoms have been omitted for clarity.

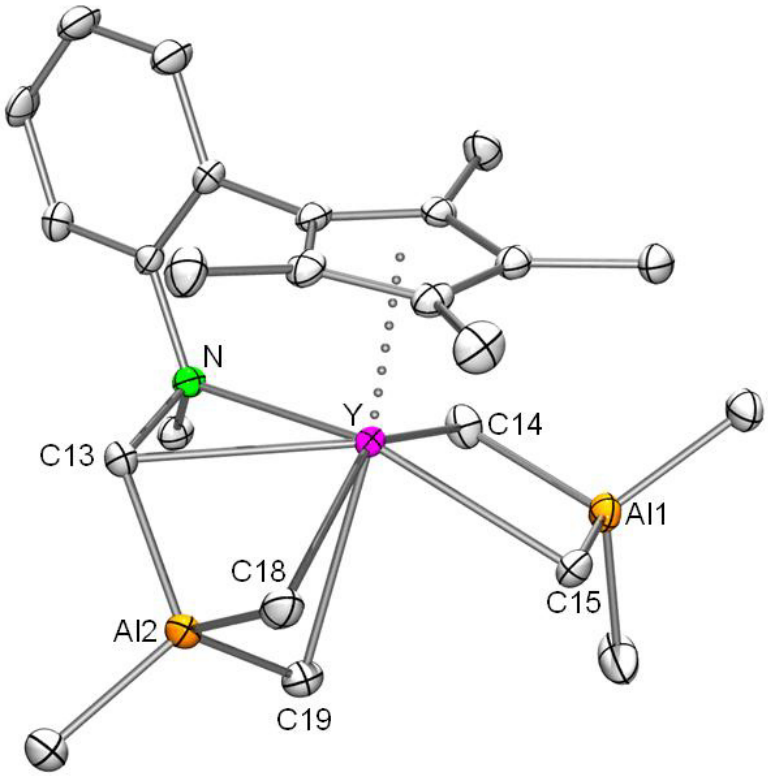

Figure S19: Molecular structure of [(Cp^{AMe}\{μ-CH_2\}$AlMe_3$)Y($AlMe_4$)] (**5c**); atomic displacement parameters are set at the 50% level; hydrogen atoms have been omitted for clarity.

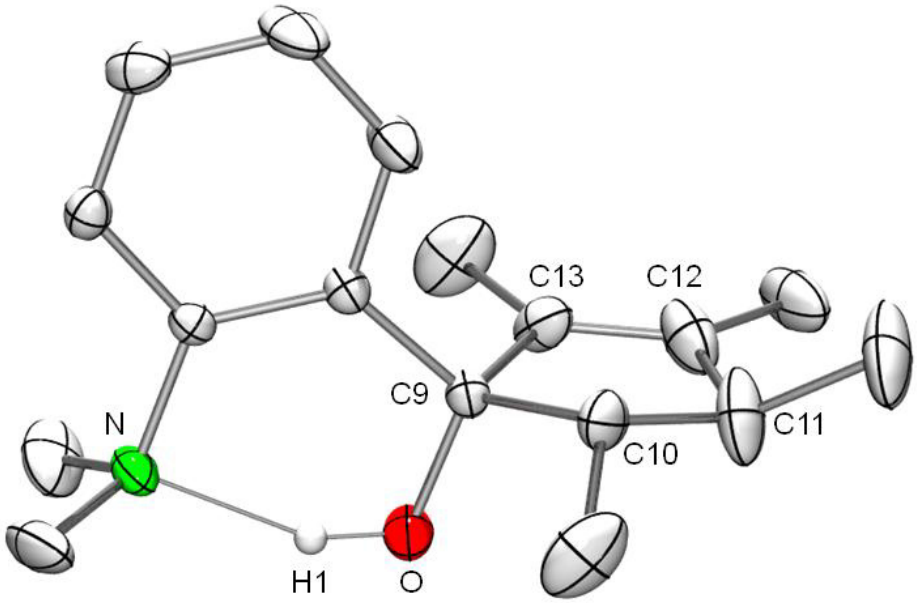

Figure S20: Molecular structure of 1-[1-(*N*,*N*-dimethylanilinyl)]-2,3,4,5-tetramethyl-cyclopenten-1-ol, which is the precursor of HCp^{AMe2}. Atomic displacement parameters are set at the 50% level; hydrogen atoms except from the hydroxyl group have been omitted for clarity. It crystallizes in the monoclinic space group $P2_1/n$, with cell parameters: a = 8.28110(10), b = 20.5270(4), c = 9.1870(2) [Å]; α = 90.00, β = 98.7790(10), γ = 90.00 [°]. Selected bond length (Å): C10–C11 = 1.495(3), C10–C11 = 1.510(4), C12–C13 = 1.370(4), C9–O = 1.421(2), O–H1 = 0.86(3); CCDC = 950316.

Paper II

ELSEVIER LICENSE
TERMS AND CONDITIONS

Apr 07, 2015

This is a License Agreement between Lars Jende ("You") and Elsevier ("Elsevier") provided by Copyright Clearance Center ("CCC"). The license consists of your order details, the terms and conditions provided by Elsevier, and the payment terms and conditions.

All payments must be made in full to CCC. For payment instructions, please see information listed at the bottom of this form.

Supplier	Elsevier Limited The Boulevard,Langford Lane Kidlington,Oxford,OX5 1GB,UK
Registered Company Number	1982084
Customer name	Lars Jende
Customer address	Eichhaldenstr 23 Tuebingen, DE 72074
License number	3603710036352
License date	Apr 07, 2015
Licensed content publisher	Elsevier
Licensed content publication	Journal of Organometallic Chemistry
Licensed content title	Yttrium half-sandwich complexes bearing the 2-(N,N-dimethylamino)ethyl-tetramethylcyclopentadienyl ligand
Licensed content author	None
Licensed content date	1 November 2013
Licensed content volume number	744
Licensed content issue number	n/a
Number of pages	8
Start Page	74
End Page	81
Type of Use	reuse in a thesis/dissertation
Portion	full article
Format	electronic
Are you the author of this Elsevier article?	Yes
Will you be translating?	No
Title of your thesis/dissertation	Donor-Substituted Cyclopentadienyl Ligands in Rare-Earth Metal-Based Isoprene Polymerization
Expected completion date	May 2015
Estimated size (number of pages)	108
Elsevier VAT number	GB 494 6272 12
Permissions price	0.00 EUR
VAT/Local Sales Tax	0.00 EUR / 0.00 GBP
Total	0.00 EUR
Terms and Conditions	

Journal of Organometallic Chemistry 744 (2013) 74–81

Contents lists available at SciVerse ScienceDirect

Journal of Organometallic Chemistry

journal homepage: www.elsevier.com/locate/jorganchem

Yttrium half-sandwich complexes bearing the 2-(*N*,*N*-dimethylamino) ethyl-tetramethylcyclopentadienyl ligand

Lars N. Jende, Cäcilia Maichle-Mössmer, Christoph Schädle, Reiner Anwander*

Institut für Anorganische Chemie, Universität Tübingen, Auf der Morgenstelle 18, D-72076 Tübingen, Germany

ARTICLE INFO

Article history:
Received 10 April 2013
Received in revised form
2 May 2013
Accepted 3 May 2013

Dedicated to Professor Wolfgang A. Herrmann on the occasion of his 65th Birthday.

Keywords:
Alkyl
Silylamide
Cyclopentadienyl
Donor-functionalization
Yttrium
SiH activation

ABSTRACT

The synthesis of bis(dimethylsilyl)amide and dimethyl half-sandwich complexes of yttrium bearing the 2-(*N*,*N*-dimethylamino)ethyl-tetramethylcyclopentadienyl ligand revealed unusual Si–H activation reactions and *ate* complex formation, respectively. Protonolysis of complex $Y[N(SiHMe_2)_2]_3(thf)_2$ with cyclopentadiene $C_5Me_4HCH_2CH_2NMe_2$ (HCp^{NMe2}) at elevated temperature yielded complex $Cp^{NMe2}Y[\eta^2\text{-}SiMe_2(NSiHMe_2)_2](thf)$ featuring a four-membered metallacycle. The bis(amido) ligand $[\eta^2\text{-}SiMe_2(NSiHMe_2)_2]^{2-}$ is shown to form via separation of H_2SiMe_2. In contrast, the salt metathesis reaction of $YCl_3(thf)_3$ with $LiN(SiHMe_2)_2$ and $LiCp^{NMe2}$ in a 1/2/1 ratio at ambient temperature generated the non-activated complex $Cp^{NMe2}Y[N(SiHMe_2)_2]_2$, exhibiting a distinct ligand activation at elevated temperatures, as evidenced by a comprehensive NMR spectroscopic study. Application of a sequential salt metathesis protocol involving $YCl_3(thf)_3$, $LiCp^{NMe2}$, and LiMe led to the isolation of ate complexes $[Cp^{NMe2}YCl_2]_2[LiCl(thf)_2]$ and $[Cp^{NMe2}YMe_2(LiMe)]_2$. Aforementioned half-sandwich complexes were all characterized by X-ray structure analyses and the respective silylamido and methyl derivatives are demonstrated to produce the half-sandwich yttrium bis(tetramethylaluminate) complex $[Cp^{NMe2Al\text{-}Me3}Y(AlMe_4)_2]$ in the presence of excess trimethylaluminium, by NMR spectroscopic studies.

1. Introduction

Monocyclopentadienyl or half-sandwich-type complexes emerged as a prolific field in organorare-earth metal chemistry [1]. Particularly, highly reactive alkyl, hydrido, and amido derivatives and their cationic variants have revealed unique catalytic potential in polymerization reactions [1]. Approximately ten years ago, we set out to use tetramethylaluminato ligands as thermally robust alkyls in disguise and found that they are ideally suited to stabilize rare-earth metal half-sandwich complexes [2]. The corresponding complexes $Cp^RLn(AlMe_4)_2$ represent the first entries of the **L**Ln(III) bis(tetramethylaluminate)-based postmetallocene library (**L** = monoanionic ancillary ligand), which is currently exploited for 1,3-diene polymerization [3]. Furthermore, donor-functionalized cyclopentadienyl ligands often ensure the formation of monolanthanide complexes via additional intramolecular coordination [1,4]. Amino functionalities are particularly effective for rare-earth metal(III) centres due to a good HSAB match and optimal steric shielding [5]. To date, bis(aluminate) complexes $Cp^RLn(AlMe_4)_2$ have been synthesized according to two main reaction sequences (Scheme 1, A and B). While route A exploits the thermal stability of homoleptic tetramethylaluminate complexes $Ln(AlMe_4)_3$ [6], route B refers to the well-defined bis(dimethylsilyl)amide derivatives $Ln[N(SiHMe_2)_2]_3(thf)_x$ (*extended silylamide route*) [7]. Herein we examined synthesis strategies B and C for assessing the feasibility of yttrium bis(aluminate) complexes $Cp^{NMe2}Y(AlMe_4)_2$, with Cp^{NMe2} designating $\eta^5\text{-}C_5Me_4CH_2CH_2NMe_2$ (1-[2-(*N*,*N*-dimethylamino)-ethyl]-2,3,4,5-tetramethyl-cyclopentadienyl) [8].

2. Results and discussion

2.1. Route B

Aiming at a bis(aluminate) half-sandwich complex with an amino-coordinated yttrium centre, we initially focused on pre-coordinating the cyclopentadienyl ligand in a $\eta^5{:}\kappa^1$ fashion to the rare-earth metal. Thus formed complex $Cp^{NMe2}Y[N(SiHMe_2)_2]_2$ should engage in a trimethylaluminum-promoted silylamido/aluminato exchange under mild conditions and formation of the corresponding hydrocarbyl complexes [2]. It is noteworthy that very recently half-sandwich rare-earth metal bis(dimethylsilyl)amide complexes were successfully tested in styrene polymerization upon activation with perfluorated organborate salts ($[Ph_3C][B(C_6F_5)_4]$, $[PhNMe_2H][B(C_6F_5)_4]$ [9,10]. However, the activity was low and

* Corresponding author.
E-mail address: reiner.anwander@uni-tuebingen.de (R. Anwander).

0022-328X/$ – see front matter © 2013 Elsevier B.V. All rights reserved.
http://dx.doi.org/10.1016/j.jorganchem.2013.05.002

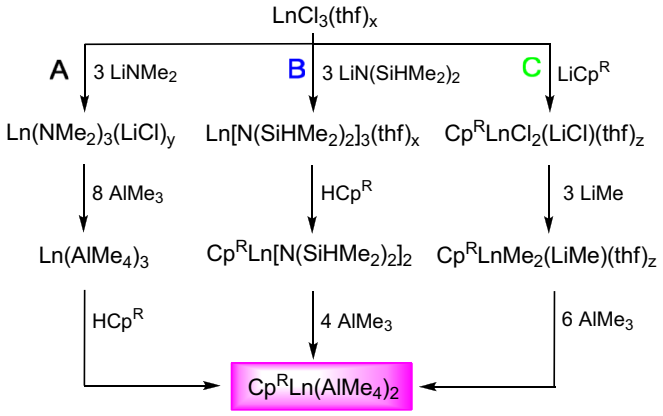

Scheme 1. Protocols considered for the synthesis of complexes $Cp^{R}Ln(AlMe_4)_2$.

addition of trialkylaluminum was necessary to form a ternary catalyst system of complex/borate/AlR_3 (AlR_3; R = Me, ^{i}Bu). The protonolysis reaction of yttrium bis(dimethylsilyl)amide complex $Y[N(SiHMe_2)_2]_3(thf)_2$ [7a] with one equivalent of the N-donor functionalized cyclopentadiene HCp^{NMe2} in toluene at 150 °C yielded the Si–H bond activated complex $Cp^{NMe2}Y[\eta^2SiMe_2(NSiHMe_2)_2](thf)$ (**1**) in moderate yields (68%) (Scheme 2). As previously observed for the synthesis of half-sandwich complex $(C_5Me_5)Y[N(SiHMe_2)_2]_2$ [2] the silylamine elimination took place only at elevated temperature (according to an ^{1}H NMR spectroscopic study the reaction did not occur below 70 °C).

Single crystals of **1** suitable for X-ray diffraction analysis were grown from saturated toluene solutions at −35 °C (space group *P*-1, Fig. 1). The yttrium centre is $\eta^5{:}\kappa^1$ coordinated by the N-donor substituted cyclopentadienyl ligand via the Cp ring and the nitrogen atom. The dianionic bisamido ligand $[SiMe_2(NSiHMe_2)_2]^{2-}$ coordinates in a η^2 fashion via the two nitrogen atoms, while an additional thf molecule completes the coordination sphere of the yttrium centre.

The geometry of complex **1** is best described as distorted trigonal bipyramidal, with the nitrogen atoms N1 and N3 in the apical position disclosing an angle of 145.2° at the metal centre, while the centroid of the cyclopentadienyl together with the nitrogen atom N2 and the oxygen atom of the thf molecule are in the equatorial positions with angles close to trigonal planar (118.0, 120.1 and 121.5°). Interestingly, both Si–H units are oriented towards the electrophilic Y^{3+} centre, but Y···HSi β-agostic interactions can be ruled out since the Y···H distances are longer than 3.7 Å. The absence of such secondary interactions is also evidenced by the lack of Si–H stretching vibrations at lower frequencies (2000–1800 cm^{-1}) [11]. The most striking feature of complex **1** is the generation of the chelating (dimethylsilylene)-bis(dimethylsilylamido) ligand itself, although such Si–H bond activation along with the formation of a new Si–N bond under elimination of H_2SiMe_2 has been observed previously. In 2009, Yuen and Marks observed the generation of a bidentate

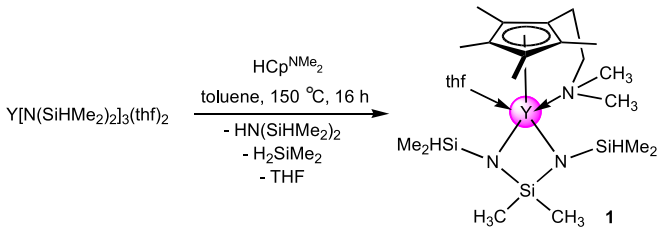

Scheme 2. Synthesis of the bisamido yttrium half-sandwich complex **1**.

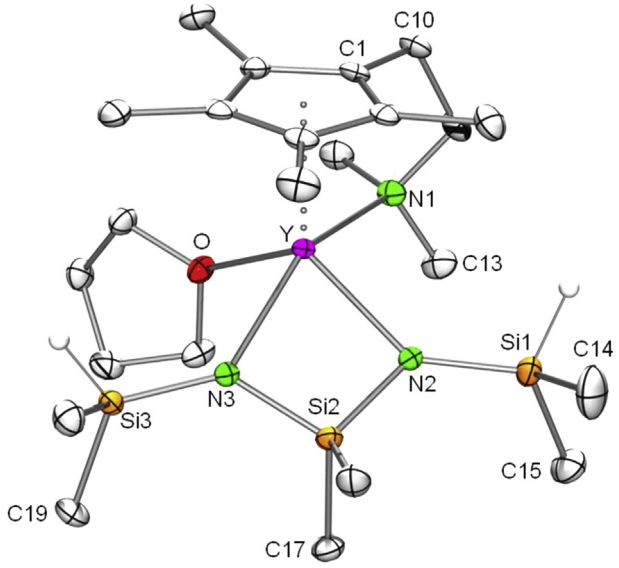

Fig. 1. ORTEP view of the molecular structure of **1**. Atomic displacement parameters are set at the 50% probability level. Hydrogen atoms (except for SiH) are omitted for clarity. Selected bond lengths (Å) and angles (°) for **1**: Y–Cp_{cent} = 2.381, Y–O = 2.388(4), Y–N1 = 2.629(3), Y–N2 = 2.249(3), Y–N3 = 2.276(3), Si1–N2 = 1.719(3), Si3–N3 = 1.719(3), Si2–N2 = 1.694(4), Si2–N3 = 1.683(3), N1–Y–N2 = 93.8(1), N2–Y–N3 = 71.6(1), N1–Y–N3 = 145.2(1), N1–Y–O = 77.5(1), O–Y–N3 = 83.8(1), Cp_{cent}–Y–N2 = 120.1(1), Cp_{cent}–Y–O = 118.0(1), O–Y–N2 = 121.5(1).

amido-amine ligand during a transamination protocol, utilizing Nd $[N(SiMe_3)_2]_3$ and $HN(SiHMe_2)_2$ for the synthsis of $Nd[N(SiHMe_2)_2]_3$. The formation of monoanionic $[SiMe_2(NSiHMe_2)(NHSiHMe_2)]^-$ ligand was confirmed by a ligand exchange reaction with a binucluear lanthanum complex and subsequent X-ray diffraction analysis (Chart 1, **A**) [12]. The same divalent ligand as present in complex **1** was reported by Buffet and Okuda in 2011, to result from a protonolysis reaction of $Sc[N(SiHMe_2)_2]_3(thf)$ with Me_3[12]aneN$_4$ in C_6D_6 at 80 °C (Chart 1, **B**) [13]. Very recently, Chen et al. were able to isolate the cationic amidinate scandium amide complex [(PhC{N-2,6-$^{i}Pr_2C_6H_3$}$_2$)Sc(N{SiHMe$_2$}{SiMe$_2$N(SiHMe$_2$)$_2$})(thf)$_2$][B(C_6F_5)$_4$] (Chart 1, **C**) [10a]. Treatment of the corresponding amidinate scandium bis(dimethylsilyl)amide complex with $[Ph_3C][B(C_6F_5)_4]$ in an aromatic solvent initiated the unexpected Si–H activation, but single crystals suitable for X-ray diffraction could only be obtained after addition of thf.

The metrical parameters of the bidentate bis(amido) (**1** and **B**) and amido-amine (**A**) are illustrated in Chart 2. The position of the hydrogen atoms is given by the torsion angle (H–Si–N–M, underlined) and bond lengths are set in brackets (Å).

The previously assumed elimination of dimethylsilane (during the synthesis of compound **B**), could be unambiguously proven by ^{1}H and ^{1}H–^{1}H COSY NMR spectroscopy in our reaction, showing a sharp septet at 4.03 ppm for the Me_2SiH_2 protons which couples with the triplet at 0.07 ppm of the Me_2SiH_2 protons. Furthermore, the ^{1}H NMR spectrum of complex **1** showed the expected set of signals for the coordinated Cp^{NMe2} ligand. The two aminomethyl groups appear as a singlet at 1.95 ppm and the four methyl groups of the Cp ring display two singlets at 2.18 and 2.4 ppm. The signals of the four ethylene-bridge protons are found as two multiplets at 2.42 and 2.57 ppm. The Si*H* protons of the bis(amido) ligand are detected at 5.18 ppm, while the silyl methyl groups give a broad signal at 0.54 ppm (ESI, Fig. S1).

Efforts to synthesize the half-sandwich yttrium bis(dimethylsilyl)amide complex by applying a one-pot salt metathesis protocol, that is subsequent addition of $LiCp^{NMe2}$ and two

equivalents of lithium bis(dimethylsilyl)amide to a stirring suspension of $YCl_3(thf)_{3.5}$ in toluene, resulted in an oily product (Scheme 3). However, ^1H, ^{13}C and $^1H-^{13}C$ HSQC NMR spectroscopic investigations pointed to $[Cp^{NMe2}Y(N\{SiHMe_2\}_2)_2]$ (**2**) as the main product with minor impurities of other metal bis(dimethylsilyl) amide derivatives. The methyl groups of the cyclopentadienyl ligand appeared as three singlets at 2.40, 2.23 and 2.12 ppm, slightly shifted upfield in comparison to complex **2**, while the four protons of the ethylene bridge showed only one multiplet at 2.42 ppm. The four Si*H* protons of the two silylamido ligands produced a multiplet at 4.76 ppm and the corresponding methyl groups a sharp doublet at 0.47 ppm, evidencing the absence of any Si–H activation comparable to complex **1** (ESI, Fig. S3).

Half-sandwich bis(dimethylsilyl)amide complexes of the rare-earth elements such as complex **2** are highly soluble in aromatic and aliphatic solvents. Hence, X-ray structure analyses are so far limited to scandium complexes $(CpMe_4R)Sc[N(SiHMe_2)_2]_2$ (R = Me, $SiMe_3$) [9] and the yttrium thf adduct $(C_5Me_5)Y[N(SiHMe_2]_2(thf)$ [14]. However, we were able to obtain single crystals of $(Cp^{NMe2})Y[N(SiHMe_2]_2$ suitable for an X-ray diffraction analysis by adding a small amount of thf to a concentrated solution of **2** in pentane at −35 °C. Interestingly, tetrahydrofuran is neither coordinated towards the metal centre nor included in the unit cell. Complex **2** crystallized in the monolinic space group $P2_1$ with three independent molecules in the crystal lattice. Molecule 1 is representatively shown in Fig. 2 and selected bond distances and angles are given in Table 1. As in complex **1**, the yttrium metal centre is coordinated by the donor-substituted cyclopentadienyl ligand in a $\eta^5{:}\kappa^1$ fashion. Due to the lower coordination number of the yttrium centre (formally 6-coordinate), the $Y-C_{Cp}$ distances (2.624(2)–2.697(2) Å) as well as the Y–N1 distance (2.575(2) vs 2.629(3) Å) are slightly shorter than in complex **1** (formally 7-coordinate). The two bis(dimethylsilyl)amido ligands are asymmetrically η^1-coordinated via the nitrogen atoms (Y–N2 = 2.265(1) Å, Y–N3 = 2.269(1) Å), indicative of monoagostic Y–SiH interactions. Distinct Y···Si distances (Si1, 3.0811(5) Å, Si4, 3.1027(4) Å versus Si2, 3.649 Å and Si3, 3.679 Å) and concomitantly distinct Y–N–Si angles (101.41(7)° and 101.83(7)° vs 133.15(8)° and 135.11(8)°) are in agreement with such secondary interactions, which were also detected in complex $(C_5Me_5)Y[N(SiHMe_2]_2(thf)$ (Y···Si2 = 3.0929(8) Å, Y–N1–Si2 = 102.15(10)° vs Y···Si1 = 3.636(1) Å, Y–N1–Si1 = 132.44(12)°) [14]

Since bis(amido) half-sandwich complex **2** is isolable, we reckoned that the formation of SiH-activated complex **1** is thermally induced. By performing a variable temperature NMR study, compound **2** was heated to 150 °C in steps of 10 °C at a time. Surprisingly, at 130 °C not only Si–H but also C–H activation was observed. After 2 h at 150 °C transformation to the activated complex **3** was completed with the integration of the proton signals staying constant. In addition, $^1H-^{13}C$ HSQC, $^1H-^{13}C$ HMBC and $^1H-^1H$ COSY NMR spectroscopic investigations of **3** indicated the formation of a new Si–C bond between one aminomethyl and one dimethylsilylamido group (ESI, Figs. S5–8). The COSY spectrum clearly revealed the coupling of two Si*H* protons at 4.72 ppm with twelve methyl protons, which appear as two discrete doublets at 0.42 and 0.38 ppm, in accordance with an intact dimethylsilylamido ligand. On the other hand a single Si*H* proton at 4.79 ppm, coupling to six methyl protons at 0.45 and 0.41 ppm, and the appearance of two sharp singlets of uncoupled methyl groups indicated the formation of a $[N(SiHMe_2)(SiRMe_2)]^-$ moiety. In the ^1H NMR, only five singlets corresponding to the methyl groups appeared, while two new doublets were found for the $N-CH_2-Si$ moiety at 1.95 and 1.86 ppm with a $^2J_{HH}$ coupling constant of 14.3 Hz. The new Si–C bond was confirmed via $^1H-^{13}C$ HMBC NMR spectroscopy, showing a $^3J_{HC}$ coupling of the $CH_2-Si(CH_3)_2$ moiety. Given these NMR results we concluded that complex **3** has the molecular composition $[(\eta^5{:}\kappa^1{:}\eta^1)(C_5Me_4C_2H_4NMe-CH_2SiMe_2NSiHMe_2)]Y[N(SiHMe_2)_2]$ (Scheme 3). A similar thermally induced hydrogen elimination and interligand coupling has been observed previously between the Si–H bond of the $N(SiHMe_2)_2$ ligand and the C–H bond of the cyclopentadienyl ligand in complex $(C_5H_5)_2Zr[N(SiHMe_2)tBu][N(SiHMe_2)_2]$ to form constrained-geometry-like $[Me_2Si(C_5H_4)N(SiHMe_2)](C_5H_5)Zr[N(SiHMe_2)tBu]$ [15].

2.2. Route C

Previously, Schumann et al. obtained ate complex $[Li(tmeda)_2][(C_5Me_5)Lu(CH_3)_3]$ from a mixture of $LuCl_3$, $Na(C_5Me_5)$ and $LiCH_3$ (1/1/3) in thf/tmeda [16]. Following a similar synthesis procedure, the salt metathesis reaction of $LiCp^{NMe2}$ with $YCl_3(thf)_{3.5}$ afforded the trimetallic *ate* complex $[Cp^{NMe2}YCl_2]_2[LiCl(thf)_2]$ (**4**), which could be converted into the dimeric *ate* complex $[Cp^{NMe2}YMe_2(MeLi)]_2$ (**5**) in the presence of an excess methyllithium in toluene (Scheme 4).

Both complexes could be obtained as single crystals suitable for X-ray diffraction analyses from a saturated toluene solution at −35 °C. Complex **4** crystallized in the monoclinic space group *C*2/c with four molecules in the unit cell including one molecule of toluene per complex. The solid-state structure of complex **4** is identical with the yttrium chloro *ate* complex bearing an anilinyl

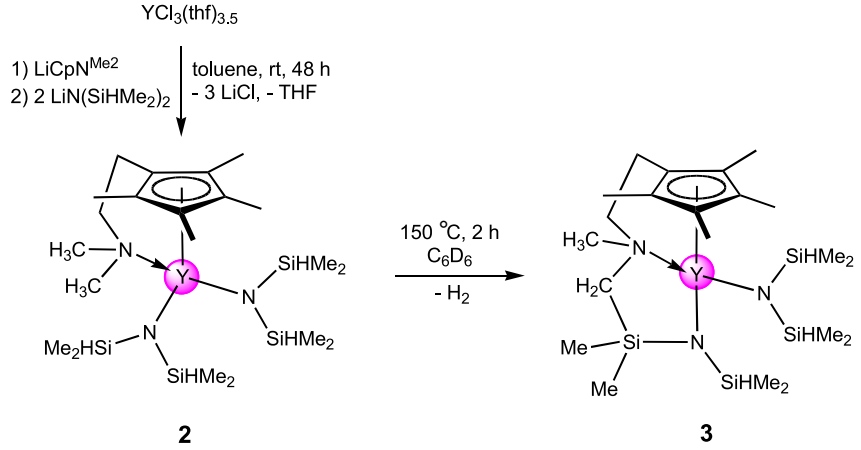

2 **3**

Scheme 3. Synthesis of half-sandwich complex **2** and proposed formation of complex **3** via a thermally induced Si–H activation.

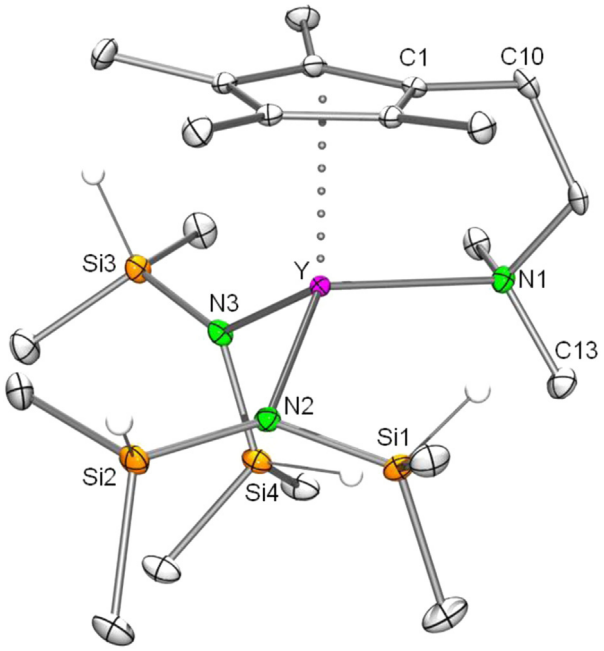

Fig. 2. ORTEP view of the molecular structure of **2**. Atomic displacement parameters are set at the 50% probability level. Hydrogen atoms (except for SiH) are omitted for clarity. For selected bond lengths and angles, see Table 1.

substituted cyclopentadienyl ligand $[(C_5Me_4\text{-}C_6H_4\text{-}o\text{-}NMe_2)YCl_2]_2[LiCl(thf)_2]$ [17] and displays the same trinuclear core as the yttrium chloro complex $[(L)YCl_2(thf)_2]_2[LiCl(thf)_2]$ (L = 2-phenyl-1,4,5,6,7,8-hexhydroazulenyl) [18], which contains two thf molecules coordinating towards the yttrium metal centre instead of the intramolecular nitrogen function. Two yttrium and one lithium metal centres are bridged by three μ_2-Cl and two μ_3-Cl anions (Fig. 3). The N-donor functionalized cyclopentadienyl ligand coordinates to the yttrium metal centres in a $\eta^5{:}\kappa^1$ fashion, generating a distorted octahedral geometry, while the lithium ion is additionally coordinated by two thf molecules. The Y–Cl1 (2.750(1) Å), Y–Cl2 (2.717(1) Å), Y–Cl2′ (2.813(1) Å) and Y–Cl3 (2.622(1) Å) bond lengths are comparable to those found in $[(C_5Me_4C_6H_4\text{-}o\text{-}NMe_2)YCl_2]_2[LiCl(thf)_2]$ [17] with the shortest contact towards the μ_2 chloride bridging yttrium and lithium. The Y–N distance of 2.571(3) Å is slightly shorter than in the anilinyl complex (2.612(3) Å), most likely due to the higher flexibility of the C_2 spacer between the nitrogen and the cyclopentadienyl ring. The NMR spectra of complex **4** revealed only broad signals indicating that the trinuclear structure is not stable in solution at ambient temperature. Also the elemental analysis showed low carbon and hydrogen values, which we interpret by the loss of solvent molecules upon drying under vacuum.

The methyl-exchanged *ate* complex $[Cp^{NMe2}YMe_2(MeLi)]_2$ (**5**) crystallized in the triclinic space group *P*-1 with one molecule per unit cell (Fig. 4). The yttrium metal centre is $\eta^5{:}\kappa^1$ coordinated by the N-donor substituted cyclopentadienyl ligand as previously described for complexes **2** and **4**. In addition, three methyl groups coordinate to the yttrium centre which bridge to the lithium atoms either in a μ_2 (C15/C16) or μ_3 (C14) fashion. The geometry around the formally 7-coordinate yttrium metal is best described as distorted square pyramidal, while the lithium is coordinated tetrahedrally by four methyl groups. The average Y–Cp bond distance of 2.656 Å is comparable to that in complex **1** (2.669 Å), whereas the nitrogen donor forms a Y–N contact of 2.587(2) Å, which is slightly shorter than in compound **1** (2.629(3) Å). As expected, the Y–C bond lengths with the μ_2-CH_3 groups (2.504(5) and 2.514(5) Å) are shorter than with the μ_3- bridging methyl group (2.554(3) Å). The same tendency can also be observed for the Li–C(methyl) bond lengths, where the Li–C15 and Li–C16′ distances (2.171(7) and 2.180(7) Å) are shorter than the Li–C14 and Li–C14′ distances of 2.282(8) and 2.247(9) Å, respectively. The Li–C bond length in the distorted cubane structure of $[LiCH_3]_4$ is 2.28 Å [19]. Other half-sandwich rare-earth metal methyl complexes authenticated by X-ray structure analysis include $[(C_5Me_5)Y(CH_3)_2]_3$ [20], $(C_5Me_5)Sc(CH_3)_2(t\text{-}Bu_3P{=}O)$ [21], $[(C_5Me_4SiMe_3)Sc(CH_3)_2]_2$ [3e], and ate complex $[Li(tmeda)_2][(C_5Me_5)Lu(CH_3)_3]$ [16].

Complex **5** represents a rare case in which lithium atoms are bound to four carbon atoms only (no donor coordination). Unfortunately, complex **5** was separated as single crystals only in low yields as a side product in attempts to synthesize the bis(tetramethylaluminate) half-sandwich yttrium complex, requiring the use of pre-isolated complex **4**. Therefore further analysis was limited to ^{1}H NMR spectroscopy which revealed three sharp singlets for the six methyl groups at 2.26, 2.23 and 2.14 ppm and a multiplet for the ethylene sidearm protons at 2.41 ppm for the Cp^{NMe2} ligand. The μ_2 bridging methyl groups showed a sharp singlet at −0.20 ppm, while the μ_3 coordinated methyls appeared as a broad singlet at −0.28 ppm (ESI, Fig. S9).

Complex **1** and **5,** as well as the bis(dimethylsilyl)amide compound **2** were tested as precursors for the synthesis of the half-sandwich yttrium bis(tetramethylaluminate) complex **6** (Scheme

Table 1
Selected bond lengths (Å) and angles (°) for **2**.

Molecule1		Molecule 2		Molecule 3	
Bond length (Å)					
Y1–C_{Cp}1	2.624(2)–2.697(2)	Y2–C_{Cp}101	2.632(2)–2.717(2)	Y3–C_{Cp}201	2.640(2)–2.699(2)
Y1–N1	2.575(2)	Y2–N101	2.584(2)	Y3–N201	2.579(1)
Y1–N2	2.265(1)	Y2–N103	2.262(1)	Y3–N202	2.270(2)
Y1–N3	2.269(1)	Y2–N102	2.265(1)	Y3–N203	2.275(1)
Y1–Si1	3.0811(5)	Y2–Si7	3.0496(5)	Y3–Si9	3.0699(5)
Y1–Si4	3.1027(5)	Y2–Si5	3.1063(5)	Y3–Si11	3.0776(5)
Bond angle (°)					
N1–Y1–N2	125.08(5)	N101–Y2–N103	129.16(5)	N201–Y3–N202	129.90(5)
N1–Y1–N3	98.92(5)	N101–Y2–N102	95.66(5)	N201–Y3–N203	95.55(5)
N2–Y1–N3	102.73(5)	N102–Y2–N103	102.06(5)	N202–Y3–N203	101.86(5)
Y1–N2–Si1	101.41(7)	Y2–N102–Si5	102.12(6)	Y3–N202–Si9	100.91(7)
Y1–N2–Si2	133.15(8)	Y2–N102–Si6	135.08(7)	Y3–N202–Si10	133.16(8)
Y1–N3–Si3	135.11(8)	Y2–N103–Si7	100.01(7)	Y3–N203–Si11	100.32(6)
Y1–N3–Si4	101.83(7)	Y2–N103–Si8	133.01(8)	Y3–N203–Si12	136.71(8)

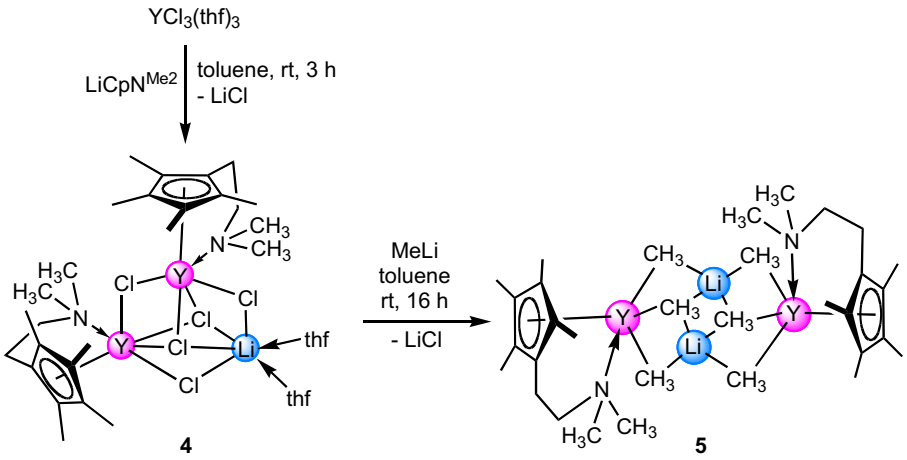

Scheme 4. Synthesis of yttrium half-sandwich chloro (**4**) and methyl (**5**) ate complexes.

5). Using C_6D_6, the silylamide complexes were transferred to a Teflon sealed *J. Young* NMR tube and an excess of trimethylaluminium was added. However, the interpretation of the NMR spectra was challenging due to an equilibrium of the amido/aluminate exchange. Nevertheless, a more straightforward synthesis of $(Cp^{NMe2AlMe3})Y(AlMe_4)_2$ was possible by applying a protonolysis reaction of the homoleptic yttrium aluminate complex $Y(AlMe_4)_3$ with HCp^{NMe2} at lower temperatures (route A, Scheme 1) [22]. Comparison of the proton NMR spectra obtained from the reactions shown in Scheme 5 disclosed the formation of a half-sandwich yttrium bis(tetramethylaluminate) complex, where the N-donor coordinates to trimethylaluminium instead of the expected intramolecular coordination toward the yttrium metal centre (ESI, Fig. S10). Identical signals for the methyl groups of the Cp^{NMe2} ligand were found as singlets at 1.82, 1.93 and 2.02 ppm as well as two multiplets at 2.24 and 2.77 ppm for the ethylene sidearm protons. The protons of the aluminate moieties showed a sharp doublet at −0.22 ppm with a H–Y scalar coupling of $^2J_{YH} = 2.15$ Hz. An additional singlet for the donor coordinated trimethylaluminum was detected at −0.32 ppm. Separation of the desired product **6** from the aluminium by-products $[Me_2AlN(SiHMe_2)_2]_2$ or $[Me_2Si\{Me_2AlNSiHMe_2\}_2]$ via fractional recrystalization might be feasible, but was not attempted in the work.

3. Conclusion

Formation of the SiH-activated complex $Cp^{NMe2}Y[\eta^2SiMe_2(N\text{-}SiHMe_2)_2](thf)$ via protonolysis of $Y[N(SiHMe_2)_2]_3(thf)_2$ with the donor-functionalized cyclopentadiene $C_5Me_4HCH_2CH_2NMe_2$ (HCp^{NMe2}) seems to be driven by elevated temperatures and/or the presence of a donor functionality (NMe_2, thf). The generation of the dianionic bis(amido) ligand $[\eta^2\text{-}SiMe_2(NSiHMe_2)_2]$ which occurs via separation of H_2SiMe_2, has been shown previously. The desired half-sandwich complex $(Cp^{NMe2})Y[N(SiHMe_2)_2]_2$ is accessible via application of a sequential salt metathesis protocol utilizing $YCl_3(thf)_3$, $LiN(SiHMe_2)_2$ and $LiCp^{NMe2}$ in a 1/2/1 ratio at ambient temperature. Complex $(Cp^{NMe2})Y[N(SiHMe_2)_2]_2$ engages in a distinct ligand activation at elevated temperatures predominantly

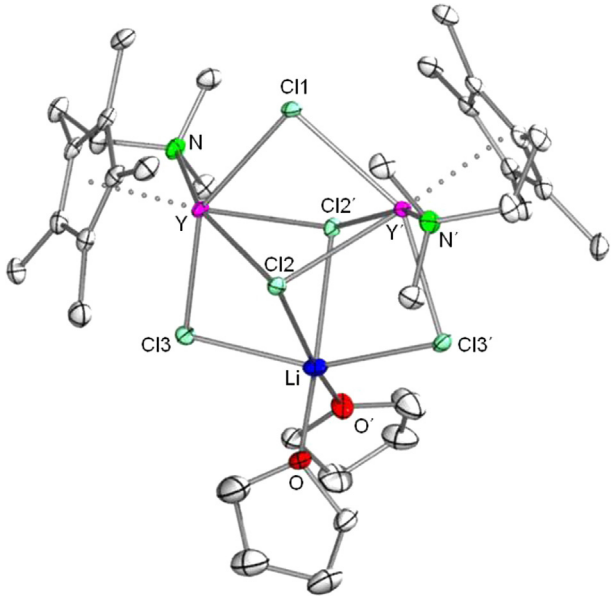

Fig. 3. ORTEP view of the molecular structure of **4**. Atomic displacement parameters are set at the 50% probability level. Hydrogen atoms are omitted for clarity. Selected bond lengths (Å) and angles (°) for **1**: Y–Cp_{cent} = 2.356, Y–N = 2.571(3), Y–Cl1 = 2.7502(9), Y–Cl2 = 2.717(1), Y–Cl2′ = 2.813(1), Y–Cl3 = 2.622(1), Li–O = 1.963(7), Li–Cl3 = 2.631(2), N–Y–Cl1 = 100.25(8), N–Y–Cl2 = 157.66(8), N–Y–Cl2′ = 80.63(8), N–Y–Cl3 = 91.86(8), Cl3-Li–Cl3′ = 155.3(4), O–Li–O′ = 95.9(4).

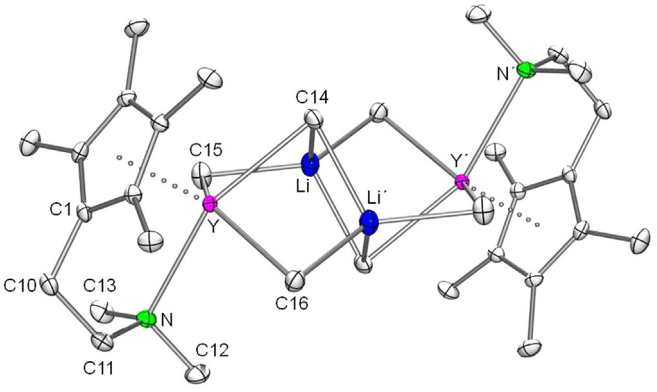

Fig. 4. ORTEP view of the molecular structure of **5**. Atomic displacement parameters are set at the 50% probability level. Hydrogen atoms are omitted for clarity. Selected bond lengths (Å) and angles (°) for **1**: Y–Cp_{av} = 2.656, Y–Cp_{cent} = 2.366, Y–N = 2.587(2), Y–C15 = 2.514(5), Y–14 = 2.554(3), Y–C16 = 2.504(5), Li–C15 = 2.171(7), Li–C16′ = 2.180(7), Li–C14 = 2.282(8), Li–C14′ = 2.247(9), Li–Li = 2.749, N–Y–C15 = 87.3(1), N–Y–C14 = 154.7(1), N–Y–C16 = 85.3(1), C14–Y–C15 = 83.6(1), C14–Y–C16 = 83.8(1), C15–Y–C16 = 133.1(1).

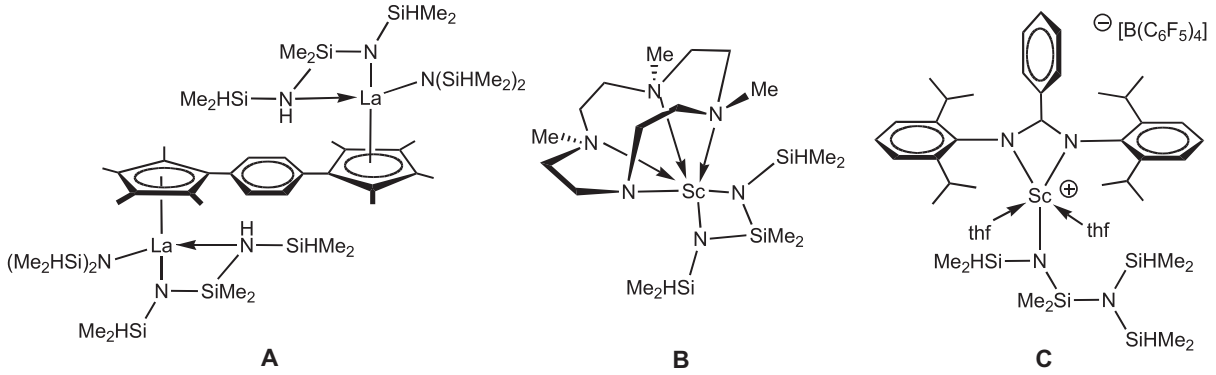

Chart 1. Structurally authenticated Si–H activation products involving rare-earth metal bis(dimethylsilyl)amide complexes [**12**,**13**,**10a**].

involving the dimethylamino functionality and formation of complex $[(C_5Me_4C_2H_4NMeCH_2–SiMe_2NSiHMe_2)Y\{N(SiHMe_2)_2\}]$. Both half-sandwich silylamido complexes exhibit amido-aluminate exchange upon treatment with trimethylaluminium producing the half-sandwich bis(tetramethylaluminate) complex ($Cp^{NMe2AlMe3}$)$Y(AlMe_4)_2$. Importantly, the concomitant generation of diverse aluminium silylamide byproducts hampers the purification of complex ($Cp^{NMe2AlMe3}$)$Y(AlMe_4)_2$, which makes the protonolysis reaction of $Y(AlMe_4)_3$ with HCp^{NMe2} a superior route. Details of the latter route will be elaborated in another contribution. The least suitable seems the protocol following the reaction sequence "$YCl_3(thf)_3 + LiCp^{NMe2} + LiMe + AlMe_3$" along which the formation of ate complexes as shown for the isolation of complexes $[Cp^{NMe2}YCl_2]_2[LiCl(thf)_2]$ and $[(Cp^{NMe2})YMe_2(MeLi)]_2$. Nevertheless, complex $[(Cp^{NMe2})YMe_2(MeLi)]_2$ features a rare example of a structurally authenticated rare-earth metal half-sandwich dimethyl complex.

4. Experimental section

4.1. General remarks

All operations were performed with rigorous exclusion of air and water, using standard *Schlenk*, high-vacuum, and argon glovebox techniques (MBraun MB 200B; <1 ppm O_2, <1 ppm H_2O). Hexane, pentane, toluene and thf were purified by using *Grubbs* columns (MBraun SPS-800, solvent purification system) and stored in a glovebox. C_6D_6 and C_7D_8 were obtained from *Aldrich*, dried over Na for 24 h, and filtered. $AlMe_3$ was purchased from *Aldrich* and used as received. $Y[N(SiHMe_2)_2]_3(thf)_2$ was prepared according to literature method [7c]. HCp^{NMe2} (Cp^{NMe2} = 1-[2-(*N*,*N*-dimethylamino)-ethyl]-2,3,4,5-tetramethyl-cyclopentadienyl) was synthesized as described in literature [8]. The NMR spectra of air and moisture sensitive compounds were recorded by using *J. Young* valve NMR tubes at 25 °C on a *Bruker* DMX-400 Advance (^{1}H: 400.13 Hz; ^{13}C: 100.61 MHz). ^{1}H and ^{13}C shifts are referenced to internal solvent resonances and reported in *parts per million* relative to TMS. IR spectra were recorded between 4000 cm^{-1} and 400 cm^{-1} on a NICOLET 6700 FTIR spectrometer using a DRIFT chamber with dry KBr/sample mixtures and KBr windows. For the latter the collected data were converted using the Kubelka-Munk refinement. Elemental analyses were performed on an *Elementar Vario MICRO cube*.

4.2. Synthesis of $(C_5Me_4CH_2CH_2NMe_2)Y[\eta^2\text{-}Me_2Si(NSiHMe_2)_2](thf)$ (**1**)

In a glovebox, HCp^{NMe2} (193 mg, 1.00 mmol) was added dropwise to a stirred solution of $Y[N(SiHMe_2)_2]_3(thf)_2$ (628 mg, 1.00 mmol) in 10 mL of toluene. The mixture was transferred to a pressure tube and stirred for 16 h at 150 °C. After evaporation of the solvent, the crude product was redissolved in toluene and hexane. Crystallization from a solution in hexane/toluene at −35 °C gave single crystals of **2** suitable for X-ray diffraction analysis (379 mg, 0.68 mmol, 68%). ^{1}H NMR (400 MHz, C_6D_6, 25 °C): δ = 5.18 (sept, 2H, $^3J_{HH}$ = 3.00 Hz, Si*H*CH_3), 3.65 (m, 4H, THF), 2.57 (m, 2H, N*C*$H_2$$CH_2$Cp), 2.42 (t, 2H, $^3J_{HH}$ = 6.13 Hz NCH_2*C*H_2Cp), 2.38 (s, 6H, *C*H_3Cp), 2.18 (s, 6H, *C*H_3Cp), 1.95 (s, 6H, *C*H_3N), 1.48 (m, 4H, THF), 0.54 (br, 18H, SiH(*C*H_3)$_2$), Si(*C*H_3)$_2$). ^{13}C NMR (126 MHz, C_6D_6, 25 °C): δ = 119.9 (*C*$_5$(CH$_3$)$_4$), 118.0 (*C*$_5$(CH$_3$)$_4$), 116.2 (*C*$_5$(CH$_3$)$_4$), 69.1 (THF), 64.1 (N*C*$H_2$$CH_2$), 45.7 (*C*$H_3$N), 25.2 (THF), 22.8 ($CH_2$*C*$H_2$Cp), 11.5 (C$_5$(*C*H$_3$)$_4$), 11.3 (C$_5$(*C*H$_3$)$_4$), 7.9 (Si(*C*$H_3$)$_2$), 4.2 (SiH(*C*$H_3$)$_2$). IR ($cm^{-1}$): 2959 s, 2923 s, 2852 s, 2724 w, 2669 w, 2047 w (SiH), 1459 s, 1377 s, 1303 w, 1155 w, 722 w. Element analysis calcd (%) for $C_{23}H_{50}N_3OSi_3Y$ (557.23): C 49.52, H 9.03, N 7.53; found: C 49.45, H 9.05, N 7.57.

4.3. Synthesis of $[(C_5Me_4CH_2CH_2NMe_2)Y\{N(SiHMe_2)_2\}_2]$ (**2**)

In a glovebox $LiCp^{NMe2}$ (100 mg, 0.50 mmol) was added to a suspension of $YCl_3(thf)_3$ (224 mg, 0.50 mmol) in 4 mL of toluene.

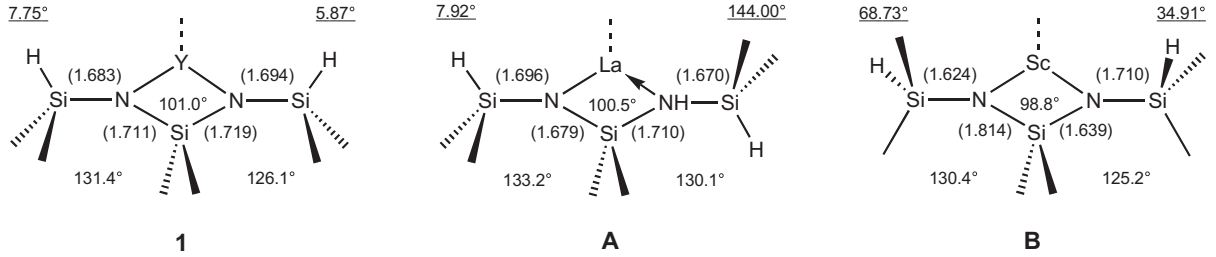

Chart 2. Structural parameters (torsion angles H–Si–N–M, underlined; bond lengths [Å], in brackets) and coordination modes of bidentate bis(amido) (**1** and **B**) and amido-amine (**A**) ligands as originated from Si–H activation.

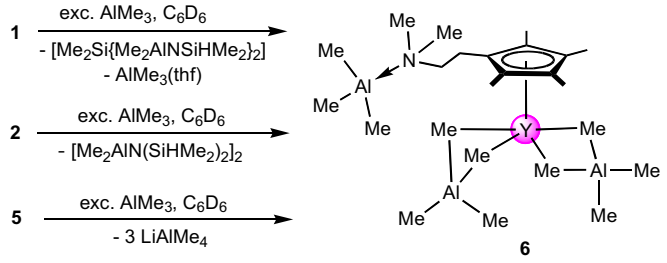

Scheme 5. Synthesis of the yttrium half-sandwich bis(tetramethylaluminate) complex **6**.

The mixture was stirred for 4 h and $LiN(SiHMe_2)_2$ (139 mg, 1.00 mmol, 2 equiv) was added. Then the reaction mixture was stirred another 16 h at ambient temperature. After evaporation of the solvent, the crude mixture was dissolved in hexane and LiCl was removed via centrifugation and filtration. After removal of the solvent the title compound was isolated as yellow oil (179 mg, 0.33 mmol, 66%). Single crystals suitable for X-ray diffraction analysis were grown from a saturated pentane solution with a small addition of thf at −35 °C. ^{1}H NMR (400 MHz, C_6D_6, 25 °C): δ = 4.76 (m, 4H, Si*H*CH$_3$), 2.42 (m, 4H, NC*H*$_2$C*H*$_2$Cp), 2.40 (s, 6H, C*H*$_3$Cp), 2.23 (s, 6H, C*H*$_3$Cp), 2.11 (s, 6H, C*H*$_3$N), 0.47 (d, 24H, $^3J_{HH}$ = 3.00 Hz, SiH(C*H*$_3$)$_2$). ^{13}C NMR (126 MHz, C_6D_6, 25 °C): δ = 119.8 (C_5(CH$_3$)$_4$), 119.4 (C_5(CH$_3$)$_4$), 116.6 (C_5(CH$_3$)$_4$), 65.3 (NCH$_2$CH$_2$), 47.1 (*C*H$_3$N), 22.9 (NCH$_2$CH$_2$Cp), 12.2 (C_5(CH$_3$)$_4$), 11.8 (C_5(*C*H$_3$)$_4$), 3.2 (SiH(*C*H$_3$)$_2$). IR (cm^{-1}): 2955 s, 2917 br, 2852 s, 2059 w (SiH), 1460 s, 1377 s, 1304 w, 1155 w, 897 w, 722 w. Element analysis calcd (%) for $C_{21}H_{50}N_3Si_4Y$ (545.89): C 46.20, H 9.23, N 7.70; found: C 45.65, H 9.38, N 7.49.

4.4. Synthesis of [(η^5:κ^1:η^1)(C_5Me_4–C_2H_4–NMe–CH_2–$SiMe_2NSiHMe_2$)]Y[N(SiHMe$_2$)$_2$] (**3**)

Compound **2** was transferred to a Teflon sealed *J. Young* NMR tube using C_6D_6 and heated up to 150 °C in steps of 10 °C. After 2 h at 150 °C, the integration of the proton signals in the ^{1}H NMR spectrum stayed constant and additional ^{1}H–^{13}C HSQC, ^{1}H–^{13}C HMBC and ^{1}H–^{1}H COSY NMR spectra were recorded to identify the product. Detailed NMR analysis is presented in the supporting information. ^{1}H NMR (400 MHz, C_6D_6, 25 °C): δ = 4.79 (sept, 1H Si*H*CH$_3$), 4.72 (m, 2H, Si*H*CH$_3$), 3.06 (m, 1H, NC*H*$_2$CH$_2$Cp), 2.57–2.43 (m, 2H, NCH$_2$C*H*$_2$Cp), 2.37–2.32 (m, 1H, NC*H*$_2$C*H*$_2$Cp), 2.31 (s, 3H, C*H*$_3$Cp), 2.30 (s, 3H, C*H*$_3$Cp), 2.27 (s, 3H, C*H*$_3$Cp), 2.11 (s, 3H, NC*H*$_3$), 1.95 (d, 1H, $^2J_{HH}$ = 14.3 Hz, N–C*H*$_2$–Si), 1.86 (d, 1H, $^2J_{HH}$ = 14.3 Hz, N–C*H*$_2$–Si), 0.45 (d, 3H, $^3J_{HH}$ = 3.00 Hz, N(SiH{C*H*$_3$}$_2$)(SiR{CH$_3$}$_2$)), 0.43 (d, 6H, $^3J_{HH}$ = 3.00 Hz, N(SiH{C*H*$_3$}$_2$)$_2$), 0.41 (d, 3H, $^3J_{HH}$ = 3.00 Hz, N(SiH{C*H*$_3$}$_2$)$_2$), 0.39 (d, 3H, $^3J_{HH}$ = 3.00 Hz, N(SiH{C*H*$_3$}$_2$)(SiR{CH$_3$}$_2$)), 0.28 (d, 3H, NSiR{C*H*$_3$}$_2$), 0.15 (d, 3H, NSiR{C*H*$_3$}$_2$). ^{13}C NMR (126 MHz, C_6D_6, 25 °C): δ = 121.0, 118.5, 118.5, 117.1 (C_5(CH$_3$)$_4$), 116.7 (C_5(CH$_3$)$_4$), 64.9 (NCH$_2$CH$_2$), 53.7 (NCH$_2$Si), 48.5 (NCH$_3$), 23.1 (CpCH$_2$), 11.9, 11.8, 11.6, 11.4 (Cp(*C*H$_3$)$_4$), 4.7, 4.4 (SiR{*C*H$_3$}$_2$), 3.6, 3.4 (SiH{*C*H$_3$}$_2$), 3.4, 3.0 (SiH{CH$_3$}$_2$).

4.5. Synthesis of [($C_5Me_4CH_2CH_2NMe_2$)YCl_2]$_2$[LiCl(thf)$_2$] (**4**)

To a suspension of YCl_3(thf)$_{3.5}$ (224 mg, 0.50 mmol) in 4 mL toluene $LiCp^{NMe}$ (100 mg, 0.50 mmol) was added and the mixture was stirred for 3 h at ambient temperature. After evaporation of the solvent, the crude product was dissolved in toluene and LiCl was removed via centrifugation and filtration. Single crystals of **4** suitable for X-ray diffraction analysis were grown from saturated toluene solution at −35 °C (191 mg, 0.21 mmol, 86%). ^{1}H NMR in toluene-d$_8$ at ambient temperature only showed the thf signals at 3.81 and 1.38 ppm and broad signals in the expected area from 2.85 ppm to 2.03 ppm for the Cp^{NMe2} ligand indicating fluxional behaviour and cluster rearrangement in solution. IR (cm^{-1}): 2963 s, 2910 s, 2875 sh, 2797 w, 1468 s, 1452 s, 1377 m, 1062 sh, 1032 s, 1009 m, 914 m, 890 w, 857 w.

4.6. Synthesis of [($C_5Me_4CH_2CH_2NMe_2$)YMe_2(MeLi)]$_2$ (**5**)

Without further analysis, complex **4** (178 mg, 0.20 mmol, 1 equiv) was dissolved in 4 mL toluene and MeLi (33 mg, 1.20 mmol, 3 equiv) was added. The reaction mixture was stirred for 16 h at ambient temperature. After evaporation of the solvent, the crude mixture was dissolved in toluene and LiCl was removed via centrifugation and filtration. Removal of the solvent gave complex **5** as a white powder (84 mg, 0.16 mmol, 63%). Single crystals of complex **5** were grown from a saturated toluene solution at −35 °C in very low yield. ^{1}H NMR (400 MHz, C_6D_6, 25 °C): δ = 2.41 (m, 8H, NC*H*$_2$C*H*$_2$Cp), 2.26 (s, 12H, C*H*$_3$Cp), 2.23 (s, 12H, C*H*$_3$Cp), 2.14 (s, 12H, C*H*$_3$N), −0.20 (s, 12H Y(C*H*$_3$)$_2$), −0.28 (s, 6H YC*H*$_3$). Element analysis calcd (%) for $C_{32}H_{62}Li_2N_2Y$ (666.54): C 57.66, H 9.38, N 4.20; found: C 57.80, H 8.72, N 4.18.

4.7. X-ray crystallography and crystal structure determination of **1**, **2**, **4**, and **5**

Single-crystals suitable for X-ray diffraction measurements were selected in a glovebox, covered in Paratone-N (Hampton Research) and mounted on a glass fibre. The crystal data for complexes **1** and **5** were collected on a STOE IPDS 2T diffractometer using graphite-monochromated Mo-Kα radiation (λ = 0.71073 Å) at 173(2) K performing ω-scans in two orthogonal φ positions. Data collection for **2** and **4** and was performed on a Bruker APEX DUO diffractometer at 100(2) K using graphite-monochromated Mo Kα radiation (λ = 0.71073 Å) performing 182° ω-scans in four orthogonal φ positions. Raw data were collected using the program SMART [23] and integrated and reduced with the program SAINT [24]. Corrections for absorption effects were applied using SHELXTL [25] and/or SADABS [26] Structure solutions and refinements were performed using the programs SHELXS [27] and SHELXL [28]. The structures in this article are represented using the program ORTEP-III [29]. All CIF files were checked at http://www.checkcif.iucr.org/. For further experimental details on refinement and crystallographic data see Table 2.

Table 2
Crystallographic data for complexes **1**, **2**, **4** and **5**.

	1[1]	**2**[2]	**4**[2]	**5**[1]
Formular	$C_{23}H_{50}N_3OSi_3Y$	$C_{21}H_{50}N_3Si_4Y$	$C_{48}H_{76}Cl_5LiN_2O_2Y_2$	$C_{32}H_{62}Li_2N_2Y_2$
Fw	557.84	545.91	1075.12	666.54
Temp (K)	173(2)	100(2)	100(2)	173(2)
Cryst syst	triclinic	monoclinic	monoclinic	triclinic
Space group	*P*-1	$P2_1$	*C*2/c	*P*-1
a (Å)	9.7070(11)	17.6834(3)	20.768(4)	8.3296(11)
b (Å)	10.3817(12)	15.4709(3)	11.4600(19)	8.4946(11)
c (Å)	16.2848(19)	18.2584(4)	24.675(4)	13.4840(17)
α (deg)	89.882(9)	90	90.00	77.170(10)
β (deg)	91.109(9)	113.2410(10)	106.958(4)	84.982(10)
γ (deg)	115.303(8)	90	90.00	69.093(10)
Vol (Å^3)	1483.3(3)	4589.76(16)	5617.3(7)	2844.65(17)
Z	2	6	4	1
ρ_{calcd} (mg/mm^3)	1.249	1.185	1.271	1.274
μ (mm^{-1})	2.106	2.075	2.328	3.343
*R*1[a]	0.0858	0.0364	0.0718	0.0636
*wR*2[b]	0.0995	0.0476	0.1381	0.0890
GOF (on F^2)[a]	1.167	0.822	1.056	1.209

[a] R1 = $\Sigma(||F_o| - |F_c||)/\Sigma|F_o|$; [b] *wR*2 = $\{\Sigma[w(F_o^2 - F_c^2)^2/\Sigma[w(F_o^2)^2]\}^{1/2}$; GOF = $\{\Sigma[w(F_o^2 - F_c^2)^2]/(n-p)\}^{1/2}$.
[1] STOE IPDS 2T diffractometer; [2] Bruker APEX DUO diffractometer.

Acknowledgement

Support from the German Science Foundation is gratefully acknowledged.

Appendix A. Supplementary data

NMR spectra and CIF files giving full crystallographic data for complexes **1**, **2**, **4**, and **5**. CCDC 930897–930899 and 933280, contain the supplementary crystallographic data for this paper. These data can be obtained free of charge via http://www.ccdc.cam.ac.uk/data_request/cif.

Appendix B. Supplementary data

Supplementary data related to this article can be found at http://dx.doi.org/10.1016/j.jorganchem.2013.05.002.

References

[1] (a) S. Arndt, J. Okuda, Chem. Rev. 102 (2002) 1953;
(b) A. Fischbach, R. Anwander, Adv. Polym. Sci. 204 (2006) 155;
(c) Z. Hou, Bull. Chem. Soc. Jpn. 76 (2003) 2253;
(d) J. Okuda, Dalton Trans. (2003) 2367;
(e) M. Zimmermann, R. Anwander, Chem. Rev. 110 (2010) 6194.
[2] R. Anwander, M.G. Klimpel, H. Martin Dietrich, D.J. Shorokhov, W. Scherer, Chem. Comm. (2003) 1008.
[3] (a) M. Zimmermann, K.W. Törnroos, R. Anwander, Angew. Chem. 120 (2008) 9702. Angew. Chem. Int. Ed. 47 (2008) 775;
(b) M. Zimmermann, J. Volbeda, K. W. Törnroos, R. Anwander, C. R. Chim. 13 (2010) 651; (c) M. Zimmermann, K.W. Törnroos, H. Sitzmann, R. Anwander, Chem. Eur. J. 14 (2008) 7266.(d) R. Litlabø, M. Enders, K.W. Törnroos, R. Anwander, Organometallics 29 (2010) 2588;
(e) D. Robert, T.P. Spaniol, J. Okuda, Eur. J. Inorg. Chem. (2008) 2801.
[4] For rare-earth metal(III) half-sandwich complexes with side chains carrying neutral N-donors, see: (a) T.K. Panda, C.G. Hrib, P.G. Jones, J. Jenter, P.W. Roesky, M. Tamm, Eur. J. Inorg. Chem. 2008 (2008) 4270.(b) X. Li, M. Nishiura, L. Hu, K. Mori, Z. Hou, J. Am. Chem. Soc. 131 (2009) 13870;
(c) D.J. Beetstra, A. Meetsma, B. Hessen, J.H. Teuben, Organometallics 22 (2003) 4372;
(d) I.L. Fedushkin, S. Dechert, H. Schumann, Organometallics 19 (2000) 4066;
(e) H. Schumann, K. Herrmann, F. Erbstein, Z. Naturforsch. B. Chem. Sci. 58 (2003) 832.
[5] For rare-earth metal-based metallocene derivatives carrying amino-functionalized cyclopentadienyl ligands, see: (a) W.A. Herrmann, R. Anwander, F.C. Munck, W. Scherer, Chem. Ber. 126 (1993) 331;
(b) G.A. Molander, H. Schumann, E.C.E. Rosenthal, J. Demtschuk, Organometallics 15 (1996) 3817;
(c) H. Schumann, E.C.E. Rosenthal, J. Demtschuk, G.A. Molander, Organometallics 17 (1998) 5324;
(d) A.T. Trifonov, T.P. Spaniol, J. Okuda, Eur. J. Inorg. Chem. 2003 (2003) 926.
[6] (a) W.J. Evans, R. Anwander, J.W. Ziller, Organometallics 14 (1995) 1107;
(b) M. Zimmermann, N.Å. Frøystein, A. Fischbach, P. Sirsch, H.M. Dietrich, K.W. Törnroos, E. Herdtweck, R. Anwander, Chem. Eur. J. 13 (2007) 8784;
(c) G. Occhipinti, C. Meermann, H.M. Dietrich, R. Litlabø, F. Auras, K.W. Törnroos, C. Maichle-Mössmer, V.R. Jensen, R. Anwander, J. Am. Chem. Soc. 133 (2011) 6323.
[7] (a) W.A. Herrmann, R. Anwander, F.C. Munck, W. Scherer, V. Dufaud, N.W. Huber, G.R.J. Artus, Z. Naturforsch. Teil B 49 (1994) 1789;
(b) R. Anwander, O. Runte, J. Eppinger, G. Gerstberger, E. Herdtweck, M. Spiegler, J. Chem. Soc. Dalton Trans. (1998) 847;
(c) W.A. Herrmann, F.C. Munck, G.R.J. Artus, O. Runte, R. Anwander, Organometallics 16 (1997) 682.
[8] P. Jutzi, J. Dahlhaus, Synthesis 7 (1993) 684.
[9] Y. Luo, X. Feng, Y. Wang, S. Fan, J. Chen, Y. Lei, H. Liang, Organometallics 30 (2011) 3270.
[10] For bis(silylamide) complexes bearing amidinate/aminopyridinate ligands in isoprene polymerization, see: (a) F. Chen, S. Fan, Y. Wang, J. Chen, Y. Luo, Organometallics 31 (2012) 3730;
(b) C. Döring, W.P. Kretschmer, T. Bauer, R. Kempe, Eur. J. Inorg. Chem. (2009) 4255;
(c) Y. Luo, S. Fan, J. Yang, J. Fang, P. Xu, Dalton Trans. 40 (2011) 3053.
[11] J. Eppinger, M. Spiegler, W. Hieringer, W.A. Herrmann, R. Anwander, J. Am. Chem. Soc. 122 (2000) 3080. and references cited therein.
[12] H.F. Yuen, T.J. Marks, Organometallics 28 (2009) 2423.
[13] J.-C. Buffet, J. Okuda, Dalton Trans. 40 (2011) 7748.
[14] B.B. Lazarov, F. Hampel, K.C. Hultzsch, Z. Anorg. Allg. Chem. 633 (2007) 2367.
[15] K. Yan, A. Ellern, A.D. Sadow, J. Am. Chem. Soc. 134 (2012) 9154.
[16] H. Schumann, I. Albrecht, J. Pickardt, E. Hahn, J. Organomet. Chem. 276 (1984) c5.
[17] Z. Jian, W. Zhao, X. Liu, X. Chen, T. Tang, D. Cui, Dalton Trans. 39 (2010) 6871.
[18] G. Paolucci, M. Vignola, A. Zanella, V. Bertolasi, E. Polo, S. Sostero, Eur. J. Inorg. Chem. (2006) 4104.
[19] W. Schlenk, J. Holtz, Ber. Dtsch. Chem. Ges. 50 (1917) 262;
(b) E. Weiss, E.A.C. Lucken, J. Orgnomet. Chem. 2 (1964) 197.
[20] H.M. Dietrich, H. Grove, K.W. Törnroos, R. Anwander, J. Am. Chem. Soc. 128 (2006) 1458.
[21] L.D. Henderson, G.D. MacInnis, W.E. Piers, M. Parvez, Can. J. Chem. 82 (2004) 162.
[22] L.N. Jende, R. Anwander, unpublished results.
[23] SMART, v.5.054, Data Collection Software for Bruker AXS CCD, Bruker AXS Inc., Madison, WI, 1999.
[24] SAINT, v. 6.45A, Data Integration Software for Bruker AXS CCD, Bruker AXS Inc., Madison, WI, 2002.
[25] SHELXTL, v. 6.14, Structure Determination Software Suite, Bruker AXS Inc., Madison, WI, 2000.
[26] G.M. Scheldrick, SADABS, v. 2001/1, University of Göttingen, Germany, 2001.
[27] G.M. Scheldrick, SHELXS-97, Program for Crystal Structure Solution, University of Göttingen, Germany, 1997.
[28] G.M. Scheldrick, SHELXL-97, Program for Crystal Structure Refinement, University of Goettingen, Germany, 1997.
[29] L.J. Farrugia, J. Appl. Cryst. 30 (1997) 565.

Supporting Information

Yttrium half-sandwich complexes bearing the 2-(*N*,*N*-dimethylamino)ethyl-tetramethylcyclopentadienyl ligand

Lars N. Jende,[a] Cäcilia Maichle-Mössmer,[a] Christoph Schädle,[a] and Reiner Anwander[a]

[a]Institut für Anorganische Chemie, Universität Tübingen, Auf der Morgenstelle 18A, D-72076 Tübingen, Germany

[*]Corresponding authors: E-mail: reiner.anwander@uni-tuebingen.de

Contents

Figure S1: ^{1}H NMR spectrum (C_6D_6, 25 °C) of complex**1**

Figure S2: ^{13}C NMR spectrum (C_6D_6, 25 °C) of complex **1**

Figure S3: ^{1}H NMR spectrum (C_6D_6, 25 °C) of complex **2**

Figure S4: ^{13}C NMR spectrum (C_6D_6, 25 °C) of complex **2**

Figure S5: ^{1}H NMR spectrum (C_6D_6, 25 °C) of compound **3**

Figure S6: ^{13}C NMR spectrum (C_6D_6, 25 °C) of compound **3**

Figure S7: 2D ^{1}H-^{13}C HSQC NMR spectrum (C_6D_6, 25 °C) of compound **3**

Figure S8: 2D ^{1}H-^{13}C HMBC NMR spectrum (C_6D_6, 25 °C) of compound **3**

Figure S9: ^{1}H NMR spectrum (C_6D_6, 25 °C) of complex **5**

Figure S10: ^{1}H NMR spectra (C_6D_6, 25 °C) from reaction of complex **1** and **2** with $AlMe_3$ compared with spectrum of $Cp^{NMe2AlMe3}Y(AlMe_4)_2$

Note: Solvent impurities like pentane, hexane and tetrahydrofurane (thf) are marked with an asterisk (*) in the NMR spectra except donor solvents coordinating towards a metal centre.

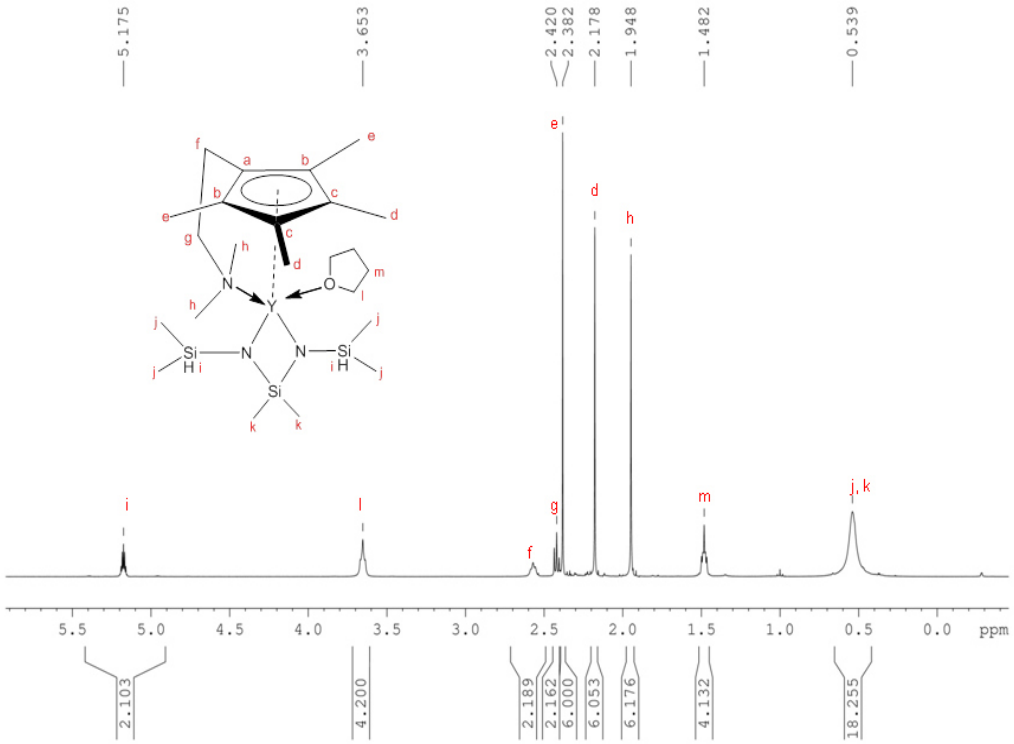

Figure S1: ^{1}H NMR spectrum (C_6D_6, 25 °C) of complex **1**

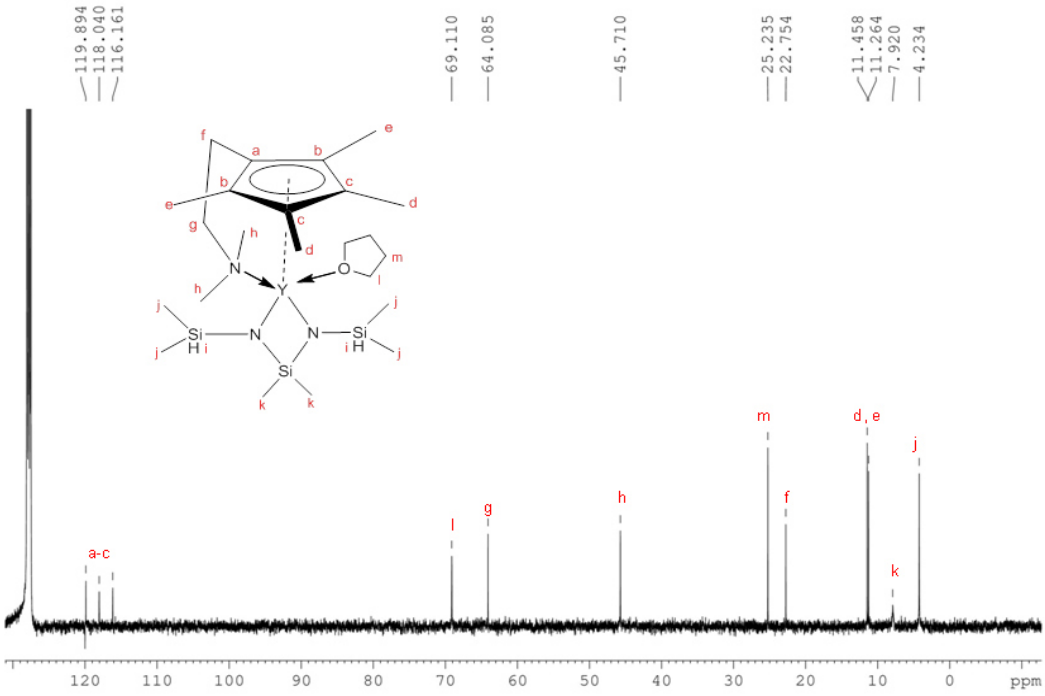

Figure S2: ^{13}C NMR spectrum (C_6D_6, 25 °C) of complex **1**

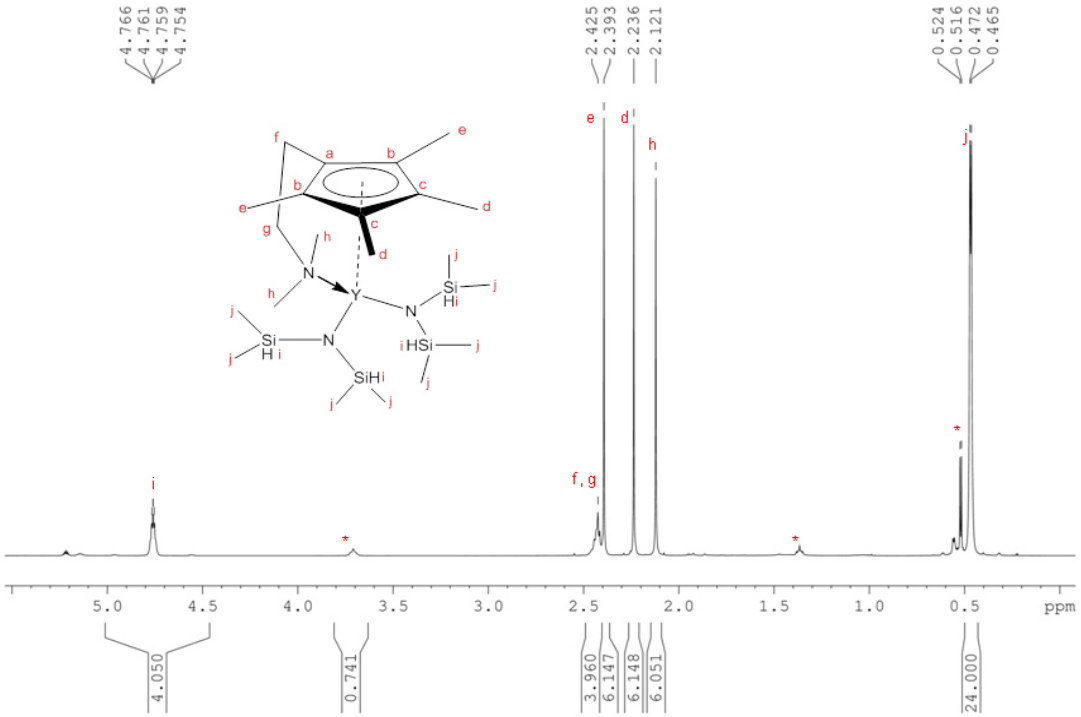

Figure S3: ^{1}H NMR spectrum (C_6D_6, 25 °C) of complex **2**

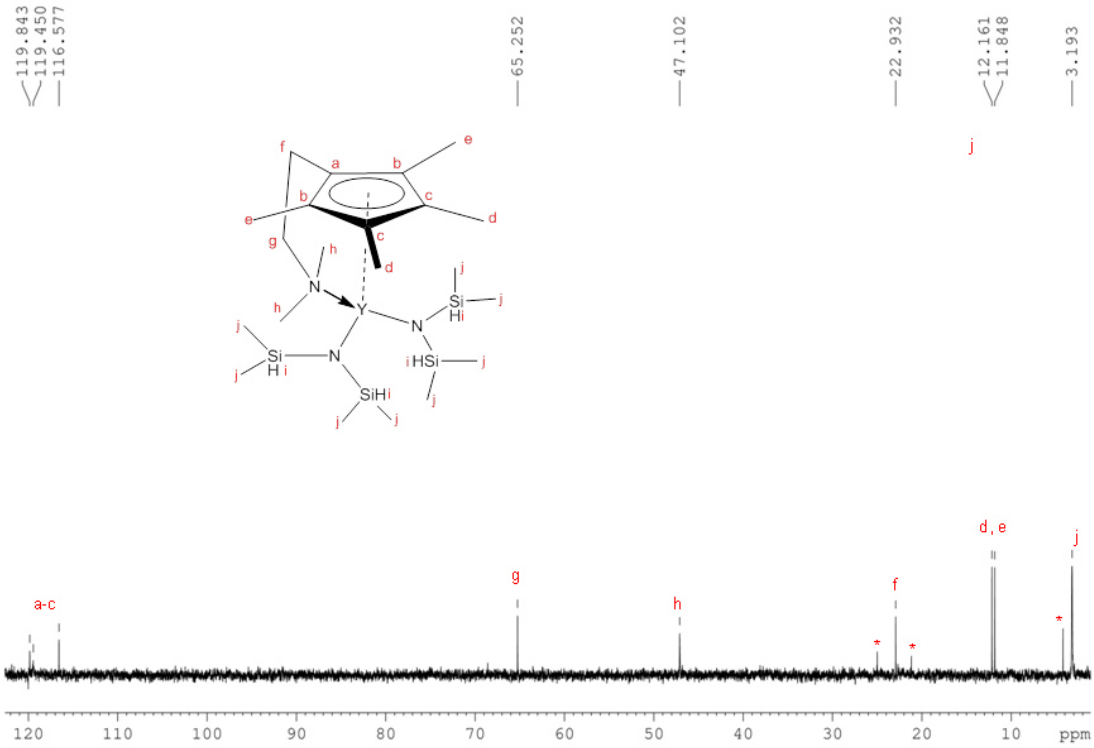

Figure S4: ^{13}C NMR spectrum (C_6D_6, 25 °C) of complex **2**

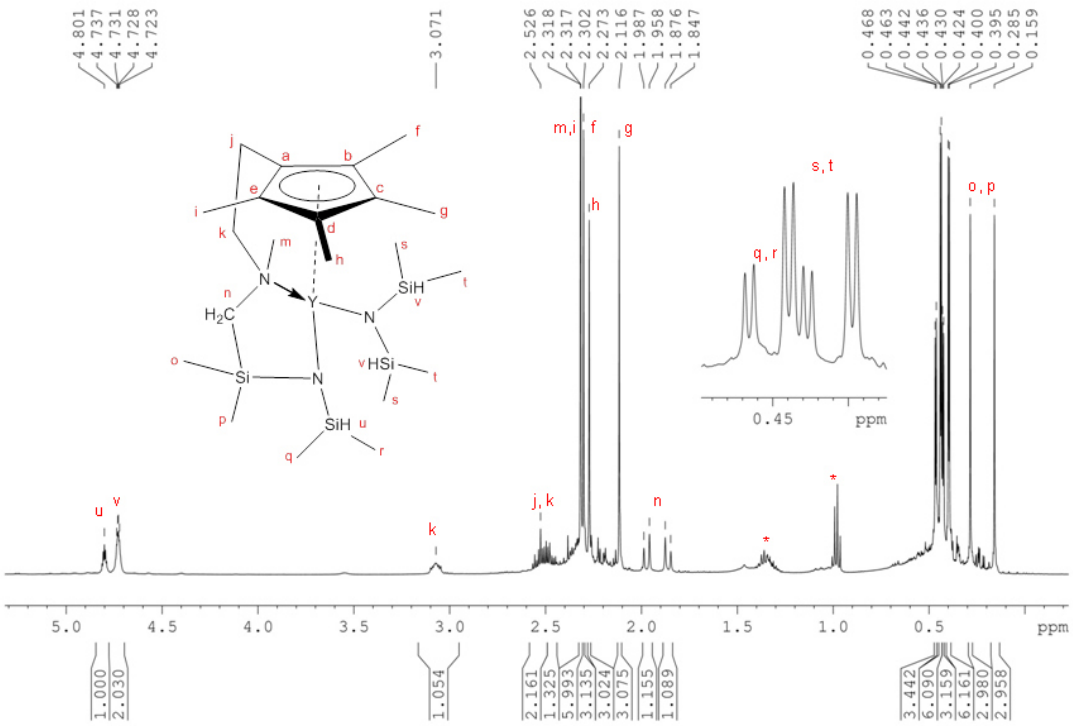

Figure S5: ^{1}H NMR spectrum (C_6D_6, 25 °C) of compound **3**

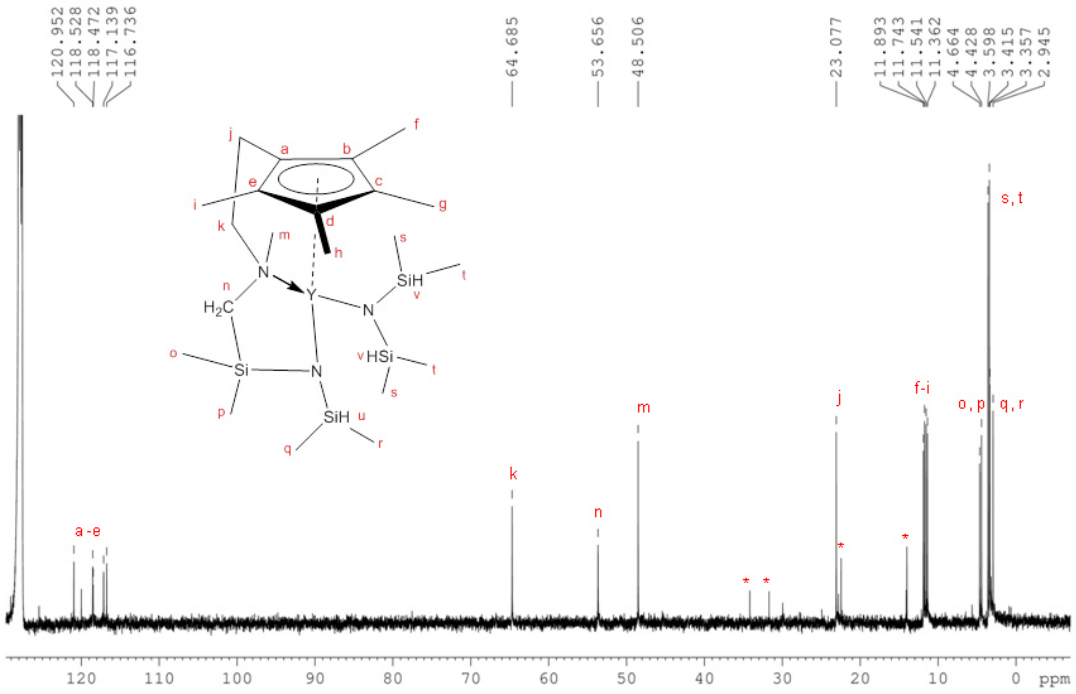

Figure S6: ^{13}C NMR spectrum (C_6D_6, 25 °C) of compound **3**

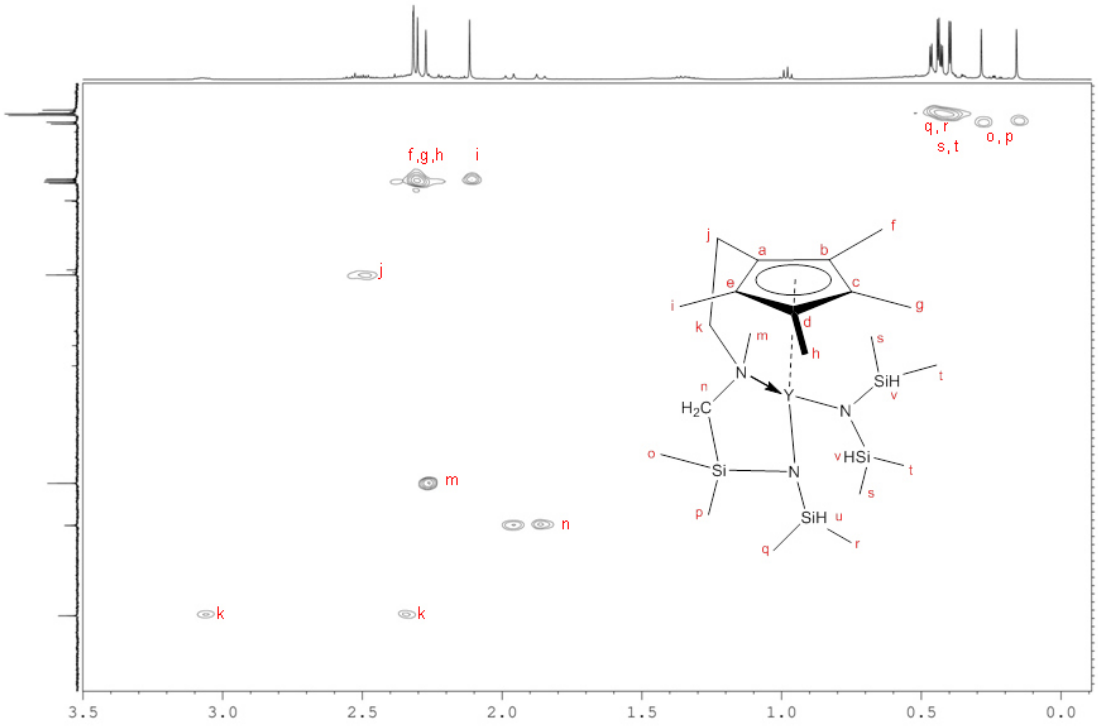

Figure S7: 2D ^{1}H-^{13}C HSQC NMR spectrum (C_6D_6, 25 °C) of compound **3**

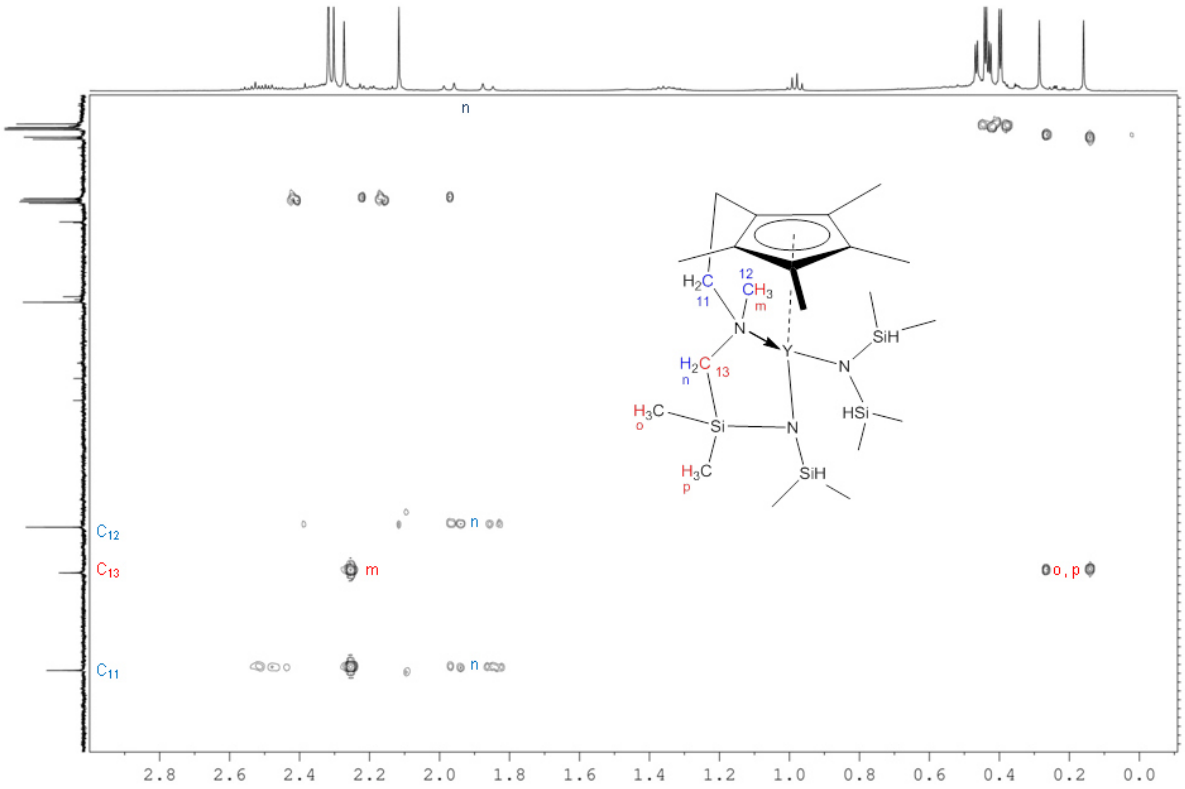

Figure S8: 2D ^{1}H-^{13}C HMBC NMR spectrum (C_6D_6, 25 °C) of compound **3**

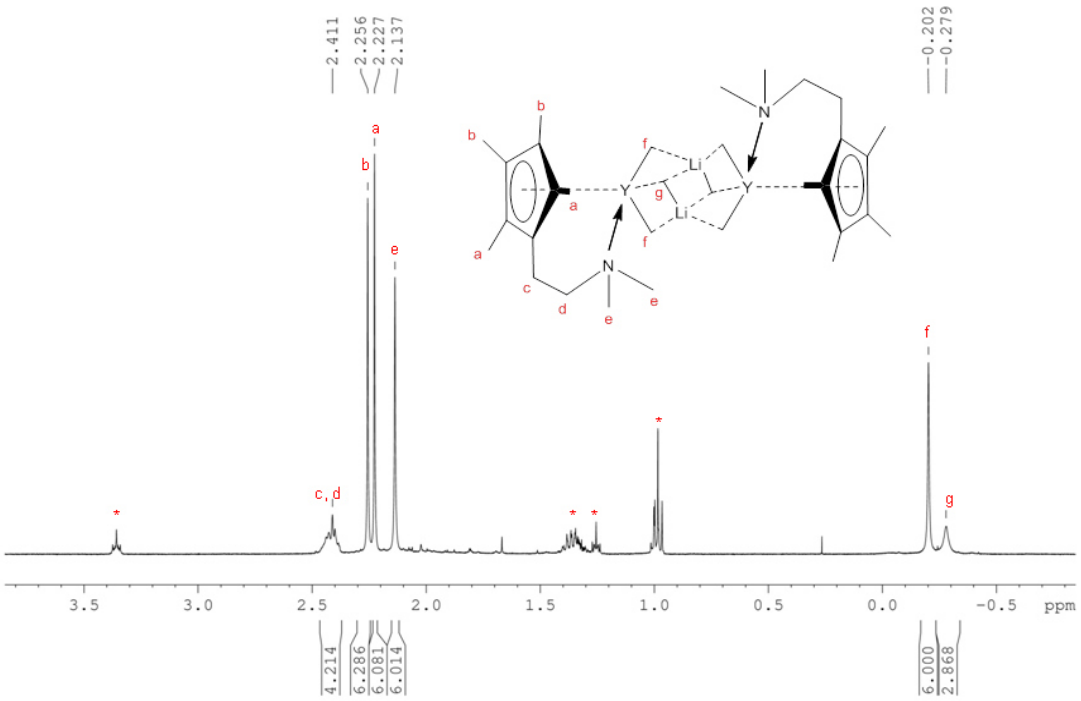

Figure S9: ^{1}H NMR spectrum (C_6D_6, 25 °C) of complex **5**

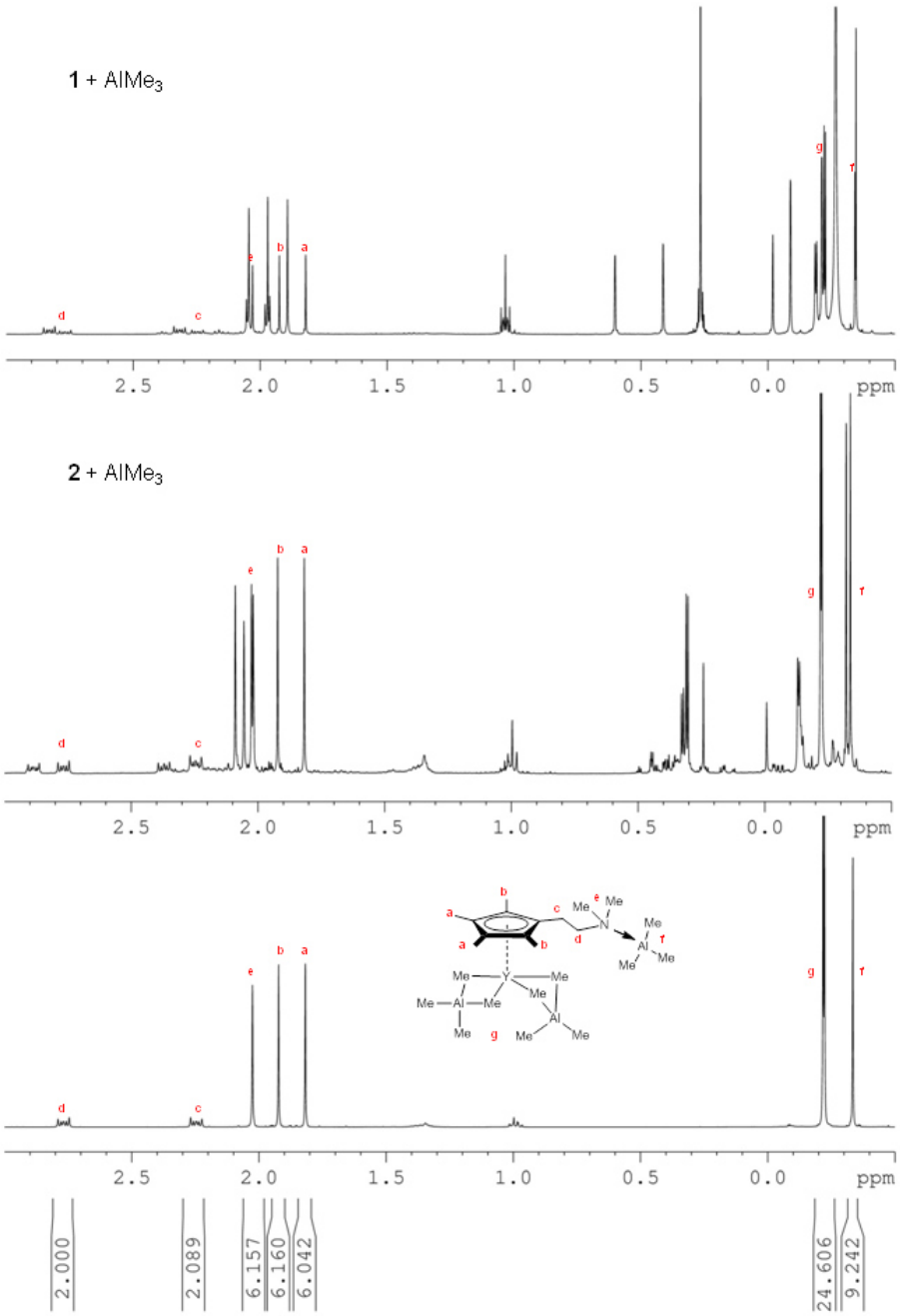

Figure S10: ^{1}H NMR spectra (C_6D_6, 25 °C) from reaction of complex **1** and **2** with $AlMe_3$ compared with that of $Cp^{NMe2AlMe3}Y(AlMe_4)_2$

Paper III

Title: Rare-Earth-Metal Allyl Complexes Supported by the [2-(N,N-Dimethylamino)ethyl]tetramethylcyclopentadienyl Ligand: Structural Characterization, Reactivity, and Isoprene Polymerization

Author: Lars N. Jende, Christoph O. Hollfelder, Cäcilia Maichle-Mössmer, et al

Publication: Organometallics

Publisher: American Chemical Society

Date: Jan 1, 2015

PERMISSION/LICENSE IS GRANTED FOR YOUR ORDER AT NO CHARGE

This type of permission/license, instead of the standard Terms & Conditions, is sent to you because no fee is being charged for your order. Please note the following:

- Permission is granted for your request in both print and electronic formats, and translations.
- If figures and/or tables were requested, they may be adapted or used in part.
- Please print this page for your records and send a copy of it to your publisher/graduate school.
- Appropriate credit for the requested material should be given as follows: "Reprinted (adapted) with permission from (COMPLETE REFERENCE CITATION). Copyright (YEAR) American Chemical Society." Insert appropriate information in place of the capitalized words.
- One-time permission is granted only for the use specified in your request. No additional uses are granted (such as derivative works or other editions). For any other uses, please submit a new request.

If credit is given to another source for the material you requested, permission must be obtained from that source.

ORGANOMETALLICS

Article

pubs.acs.org/Organometallics

Rare-Earth-Metal Allyl Complexes Supported by the [2-(*N*,*N*-Dimethylamino)ethyl]tetramethylcyclopentadienyl Ligand: Structural Characterization, Reactivity, and Isoprene Polymerization

Lars N. Jende, Christoph O. Hollfelder, Cäcilia Maichle-Mössmer, and Reiner Anwander*

Institut für Anorganische Chemie, Universität Tübingen, Auf der Morgenstelle 18, D-72076 Tübingen, Germany

Supporting Information

ABSTRACT: Rare-earth-metal half-sandwich allyl complexes bearing an amino-functionalized cyclopentadienyl ligand (Cp^{NMe2} = 1-[2-(*N*,*N*-dimethylamino)ethyl]-2,3,4,5-tetramethylcyclopentadienyl) were synthesized in a two-step salt-metathesis reaction. Treatment of $LnCl_3(THF)_x$ with $LiCp^{NMe2}$, followed by an in situ reaction with the Grignard reagent C_3H_5MgCl, generated the bis(allyl) half-sandwich complexes $Cp^{NMe2}Ln(\eta^3\text{-}C_3H_5)_2$ only for the smaller rare-earth metals (Ln = Y, Ho, Lu) in good yields (82−88%). In case of the larger neodymium, the dimeric mono(allyl) chlorido half-sandwich complex $[Cp^{NMe2}Nd(\eta^3\text{-}C_3H_5)(\mu\text{-}Cl)]_2$ was obtained in 68% yield. All complexes show moderate to high activity in isoprene polymerization upon cationization with organoborates $[Ph_3C][B(C_6F_5)_4]$ and $[PhNMe_2H][B(C_6F_5)_4]$, the yttrium, holmium, and neodymium metal centers yielding mainly 3,4-microstructures (maximum 79%). Addition of 10 equiv of $AlMe_3$ to the catalyst systems $Cp^{NMe2}Ln(\eta^3\text{-}C_3H_5)_2$ (Ln = Y, Ho)/$[PhNMe_2H][B(C_6F_5)_4]$ and $[Cp^{NMe2}Nd(\eta^3\text{-}C_3H_5)(\mu\text{-}Cl)]_2$/$[PhNMe_2H][B(C_6F_5)_4]$ switched the polyisoprene stereoregularity from 3,4-specific to trans-1,4-selective (maximum 85%). The use of Al^iBu_3 instead led to polymers with mainly cis-1,4-microstructure for the monomeric yttrium and holmium complexes (maximum 74%). Treatment of the bis(allyl) complexes with Et_2AlCl (as cocatalyst) did not provide active species for isoprene polymerization but led to [allyl] → [Cl] exchange and isolation of the hexameric rare-earth-metal clusters $[\{(Cp^{NMe2AlEt3})_2(Cp^{NMe2})Ln_3(\mu_2\text{-}Cl)_3(\mu_3\text{-}Cl)_2\}(\mu_2\text{-}Cl)]_2$ (Ln = Y, Ho). The complexes $Cp^{NMe2}Ln(\eta^3\text{-}C_3H_5)_2$ (Ln = Y, Ho, Lu), $[Cp^{NMe2}Nd(\eta^3\text{-}C_3H_5)(\mu\text{-}Cl)]_2$, and $[\{(Cp^{NMe2AlEt3})_2(Cp^{NMe2})Ln_3(\mu_2\text{-}Cl)_3(\mu_3\text{-}Cl)_2\}(\mu_2\text{-}Cl)]_2$ (Ln = Y, Ho) were analyzed by X-ray crystallography.

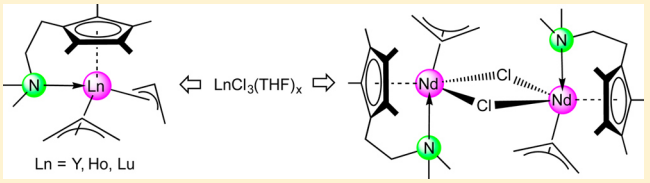

INTRODUCTION

The development of rare-earth-metal (Ln) based single-site initiators for polymerization reactions has been closely related to the progress in group 4 metal based homogeneous Ziegler−Natta catalysis.[1] Most striking was the discovery by Marks and Schumann et al. that lanthanidocene complexes revealed high catalytic activity in ethylene polymerization without further activation by cocatalysts (so-called single-component catalysts).[2,3] The introduction of dianionic bidentate amido-cyclopentadienyl ligands by Bercaw and Shapiro, such as in scandium complexes $[(C_5Me_4SiMe_2NCMe_3)Sc(PMe_3)_2(\mu\text{-}R)]_2$ (R = H, alkyl), marked another milestone.[4] This approach, which implies enhanced reactivity through electronically and sterically less saturated metal centers, was adopted by the Dow and Exxon Chemical Cos. for group 4 metal centers as the first "constrained geometry" catalysts (CGC).[5,6] Since then, a series of rare-earth-metal(III) complexes of this type have been reported,[7] but as they exist by nature only as mono(alkyl) or -(hydride) species, these complexes generally display no activity in 1,3-diene polymerization. The rare examples that can polymerize 1,3-butadiene and isoprene are limited to the dimeric complexes $[(C_5Me_4)_2Ln(\mu\text{-}Me)_2AlMe_2]_2$[8−11] and $[(C_5Me_4)SiMe_2P(Cy)Ln(CH_2SiMe_3)]_2$[12] (Ln = Y, Lu; Cy = cyclohexyl), requiring activation with 1 equiv of cocatalyst, thus forming a dimeric mono(alkyl) monocation as the active species, and the *ansa*-neodymocene complex $[(CpCMe_2Flu)Nd(\mu^3\text{-}C_3H_5)(thf)]$ (Cp = cyclopentadienyl, Flu = fluorenyl),[13,14] representing a single-component catalyst which also terpolymerizes conjugated dienes with styrene and ethylene. The need for a remaining reactive metal−carbon bond upon activation led to extensive investigations of half-sandwich rare-earth-metal bis(hydrocarbyl) complexes of the $[(\mathbf{L})Ln^{III}R_2(Do)_x]$ type, bearing a monoanionic ancillary ligand (**L**) and σ-bonded alkyl groups (R = Me, CH_2SiMe_3, CH_2Ph, $CH_2C_6H_4\text{-}o\text{-}NMe_2$), as versatile polymerization initiators.[15,16] Due to the sterically unsaturated Ln(III) centers, incorporation of neutral donor ligands (Do) was frequently observed.[15,16]

In contrast, donor side arm substituted cyclopentadienyls, fluorenyls, and indenyls as monoanionic ancillary ligands can mimic a constrained geometry configuration, thus accomplishing "solvent free", highly stable precatalysts with well-defined reaction sites.[17−33] Very recently, Cui et al. reported on the synthesis and characterization of a series of linked-half-sandwich rare-earth-metal bis(allyl) complexes and demonstrated their excellent catalytic performance in the polymerization of 1,3-diene and styrene, following cationization with organoborate activators in the presence or absence of

Received: July 15, 2014
Published: December 24, 2014

DOI: 10.1021/om500725g
Organometallics 2015, 34, 32−41

trialkylaluminum.[17,18,20,24] Worth emphasizing is a comprehensive study on isoprene polymerization promoted by the *N*,*N*-dimethylanilinyl-substituted half-sandwich rare-earth-metal complexes $[(C_5Me_4C_6H_4\text{-}o\text{-}NMe_2)Ln(\eta^3\text{-}C_3H_5)_2]$ (Ln = Y, Nd, Gd, Dy) back in 2010.[24] Activation of the respective gadolinium complex with $[PhNMe_2H][B(C_6F_5)_4]$ and 10 equiv of $AlMe_3$ produced the first rare-earth-metal bis(allyl) system that polymerizes isoprene in a living fashion (PDI = 1.11). While the moderate cis-1,4 selectivity of 83% could be increased to 99% via addition of $AliBu_3$, the capability of the organoaluminum compound to act as a chain-transfer agent was revealed by up to eight growing polymer chains per gadolinium center (800% catalytic efficiency). In the same year, the group of Cui reported the bis(allyl) lutetium complex $[(C_5Me_4C_6H_4N)Lu(\eta^3\text{-}C_3H_5)_2]$, bearing a pyridyl-substituted cyclopentadienyl ancillary ligand, to initiate highly cis-1,4-selective (99%) butadiene and purely syndiotactic (*rrrr* >99%) styrene polymerization on activation with the trityl borate agent $[Ph_3C][B(C_6F_5)_4]$.[17] The latter cationic lutetium CGC catalyst was also employed for the terpolymerization of styrene with 1,3-butadiene and isoprene, allowing outstanding control over regio- and stereoregularity as well as block copolymer formation.[20] Previous studies on bis(allyl) rare-earth-metal half-sandwich complexes also feature Taube's complex $[(C_5Me_5)Nd(\eta^3\text{-}C_3H_5)_2(C_4H_8O_2)_{0.7}]$, which upon activation with MAO (Al/Nd = 30) produced polybutadiene with cis contents as high as 66%.[34] The latter dioxane complex was obtained via protonolysis employing $[Nd(\eta^3\text{-}C_3H_5)_3(C_4H_8O_2)]$ and HC_5Me_5.

Recently, our group developed a bis(tetramethylaluminate)-based library of $[(\mathbf{L})Ln^{III}(AlMe_4)_2]$-type complexes, particularly to be exploited for 1,3-diene polymerization. The respective monoanionic ancillary ligands **L** also comprise N-donor-functionalized quinolyl-,[35] aminophenyl-,[35] and dimethylaminoethyl-cyclopentadienyl ligands[36] (Cp^{Q}, Cp^{ANMe2}, and Cp^{NMe2}).[37−41] Triggered by the interesting catalytic properties of the bis(allyl) complexes presented by Cui, we set out to examine Cp^{NMe2}-supported rare-earth-metal bis(allyl) complexes. Here, we focused on the implications of a flexible C_2 spacer between the cyclopentadienyl and N-donor moieties, and whether [allyl] → [organoaluminum] exchanges under formation of identifiable alkylaluminate species can be observed as Evans reported for $[\{C_5Me_4SiMe_2(CH_2CH{=}CH_2)\}_2Y(\eta^3\text{-}C_3H_5)]$.[42] In addition, the performance in isoprene polymerization upon activation with perfluorated organoborate compounds was tested and compared with the performance of half-sandwich bis(aluminate) complexes.

RESULTS AND DISCUSSION

The salt-metathesis reaction of $LnCl_3(THF)_x$ with $[C_5Me_4C_2H_4NMe_2]Li$ at ambient temperature for 4 h, followed by an in situ reaction with the Grignard reagent C_3H_5MgCl for another 16 h, generated the bis(allyl) half-sandwich complexes $[Cp^{NMe2}Ln(\eta^3\text{-}C_3H_5)_2]$ (**1**) in high yields (82−88%) for the smaller rare-earth metals (Ln = Y (**1a**), Ho (**1b**), Lu (**1c**)) (Scheme 1). In the case of the larger neodymium, only the dimeric mono(allyl) chlorido half-sandwich complex $[Cp^{NMe2}Nd(\eta^3\text{-}C_3H_5)(\mu\text{-}Cl)]_2$ (**2**) was obtained under identical reaction conditions. We assume that the presence of two bridging chlorido ligands sterically disfavors any complete displacement by allyl moieties. Although the elemental analyses of samples, obtained from the reaction of isolated complex **2** with another 1 equiv of C_3H_5MgCl, showed increased

Scheme 1. Synthesis of Rare-Earth-Metal Bis(allyl) Complexes 1 and the Dimeric Neodymium Mono(allyl) Chlorido Half-Sandwich Complex 2

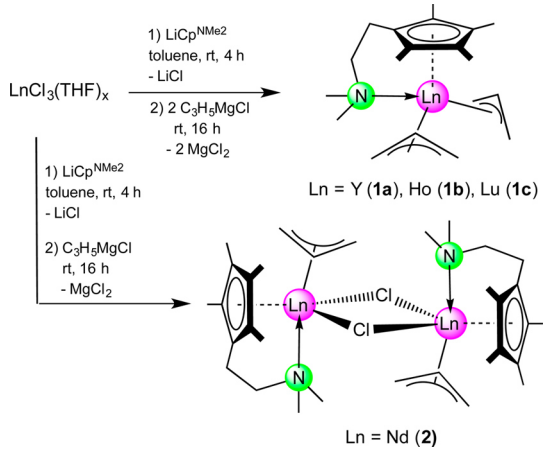

hydrogen and carbon values indicative of further chlorido allyl exchange, no crystalline products could be obtained. Attempts to isolate the respective complexes with the largest rare-earth-metal, lanthanum, failed.

The ^1H NMR spectra of the diamagnetic complexes **1a** (Y) and **1b** (Lu) show the expected sets of signals for the cyclopentadienyl ligand. In particular, three singlets for the methyl groups and two multiplets for the ethyl spacer were detected. The methine proton of the allyl group in compound **1a** gave a doublet of quintets at 6.31 ppm. The signal splitting of the quintet ($^3J_{HH}$ = 12.36 Hz) is clearly attributable to a two-bond $^1H-^{89}Y$ scalar coupling ($^2J_{YH}$ = 1.36 Hz). The resonance of the corresponding methylene protons appeared at 3.04 ppm as a rather broad doublet, implying fast exchange of the terminal allylic protons (H_{syn} and H_{anti}). The allyl groups of the lutetium complex **1c** gave a quintet at 6.37 ppm ($^3J_{HH}$ = 12.36 Hz) and a sharp doublet at 3.07 ppm ($^3J_{HH}$ = 12.36 Hz) for the methine and methylene protons, respectively.

Single crystals of complexes **1** suitable for X-ray crystallography were grown from saturated toluene/*n*-hexane solutions at −35 °C. The complexes are isostructural and crystallize in the monoclinic space group $P2_1$. The representative molecular structure of **1a** is shown in Figure 1, and selected bond distances and angles for complexes **1** are given in Table 1. The ancillary ligand coordinates to the Ln^{III} center in a η^5/κ^1 fashion

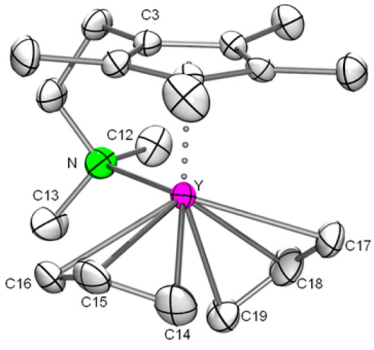

Figure 1. Molecular structure of $[Cp^{NMe2}Y(C_3H_5)_2]$ (**1a**), representative of isostructural complexes **1**. Atomic displacement parameters are set at the 50% probability level; hydrogen atoms are omitted for clarity.

DOI: 10.1021/om500725g
Organometallics 2015, 34, 32−41

Table 1. Selected Bond Lengths (Å) and Angles (deg) of 1a, 1b, 1c, and 2

	1a (Y)	1b (Ho)	1c (Lu)	2 (Nd)
Ln−C14	2.609(4)	2.604(6)	2.575(4)	2.666(5)
Ln−C15	2.625(5)	2.617(7)	2.581(4)	2.702(4)
Ln−C16	2.610(5)	2.604(6)	2.572(4)	2.685(5)
Ln−C17	2.590(5)	2.587(7)	2.534(4)	
Ln−C18	2.614(7)	2.615(14)	2.545(8)	
Ln−C19	2.663(7)	2.660(13)	2.633(9)	
Ln−Cl				2.796(1)
Ln−Cl′				2.874(1)
Ln−N	2.583(4)	2.566(6)	2.550(4)	2.666(3)
Ln−Cp	2.593(4)−2.705(6)	2.589(6)−2.70(1)	2.557(3)−2.669(7)	2.686(4)−2.801(4)
$Ln-Cp_{av}$	2.653	2.645	2.627	2.738
$Ln-Ct_1$	2.363	2.353	2.322	2.459
$Ct_1-Ln-Ct_2$	109.93	109.64	109.53	106.89
$Ct_1-Ln-Ct_3$	131.81	131.36	131.62	
$Ct_2-Ln-Ct_3$	108.40	108.64	108.12	
Ct_1-Ln-N	96.99	97.43	98.21	94.02
Ct_2-Ln-N	109.77	109.69	110.2	112.45
Ct_3-Ln-N	96.47	96.82	96.34	
$Ct_1-Ln-Cl$				101.44
$Ct_1-Ln-Cl'$				166.54
$Ct_2-Ln-Cl$				118.11
$Ct_2-Ln-Cl'$				86.30
N−Ln−Cl				119.09(8)
N−Ln−Cl′				78.04(8)
Cl−Ln−Cl′				73.75(3)

via the Cp ring and the nitrogen atom of the amino group, generating a constrained geometry, while the two allyl moieties bind the rare-earth-metal atom in π-η^3 modes. Due to the constrained geometry the Cp ring is slightly tilted, with the shortest Ln−C distance involving the C3 carbon atom (**1a**, 2.593(4) Å; **1b**, 2.589(6) Å; **1c**, 2.557(3) Å). The two allyl ligands show distinct bonding toward the Ln^{III} centers. While the terminal (C_{AT}) and central (C_{AC}) carbon atoms of one allyl ligand (C14−C16) reveal similar Ln−C_{AT} and Ln−C_{AC} bond lengths (**1a**, average 2.615 Å; **1b**, average 2.608 Å; **1c**, average 2.576 Å), the second allyl ligand features one significantly elongated Ln−C_{AT} distance (C19: **1a**, 2.663(7) Å, **1b**, 2.660(13) Å; **1c**, 2.633(9) Å). The overall ligand arrangement is comparable with that of the *N*,*N*-dimethylanilinyl-substituted half-sandwich rare-earth complexes [$(C_5Me_4C_6H_4$-*o*-$NMe_2)Ln(\eta^3$-$C_3H_5)_2$] (Ln = Y, Lu).[24]

The bond angles $Ct_2-Ln-Ct_3$ involving the allyl centroids (**1a**, 108.40°; **1b**, 108.64°; **1c**, 108.12°) are smaller than in the nonfunctionalized rare-earth-metal bis(allyl) complexes [$(C_5Me_4R)Sc(\eta^3$-$C_3H_5)_2$] (R = $SiMe_3$, 119.11°; R = Me, 115.09)[43] but somewhat elongated in comparison to [$(C_5Me_4C_6H_4$-*o*-$NMe_2)Ln(\eta^3$-$C_3H_5)_2$] (Y, 106.9°; Lu, 106.0°).[24] Furthermore, the bite angles between the cyclopentadienyl centroid and the nitrogen atom Ct_1-Ln-N (**1a**, 96.99°; **1b**, 97.43°; **1c**, 98.21°) are slightly wider than in the anilinyl-functionalized complexes (Y, 95.4°; Lu, 96.7°).[24]

Single crystals of the neodymium complex **2** were also grown from a saturated toluene/*n*-hexane mixture at −35 °C. The complex crystallizes in the triclinic space group $P\bar{1}$ with one molecule of toluene in the unit cell. An X-ray structure analysis of **2** revealed the dimeric structure [$Cp^{NMe2}Nd(\eta^3$-$C_3H_5)(\mu$-$Cl)]_2$ with bridging chlorido ligands (Figure 2, Table 1). The N-donor-functionalized cyclopentadienyl ligand and the allyl group display the expected η^5/κ^1 and π-η^3 coordination modes, respectively, with a Ct_1-Nd-N bite angle of 94.02° and Nd−C_A distances ranging from 2.666(5) to 2.702(4) Å. The coordination geometry of the neodymium centers is best described as distorted trigonal bipyramidal, with the Cp centroid and one chlorine atom in the apical positions, while the other chlorine atom, the allyl group, and the nitrogen atom span the equatorial plane. The bond length between the neodymium atom and the chlorine atom trans to the Cp ring, Nd−Cl′ (2.874(1) Å), is markedly longer than the neodymium−chlorine bond in the trigonal plane (Nd−Cl = 2.796(1) Å). Comparable Nd−Cl distances were found in [$\{Nd(\eta^3$-$C_3H_5)_2(\mu$-$Cl)(THF)_2\}_2$][44] (2.822(1)/2.874(1) Å) and [$\{Nd(AlMe_4)(\mu$-$Cl)\{1,2,4$-$(Me_3C)_3C_5H_2\}\}_2$][38] (2.7807(6)/2.8077(6) Å).

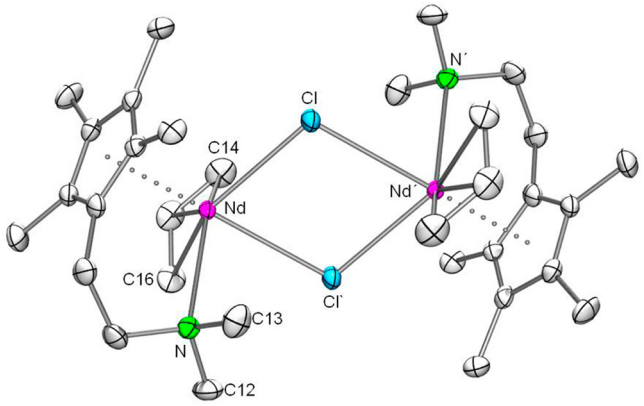

Figure 2. Molecular structure of [$Cp^{NMe2}Nd(\eta^3$-$C_3H_5)(\mu_2$-$Cl)]_2$ (**2**). Atomic displacement parameters are set at the 50% probability level; hydrogen atoms are omitted for clarity.

DOI: 10.1021/om500725g
Organometallics 2015, 34, 32−41

Reactivity toward Et_2AlCl. Activation of rare-earth-metal alkyl or hydride complexes with Lewis acidic diethylaluminum chloride as a "weakly cationizing" cocatalyst is known to form promising catalysts for stereoregular 1,3-diene polymerization.[45,46] In particular, Ln/Al heterobimetallic complexes such as $[Ln(AlMe_4)_3]$,[47,48] $[LnAl_3Me_8(O_2CC_6H_2iPr_3\text{-}2,4,6)_4]$,[49] and $[Ln(AlMe_3)_n(OR)_3]$[50] (R = neopentyl, $C_6H_3iPr_2$-2,6) activated with chlorination reagents such as Et_2AlCl and Ph_3CCl give catalysts for highly cis selective isoprene polymerization. However, active species for the polymerization of isoprene were not formed upon treatment of complexes **1** with Et_2AlCl in 1:0.5, 1:1, 1:1.5, and 1:2 molar ratios.

Addition of 2 equiv of Et_2AlCl to a solution of **1a,b** in deuterated benzene led to full [allyl] → [Cl] exchange under the formation of $[\{(Cp^{NMe2AlEt3})_2(Cp^{NMe2})Ln_3(\mu_2\text{-}Cl)_3(\mu_3\text{-}Cl)_2\}(\mu_2\text{-}Cl)]_2$ (Ln = Y (**3a**), Ho (**3b**); Scheme 2). ^{1}H NMR spectroscopic investigations were not conclusive, probably due to cluster rearrangements and coordination switch of the hemilabile donor function of the cyclopentadienyl ligand at the Lewis acidic Ln(III) and Al(III) centers. Single crystals of **3** suitable for X-ray structure analysis were obtained when pentane was added to a benzene solution which was then cooled to −35 °C. Complexes **3** crystallize in the triclinic space group $P\bar{1}$ with varying amounts of solvent molecules. Since the crystallographic data of the yttrium complex **3a** were of low quality (only allowing the assignment of a connectivity structure; see the Supporting Information), ORTEP drawings of the holmium structure **3b** are shown in Figure 3. Both complexes share the same core structure, which can be best described as two distorted hexagonal bipyramids $[Ln_3Cl_5]$ linked by two chlorido (C16) ligands (Figure 3A).[51] The resulting hexalanthanide cluster $[Ln_6Cl_{12}]$ adopts a chairlike geometry (Figure 3B). Each $[Ln_3Cl_5]$ unit implements three μ_2- and two μ_3-chlorido ligands with Ln−Cl distances of 2.6672(2)−2.7048(2) and 2.7639(2)−2.8486(2) Å, respectively. With regard to the μ_3-chlorido ligands, the contacts involving Cl1 are significantly shorter (2.7639(2)−2.8018(3) Å). Similar cluster arrangements were found previously for the earlier ("larger") lanthanides in the presence of small anions (X) such as halo, cyano, borohydro, and hydroxy, which favorably act as bridging ligands.[52] Examples include $[Nd_6(2,4\text{-}C_7H_{11})_6Cl_{12}(thf)_2]$,[51] $[Ln_6(C_5Me_5)_6Cl_{12}(thf)_2]$ (Ln = Nd, Sm),[53] $[Ln_6(C_5Me_4nPr)_6(BH_4)_{12-x}Cl_x(thf)_2]$ (Ln = Sm, Nd; x = 0, 5, 10),[54] and $[Sm_6(C_5Me_5)_6Cl_{10}(OH)_2(thf)_2]$.[55] The yttrium complex $[Y_6(L)_6Cl_6(OH)_6(thf)_2]$ (L = 2-phenyl-1,4,5,6,7,8-hexahydroazulenyl) represents a rare example of a $[Ln_6X_{12}]$ cluster with a smaller rare-earth-metal center.[56] Herein the hydroxo ligands occupy the two μ_3 and one μ_2 position in the trimeric subunit. In addition to the η^5-coordinated cyclopentadienyl ligand, two of the metal centers in each triangle accommodate five anionic ligands X, while the third has only contact to four X. The latter metal center is additionally coordinated by one thf donor ligand to achieve steric saturation. This way, each metal center has a coordination number of 8. In contrast, the vacant position at Ho3 in complex **3b** is occupied by the nitrogen donor functionality of the cyclopentadienyl ligand, accomplishing a chelating η^5/κ^1 coordination mode (Ho3−N3 = 2.5162(3) Å). The other metal centers (Ho1/Ho2) are η^5 coordinated by the Cp^{NMe2} ligand, while their donor functions are attached to triethylaluminum (N1/2−Al1/2 = 2.0683(2)/2.0612(2) Å). This coordination mode of the Cp^{NMe2} ligand was previously detected in the half-sandwich bis(tetramethylaluminate) complexes $[\{Cp^{NMe2AlMe3}\}Ln(AlMe_4)_2]$ (Ln = Y, La, Nd).[57]

Scheme 2. Allyl−Chlorido Exchange: Synthesis of Complexes $[\{(Cp^{NMe2AlEt3})_2(Cp^{NMe2})Ln_3(\mu_2\text{-}Cl)_3(\mu_3\text{-}Cl)_2\}(\mu_2\text{-}Cl)]_2$ (3)

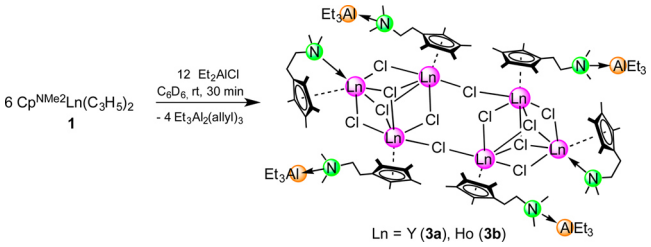

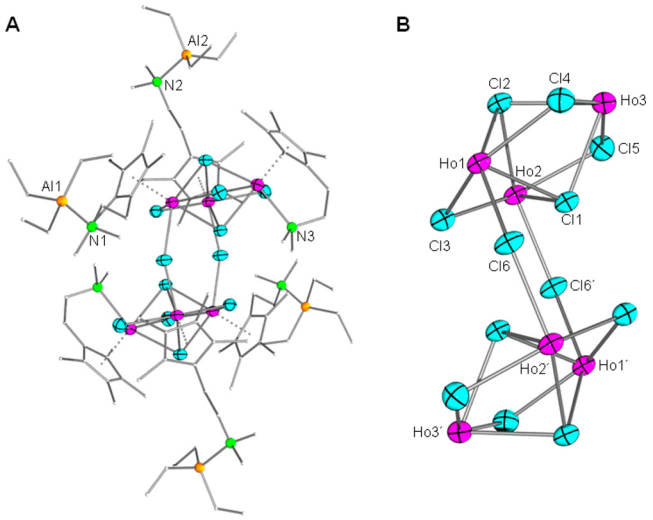

Figure 3. (A) Molecular structure of complex **3b**. Atomic displacement parameters are set at the 50% probability level; hydrogen atoms are omitted for clarity. Aluminum, carbon, and nitrogen atoms are shown with a ball and stick representation. The disorders of the ethyl groups at the aluminum atoms and in the side arm functionality are not shown. (B) Core structure of the hexameric complex. Atomic displacement parameters are set at the 50% probability level. Selected bond distances (Å) and angles (deg): Ho1/2/3−Cl1 2.7885(2)/2.8018(3)/2.7639(2), Ho1/2/3−Cl2 2.8406(3)/2.8486(2)/2.8004(3), Ho1−Cl3/4 2.6672(2)/2.6998(2), Ho2−Cl3/5 2.6771(2)/2.6839(2), Ho3−Cl4/5 2.7048(2)/2.7022(2), Ho1−Cl6 2.6951(3), Ho2−Cl6′ 2.7007(2), Ho3−N3 2.5162(3), Al1/2−N1/2 2.0683(2)/2.0612(2), Cl3/4/5−Ho1/3/2−Cl4/5/3 145.037(14)/145.330(13)/145.330(13), Ho1/2/3−Cl3/5/4−Ho2/3/1 90.298(11)/90.298(11)/ 90.616(13), Ho1/2/3−Cl3/5/4−Ho2/3/1 95.732(13)/94.209(16)/93.830(14), Ho1/2/3−Cl2−Ho2/3/1 88.314(12)/88.611(13)/88.810(11), Ho1−Cl6−Ho2′ 140.437(17), N3−Ho3−Cl1/2/4/5 82.62(4)/154.55(4)/93.98(5)/96.38(5).

Polymerization of Isoprene. The bis(allyl) complexes **1** and the dimeric mono(allyl) chlorido complex **2** were tested as precatalysts in the polymerization of isoprene. Upon cationization with the organoborate reagents $[Ph_3C][B(C_6F_5)_4]$ (**A**) and $[PhNMe_2H][B(C_6F_5)_4]$ (**B**) as cocatalysts, the monomeric complexes **1** displayed moderate to high activity, producing polyisoprenes with microstructures that were affected by the rare-earth-metal center rather than the cocatalyst (Table 2, Figure 4). The yttrium- and holmium-based catalyst systems **1a**/**A**, **1a**/**B**, **1b**/**A**, and **1b**/**B** produced polymers with dominant 3,4 -sequences, as detected by ^{1}H NMR spectroscopy (Table 2, runs 1, 2, 5, and 6). Determination of the accurate cis

DOI: 10.1021/om500725g
Organometallics 2015, 34, 32−41

Table 2. Selected Examples of Isoprene Polymerization at 40 °C

entry[a]	precat.	cocat.[b]	time (min)	yield (%)	*cis*-1,4[c]	*trans*-1,4[c]	3,4[c]	$10^4 M_n$[d]	M_w/M_n[d]
1	$(Cp^{NMe2})Y(C_3H_5)_2$ (**1a**)	**A**	120	19	6	15	79	0.9	1.15
2	$(Cp^{NMe2})Y(C_3H_5)_2$ (**1a**)	**B**	120	20	4	21	75	1.0	1.09
3	$(Cp^{NMe2})Y(C_3H_5)_2$ (**1a**)	**B**/$AlMe_3$	30	>99	<1	71	29	5.4	1.24
4	$(Cp^{NMe2})Y(C_3H_5)_2$ (**1a**)	**B**/Al*i*Bu_3	60	>99	74	<1	26	1.5	1.19
5	$(Cp^{NMe2})Ho(C_3H_5)_2$ (**1b**)	**A**	120	16	11	12	77	1.23	1.17
6	$(Cp^{NMe2})Ho(C_3H_5)_2$ (**1b**)	**B**	120	17	7	17	76	1.23	1.13
7	$(Cp^{NMe2})Ho(C_3H_5)_2$ (**1b**)	**B**/$AlMe_3$	30	>99	<1	72	28	4.0	1.24
8	$(Cp^{NMe2})Ho(C_3H_5)_2$ (**1b**)	**B**/Al*i*Bu_3	60	>99	74	<1	26	1.0	1.25
9	$(Cp^{NMe2})Lu(C_3H_5)_2$ (**1c**)	**A**	120	97	27	34	39	2.4	1.04
10	$(Cp^{NMe2})Lu(C_3H_5)_2$ (**1c**)	**B**	120	81	32	31	37	2.6	1.04
11	$(Cp^{NMe2})Lu(C_3H_5)_2$ (**1c**)	**B**/$AlMe_3$	30	>99	4	51	45	3.3	1.39
12	$(Cp^{NMe2})Lu(C_3H_5)_2$ (**1c**)	**B**/Al*i*Bu_3	60	>99	40	25	35	1.0	1.72
13	$[(Cp^{NMe2})Nd(\mu\text{-}Cl)(C_3H_5)]_2$ (**2**)	**A**	120	>99	5	29	66	4.3	1.10
14	$[(Cp^{NMe2})Nd(\mu\text{-}Cl)(C_3H_5)]_2$ (**2**)	**B**	120	>99	6	30	64	4.7	1.11
15	$[(Cp^{NMe2})Nd(\mu\text{-}Cl)(C_3H_5)]_2$ (**2**)	**B**/$AlMe_3$	30	>99	<1	85	15	4.3	1.06
16	$[(Cp^{NMe2})Nd(\mu\text{-}Cl)(C_3H_5)]_2$ (**2**)	**B**/Al*i*Bu_3	60	>99	5	10	85	1.2	1.29
17[e]	$(Cp^{NMe2AlMe3})Y(AlMe_4)_2$ (**4**)	**A**	120	>99	<1	77	23	2.7	1.11
18[e]	$(Cp^{NMe2AlMe3})Y(AlMe_4)_2$ (**4**)	**B**	120	>99	4	75	21	2.7	1.22

[a]Conditions: 0.02 mmol of catalyst, [complex]/[cocat] = 1/1, 8 mL of solvent, 20 mmol of isoprene. [b]Cocatalyst: **A**, $[Ph_3C][B(C_6F_5)_4]$; **B**, $[PhNMe_2H][B(C_6F_5)_4]$. [c]Determined by ^1H and ^{13}C NMR spectroscopy in $CDCl_3$. [d]Determined by means of size-exclusion chromatography (SEC) against polystyrene standards. [e][Ln]/[cocat]/[isoprene] = 1/1/500, 4 mL of solvent.

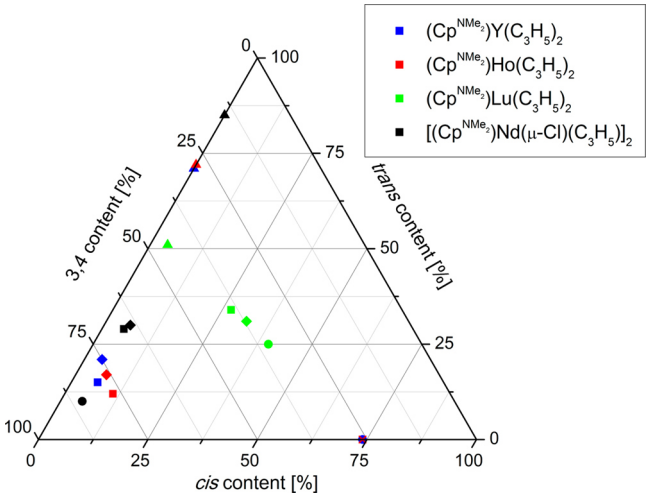

Figure 4. Ternary plot of the microstructures of the polyisoprenes obtainend from precatalysts **1** and **2** upon activation with **A** (■), **B** (◆), **B**/$AlMe_3$ (▲), and **B**/Al^iBu_3 (●) (see Table 2).

and trans contents of the 1,4-units by ^{13}C NMR spectroscopy is hampered by the high contents of atactic 3,4-polyisoprene, leading to broad signals (Figure S14, Supporting Information). Furthermore, in contrast to our intensely studied aluminate precatalysts,[37−39] the selectivity of the allyl complexes is very sensitive toward small (salt) impurities. The lutetium complex **1c** gave polymers with almost equal amounts of *cis*-1,4-, *trans*-1,4-, and 3,4-polyisoprene units (Table 2, runs 9 and 10). The dimeric neodymium complex **2** did not display any activity when a [Ln]:[cocat.] ratio of 1:1 was applied, indicating the displacement of both allyl moieties. However, upon activation of complex **2** with 1 equiv of **A** or **B**, polyisoprenes with a dominant 3,4-microstructure were produced (Table 2, runs 13 and 14). The high 3,4-content is proposed to result from an enhanced steric encumbrance at the CGC metal center in comparison to donor side arm free half-sandwich complexes, which produce predominantly *trans*-1,4-polyisoprene.[37−39] The molecular weight distributions of all obtained polyisoprenes are very narrow (1.04−1.17), suggesting polymerization in a living fashion.

In this context it is worth mentioning that the rare-earth-metal CGC $[(C_5Me_4)SiMe_2(NCMe_3)Sc(PMe_3)_2(\mu_2\text{-}H)_2]$ polymerizes not only ethylene but also higher α-olefins[4] and that the first isospecific 3,4-polymerization (100% 3,4; *mmmm* >99%) of isoprene was achieved by applying the binuclear complexes $[(C_5Me_4)SiMe_2P(Cy)Ln(CH_2SiMe_3)]_2$ (Ln = Y, Lu; Cy = cyclohexyl) bearing a dianionic phosphido-substituted cyclopentadienyl ligand.[12] Furthermore, the rare-earth-metal postmetallocene bis(alkyl) complexes $[\{PhC(NC_6H_4iPr_2\text{-}2,6)_2\}Y(o\text{-}CH_2C_6H_4NMe_2)_2]$,[58] $[L^{1/2}Sc(CH_2SiMe_3)_2]$[59] ($L^1$ = 2,5-bis((pyrrolidin-1-yl)methylene)-pyrrolyl, L^2 = 2,5-bis-((piperidino)methylene)-pyrrolyl), and $[\{2,6\text{-}R_2C_6H_3NCH_2C(CH_2{-}SiMe_3){=}NC_6H_3R_2\text{-}2,6\}Ln(CH_2SiMe_3)_2(THF)]$[60] (Ln = Sc, Y, Lu; R = Me, *i*Pr) were reported to polymerize isoprene in high 3,4-regioselectivity on activation with cocatalyst **A**. For the latter complexes, DFT calculations demonstrated a favorable η^2 coordination of the monomer to the metal center, leading to the 3,4-insertion product. The tendency for 3,4-polyisoprene formation in the presence of sterically demanding ligands was also presented in an investigation of the structure−reactivity relationship of half-sandwich bis(alkyl) scandium complexes, bearing nonfunctionalized and heteroatom-substituted cyclopentadienyl ligands.[33]

It has been shown earlier that the addition of trialkylaluminum compounds to binary catalyst systems has a drastic effect on the activity as well as the regio- and stereoselectivity.[24,58,61] Hence, in subsequent reactions, 10 equiv of each of the trialkylaluminum compounds AlR_3 (R = Me, ^{i}Bu) was added to the catalyst systems utilizing cocatalyst $[PhNMe_2H][B(C_6F_5)_4]$ (**B**), in order to investigate the implications for activity and selectivity. In case of the lutetium complex **1c** and addition of $AlMe_3$, a decrease in the cis-1,4-content to 4% in the resulting polymer was observed, while the trans-1,4- and the 3,4-microstructure contents increased to 51% and 45%, respectively. The use of Al*i*Bu_3 instead caused only minor changes in

DOI: 10.1021/om500725g
Organometallics 2015, 34, 32−41

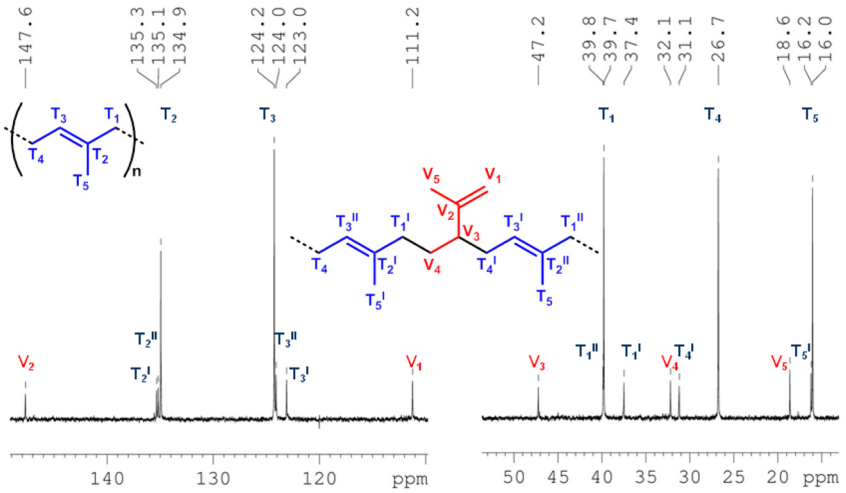

Figure 5. Olefinic and aliphatic regions of the ^{13}C NMR spectrum (101 MHz, 25 °C, $CDCl_3$, σ 77.0 ppm) of polyisoprene obtained with the catalyst system **2**/**B**/$AlMe_3$ (Table 2, run 15).

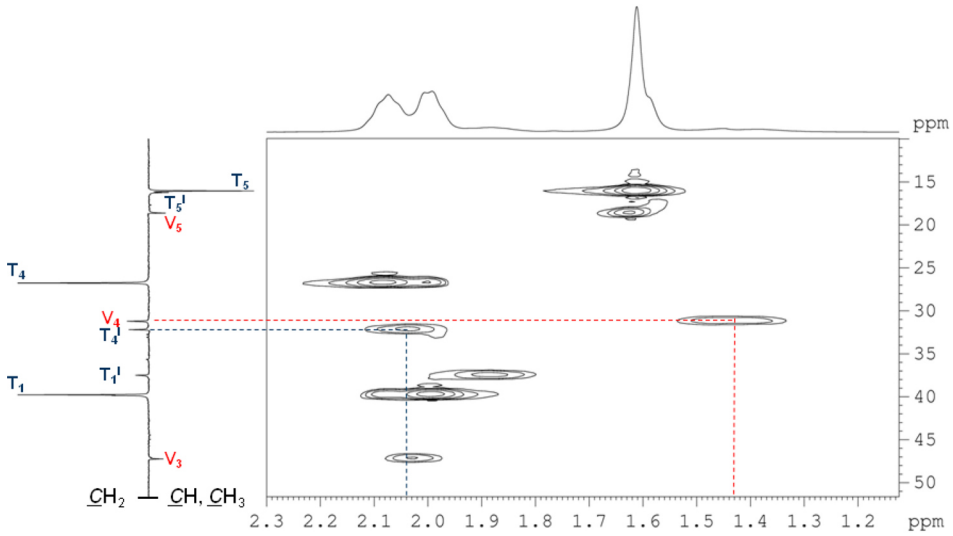

Figure 6. Aliphatic region of the $^1H-^{13}C$ HSQC NMR spectrum (25 °C, $CDCl_3$, σ 77.0 ppm/7.26 ppm) of polyisoprene obtained with the catalyst system **2**/**B**/$AlMe_3$ (run 15). The ^{13}C (DEPT 135) NMR spectrum is shown on the left edge of the contour plot, while the ^1H NMR spectrum is shown at the top.

the stereoregularity, while in both cases a broadening of the molecular weight distribution was found (Table 2, runs 11 and 12). In contrast, the yttrium-based (**1a**) and holmium-based (**1b**) systems were dramatically influenced by the choice of trialkylaluminum reagent. While addition of $AlMe_3$ resulted in moderate trans-1,4-selectivity of 71% (**1a**) and 72% (**1b**) (runs 3 and 7), the use of $AliBu_3$ provided polyisoprene with moderate contents of cis-1,4-microstructure in both cases (74%, runs 4 and 8). This is in agreement with the findings on $[(C_5Me_4C_6H_4\text{-}o\text{-}NMe_2)Y(\eta^3\text{-}C_3H_5)_2]$/**A** based catalyst systems, where the addition of $AlMe_3$ led to 70% *trans*-1,4-polyisoprene and $AliBu_3$ produced 75% *cis*-1,4-polyisoprene.[24] Furthermore, the decrease of the polymer molecular weights with consistently low molecular weight distributions in the presence of $AliBu_3$ (runs 4, 8, 12, and 16) are in agreement with its chain-transfer capability,[24] ideally leading to a so-called "immortal" polymerization.[62,63] Interestingly, for the catalyst system **2**/**B** only a shift toward 1,4-selectivity was observed upon addition of $AlMe_3$ (85% trans, Table 2, run 15), while $AliBu_3$ increased the 3,4-selectivity up to 85% (Table 2, run 16).

In contrast to the case for natural rubber (*Hevea*; 100% *cis*-1,4-PIP) and gutta-percha (100% *trans*-1,4-PIP), synthetic rubbers often not only reveal a mixture of 1,4-units but also incorporate 3,4-microstructures. Depending on the amount and tacticity of the 3,4-units, distinct NMR shifts of adjacent isoprene units are observed, making structure analysis a challenging task.[64] On the other hand, systematic incorporation of 3,4-units has been proven to influence the physicochemical properties of such rubbers, as has been shown for the increase in wet skid resistance coupled with balanced abrasion and rolling resistance properties of produced tire treads.[65] However, the majority of publications on the structural NMR analysis of polyisoprenes have dealt with the incorporation of 3,4-units in polymers with pronounced cis-1,4-microstructure.[66−69] The catalytic system **2**/**B**/$AlMe_3$ (Table 2, run 15) produced polyisoprene with predominant trans-1,4-regularity but also featured 15% of 3,4-units as determined by ^1H NMR spectroscopy. The ^{13}C NMR gave sharp resonances for both the trans-1,4- (**T**) and the 3,4-units (**V**) but no indication of

DOI: 10.1021/om500725g
Organometallics 2015, 34, 32−41

any cis-1,4-microstructures (signals at 23.4, 26.4, and 32.2 ppm in the aliphatic region) (Figure 5).

The integral ratio of the peaks assigned to the 3,4-units at 18.6, 47.2, 111.2, and 147.6 fits the presence of single isolated 3,4-units incorporated into the trans-1,4-polymer chain, as shown in Figure 5. To correlate the remaining signals, a two-dimensional $^{1}H-^{13}C$ HSQC NMR spectrum was recorded (Figure 6). This allowed us to verify that the ^{13}C NMR signal at 32.1 ppm is the $\mathbf{V}_4$ carbon of the 3,4-unit correlating with the broad doublet at 1.43 ppm in the ^{1}H NMR spectrum and that the peak at 31.1 ppm belongs to the $\mathbf{T}_4^{I}$ carbon. As far as we are aware, this type of polyisoprene microstructure and its corresponding NMR data have not been described in detail to date. Such polymers might open up interesting avenues for selective functionalization of the pendant vinylic groups.

With the aim of gaining more knowledge about the effect of the trialkylaluminum compounds, the reaction of the diamagnetic yttrium bis(allyl) complex $[Cp^{NMe2}Y(\eta^3\text{-}C_3H_5)_2]$ (**1a**) with $AlMe_3$ was investigated by NMR experiments (see the Supporting Information). To this end, **1a** was charged into an NMR tube fitted with a J. Young valve, dissolved in C_6D_6, and blended with 10 equiv of trimethylaluminum (Scheme 3, **I**). Disappearance of the quintet at 6.31 ppm and the doublet at 3.04 ppm in the ^{1}H NMR spectrum indicated a rapid displacement of the η^3-coordinated allyl ligands (**i**, Figure 7a). After evaporation of the volatiles, a clean spectrum of the reaction products was obtained, suggesting the formation of two different species (Figure 7b). A closer examination of the obtained data unambiguously verified one of the species as the yttrium half-sandwich bis(tetramethylaluminate) complex $[Cp^{NMe2AlMe3}Y(AlMe_4)_2]$ (**4**) reported recently (Figure 7c).[57,70]

Scheme 3. Allyl−Alkyl Exchange: Synthesis of the Rare-Earth-Metal Bis(aluminate) Half-Sandwich Complex $[Cp^{NMe2AlMe3}Y(AlMe_4)_2]$ (4)[70]

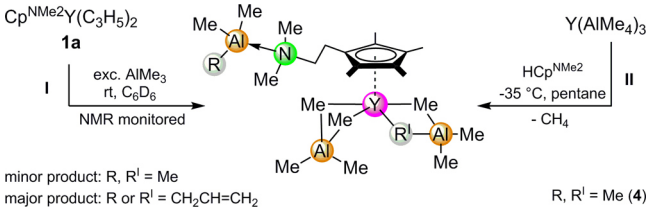

The second reaction product could not be isolated. It is likely that the nitrogen-functionalized side arm coordinates to a trialkylaluminum instead of the rare-earth-metal center, as indicated by the separation of the ethylene-linker proton signals (**ii**) in the ^{1}H NMR spectra. Furthermore, the appearance of two multiplets at 5.66 and 5.10 ppm (**iii**) with a proton integral ratio of 1:2 may belong to one remaining allyl ligand σ-bonded to a metal center either as $AlMe_2R$ (R = CH_2CHCH_2) coordinated by the nitrogen atom or as a bridging anion of a $[AlMe_3R]^-$ moiety (Scheme 3).[71,72]

In order to work out if a half-sandwich bis(aluminate) species represents the real precatalyst, the complex $[Cp^{NMe2AlMe3}Y(AlMe_4)_2]$ (**4**) was synthesized by applying the protonolysis protocol with the homoleptic tetramethylaluminate yttrium complex as the precursor (Scheme 3, **II**) and tested in isoprene polymerization after cationization with the borate reagents **A** and **B**. Both polymerization reactions produced polyisoprene with moderate trans-1,4-microstructures of 77% and 75%, while the cis-1,4-contents were very low (Table 2, runs 17 and 18), which is comparable to those for the catalyst systems **1**/**B**/$AlMe_3$ of yttrium and holmium. It is important to note that none of the cationized species could be unambiguously identified and that the excess amount of trimethylaluminum in the ternary catalyst systems might have further implications for the activation sequence.

CONCLUSIONS

Linked half-sandwich rare-earth-metal bis(allyl) complexes $Cp^{NMe2}Ln(\eta^3\text{-}C_3H_5)_2$, bearing an amino-functionalized tetramethylcyclopentadienyl ancillary ligand, are accessible in a straightforward one-pot synthesis by using a two-step salt-metathesis protocol for the smaller rare-earth metals yttrium, holmium, and lutetium. When the same reaction sequence was employed, the larger neodymium metal led to the mono(allyl)

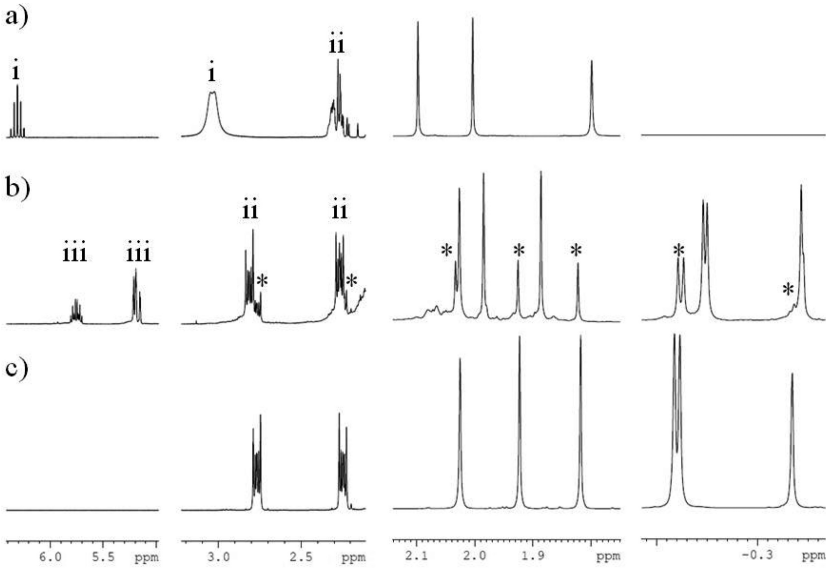

Figure 7. Regions of the ^{1}H NMR spectra (400 MHz, 25 °C, C_6D_6) of (a) pure $[Cp^{NMe2}Y(\eta^3\text{-}C_3H_5)_2]$ (**1a**), (b) reaction product of $[Cp^{NMe2}Y(\eta^3\text{-}C_3H_5)_2]$ with 10 equiv of $AlMe_3$ after evaporation of volatiles, and (c) $[Cp^{NMe2AlMe3}Y(AlMe_4)_2]$ (**4**).

DOI: 10.1021/om500725g
Organometallics 2015, 34, 32−41

chlorido complex $[Cp^{NMe2}Nd(\eta^3\text{-}C_3H_5)(\mu\text{-}Cl)]_2$. Upon activation with $[PhNMe_2H][B(C_6F_5)_4]$, the yttrium and holmium bis(allyl) complexes showed moderate activity for mainly 3,4-selective isoprene polymerization. In the presence of 10 equiv of AlR_3, the activities increased and dramatic shifts toward 1,4-selectivity were observed. The addition of an excess of Al*i*Bu$_3$ led to mainly cis-1,4-regulated polyisoprene, while the use of $AlMe_3$ produced polymers with dominant trans-1,4-microstructure. NMR spectroscopic studies of the mixture $Cp^{NMe2}Y(\eta^3\text{-}C_3H_5)_2/AlMe_3$ revealed rapid [allyl] → [aluminate] exchange (allyl/methyl scrambling) with loss of the constrained geometry conformation involving the formation of complexes such as $Cp^{NMe2AlMe3}Y(AlMe_4)_2$.[70] In accordance with the NMR study, the catalyst systems $Cp^{NMe2}Y(\eta^3\text{-}C_3H_5)_2/[PhNMe_2H][B(C_6F_5)_4]/AlMe_3$ and $Cp^{NMe2AlMe3}Y(AlMe_4)_2/[PhNMe_2H][B(C_6F_5)_4]$ showed similar performance. Apparently, trialkylaluminum reagents are less prone to disrupt the chelate coordination of more rigid CG complexes such as Cui's anilinyl-type complexes $[(C_5Me_4C_6H_4\text{-}o\text{-}NMe_2)Ln(\eta^3\text{-}C_3H_5)_2]$, which afford high cis-1,4 selectivtiy.[24] Treatment of the bis(allyl) complexes with dialkylaluminum chloride as a cocatalyst did not afford initiators for isoprene polymerization but complete [allyl] → [Cl] exchange. As revealed by the X-ray diffraction analyses of the hexameric clusters $[\{(Cp^{NMe2AlEt3})_2(Cp^{NMe2})Ln_3Cl_5\}(\mu_2\text{-}Cl)]_2$ (Ln = Y, Ho), the donor functionality of the ancillary ligand Cp^{NMe} exhibits hemilability in the presence of Lewis acids (here $AlEt_3$): four of the Cp^{NMe} groups coordinate in a η^5 mode to the metal center with a dangling amine group attached to triethylaluminum (formed from $ClAlEt_2$), while the remaining two groups are bonded to the rare-earth-metal center in a chelating η^5/κ^1 fashion.

EXPERIMENTAL SECTION

General Remarks. All operations were performed with rigorous exclusion of air and water, using standard Schlenk, high-vacuum, and argon glovebox techniques (MBraun MB 200B; <1 ppm of O_2, <1 ppm of H_2O). *n*-Hexane, toluene, and THF were purified by using Grubbs columns (MBraun SPS-800, solvent purification system) and stored in a glovebox. C_6D_6 and toluene-d_8 were obtained from Aldrich, dried over Na for 24 h, and filtered. $CDCl_3$ and $AlMe_3$ were purchased from Aldrich and used as received. Homoleptic $Y(AlMe_4)_3$ was prepared according to literature methods.[73] HCp^{NMe2} (Cp^{NMe2} = 1-[2-(*N*,*N*-dimethylamino)ethyl]-2,3,4,5-tetramethylcyclopentadienyl) was synthesized as described in the literature.[36] Isoprene was obtained from Aldrich, dried over trioctylaluminum, and vacuum-transferred prior to use. $[Ph_3C][B(C_6F_5)_4]$ (**A**) and $[PhNMe_2H][B(C_6F_5)_4]$ (**B**) were purchased from Boulder Scientific Co. and used without any further purification. C_3H_5MgCl (1.7 M solution in THF) was purchased from Aldrich and used as received. The NMR spectra of air- and moisture-sensitive compounds were recorded by using J. Young valve NMR tubes at 25 °C on a Bruker AVII+400 (^{1}H, 400.13 Hz; ^{13}C, 100.61 MHz). ^{1}H and ^{13}C shifts are referenced to internal solvent resonances and reported in parts per million relative to TMS. IR spectra were recorded between 4000 and 400 cm^{-1} on a NICOLET 6700 FTIR spectrometer using a DRIFT chamber with dry KBr/sample mixtures and KBr windows. The collected data were converted using the Kubelka–Munk refinement. Elemental analyses were performed on an Elementar Vario MICRO cube. The crystalline materials were dried under vacuum for several hours before analysis; however, the solvent molecules incorporated into the crystal lattice of complexes **2** and **3** could not be removed under these conditions and hence were allowed for the calculation of the theoretical values. The molar masses (M_w and M_n) of the polymers were determined by size-exclusion chromatography (SEC). Sample solutions (1.0 mg of polymer per mL of THF) were filtered through a 0.45 μm syringe filter prior to injection. SEC was performed with a pump supplied by Viscotek (GPCmax VE 2001), employing ViscoGEL columns. Signals were detected by means of a triple detection array (TDA 305) and calibrated against polystyrene standards (M_w/M_n < 1.15). The flow rate was set to 1.0 mL min^{-1}. The microstructure of the polyisoprenes was examined by means of ^{1}H, ^{13}C, and two-dimensional ^{1}H–^{13}C HSQC NMR experiments on the Bruker AVII+400 spectrometer at ambient temperature, using $CDCl_3$ as solvent.

General Procedure for the Synthesis of $(C_5Me_4CH_2CH_2NMe_2)Ln(C_3H_5)_2$ (1). *Route A.* In a glovebox, $LiCp^{NMe2}$ was suspended in 4 mL of toluene and added dropwise to a stirred suspension of $LnCl_3(THF)_x$ in 4 mL of toluene. The mixture was stirred for 4 h, and C_3H_5MgCl in THF (1.7 M) was added. After complete addition the reaction mixture was stirred for another 16 h at ambient temperature. After evaporation of the solvent, the crude mixture was redissolved in toluene and LiCl and $MgCl_2$ were removed via centrifugation and filtration. The clear solution was reduced to 3 mL, layered with *n*-hexane, and stored at −35 °C to yield crystalline complexes **1**, which were further purified by repeated recrystallization from saturated *n*-hexane solutions at −35 °C.

Alternatively, the following route was successfully tested for the yttrium and holmium complexes.

Route B. In a glovebox, $LiCp^{NMe2}$ was added to a stirred suspension of $LnCl_3(THF)_x$ in 4 mL of THF chilled to −35 °C. After 0.5 h at ambient temperature the solution became clear and C_3H_5MgCl in THF (1.7 M) was added. The reaction mixture was stirred another 1 h at ambient temperature, and 0.5 mL of dioxane was added. After 1 h, the precipitated $MgCl_2$–dioxane adduct was removed via centrifugation and filtration. The solvent was evaporated and the crude product extracted with *n*-hexane. For crystallization of complexes **1** the clear solution was reduced to 3 mL and stored at −35 °C.

*Synthesis of $(C_5Me_4CH_2CH_2NMe_2)Y(C_3H_5)_2$ (**1a**).* Following synthesis route A described above, $LiCp^{NMe2}$ (199 mg, 1.00 mmol), $YCl_3(THF)_{3.5}$ (448 mg, 1.00 mmol), and C_3H_5MgCl (1.18 mL, 2.00 mmol, 1.7 M in THF) yielded **1a** (319 mg, 0.88 mmol, 88%) as slightly yellow crystals. Following synthesis route B described above, $LiCp^{NMe2}$ (66 mg, 0.33 mmol), $YCl_3(THF)_{3.5}$ (148 mg, 0.33 mmol), and C_3H_5MgCl (0.39 mL, 0.66 mmol, 1.7 M in THF) yielded **1a** (102 mg, 0.28 mmol, 85%) as slightly yellow crystals. ^{1}H NMR (400 MHz, C_6D_6, 25 °C): σ 6.31 (dquin, 2 H, $^3J_{HH}$ = 12.36 Hz, $^2J_{YH}$ = 1.36 Hz, CH_2CHCH_2), 3.04 (d(br), 8 H, CH_2CHCH_2), 2.32–2.24 (m, 4 H, NCH_2CH_2Cp), 2.10 (s, 6 H, CH_3Cp), 2.00 (s, 6 H, CH_3Cp), 1.80 (s, 6 H, CH_3N). ^{13}C NMR (101 MHz, C_6D_6, 25 °C): σ 147.9 (CH_2CHCH_2), 120.0, 117.9, 113.8 ($C_5(CH_3)_4$), 68.8 (CH_2CHCH_2), 64.7 (NCH_2CH_2), 46.9 (CH_3N), 22.8 (CH_2CH_2Cp), 11.8, 11.4 ($C_5(CH_3)_4$). IR (cm^{-1}): 3068 m, 3000 m, 2970 m, 2952 m, 2904 br, 2864 br, 2833 br, 2802 m, 2723 m, 1545 s, 1461 s, 1438 br, 1376 w, 1367 w, 1244 m, 1230 s, 1029 m, 1008 m, 909 m, 765 s, 752 m, 715 m, 680 s, 576 w. Anal. Calcd for $C_{19}H_{32}NY$ (363.37): C, 62.80; H, 8.88; N, 3.85. Found: C, 62.18; H, 8.73; N, 3.91.

*Synthesis of $(C_5Me_4CH_2CH_2NMe_2)Ho(C_3H_5)_2$ (**1b**).* Following synthesis route A described above, $LiCp^{NMe2}$ (199 mg, 1.00 mmol), $HoCl_3(THF)_3$ (509 mg, 1.00 mmol), and C_3H_5MgCl (1.18 mL, 2.00 mmol, 1.7 M in THF) yielded **1b** (360 mg, 0.82 mmol, 82%) as orange crystals. Following synthesis route B described above, $LiCp^{NMe2}$ (66 mg, 0.33 mmol), $HoCl_3(THF)_3$ (168 mg, 0.33 mmol), and C_3H_5MgCl (0.39 mL, 0.66 mmol, 1.7 M in THF) yielded **1b** (120 mg, 0.27 mmol, 83%) as orange crystals. IR (cm^{-1}): 3068 m, 3006 m, 2974 m, 2952 m, 2909 br, 2852 br, 2800 m, 2723 m, 1546 s, 1461 s, 1440 s, 1376 w, 1367 w, 1244 m, 1227 s, 1028 m, 1007 m, 909 m, 766 s, 718 m, 685 s, 571 w. Anal. Calcd for $C_{19}H_{32}NHo$ (439.39): C, 51.94; H, 7.34; N, 3.19. Found: C, 51.42; H, 6.84; N, 3.15.

*Synthesis of $(C_5Me_4CH_2CH_2NMe_2)Lu(C_3H_5)_2$ (**1c**).* Following synthesis route A described above, $LiCp^{NMe2}$ (199 mg, 1.00 mmol), $LuCl_3(THF)_3$ (497 mg, 1.00 mmol), and C_3H_5MgCl (1.18 mL, 2.00 mmol, 1.7 M in THF) yielded **1c** (369 mg, 0.87 mmol, 87%) as slightly yellow crystals. ^{1}H NMR (400 MHz, C_6D_6, 25 °C): σ 6.37 (quin, 2 H, $^3J_{HH}$ = 12.36 Hz, CH_2CHCH_2), 3.07 (d, 8H, $^3J_{HH}$ = 12.36 Hz, CH_2CHCH_2), 2.31–2.22 (m, 4 H, NCH_2CH_2Cp), 2.09 (s, 6 H, CH_3Cp), 2.01 (s, 6 H, CH_3Cp), 1.79 (s, 6 H, CH_3N). ^{13}C NMR (101

DOI: 10.1021/om500725g
Organometallics 2015, 34, 32–41

MHz, C_6D_6, 25 °C): σ 149.1 (CH_2CHCH_2), 125.7, 116.6, 112.9 ($C_5(CH_3)_4$), 68.3 (CH_2CHCH_2), 64.9 (NCH_2CH_2), 47.4 (CH_3N), 22.5 (CH_2CH_2Cp), 11.7, 11.3 ($Cp(CH_3)_4$). IR (cm^{-1}): 3068 m, 3001 m, 2970 m, 2951 m, 2908 br, 2853 br, 2802 m, 2723 m, 1545 s, 1461 s, 1440 s, 1376 w, 1367 w, 1244 m, 1229 s, 1029 m, 1007 m, 909 m, 765 s, 753 m, 715 m, 680 s, 576 w. Anal. Calcd for $C_{19}H_{32}NLu$ (449.43): C, 50.78; H, 7.18; N, 3.12. Found: C, 50.18; H, 7.10; N, 3.08.

Synthesis of [(C5Me4CH2CH2NMe2)Nd(C3H5)(μ-Cl)]2 (2). Following synthesis route A described above, $LiCp^{NMe2}$ (199 mg, 1.00 mmol), $NdCl_3(thf)_{1.75}$ (370 mg, 1.00 mmol), and C_3H_5MgCl (1.18 mL, 2.00 mmol, 1.7 M in THF) yielded **3** (281 mg, 0.34 mmol, 68%) as green crystals. IR (cm^{-1}): 3066 w, 2953 m, 2938 m, 2901 s, 2865 s, 2835 m, 2823 m, 2802 m, 2723 w, 1544 s, 1462 s, 1431 m, 1376 w, 1245 m, 1036 w, 1014 m, 912 m, 779 s, 766 m, 737 m, 681 s. Anal. Calcd for $C_{32}H_{54}Cl_2N_2Nd_2$·(toluene) (918.31): C, 51.01; H, 6.81; N, 3.05. Found: C, 51.14; H, 6.86; N, 2.98.

General Procedure for the Synthesis of [{(C5Me4CH2CH2NMe2AlEt3)2(C5Me4CH2CH2NMe2)Ln3(μ2-Cl)3(μ3-Cl)2}(μ2-Cl)]2 (3). Et_2AlCl was diluted in 0.5 mL of C_6D_6 and added to a solution of complex **1** in 0.5 mL of C_6D_6. The mixture was charged with pentane via the vapor diffusion method at ambient temperature until small crystals appeared. For crystal growth the solution was then stored at −35 °C for several days.

Synthesis of [{(Cp^NMe2AlEt3)2(Cp^NMe2)Y3Cl5}(μ-Cl)]2 (3a). Following the procedure described above, complex **1a** (25 mg, 0.069 mmol) and Et_2AlCl (16.6 mg, 0.138 mmol) yielded **3a** (19 mg, 0.007 mmol, 64%) as colorless crystals. IR (cm^{-1}): 3058 vw(sh), 2972 s, 2922 s, 2894 s, 2855 s, 2791 m, 2728 w, 2633 w, 2279 w, 1467 s, 1452 s, 1408 m, 1378 w, 1328 w, 1272 w, 1241 w, 1228 w, 1189 w, 1137 w, 1098 w, 1064 w, 1027 m, 1009 m, 988 m, 950 m, 913 w, 856 w, 803 w, 765 w, 668 m, 647 s, 634 s. Anal. Calcd for for $C_{102}H_{192}Al_4Cl_{12}N_6Y_6$ (2569.45): C, 47.68; H, 7.53; N, 3.27. Calcd for **3a**·$(benzene)_2$: C, 50.23; H, 7.54; N, 3.08. Found: C, 51.16; H, 7.83; N, 3.35. Multiple attempts to obtain a more satisfactory microanalysis failed.

Synthesis of [{(Cp^NMe2AlEt3)2(Cp^NMe2)Ho3Cl5}(μ-Cl)]2 (3b). Following the procedure described above, complex **1b** (25 mg, 0.057 mmol) and Et_2AlCl (13.7 mg, 0.114 mmol) yielded **3b** (24 mg, 0.008 mmol, 83%) as pink crystals. IR (cm^{-1}): 3063 vw(sh), 2973 s, 2922 s, 2893 s, 2855 s, 2791 m, 2728 w, 2634 w, 2279 w, 1467 s, 1452 s, 1408 m, 1378 w, 1328 w, 1272 w, 1241 w, 1228 w, 1189 w, 1137 w, 1098 w, 1064 w, 1027 m, 1009 m, 988 m, 950 m, 913 w, 856 w, 856 w, 804 w, 766 w, 667 m, 647 s, 633 s. Anal. Calcd for $C_{102}H_{192}Al_4Cl_{12}Ho_6N_6$ (3025.60): C, 40.49; H, 6.40; N, 2.78. Calcd for **3b**·2(benzene): C, 43.03; H, 6.46; N, 2.64. Found: C, 43.26; H, 6.14; N, 2.71.

Polymerization of Isoprene. A detailed polymerization procedure (Table 2, run 1) is described as a typical example. $[Ph_3C][B(C_6F_5)_4]$ (**A**; 18 mg, 0.02 mmol, 1 equiv) was added to a solution of **1a** (7.27 mg, 0.02 mmol) in toluene (8 mL), and the mixture was aged at ambient temperature for 30 min. After the addition of isoprene (1.36 g, 20 mmol), the polymerization was carried out at 40 °C for 2 h. The reaction was terminated by pouring the polymerization mixture into 200 mL of methanol containing 0.1% (w/w) 2,6-di-*tert*-butyl-4-methylphenol as a stabilizer and stirred for 12 h. The polymer was washed with methanol and dried under vacuum at ambient temperature to constant weight. In case of the ternary catalyst system (example Table 2, run 3), the precatalyst was mixed with the trialkylaluminum compound for 30 min prior to activation with the cocatalyst. The polymerization was following the procedure described above.

Crystallographic Details. Single crystals suitable for X-ray diffraction measurements were selected in a glovebox, covered in Parabar 10312 (previously known as Paratone-N), and mounted on a glass fiber. The crystal data for the complexes were collected on a STOE IPDS II diffractometer using graphite-monochromated Mo K_α radiation (λ = 0.71073 Å) at 173(2) K performing φ scans. Raw data were collected, integrated, and reduced using the program package X-Area.[74] Corrections for absorption effects were applied using Platon/Mulabs.[75] Structure solutions and refinements were performed using the programs SHELXS[76] and SHELXL.[77] The structures in this article are represented using the program ORTEP-III.[78] For further experimental details on refinement and crystallographic data see Table S1 (Supporting Information).

■ ASSOCIATED CONTENT

Supporting Information

CIF files giving full crystallographic data for complexes **1**, **2**, and **3b**, ^1H, ^{13}C, and 2D $^1H-^{13}C$ HSQC NMR spectra of compounds **1a** (Figures S1−S3), **1c** (Figures S4−S6), and **4** (Figures S7 and S8), ^1H NMR reaction spectra of **1a** with $AlMe_3$ (Figure S9), ORTEP representations of **1b** (Figure S10), **1c** (Figure S11), **3a** (Figure S12), and **3b** (Figure S13), crystallographic data for complexes **1**−**3** (Table S1), ^1H and ^{13}C NMR data for polyisoprene from run 11 (Table S2), and ^{13}C NMR spectra from polyisoprenes obtained from precatalyst **1a** under various conditions (Figure S14). This material is available free of charge via the Internet at http://pubs.acs.org. Crystallographic data have also been deposited at the Cambridge Crystallographic Data Centre under CCDC reference numbers 974988 (**1a**), 974989 (**1b**), 974990 (**2**), 974991 (**1c**), and 994213 (**3b**), which can be obtained free of charge via www.ccdc.cam.ac.uk/data_request/cif.

■ AUTHOR INFORMATION

Corresponding Author

*E-mail for R.A.: reiner.anwander@uni-tuebingen.de.

Notes

The authors declare no competing financial interest.

■ ACKNOWLEDGMENTS

We are grateful to the German Science Foundation for support (Grant No. AN 238/14-2).

■ REFERENCES

(1) Brintzinger, H. H.; Fischer, D.; Mülhaupt, R.; Rieger, B.; Waymouth, R. M. *Angew. Chem., Int. Ed.* **1995**, *34*, 1143.
(2) Nakayama, Y.; Yasuda, H. *J. Organomet. Chem.* **2004**, *689*, 4489.
(3) Gromada, J.; Carpentier, J.-F.; Mortreux, A. *Coord. Chem. Rev.* **2004**, *248*, 397.
(4) Shapiro, P. J.; Bunel, E.; Schaefer, W. P.; Bercaw, J. E. *Organometallics* **1990**, *9*, 867.
(5) Stevens, J. C.; Timmers, F. J.; Rosen, G. W.; Knight, G. W.; Lai, S. Y. Eur. Pat. Appl. EP 0 416 815 A2, 1991.
(6) Canich, J. A. Eur. Pat. Appl. EP 0 420 436 A1, 1991.
(7) Okuda, J. *Dalton Trans.* **2003**, 2367.
(8) Kaita, S.; Doi, Y.; Kaneko, K.; Horiuchi, A. C.; Wakatsuki, Y. *Macromolecules* **2004**, *37*, 5860.
(9) Kaita, S.; Hou, Z.; Nishiura, M.; Doi, Y.; Kurazumi, J.; Horiuchi, A. C.; Wakatsuki, Y. *Macromol. Rapid Commun.* **2003**, *24*, 179.
(10) Kaita, S.; Hou, Z.; Wakatsuki, Y. *Macromolecules* **1999**, *32*, 9078.
(11) Kaita, S.; Yamanaka, M.; Horiuchi, A. C.; Wakatsuki, Y. *Macromolecules* **2006**, *39*, 1359.
(12) Zhang, L.; Luo, Y.; Hou, Z. *J. Am. Chem. Soc.* **2005**, *127*, 14562.
(13) Kirillov, E.; Lehmann, C. W.; Razavi, A.; Carpentier, J.-F. *J. Am. Chem. Soc.* **2004**, *126*, 12240.
(14) Rodrigues, A.-S.; Kirillov, E.; Vuillemin, B.; Razavi, A.; Carpentier, J.-F. *Polymer* **2008**, *49*, 2039.
(15) Arndt, S.; Okuda, J. *Chem. Rev.* **2002**, *102*, 1953.
(16) Zimmermann, M.; Anwander, R. *Chem. Rev.* **2010**, *110*, 6194.
(17) Jian, Z.; Tang, S.; Cui, D. *Chem. Eur. J.* **2010**, *16*, 14007.
(18) Jian, Z.; Cui, D.; Hou, Z. *Chem. Eur. J.* **2012**, *18*, 2674.
(19) Panda, T. K.; Hrib, C. G.; Jones, P. G.; Jenter, J.; Roesky, P. W.; Tamm, M. *Eur. J. Inorg. Chem.* **2008**, *2008*, 4270.
(20) Jian, Z.; Tang, S.; Cui, D. *Macromolecules* **2011**, *44*, 7675.
(21) Beetstra, D. J.; Meetsma, A.; Hessen, B.; Teuben, J. H. *Organometallics* **2003**, *22*, 4372.

DOI: 10.1021/om500725g
Organometallics 2015, 34, 32−41

(22) Jian, Z.; Petrov, A. R.; Hangaly, N. K.; Li, S.; Rong, W.; Mou, Z.; Rufanov, K. A.; Harms, K.; Sundermeyer, J.; Cui, D. *Organometallics* **2012**, *31*, 4267.
(23) Otero, A.; Fernández-Baeza, J.; Antiñolo, A.; Lara-Sánchez, A.; Martínez-Caballero, E.; Tejeda, J.; Sánchez-Barba, L. F.; Alonso-Moreno, C.; López-Solera, I. *Organometallics* **2008**, *27*, 976.
(24) Jian, Z.; Cui, D.; Hou, Z.; Li, X. *Chem. Commun.* **2010**, *46*, 3022.
(25) Wang, Y.; Lei, Y.; Chi, S.; Luo, Y. *Dalton Trans.* **2013**, *42*, 1862.
(26) Jian, Z.; Zhao, W.; Liu, X.; Chen, X.; Tang, T.; Cui, D. *Dalton Trans.* **2010**, *39*, 6871.
(27) Royo, B.; Peris, E. *Eur. J. Inorg. Chem.* **2012**, *2012*, 1309.
(28) Pan, Y.; Rong, W.; Jian, Z.; Cui, D. *Macromolecules* **2012**, *45*, 1248.
(29) Wang, B.; Cui, D.; Lv, K. *Macromolecules* **2008**, *41*, 1983.
(30) Wang, B.; Wang, D.; Cui, D.; Gao, W.; Tang, T.; Chen, X.; Jing, X. *Organometallics* **2007**, *26*, 3167.
(31) Wang, B.; Tang, T.; Li, Y.; Cui, D. *Dalton Trans.* **2009**, 8963.
(32) Rufanov, K. A.; Petrov, A. R.; Kotov, V. V.; Laquai, F.; Sundermeyer, J. *Eur. J. Inorg. Chem.* **2005**, *2005*, 3805.
(33) Li, X.; Nishiura, M.; Hu, L.; Mori, K.; Hou, Z. *J. Am. Chem. Soc.* **2009**, *131*, 13870.
(34) Taube, R.; Maiwald, S.; Sieler, J. *J. Organomet. Chem.* **2001**, *621*, 327.
(35) Enders, M.; Rudolph, R.; Pritzkow, H. *Chem. Ber.* **1996**, *129*, 459.
(36) Jutzi, P.; Dahlhaus, J.; Bangel, M. *J. Organomet. Chem.* **1993**, *460*, C13.
(37) Zimmermann, M.; Volbeda, J.; Törnroos, K. W.; Anwander, R. *C. R. Chim.* **2010**, *13*, 651.
(38) Zimmermann, M.; Törnroos, K. W.; Sitzmann, H.; Anwander, R. *Chem. Eur. J.* **2008**, *14*, 7266.
(39) Zimmermann, M.; Törnroos, K. W.; Anwander, R. *Angew. Chem., Int. Ed.* **2008**, *47*, 775.
(40) Zimmermann, M.; Frøystein, N. Å.; Fischbach, A.; Sirsch, P.; Dietrich, H. M.; Törnroos, K. W.; Herdtweck, E.; Anwander, R. *Chem. Eur. J.* **2007**, *13*, 8784.
(41) Litlabø, R.; Enders, M.; Törnroos, K. W.; Anwander, R. *Organometallics* **2010**, *29*, 2588.
(42) Evans, W. J.; Kozimor, S. A.; Brady, J. C.; Davis, B. L.; Nyce, G. W.; Seibel, C. A.; Ziller, J. W.; Doedens, R. J. *Organometallics* **2005**, *24*, 2269.
(43) Yu, N.; Nishiura, M.; Li, X.; Xi, Z.; Hou, Z. *Chem. Asian J.* **2008**, *3*, 1406.
(44) Maiwald, S.; Taube, R.; Hemling, H.; Schumann, H. *J. Organomet. Chem.* **1998**, *552*, 195.
(45) Fischbach, A.; Anwander, R. *Adv. Polym. Sci.* **2006**, *204*, 155.
(46) Friebe, L.; Nuyken, O.; Obrecht, W. *Adv. Polym. Sci.* **2006**, *204*, 1.
(47) Fischbach, A.; Klimpel, M. G.; Widenmeyer, M.; Herdtweck, E.; Scherer, W.; Anwander, R. *Angew. Chem., Int. Ed.* **2004**, *43*, 2234.
(48) Meermann, C.; Törnroos, K. W.; Nerdal, W.; Anwander, R. *Angew. Chem., Int. Ed.* **2007**, *46*, 6508.
(49) Fischbach, A.; Perdih, F.; Herdtweck, E.; Anwander, R. *Organometallics* **2006**, *25*, 1626.
(50) Fischbach, A.; Meermann, C.; Eickerling, G.; Scherer, W.; Anwander, R. *Macromolecules* **2006**, *39*, 6811.
(51) Sieler, J.; Simon, A.; Peters, K.; Taube, R.; Geitner, M. *J. Organomet. Chem.* **1989**, *362*, 297.
(52) Anwander, R. *Angew. Chem., Int. Ed.* **1998**, *37*, 599.
(53) Barnea, E.; Averbuj, C.; Kapon, M.; Botoshansky, M.; Eisen, M. S. *Eur. J. Inorg. Chem.* **2007**, *2007*, 4535.
(54) Bonnet, F.; Visseaux, M.; Barbier-Baudry, D.; Hafid, A.; Vigier, E.; Kubicki, M. M. *Inorg. Chem.* **2004**, *43*, 3682.
(55) Evans, W. J.; Champagnea, T. M.; Davisa, B. L.; Allena, N. T.; Nycea, G. W.; Johnstona, M. A.; Lina, Y.-C.; Khvostova, A.; Zillera, J. W. *J. Coord. Chem.* **2006**, *59*, 1069.
(56) Paolucci, G.; Vignola, M.; Zanella, A.; Bertolasi, V.; Polo, E.; Sostero, S. *Eur. J. Inorg. Chem.* **2006**, *2006*, 4104.
(57) Jende, L. N.; Maichle-Mössmer, C.; Anwander, R. *Chem. Eur. J.* **2013**, *19*, 16321.
(58) Zhang, L.; Nishiura, M.; Yuki, M.; Luo, Y.; Hou, Z. *Angew. Chem., Int. Ed.* **2008**, *47*, 2642.
(59) Wang, L.; Liu, D.; Cui, D. *Organometallics* **2012**, *31*, 6014.
(60) Du, G.; Wei, Y.; Ai, L.; Chen, Y.; Xu, Q.; Liu, X.; Zhang, S.; Hou, Z.; Li, X. *Organometallics* **2011**, *30*, 160.
(61) Ajellal, N.; Furlan, L.; Thomas, C. M.; Casagrande, O. L.; Carpentier, J.-F. *Macromol. Rapid Commun.* **2006**, *27*, 338.
(62) Inoue, S. *J. Macromol. Sci., Part A: Chem.* **1988**, *25*, 571.
(63) Inoue, S. *J. Polym. Sci., Part A: Polym. Chem.* **2000**, *38*, 2861.
(64) Tanaka, Y.; Sato, H.; Ogura, A.; Nagoya, I. *J. Polym. Sci., Part A: Polym. Chem. Ed.* **1976**, *14*, 73.
(65) Yao, C.; Liu, D.; Li, P.; Wu, C.; Li, S.; Liu, B.; Cui, D. *Organometallics* **2014**, *33*, 684.
(66) Makhiyanov, N. *Polym. Sci. Ser. A* **2014**, *56*, 241.
(67) Makhiyanov, N.; Akhmetov, I. G.; Vagizov, A. M. *Polym. Sci. Ser. A* **2012**, *54*, 942.
(68) Qiu, Z. W.; Chen, X.; Sun, B.; Zhou, Z.; Wang, F. *J. Macromol. Sci. Part A: Chem.* **1988**, *25*, 127.
(69) Xie, D.; Sun, Q. *Chin. J. Polym. Sci.* **1987**, *5*, 114.
(70) Jende, L. N.; Maichle-Mössmer, C.; Schädle, C.; Anwander, R. *J. Organomet. Chem.* **2013**, *744*, 74.
(71) Lichtenberg, C.; Robert, D.; Spaniol, T. P.; Okuda, J. *Organometallics* **2010**, *29*, 5714.
(72) Abrams, M. B.; Yoder, J. C.; Loeber, C.; Day, M. W.; Bercaw, J. E. *Organometallics* **1999**, *18*, 1389.
(73) Evans, W. J.; Anwander, R.; Ziller, J. W. *Organometallics* **1995**, *14*, 1107.
(74) *X-Area*, V. 155; Stoe & Cie GmbH: Darmstadt, Germany, 2009.
(75) Spek, A. *Acta Crystallogr., Sect. D* **2009**, *65*, 148.
(76) Sheldrick, G. M. *SHELXS-97 Program for crystal structure solution*; University of Göttingen, Göttingen, Germany, 1997.
(77) Scheldrick, G. M. *SHELXL-97 Program for crystal structure refinement*; University of Göttingen, Göttingen, Germany, 1997.
(78) Farrugia, L. J. *J. Appl. Crystallogr.* **1997**, *30*, 565.

DOI: 10.1021/om500725g
Organometallics 2015, 34, 32−41

Supporting Information

Rare-Earth Metal Bis(allyl) Complexes Supported by the [2-(*N*,*N*-Dimethylamino)ethyl]tetramethylcyclopentadienyl Ligand: Structural Characterization, Reactivity, and Isoprene Polymerization

Lars N. Jende, Christoph O. Hollfelder, Cäcilia Maichle-Mössmer, and Reiner Anwander*

Figure S1. ^{1}H NMR spectrum (C_6D_6, 25 °C) of complex **1a**

Figure S2. ^{13}C NMR spectrum (C_6D_6, 25 °C) of complex **1a**

Figure S3. 2D ^{1}H-^{13}C HSQC NMR spectrum (C_6D_6, 25 °C) of complex **1a**

Figure S4. ^{1}H NMR spectrum (C_6D_6, 25 °C) of complex **1c**

Figure S5. ^{13}C NMR spectrum (C_6D_6, 25 °C) of complex **1c**

Figure S6. 2D ^{1}H-^{13}C HSQC NMR spectrum (C_6D_6, 25 °C) of complex **1c**

Figure S7. ^{1}H NMR spectrum (C_6D_6, 25 °C) of complex **4**

Figure S8. ^{13}C NMR spectrum (C_6D_6, 25 °C) of complex **4**

Figure S9. ^{1}H NMR reaction spectra of [$Cp^{NMe2}Y(C_3H_5)_2$] (**1a**) with $AlMe_3$

Figure S10. Molecular structure of [$Cp^{NMe2}Ho(C_3H_5)_2$] (**1b**)

Figure S11. Molecular structure of [$Cp^{NMe2}Lu(C_3H_5)_2$] (**1c**)

Figure S12. Molecular structure of [{($Cp^{NMe2AlEt3}$)$_2$(Cp^{NMe2})Y_3Cl_5}(μ-Cl)]$_2$ (**3a**)

Figure S13. Molecular structure of [{($Cp^{NMe2AlEt3}$)$_2$(Cp^{NMe2})Ho_3Cl_5}(μ-Cl)]$_2$ (**3b**)

Table S1. Crystallographic data for complexes **1**, **2**, and **3**

Table S2. ^{1}H and ^{13}C NMR data of polyisoprene obtained from **2**/**B**/$AlMe_3$

Figure S14. ^{13}C NMR spectra of polyisoprenes obtained with pre-catalyst **1a**

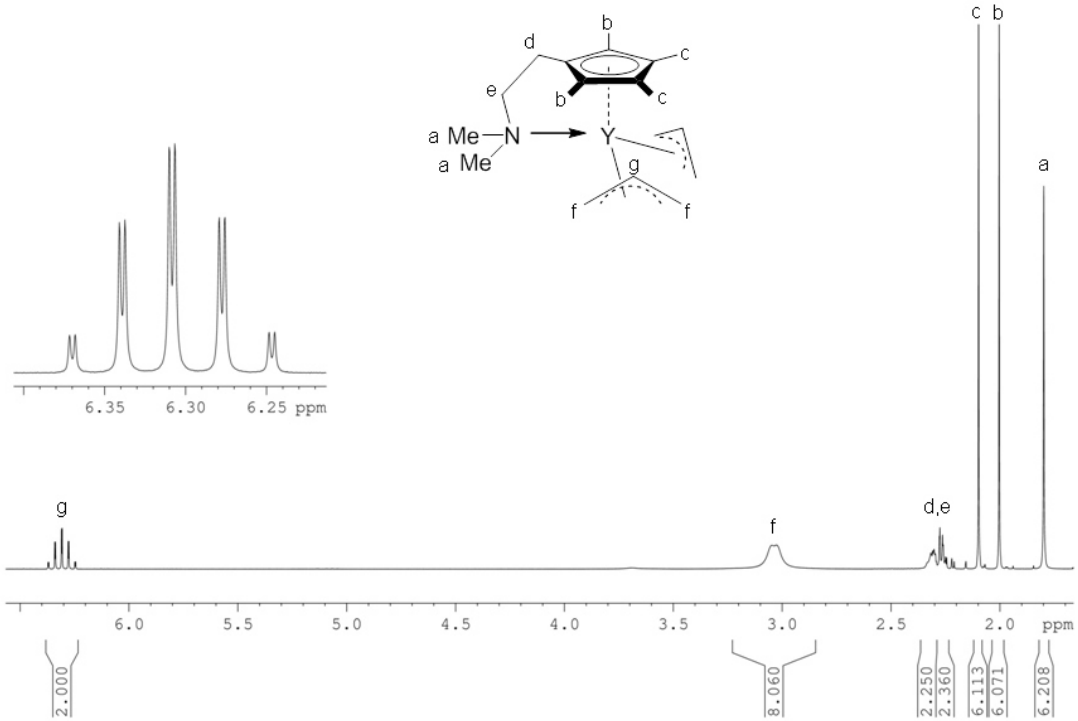

Figure S1. ^{1}H NMR spectrum (C_6D_6, 25 °C) of complex **1a**.

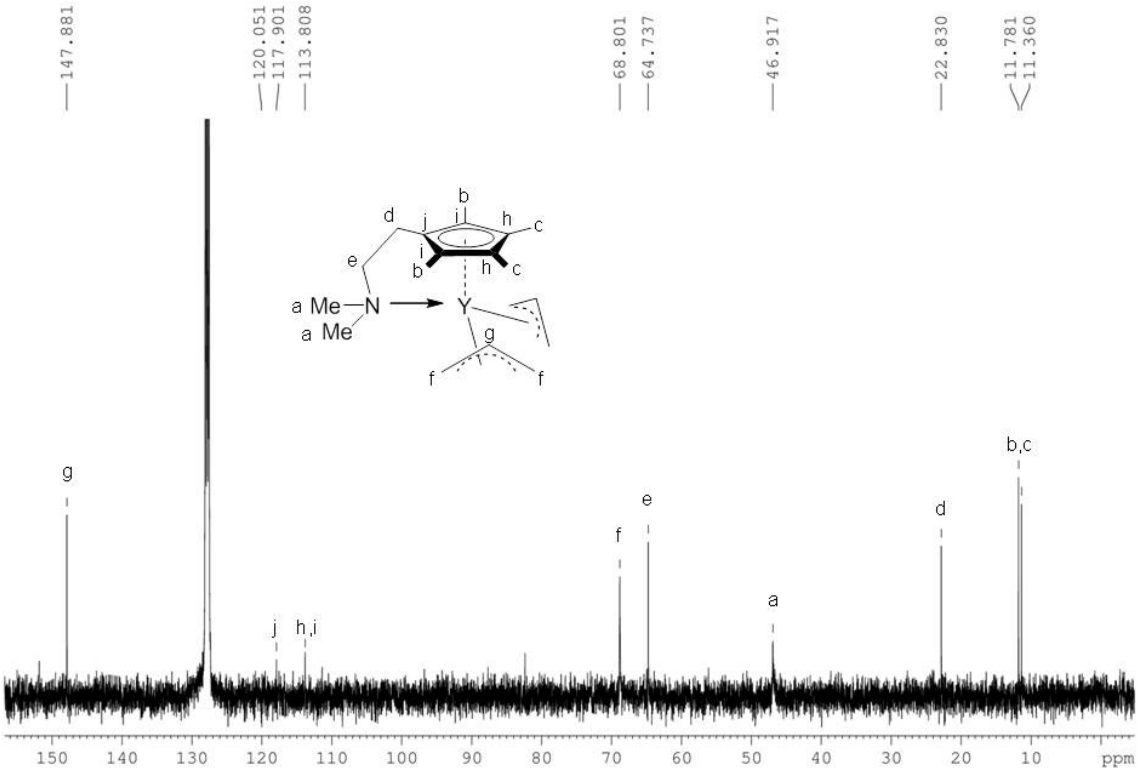

Figure S2. ^{13}C NMR spectrum (C_6D_6, 25 °C) of complex **1a**.

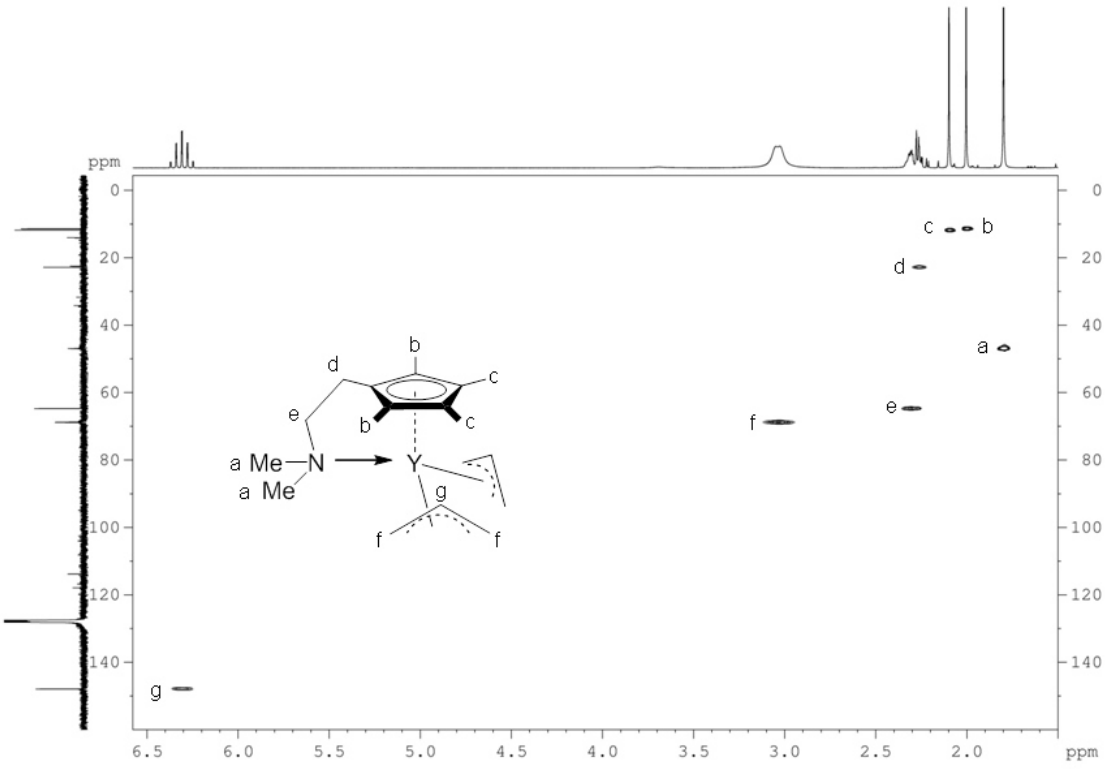

Figure S3. 2D ^{1}H-^{13}C HSQC NMR spectrum (C_6D_6, 25 °C) of complex **1a**.

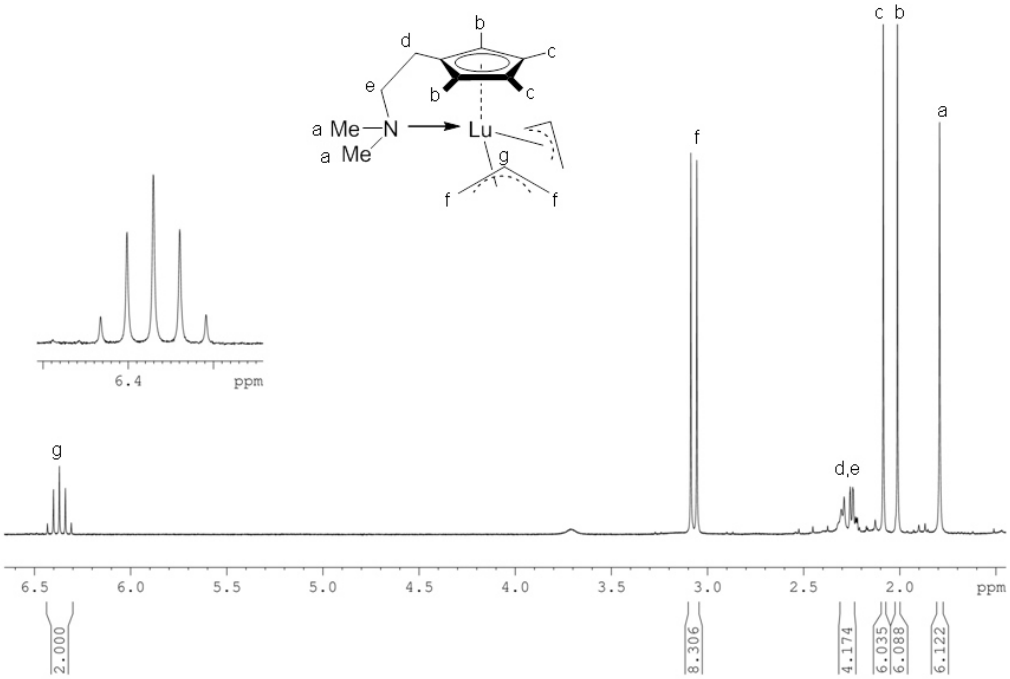

Figure S4. ^{1}H NMR spectrum (C_6D_6, 25 °C) of complex **1c**.

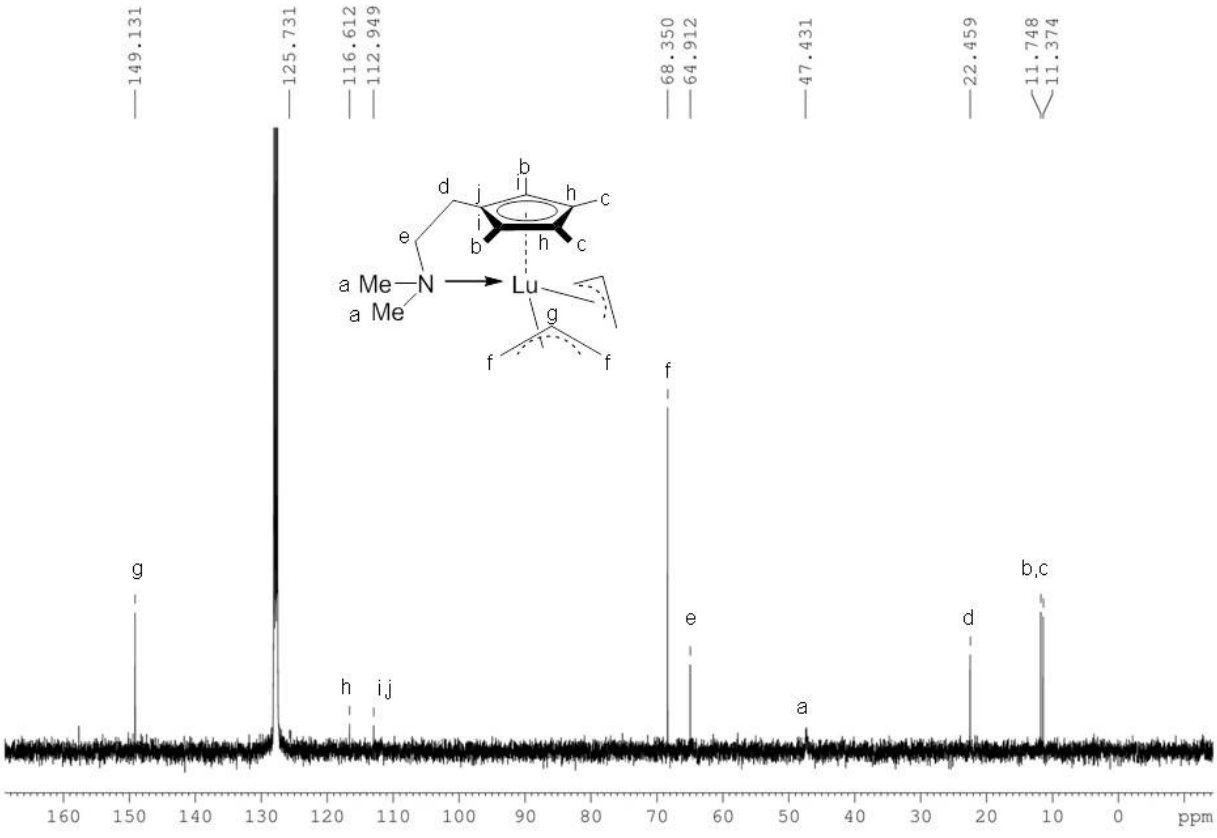

Figure S5. ^{13}C NMR spectrum (C_6D_6, 25 °C) of complex **1c**.

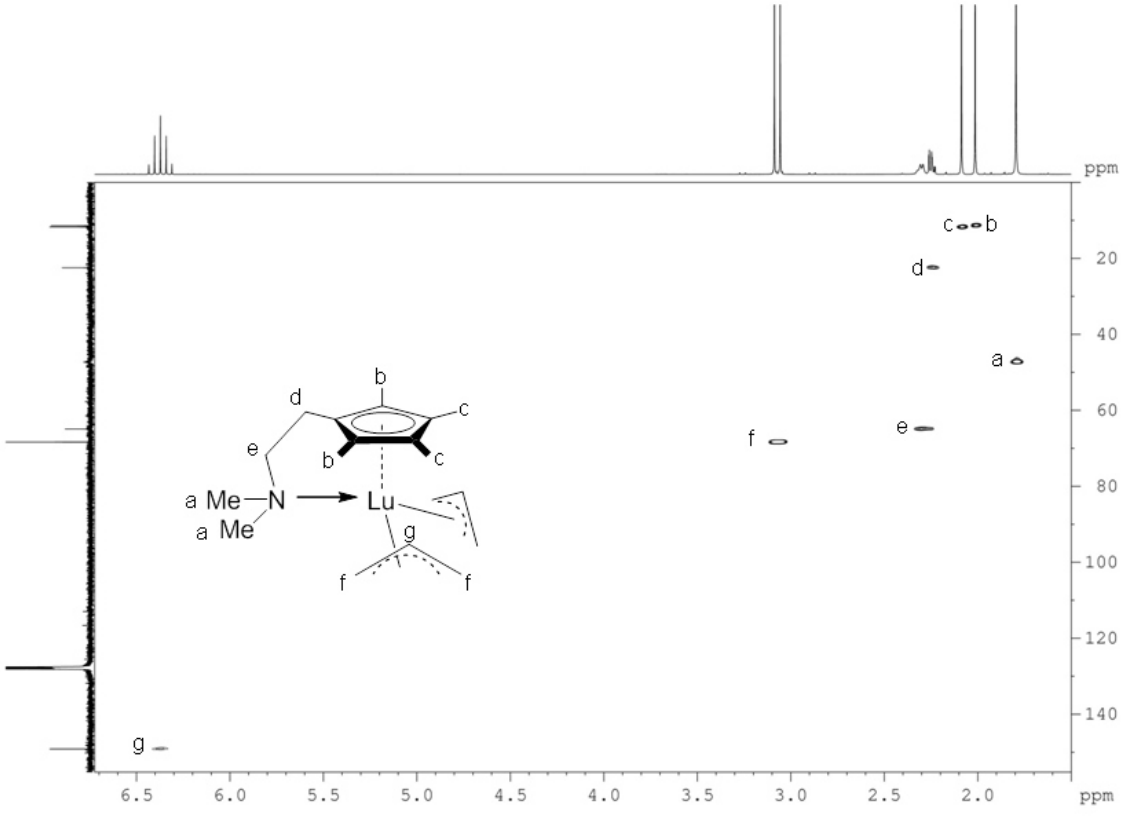

Figure S6. 2D ^{1}H-^{13}C HSQC NMR spectrum (C_6D_6, 25 °C) of complex **1c**.

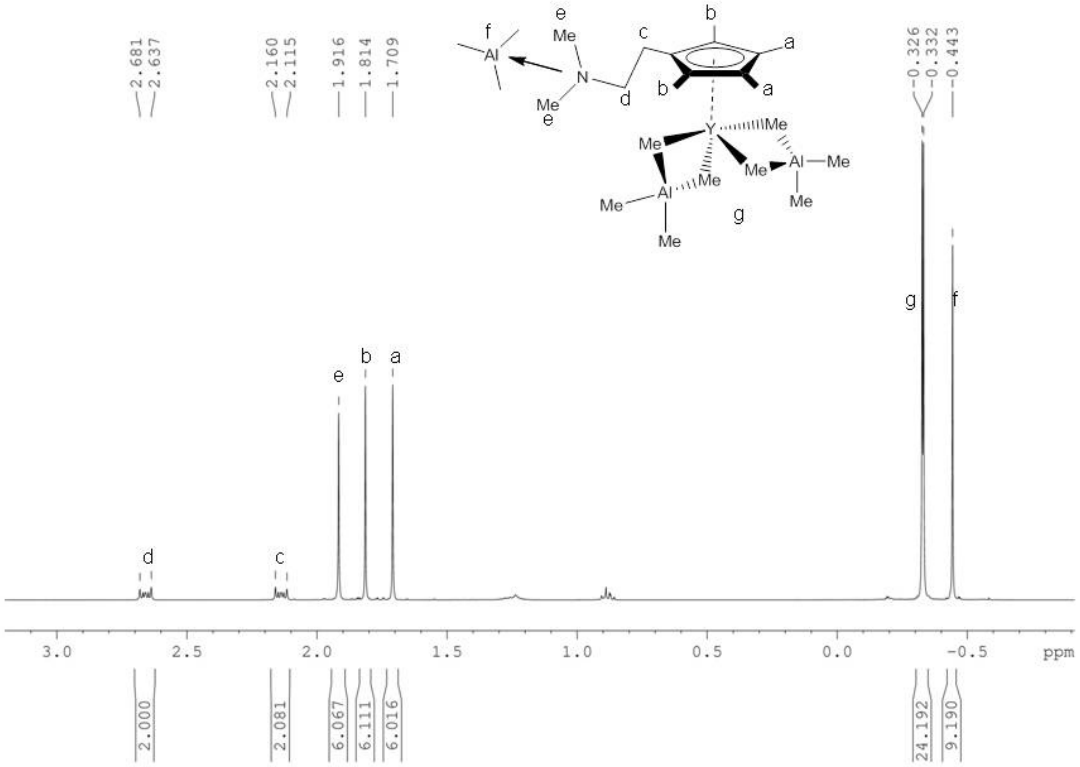

Figure S7. ^{1}H NMR spectrum (C_6D_6, 25 °C) of complex **4**.

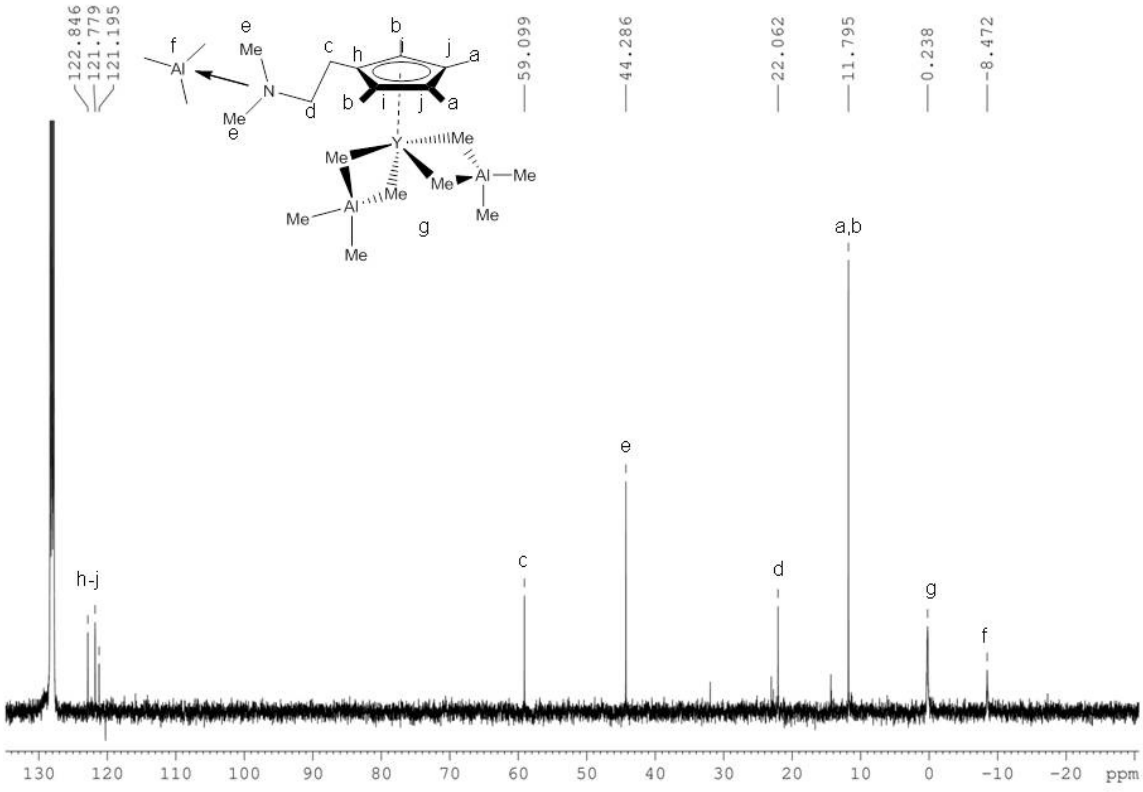

Figure S8. ^{13}C NMR spectrum (C_6D_6, 25 °C) of complex **4**.

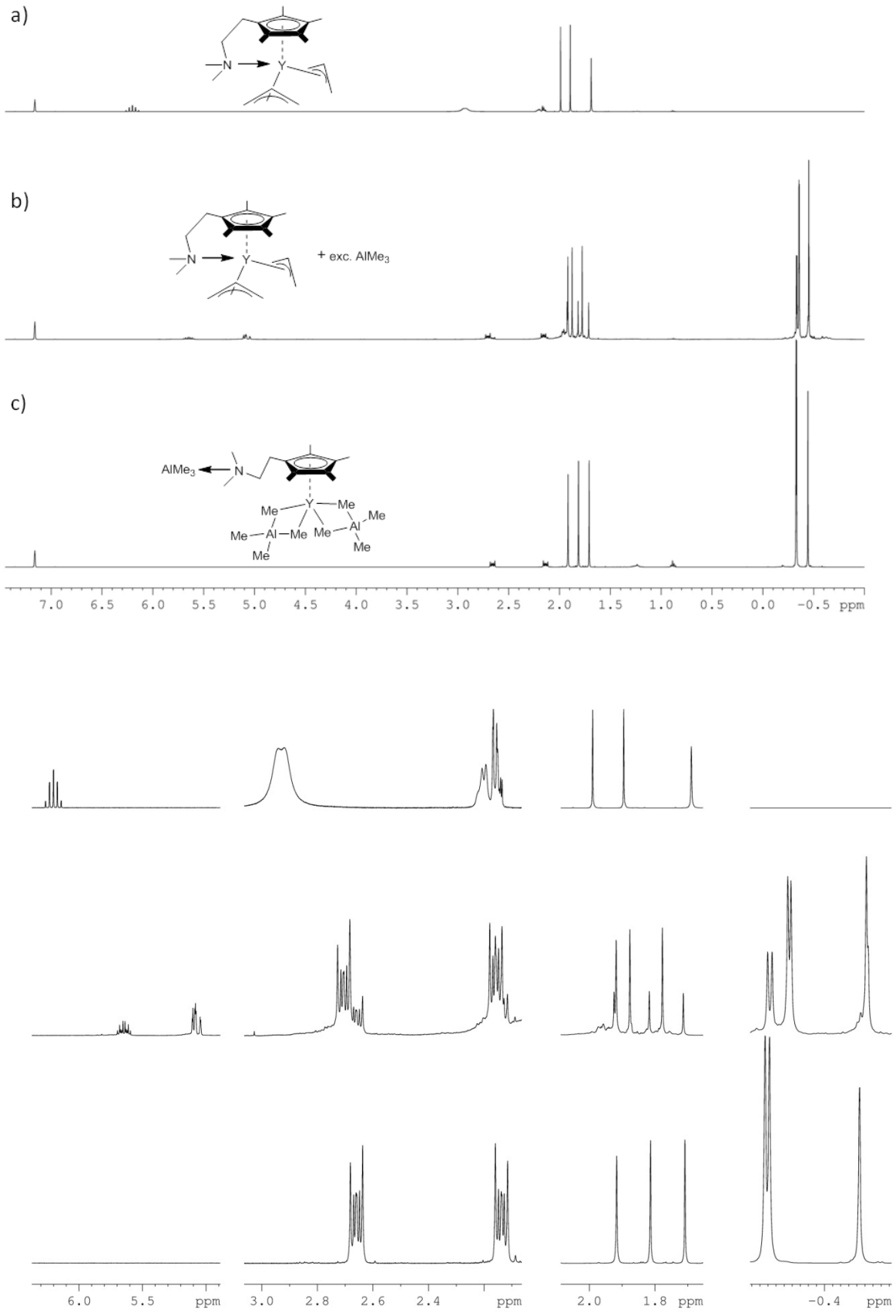

Figure S9. Top) ^{1}H NMR spectra (400 MHz, 25 °C, C_6D_6) of a) pure [$Cp^{NMe2}Y(\eta^3\text{-}C_3H_5)_2$] (**1a**); b) reaction product of [$Cp^{NMe2}Y(\eta^3\text{-}C_3H_5)_2$] with 10 eq. $AlMe_3$ after evaporation of volatiles; c) [$Cp^{NMe2AlMe3}Y(AlMe_4)_2$] (**4**). Bottom) selected regions.

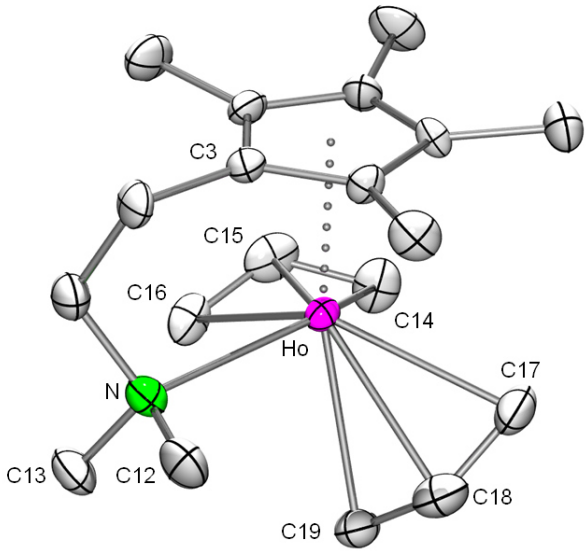

Figure S10. Molecular structure of $[Cp^{NMe2}Ho(C_3H_5)_2]$ (**1b**); atomic displacement parameters set at the 50% level; hydrogen atoms omitted for clarity.

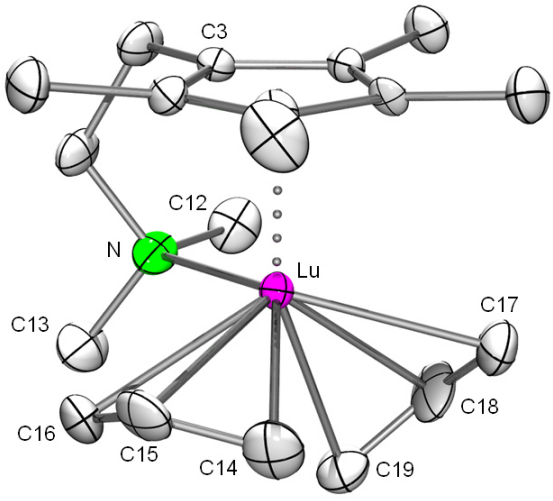

Figure S11. Molecular structure of $[Cp^{NMe2}Lu(C_3H_5)_2]$ (**1c**); atomic displacement parameters set at the 50% level; hydrogen atoms omitted for clarity.

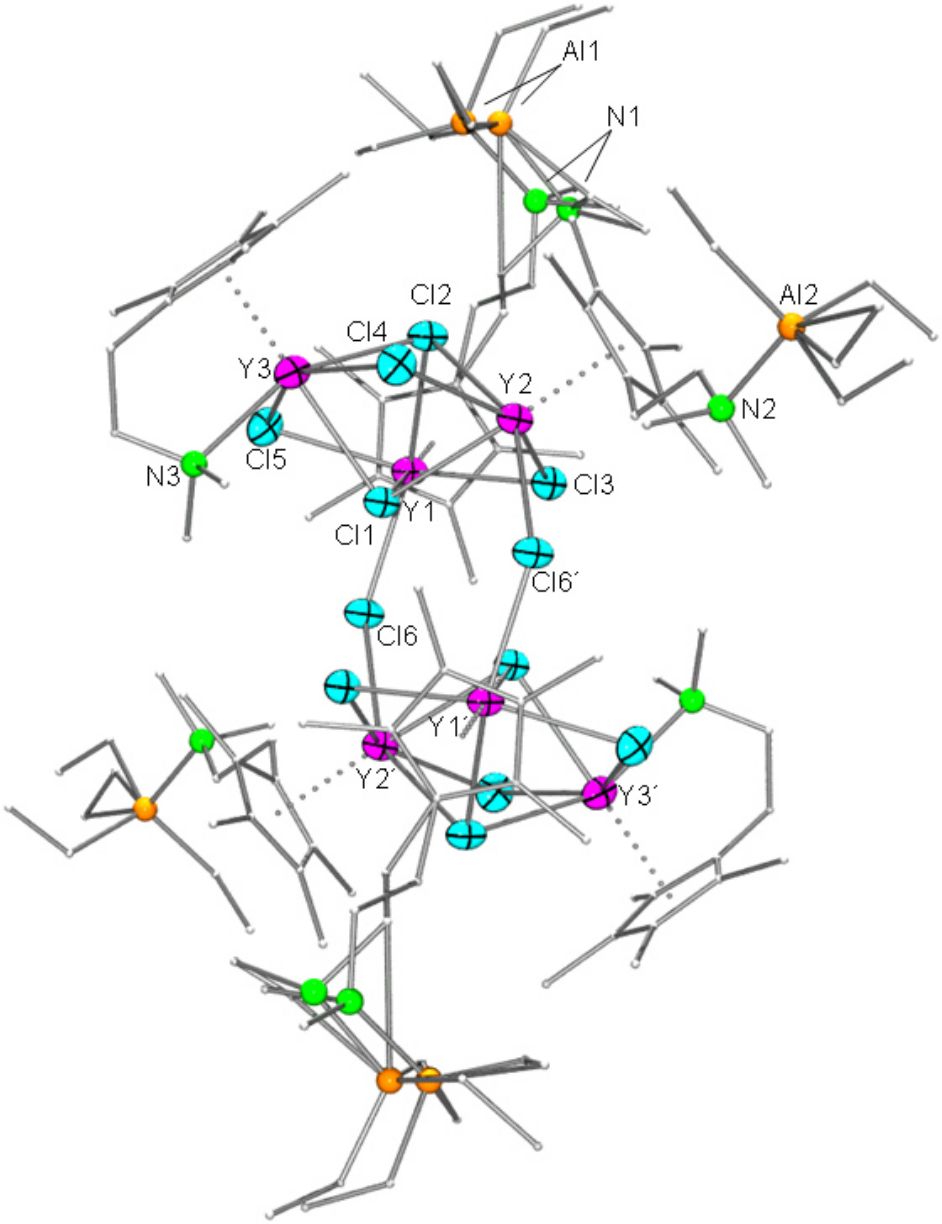

Figure S12. Molecular structure of $[\{(Cp^{NMe2AlEt3})_2(Cp^{NMe2})Y_3Cl_5\}(\mu\text{-}Cl)]_2$ (**3a**); atomic displacement parameters set at the 50% level; aluminum, carbon, and nitrogen atoms are shown as ball-stick representation; hydrogen atoms have for clarity. Disorders of the cyclopentadienyl sidearm and of the ethyl groups at the aluminum centers are shown.

Cell parameters (*P*-1): a = 13.9232, b = 17.0282, c = 18.0040 [Å]; α = 65.191, β = 67.445, γ = 89.805 [°].

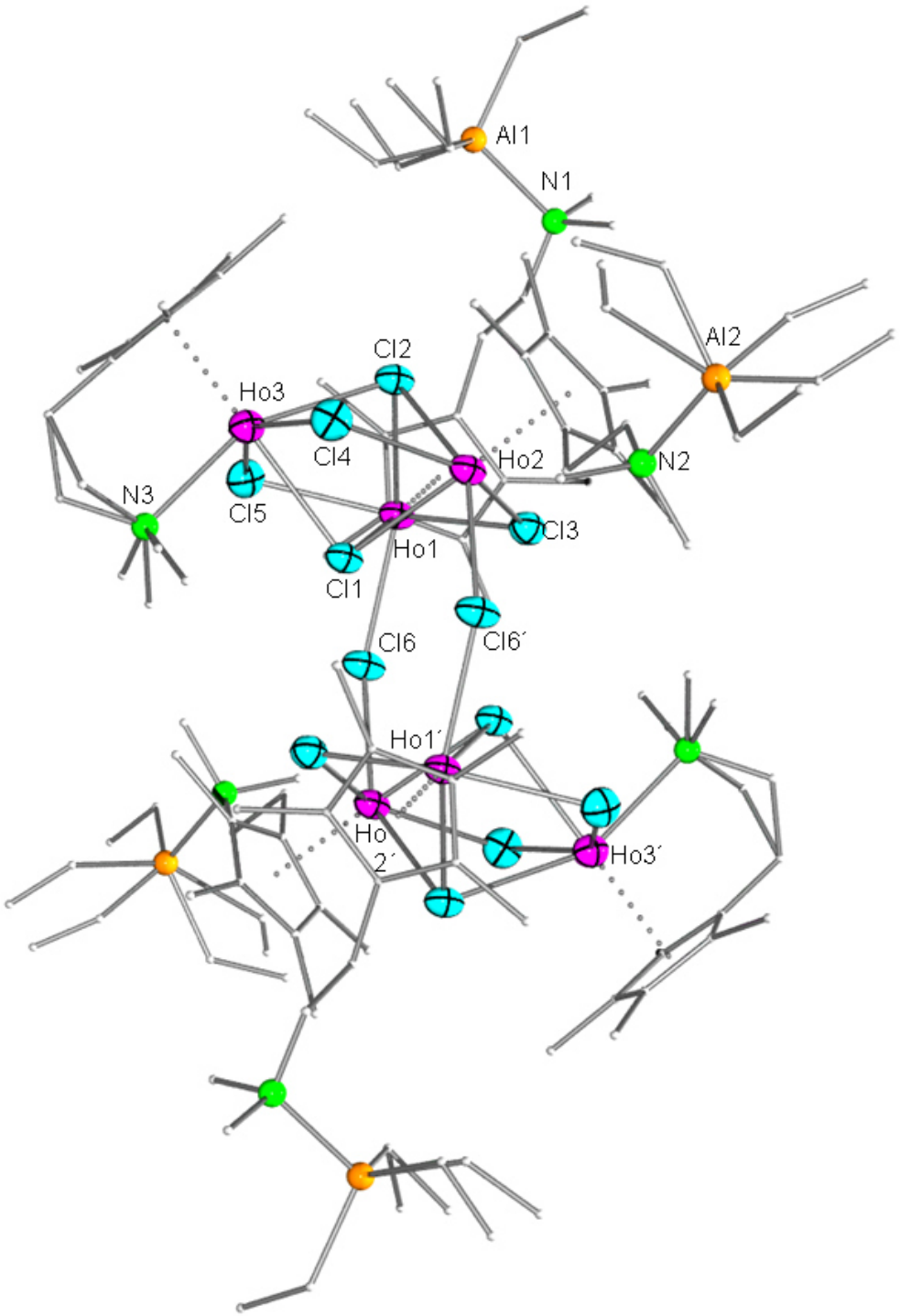

Figure S13. Molecular structure of $[\{(Cp^{NMe2AlEt3})_2(Cp^{NMe2})Ho_3Cl_5\}(\mu\text{-}Cl)\}]_2$ (**3b**); atomic displacement parameters set at the 50% level; aluminum, carbon, and nitrogen atoms are shown as ball-stick representation; hydrogen atoms omitted for clarity. Disorders of the cyclopentadienyl sidearm at N3 and of the ethyl groups at the aluminum centers are shown.

Table S1. Crystallographic data for complexes **1**, **2**, and **3**

	1a (Ln = Y)	**1b** (Ln = Ho)	**1c** (Ln = Lu)	**2** (Ln = Nd)	**3b** (Ln = Ho)·$(C_6H_6)_4$
Formular	$C_{19}H_{32}NY$	$C_{19}H_{32}NHo$	$C_{19}H_{32}NLu$	$C_{39}H_{62}Cl_2N_2Nd_2$	$C_{126}H_{216}Al_4Cl_{12}Ho_6N_6$
Fw	363.37	439.39	449.43	918.29	3337.94
temp (K)	173(2)	173(2)	173(2)	173(2)	173(2)
cryst syst	monoclinic	monoclinic	monoclinic	triclinic	triclinic
space group	$P2_1$	$P2_1$	$P2_1$	P-1	P-1
a (Å)	8.4644(4)	8.4569(8)	8.4482(9)	8.7736(9)	14.0630(11)
b (Å)	13.9975(5)	13.9798(13)	13.9076(10)	10.4931(15)	17.0674(12)
c (Å)	8.5546(4)	8.5604(8)	8.5517(9)	12.2435(15)	17.9374(14)
α (deg)	90.00	90.00	90.00	67.958(11)	66.845(6)
β (deg)	114.260(3)	114.331(7)	114.482(8)	81.853(9)	68.304(6)
γ (deg)	90.00	90.00	90.00	74.973(10)	88.529(6)
vol ($Å^3$)	924.05(7)	922.17(15)	914.44(15)	1007.8(2)	3641.8(5)
Z	2	2	2	1	1
ρ_{calcd} (mg/mm^3)	1.306	1.582	1.632	1.513	1.522
μ (mm^{-1})	3.151	4.285	5.393	2.707	3.508
R_1(all) [a]	0.0416	0.0304	0.0198	0.0430	0.0498
wR_2(all) [b]	0.0928	0.0677	0.0399	0.0919	0.1027
GOF (on F^2) [c]	1.154	1.052	1.051	1.223	1.100

[a] $R1 = \Sigma(||F_0|-|F_c||)/\Sigma|F_0|$; [b] $wR2 = \{\Sigma[w(F_0^2-F_c^2)^2/\Sigma[w(F_0^2)^2]\}^{1/2}$; [c] GOF = $\{\Sigma[w(F_0^2-F_c^2)^2]/(n-p)\}^{1/2}$.

Table S2. NMR data of *trans*-1,4- (**T**) and 3,4- (**V**) units of polyisoprene obtained from **2**/**B**/$AlMe_3$.

Position	^{13}C	^{1}H	Position	^{13}C	^{1}H
T_5	16.0	1.61	T_5^I	16.2	n.d.
T_4	26.7	2.08	T_4^I	32.1	2.04
T_1	39.7	2.00	T_1^I	37.4	1.89
T_3	124.2	5.13	T_3^I	123.0	5.09
T_2	134.9	–	T_2^I	135.3	–
V_5	18.6	1.63	T_5^{II}	n.d.	n.d.
V_4	31.3	1.43	T_4^{II}	n.d.	n.d.
V_3	47.2	2.03	T_1^{II}	39.8	n.d.
V_1	111.2	4.71	T_3^{II}	124.0	n.d.
V_2	147.6	–	T_2^{II}	135.1	–

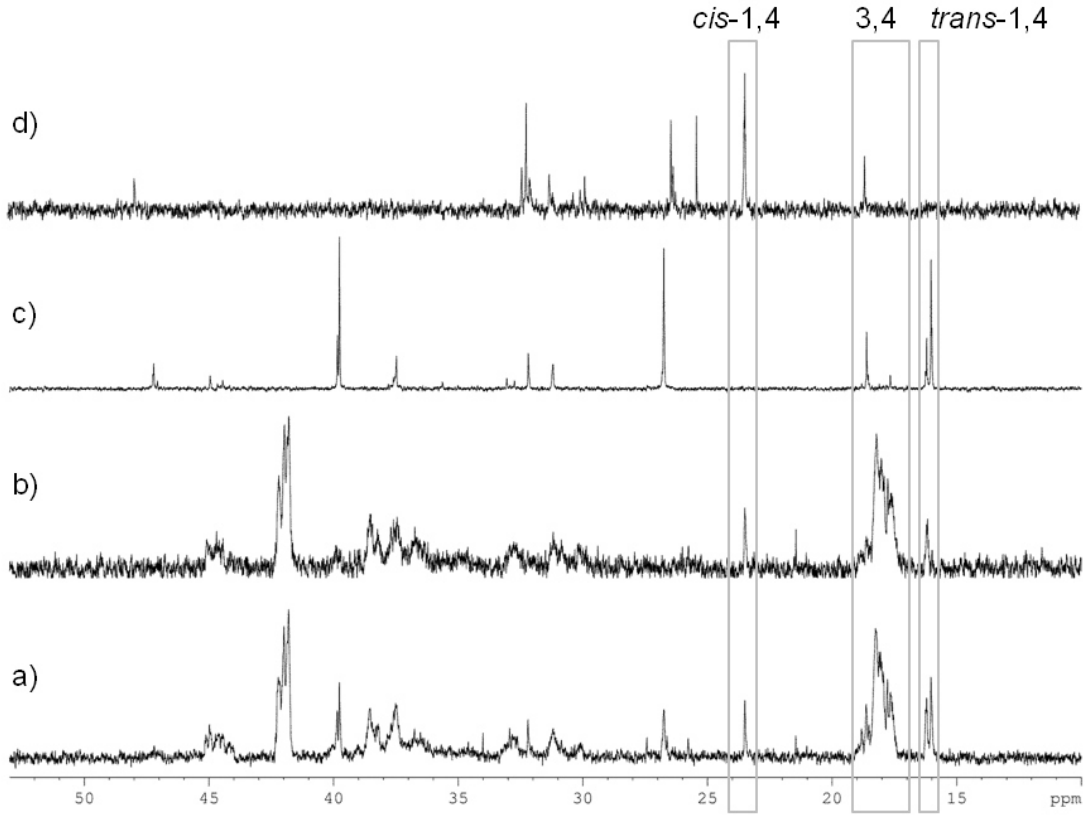

Figure S14. ^{13}C NMR ($CDCl_3$, 25 °C) spectra of polyisoprenes obtained from pre-catalyst **1a** activated with co-catalyst **A** (a), **B** (b), **B** with 10 equiv $AlMe_3$ (c) and **B** with 10 equiv Al*i*Bu_3 (d).

Paper IV

ORGANOMETALLICS

Article

pubs.acs.org/Organometallics

C–H Bond Activation and Isoprene Polymerization by Rare-Earth-Metal Tetramethylaluminate Complexes Bearing Formamidinato N-Ancillary Ligands

Shima Hamidi,[†] Lars N. Jende,[‡] H. Martin Dietrich,[‡] Cäcilia Maichle-Mössmer,[‡] Karl W. Törnroos,[§] Glen B. Deacon,*[,†] Peter C. Junk,*[,∥] and Reiner Anwander*[,‡]

[†]School of Chemistry, Monash University, 3800 Clayton, Victoria, Australia

[‡]Institut für Anorganische Chemie, Universität Tübingen, Auf der Morgenstelle 18, D-72076 Tübingen, Germany

[§]Department of Chemistry, University of Bergen, Allégaten 41, N-5007 Bergen, Norway

[∥]School of Pharmacy & Molecular Sciences, James Cook University, Townsville, Queensland 4811, Australia

Supporting Information

ABSTRACT: The bimetallic formamidinate complexes Ln(Form)$(AlMe_4)_2$ (Ln = Y, Form (ArNCHNAr) = EtForm (Ar = 2,6-$Et_2C_6H_3$), MesForm (Ar = 2,4,6-$Me_3C_6H_2$), DippForm (Ar = 2,6-$iPr_2C_6H_3$), *t*BuForm (Ar = 2-*t*BuC_6H_4); Ln = La, Form = DippForm, *t*BuForm) were obtained in high yield by protonolysis reactions between formamidines (FormH) and homoleptic rare-earth-metal tetramethylaluminates $Ln(AlMe_4)_3$. Y(Form)$(AlMe_4)_2$ (Form = EtForm, DippForm) were also prepared by treatment of Y(Form)$[N(SiHMe_2)_2]_2$(thf) with trimethylaluminum after the former were prepared by the protonolysis of $Y[N(SiHMe_2)_2]_3(thf)_2$ complexes with EtFormH or DippFormH. The monomeric six-coordinate complexes Ln(Form)$(AlMe_4)_2$ (Ln = Y, Form = EtForm, MesForm, DippForm, *t*BuForm; Ln = La, Form = DippForm, *t*BuForm) show similar molecular structures with distorted-octahedral geometry and bidentate (N,N′) Form and $AlMe_4$ ligands. The complex [La(EtFormAlMe_3)$(AlMe_4)_2$]$(C_7H_8)_{1.5}$ from a protonolysis reaction between $La(AlMe_4)_3$ and EtFormH has the EtForm ligand adopting a configuration in which one nitrogen and one aryl substituent are coordinated to the eight-coordinate lanthanum center in an η^1(N):η^6(arene) manner. From the reaction of $La(AlMe_4)_3$ with MesFormH, C–H bond activation of an *o*-methyl group of the mesityl moiety occurred, yielding [La{η^1(N):η^6(Ar)-Me_2CH_2FormAlMe_3}$(AlMe_3)(AlMe_4)$][La(Me_2CH_2FormAlMe_3)$(AlMe_3)$-$(AlMe_4)$]$(C_6H_{14})_{1.5}$ (Me_2CH_2Form = MesForm-H(*o*-Me)), in which two linkage isomers of Me_2CH_2Form were observed. Investigations were carried out on the compounds [Ln(Form)$(AlMe_4)_2$] (Ln = Y, La; Form = EtForm, DippForm) as precatalysts activated by $[Ph_3C][B(C_6F_5)_4]$ or $[PhNMe_2H][B(C_6F_5)_4]$ in isoprene polymerization. While the lanthanum complexes showed narrower molecular weight distributions (PDI < 1.2), a stereodirecting role was evidenced for the cocatalysts (trityl borate, maximum 87% trans-1,4-selectivity; anilinium borate, maximum 82% cis-1,4-selectivity).

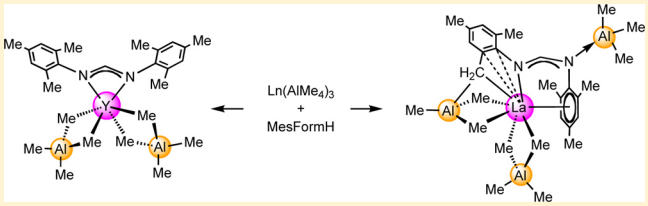

INTRODUCTION

Among the approaches to replace the cyclopentadienyl family of ligands in rare-earth-metal chemistry, N-coordinating ancillary ligands have attracted considerable attention during the past few years.[1−7] For instance, bidentate amidinato and guanidinato ligands can be exploited in so-called post-metallocene (or non-cyclopentadienyl) complexes.[8−23] Significantly, a number of complexes containing N-coordinating ligands, e.g. guanidinato,[3] benzamidinato,[12,15,24] aminopyridinato,[25] diamido pyridine and iminoamido pyridine,[26] nacnac,[27] and others,[28−34] activated by cocatalysts such as organoaluminum or organoboron compounds, show promising catalytic activity in the polymerization of 1,3-dienes and α-olefins, relatively similar to cyclopentadienyl complexes.

The formamidine proligands *N*,*N*′-bis(aryl)formamidines, ArN═CH-NHAr (Ar = aryl), can be prepared in high yields from addition of triethyl orthoformate to a substituted aniline. Variation of the substituents on the aryl rings can modulate the steric and electronic effects of the ligands as well as their solubilities.[8,35−37] A range of sterically different tris(formamidinato) rare-earth-metal(III) complexes has been reported previously, mostly synthesized by the redox transmetalation/protonolysis (RTP) route.[8,9,13] However, the bulkiest ligand caused C–F bond activation to give [Ln(Form)$_2$F(thf)] complexes, derived from tetrafluorobenzyne elimination from a putative [Ln(Form)$_2C_6F_5$(thf)] intermediate.[8,9]

The steric tunability of formamidinato ligands would make mixed rare-earth-metal/aluminum formamidinate complexes structurally interesting, as N-donors have a strong affinity for both metals,[38−40] and such bimetallics could serve as precatalysts in

Special Issue: Recent Advances in Organo-f-Element Chemistry

Received: October 26, 2012
Published: January 9, 2013

   dx.doi.org/10.1021/om301010m | *Organometallics* 2013, 32, 1209−1223

olefin polymerization. We now report syntheses, structures, and catalysis in isoprene polymerization of a series of formamidinato rare-earth-metal tetramethylaluminate complexes. In one instance, C−H bond activation was observed. The homoleptic $Ln(AlMe_4)_3$ (Ln = La, Nd, Y, Lu) complexes are convenient precursors for generating a variety of heterobimetallic Ln/Al complexes, currently used to build a LLn^{III}bis(tetramethylaluminate)-based post-metallocene library (L = ancillary ligand).[41] The latter *aluminate route* also features dianionic[38,42] and monoanionic N-ancillary ligands such as tris(pyrazolyl)borato (Tp)[NNN]$^-$,[43] benzamidinato [RNC(Ph)NR]$^-$ (Chart 1, **I**),[24,44] triazenido [RNNNR]$^-$ (Chart 1, **II**),[45]

Chart 1. Structurally Characterized Rare-Earth-Metal Bis(tetramethylaluminate) Complexes with N-Ancillary Ligands

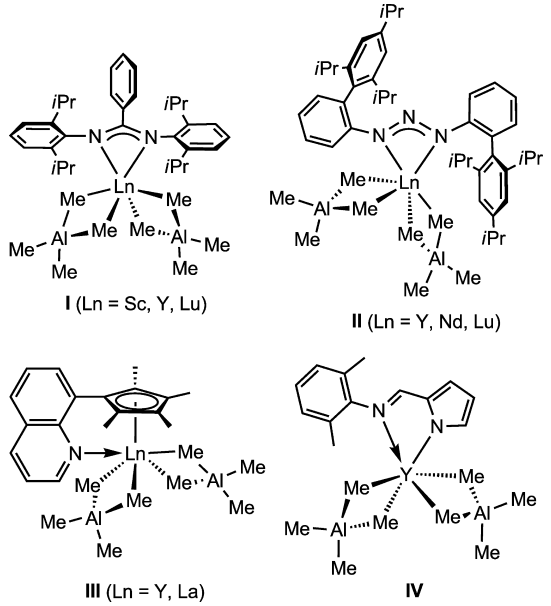

quinolyl-substituted cyclopentadienyl (Cp^Q) (Chart 1, **III**),[46] and iminopyrrolyl (Chart 1, **IV**).[47]

Rare-earth-metal silylamide complexes also provide suitable reagents for the stepwise synthesis of Ln/Al complexes,[48,49] since a number of complexes with mixed silylamido/N-coordinating ligands have been reported.[14,23,28,40,50] Both of these routes have been employed in the present study.

RESULTS AND DISCUSSION

Synthesis and Characterization of Formamidinato Rare-Earth-Metal(III) Tetramethylaluminate Complexes. From the rare-earth metals, La and Y were chosen as representative of larger and smaller sizes, respectively, as their Ln^{3+} ions are diamagnetic, facilitating NMR characterization. First, protonolysis of tris{bis(dimethylsilyl)amido}bis(tetrahydrofuran)-yttrium[49] with *N*,*N*′-bis(2,6-diethylphenyl)formamidine (EtFormH) and *N*,*N*′-bis(2,6-diisopropylphenyl)formamidine (DippFormH) yielded the corresponding $Y(Form)[N(SiHMe_2)_2]_2(thf)$ complexes (Form = EtForm (**1a**), DippForm (**1b**); thf = tetrahydrofuran) (Scheme 1, (i)). Treatment of **1a**,**b** with trimethylaluminum led to formation of the corresponding $Y(Form)(AlMe_4)_2$ complexes (Form = EtForm (**2a**), DippForm (**4a**)) with elimination of $[AlMe_2\{N(SiHMe_2)_2\}]$[49] (Scheme 1, (ii)). It was also possible to prepare $[Y(EtForm)_2\{N(SiHMe_2)_2\}]$

Scheme 1. Synthesis of $[Ln(Form)(AlMe_4)_2]$ Complexes

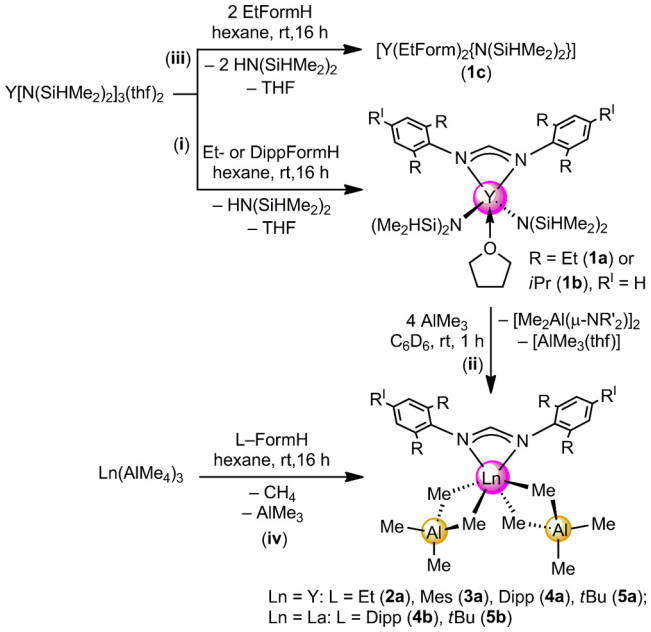

(**1c**) by a double protonolysis of $Y[N(SiHMe_2)_2]_3(thf)_2$ (Scheme 1, (iii)).

As a general route to $Ln(Form)(AlMe_4)_2$ (Ln = La, Y) complexes, use of homoleptic $Ln(AlMe_4)_3$[51] species proved more satisfactory. Thus, protonolysis of these complexes with several formamidines gave $Ln(Form)(AlMe_4)_2$ (Ln = Y, Form = EtForm (**2a**), MesForm (**3a**), DippForm (**4a**), *t*BuForm (**5a**); Ln = La, Form = DippForm (**4b**), *t*BuForm (**5b**); MesForm = *N*,*N*′-bis(2,4,6-trimethylphenyl)formamidinate, *t*BuForm = *N*,*N*′-bis(2-*tert*-butylphenyl)formamidinate) (Scheme 1, (iv)).

The strong Lewis acid Al^{3+} has a high affinity for nitrogen donor ligands.[38,52,53] Competition between the Lewis acidic Al^{3+} and the rare-earth-metal ions for N-donor ligands is well documented.[38,41,43,45] However, no isolated byproducts of formamidinato aluminum species such as $[Me_2Al\{\mu\text{-Form}\}(\mu\text{-Me})AlMe_2]$ and $[Al(Form)Me_2]$ were observed in any case, thereby simplifying isolation of pure complexes.

All aluminate compounds were obtained in reasonable yields (65−72%), and their purity was established by elemental analysis and proton and carbon NMR as well as IR spectroscopy, except that satisfactory hydrogen analyses could not be obtained for **2b**, **3bc** , **4a**, and **5a** nor a carbon analysis for **5a**. All complexes (except for **1c**) were crystallized from hexane or toluene and their structures determined by single-crystal X-ray diffraction.

The yttrium centers in $Y(Form)[N(SiHMe_2)_2]_2(thf)$ complexes **1a**,**b** reveal a similar coordination environment involving four nitrogen atoms, two from the formamidinato and two from the bis(dimethylsilyl)amido ligand, and one tetrahydrofuran molecule (Figure 1). The X-ray structures of mono- and bis(silylamido) rare-earth-metal compounds with ancillary nitrogen-donor ligands coordinated to the metals are well-established.[10,12,14,15,20−23] The coordination geometry of the yttrium center in both cases is best described as distorted trigonal bipyramidal. The two nitrogen atoms of the silylamido ligands are approximately coplanar with the yttrium atom and atom N1 of the formamidinato ligand. The oxygen atom of the thf molecule and the N2 atom of the formamidinato ligand are

dx.doi.org/10.1021/om301010m | *Organometallics* 2013, 32, 1209−1223

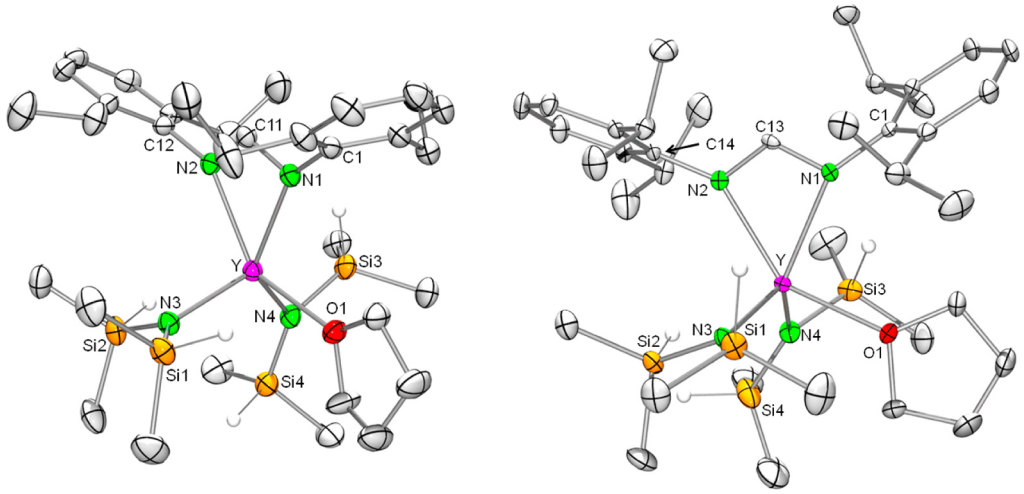

Figure 1. Perspective ORTEP views of the molecular structures of **1a** (left) and **1b** (right). Atomic displacement parameters are set at the 30% level. Hydrogen atoms (except Si−H) are omitted for clarity. The disorders of the tetrahydrofuran ligand (**1a**) and of the methyl groups at Si4 (**1b**) are not shown. For selected bond lengths and angles, see Table 1.

located above and below the plane (O1−Y−N2 = 142.1(1)° in **1a** and 143.4(2)° in **1b**), similar to the arrangement in Y[PhC(N-C_6H_3*i*Pr_2-2,6)$_2$](CH_2SiMe_3)$_2$(thf), (O1−Y−N2 = 142.97(9)°).[15] The silylamido ligands are asymmetrically coordinated to the metal center, owing to Y···(Si−H) interactions[50] of both silylamido ligands, in a manner similar to that for (aminopyridinato)bis(dimethylsilylamido)scandium complexes.[28] There is one shorter Y···Si distance for each ligand (Y···Si2 = 3.107(2) Å and Y···Si3 = 3.144(2) Å vs Y···Si1 = 3.526(2) Å and Y···Si4 = 3.550(2) Å in **1a**; Y···Si2 = 3.052(2) Å and Y···Si3 = 3.134(2) Å vs Y···Si1 = 3.663(2) Å and Y···Si4 = 3.658(2) Å in **1b**). Due to these asymmetrical *β*-agostic interactions, the Ln−N−Si angles within each amido ligand are different (Y−N3−Si1 = 126.7(2)° vs Y−N3−Si2 = 103.8(2)° and Y−N4−Si3 = 105.1(2)° vs Y−N4−Si4 = 127.3(2)° in **1a**; Y−N3−Si1 = 134.0(2)° vs Y−N3−Si2 = 100.0(2)° and Y−N4−Si3 = 103.7(2)° vs Y−N4−Si4 = 132.9(3)° in **1b**). In both **1a** and **1b**, the N−C(backbone) bond lengths and N1−C−N2 backbone angles are very similar (Table 1). The distances between yttrium and the Form nitrogen atoms (Y−N = 2.373(4) Å and 2.368(4) Å in **1a**; Y−N = 2.361(4) and 2.423(4) Å in **1b**) are consistent with the Y−N(amidinato) bond lengths in Y[PhC(N-C_6H_3*i*Pr_2-2,6)$_2$](CH_2SiMe_3)$_2$(thf) (2.339(3) and 2.369(2) Å) and Y[CyC(N-$C_6H_3Me_2$-2,6)$_2$](CH_2SiMe_3)$_2$(thf)$_2$ (2.375(7) Å)[10,15] and also in Y[pTolC(N-C_6H_3*i*Pr_2-2,6)$_2$][N($SiHMe_2$)$_2$]$_2$(thf) (2.412(3) and 2.351(2) Å).[14] The N1−Y−N2 bite angles (**1a**, 57.2(1)°; **1b**, 56.5(2)°) are similar to those of Y[PhC(N-C_6H_3*i*Pr_2-2,6)$_2$](CH_2SiMe_3)$_2$(thf)] (57.27(9)°) and Y[CyC(N-$C_6H_3Me_2$-2,6)$_2$](CH_2SiMe_3)$_2$(thf)$_2$ (55.8(3)°).

All bis(tetramethylaluminate) rare-earth metal complexes **2a**, **3a**, **4a**,**b**, and **5a**,**b** show similar molecular arrangements, with yttrium (**4a**) and lanthanum (**4b**) DippForm derivatives (monoclinic space group $P2_1/n$) being isotypic, as are yttrium (**5a**) and lanthanum (**5b**) *t*BuForm derivatives (triclinic space group $P\bar{1}$). In each complex the rare-earth-metal atom and each of the two Al atoms are bridged by two methyl groups (Figure 2). The six-coordinate rare-earth metal is ligated by two nitrogen atoms of the formamidinato ligand and two methyl carbons of each of the η^2-coordinated tetramethylaluminato moieties and adopts a distorted-octahedral geometry. In all the above complexes both [$AlMe_4$] ligands coordinate in the commonly observed η^2 fashion to form an almost planar heterobimetallic LnC_2Al unit.

Table 1. Selected Interatomic Distances (Å) and Angles (deg) of 1a,b[a]

	1a		
	molecule 1	molecule 2	1b
	Bond Lengths		
Y···Si1(5)	3.526(2)	3.600(2)	3.663(2)
Y···Si2(6)	3.107(2)	3.052(2)	3.052(2)
Y···Si3(7)	3.144(2)	3.140(2)	3.134(2)
Y···Si4(8)	3.550(2)	3.641(2)	3.658(2)
Y−N1(5)	2.373(4)	2.350(3)	2.423(4)
Y−N2(6)	2.368(4)	2.375(3)	2.361(4)
Y−N3(7)	2.240(4)	2.257(4)	2.259(4)
Y−N4(8)	2.249(4)	2.261(4)	2.269(4)
Y−O1(2)	2.374(4)	2.360(4)	2.354(4)
C11−N1(5)	1.322(6)	1.316(6)	
C13−N1			1.322(6)
C11−N2(6)	1.325(6)	1.326(6)	
C13−N2			1.318(7)
	Bond Angles		
N3(7)−Y−N4(6)	117.1(1)	130.3(2)	120.3(2)
N1(5)−Y− N2(6)	57.2(1)	57.1(1)	56.5(2)
N1(5)−Y−N3(7)	111.9(1)	113.8(1)	111.9(1)
N2(6)−Y−N4(8)	115.2(1)	115.9(1)	115.2(1)
N2(6)−Y−O1(2)	142.1(1)	139.9(1)	143.4(2)
Y−N3(7)−Si1(5)	126.7(2)	130.7(2)	134.0(2)
Y−N3(7)−Si2(6)	103.8(2)	104.3(2)	100.0(2)
Y−N4(8)−Si3(7)	105.1(2)	100.3(2)	103.7(2)
Y−N4(8)−Si4(8)	127.3(2)	133.3(2)	132.9(3)
N1(5)−C11−N2(6)	118.0(5)	117.5(4)	
N1−C13−N2			118.2(5)

[a]Where pairs of atom numbers are given, those without parentheses are for molecule 1 and those in parentheses are for molecule 2.

All Ln−C bond lengths are in the expected range (Table 2 averages: **2a**, 2.52 Å; **3a**, 2.54 Å; **4a**, 2.55 Å; **5a**, 2.54 Å; **4b**, 2.69 Å; **5b**, 2.69 Å).[51,54] These averages for Y−C are marginally larger than those reported for the triazenide complex Y[(Tph)$_2$$N_3$]($AlMe_4$)$_2$ (2.49 Å (av))[45] and closer to those for the benzamidinate complex Y[PhC(N-C_6H_3*i*Pr_2-2,6)$_2$]($AlMe_4$)$_2$ (2.53 Å (av)) (see also Chart 1, **II** and **I**).[24] The Ln−N bonds in **4b** and **5b** are on average 0.14 Å longer than those in **2a**−**5a**. This value

dx.doi.org/10.1021/om301010m | *Organometallics* 2013, 32, 1209−1223

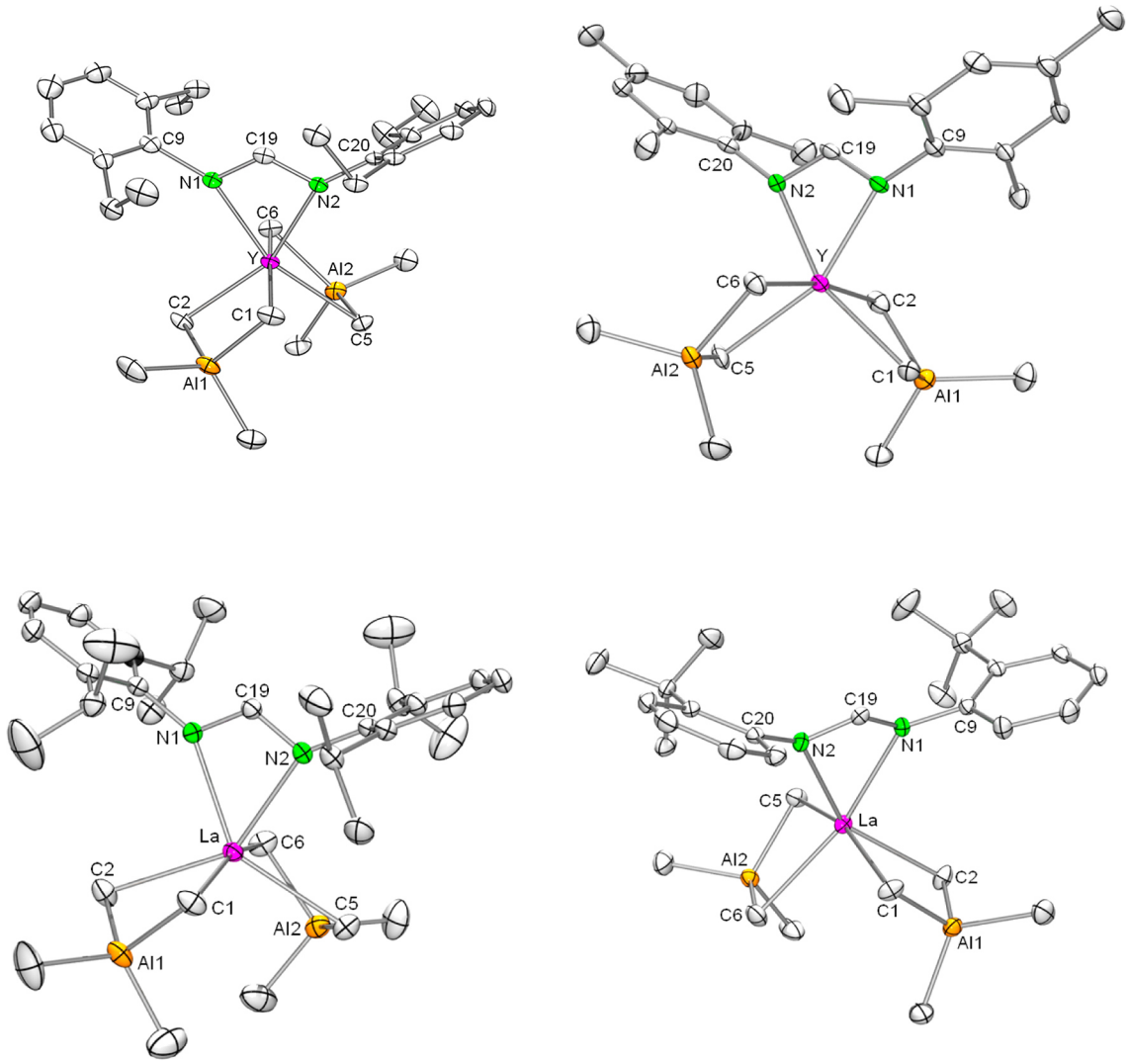

Figure 2. Perspective ORTEP views of the molecular structures of **2a** (top, left), **3a** (top, right), **4b** (bottom, left), and **5b** (bottom, right). Atomic displacement parameters are set at the 30% level. Hydrogen atoms and the solvent molecules are omitted for clarity. The disorder of one of the isopropyl groups of the DippForm ligand of complex **4b** is not shown. Not depicted are complexes **4a** and **5a**, which show similar molecular structures. For selected bond lengths and angles, see Table 2.

corresponds well with the 0.13 Å difference between the ionic radii of yttrium and lanthanum.[55] Furthermore, the La−C bonds in **4b** and **5b** are on average 0.15 Å longer than the respective Y−C bonds. In most complexes, chelation of the Form ligand is symmetrical. A noteworthy exception is **2a**, which shows a considerable 0.13 Å difference between the Y−N bond lengths and a larger N1−Y−N2 bite angle (65.4(1)°). The bond lengths and angles in **3a**−**5a** are also relatively close to those of Y[PhC(N-C_6H_3*i*Pr_2-2,6)$_2$]-($AlMe_4$)$_2$ (Y−N = 2.3157(15) Å, N1−Y−N2 = 57.51(8)°),[24] while the N1−La−N2 angles of **4b** and **5b** are close to the related angle of the triazenido ligand in Y[$(Tph)_2N_3$]($AlMe_4$)$_2$ (N1−Y−N3 = 54.6(1)°).[45,56] In both yttrium and lanthanum complexes the two N−C(backbone) bond lengths (∼1.32 Å) and N1−C−N2 backbone angles (∼118°) are almost equivalent. The latter are larger than the corresponding angles in the triazenide (109.9(3)°) and benzamidinate compounds (112.0(2)°).

The N−H stretching absorption of the formamidines at 3300−3100 cm^{-1} is not observed in the IR spectra of the complexes, indicating complete deprotonation, and a strong absorption assignable to the C−C stretching vibration of a metal-coordinated formamidinato group is detected at 1503 cm^{-1}. The IR spectra of **1a**−**c** show the presence of two distinct ν(SiH) bands at 2084/2074/2061 and 1929/1931/1926 cm^{-1}, respectively, as observed for other rare-earth-metal bis(dimethylsilyl)amide complexes.[49] The strong band at around 690 cm^{-1} in all aluminate moieties is assigned to an Al−C stretching absorption.[57]

In the IR spectra of all tetramethylaluminate complexes CH asymmetrical stretching, CH symmetrical stretching, and a Fermi resonance mode of methyl groups attached to aluminum centers appear as three bands (or two broad overlapping) at 2900−2790 cm^{-1}.[58]

The ambient-temperature ^{1}H NMR spectra of **1a**−**c** and **2a**−**5a** show a doublet for the CH backbone resonance due to the scalar ^{1}H−^{89}Y coupling ($^3J_{YH}$ = 4.6 Hz).[50] Furthermore, the ^{1}H NMR spectra of **2a**, **4a**,**b**, and **5a**,**b** at ambient temperature exhibit a sharp resonance for the aluminum−methyl groups (δ −0.24, −0.24, 0.00, −0.05, and −0.05 ppm, respectively), consistent with rapid bridge−terminal exchange at ambient temperature. In the case of the yttrium derivatives (**2a**, **4a**, and **5a**) the observed splitting of the ^{1}H methyl resonance for the [$AlMe_4$]

dx.doi.org/10.1021/om301010m | *Organometallics* 2013, 32, 1209−1223

Table 2. Selected Interatomic Distances (Å) of 2a,b, 3a, 4a,b, and 5a,b

	2a	3a	4a	5a	2b	4b	5b
Ln−C1	2.403(4)	2.542(7)	2.548(5)	2.568(2)	2.705(4)	2.694(4)	2.702(3)
Ln−C2	2.606(5)	2.540(7)	2.553(5)	2.510(2)	2.782(4)	2.710(3)	2.670(3)
Ln−C5	2.710(5)	2.518(6)	2.555(5)	2.526(2)	2.715(4)	2.693(4)	2.680(3)
Ln−C6	2.343(4)	2.548(6)	2.531(5)	2.541(2)	2.703(4)	2.669(4)	2.720(3)
Ln−N1	2.428(4)	2.338(5)	2.343(4)	2.340(2)	3.861(3)[a]	2.478(2)	2.500(2)
Ln−N2	2.293(3)	2.337(5)	2.345(4)	2.332(2)	2.524(3)	2.482(2)	2.457(2)
Ln···Al1[a]	3.075(2)	3.091(2)	3.084(2)	3.080(7)	3.301(2)	3.172(2)	3.234(2)
Ln···Al2[a]	2.875(2)	3.098(2)	3.083(2)	3.092(7)	3.296(2)	3.196(2)	3.255(2)
Al1−C1	2.091(5)	2.067(7)	2.079(5)	2.091(2)	2.068(4)	2.080(4)	2.091(3)
Al1−C2	2.051(5)	2.078(8)	2.075(6)	2.070(2)	2.055(4)	2.066(4)	2.077(3)
Al1−C3	2.042(6)	1.958(8)	1.973(6)	1.972(3)	1.968(4)	1.980(5)	1.972(3)
Al1−C4	1.989(6)	1.982(7)	1.952(7)	1.960(3)	1.981(5)	1.957(5)	1.964(3)
Al2−C5	2.002(5)	2.076(7)	2.077(6)	2.083(2)	2.082(5)	2.076(4)	2.093(3)
Al2−C6	2.255(6)	2.082(6)	2.091(5)	2.063(2)	2.078(5)	2.081(4)	2.065(3)
Al2−C7	2.038(6)	1.965(8)	1.963(6)	1.960(3)	1.971(5)	1.955(4)	1.966(3)
Al2−C8	1.903(5)	1.972(7)	1.975(6)	1.959(3)	1.970(6)	1.988(5)	1.963(4)
C(backbone)−N1	1.403(5)	1.320(8)	1.313(6)	1.324(3)	1.316(4)	1.324(3)	1.324(3)
C(backbone)−N2	1.464(6)	1.339(8)	1.326(6)	1.331(3)	1.324(4)	1.323(4)	1.335(3)

[a]Not bonding.

moieties is clearly attributable to a $^{1}H-^{89}Y$ scalar coupling ($^{2}J_{YH}$ = 3 Hz) as well. These resonances are shifted to lower frequencies in comparison with the corresponding homoleptic precursors.[51,54] When the temperature was lowered from +25 to −80 °C in toluene-d_8, the signals of yttrium complex **2a** in a similar manner to that for half-sandwich bis(tetramethyl)aluminate complexes[41,48] and the complex $Y[(Tph)_2N_3](AlMe_4)_2$[45] did not reveal any further resolution and did not show the decoalescence of the methyl resonance.

The relatively larger backbone angle along with the different donor abilities of amidinato ligands in comparison to triazenido ligands are plausible reasons why formamidinato aluminum compounds were not isolated in contrast to the triazenide system,[45,56] and these factors facilitated the isolation of formamidinato bis(tetramethylaluminato) rare-earth-metal complexes.

In contrast to the preceding formamidinate complexes, $[La(EtFormAlMe_3)(AlMe_4)_2](C_7H_8)_{1.5}$ (**2b**), which was obtained following a similar protonolysis reaction from EtFormH and $La(AlMe_4)_3$, has a metal−π-arene interaction (Scheme 2).

Scheme 2. Contrasting Outcomes of the Syntheses of 2a,b

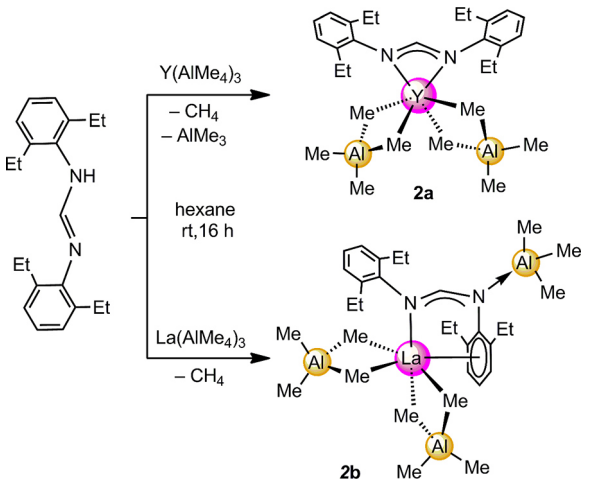

In complex **2b** the EtForm ligand adopts a configuration in which one nitrogen and one aryl substituent are coordinated to the lanthanum atom in an η^1(N):η^6(arene) manner to give eight-coordination, in contrast to the normal N,N′-chelating mode in six-coordinate **2a** with the smaller Y^{3+}, which gives more stable complexes in comparison to La^{3+} because of the higher charge/size value. In addition the η^6(arene)−La interaction may provide greater steric saturation than a single N−La bond. The second nitrogen donor binds to aluminum. This provides a rare case in the present study where Al competes with a rare-earth metal for a formamidinato nitrogen atom. Although η^6(arene) interactions are known in lanthanum complexes,[59] this rearranging of amidinato ligands has not been observed previously for rare-earth metals[1] and is quite rare for guanidinato ligands,[60] but it is common in group 1, 2, and 13 (In and Tl) derivatives.[37,61] The La−C(arene) distances (Figure 3) fall in the same ranges of those of $La(OC_6H_3Ph_2\text{-}2,6)_3$ (3.107(7)−3.274(7) Å) and $La_2(NHiPr_2C_6H_3\text{-}2,6)_6$ (2.972(3)−3.209(4) Å).[59a,b]

Chelation (η^1, η^6) of lanthanum by the EtForm ligand is accompanied by C−N bond lengths suggestive of delocalization (1.316(4) and 1.324(4) Å), rather similar to the case for alkali-metal amidinate complexes with similar ligands.[37,62] The NCN backbone angle of **2b** (126.1(3)°) also correlates well with those of alkali-metal complexes with η^1(N):η^6(arene)-bonded ligands (e.g., K[(η^6-Mes)NC(H)N(Mes)][(η^6-Mes)NHC(H)N(Mes)] N−C(backbone)−N = 126.3(2)°)[62] and is larger than for **4b** and **5b**. The La−N2 interaction (2.524(3) Å) and the average La−C(aluminato) bond length (2.73 Å) are slightly longer than those of **4b** and **5b** (Table 2).

The ^{1}H NMR spectrum of **2b** in toluene-d_8 at ambient temperature shows three discrete sets of CH_2 signals caused by a shift of the CH_2 hydrogen atoms of the ethyl groups attached to the asymmetrically coordinated aromatic ring. The signal at 2.25 ppm is assignable to CH_2 groups belonging to the uncoordinated aromatic ring (C(9)−C(14)), while resonances shifted to higher values (2.46 and 3.22 ppm) are attributable to CH_2 groups of the ring π-bonded to lanthanum. There are two single resonances (−0.46 and −0.53 ppm) for the aluminum−methyl groups of $[AlMe_4]$ and $AlMe_3$, respectively. A low-temperature ^{1}H NMR spectrum (−52 °C) of complex **2b** in toluene-d_8 showed decoalescence of the signals of the eight

dx.doi.org/10.1021/om301010m | Organometallics 2013, 32, 1209−1223

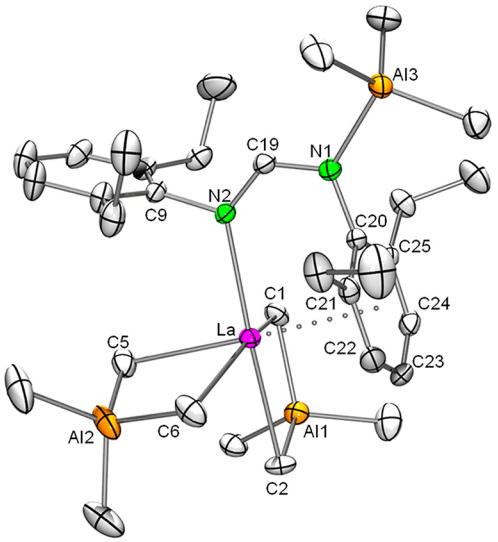

Figure 3. Perspective ORTEP view of the molecular structure of **2b**. Atomic displacement parameters are set at the 30% level. Hydrogen atoms and the solvent molecules are omitted for clarity. Selected bond distances (Å): La1−C20 = 3.068(3), La1−C21 = 3.084(3), La1−C22 = 3.090(4), La1−C23 = 3.110(4), La1−C25 = 3.143(3), La1−C24 = 3.144(4), Al3−N1 = 1.989(3), Al3−C30 = 1.980(5), Al3−C31 = 1.984(5), Al3−C32 = 1.976(4) Å. For further selected bond lengths and angles, see Table 2.

methyl groups of the two $[AlMe_4]$ ligands but one sharp signal for the nitrogen bound $AlMe_3$ (Experimental Section).

Addition of the homoleptic precursor $La(AlMe_4)_3$ to 1 equiv of MesFormH in hexane gave a yellow solution, from which the complex $[La\{\eta^1(N):\eta^6(Ar)\text{-}Me_2CH_2FormAlMe_3\}(AlMe_3)(AlMe_4)][La(Me_2CH_2FormAlMe_3)(AlMe_3)(AlMe_4)](C_6H_{14})_{1.5}$ (**3bc**; Me_2CH_2Form = MesForm-H(*o*-Me)) crystallized in the triclinic space group $P\bar{1}$ (Scheme 3). Compound **3bc** exhibits

Scheme 3. Syntheses of 3b,c Showing Distinct Me_2CH_2Form Coordination

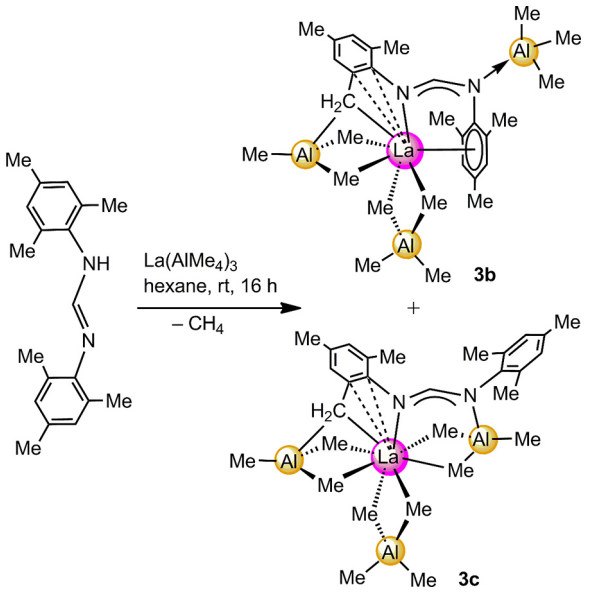

cocrystallization of two discrete molecules (**3b** + **3c**, 1:1) in the unit cell with 1.5 hexane molecules in the lattice (Figure 4). Isolation of the crystals and evaporation of the yellow filtrate resulted in a residue of the pure $La[\eta^1(N):\eta^6(Ar)\text{-}Me_2CH_2FormAlMe_3](AlMe_3)(AlMe_4)$ (**3b**) (Scheme 3). Complexes **3b,c** are linkage isomers, and the Me_2CH_2Form ligand in **3b** is in a configuration similar to that of compound **2b** with η^6 coordination of an aryl group to the lanthanum atom and a metal-to-arene centroid distance of 2.768 Å, relatively close to that of **2b** (2.774 Å). However, compound **3c** exhibits a different form of Me_2CH_2Form (Table 3).

The coordination number in **3b** is 10, the complex containing the $\eta^1(N):\eta^6(arene)$ binding mode of Me_2CH_2Form, while **3c** has 9-coordination, with $AlMe_3$ bridging a nitrogen donor atom and the lanthanum atom via two methyl groups. The structures of **3b,c** differ from that of **2b** (and **2a**) owing to C−H bond activation of an *o*-methyl group of the mesityl moiety. The resulting (RCH_2^-) moiety bridges Al and La in a μ_2 fashion, creating a pseudo-aluminate species.

Each of the structures of **3b,c** exhibits three methylaluminum moieties: namely, $[AlMe_4]$, $[AlMe_3RCH_2]$, and $AlMe_3$. In each molecule the $[AlMe_4]^-$ ligand is coordinated to the La atom in the common η^2 fashion to form a $[La(\mu\text{-}CH_3)_2Al]$ unit with a La1−C1−Al1−C2 torsion angle of 4.14(3)° in **3b** and a smaller La2−C30−Al4−C31 angle of 0.58(4)° in **3c**. The $[AlMe_3RCH_2]^-$ moiety coordinates through a methylene and two bridging methyl groups to the lanthanum metal center. The La−(μ-CH_2) bond lengths (**3b**, La1−C5 = 2.851(7) Å; **3c**, La2−C34 = 2.815(7) Å) are shorter than the La−(μ-CH_3) bond lengths (Table 3). The La−(μ-Me) bonds of this η^3-coordinated $[AlMe_3RCH_2]$ ligand (average 2.92 Å in **3b** and 2.96 Å in **3c**) are longer than the bonds of the η^2-coordinated $[AlMe_4]$ ligand (average 2.75 Å in **3b** and 2.73 Å in **3c**), consistent with observations for homoleptic $La(AlMe_4)_3$ (average η^3-coordinated, 2.88 Å; average η^2-coordinated, 2.70 Å).[51] Remarkably, the La−N and La−CH_2 bonds anchor two aromatic carbons in possible bonding positions. This rare multihapto NC_3 bonding of the lanthanum atoms has only been reported in a lanthanum complex with chelating *o*-(dimethylamino)benzyl ligands.[63] The La−C bond lengths of the anchored aromatic carbon atoms (C9, C10/C38, C43) are consistent with or shorter than typical La−π(C) values.[59] For comparison, the smaller yttrium(III) was previously shown to engage in a respective NC_2 bonding involving a η^2-coordinated $[AlMe_3RCH_2]$ ligand.[38] The nature of the $AlMe_3$ group is different in **3b,c**. In the former there is N−$AlMe_3$ bonding similar to that in **2b** and no interaction of the methyl groups of $AlMe_3$ with the La center. However, in **3c** the N−$AlMe_3$ group binds via two bridging methyl groups to the La atom.

The most striking structural characteristic of compounds **3b,c** is the presence of a methylene ligand, which increases the coordination saturation of the lanthanum center and helps anchor the η^2 binding of two aromatic carbon atoms. The structures show the product of a ligand metalation involving σ-bond metathesis between Al−CH_3 and a C−H bond of the aromatic methyl group together with loss of methane and the formation of four- and five-membered metallacycles. The La−CH_2 contacts are nearly equidistant (La1−C5 = 2.851(7) Å in **3b** and La2−C34 = 2.815(7) Å in **3c**) and are in the range of the previously observed La−CH_2 bonds.[43b,64−67] For lanthanum and yttrium mono-C_5Me_5 complexes, single and multiple C−H bond activation was established when using tetramethylaluminate functionalities.[66,68] Furthermore, C−H bond activation and metalation of the isopropyl methyl groups have been documented in the case of the pyridine-supported complexes (BDPPpyr-H)-Y[(μ-Me)$AlMe_2$]$_2$ and (BDPPpyr-H)Lu[(μ-Me)$AlMe_2$](thf)

dx.doi.org/10.1021/om301010m | *Organometallics* 2013, 32, 1209−1223

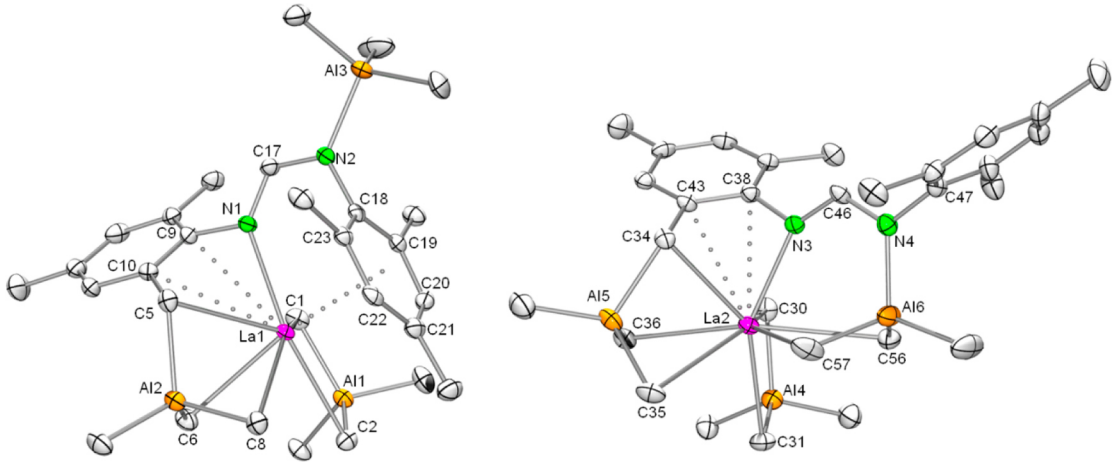

Figure 4. Perspective ORTEP views of the molecular structures of **3b** (left) and **3c** (right). Atomic displacement parameters are set at the 30% level. Hydrogen atoms and the solvent molecules are omitted for clarity. For selected bond lengths and angles, see Table 3.

(H_2BDPPpyr = 2,6-bis-(((2,6-diisopropylphenyl)amino)methyl)-pyridine),[38] and also in scandium complexes supported by nacnac (β-diketiminato) ligands containing bulky 2,6-diisopropylphenyl substituents.[69]

The NCN backbone angle of **3b** (122.6(6)°) is less than that of **2b** (126.2(3)°), most likely due to the less sterically demanding character of Me_2CH_2Form in comparison with EtForm. The CNC backbone bond lengths in both **3b** and **3c** (Table 3) are in the routinely observed range (1.316(7)−1.333(5) Å).[8,9,13,23]

In the ^{1}H NMR spectrum of complex **3bc** in C_6D_6, at ambient temperature, six separate peaks (−0.56, −0.41, −0.28, −0.20, −0.17, −0.14 ppm) can be assigned to [$AlMe_3$]/[$AlMe_4$] moieties. The residue after isolation of **3bc** is considered to be pure **3b** because of the observation of only three peaks at low frequencies (−0.56, −0.41, −0.28 ppm) similar to the corresponding chemical shifts (−0.53, −0.46 ppm) of **2b**. The characteristic pattern of four methylene doublets in the ^{1}H NMR spectrum of **3bc** in C_6D_6 and two methylene doublets in **3b** is clearly indicative of the outcome of this reaction. The doublets at 2.65, 2.34, 1.27, and 1.23 ppm ($^2J_{HH}$ = 15.5 Hz) in **3bc** and 2.34 and 1.27 ppm in **3b** ($^2J_{HH}$ = 15.5 Hz) are assignable to the diastereotopic La−CH_2 methylene protons. The ^{13}C NMR spectrum of compound **3bc** in C_6D_6 indicates two distinctive peaks belonging to CH_2 at 24.9 and 27.6 ppm, while in **3b** merely 27.6 ppm is observed, consistent with the proposed products of this reaction.

Polymerization of Isoprene. The new post-metallocene catalyst families based on donor-functionalized chelating non-cyclopentadienyl ligands (e.g., imines, amides) have received significant attention in the field of polymer science during the past few years.[2−5,70,71] In the field of organo−rare-earth-metal chemistry, most of these are bis(alkyl) (R = CH_2SiMe_3) complexes of the [Ln^{III}(Solv)(**L**)R_2] type containing monoanionic N-ancillary ligands ($\mathbf{L}^-$).[7] For isoprene polymerization, the complexes are activated by treatment with boron cocatalysts, often in the presence of trialkylaluminum.[32−34,72,73] Surprisingly, even when the formation of a heterobimetallic complex as a precatalyst is proposed, isolation of the discrete bis(aluminate) post-metallocene complexes is scarce. To our knowledge, the complexes [$PhC(NC_6H_3iPr_2$-2,6)$_2$]Y($AlMe_4$)$_2$,[24] [$(Tph)_2N_3$]-Ln($AlMe_4$)$_2$ (Ln = La, Nd, Y),[45] and (Cp^Q)Ln($AlMe_4$)$_2$[46] represent the only complexes of this type tested in isoprene polymerization (Chart 1, **I**−**III**). In order to extend these investigations, we carried out preliminary tests on compounds **2a**,**b** and **4a**,**b** as precatalysts activated by [Ph_3C][$B(C_6F_5)_4$] (**A**) or [$PhNMe_2H$]-[$B(C_6F_5)_4$] (**B**) in isoprene polymerization. Furthermore, 1 equiv of $AlMe_3$ was added to the binary catalyst system to determine the effect of excess trialkylaluminum. The polymerization results are summarized in Table 4. For all activations of complexes **2a**,**b** and **4a**,**b** colorless solutions changed to orange independent of the boron activator, a common feature in such systems.

The stereoselectivity of the polymerization reactions performed with yttrium aluminate precatalysts (**2a** and **4a**) was highly affected by the choice of cocatalyst. Initiators applying the cocatalyst trityl borate [Ph_3C][$B(C_6F_5)_4$] (**A**) display relatively high trans-1,4-selectivities up to 84% (Table 4, runs 1 and 5), while activation with anilinium borate [$PhNMe_2H$][B-(C_6F_5)$_4$] (**B**) exhibits less selective polymers with moderate cis-1,4-content (Table 4, runs 2 and 6). When 1 equiv of $AlMe_3$ was added to the trityl borate (**A**) activated catalysts, no significant effect in stereoselectivity was observed (Table 4, runs 3 and 7). In contrast, the addition of trimethylaluminum to the binary catalyst systems **2a**/**B** and **4a**/**B** increases the trans-1,4-selectivity from 13.0% to 44.5% and from 15.9% to 87.0%, respectively (Table 4, runs 4 and 8). However, all polymers produced from yttrium aluminates show comparatively broad molecular weight distributions (1.53−2.69).

The activation of the lanthanum complexes **2b** and **4b** with [Ph_3C][$B(C_6F_5)_4$] (**A**) led to catalysts producing polyisoprene with mainly trans-1,4-content (runs 9 and 13), whereby a higher selectivity for the smaller EtForm complexes is observed, comparable with that of the yttrium species (**2a** vs **4a**). In contrast, a switch from trans-1,4-polymer (**2b**, 69.6% trans; Table 4, run 10) to cis-1,4-polymer (**4b**, 81.8% cis; Table 4, run 14) could be reproducibly observed when anilinium borate (**B**) was used as a cocatalyst. The addition of trimethylaluminum had no significant effect on the trans-1,4-selective catalyst systems but changes the cis-1,4-selective system **4b**/[$PhNMe_2H$]-[$B(C_6F_5)_4$] toward trans-1,4-selectivity (81.8% cis versus 61.1% trans; Table 4, runs 14 and 16). The trans-1,4-selectivity of **2b**, which already has an $AlMe_3$ molecule coordinated to a nitrogen atom in the structure (Figure 3), does not change significantly after addition of trimethylaluminum (Scheme 2, Table 4, runs 9−12). The increases in trans formation for **2a**/**B**, **4a**/**B**, and **4b**/**B** on addition of $AlMe_3$ (runs 4, 8, and 16) might be a result of the formation of a precatalyst species similar to **2b** (Scheme 2), whereby the additional $AlMe_3$ is complexed by one nitrogen

dx.doi.org/10.1021/om301010m | *Organometallics* 2013, 32, 1209−1223

Table 3. Selected Interatomic Distances (Å) and Angles (deg) of 3b,c

	3b	3c
Bond Lengths[a]		
La1(2)−C1(30)	2.702(7)	2.719(7)
La1(2)−C2(31)	2.807(7)	2.744(7)
La1(2)−C5(34)	2.851(7)	2.815(7)
La1(2)−C6(35)	2.959(7)	3.080(8)
La1(2)−C8(36)	2.942(7)	2.976(7)
La1−C18	3.036(6)	
La1−C19	3.078(6)	
La1−C20	3.092(7)	
La1−C21	3.158(7)	
La1−C22	3.131(6)	
La1−C23	3.109(6)	
La1(2)−C9(38)	3.087(6)	2.899(6)
La1(2)−C10(43)	3.233(7)	2.984(7)
La2−C56		3.081(8)
La2−C57		2.850(8)
La1(2)−N1(3)	2.467(5)	2.434(5)
La1(2)···Al1(4)	3.314(3)	3.295(3)
La1(2)···Al2(5)	2.999(3)	3.0514(3)
La1(2)···Al3(6)	5.784(3)	3.3832(3)
N2(4)−Al3(6)	1.971(6)	1.916(6)
Al1(4)−C1(30)	2.053(7)	2.063(8)
Al1(4)−C2(31)	2.046(7)	2.059(8)
Al1(4)−C3(32)	1.972(7)	1.970(9)
Al1(4)−C4(33)	1.967(8)	1.978(8)
Al2(5)−C5(34)	2.068(7)	2.095(7)
Al2(5)−C6(35)	2.038(7)	2.023(8)
Al2(5)−C7(37)	1.950(7)	1.928(9)
Al2(5)−C8(36)	2.030(7)	2.038(8)
Al6−C56		2.013(9)
Al6−C57		2.037(9)
C(backbone)−N1(N3)	1.313(8)	1.320(8)
C(backbone)−N2(N4)	1.313(8)	1.325(8)
Bond Angles		
N1(3)−La1(2)−N2(4)	122.6(6)	120.9(6)
Al1(4)−C1(30)−La1(2)	87.3(2)	85.9(2)
Al1(4)−C2(31)−La1(2)	84.6(2)	85.4(2)
Al2(5)−C5(34)−La1(2)	73.2(2)	75.3(2)
Al2(5)−C6(35)−La1(2)	71.1(2)	70.0(2)
Al2(5)−C8(36)−La1(2)	71.5(2)	72.3(2)
Al6−C56−La2		80.3(3)
Al6−C57−La2		85.9(3)
C1(30)−La1(2)−C2(31)	76.1(2)	77.2(2)
C1(30)−Al1(4)−C2(31)	111.8(3)	111.5(3)
C5(34)−La1(2)−C6(35)	67.32(19)	68.5(2)
C5(34)−Al2(5)−C6(35)	103.4(3)	107.7(3)
C56−La2−C57		69.0(3)
C56−Al6−C57		112.3(3)
N1(3)−C(H)−N2(4)	122.6(6)	120.9(6)

[a]Where pairs of atom numbers are given, those without parentheses are for **3b** and those in parentheses are for **3c**.

from the formamidinato ligand and the Ln metal center is now changed to η^1(N) and η^6(arene) coordination. All polymers produced by lanthanum complexes reveal narrow molecular weight distributions lower than 1.3 and suggest a living fashion by complete consumption of the monomer. Moreover, selected polymerizations were repeated with 1 h reaction times, affording lower M_w/M_n values down to 1.07 without affecting the stereoselectivity. One typical example is given in Table 4, run 17, representing the reproducibility of these polymerizations.

The influence of addition of alkylaluminum cocatalysts has been investigated previously for complexes including N-coordinating ancillary ligands.[24,28,32,33] Due to the formation of $[AlR_4]^-$ moieties as active species upon addition of alkylaluminum derivatives to the initiators, a switch to cis-1,4-selectivity was mostly observed, especially for less sterically saturated metal centers.[24,28] For complexes **2a,b** and **4a,b** already having $[AlMe_4]^-$ moieties in the structure, the switch between cis and trans species is independent of the size of the metal cation or the bulkiness of the ligand. Although the complexes under investigation display high polymerization activity when activated with borate cocatalysts, the stereoselectivities did not exceed 90%. Table 5 summarizes important polymerization performances of the related rare-earth-metal bis(tetramethylaluminate) complexes depicted in Chart 1. Clearly, the implications of the metal size for the cis/trans selectivity deserve special attention. While a metal center as small as Sc(III) gives high cis-1,4-selectivity (run 1, 94%), polyisoprene with high trans-1,4-selectivity is favorably produced at the large La(III) center (run 7, 92%). The cis-directing behavior of the complex $[PhC(NC_6H_3iPr_2\text{-}2,6)_2]Y(AlMe_4)_2$ (**I$_Y$**) (Table 5, run 2, C_6H_5Cl)[24] is striking in comparison with that of Y(DippForm)$(AlMe_4)_2$ (**4a**) (Table 4, run 5, toluene), which produced mainly *trans*-1,4-polyisoprene. These two complexes differ only in that the former carries a phenyl group in the ligand backbone. Generally, the high trans stereoselectivities observed for the half-sandwich bis(aluminate)/cocatalyst systems $(C_5Me_5)La(AlMe_4)_2$/**A** (trans-1,4 content 95.2%, M_w/M_n = 1.05, −30 °C preformation) and $(C_5Me_5)La(AlMe_4)_2/B(C_6F_5)_3$ (trans-1,4 content 99.5%, M_w/M_n = 1.18) remain unmatched.[41]

CONCLUSIONS

Formamidines (FormH) feature a suitable and versatile N-ancillary ligand set for the synthesis of heteroleptic LnAl bimetallic hydrocarbyl complexes. Post-metallocene-type complexes Ln(Form)$(AlMe_4)_2$ (Form (ArNCHNAr) = EtForm (Ar = 2,6-$Et_2C_6H_3$), MesForm (Ar = 2,4,6-$Me_3C_6H_2$), DippForm (Ar = 2,6-$iPr_2C_6H_3$), *t*BuForm (Ar = 2-*t*BuC_6H_4)) can be obtained favorably via methane elimination utilizing homoleptic Ln$(AlMe_4)_3$ or by successive silylamine elimination/silylamido elimination employing $Ln[N(SiHMe_2)_2]_3(thf)_2$ and $AlMe_3$, respectively. While the isolated yttrium complexes show η^1-(N):η^1(N′)-coordinated Form ligands throughout, the lanthanum congeners revealed distinct coordination chemistry depending on the substituents on the aryl rings of the Form ligands. Less bulky aryl substituents (Me, Et) favor a η^1(N):η^6(arene) ligation, as observed in La(EtFormAlMe_3)$(AlMe_4)_2$. This configurational switch is probably caused by the successful competition of released Lewis acidic trimethylaluminum for a N(Form) coordination site, meaning that the large and hence mildly Lewis acidic La(III) center is abandoning η^1(N):η^1(N′) bonding in favor of the η^1(N):η^6(arene) mode. Further, the lanthanum derivatives can engage in C−H bond activation reactions of the aryl substituents, as shown for La(Me_2CH_2FormAlMe_3)$(AlMe_3)(AlMe_4)$ (Me_2CH_2Form = MesForm-H(*o*-Me)). These C−H activation reactions are facilitated by the high mobility of the aluminate methyl groups. Although there is a potential competition between Al(III) and La(III) for the nitrogen atoms of the formamidinato ligands, no byproducts of formamidinato aluminum species were isolated in any case. On activation with the borate $[Ph_3C][B(C_6F_5)_4]$ or $[PhNMe_2H][B(C_6F_5)_4]$, the

dx.doi.org/10.1021/om301010m | *Organometallics* 2013, 32, 1209−1223

Table 4. Isoprene Polymerization of Formamidinate Complexes under Study

entry[a]	precat.	cocat.[b]	yield (%)	cis-1,4[c]	3,4[c]	trans-1,4[c]	M_n[d] (×10⁴)	M_w/M_n[d]
1	Y(EtForm)$(AlMe_4)_2$ (**2a**)	**A**	>99	8.8	7.0	84.2	8.3	1.71
2	Y(EtForm)$(AlMe_4)_2$ (**2a**)	**B**	>99	58.2	28.8	13.0	11.7	2.69
3	Y(EtForm)$(AlMe_4)_2$ (**2a**)	**A**/$AlMe_3$	>99	16.4	6.8	76.8	6.9	1.61
4	Y(EtForm)$(AlMe_4)_2$ (**2a**)	**B**/$AlMe_3$	>99	42.7	12.8	44.5	9.0	2.00
5	Y(DippForm)$(AlMe_4)_2$ (**4a**)	**A**	>99	15.6	8.1	76.3	2.6	1.96
6	Y(DippForm)$(AlMe_4)_2$ (**4a**)	**B**	>99	53.6	30.5	15.9	7.7	2.05
7	Y(DippForm)$(AlMe_4)_2$ (**4a**)	**A**/$AlMe_3$	>99	10.4	8.7	80.9	5.3	1.91
8	Y(DippForm)$(AlMe_4)_2$ (**4a**)	**B**/$AlMe_3$	>99	5.2	7.8	87.0	6.3	1.53
9	La(EtFormAlMe_3)$(AlMe_4)_2$ (**2b**)	**A**	>99	9.7	8.6	81.6	14.6	1.18
10	La(EtFormAlMe_3)$(AlMe_4)_2$ (**2b**)	**B**	>99	17.8	12.6	69.6	9.4	1.13
11	La(EtFormAlMe_3)$(AlMe_4)_2$ (**2b**)	**A**/$AlMe_3$	>99	17.0	15.2	67.8	13.7	1.13
12	La(EtFormAlMe_3)$(AlMe_4)_2$ (**2b**)	**B**/$AlMe_3$	>99	17.9	12.0	70.1	9.8	1.14
13	La(DippForm)$(AlMe_4)_2$ (**4b**)	**A**	>99	31.5	5.9	62.6	7.2	1.19
14	La(DippForm)$(AlMe_4)_2$ (**4b**)	**B**	>99	81.8	5.7	12.5	8.4	1.27
15	La(DippForm)$(AlMe_4)_2$ (**4b**)	**A**/$AlMe_3$	>99	32.3	5.7	62.0	8.7	1.18
16	La(DippForm)$(AlMe_4)_2$ (**4b**)	**B**/$AlMe_3$	>99	35.1	3.8	61.1	8.5	1.19
17[e]	La(EtFormAlMe_3)$(AlMe_4)_2$ (**2b**)	**B**/$AlMe_3$	>99	16.3	16.3	67.4	8.2	1.07

[a]Conditions: 0.02 mmol of precatalyst, [Ln]/[cocat] = 1/1, 8 mL of solvent toluene, 20 mmol of isoprene, 24 h. [b]Cocatalyst: **A**, $[Ph_3C][B(C_6F_5)_4]$; **B**, $[PhNMe_2H][B(C_6F_5)_4]$. [c]Determined by ^{13}C NMR spectroscopy in $CDCl_3$. [d]Determined by means of size-exclusion chromatography (SEC) against polystyrene standards. [e]The polymerization reaction was quenched after 1 h.

Table 5. Isoprene Polymerization Promoted by Selected Rare-Earth-Metal Bis(tetramethylaluminate) Complexes Bearing N-Ancillary Ligands (cf. Chart 1)

entry[a]	precat.	cocat.[b]	yield (%)	cis-1,4[c]	3,4[c]	trans-1,4[c]	M_n[d] (×10⁴)	M_w/M_n[d]	ref
1[e]	$[PhC(NC_6H_3iPr_2\text{-}2,6)_2]Sc(AlMe_4)_2$ ($\mathbf{I_{Sc}}$)	**A**	98	94	5	1	8.03	1.56	44
2[f]	$[PhC(NC_6H_3iPr_2\text{-}2,6)_2]Y(AlMe_4)_2$ ($\mathbf{I_Y}$)	**A**	>99	77.8	22	0.2	6.8	1.8	24
3[f]	$[PhC(NC_6H_3iPr_2\text{-}2,6)_2]Y(AlMe_4)_2$ ($\mathbf{I_Y}$)	**A**/$AlMe_3$	>99	92	6	2	7.5	1.6	24
4	$[(Tph)_2N_3]Y(AlMe_4)_2$ ($\mathbf{II_Y}$)	**A**	>99	49.6	9.4	41.0	8.0	1.41	45
5	$[(Tph)_2N_3]Y(AlMe_4)_2$ ($\mathbf{II_Y}$)	**B**	>99	57.5	11.1	31.4	6.0	1.52	45
6	$[(Tph)_2N_3]La(AlMe_4)_2$ ($\mathbf{II_{La}}$)	**A**	>99	16.1	3.0	81.0	6.0	1.28	45
7	$[(Tph)_2N_3]La(AlMe_4)_2$ ($\mathbf{II_{La}}$)	**B**	>99	6.3	2.1	91.7	7.0	1.30	45
8[g]	$(Cp^Q)Y(AlMe_4)_2$ ($\mathbf{III_Y}$)	**A**	>99	1.3	12.8	85.9	74	1.14	46
9[g]	$(Cp^Q)Y(AlMe_4)_2$ ($\mathbf{III_Y}$)	**B**	>99	3.8	21.4	74.7	35	1.12	46
10[h]	$(Cp^Q)Y(AlMe_4)_2$ ($\mathbf{III_Y}$)	**A**	19	-	9.9	90.1	61	1.91	46
11[h]	$(Cp^Q)Y(AlMe_4)_2$ ($\mathbf{III_Y}$)	**B**	>99	1.3	12.8	85.9	74	1.14	46
12[i]	$(Cp^Q)La(AlMe_4)_2$ ($\mathbf{III_{La}}$)	**B**	>99	19.6	9.5	70.9	39	1.21	46
15[j]	$(Cp^Q)La(AlMe_4)_2$ ($\mathbf{III_{La}}$)	**B**	>99	2.1	4.9	93.1	93	1.11	46

[a]Conditions unless otherwise specified: 0.02 mmol of precatalyst, [Ln]/[cocat] = 1/1, 8 mL of solvent toluene, 20 mmol of isoprene, 24 h. [b]Cocatalyst: **A**, $[Ph_3C][B(C_6F_5)_4]$; **B**, $[PhNMe_2H][B(C_6F_5)_4]$. [c]Determined by ^{13}C NMR spectroscopy in $CDCl_3$. [d]Determined by means of size-exclusion chromatography (SEC) against polystyrene standards. [e]Conditions: 10 mmol of isoprene, 2 min, 25 °C. [f]Conditions: C_6H_5Cl, 1.022 g of isoprene, 10 min, 25 °C, T_g = −57 °C. [g]Conditions: 2 h. [h]Conditions: hexane, 2 h. [i]Conditions: 2 h. [j]Conditions: hexane, 24 h.

complexes Y(EtForm)$(AlMe_4)_2$, Ln(DippForm)$(AlMe_4)_2$ (Ln = Y, La), and La(EtFormAlMe_3)$(AlMe_4)_2$ efficiently initiated the polymerization of isoprene. In particular, the lanthanum-based catalysts produced polyisoprene of narrow molecular weight distribution (PDI < 1.2) at ambient temperature. The general tendency for trans-1,4-selectivity is clearly seen in the presence of the trityl borate cocatalyst (maximum 87%), while the anilinium borate cocatalyst favors cis-1,4-selectivity (maximum 82%).

EXPERIMENTAL SECTION

General Considerations. Syntheses and catalytic operations were carried out under an inert atmosphere of dry argon using standard Schlenk, high-vacuum, and glovebox techniques (MBraun MBLab; <1 ppm O_2, <1 ppm H_2O). Hexane, toluene, and tetrahydrofuran were purified by using Grubbs columns (MBraun SPS, solvent purification system) and stored in a glovebox. The starting materials Ln$(AlMe_4)_3$ (Ln = La, Y),[51,54] Y$[N(SiHMe_2)_2]_3(thf)_2$,[74] and formamidine compounds (EtFormH, DippFormH, MesFormH, and *t*BuFormH)[35,36] were prepared by the literature methods. C_6D_6 and toluene-d_8 were obtained from Aldrich, dried over Na for 24 h, and filtered. $CDCl_3$ and $AlMe_3$ were purchased from Aldrich and used as received. Isoprene was obtained from Aldrich, degassed, dried over activated 4 Å molecular sieves, and vacuum-transferred three times prior to use. The borate cocatalysts $[Ph_3C][B(C_6F_5)_4]$ (**A**) and $[PhNMe_2H][B(C_6F_5)_4]$ (**B**) were purchased from Boulder Scientific Co. and were used without any further purification. The NMR spectra of air- and moisture-sensitive compounds in C_6D_6 or toluene-d_8 solutions were recorded by using J. Young valve NMR tubes at +25/−52 °C on a Bruker AVANCE-DMX400 (^1H, 400.13 MHz; ^{13}C, 100.62 MHz) or Bruker

dx.doi.org/10.1021/om301010m | *Organometallics* 2013, 32, 1209−1223

BIOSPIN-AV500 instrument (^{1}H, 500.13 MHz; ^{13}C, 125.77 MHz). ^{1}H and ^{13}C chemical shifts are referenced to internal solvent resonances and reported relative to TMS. Elemental analyses (C, H, N) were performed using an Elementar Vario MICRO cube. IR spectra were recorded between 4000 and 400 cm^{-1} on a Nicolet 6700 FTIR spectrometer using a DRIFT chamber with dry KBr/sample mixtures and KBr windows. The collected data were converted using the Kubelka−Munk refinement. The molar masses (M_w and M_n) of the polymers were determined by size-exclusion chromatography (SEC). Sample solutions (1.0 mg of polymer/mL of thf) were filtered through a 0.2 μm syringe filter prior to injection. SEC was performed with a pump supplied by Viscotek (GPCmax VE 2001), employing ViscoGEL columns. Signals were detected by means of a triple detection array (TDA 302) and calibrated against polystyrene standards (M_w/M_n < 1.15). The flow rate was set to 1.0 mL min^{-1}. The microstructure of the polyisoprenes was examined by means of ^{1}H and ^{13}C NMR experiments on the AV400 and AV500 spectrometers at ambient temperature, using $CDCl_3$ as solvent. *Caution!* Aluminate compounds and volatiles containing trimethylaluminum react violently when exposed to air; concentrated solutions of organoaluminum and fluorinated boron compounds and their solid reaction products are highly shock sensitive.[41] For some of the tetramethylaluminate complexes, we could not obtain satisfactory carbon (**5a**) and hydrogen analyses (**2b**, **3bc** , **4a**, and **5a**).

General Procedure for the Synthesis of Complexes 1−5. In a glovebox, a solution of $Y[N(SiHMe_2)_2]_3(thf)_2$ or $Ln(AlMe_4)_3$ (Ln = Y, La) in 5 mL of hexane was added dropwise to a suspension of the formamidine reagents HL in 5 mL of hexane with vigorous stirring. Instant gas formation was observed in the case of $Ln(AlMe_4)_3$. The clear solution was stirred overnight at ambient temperature and then evaporated to dryness under oil pump vacuum. The powder was dissolved in hexane or toluene (only for compounds **2b** and **3bc**) and crystallized at −40 °C. The pure crystalline product was generally obtained after 1 day. All the characterizations were performed on the crystalline compounds.

*Y(EtForm)[N(SiHMe$_2$)$_2$]$_2$(thf) (**1a**).* Following the procedure described above, $Y[N(SiHMe_2)_2]_3(thf)_2$ (100 mg, 0.16 mmol) and EtFormH (48 mg, 0.16 mmol) were reacted. Recrystallization of the product from hexane yielded 45 mg (38%) of **1a** as colorless crystals suitable for X-ray crystallography. DRIFT (KBr, cm^{-1}): 2961 m br, 2927 m, 2896 w, 2084 m, 1929 w, 1520 s, 1446 s, 1374 w, 1325 w, 1279 m, 1243 m, 1199 m, 1105 w, 1047 m br, 900 s br, 838 m, 789 w, 762 m, 683 w, 609 w. ^{1}H NMR (400.13 MHz, C_7D_8, 25 °C): δ 7.88 (d, $^3J_{YH}$ = 4.6 Hz, 1 H, NC(H)N), 7.00−7.13 (m, 6H, Ar), 5.06 (m, $^3J_{HH}$ = 2.9 Hz, 4H, SiH), 3.76 (t, 4H, α-CH_2, thf), 2.65 (q, 8H, CH_2), 1.36 (t, 4H, β-CH_2, thf), 1.13 (t, 12H, CH_3), 0.29 (s br, 24H, $Si(CH_3)_2$) ppm. ^{13}C NMR (100.62 MHz, C_7D_8, 25 °C): δ 177.9 (NC(H)N), 145.2 (Ar-C), 137.9 (Ar-C), 125.4 (Ar-CH), 123.9 (Ar-CH), 69.1 (α-CH_2, thf), 25.1 (β-CH_2, thf), 25.0 (CH), 14.5 (CH_3), 2.1 (s br, $Si(CH_3)_2$) ppm. Anal. Calcd for $C_{33}H_{63}N_4OSi_4Y$: C, 54.06; H, 8.66; N, 7.64. Found: C, 53.45; H, 9.09; N, 7.32.

*Y(DippForm)[N(SiHMe$_2$)$_2$]$_2$(thf) (**1b**).* Following the procedure described above, $Y[N(SiHMe_2)_2]_3(thf)_2$ (100 mg, 0.16 mmol) and DippFormH (57 mg, 0.16 mmol) were reacted. Recrystallization of the product from hexane yielded 50 mg (40%) of **1b** as colorless crystals suitable for X-ray crystallography. DRIFT (KBr, cm^{-1}): 2959 s, 2923 m, 2867 m, 2074 m, 1931 w, 1664 s, 1587 w, 1526 m, 1461 m, 1382 w, 1321 w, 1286 m, 1254 m, 1182 w, 1018 m br, 897 s, 838 m, 800 s br, 766 m, 678 w, 610 w. ^{1}H NMR (400.13 MHz, C_6D_6, 25 °C): δ 8.22 (d, $^3J_{YH}$ = 4.6, 1H, NC(H)N), 7.06−7.14 (m, 6H, Ar), 5.07 (sep,, $^3J_{HH}$ = 2.9 Hz, 4H, SiH), 3.76 (t, 4H, α-CH_2, thf), 3.66 (sep, $^3J_{HH}$ = 6.9 Hz, 4H, CH), 1.36 (t, 4H, β-CH_2, thf), 1.19 (br, 24H, CH_3), 0.29 (s br, $^3J_{HH}$ = 2.9 Hz, 24H, $Si(CH_3)_2$) ppm. ^{13}C NMR (100.62 MHz, C_6D_6, 25 °C): δ 170.1 (NC(H)N), 143.1 (Ar-C), 124.9 (Ar-CH), 123.9 (Ar-CH), 65.07 (β-CH_2, thf), 27.9 (CH), 24.8 (s br α-CH_2, thf + CH_3), 3.3 (s br, $Si(CH_3)_2$) ppm. Anal. Calcd for $C_{37}H_{71}N_4OSi_4Y$: C, 56.31; H, 9.07; N, 7.09. Found: C, 56.40; H, 8.99; N, 7.03.

*[Y(EtForm)$_2${N(SiHMe$_2$)$_2$}] (**1c**).* Following the procedure described above, $Y[N(SiHMe_2)_2]_3(thf)_2$ (100 mg, 0.16 mmol) and EtFormH (96 mg, 0.31 mmol) were reacted. Recrystallization of the product from hexane yielded 48 mg (36%) of **1c** as colorless crystals not suitable for X-ray crystallography. DRIFT (KBr, cm^{-1}): 2965 s, 2931 m, 2872 w, 2060 m, 1925 w, 1523 s, 1448 s, 1374 w, 1323 w, 1280 s, 1245 m, 1199 m, 1105 w, 946 w, 894 s br, 840 w, 797 w, 759 m, 689 w, 610 w. ^{1}H NMR (400.13 MHz, C_6D_6, 25 °C): δ = 8.01 (d, $^3J_{YH}$ = 4.6 Hz, 2H, NC(H)N), 7.16 (s br, 12H, Ar), 5.16 (m, $^3J_{HH}$ = 2.9 Hz, 2H, SiH), 2.77 (q, 16H, CH_2), 1.23 (t, 24H, CH_3), 0.24 (s br, $^3J_{HH}$ = 2.9, 12H, $Si(CH_3)_2$) ppm. ^{13}C NMR (100.62 MHz, C_6D_6, 25 °C): δ 170.77 (NC(H)N), 145.8 (Ar-C), 137.6 (Ar-C), 125.6 (Ar-CH), 124.4 (Ar-CH), 25.2 (CH_2), 14.72 (CH_3), 2.29 ($Si(CH_3)_2$) ppm. Anal. Calcd for $C_{46}H_{68}N_5Si_2Y$: C, 66.08; H, 8.20; N, 8.38. Found: C, 65.92; H, 8.12; N, 8.33.

*Y(EtForm)(AlMe$_4$)$_2$ (**2a**).* Following the procedure described above, $Y(AlMe_4)_3$ (150 g, 0.43 mmol) and EtFormH (140 mg, 0.45 mmol) were reacted. Recrystallization of the product from hexane yielded 184 mg (65%) of **2a** as colorless crystals not suitable for X-ray crystallography. DRIFT (KBr, cm^{-1}): 2966 m, 2926 m, 2885 w, 1507 s, 1448 m, 1374 w, 1327 w, 1274 m, 1191 w, 1107 w, 772 w, 719 s, 696 s, 611 w, 571 w, 550 w. ^{1}H NMR (400.13 MHz, C_6D_6, 25 °C): δ 7.63 (d, $^3J_{Y,H}$ = 4.6 Hz, 1H, NC(H)N), 6.94−6.99 (m, 6H, Ar), 2.56 (q, $^3J_{HH}$ = 7.4 Hz, 8H, CH_2), 1.12 (t, $^3J_{HH}$ = 7.4 Hz, 12H, CH_3), −0.24 (d, $^3J_{YH}$ = 3 Hz, 24 H, $Al(CH_3)_4$) ppm. ^{13}C NMR (100.62 MHz, C_7D_8, 25 °C): δ 172.8 (NC(H)N), 144.0 (Ar-C), 137.6 (Ar-C), 126.4 (Ar-CH), 125.3 (Ar-CH), 25.2 (CH_2), 15.2 (CH_3), 1.8 (s br, $Al(CH_3)_4$) ppm. Anal. Calcd for $C_{29}H_{51}N_2Al_2Y$: C, 61.04; H, 9.01; N, 4.91. Found: C, 60.25; H, 8.46; N, 4.96. This compound was also formed by addition of $AlMe_3$ (4.03 mg, 0.056 mmol) to **1a** (10 mg, 0.014 mmol) in C_6D_6 in a J. Young valve NMR tube at 25 °C. When the temperature was lowered from +25 to −80 °C in toluene-d_8, the signals of complex **2a** did not reveal any decoalescence of the $[Al(CH_3)_4]$ resonance.

*[La(EtFormAlMe$_3$)(AlMe$_4$)$_2$](C$_7$H$_8$)$_{1.5}$ (**2b**).* Following the procedure described above, $La(AlMe_4)_3$ (145 mg, 0.35 mmol) and EtFormH (112 mg, 0.36 mmol) were reacted. Recrystallization of the product from toluene yielded 160 mg (56%) of **2b** as colorless crystals suitable for X-ray crystallography from an orange solution. DRIFT (KBr, cm^{-1}): 2969 m, 2919 m, 2889 w, 1536 s, 1442 m, 1362 w, 1330 w, 1189 m, 1106 w, 841 w, 762 w, 694 s br, 587 m, 568 w, 545 w, 520 w. ^{1}H NMR (500.13 MHz, C_7D_8, 25 °C): δ 7.64 (s br, 1H, NC(H)N), 7.03 - 6.76 (m, 6H, Ar), 3.22 (q, , $^3J_{HH}$ = 7.4 Hz, 2H, CH_2), 2.46 (q, $^3J_{HH}$ = 7.4 Hz, 2H, CH_2), 2.25 (q, $^3J_{HH}$ = 7.4 Hz, 4H, CH_2), 1.06 (t, $^3J_{HH}$ = 7.4 Hz, 6 H, CH_3), 0.98 (t, $^3J_{HH}$ = 7.4 Hz, 6H, CH_3), −0.46 (s br, 24H, $Al(CH_3)_4$), −0.53 (s, 9H, $Al(CH_3)_3$) ppm. ^{1}H NMR (500.13 MHz, C_7D_8, −52 °C): δ 7.64 (s br, 1H, NC(H)N), 7.18 (d, 1H, *m*-Ar-H), 6.87 (t, 1H, *p*-Ar-H), 6.76 (d, 1H, *m*-Ar-H), 6.67 (d, 1H, *m*-Ar-H), 6.62 (t, 1H, *p*-Ar-H), 6.12 (d, 1H, *m*-Ar-H), 3.22 (m, 2H, CH_2), 2.46 (m, 2H, CH_2), 2.33 (m, 2H, CH_2), 2.26 (m, 2H, CH_2), 1.06 (t, 6H, CH_3), 0.98 (t, 6H, CH_3), −0.12 (s br, 3H, $Al(CH_3)_4$), −0.13 (s br, 3H, $Al(CH_3)_4$), −0.28 (s br, 3H, $Al(CH_3)_4$), −0.31 (s, 9H, $Al(CH_3)_3$), −0.45 (s br, 3H, $Al(CH_3)_4$), −0.46 (s br, 3H, $Al(CH_3)_4$), −0.50 (s br, 3H, $Al(CH_3)_4$), −0.51 (s, 3H, $Al(CH_3)_4$), −0.68 (s, 3H, $Al(CH_3)_4$) ppm. ^{13}C NMR (125.77 MHz, C_7D_8, 25 °C): δ 169.0 (NC(H)N), 155.5 (Ar), 146.7 (Ar), 141.9 (Ar), 139.4 (Ar), 131.4 (Ar), 130.0 (Ar), 129.2 (Ar), 128.3 (Ar), 26.1 (CH_2), 25.1 (CH_2), 16.22 (CH_3), 12.9 (CH_3), −7.1 (s br, $Al(CH_3)_3$ and $Al(CH_3)_4$) ppm. Anal. Calcd for $C_{32}H_{60}N_2Al_3La\cdot(C_7H_8)_{1.5}$: C, 61.44; H, 8.73; N, 3.37. Anal. Calcd for $C_{32}H_{60}N_2Al_3La\cdot C_7H_8$: C, 59.68; H, 8.73; N, 3.57. Found: C, 59.13; H, 7.57; N, 3.61 (microanalysis revealed that half a toluene molecule in the lattice was lost upon drying the sample in vacuo).

*Y(MesFormAlMe$_3$)(AlMe$_4$)$_2$ (**3a**).* Following the procedure described above, $Y(AlMe_4)_3$ (100 mg, 0.28 mmol) and MesFormH (80 mg, 0.28 mmol) were reacted. Recrystallization of the product from hexane yielded 132 mg (65%) of **3a** as colorless crystals suitable for X-ray crystallography. DRIFT (KBr, cm^{-1}): 2922 m br, 2886 m, 2864 m, 1510 s, 1477 s, 1376 w, 1304 w, 1267 s, 1224 m, 1187 m, 1161 w, 1031 w, 968 w, 922 w, 854 m, 720 s, 692 s br, 572 m, 533 w. ^{1}H NMR (400.13 MHz, C_6D_6, 25 °C): δ 7.74 (d, $^3J_{YH}$ = 4.6 Hz, 1H, NC(H)N), 6.74 (br s, 4H, Ar), 2.13 (s, 6H; *p*-CH_3), 2.11 (s, 12H; *o*-CH_3), −0.09 (d, $^3J_{YH}$ = 3 Hz, 24H, $Al(CH_3)_4$) ppm. ^{13}C NMR (100.62 MHz, C_6D_6, 25 °C): δ 172.9 (NC(H)N), 143.1 (Ar-C), 134.06 (Ar-C), 131.43 (Ar-C), 129.52 (Ar-C), 20.5 (CH_3), 19.8

(CH_3), 1.89 (br $Al(CH_3)_4$). Anal. Calcd for $C_{27}H_{47}N_2Al_2Y$: C, 59.77; H, 8.73; N, 5.16. Found: C, 59.52; H, 8.25; N, 5.08.

*[La{η^1(N):η^6(Ar)-$Me_2CH_2FormAlMe_3$}($AlMe_3$)($AlMe_4$)][La($Me_2CH_2FormAlMe_3$)($AlMe_3$)($AlMe_4$)](C_6H_{14})$_{1.5}$ (**3bc**) and La[η^1(N):η^6(Ar)-$Me_2CH_2FormAlMe_3$]($AlMe_3$)($AlMe_4$) (**3b**).* Following the procedure described above, $La(AlMe_4)_3$ (100 mg, 0.25 mmol) and MesFormH (70 mg, 0.25 mmol) were reacted. Crystallization of the product from toluene yielded first 76 mg (44%) of **3bc** as colorless crystals suitable for X-ray crystallography from a yellow solution. After filtering, drying of the yellow filtrate in vacuo gave 57 mg (35%) of **3b** as a residue of the pure compound. Characterization data for **3bc** are as follows: DRIFT (KBr, cm^{-1}) 2921 m br, 2882 m, 1552 s, 1468 m, 1379 w, 1322 m, 1210 m br, 1186 m br, 1106 w, 1032 w, 968 w, 941 w, 854 m, 692 s br, 570 m br, 533 w, 506 w. ^{1}H NMR (400.13 MHz, C_6D_6, 25 °C): δ 7.74 (s, 1H, NC(H)N, **3b**), 6.80 (s, 1H, Ar, **3c**), 6.75 (s, 2H, Ar, **3b**), 6.73 (s, 1H, Ar, **3c**), 6.63 (s, 1H, Ar, **3b**), 6.58 (s, 1H, Ar), 6.57 (s, 1H, NC(H)N, **3c**), 6.53 (s, 1H, Ar, **3b**), 6.47 (s, 1H, Ar, **3c**), 2.65 (d, $^2J_{HH}$ = 15.5 Hz, 1H, CH_2, 3c), 2.34 (d, $^2J_{HH}$ = 15.5 Hz, 1H, CH_2, **3b**), 2.26 (s, 3H; CH_3, **3b**), 2.25 (s, 3H, CH_3, **3b**), 2.12 (s, 3H, CH_3, **3c**), 2.09 (s, 3H, CH_3, **3c**), 2.00 (s, 3H, CH_3, **3c**), 1.99 (s, 3H, CH_3, **3c**), 1.97 (s, 3H, CH_3, **3c**), 1.93 (s, 3H, CH_3, **3b**), 1.81 (s, 3H, CH_3, **3c**), 1.77 (d, $^2J_{HH}$ = 15.5 Hz, 1H, CH_2, **3c**), 1.73 (s, 3H, CH_3, **3b**), 1.27 (d, 1H, CH_2, $^2J_{HH}$ = 15.5 Hz, **3b**), 1.23 (m, 8H, CH_2 of hexane), 0.88 (t, 6H, CH_3 of hexane), −0.14 (s br, 9H, $Al(CH_3)_3$, **3c**), −0.18 (s br, 12H, $Al(CH_3)_4$, **3c**), −0.20 (s br, 9H, $Al(CH_3)_3$, **3c**), −0.28 (s br, 9H, $Al(CH_3)_3$, **3b**), −0.41 (s br, 9H, $Al(CH_3)_3$, **3b**), −0.56 (s br, 12H, $Al(CH_3)_4$, **3b**) ppm. ^{13}C NMR (100.62 MHz, C_6D_6, 25 °C): δ 166.1 (NC(H)N, **3b**), 164.4 (NC(H)N, **3c**), 154.9−127.2 (Ar-C, **3b** + **3c**), 32.3 (CH_3, hex), 27.6 (CH_2, **3b**), 24.9 (CH_2, **3c**), 23.4 (CH_2, hex), 21.8 (CH_3, **3b**), 21.3 (br, 2 CH_3, **3c**), 21.2 (br, CH_3, **3b**), 20.3 (CH_3, **3c**), 19.6 (CH_3, **3b**), 19.5 (br, 2 CH_3, **3c**), 19.2 (CH_3, **3c**), 18.9 (CH_3, **3b**), 14.7 (CH_2, hex), 4.9 (br, $Al(CH_3)_4$, **3c**), 2.9 (br, $Al(CH_3)_4$, **3b**), −0.1 (br, $Al(CH_3)_3$, **3b**), −1.6 ($Al(CH_3)_3$, **3c**), −1.7 ($Al(CH_3)_3$, **3c**), −6.3 (br, $Al(CH_3)_3$, **3a**) ppm. Anal. Calcd for $C_{58}H_{104}N_4Al_6La_2{\cdot}C_6H_{14}$: C, 55.57; H, 8.60; N, 4.05. Calcd for $C_{58}H_{104}N_4Al_6La_2{\cdot}1.5C_6H_{14}$: C, 56.41; H, 8.83; N, 3.93. Found: C, 56.20; H, 7.09; N, 4.29 (the microanalysis suggests 1.5 hexane molecule in the lattice, in accordance with the crystal structure, while the ^{1}H NMR of **3bc** showed that half of a hexane molecule from the lattice was lost upon drying the sample in vacuo prior to dissolution).

Characterization data for **3b** are as follows: DRIFT (KBr, cm^{-1}) 2914 m br, 2881 w, 1541 s, 1468 m, 1380 w, 1327 m, 1211m, 1184 m, 1150 w, 1032 w, 968 w, 941 w, 851 w, 692 s br, 574 m, 533 w, 522 w, 503 w; ^{1}H NMR (400.13 MHz, C_6D_6, 25 °C): δ 7.74 (s, 1H, NC(H)N), 6.75 (s, 1H, Ar), 6.63 (s, 1H, Ar), 6.53 (s, 1H, Ar), 6.47 (s, 1H, Ar), 2.34 (d, $^2J_{HH}$ = 15.5 Hz, 1H, CH_2), 2.26 (s, 3H, *p*-CH_3), 2.25 (s, 3H, *p*-CH_3), 1.99 (s, 3H, *o*-CH_3), 1.93 (s, 3H, *o*-CH_3), 1.73 (s, 3H, *o*-CH_3), 1.27 (d, $^2J_{HH}$ = 15.5 Hz, 1H, CH_2), −0.28 (s br, 9H, $Al(CH_3)_3$), −0.41 (s br, 9H, $Al(CH_3)_3$), −0.56 (s br, 12H, $Al(CH_3)_4$) ppm; ^{13}C NMR (100.62 MHz, C_6D_6, 25 °C): δ 166.14 (NC(H)N), 154.9 (Ar-C), 148.1 (Ar-C), 140.7 (Ar-C), 140.08 (Ar-C), 138.8 (Ar-C), 138.5 (Ar-CH), 135.1 (Ar-CH), 134.8 (Ar-CH), 133.5 (Ar-C), 131.6 (Ar-C), 129.8 (Ar-CH), 127.2 (Ar-CH), 27.6 (CH_2), 21.8 (CH_3), 21.2 (CH_3), 20.3 (CH_3), 19.6 (CH_3), 18.9 (CH_3), 2.9 (br $Al(CH_3)_4$), −0.1 ($Al(CH_3)_3$), −6.3 (s br, $Al(CH_3)_3$) ppm. Anal. Calcd for $C_{29}H_{52}N_2Al_3La$: C, 53.70; H, 8.08; N, 4.32. Found: C, 53.34; H, 7.19; N, 4.38.

*Y(DippForm)($AlMe_4$)$_2$ (**4a**).* Following the procedure described above, $Y(AlMe_4)_3$ (164 mg, 0.46 mmol) and DippFormH (171 mg, 0.46 mmol) were reacted. Recrystallization of the product from hexane yielded 185 mg (64%) of **4a** as colorless crystals suitable for X-ray crystallography. DRIFT (KBr, cm^{-1}): 2961 s, 2925 m, 2888 m, 1513 s, 1456 m, 1442 m, 1383 w, 1362 w, 1316 m, 1271 s, 1189 m, 1100 w, 805 m, 774 w, 759 w, 697 s br, 616 w, 575 w. ^{1}H NMR (400.13 MHz, C_6D_6, 25 °C): δ 8.05 (d, $^3J_{YH}$ = 4.6, 1H, NC(H)N), 7.06 (s br, 6H, Ar), 3.24 (sep, $^3J_{HH}$ = 6.9 Hz, 4H, CH), 1.12 (d, $^3J_{HH}$ = 78.4 Hz, 24H, CH_3), −0.24 (s, $^3J_{YH}$ = 3 Hz, 24H, $Al(CH_3)_4$) ppm. ^{13}C NMR (100.62 MHz, C_6D_6, 25 °C): δ 172.4 (NC(H)N), 142.5 (Ar-C), 142.3 (Ar-C), 125.9 (Ar-CH), 124.1 (Ar-CH), 28.6 (CH), 25.5 and 23.5 (CH_3), 2.1 (s br, $Al(CH_3)_4$) ppm. Anal. Calcd for $C_{33}H_{59}N_2Al_2Y$: C, 63.24; H, 9.49; N, 4.47. Found: C, 62.83; H, 8.61; N, 4.56. This compound was also formed by addition of $AlMe_3$ (3.65 mg, 0.051 mmol) to **1b** (10 mg, 0.0126 mmol) in C_6D_6 in a J. Young valve NMR tube at 25 °C.

*La(DippForm)($AlMe_4$)$_2$ (**4b**).* Following the procedure described above, $La(AlMe_4)_3$ (0.12 g, 0.29 mmol) and DippFormH (0.11 g, 0.31 mmol) were reacted. Recrystallization of the product from hexane yielded 140 mg (66%) of **4b** as colorless crystals suitable for X-ray crystallography. DRIFT (KBr, cm^{-1}): 2961 s, 2926 m, 2882 m, 1512 s, 1460 m, 1442 m, 1382 w, 1362 w, 1315 m, 1271 s, 1189 m, 1100 w, 804 m, 773 w, 759 w, 697 s br, 615 w, 576 w. ^{1}H NMR (400.13 MHz, C_6D_6, 25 °C): δ 8.17 (s br, 1H, NC(H)N), 7.06 (s br, 6H, Ar), 3.27 (sep, $^3J_{HH}$ = 6.9 Hz, 4H, CH), 1.12 (s br, 24H, CH_3), 0.00 (s br, 24H, $Al(CH_3)_4$) ppm. ^{13}C NMR (100.62 MHz, C_6D_6, 25 °C): δ 175.3 (NC(H)N), 143.8 (Ar-C), 142.8 (Ar-C), 126.1 (Ar-CH), 124.1 (Ar-CH), 29.0 (CH), 25.3 and 23.9 (CH_3), 4.8 (s br, $Al(CH_3)_4$) ppm. Anal. Calcd for $C_{33}H_{59}N_2Al_2La$: C, 58.57; H, 8.79; N, 4.14. Found: C, 58.57; H, 8.96; N, 4.09.

*Y(tBuForm)($AlMe_4$)$_2$ (**5a**).* Following the procedure described above, $Y(AlMe_4)_3$ (100 mg, 0.28 mmol) and *t*BuFormH (86 mg, 0.28 mmol) were reacted. Recrystallization of the product from hexane yielded 124 mg (77%) of **5a** as colorless crystals suitable for X-ray crystallography. DRIFT (KBr, cm^{-1}): 2958 m br, 2927 m, 2889 w, 1502 s, 1480 s, 1438 m, 1390 w, 1357 w, 1291 s, 1277 m, 1213 m br, 1085 w, 1055 w, 946 w, 774 m, 754 s, 720 s, 699 s br, 569 m, 518 w. ^{1}H NMR (400.13 MHz, C_6D_6, 25 °C): δ 7.66 (d, $^3J_{Y,H}$ = 4.6 Hz, 1H, NC(H)N), 7.29 (dd, 2H, Ar), 7.10 (td, 2H, Ar), 7.01 (td, 2H, Ar), 6.69 (dd, 2H, Ar), 1.34 (s br, 18 H, CH_3), −0.05 (d, $^3J_{YH}$ = 3 Hz, 24 H, $Al(CH_3)_4$) ppm. ^{13}C NMR (100.62 MHz, C_6D_6, 25 °C): δ 169.3 (NC(H)N), 144.7 (Ar-C), 144.2 (Ar-C), 127.2 (Ar-CH), 127.1 (Ar-CH), 126.6 (Ar-CH), 125.8 (Ar-CH), 35.4 (C), 31.7 (CH_3), 2.5 (s br, $Al(CH_3)_4$) ppm. Anal. Calcd for $C_{29}H_{51}N_2Al_2Y$: C, 61.04; H, 9.01; N, 4.91. Found: C, 62.46; H, 8.29; N, 5.24.

*La(tBuForm)($AlMe_4$)$_2$ (**5b**).* Following the procedure described above, $La(AlMe_4)_3$ (0.05 g, 0.12 mmol) and *t*BuFormH (38 mg, 0.12 mmol) were reacted. Recrystallization of the product from hexane yielded 68 mg (72%) of **5b** as colorless crystals suitable for X-ray crystallography. DRIFT (KBr, cm^{-1}): 2966 m br, 2922 m, 2888 w, 1503 s, 1478 s, 1438 m, 1388 w, 1354 w, 1291 s, 1279 m, 1210 m br, 1085 w, 1055 w, 942 w, 773 m, 754 m, 716 s, 697 s br, 610 w, 569 m, 518 w. ^{1}H NMR (400.13 MHz, C_6D_6, 25 °C): δ 7.96 (s, 1H, NC(H)N), 7.13 (dd, 2H, Ar), 7.10 (td, 2H, Ar), 7.00 (td, 2H, Ar), 6.69 (dd, 2H, Ar), 1.37 (s, 18H, CH_3), −0.05 (s, 24H, $Al(CH_3)_4$) ppm. ^{13}C NMR (100.62 MHz, C_6D_6, 25 °C): δ 166.1 (NC(H)N), 148.6 (Ar-C), 143.7 (Ar-C), 127.4 (Ar-CH), 127.1 (Ar-CH), 126.6 (Ar-CH), 125.5 (Ar-CH), 35.5 (C), 31.8 (CH_3), 4.9 (s br, $Al(CH_3)_4$) ppm. Anal. Calcd for $C_{29}H_{51}N_2Al_2La$: C, 56.12; H, 8.28; N, 4.51. Found: C, 55.75; H, 8.52; N, 4.38.

Polymerization of Isoprene. A detailed polymerization procedure (Table 4, run 1) is described as a typical example. $[Ph_3C][B(C_6F_5)_4]$ (**A**, 18 mg, 0.02 mmol, 1 equiv) was added to a solution of **2a** (11 mg, 0.02 mmol) in toluene (8 mL), and the mixture was aged at ambient temperature for 30 min. After the addition of isoprene (2.0 mL, 20 mmol), the polymerization was carried out at ambient temperature for 24 h. The reaction was terminated by pouring the polymerization mixture into a large quantity of acidified 2-propanol containing 0.1% (w/w) 2,6-di-*tert*-butyl-4-methylphenol as a stabilizer. The polymer was washed with 2-propanol and dried under vacuum at ambient temperature to constant weight. The polymer yield was determined gravimetrically.

X-ray Crystallography and Crystal Structure Determination of 1a,b, 2a,b, 3bc, 3a, 4a,b, and 5a,b. Crystals suitable for diffraction experiments were selected in a glovebox and mounted in Paratone-N oil inside a nylon loop. Data collection was done at 173(2) K on a STOE IPD II diffractometer using graphite-monochromated Mo Kα radiation (λ = 0.71073 Å), performing ω scans in two φ positions. Structure solutions and refinements were performed using the programs SHELXS-97[75] and SHELXL-97[76] through the graphical interface X-Seed, which was also used to generate the figures. All CIF files were checked at http://www.checkcif.iucr.org/. For further experimental details on refinement and crystallographic data see Table 6.

Table 6. Crystallographic Data for Compounds 1a,b, 2a,b, 3bc, 3a, 4a,b, and 5a,b

	1a	1b	2a	2b	3bc
formula	$C_{33}H_{63}N_4OSi_4Y$	$C_{37}H_{71}N_4OSi_4Y$	$C_{29}H_{51}Al_2N_2Y$	$C_{42.50}H_{72}Al_3LaN_2$	$C_{64}H_{118}Al_6La_2N_4$
fw	733.14	789.25	570.59	830.87	1383.32
color/habit	none/block	none/block	none/block	none/block	none/block
crystal dimens, mm^3	0.30 × 0.22 × 0.20	0.70 × 0.25 × 0.25	0.60 × 0.50 × 0.35	0.35 × 0.25 × 0.25	0.50 × 0.40 × 0.10
cryst syst	triclinic	monoclinic	triclinic	monoclinic	triclinic
space group	$P\bar{1}$	$P2_1/c$	$P\bar{1}$	$P2_1/c$	$P\bar{1}$
a, Å	12.1707(6)	18.758(4)	11.5677(11)	20.3515(14)	10.238(2)
b, Å	19.6297(10)	11.075(2)	12.5648(11)	18.6499(11)	14.998(3)
b, Å	20.3094(10)	21.964(4)	12.6101(11)	12.4888(8)	27.636(6)
α, deg	61.861(4)	90.00	112.244(7)	90.00	75.10(3)
β, deg	87.197(4)	93.14(3)	102.724(7)	96.487(5)	79.68(3)
γ, deg	77.763(4)	90.00	91.594(3)	90.00	74.01(3)
V, $Å^3$	4174.0(4)	4556.4(16)	1642.2(3)	4709.8(5)	3915.3(13)
Z	4	4	2	4	2
T, K	173(2)	173(2)	173(2)	173(2)	173(2)
D_{calcd}, g/cm^3	1.167	1.151	1.156	1.172	1.173
μ, mm^{-1}	1.540	1.415	1.849	0.990	1.178
$F(000)$	1568	1696	608	1748	1444
θ range, deg	2.85−25.35	4.71−27.10	2.69−26.37	3.28−27.10	2.44−27.50
index ranges (h, k, l)	−14 to +14, −23 to +23, −23 to +24	−24 to +24, −14 to +14, −28 to +28	−15 to +15, −15 to +15, −15 to +15	−26 to +26, −23 to +23, −16 to +15	−13 to +13, −19 to +17, −35 to +35
no. of rflns collected	55191	64335	24081	68345	38479
no. of indep rflns/R_{int}	15293/0.0630	9983/0.1667	6685/0.1009	10354/0.0652	17822/0.0612
no. of obsd rflns ($I > 2\sigma(I)$)	13705	7522	6369	8714	12270
no. of data/restraints/params	15293/23/849	9983/2/463	6685/56/305	10354/75/469	17822/0/707
R1/wR2 ($I > 2\sigma(I)$)[a]	0.0841/0.1229	0.0954/0.1522	0.0696/0.1720	0.0474/0.0871	0.0708/0.1557
R1/wR2 (all data)[a]	0.0946/0.1256	0.1318/0.1641	0.0727/0.1746	0.0612/0.0916	0.1151/0.1738
GOF (on F^2)[a]	1.433	1.244	1.139	1.140	1.078
largest diff peak and hole (e $Å^{-3}$)	0.39/−0.62	1.67/−0.94	1.79/−1.74	0.94/−0.86	2.22/−1.20
	3a	**4a**	**4b**	**5a**	**5b**
formula	$C_{27}H_{47}Al_2N_2Y$	$C_{33}H_{59}Al_2N_2Y$	$C_{33}H_{59}Al_2LaN_2$	$C_{29}H_{51}Al_2N_2Y$	$C_{29}H_{51}Al_2LaN_2$
fw	542.54	626.69	676.69	570.61	620.59
color/habit	none/block	none/block	none/block	none/block	none/block
crystal dimens, mm^3	0.50 × 0.40 × 0.30	0.45 × 0.20 × 0.10	0.40 × 0.20 × 0.20	0.40 × 0.20 × 0.10	0.35 × 0.30 × 0.25
cryst syst	monoclinic	monoclinic	monoclinic	triclinic	triclinic
space group	$C2$	$P2_1/n$	$P2_1/n$	$P\bar{1}$	$P\bar{1}$
a, Å	28.475(6)	13.249(3)	13.323(3)	9.2439(3)	9.2922(19)
b, Å	9.796(2)	16.148(3)	16.235(3)	12.2091(4)	12.290(3)
b, Å	24.756(5)	17.544(4)	17.615(4)	16.2281(5)	16.392(3)
α, deg	90.00	90.00	90.00	110.156(2)	109.91(3)
β, deg	114.67(3)	100.35(3)	99.65(3)	93.658(2)	94.15(3)
γ, deg	90.00	90.00	90.00	106.790(2)	105.93(3)

dx.doi.org/10.1021/om301010m | Organometallics 2013, 32, 1209−1223

Table 6. continued

	3a	4a	4b	5a	5b
V, Å^3	6275(2)	3692.4(13)	3756.2(13)	1618.63(9)	1663.7(6)
Z	8	4	4	2	2
T, K	173(2)	173(2)	173(2)	173(2)	173(2)
D_{calcd} g/cm^3	1.149	1.127	1.197	1.171	1.239
μ, mm^{-1}	1.930	1.648	1.205	1.874	1.354
F(000)	2304	1344	1416	608	644
θ range, deg	3.25−27.50	4.72−27.10	4.78−28.28	1.88−27.50	4.92−22.18
index ranges (h, k, l)	−36 to +36, −12 to +12, −32 to +29	−16 to +16, −20 to +20, −22 to +22	−17 to +17, −21 to +21, −21 to +23	−11 to +12, −15 to +15, −21 to +21	−12 to +12, −16 to +16, −22 to +22
no. of rflns collected	51917	55342	28586	39939	23132
no. of indep rflns/R_{int}	14434/0.1185	8105/0.1533	9204/0.0557	7405/0.0386	8876/0.0490
no. of obsd rflns ($I > 2\sigma(I)$)	12078	6414	7662	6232	7632
no. of data/restraints/params	14434/1/598	8105/0/355	9204/0/427	7405/0/317	8876/0/321
R1/wR2 ($I > 2\sigma(I)$)[a]	0.0745/0.1454	0.0902/0.1360	0.0398/0.0825	0.0335/0.0846	0.0350/0.0723
R1/wR2 (all data)[a]	0.0945/0.1534	0.1183/0.1439	0.0534/0.0869	0.0472/0.0896	0.0463/0.0754
GOF (on F^2)[a]	1.200	1.309	1.081	1.073	1.040
largest diff peak and hole (e Å^{-3})	1.10/−1.27	0.46/−0.92	0.80/−0.99	0.33/−0.40	0.92/−0.77

[a] $R1 = \sum(||F_o| - |F_c||)/\sum|F_o|$; $wR2 = \{\sum[w(F_o^2 - F_c^2)^2]/\sum[w(F_o^2)^2]\}^{1/2}$; $GOF = \sum[w(F_o^2 - F_c^2)^2]/(n - p)\}^{1/2}$.

Variata are as follows. **1a**: Two discrete molecules were observed in the asymmetric unit. One thf was modeled as disordered with C atom position C31 (refined occupancy 0.54:0.46). DELU and SIMU restrains were applied on C63, C64, C65 and C66. **1b**: Methyl carbons on Si4 were modeled as disordered on C30, C30A, C31, and C31A (refined occupancy 0.64:0.36), and EADP and DFIX commands were applied on them. **2a**: SIMU and DELU commands were applied for C9, C10, C11, C12, C13, and C14. The EADP command was applied on C28 and C29. The DFIX command was used for C17 and C18 and also C25 and C28. The DFIX command was used for C19 and H19, C1 and H1A, and also C6 and H6A. **2b**: 1.5 toluene molecules in the lattice were modeled. SIMU and DELU were applied on C101 C102, C103, C10a, C10b, C10c, C100, and C40 as well as C26 and C31. The ISOR command was applied on C26, C31, and C40. **3a**: Two discrete molecules were observed in the asymmetric unit. TWIN and BASF commands were applied. **3bc**: Two discrete molecules were observed in the asymmetric unit as discussed above.

■ ASSOCIATED CONTENT

Supporting Information

CIF files giving full crystallographic data for complexes **1a,b**, **2a,b**, **3bc**, **3a**, **4a,b**, and **5a,b** and a table giving selected bond angles of **2a,b**, **3a**, **4a,b**, and **5a,b**. This material is available free of charge via the Internet at http://pubs.acs.org. Crystallographic data have also been deposited at the Cambridge Crystallographic Data Centre under CCDC reference numbers 907682−907691 and can be obtained free of charge via www.ccdc.cam.ac.uk/data_request/cif.

■ AUTHOR INFORMATION

Corresponding Author

*E-mail: glen.deacon@monash.edu (G.B.D.); peter.junk@jcu.edu.au (P.C.J.); reiner.anwander@uni-tuebingen.de (R.A.).

Notes

The authors declare no competing financial interest.

■ ACKNOWLEDGMENTS

This work was performed with the support of ARC grant DP0984775. S.H. is grateful to the School of Chemistry at Monash for a scholarship. We also acknowledge support from the German Science Foundation.

■ REFERENCES

(1) (a) Edelmann, F. T. *Coord. Chem. Rev.* **1994**, *137*, 403−481. (b) Edelmann, F. T. Advances in the Coordination Chemistry of Amidinate and Guanidinate Ligands. In *Advances in Organometallic Chemistry*; Hill, A. F., Fink, M. J., Eds.; Academic Press: New York, 2008; Vol. 57, pp 183−352. (c) Edelmann, F. T. *Chem. Soc. Rev.* **2009**, *38*, 2253−2268. (d) Edelmann, F. T. *Chem. Soc. Rev.* **2012**, *41*, 7657−7672.

(2) Edelmann, F. T.; Freckmann, D. M. M.; Schumann, H. *Chem. Rev.* **2002**, *102*, 1851−1896.

(3) Piers, W. E.; Emslie, D. J. H. *Coord. Chem. Rev.* **2002**, *233−234*, 131−155.

(4) Gade, L. H. *Acc. Chem. Res.* **2002**, *35*, 575−582.

(5) Kempe, R. *Angew. Chem., Int. Ed.* **2000**, *39*, 468−493.

(6) Fischbach, A.; Anwander, R. *Adv. Polym. Sci.* **2006**, *204*, 155−281.

(7) Zimmermann, M.; Anwander, R. *Chem. Rev.* **2010**, *110*, 6194−6259.

(8) Cole, M. L.; Deacon, G. B.; Forsyth, C. M.; Junk, P. C.; Konstas, K.; Wang, J. *Chem. Eur. J.* **2007**, *13*, 8092−8110.

(9) Cole, M. L.; Deacon, G. B.; Junk, P. C.; Konstas, K. *Chem. Commun.* **2005**, 1581−1583.

(10) Luo, Y.; Wang, X.; Chen, J.; Luo, C.; Zhang, Y.; Yao, Y. *J. Organomet. Chem.* **2009**, *694*, 1289−1296.

(11) Bambirra, S.; Meetsma, A.; Hessen, B. *Organometallics* **2006**, *25*, 3454−3462.
(12) Bambirra, S.; Bouwkamp, M. W.; Meetsma, A.; Hessen, B. *J. Am. Chem. Soc.* **2004**, *126*, 9182−9183.
(13) Cole, M. L.; Junk, P. C. *Chem. Commun.* **2005**, 2695−2697.
(14) Aubrecht, K. B.; Chang, K.; Hillmyer, M. A.; Tolman, W. B. *J. Polym. Sci., Part A: Polym. Chem.* **2001**, *39*, 284−293.
(15) Bambirra, S.; van Leusen, D.; Meetsma, A.; Hessen, B.; Teuben, J. H. *Chem. Commun.* **2003**, 522−523.
(16) Luo, Y.; Yao, Y.; Shen, Q.; Sun, J.; Weng, L. *J. Organomet. Chem.* **2002**, *662*, 144−149.
(17) Zhou, L.; Yao, Y.; Zhang, Y.; Xue, M.; Chen, J.; Shen, Q. *Eur. J. Inorg. Chem.* **2004**, 2167−2172.
(18) Jing-Lei, C.; Ying-Ming, Y.; Yun-Jie, L.; Li-Ying, Z.; Yong, Z.; Qi, S. *J. Organomet. Chem.* **2004**, *689*, 1019−1024.
(19) Zhou, Y.; Yap, G. P. A.; Richeson, D. S. *Organometallics* **1998**, *17*, 4387−4391.
(20) Ge, S.; Meetsma, A.; Hessen, B. *Organometallics* **2008**, *27*, 3131−3135.
(21) Luo, Y.; Fan, S.; Yang, J.; Fang, J.; Xu, P. *Dalton Trans.* **2011**, *40*, 3053−3059.
(22) Luo, Y.; Xu, P.; Lei, Y.; Zhang, Y.; Wang, Y. *Inorg. Chim. Acta* **2010**, *363*, 3597−3601.
(23) Deacon, G. B.; Forsyth, C. M.; Junk, P. C.; Wang, J. *Inorg. Chem.* **2007**, *46*, 10022−10030.
(24) Zhang, L.; Nishiura, M.; Yuki, M.; Luo, Y.; Hou, Z. *Angew. Chem., Int. Ed.* **2008**, *47*, 2642−2645.
(25) Kretschmer, W. P.; Meetsma, A.; Hessen, B.; Schmalz, T.; Qayyum, S.; Kempe, R. *Chem. Eur. J.* **2006**, *12*, 8969−8978.
(26) Zimmermann, M.; Törnroos, K. W.; Waymouth, R. M.; Anwander, R. *Organometallics* **2008**, *27*, 4310−4317.
(27) Hayes, P. G.; Piers, W. E.; McDonald, R. *J. Am. Chem. Soc.* **2002**, *124*, 2132−2133.
(28) Döring, C.; Kretschmer, W. P.; Bauer, T.; Kempe, R. *Eur. J. Inorg. Chem.* **2009**, 4255−4264.
(29) Bambirra, S.; van Leusen, D.; Tazelaar, C. G. J.; Meetsma, A.; Hessen, B. *Organometallics* **2007**, *26*, 1014−1023.
(30) Bambirra, S.; van Leusen, D.; Meetsma, A.; Hessen, B.; H. Teuben, J. *Chem. Commun.* **2001**, 637−638.
(31) Wang, D.; Li, S.; Liu, X.; Gao, W.; Cui, D. *Organometallics* **2008**, *27*, 6531−6538.
(32) Yang, Y.; Wang, Q.; Cui, D. *J. Polym. Sci., Part A: Polym. Chem.* **2008**, *46*, 5251−5262.
(33) Yang, Y.; Liu, B.; Lv, K.; Gao, W.; Cui, D.; Chen, X.; Jing, X. *Organometallics* **2007**, *26*, 4575−4584.
(34) Luo, Y.; Nishiura, M.; Hou, Z. *J. Organomet. Chem.* **2007**, *692*, 536−544.
(35) Roberts, R. M. *J. Org. Chem.* **1949**, *14*, 277−284.
(36) Kuhn, K. M.; Grubbs, R. H. *Org. Lett.* **2008**, *10*, 2075−2077.
(37) Junk, P. C.; Cole, M. L. *Chem. Commun.* **2007**, 1579−1590.
(38) Zimmermann, M.; Estler, F.; Herdtweck, E.; Törnroos, K. W.; Anwander, R. *Organometallics* **2007**, *26*, 6029−6041.
(39) Duchateau, R.; van Wee, C. T.; Meetsma, A.; van Duijnen, P. T.; Teuben, J. H. *Organometallics* **1996**, *15*, 2279−2290.
(40) Döring, C.; Kempe, R. *Eur. J. Inorg. Chem.* **2009**, 412−418.
(41) (a) Le Roux, E.; Nief, F.; Jaroschik, F.; Törnroos, K. W.; Anwander, R. *Dalton Trans.* **2007**, 4866−4870. (b) Zimmermann, M.; Törnroos, K. W.; Anwander, R. *Angew. Chem., Int. Ed.* **2008**, *47*, 775−778. (c) Zimmermann, M.; Törnroos, K. W.; Sitzmann, H.; Anwander, R. *Chem. Eur. J.* **2008**, *14*, 7266−7277. (d) Robert, D.; Spaniol, T. P.; Okuda, J. *Eur. J. Inorg. Chem.* **2008**, 2801−2809. (e) Zimmermann, M.; Volbeda, J.; Törnroos, K. W.; Anwander, R. *C. R. Chim.* **2010**, *13*, 651−660.
(42) (a) Zimmermann, M.; Törnroos, K. W.; Anwander, R. *Organometallics* **2006**, *25*, 3593−3598. (b) Zimmermann, M.; Törnroos, K. W.; Anwander, R. *Angew. Chem., Int. Ed.* **2007**, *46*, 3126−3130.
(43) (a) Zimmermann, M.; Takats, J.; Kiel, G.; Törnroos, K. W.; Anwander, R. *Chem. Commun.* **2008**, 612−614. (b) Litlabø, R.; Zimmermann, M.; Saliu, K.; Takats, J.; Törnroos, K. W.; Anwander, R. *Angew. Chem., Int. Ed.* **2008**, *47*, 9560−9564.
(44) Chen, F.; Fan, S.; Wang, Y.; Chen, J.; Luo, Y. *Organometallics* **2012**, *31*, 3730−3735.
(45) Litlabo, R.; Lee, H. S.; Niemeyer, M.; Törnroos, K. W.; Anwander, R. *Dalton Trans.* **2010**, *39*, 6815−6825.
(46) Litlabø, R.; Enders, M.; Törnroos, K. W.; Anwander, R. *Organometallics* **2010**, *29*, 2588−2595.
(47) Kaneko, H.; Dietrich, H. M.; Schädle, C.; Tsurugi, H.; Törnroos, K. W.; Mashima, K.; Anwander, R. Submitted for publication.
(48) Anwander, R.; Klimpel, M. G.; Dietrich, H. M.; Shorokhov, D. J.; Scherer, W. *Chem. Commun.* **2003**, 1008−1009.
(49) Anwander, R.; Runte, O.; Eppinger, J.; Gerstberger, G.; Herdtweck, E.; Spiegler, M. *J. Chem. Soc., Dalton Trans.* **1998**, 847−858.
(50) (a) Görlitzer, H. W.; Spiegler, M.; Anwander, R. *J. Chem. Soc., Dalton Trans.* **1999**, 4287−4288. (b) Schmidt, J. A. R.; Arnold, J. *Chem. Commun.* **1999**, 2149−2150. (c) Hultzsch, K. C.; Gribkov, D. V.; Hampel, F. *J. Organomet. Chem.* **2005**, *690*, 4441−4452. (d) Cui, C.; Shafir, A.; Schmidt, J. A. R.; Oliver, A. G.; Arnold, J. *Dalton Trans.* **2005**, 1387−1393. (e) Alaaeddine, A.; Amgoune, A.; Thomas, C. M.; Dagorne, S.; Bellemin-Laponnaz, S.; Carpentier, J.-F. *Eur. J. Inorg. Chem.* **2006**, 3652−3658. (f) Cheng, J.; Takats, J.; Ferguson, M. J.; McDonald, R. *J. Am. Chem. Soc.* **2008**, *130*, 1544−1545. (g) Lazarov, B. B.; Hampel, F.; Hultzsch, K. C. *Z. Anorg. Allg. Chem.* **2007**, *633*, 2367−2373.
(51) (a) Zimmermann, M.; Frøystein, N. Å.; Fischbach, A.; Sirsch, P.; Dietrich, H. M.; Törnroos, K. W.; Herdtweck, E.; Anwander, R. *Chem. Eur. J.* **2007**, *13*, 8784−8800. (b) Occhipinti, G.; Meermann, C.; Dietrich, H. M.; Litlabø, R.; Auras, F.; Törnroos, K. W.; Maichle-Mössmer, C.; Jensen, V. R.; Anwander, R. *J. Am. Chem. Soc.* **2011**, *133*, 6323−6337.
(52) Knijnenburg, Q.; Smits, J. M. M.; Budzelaar, P. H. M. *Organometallics* **2006**, *25*, 1036−1046.
(53) Bruce, M.; Gibson, V. C.; Redshaw, C.; Solan, G. A.; White, A. J. P.; Williams, D. J. *Chem. Commun.* **1998**, 2523−2524.
(54) Evans, W. J.; Anwander, R.; Ziller, J. W. *Organometallics* **1995**, *14*, 1107−1109.
(55) Shannon, D. R. *Acta Crystallogr., Sect. A* **1976**, *32*, 751.
(56) Hauber, S.-O.; Lissner, F.; Deacon, G. B.; Niemeyer, M. *Angew. Chem., Int. Ed.* **2005**, *44*, 5871−5875.
(57) Yamamoto, J.; Wilkie, C. A. *Inorg. Chem.* **1971**, *10*, 1129−1133.
(58) Soto, C.; Wu, R.; Bennett, D. W.; Tysoe, W. T. *Chem. Mater.* **1994**, *6*, 1705−1711.
(59) For examples, see: (a) Deacon, G. B.; Feng, T. C.; Forsyth, C. M.; Gitlits, A.; Hockless, D. C. R.; Shen, Q.; Skelton, B. W.; White, A. H. *Dalton Trans.* **2000**, 961−966. (b) Giesbrecht, G. R.; Gordon, J. C.; Clark, D. L.; Hay, P. J.; Scott, B. L.; Tait, C. D. *J. Am. Chem. Soc.* **2004**, *126*, 6387−6401. (c) Cassani, M. C.; Duncalf, D. J.; Lappert, M. F. *J. Am. Chem. Soc.* **1998**, *120*, 12958−12959. (d) Thiele, K. H.; Bambirra, S.; Sieler, J.; Yelonek, S. *Angew. Chem., Int. Ed.* **1998**, *37*, 2886−2888. (e) Gerber, L. C. H.; Le Roux, E.; Törnroos, K. W.; Anwander, R. *Chem. Eur. J.* **2008**, *14*, 9555−9564. (f) Filatov, A. S.; Rogachev, A. Y.; Petrukhina, M. A. *J. Mol. Struct.* **2008**, *890*, 116−122. (g) Butcher, R. J.; Clark, D. L.; Grumbine, S. K.; Vincent-Hollis, R. L.; Scott, B. L.; Watkin, J. G. *Inorg. Chem.* **1995**, *34*, 5468−5476.
(60) Heitmann, D.; Jones, C.; Junk, P. C.; Lippert, K.-A.; Stasch, A. *Dalton Trans.* **2007**, 187−189.
(61) For examples, see: (a) Jones, C.; Mills, D.; Rivard, E.; Stasch, A.; Woodul, W. *J. Chem. Crystallogr.* **2010**, *40*, 965−969. (b) Cole, M. L.; Davies, A. J.; Jones, C.; Junk, P. C. *J. Organomet. Chem.* **2007**, *692*, 2508−2518. (c) Cole, M. L.; Junk, P. C. *J. Organomet. Chem.* **2003**, *666*, 55−62. (d) Jones, C.; Junk, P. C.; Platts, J. A.; Rathmann, D.; Stasch, A. *Dalton Trans.* **2005**, 2497−2499.
(62) Baldamus, J.; Berghof, C.; Cole, M. L.; Evans, D. J.; Hey-Hawkins, E.; Junk, P. C. *Dalton Trans.* **2002**, 2802−2804.
(63) Harder, S. *Organometallics* **2005**, *24*, 373−379.
(64) Evans, W. J.; Perotti, J. M.; Ziller, J. W. *Inorg. Chem.* **2005**, *44*, 5820−5825.

(65) Tazelaar, C. G. J.; Bambirra, S.; van Leusen, D.; Meetsma, A.; Hessen, B.; Teuben, J. H. *Organometallics* **2004**, *23*, 936−939.
(66) Dietrich, H. M.; Törnroos, K. W.; Anwander, R. *J. Am. Chem. Soc.* **2006**, *128*, 9298−9299.
(67) Bambirra, S.; Perazzolo, F.; Boot, S. J.; Sciarone, T. J. J.; Meetsma, A.; Hessen, B. *Organometallics* **2008**, *27*, 704−712.
(68) Dietrich, H. M.; Grove, H.; Törnroos, K. W.; Anwander, R. *J. Am. Chem. Soc.* **2006**, *128*, 1458−1459.
(69) For examples, see: (a) Hayes, P. G.; Piers, W. E.; Lee, L. W. M.; Knight, L. K.; Parvez, M.; Elsegood, M. R. J.; Clegg, W. *Organometallics* **2001**, *20*, 2533−2544. (b) Knight, L. K.; Piers, W. E.; Fleurat-Lessard, P.; Parvez, M.; McDonald, R. *Organometallics* **2004**, *23*, 2087−2094. (c) Knight, L. K.; Piers, W. E.; McDonald, R. *Organometallics* **2006**, *25*, 3289−3292.
(70) Gibson, V. C.; Spitzmesser, S. K. *Chem. Rev.* **2002**, *103*, 283−316.
(71) (a) Britovsek, G. J. P.; Gibson, V. C.; Wass, D. F. *Angew. Chem., Int. Ed.* **1999**, *38*, 428−447. (b) Labinger, J. A.; Bercaw, J. E. *Nature* **2002**, *417*, 507−514. (c) Agapie, T. *Coord. Chem. Rev.* **2011**, *255*, 861−880. (d) Lin, S.; Agapie, T. *Synlett.* **2011**, *1*, 1−5. (e) Sita, L. R. *Angew. Chem., Int. Ed.* **2011**, *50*, 6963−6965. (f) Choi, J.; MacArthur, A. H. R.; Brookhart, M.; Goldman, A. S. *Chem. Rev.* **2011**, *111*, 1761−1779. (g) Gladysz, J. A.; Ball, Z. T.; Bertrand, G.; Blum, S. A.; Dong, V. M.; Dorta, R.; Hahn, F. E.; Humphrey, M. G.; Jones, W. D.; Klosin, J.; Manners, I.; Marks, T. J.; Mayer, J. M.; Rieger, B.; Ritter, J. C.; Sattelberger, A. P.; Schomaker, J. M.; Yam, V. W.-W. *Organometallics* **2012**, *31*, 1−8.
(72) Li, S.; Cui, D.; Li, D.; Hou, Z. *Organometallics* **2009**, *28*, 4814−4822.
(73) Li, S.; Miao, W.; Tang, T.; Dong, W.; Zhang, X.; Cui, D. *Organometallics* **2008**, *27*, 718−725.
(74) Herrmann, W. A.; Munck, F. C.; Artus, G. R. J.; Runte, O.; Anwander, R. *Organometallics* **1997**, *16*, 682−688.
(75) Scheldrick, G. M., *SHELXS-97: Program for crystal structure solution*; University of Göttingen, Göttingen, Germany, 1997.
(76) Scheldrick, G. M., *SHELXL-97: Program for crystal structure refinement*; University of Göttingen, Göttingen, Germany, 1997.

Supplementary Data

C–H Bond Activation and Isoprene Polymerization by Rare-Earth Metal Tetramethylaluminate Complexes Bearing Formamidinato *N*-Ancillary Ligands

Shima Hamidi,[a] Lars N. Jende,[b] M. H. Dietrich,[b] Caecilia Maichle-Moessmer,[b] Karl W. Törnroos,[c] Glen B. Deacon,[a,] Peter C. Junk,[d,]* and Reiner Anwander[b,]**

Table S1: Selected bond angles (deg) of **2a**, **2b**, **3c**, **4a**, **4b**, **5a**, and **5b**

Bond Angles (deg)							
N1–Ln–N2	65.4(1)	59.0(2)	57.8(1)	58.34(6)	-	54.68(8)	54.80(7)
Al1–C1–Ln	86.1(2)	83.5(2)	82.9(2)	82.08(7)	86.4(1)	82.2(1)	83.8(1)
A11–C2–Ln	81.7(2)	83.4(2)	82.9(2)	83.93(8)	84.6(1)	82.11)	84.9(1)
Al2– C5–Ln	73.5(2)	84.2(2)	82.8(2)	83.68(8)	85.7(2)	83.1(1)	85.03(9)
Al2–C6–Ln	77.4(2)	83.3(2)	83.1(2)	83.68(8)	86.1(2)	83.6(1)	84.5(1)
C1–Ln–C2	83.1(2)	82.7(2)	81.5(2)	83.65(7)	77.0(1)	76.6(1)	79.3(1)
C1–Al1–C2	106.8(2)	108.1(3)	106.6(2)	108.94(9)	111.9(2)	107.8(2)	110.6(1)
C5–Ln–C6	91.3(2)	83.2(2)	81.8(2)	82.76(8)	77.8(1)	77.2(1)	78.61(9)
C5–Al2–C6	116.5(2)	107.9(3)	106.1(2)	107.76(9)	109.8(2)	107.1(2)	110.7(1)
N1–C(backbone)–N2	125.8(3)	119.9(5)	118.4(4)	118.1(2)	126.1(3)	118.8(3)	118.2(2)

Paper V

JOHN WILEY AND SONS LICENSE
TERMS AND CONDITIONS

Apr 07, 2015

This Agreement between Lars Jende ("You") and John Wiley and Sons ("John Wiley and Sons") consists of your license details and the terms and conditions provided by John Wiley and Sons and Copyright Clearance Center.

License Number	3603710971825
License date	Apr 07, 2015
Licensed Content Publisher	John Wiley and Sons
Licensed Content Publication	European Journal of Inorganic Chemistry
Licensed Content Title	Organoaluminum and -gallium Formamidinate Complexes
Licensed Content Author	Shima Hamidi,H. Martin Dietrich,Daniel Werner,Lars N. Jende,Cäcilia Maichle-Mössmer,Karl W. Törnroos,Glen B. Deacon,Peter C. Junk,Reiner Anwander
Licensed Content Date	Mar 8, 2013
Pages	7
Type of use	Dissertation/Thesis
Requestor type	Author of this Wiley article
Format	Electronic
Portion	Full article
Will you be translating?	No
Title of your thesis / dissertation	Donor-Substituted Cyclopentadienyl Ligands in Rare-Earth Metal-Based Isoprene Polymerization
Expected completion date	May 2015
Expected size (number of pages)	108
Requestor Location	Lars Jende Eichhaldenstr 23 Tuebingen, Germany 72074 Attn: Lars Jende
Billing Type	Invoice
Billing Address	Lars Jende Eichhaldenstr 23 Tuebingen, Germany 72074 Attn: Lars Jende
Total	0.00 EUR

EurJIC European Journal of Inorganic Chemistry

ChemPubSoc Europe

FULL PAPER

DOI:10.1002/ejic.201201515

Organoaluminum and -gallium Formamidinate Complexes

Shima Hamidi,[a] H. Martin Dietrich,[b] Daniel Werner,[a] Lars N. Jende,[b] Cäcilia Maichle-Mössmer,[b] Karl W. Törnroos,[c] Glen B. Deacon,*[a] Peter C. Junk,*[d] and Reiner Anwander*[b]

Keywords: Aluminum / Gallium / X-ray diffraction / Formamidines / Bridging ligands

Dialuminum formamidinate complexes [$Me_2Al(\mu$-Form)(μ-Me)$AlMe_2$] [Form (ArNCHNAr) = EtForm (Ar = 2,6-$Et_2C_6H_3$) or DippForm (Ar = 2,6-$i Pr_2C_6H_3$)] were obtained in good yields by treatment of formamidines (FormH) with trimethylaluminum in a 1:3 stoichiometry. The products contain both a bridging Form ligand and a bridging methyl group between the two aluminum centers. [M(Form)Me_2] (M = Al, Form = DippForm, EtForm; M = Ga, Form = DippForm) were prepared in high yields by the protonolysis reactions of MMe_3 (M = Al, Ga) with formamidines (FormH) in a 1:1 stoichiometry. [Al(DippForm)Me_2] was also synthesized by other methods including concentration of the tetrahydrofuran/*n*-hexane solution of [$Me_2Al(\mu$-DippForm)(μ-Me)$AlMe_2$] to dryness and also by reaction of $AlMe_3$ with [Ga(DippForm)Me_2] in a 1:1 ratio. Partial dissociation of the dialuminum to monoaluminum complexes was detected in the ^{1}H NMR spectra of [$Me_2Al(\mu$-Form)(μ-Me)$AlMe_2$] complexes. All complexes exhibit a distorted tetrahedral stereochemistry of the Group 13 metal atoms.

Introduction

Amidinato monoanions $[R^1NC(R^2)NR^3]^-$ form a class of ligands that has long been known in the chemistry of main group, transition, and lanthanide metals.[1] Recently, they have found many applications as ancillary ligands in polymerization catalysis.[1d–1f,2] More specifically, aluminum amidinate complexes act as significant catalysts in olefin polymerization.[2h,2i,3] For example, [Al{RC(NR′)$_2$}Me_2] (R = Me or *t*Bu; R′ = *i*Pr or cyclohexyl) complexes are activated by boron reagents to form cationic aluminum complexes, which function as catalysts in ethylene polymerization.[2i] Furthermore, aluminum amidinates are of prime importance as potential reagents in organic synthesis.[1e,4] Charge delocalization across the N···C···N backbone in amidinate ligands allows for different coordination modes to metal centers, such as monodentate, bidentate, and dimetallic bridging modes.[1a,1b,1e,3a,5] A number of monoamidinato- and bisamidinato-aluminum and -gallium complexes have been synthesized[2h,2i,3,5d,6] by applying protocols such as the addition of alkylaluminum compounds to the N=C double bond in carbodiimides,[7] salt metathesis of lithium amidinates with Al or Ga halide species,[5d,6h,7,8] and deprotonation of amidines by organoaluminum compounds like trimethylaluminum.[6a,6g,6h,9] Recent formamidinate examples authenticated by X-ray structure analysis comprise [AlMe(DippForm)$_2$], [{GaI(DippForm)}$_2$], [GaI(DippForm)$_2$], [AlCl(DippForm)$_2$], [AlCl(EtForm)$_2$], and [AlMe(EtForm)$_2$] [FormH = ArN=CH–NHAr (Ar = aryl); EtForm (Ar = 2,6-$Et_2C_6H_3$), DippForm (Ar = 2,6-$i Pr_2C_6H_3$)].[5d,6g,6h] Formamidinate complexes are an interesting subclass of amidinate complexes. The formamidine proligands *N*,*N*′-bis(aryl)formamidines (FormH) can be prepared in high yields from the addition of triethyl orthoformate to a substituted aniline. Variation of the substituents on the aryl rings can modulate the steric and electronic effect of the ligands as well as their solubilities.[10]

Herein, we report the synthesis by protonolysis of $AlMe_3$ with formamidines and the structural characterization of two new classes of aluminum and gallium formamidinate complexes. These include dialuminum formamidinate complexes that feature both bridging Form ligands and a bridging methyl group, [$Me_2Al(\mu$-Form)(μ-Me)$AlMe_2$] [Form = DippForm (**1a**), EtForm (**1b**)]. We also report the synthesis by various methods and structural characterization of formamidinate complexes of dimethylaluminum (**2a** and **2b**) and -gallium (**3a**). All compounds in the current study were identified by X-ray crystal structure analysis (except for **2b**).

[a] School of Chemistry, Monash University, 3800 Clayton, Victoria, Australia
Fax: +61-3-9905-4597
E-mail: glen.deacon@monash.edu
Homepage: http://monash.edu/science/about/schools/chemistry/staff/deacon.html
[b] Institut für Anorganische Chemie, Universität Tübingen, Auf der Morgenstelle 18A, 72076 Tübingen, Germany
Fax: +49-7071-29-2436
E-mail: reiner.anwander@uni-tuebingen.de
Homepage: http://www.mnf.uni-tuebingen.de/fachbereiche/chemie/institute/anorganische-chemie/institut/ag-anwander.html
[c] Department of Chemistry, University of Bergen, Allégaten 41, 5007 Bergen, Norway
[d] School of Pharmacy & Molecular Sciences, James Cook University, Townsville, Qld 4811, Australia

Results and Discussion

Treatment of *N*,*N*′-bis(2,6-diisopropylphenyl)formamidine (DippFormH) or *N*,*N*′-bis(2,6-diethylphenyl)formamidine (EtFormH) with an excess amount of trimethylaluminum ($AlMe_3$, 3 equiv.) in *n*-hexane at ambient temperature led to instant methane evolution and subsequent formation of [$Me_2Al(\mu\text{-Form})(\mu\text{-Me})AlMe_2$] [Form = DippForm (**1a**) or EtForm (**1b**)] in good yields (76 and 82%, respectively; Scheme 1, i). Crystal structures of **1a** and **1b** both feature a six-membered dialuminum ring with both bridging *N*,*N*′-formamidinato and methyl groups (Figure 1). Compound **1a** was dissolved in a mixture of tetrahydrofuran and *n*-hexane (7:3, v/v) and left under vacuum for 5 h. The complex [Al(DippForm)Me_2] (**2a**) was isolated as colorless crystals in high yields (96%) from an *n*-hexane solution (Scheme 1, ii). On the basis of an NMR-spectroscopic-scale experiment in C_6D_6 at ambient temperature, addition of $AlMe_3$ to **2a** in a 1:1 ratio resulted in **1a** (Scheme 1, iii). Compounds **2a** and **2b** were also prepared in high yields (93 and 77%, respectively) through a protonolysis route by treatment of the relevant FormH with $AlMe_3$ (1:1 mol ratio) in *n*-hexane at ambient temperature overnight (Scheme 1, iv).

Protonolysis of trimethylgallium with DippFormH (1 equiv.) yielded **3a** (85%) as colorless crystals (Scheme 1, v), and it was fully characterized. The ^1H NMR spectrum of **3a** in C_6D_6 indicates sharp resonances of methyl groups at higher δ values (δ = 0.24 ppm) than those of **2a** (δ = –0.14 ppm). An NMR-spectroscopic-scale reaction of an excess amount (3 equiv.) of trimethylgallium with DippFormH (in C_6D_6) at ambient temperature revealed the presence of **3a** and unreacted $GaMe_3$, rather than the formation of [$Me_2Ga(\mu\text{-DippForm})(\mu\text{-Me})GaMe_2$], analogous to **1a** and **1b**. Two attempts to synthesize the putative Al/Ga dimetallic complex [$Me_2Ga(\mu\text{-DippForm})(\mu\text{-Me})AlMe_2$] were conducted, namely, by treatment of $GaMe_3$ with an equimolar amount of **2a** and reaction of $AlMe_3$ with **3a** in a 1:1 ratio (Scheme 1, vi). However, both synthesis attempts failed, and the isolated product in both cases was **2a**. This is consistent with $AlMe_3$ being a harder Lewis acid than $GaMe_3$.[11]

Partial dissociation of **1a** to **2a** and of **1b** into **2b** was detected in the ^1H NMR spectra of **1a** and **1b** in [D_8]toluene or C_6D_6. At equilibrium (Scheme 2), the ratio of **1a**/**2a** was 2:1 and of **1b**/**2b** was 2.5:1 (see the Experimental Section). To gain further insight into the equilibrium, variable-temperature ^1H NMR spectroscopic measurements in [D_8]-toluene were undertaken. The ^1H NMR spectrum of complex **1a** in [D_8]toluene at low temperature (–80 °C) showed five resonances for the Al-methyl groups, thereby revealing the presence of the $AlMe_2$ group of **2a**, bridging and terminal methyl groups of **1a**, and free $AlMe_3$ (see the Experi-

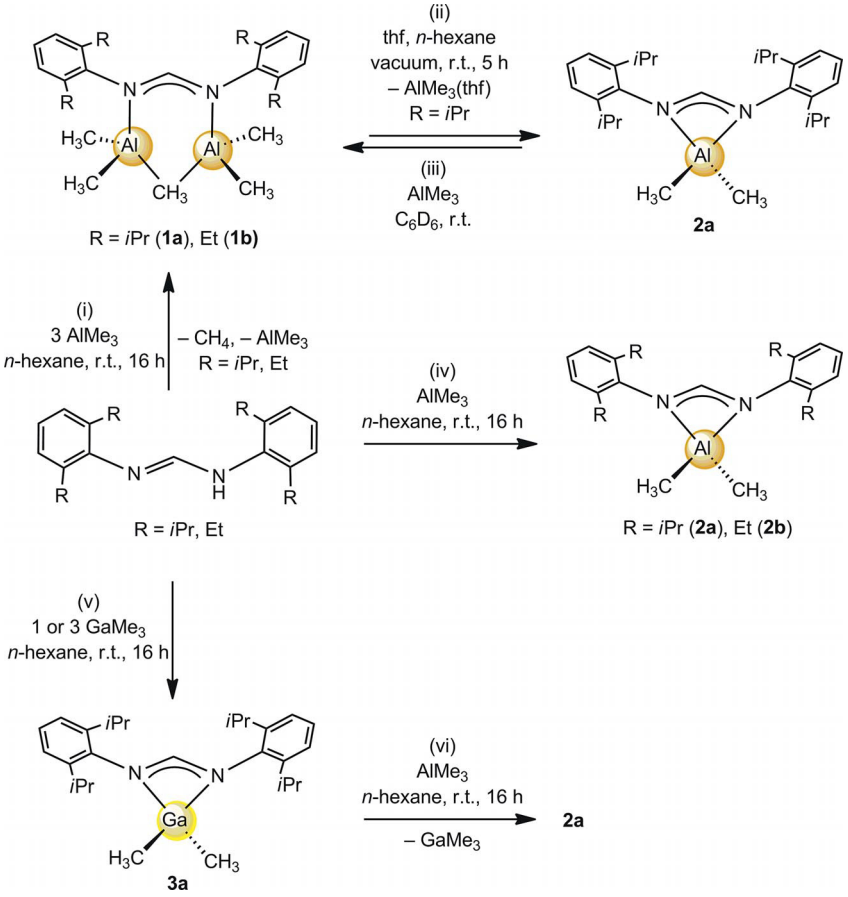

Scheme 1. Synthesis of complexes **1a**, **1b**, **2a**, **2b**, and **3a**.

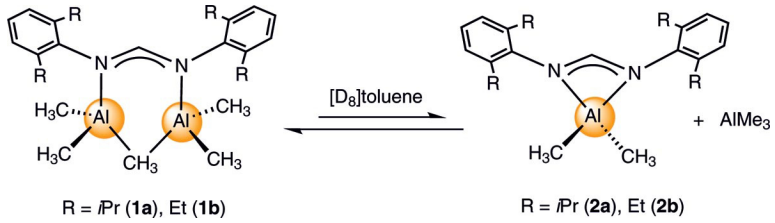

Scheme 2. Equilibria between **1a**/**1b** and **2a**/**2b**.

mental Section). The integrations of the broad resonances of free $AlMe_3$ were somewhat less than expected. Only an approximate integration could be obtained for the broad resonance of the terminal $AlMe_2$ groups of **1a**. A similar problem was encountered with one set of overlapping resonances of **1a** and **1b** obtained at room temperature.

N,*N*′-Bridging complexes analogous to those in **1a** and **1b** have been previously observed in aluminum pyrazolate (pz) complexes and structurally characterized for [$Me_2Al(\mu$-$Ph_2pz)(\mu$-$Me)AlMe_2$], [$Et_2Al(\mu$-$Ph_2pz)(\mu$-$Et)AlEt_2$], and [$(n$Pr$)_2Al(\mu$-tBu$_2$pz)(μ-nPr)Al(nPr$)_2$], which also features a three-center, two-electron μ-η^1:η^1 methyl group bridging two Al atoms.[12,13] However, there is a central five-membered ring in contrast to a six-membered ring in **1a**,**b**. At ambient temperature, they slowly decompose to form the six-membered ring dimer [{$AlMe_2(\mu$-L)}$_2$] with loss of trimethylaluminum.[12b] This gradual decomposition and loss of trimethylaluminum was not detected in the current study for solid **1a**,**b**, but was induced for **1a** by applying vacuum (10^{-2} mbar, Scheme 1, ii). The formation of compound **2a** from a solution of **1a** in thf/*n*-hexane is probably promoted by the presence of thf, which displaces a weakly bonded $AlMe_3$ through the formation of volatile $AlMe_3$(thf). From loss of $AlMe_3$, the resulting **2a** (and presumably **2b**) is monomeric with a four-membered ring, thus contrasting the behavior of the pyrazolato complexes.[12]

The N–H stretching vibration of the formamidines at 3300–3100 cm^{-1} is not observed in the IR spectra of the complexes, thus indicating complete deprotonation, and a strong absorption assignable to the C–C stretching vibration of a metal-coordinated formamidinato group is observed at 1562–1527 cm^{-1}. The strong band at around 690 cm^{-1} in **1a**, **1b**, **2a**, and **2b** is assigned to an Al–C stretching absorption.[14] In the IR spectra of all complexes, CH asymmetrical stretching, CH symmetrical stretching, and a Fermi resonance mode of methyl groups attached to metal centers appear as three bands at 2966–2827 cm^{-1}. The bending vibrations of bridging and terminal methyl groups in **1a** and **1b** give two bands at 1260–1190 cm^{-1}.[15]

The isostructural complexes [$Me_2Al(\mu$-DippForm)(μ-$Me)AlMe_2$] (**1a**) and [$Me_2Al(\mu$-EtForm)(μ-$Me)AlMe_2$] (**1b**) crystallize in the monoclinic $P2_1/n$ and $P2_1/c$ space groups, respectively (Table 2). In both complexes, two aluminum centers are bridged by a methyl group and a formamidinato ligand, whereas the arrangement about the aluminum centers is distorted tetrahedral (Figure 1). The backbone carbon atom, two nitrogen atoms and two aluminum atoms in both **1a** and **1b** lie approximately in a plane, whereas the bridging methyl group is situated 0.75 Å in **1a** and 0.83 Å in **1b** above this Al_2N_2C plane.

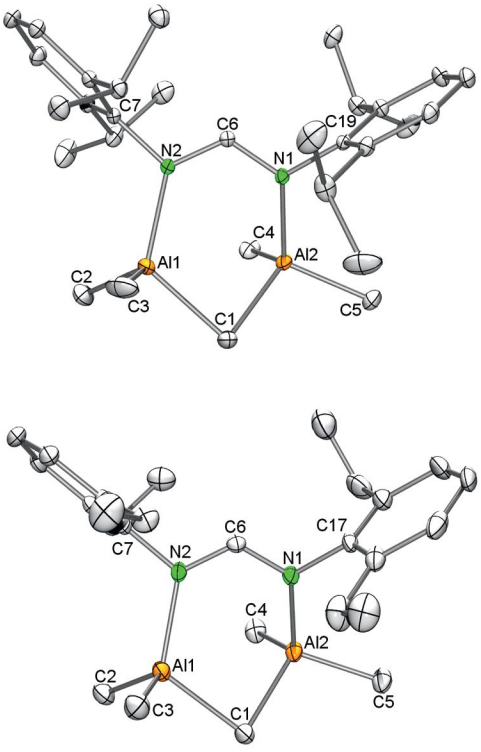

Figure 1. Perspective ORTEP views of the molecular structures of **1a** (top) and **1b** (bottom). Atomic displacement parameters are set at the 30% level. Hydrogen atoms are omitted for clarity. For selected bond lengths and angles, see Table 1.

The aryl rings are roughly perpendicular to this plane with average angles of 82.3° in both **1a** and **1b**. The Al–N bond lengths are similar in **1a** and **1b** (Table 1). In a series of structurally defined aluminum complexes with terminal and bridging Al–C bonds, the bond-length ranges are 1.94–1.98 and 2.11–2.18 Å, respectively.[12b,16] Those of **1a** and **1b** lie in the same ranges (Table 1). The Al–C–Al angles for bridging methyl groups within the six-membered rings of **1a** [91.89(4)°] and **1b** [92.5(2)°] match those observed for the five-membered rings in the aluminum pyrazolate complexes [$R_2Al(\mu$-L)(μ-R)AlR_2] (R = Me, L= 3,5-Ph_2pz, 91.8(5) Å; R = Et, L = 3,5-Ph_2pz, 90.44(12) Å; R = *n*Pr, L = 3,5-tBu$_2$pz, 89.43(12) Å).[12,13]

Table 1. Selected bond lengths [Å] and angles [°] in **1a** and **1b**.

Bond lengths [Å]	**1a**	**1b**
Al1–N2	1.9508(7)	1.960(4)
Al1–C1	2.148(1)	2.138(5)
Al1–C2	1.954(1)	1.955(4)
Al1–C3	1.966(1)	1.965(5)
Al2–N1	1.930(7)	1.920(3)
Al2–C1	2.126(1)	2.113(5)
Al2–C5	1.957(1)	1.961(4)
Al2–C4	1.962(1)	1.956(4)
C6–N1	1.316(5)	1.316(5)
C6–N2	1.321(5)	1.319(4)
Bond angles [°]		
N2–Al1–C1	116.60(4)	114.63(16)
N2–Al1–C2	110.56(5)	112.36(18)
C2–Al1–C3	116.39(7)	116.5(2)
C2–Al1–C1	105.53(5)	106.2(2)
C3–Al1–C1	98.23(6)	97.8(2)
Al1–C1–Al2	91.89(4)	92.5(2)
N1–Al2–C1	107.90(4)	106.80(18)
N1–Al2–C4	112.14(4)	111.77(17)
N1–Al2–C5	107.36(4)	105.19(16)
C4–Al2–C1	109.33(5)	109.2(2)
C5–Al2–C1	102.29(5)	104.3(2)
C5–Al2–C4	117.08(5)	118.77(19)
N1–C6–N2	123.6(4)	123.6(4)

Complexes [Al(DippForm)Me_2] (**2a**) and [Ga(DippForm)Me_2] (**3a**) are isostructural and crystallize in the monoclinic space groups $C2/c$ and $P2_1/n$, respectively (Table 2). In both **2a** and **3a**, the metal atom is a four-coordinate species with two nitrogen atoms and two methyl groups adopting a distorted tetrahedral coordination arrangement as shown in Figure 2.

The backbone carbon atom, the two nitrogen atoms, and the aluminum/gallium atom in both **2a** and **3a** lie approximately in a plane. This metallocycle plane is roughly perpendicular to the aryl rings in **2a** and **3a** (average angles between aryl rings and metallocycle planes, **2a**: 69.5°, **3a**: 73.3°).

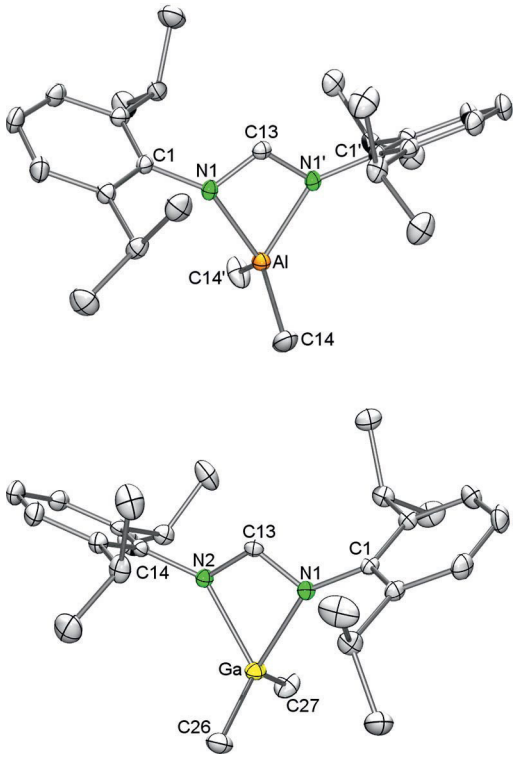

Figure 2. Perspective ORTEP views of the molecular structures of **2a** (top) and **3a** (bottom). Atomic displacement parameters are set at the 30% level. Hydrogen atoms are omitted for clarity. Selected bond lengths [Å] and angles [°] for **2a**: Al1–N1 1.955(2), Al1–C14 1.950(3), N1–C13 1.320(3); N1–Al1–N1′ 68.57(13), C14–Al1–C14′ 121.3(2), N1–C13–N1′ 113.1(3), Al1–N1–C13 89.16(17), C14–Al1–N1 112.10(13), C14′–Al1–N1 115.72(13), C14–Al1–C14′ 121.3(2). Selected bond lengths [Å] and angles [°] for **3a**: Ga1–N1 2.048(2), Ga1–N2 2.055(2), Ga1–C27 1.948(2), Ga1–C26 1.960(2), N1–C13 1.319(2), N2–C13 1.314(2); C27–Ga1–C26 127.77(11), C27–Ga1–N1 111.97(9), C26–Ga1–N1 112.47(8), C27–Ga1–N2 112.25(9), C26–Ga1–N2 110.38(9), N1–Ga1–N2 65.12(6), N2–C13–N1 113.95(16), C27–Ga1–C13 117.21(9), C26–Ga1–C13 114.99(8), N2–C13–Ga1 57.16(10), N1–C13–Ga1 56.83(9), C13–N1–Ga1 90.54(11), C13–N2–Ga1 90.34(11).

Table 2. Crystallographic data for complexes **1a**, **1b**, **2a**, and **3a**.

	1a	**1b**	**2a**	**3a**
Chemical formula	$C_{30}H_{50}Al_2N_2$	$C_{26}H_{42}Al_2N_2$	$C_{27}H_{41}AlN_2$	$C_{27}H_{41}GaN_2$
M_r	492.68	436.58	420.60	463.34
Crystal system	monoclinic	monoclinic	monoclinic	monoclinic
Space group	$P2_1/n$	$P2_1/c$	$C2/c$	$P2_1/n$
a [Å]	12.9356(5)	20.050(4)	17.698(3)	10.640(2)
b [Å]	15.0483(6)	14.536(3)	8.8444(9)	12.640(3)
c [Å]	15.9381(7)	19.180(4)	17.022(2)	19.979(4)
β [°]	90.6900(10)	106.77(3)	91.649(11)	92.91(3)
V [Å^3]	3102.3(2)	5352.2(19)	2663.3(6)	2683.5(9)
T [K]	123(2)	173(2)	173(2)	173(2)
Z	4	8	4	4
μ [mm^{-1}]	0.113	0.123	0.091	1.040
No. of reflections measured	51141	65095	16724	41050
No. of independent reflections	9076	9783	2418	6138
R_{int}	0.0305	0.1901	0.1175	0.0520
Final R_1 values [$I > 2\sigma(I)$]	0.0382	0.0808	0.0725	0.0408
Final $wR(F^2)$ values [$I > 2\sigma(I)$]	0.1069	0.1432	0.1264	0.0828
Final R_1 values (all data)	0.0406	0.1528	0.0988	0.0511
Final $wR(F^2)$ values (all data)	0.1097	0.1668	0.1349	0.0862
GoF on F^2	1.027	1.014	1.182	1.156

In complex **2a**, the Al–N bond length of 1.955(2) Å is reasonably typical for amidinato ligands coordinated to dimethylaluminum, {e.g., analogous bond lengths for [Al($CH_3C_6H_4${μ-C($NC_6H_3iPr_2$-2,6)$_2$})Me_2], 1.942(2) and 1.942(2) Å; for [Al(C_6H_3-2,6-Mes_2{μ-C($NC_6H_3iPr_2$-2,6)$_2$})-Me_2] (Mes = 2,4,6-$Me_3C_6H_2$), 1.953(4) and 1.951(4) Å; for [Al(*t*Bu{μ-C($NC_6H_3iPr_2$-2,6)$_2$})Me_2], 1.940(2) and 1.936(2) Å; for [Al(Ph{μ-C($NC_6H_3iPr_2$-2,6)$_2$})Me_2], 1.938(2) Å}.[6b,6e,6f,7b] However, the N1–C–N2 backbone angle [113.1(3)°] is larger than those of benzamidinate and acetamidinate complexes due to the lower steric constraints at the central backbone carbon atom of the formamidinato ligands[5d] [e.g., 110.3(2), 108.2(3), 107.4(2), and 109.9(2)° for the above-mentioned amidinate complexes].

For **3a**, the Ga–N bonds are approximately 0.09 Å longer than the Al–N bonds, a value similar to the difference (0.08 Å) in ionic radii.[17a] In spite of the ionic radii difference, the Al–C and Ga–C bond lengths are very similar, which can be explained by Blom and Haaland's covalent bond-length calculations (RMMS Al/Ga–C difference 0.01 Å).[17b] As expected, the N–Ga–N "bite angle" [65.12(6)] is smaller than N–Al–N of **2a** [68.57(13)]. A structurally characterized gallium amidinate complex with a four-membered ring has been previously prepared, namely, [Ga(PhC{μ-C($NC_6H_3iPr_2$-2,6)$_2$})Me_2],[6a] thus showing relatively similar gallium–nitrogen bond lengths [Ga–N 2.047(6) and 2.031(6) Å] and an N–Ga–N bite angle [64.7(2)°] relatively similar to that of **3a**. However, the backbone angle in the reported complex [110.6(7)°] is smaller than that of **3a** [113.9(2)°] owing to the enhanced steric hindrance at the central backbone carbon atoms of benzamidinato relative to formamidinato ligands.

Conclusion

Monometallic complexes [M(Form)Me_2] (M = Al, Ga) can be readily accessed by means of a protonolysis protocol by using [MMe_3] and formamidines. Depending on the stoichiometry, trimethylaluminum also produces dimetallic complexes [Me_2Al(μ-Form)(μ-Me)AlMe_2], which nicely reflects the degree of agglomeration of the homoleptic alkylmetal compounds, Al_2Me_6 versus $GaMe_3$. As shown by ^{1}H NMR spectroscopy, dimetallic complexes [Me_2Al(μ-Form)(μ-Me)AlMe_2] partially dissociate in toluene depending on the substitution pattern of the formamidinato ancillary ligand, which means that bulkier substituents involve a higher degree of dissociation. The transformation of dimetallic to monometallic species is also forced by the application of vacuum, but can be reversed by addition of trimethylaluminum. In accordance with the higher Lewis acidity of trimethylaluminum, it easily expels trimethylgallium from [Ga(DippForm)Me_2]. Attempts to prepare the Al/Ga dimetallic complex [Me_2Ga(μ-DippForm)(μ-Me)AlMe_2] failed.

Experimental Section

General Considerations: Synthetic operations were carried out under dry argon by using standard Schlenk, high-vacuum, and glovebox techniques (MBraun MBLab; <1 ppm O_2, <1 ppm H_2O). *n*-Hexane, toluene, and tetrahydrofuran were purified by using Grubbs columns (MBraun SPS, solvent purification system) and stored in a glovebox. The formamidine compounds (EtFormH and DippFormH)[10b,10c] were prepared according to literature methods. C_6D_6 and [D_8]toluene were obtained from Aldrich, dried with Na for 24 h, and filtered. $AlMe_3$ was purchased from Aldrich and used as received. The NMR spectra of air- and moisture-sensitive compounds in C_6D_6 or [D_8]toluene were recorded with J. Young valve NMR spectroscopy tubes at 25/–80 °C with a Bruker Avance DMX400 (^{1}H: 400.13 MHz; ^{13}C: 100.62 MHz) or a Bruker Biospin AV500 (^{1}H: 500.13 MHz; ^{13}C: 125.77 MHz) spectrometer; ^{1}H and ^{13}C chemical shifts are referenced to internal solvent resonances and reported relative to TMS. Elemental analyses (C, H, N) were performed with an Elementar Vario Micro cube. IR spectra were recorded between 4000 and 400 cm^{-1} with a Nicolet 6700 FTIR spectrometer by using a DRIFT chamber with dry KBr/sample mixtures and KBr windows. The collected data were converted by using the Kubelka–Munk refinement.

[Me_2Al(μ-DippForm)(μ-Me)AlMe_2] (1a): In a glovebox, a solution of $AlMe_3$ (180 mg, 2.50 mmol) in *n*-hexane (5 mL) was added dropwise to a suspension of DippFormH ligand (303 mg, 0.83 mmol) in *n*-hexane (5 mL) under vigorous stirring. Instant gas formation was observed. The clear solution was stirred at ambient temperature overnight, and then dried under an oil-pump vacuum. The powder was dissolved in *n*-hexane (5 mL) and recrystallized at –40 °C. Pure colorless crystalline product was obtained after 1 d, and all the characterizations were performed on the crystalline compound (315 mg, 77%). This compound dissociates and forms an equilibrium with compounds **2a** and $AlMe_3$ in solution. The ^{1}H NMR spectrum was recorded for the mixture and interpreted as 1 × **1a** in equilibrium with 0.5 × **2a** and 0.5 × Al(CH_3)$_3$. ^{1}H NMR (500.13 MHz, [D_8]toluene, 25 °C): δ = 7.40 [s, 1 H, NC(*H*)N, **1a**], 7.24 [s, 0.5 H, NC(*H*)N, **2a**], 6.99–6.92 (br. m, 9 H, Ar, **1a** and **2a**), 3.40 (m, $^3J_{H,H}$ = 6.9 Hz, 2 H, C*H*, **2a**), 3.38 (m, $^3J_{H,H}$ = 6.9 Hz, 4 H, C*H*, **1a**), 1.21 (d, $^3J_{H,H}$ = 6.9 Hz, 12 H, CH_3, **1a**), 1.11 (d, $^3J_{H,H}$ = 6.9 Hz, 12 H, CH_3, **2a**), 0.83 (d, $^3J_{H,H}$ = 6.9 Hz, 12 H, CH_3, **1a**), –0.25 [s, 3 H, Al(CH_3)$_2$, **2a**], –0.42 to –0.55 [br. overlapping, ca. 18 H, bridging Al(CH_3) + terminal 2 × Al(CH_3)$_2$ in **1a** and free Al(CH_3)$_3$] ppm. ^{1}H NMR (500.13 MHz, [D_8]toluene, –80 °C): δ = 7.43 [s, 1 H, NC(*H*)N, **1a**], 7.10 [s, 0.5 H, NC(*H*)N, **2a**], 7.05–6.79 (br. m, 9 H, Ar, **1a** and **2a**), 3.45 (m, 6 H, C*H*, **1a** and **2a**), 1.27 (d, $^3J_{H,H}$ = 6.9 Hz, 12 H, CH_3, **1a**), 1.15 (br. s, 12 H, CH_3, **2a**), 0.83 (d, $^3J_{H,H}$ = 6.9 Hz, 12 H, CH_3, **1a**), 0.58 [s, 3 H, Al(CH_3)$_2$, **2a**], –0.03 [s, 3 H, bridging Al(CH_3), **1a**], –0.07 [br. s, 1 H, free Al(CH_3)$_3$], –0.37 [br. s, ca. 12 H, terminal 2 × Al(CH_3)$_2$, **1a**], –0.58 [br. s, 2 H, free Al(CH_3)$_3$] ppm. ^{13}C NMR (100.61 MHz, [D_8]toluene, 25 °C): δ = 168.9 [NC(H)N, **1a**], 167.0 [NC(H)N, **2a**], 145.4 (Ar–C, **1a**), 144.3 (Ar–C, **2a**), 139.2 (Ar–C, **1a**), 138.9 (Ar–C, **2a**), 126.2 (br., Ar–CH, **1a** and **2a**), 124.2 (Ar–CH, **1a**), 123.5 (Ar–CH, **2a**), 28.2 (CH, **2a**), 27.9 (CH, **1a**), 25.8 (CH_3, **1a**), 24.2 (CH_3, **2a**), –9.9 [br., Al(CH_3)$_n$, **1a** and **2a**] ppm. DRIFT (KBr): $\tilde{\nu}$ = 2964 (m), 2927 (m), 2887 (m), 1595 (m), 1557 (s), 1463 (m), 1438 (m), 1383 (w), 1363 (w), 1323 (m), 1256 (w), 1193 (m), 1168 (w), 1110 (w), 1096 (w), 1055 (w), 1013 (w), 936 (w), 805 (m), 776 (m), 760 (m), 694 (s br), 652 (m), 608 (w), 570 (m) cm^{-1}. $C_{30}H_{50}Al_2N_2$ (492.69 g mol^{-1}): calcd. C 73.13, H 10.22, N 5.68; found C 72.55, H 10.45, N 5.62. [The above equilibrium was also evident in an NMR-spectroscopic-scale reaction of $AlMe_3$ (1.2 mg, 0.017 mmol) with **2a** (7 mg, 0.017 mmol) in C_6D_6 at ambient temperature; partial formation of **1a** was detected.]

[Me_2Al(μ-EtForm)(μ-Me)AlMe_2] (1b): According to the procedure described above for compound **1a**, $AlMe_3$ (70 mg, 0.97 mmol) was

treated with EtFormH (100 mg, 0.32 mmol). Recrystallization of the product from a solution in *n*-hexane yielded **1b** (115 mg, 82%) as colorless crystals suitable for X-ray crystallography. This compound dissociated to form an equilibrium with compounds **2b** and $AlMe_3$ in solution. The ^1H NMR spectrum was recorded for the mixture and interpreted as $1 \times$ **1b** in equilibrium with $0.4 \times$ **2b** and $0.4 \times Al(CH_3)_3$. ^1H NMR (400.13 MHz, C_6D_6, 25 °C): δ = 7.06–6.95 (br. m), overlapping 7.05 (s) and 6.97 (s) [total integration ca. 10 H, ArH **1b** and **2b**; NC(*H*)N, **2b**; NC(*H*)N, **1b**, respectively], 2.67 (q, $^3J_{H,H}$ = 7.4 Hz, 8 H, CH_2, **1b**), 2.64 (q, $^3J_{H,H}$ = 7.4 Hz, 3.2 H, CH_2, **2b**), 1.14 (t, $^3J_{H,H}$ = 7.4 Hz, 4.8 H, CH_3, **2b**), 1.07 (t, $^3J_{H,H}$ = 7.4 Hz, 12 H, CH_3, **1b**), –0.18 [s, 2.4 H, $Al(CH_3)_2$, **2b**], –0.37 [br. s, ca. 18 H, bridging $Al(CH_3)$ + 2 terminal $Al(CH_3)_2$ in **1b** and free $Al(CH_3)_3$] ppm. ^{13}C NMR (100.62 MHz, C_6D_6, 25 °C): δ = 168.9 [NC(H)N, **1b**], 167.4 [NC(H)N, **2b**], 140.8 (Ar–C, **1b**), 140.7 (Ar–C, **2b**), 139.4 (Ar–C, **1b**), 139.3 (Ar–C, **2b**), 126.6 (Ar–CH, **1b**), 126.5 (Ar–CH, **2b**), 126.2 (Ar–CH, **1b**), 125.6 (Ar–CH, **2b**), 25.7 (CH_2, **2b**), 24.9 (CH_2, **1b**), 15.3 (CH_3, **2b**), 14.9 (CH_3, **1b**), –10.7 [br., $Al(CH_3)_n$, **1b** and **2b**] ppm. DRIFT (KBr): $\tilde{\nu}$ = 2966 (m), 2932 (m), 2875 (m), 1597 (m), 1562 (s), 1450 (m), 1438 (m), 1372 (w), 1341 (w), 1323 (m), 1257 (w), 1197 (m), 1171 (w), 1106 (w), 1096 (w), 1057 (w), 1018 (w), 937 (w), 805 (w), 779 (m), 763 (m), 690 (s br), 593 (w), 569 (m) cm^{-1}. $C_{26}H_{42}Al_2N_2$ (436.59): calcd. C 71.53, H 9.70, N 6.42; found C 70.83, H 8.90, N 6.48.

[Al(DippForm)Me$_2$] (2a): This compound was synthesized according to various methods. **Method 1:** Compound **1a** (100 mg, 0.20 mmol) was dissolved in a mixture of tetrahydrofuran and *n*-hexane (10 mL, 7:3, v/v) and left under high vacuum for 5 h. The resulting powder was crystallized from *n*-hexane (5 mL), and colorless crystals of **2a** were collected in high yield, and all the characterizations was performed on the crystalline compound (81 mg, 96%) (DRIFT and ^1H NMR spectroscopic identification). **Method 2:** A solution of $AlMe_3$ in *n*-hexane (5 mL, 19.8 mg, 0.27 mmol) was added dropwise to a solution of DippFormH (100 mg, 0.27 mmol) in *n*-hexane (5 mL) under vigorous stirring. The clear solution was stirred at ambient temperature overnight, and then left under vacuum to reduce the solvent volume to 5 mL. Pure colorless crystalline product (**2a**) was obtained after 1 d at –40 °C and identified by ^1H NMR spectroscopy (106 mg, 93%). **Method 3:** $AlMe_3$ (7.8 mg, 0.11 mmol) in *n*-hexane (5 mL) was added dropwise to a solution of compound **3a** (50 mg, 0.11 mmol) in *n*-hexane (10 mL). The clear solution was stirred at ambient temperature overnight, and the solvent was reduced to 5 mL under vacuum. Pure colorless crystalline product (**2a**) was obtained after 1 d at –40 °C and identified by ^1H NMR spectroscopy (44 mg, 95%). ^1H NMR (400.13 MHz, C_6D_6, 25 °C): δ = 7.38 [s, 1 H, NC(*H*)N], 7.11 (br. m, 6 H, Ar), 3.52 (sept, $^3J_{H,H}$ = 6.9 Hz, 4 H, C*H*), 1.19 (d, $^3J_{H,H}$ = 6.9 Hz, 24 H, CH_3), –0.14 [s, 6 H, Al(CH_3)$_2$] ppm. ^{13}C NMR (100.61 MHz, C_6D_6, 25 °C): δ = 167.0 [NC(H)N], 144.3 (Ar–C), 138.9 (Ar–C), 126.2 (Ar–CH), 123.5 (Ar–CH), 28.2 (CH), 24.2 (CH_3), –9.9 [br. s, $Al(CH_3)_2$] ppm. DRIFT (KBr): $\tilde{\nu}$ = 2959 (s), 2927 (m), 2887 (m), 1593 (w), 1527 (s), 1462 (m), 1444 (m), 1383 (w), 1361 (w), 1326 (m), 1256 (m), 1223 (m), 1187 (m), 1160 (w), 1112 (w), 1099 (w), 1057 (w), 1013 (w), 933 (w), 799 (m), 776 (m), 753 (m), 694 (br. s), 658 (m), 605 (w), 547 (w) cm^{-1}. $C_{27}H_{41}AlN_2$ (420.61): calcd. C 77.10, H 9.83, N 6.66; found C 77.48, H 9.74, N 6.70.

[Al(EtForm)Me$_2$] (2b): A solution of $AlMe_3$ in *n*-hexane (5 mL, 42.0 mg, 0.58 mmol) was added dropwise to a solution of EtFormH (180 mg, 0.56 mmol) in *n*-hexane (5 mL) under vigorous stirring. The clear solution was stirred at ambient temperature overnight, and then left under vacuum to reduce the solvent volume to 5 mL. Pure colorless crystalline product (**2b**) was obtained after 1 d at –40 °C and identified by ^1H NMR spectroscopy (230 mg, 77%). ^1H NMR (400.13 MHz, C_6D_6, 25 °C): δ = 7.05 [s, 1 H, NC(*H*)N], 7.04–6.95 (m, 6 H, Ar), 2.65 (q, $^3J_{H,H}$ = 7.4 Hz, 8 H, CH_2), 1.14 (t, $^3J_{H,H}$ = 7.4 Hz, 12 H, CH_3), –0.18 [s, 6 H, $Al(CH_3)_2$] ppm. ^{13}C NMR (100.62 MHz, C_6D_6, 25 °C): δ = 167.4 [NC(H)N], 140.7 (Ar–C), 139.3 (Ar–C), 126.5 (Ar–CH), 125.6 (Ar–CH), 25.7 (CH_2), 15.3 (CH_3), –10.7 [br., $Al(CH_3)_2$] ppm. DRIFT (KBr): $\tilde{\nu}$ = 2966 (s), 2931 (m), 2889 (m), 1593 (w), 1540 (s), 1456 (s), 1436 (w), 1374 (w), 1334 (m), 1265 (m), 1222 (m), 1187 (m), 1105 (w), 1099 (w), 1057 (w), 1007 (w), 978 (w), 866 (w), 769 (m), 686 (br. s), 597 (w), 551 (w) cm^{-1}. $C_{23}H_{33}AlN_2$ (364.50): calcd. C 75.79, H 9.12, N 7.69; found C 75.73, H 9.37, N 7.79.

[Ga(DippForm)Me$_2$] (3a): A solution of $GaMe_3$ in *n*-hexane (5 mL, 31 mg, 0.27 mmol) was added dropwise to a solution of DippFormH (100 mg, 0.27 mmol) in *n*-hexane (5 mL) with vigorous stirring. Instant gas formation was observed. The clear solution was stirred at ambient temperature overnight, and then left under vacuum to reduce the solvent volume to 5 mL. Pure colorless crystalline product (**3a**) was obtained after 1 d at –40 °C (106 mg, 85%). ^1H NMR (400.13 MHz, C_6D_6, 25 °C): δ = 7.34 [s, 1 H, NC(*H*)N], 7.11 (br. s, 2 H, Ar), 7.10 (br. s, 4 H, Ar), 3.59 (sept, $^3J_{H,H}$ = 6.9 Hz, 4 H, C*H*), 1.21 (d, $^3J_{H,H}$ = 6.9 Hz, 24 H, CH_3), 0.24 [s, 6 H, Ga(CH_3)$_2$] ppm. ^{13}C NMR (100.61 MHz, C_6D_6, 25 °C): δ = 163.7 [NC(H)N], 144.7 (Ar–C), 140.46 (Ar–C), 126.2 (Ar–CH), 123.6 (Ar–CH), 28.4 (CH), 24.4 (CH_3), –4.7 [br. s, Ga(CH_3)$_2$] ppm. DRIFT (KBr): $\tilde{\nu}$ = 2960 (s), 2922 (m), 2867 (m), 1593 (w), 1542 (s), 1462 (m), 1443 (m), 1382 (w), 1362 (w), 1326 (m), 1256 (m), 1228 (m), 1199 (m), 1176 (w), 1098 (w), 1057 (w), 987 (w), 969 (w), 934 (w), 800 (m), 754 (s), 719 (w), 676 (w), 587 (w), 537 (w) cm^{-1}. $C_{27}H_{41}GaN_2$ (463.36): calcd. C 69.98, H 8.91, N 6.04; found C 70.20, H 9.10, N 6.02. [Compound **3a** was also prepared by an NMR-spectroscopic-scale reaction of $GaMe_3$ (10.3 mg, 0.09 mmol) with DippFormH (10.9 mg, 0.03 mmol) in C_6D_6 at ambient temperature (^1H NMR spectroscopic identification).]

Attempted Preparation of [Me$_2$Ga(μ-DippForm)(μ-Me)AlMe$_2$]: A solution of $GaMe_3$ in *n*-hexane (27 mg, 0.24 mmol) was added dropwise to a solution of compound **2a** (100 mg, 0.24 mmol) in *n*-hexane (5 mL) under vigorous stirring. The clear solution was stirred at ambient temperature overnight, and then left under vacuum to reduce the solvent volume to 5 mL. The synthesis attempt to obtain [Me_2Ga(μ-DippForm)(μ-Me)$AlMe_2$] failed, and the pure colorless crystalline product of the starting material (**2a**) was collected after 1 d at –40 °C (88 mg, 87%) (^1H NMR spectroscopic identification). Also, $AlMe_3$ (7.8 mg, 0.11 mmol) in *n*-hexane (5 mL) was added dropwise to a solution of compound **3a** (50 mg, 0.11 mmol) in *n*-hexane (10 mL). The clear solution was stirred at ambient temperature overnight, and the solvent was reduced to 5 mL under vacuum. However, no trace of [Me_2Ga(μ-DippForm)(μ-Me)$AlMe_2$] was observed, and pure colorless crystalline product (**2a**) was obtained after 1 d at –40 °C and identified by ^1H NMR spectroscopy (44 mg, 95%).

X-ray Crystallography and Crystal-Structure Determination of 1a, 1b, 2a, and 3a: Crystals suitable for diffraction experiments were selected in a glovebox and mounted in Paratone-N oil inside a nylon loop. Data collection for **1b**, **2a**, and **3a** was performed with a STOE-IPDS II system. Structure solutions and refinements were performed with the programs SHELXS-97[18] and SHELXL-97[19] through the graphical interface X-Seed,[20] which was also used to generate the figures. Data collection for **1a** was performed with a Bruker APEX2 Ultra TXS Pt^{135} CCD diffractometer by using graphite-monochromated Mo-K_α radiation (λ = 0.71073 Å) performing 182° ω scans in four orthogonal ϕ positions. Raw data

were collected by using the program SMART[21] and integrated and reduced with the program SAINT.[22] Corrections for absorption effects were applied by using SHELXTL[23] and/or SADABS.[24] For **1b**, two discrete molecules were observed in the asymmetric unit. One methyl group that belonged to an ethyl group was modeled as disordered with C atom position C26 (refined occupancy 0.64:0.36). DELU and SIMU restraints were applied on C26 and C26A. For **3a**, two methyl groups that belong to an isopropyl group were modeled as disordered with C atom positions C11 and C12 (refined occupancy 0.86:0.14). EADP restraints were applied on C11 and C11A as well as C12 and C12A. All CIF files were checked at http://www.iucr.org/. Further details of the refinement and crystallographic data are listed in Table 2 and in the CIF files. CCDC-915552 (**1a**), 915553 (**1b**), 915554 (**2a**), and 915555 (**3a**) contain the supplementary crystallographic data for this paper. These data can be obtained free of charge from The Cambridge Crystallographic Data Centre via www.ccdc.cam.ac.uk/data_request/cif.

Acknowledgments

This work was performed with the support of the Australian Research Council (ARC) (grant DP0984775). S. H. is grateful to the School of Chemistry at Monash for a scholarship. We also acknowledge support from the German Science Foundation.

[1] a) J. Barker, M. Kilner, *Coord. Chem. Rev.* **1994**, *133*, 219–300; b) F. T. Edelmann, *Coord. Chem. Rev.* **1994**, *137*, 403–481; c) F. T. Edelmann, *Chem. Soc. Rev.* **2009**, *38*, 2253–2268; d) T. Y. Her, C. C. Chang, L. K. Liu, *Inorg. Chem.* **1992**, *31*, 2291–2294; e) F. T. Edelmann, *Chem. Soc. Rev.* DOI: 10.1039/c2cs35180c; f) F. T. Edelmann, *Adv. Organomet. Chem.* **2009**, *57*, 183–352.

[2] a) K. B. Aubrecht, M. A. Hillmyer, W. B. Tolman, *Macromolecules* **2002**, *35*, 644–650; b) J. R. Hagadorn, J. Arnold, *J. Chem. Soc., Dalton Trans.* **1997**, 3087–3096; c) F. Benetollo, G. Cavinato, L. Crosara, F. Milani, G. Rossetto, C. Scelza, P. Zanella, *J. Organomet. Chem.* **1998**, *555*, 177–185; d) J. C. Flores, J. C. W. Chien, M. D. Rausch, *Organometallics* **1995**, *14*, 1827–1833; e) J. C. Flores, J. C. W. Chien, M. D. Rausch, *Organometallics* **1995**, *14*, 2106–2108; f) V. Volkis, M. Shmulinson, C. Averbuj, A. Lisovskii, F. T. Edelmann, M. S. Eisen, *Organometallics* **1998**, *17*, 3155–3157; g) J. M. Decker, S. J. Geib, T. Y. Meyer, *Organometallics* **1999**, *18*, 4417–4420; h) S. Dagorne, I. A. Guzei, M. P. Coles, R. F. Jordan, *J. Am. Chem. Soc.* **2000**, *122*, 274–289; i) M. P. Coles, R. F. Jordan, *J. Am. Chem. Soc.* **1997**, *119*, 8125–8126.

[3] a) D. A. Kissounko, M. V. Zabalov, G. P. Brusova, D. A. Lemenovskii, *Russ. Chem. Rev.* **2006**, *75*, 351–374; b) G. Talarico, P. H. M. Budzelaar, *Organometallics* **2000**, *19*, 5691–5695; c) J. Grundy, M. P. Coles, P. B. Hitchcock, *J. Organomet. Chem.* **2002**, *662*, 178–187.

[4] C.-C. Chang, J.-H. Chen, B. Srinivas, M. Y. Chiang, G.-H. Lee, S.-M. Peng, *Organometallics* **1997**, *16*, 4980–4984.

[5] a) J. A. R. Schmidt, J. Arnold, *J. Chem. Soc., Dalton Trans.* **2002**, 3454–3461; b) M. P. Coles, *Dalton Trans.* **2006**, 985–1001; c) C. A. Nijhuis, E. Jellema, T. J. J. Sciarone, A. Meetsma, P. H. M. Budzelaar, B. Hessen, *Eur. J. Inorg. Chem.* **2005**, 2089–2099; d) C. Jones, P. C. Junk, M. Kloth, K. M. Proctor, A. Stasch, *Polyhedron* **2006**, *25*, 1592–1600.

[6] a) J. Barker, N. C. Blacker, P. R. Phillips, N. W. Alcock, W. Errington, M. G. H. Wallbridge, *J. Chem. Soc., Dalton Trans.* **1996**, 431–437; b) J. A. R. Schmidt, J. Arnold, *Organometallics* **2002**, *21*, 2306–2313; c) A. L. Brazeau, G. A. Dilabio, K. A. Kreisel, W. Monillas, G. P. A. Yap, S. T. Barry, *Dalton Trans.* **2007**, 3297–3304; d) C. N. Rowley, G. A. DiLabio, S. T. Barry, *Inorg. Chem.* **2005**, *44*, 1983–1991; e) R. T. Boere, M. L. Cole, P. C. Junk, *New J. Chem.* **2005**, *29*, 128–134; f) F. Qian, K. Liu, H. Ma, *Dalton Trans.* **2010**, *39*, 8071–8083; g) L. A. Lesikar, A. F. Richards, *Polyhedron* **2010**, *29*, 1411–1422; h) M. L. Cole, A. J. Davies, J. Cameron, P. C. Junk, A. Stasch, *Polyhedron*, in press.

[7] a) M. P. Coles, D. C. Swenson, R. F. Jordan, V. G. Young, *Organometallics* **1997**, *16*, 5183–5194; b) M. P. Coles, D. C. Swenson, R. F. Jordan, V. G. Young, *Organometallics* **1998**, *17*, 4042–4048.

[8] a) S. Dagorne, R. F. Jordan, V. G. Young, *Organometallics* **1999**, *18*, 4619–4623; b) D. Kottmair-Maieron, R. Lechler, J. Weidlein, *Z. Anorg. Allg. Chem.* **1991**, *593*, 111–123.

[9] a) C.-T. Chen, C.-A. Huang, Y.-R. Tzeng, B.-H. Huang, *Dalton Trans.* **2003**, 2585–2590; b) B. Clare, N. Sarker, R. Shoemaker, J. R. Hagadorn, *Inorg. Chem.* **2004**, *43*, 1159–1166; c) D. Abeysekera, K. N. Robertson, T. S. Cameron, J. A. C. Clyburne, *Organometallics* **2001**, *20*, 5532–5536.

[10] a) M. L. Cole, G. B. Deacon, C. M. Forsyth, P. C. Junk, K. Konstas, J. Wang, *Chem. Eur. J.* **2007**, *13*, 8092–8110; b) R. M. Roberts, *J. Org. Chem.* **1949**, *14*, 277–284; c) K. M. Kuhn, R. H. Grubbs, *Org. Lett.* **2008**, *10*, 2075–2077; d) P. C. Junk, M. L. Cole, *Chem. Commun.* **2007**, 1579–1590.

[11] a) R. G. Pearson, *J. Am. Chem. Soc.* **1963**, *85*, 3533–3539; b) R. G. Pearson, *Science* **1966**, *151*, 172; c) R. G. Pearson, *Chem. Br.* **1967**, 103; d) H. M. Dietrich, C. Maichle-Mössmer, R. Anwander, *Dalton Trans.* **2010**, *39*, 5783–5785.

[12] a) C. T. Sirimanne, Z. Yu, M. J. Heeg, C. H. Winter, *J. Organomet. Chem.* **2006**, *691*, 2517–2527; b) Z. Yu, J. M. Wittbrodt, M. J. Heeg, H. B. Schlegel, C. H. Winter, *J. Am. Chem. Soc.* **2000**, *122*, 9338–9339.

[13] Z. Yu, M. J. Heeg, C. H. Winter, *Chem. Commun.* **2001**, 353–354.

[14] J. Yamamoto, C. A. Wilkie, *Inorg. Chem.* **1971**, *10*, 1129–1133.

[15] C. Soto, R. Wu, D. W. Bennett, W. T. Tysoe, *Chem. Mater.* **1994**, *6*, 1705–1711.

[16] a) J. C. Huffman, W. E. Streib, *J. Chem. Soc., Chem. Commun.* **1971**, 911–912; b) S. K. Byram, J. K. Fawcett, S. C. Nyburg, R. J. O'Brien, *J. Chem. Soc. C* **1970**, 16–17; c) R. G. Vranka, E. L. Amma, *J. Am. Chem. Soc.* **1967**, *89*, 3121–3126; d) V. R. Magnuson, G. D. Stucky, *J. Am. Chem. Soc.* **1969**, *91*, 2544–2550; e) S. D. Waezsada, F.-Q. Liu, E. F. Murphy, H. W. Roesky, M. Teichert, I. Usón, H. G. Schmidt, T. Albers, E. Parisini, M. Noltemeyer, *Organometallics* **1997**, *16*, 1260–1264; f) E. Ihara, V. G. Young, R. F. Jordan, *J. Am. Chem. Soc.* **1998**, *120*, 8277–8278.

[17] a) R. D. Shannon, *Acta Crystallogr., Sect. A* **1976**, *32*, 751; b) R. Blom, A. Haaland, *J. Mol. Struct.* **1985**, *128*, 21–27.

[18] G. M. Sheldrick, *SHELXS-97, Program for crystal structure solution*, University of Göttingen, Germany **1997**.

[19] G. M. Sheldrick, *SHELXL-97, Program for crystal structure refinement*, University of Göttingen, Germany, **1997**.

[20] L. J. Barbour, *J. Supramol. Chem.* **2001**, *1*, 189–191.

[21] *SMART, Data Collection Software for Bruker AXS CCD*, v.5.054, Bruker AXS Inc., Madison, WI, **1999**.

[22] *SAINT, Data Integration Software for Bruker AXS CCD*, v. 6.45A, Bruker AXS Inc., Madison, WI, **2002**.

[23] *SHELXTL, Structure Determination Software Suite*, v. 6.14, Bruker AXS Inc., Madison, WI, **2000**.

[24] G. M. Sheldrick, *SADABS*, v. 2001/1, University of Göttingen, Germany, **2006**.

Received: December 14, 2012
Published Online: March 8, 2013

Paper VI

ORGANOMETALLICS

Communication

pubs.acs.org/Organometallics

Half-Sandwich Rare-Earth-Metal Alkylaluminate Complexes Bearing Peripheral Boryl Ligands

Nicole Dettenrieder, Christoph O. Hollfelder, Lars N. Jende, Cäcilia Maichle-Mössmer, and Reiner Anwander*

Institut für Anorganische Chemie, Eberhard Karls Universität Tübingen, Auf der Morgenstelle 18, 72076 Tübingen, Germany

Supporting Information

ABSTRACT: $[(C_5Me_5)LnMe_2]_3$ (Ln = Y, Lu) dissolve readily in a *n*-hexane/toluene mixture upon addition of 3 equiv of the organoaluminum boryl compound $[Me_2Al\{B(NDippCH)_2\}]_2$ (Dipp = $C_6H_3iPr_2$-2,6). The half-sandwich complexes $(C_5Me_5)Ln[(AlMe_3)\{B(NDippCH)_2\}]_2$ thus formed display unsymmetrical heteroaluminate coordination not only in the solid state but also at lower temperatures in solution, which is distinct from the behavior of the homoaluminate congeners $(C_5Me_5)Ln(AlMe_4)_2$. The effect of homo- versus heteroaluminate coordination is assessed in the coordinative polymerization of isoprene.

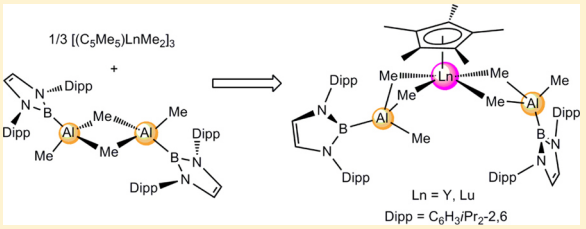

Monocyclopentadienyl rare-earth-metal alkyl complexes continue to reveal unique performance in stereospecific (co)polymerization catalysis.[1] As a consequence, much effort has been devoted to catalyst design by assessing cyclopentadienyl ring and peripheral substitution as well as type of alkyl actor ligand[2] and cocatalyst(s).[1] We and others have embarked on a strategy utilizing tetramethylaluminate ligands (Chart 1, **I**) as

Chart 1. Known Half-Sandwich Bis(alkylaluminates) I and III and Proposed Active Species II for Polymerization Reactions

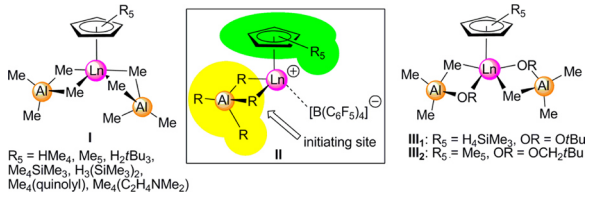

alkyls in disguise, ensuring not only thermal robustness and steric saturation but also high dynamic behavior.[3] While activation (=cationization) of complexes **I** is routinely achieved by reaction with borane/borate cocatalysts, the remaining $[AlMe_4]^-$ moiety features the initiating site (**II**): e.g., for 1,3-diene polymerization.[3d,e,h,i] It can be anticipated that the composition of the aluminate actor ligand will significantly affect the polymerization performance, which is why we set out to implement heteroaluminates ("heteroaluminates"). For monoanionic moieties X featuring either strongly electronegative donor atoms (OR (**III**),[2,4] NR_2,[5] Cl[6]) or hydrido[7] and alkynyl ligands,[8] X is found in the bridging position exclusively: that is, $Ln(\mu\text{-}X)(\mu\text{-}Me)_xAlMe_{1+y}$ ($x + y = 2$). In the case of heteroaluminates with different alkyl groups, the bulkier X is found in the peripheral position: that is, $Ln(\mu\text{-}Me)_{1+x}AlMe_yX$ ($x + y = 2$).[9]

We have recently described homoleptic heteroaluminate complexes of the type $Ln[(AlMe_3)\{B(NDippCH)_2\}]_3$ (Ln = Y, Lu; Dipp = $C_6H_3iPr_2$-2,6),[10] featuring the bulky carbanion-like boryl ligand[11] in the peripheral position. Herein we extend this study to the synthesis and characterization of the first half-sandwich complexes bearing such peripheral boryl ligands and the suitability of the resulting complexes for the polymerization of isoprene.

Half-sandwich heteroaluminate complexes $(C_5Me_5)Ln[(AlMe_3)\{B(NDippCH)_2\}]_2$ (**2** (Ln = Y), **3** (Ln = Lu)) can be obtained by applying a strategy which had previously been successful for the synthesis of the respective homoleptic derivatives. Accordingly, addition of stoichiometric amounts of $[Me_2Al\{B(NDippCH)_2\}]_2$ (**1**) to $[(C_5Me_5)LnMe_2]_3$ (Ln = Y, Lu)[12] gave complexes **2** and **3** in quantitative yields (Scheme 1). Complexes **2** and **3** were examined by X-ray crystallography and found to be isomorphous.[13] However, due to a low-quality data set collected for yttrium complex **2**, only the molecular structure of **3** will be discussed in the following. Figure 1 shows one out of two molecules $(C_5Me_5)Lu[(AlMe_3)\{B(NDippCH)_2\}]_2$ detected in the asymmetric unit. As anticipated, the two $[B(NDippCH)_2]$ moieties are terminally bonded to the aluminum atoms and are oriented nearly perpendicular to each other (∠N1B1N2−N3B2N4 = 87.1°; ∠N5B3N6−N7B4N8 = 89.3°). The $AlMe_3$ moieties, which connect the boryl entities to the lutetium center, each have two bridging methyl groups and a terminal methyl group. The terminal methyl groups are positioned in opposite directions, probably because of steric hindrance. One of the $[AlMe_2Lu]$ units is nearly planar (∠C32Lu1C33−C32Al2C33 = 13.7°; ∠C78Lu2C79−C78Al3C79 = 13.1°), while the other is remarkably bent (∠C35Lu1C36−C35Al1C36 = 51.2°;

Received: November 29, 2013
Published: March 19, 2014

   dx.doi.org/10.1021/om401163a | *Organometallics* 2014, 33, 1528−1531

Scheme 1. Synthesis of $(C_5Me_5)Ln[(AlMe_3)\{B(NDippCH)_2\}]_2$ (Ln = Y (2), Lu (3)) and Reactivity toward Tetrahydrofuran

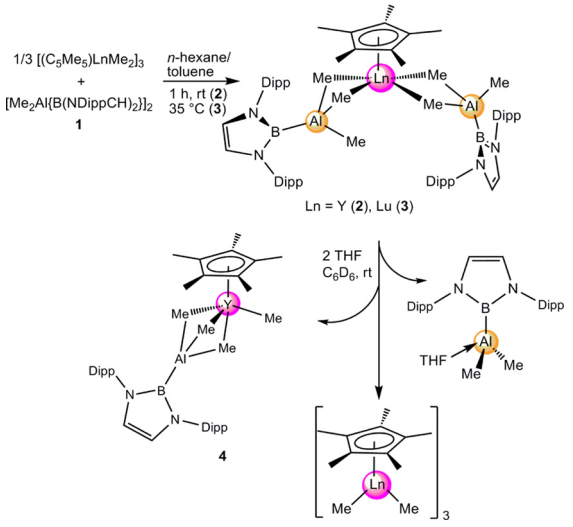

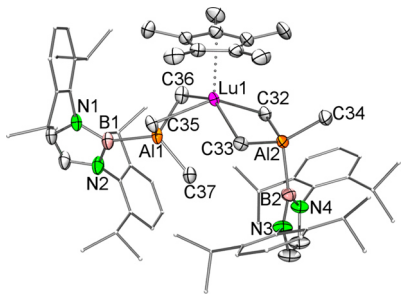

Figure 1. Molecular structure of $(C_5Me_5)Lu[(AlMe_3)\{B(NDippCH)_2\}]_2$ (3) with atomic displacement parameters set at the 50% level. The carbon atoms of the aromatic parts are shown with reduced radii. Hydrogen atoms, cocrystallized hexane, and the second molecule of the asymmetric unit have been omitted for clarity. Selected interatomic distances (Å) and angles (deg): Lu1−C32, 2.506(4); Lu1−C33, 2.504(3); Lu1−C35, 2.605(4); Lu1−C36, 2.590(4); Lu···C37, 3.381(4); Lu1···Al1, 2.917(2); Lu1···Al2, 3.059(2); ∠C32Lu1C33−C32Al2C33, 13.7; ∠C35Lu1C36−C35Al1C36, 51.2; B1−Al1, 2.137(5); B2−Al2, 2.135(5); Lu2−C78, 2.507(4); Lu2−C79, 2.509(4); Lu2−C81, 2.622(4); Lu2−C82, 2.591(4); Lu2···C83, 3.351(4); Lu2···Al3, 3.062(2); Lu2···Al4, 2.913(2); ∠C78Lu2C79−C78Al3C79, 13.1; ∠C81Lu2C82−C81Al4C82, 51.6; B3−Al4, 2.137(4); B4−Al3, 2.137(4).

∠C81Lu2C82−C81Al4C82 = 51.6°). This distinct Ln−alkylaluminate bonding is a well-known structural motif of half-sandwich rare-earth-metal bis(tetramethylaluminate), as previously revealed by $(C_5Me_5)Lu(AlMe_4)_2$,[3a] $(C_5Me_5)La(AlMe_4)_2$,[3b] $[1,3\text{-}(Me_3Si)_2C_5H_3]Ln(AlMe_4)_2$ (Ln = Y, Nd, Lu), $(C_5Me_4SiMe_3)Y(AlMe_4)_2$, and $[1,2,4\text{-}(Me_3C)_3C_5H_2]Ln(AlMe_4)_2$ (Ln = La, Nd, Sm).[3e] Moreover, the bent $[AlMe_2Lu]$ moiety in complex **3** displays further literature-known characteristics:[3] elongated Lu−(μ-CH_3) distances (Δ_{Lu-C} = 0.08−0.11 Å), a shortened Lu−Al distance (Δ_{Lu-Al} = 0.14−0.15 Å), and an additional short Lu−C(Me) contact (Lu1···C37 = 3.381(4); Lu2···C83 = 3.351(4) Å). The last observation is probably caused by steric unsaturation and is also reflected in the different angles Lu−Al−C_{term} of the two $[(AlMe_3)\{B(NDippCH)_2\}]$ ligands[3b] (∠Lu1−Al1−C37 = 84.9(2)°; ∠Lu1−Al2−C34 = 117.5(2)°; ∠Lu2−Al4−C83 = 84.0(2)°; ∠Lu2−Al3−C80 = 117.3(2)°). The B−Al distances in complex **3** (average 2.137 Å) are slightly shorter than those in our recently published homoleptic Lu complex $Lu[(AlMe_3)\{B(NDippCH)_2\}]_3$ (average 2.153 Å).[10]

$^{11}B\{^1H\}$ NMR spectra were measured for both **2** and **3**, as well as a $^1H-^{89}Y$ HSQC NMR spectrum of **2**. The boron signals appear in the expected region of 31.4 (**2**) and 31.0 (**3**) ppm (see Figures S6 and S11, Supporting Information) and are comparable to those of educt **1** (27.9 ppm) and $(THF)Me_2Al[B(NDippCH)_2]$ (31.9 ppm) (all recorded in C_6D_6).[10] The yttrium resonance of complex **2** at 144.5 ppm (see Figure S5, Supporting Information) appears at relatively low field in comparison to the published values of other(C_5Me_5)-substituted yttrium complexes,[14] which can be attributed to poor electron donation of the $Me_2Al[B(NDippCH)_2]$ ligands.[14]

Low-temperature ^1H NMR spectroscopic studies were performed both for $(C_5Me_5)Y[(AlMe_3)\{B(NDippCH)_2\}]_2$ (**2**) and $(C_5Me_5)Lu[(AlMe_3)\{B(NDippCH)_2\}]_2$ (**3**). Interestingly, the asymmetric bonding of the $[(AlMe_3)\{B(NDippCH)_2\}]$ entities as featured by the solid-state structure (Figure 1) gets nicely resolved through decoalescing methyl groups at lower temperatures. These observations are in contrast to those made for homoleptic $Ln[(AlMe_3)\{B(NDippCH)_2\}]_3$ (Ln = Y, Lu).[10] For the latter, the methyl group signal splits up at lower temperatures into two peaks with an integral ratio of 2:1 and further into three peaks with a 1:1:1 ratio, which can be explained by an intitial separation into bridging and terminal methyl groups (2:1 ratio), with a further decoalescence of the bridging methyl moieties (1:1:1).[10]

At ambient temperature, lutetium complex **3** shows a broad singlet in the high-field region, which accounts for a high fluxionality of bridging and terminal methyl groups. An analogous observation is made for the yttrium complex **2**; however, due to yttrium coupling, a doublet with a $^2J_{YH}$ coupling constant of 2.9 Hz is observed. In complex **2**, the methyl resonance of 18 protons splits up into 2 signals at about −40 °C with a ratio of 15:3, followed by a decoalescence of the larger resonance into 2 signals with a ratio of 9:6 at ca. −50 °C. The signal that corresponds to 9 protons decoalesces further at about −70 to −80 °C (ratio 3:6). At −80 °C, there are then 4 separate signals for the aluminum methyl groups, with proton ratios of 3:6:6:3. The initial splitting of the signal (15:3) at −40 °C already documents the separation of a single (terminal) methyl group from the others and shows the inequivalency of the terminal methyl groups on the $(AlMe_3)[B(NDippCH)_2]$ ligands. The final signal splitting at −80 °C with 4 signals in the ratio 3:6:6:3 indicates separate resonances for the bridging and terminal methyl groups on each ligand. Despite a different signal ordering/shifting in the low-temperature ^1H NMR spectra of Lu complex **3**, qualitatively similar observations were made as for **2** (Figure 2). For the smaller Lu(III) metal center, all decoalescence phenomena are observed at higher temperature because of enhanced steric hindrance. The single methyl resonance starts splitting up at around −20 °C with separation of one methyl group (15:3). Further splitting of the larger signal into 2 signals of 12 and 3 protons, respectively, is observed at about −25 °C. Between −30 and −40 °C, the decoalescence of the bridging methyl groups takes place to produce the final 4-signal pattern with an integral ratio of 6:6:3:3. For comparison, the low-temperature ^1H NMR spectra of half-sandwich rare-earth-metal tetramethylaluminate complexes $(C_5Me_5)Ln(AlMe_4)_2$ (**I**, Chart 1) revealed high methyl group mobility even at −85 °C, meaning that any decoalescence into bridging and terminal $AlMe_3$ signals could not be observed at all.[3] The heteroaluminate complex $(C_5Me_5)Y[(\mu\text{-}OCH_2CMe_3)(\mu\text{-}Me)AlMe_2]_2$ (**III$_2$**, Chart 1)

dx.doi.org/10.1021/om401163a | *Organometallics* 2014, 33, 1528−1531

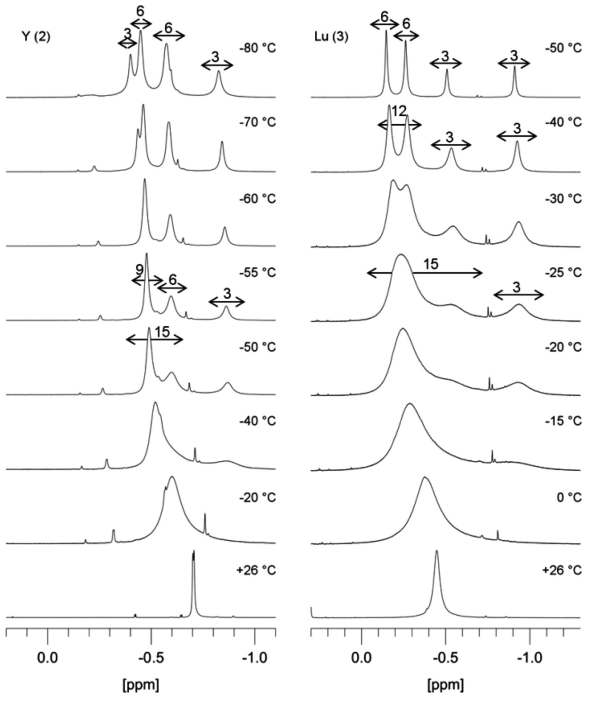

Figure 2. Low-temperature NMR spectra of $(C_5Me_5)Ln[(AlMe_3)\{B(NDippCH)_2\}]_2$ (**2**, left; **3**, right).

gave one broad $AlMe_3$ signal at ambient temperature as well but displayed a 3-signal pattern with an integral ratio of 6:6:6 in the range −30 to −80 °C, indicative of two separate signals for the terminal methyl groups and one signal for the bridging methyl groups.[2b]

The reactivity of half-sandwich complexes **2** and **3** toward THF was exploited by NMR-scale experiments in deuterated benzene as solvent. The envisaged donor-induced cleavage should proceed via separation of $(THF)Me_2Al[B(NDippCH)_2]$ and re-formation of complexes $[(C_5Me_5)LnMe_2]_3$ (Ln = Y, Lu), when using 2 equiv of THF (Scheme 1). For lutetium complex **3**, the formation of both expected products was observed without detection of any significant byproducts (see Figure S14, Supporting Information). For yttrium complex **2**, a similar cleavage reaction took place but one byproduct could be identified as well (ca. 31%). The ^{1}H NMR spectrum of this byproduct showed an integral signal ratio of about 2:15:12:12:3:9 (see also Figure S13, Supporting Information), which can be assigned to the partially donor-cleaved species $[(C_5Me_5)YMe(Me_3Al)\{B(NDippCH)_2\}]$ (**4**, Scheme 1). The signals of the metal-bonded methyl groups appear as two doublets ($^2J_{YH}$ = 2.2 and 2.0 Hz) in a 3:9 ratio. A control NMR measurement, which was performed after 3 days at ambient temperature, revealed decomposition of this species as well as of $[(C_5Me_5)YMe_2]_3$, in contrast to the case for $(THF)Me_2Al[B(NDippCH)_2]$.

Complexes **2** (Ln = Y) and **3** (Ln = Lu) were successfully tested in the polymerization of isoprene (Table 1), upon addition of borates $[Ph_3C][B(C_6F_5)_4]$ (**A**) and $[PhNMe_2H][B(C_6F_5)_4]$ (**B**) as cationizing cocatalysts (for activation with borane $B(C_6F_5)_3$ (**C**), see Table S1 in the Supporting Information). The combination **3**/**A** (run 5 in Table 1) displayed the highest activity and gave quantitative polymerization after 1 h. Exemplarily, this polymer was investigated by differential scanning calorimetry (DSC), revealing a single glass transition at −20.8 °C.

Surveying runs 1−7, in terms of microstructure, it is apparent that there is a strong tendency toward the formation of 3,4-polyisoprene if cocatalysts **A** and **B** are involved. As both cocatalysts are intended to produce a similar active species,[3h,i] the formation of similar polymers is not unexpected. However, the quite different activity situations for **3**/**A** (run 5) and **3**/**B** (run 6) are remarkable. Furthermore, the molecular weight distributions seem to be significantly cocatalyst dependent: PDI(**A**) = 1.4−1.5; PDI(**B**) = 1.2−1.3. On comparison of the obtained polymer data with our earlier results,[3e] applying $(C_5Me_5)Ln(AlMe_4)_2$ (Ln = Y, Lu) precatalysts (run 8−11 in Table 1) shows that the microstructure develops differently. In contrast to the present study, the homoaluminate-supported catalysts tend to form mainly *cis*-polyisoprene. It is striking that especially the combination $(C_5Me_5)Lu(AlMe_4)_2$/**B** is far more active than the corresponding boryl-substituted species.

For a better understanding of the cationization reaction and the involved high 3,4-polyisoprene content, the formation of the most active catalyst/cocatalyst mixture, **3**/**A**, was examined by NMR spectroscopy. The cationization reaction as depicted in eq 1 was complete after 7 min. In addition to the expected formation of 0.5 equiv of **1** and 1 equiv of Ph_3CMe as byproducts, the active species $[(C_5Me_5)Lu[(AlMe_3)\{B(NDippCH)_2\}]]^+[B(C_6F_5)_4]^-$ (**4**) gave clean and well-resolved NMR spectra.

Table 1. Selected Examples of Isoprene Polymerization at Ambient Temperature

entry[a]	precatalyst	cocatalyst[b]	*t* (h)	yield (%)	*cis*-1,4[c]	*trans*-1,4[c]	3,4[c]	M_n[d] (×10^4)	M_w/M_n[d]	ref
1	**2**	**A**	1	8.7	21.3	12.7	66.0	2.4	1.41	g
2	**2**	**A**	24	>99	49.4	5.3	45.3	9.6	1.45	g
3	**2**	**B**	1	11.2	30.7	3.3	66.8	3.8	1.22	g
4	**2**	**B**	24	>99	34.1	15.5	50.4	7.4	1.29	g
5	**3**	**A**	1	>99	21.5	17.7	60.8	4.7	1.44	g
6	**3**	**B**	1	5.5	38.6	3.2	58.2	–[e]	–[e]	g
7	**3**	**B**	24	>99	21.4	14.7	63.9	6.0	1.23	g
8[f]	$Cp^*Y(AlMe_4)_2$	**A**	24	>99	60.5	20.6	18.9	2.0	8.95	3e
9[f]	$Cp^*Y(AlMe_4)_2$	**B**	24	>99	43.5	28.7	27.8	6.0	1.59	3e
10[f]	$Cp^*Lu(AlMe_4)_2$	**A**	0.25	>99	73.9	19.7	6.4	10.0	1.49	g
11[f]	$Cp^*Lu(AlMe_4)_2$	**B**	0.25	>99	70.3	20.3	9.4	9.5	1.45	g

[a]Conditions: 0.02 mmol of precatalyst, [Ln]/[cocat] = 1/1, 7 mL of toluene, 20 mmol of isoprene, room temperature. [b]Cocatalyst: $[Ph_3C][B(C_6F_5)_4]$ (**A**); $[PhNMe_2H][B(C_6F_5)_4]$ (**B**). Polymerizations applying $B(C_6F_5)_3$ (**C**) can be found in the Supporting Information (Table S1). [c]Determined by ^{1}H and ^{13}C NMR spectroscopy in $CDCl_3$. [d]Determined by means of size-exclusion chromatography (SEC) against polystyrene standards. [e]Not determined due to low yield. [f]Polymerizations at 40 °C. [g]This work.

dx.doi.org/10.1021/om401163a | *Organometallics* 2014, 33, 1528−1531

$$(C_5Me_5)Lu[(AlMe_3)\{B(NDippCH)_2\}]_2 + \mathbf{A} \rightarrow 0.5\ \mathbf{1} + [(C_5Me_5)Lu[(AlMe_3)\{B(NDippCH)_2\}]]^+[B(C_6F_5)_4]^- + Ph_3CMe \quad (1)$$

In comparison to the spectra of nonactivated **3**, the integrals of the signals assigned to the $(AlMe_3)[B(NDippCH)_2]$ ligands were cut in half, which proves complete separation of one of these ligands. The signals assigned to the remaining $(AlMe_3)$-$[B(NDippCH)_2]$ ligand split up, implying hindered rotation. The latter phenomenon might reflect the coordination of one of the aryl moieties to the cationized metal center in **4**, which would also explain a decreased polymerization rate and a 3,4-selectivity (see Figure S15 in the Supporting Information). In addition, the ^{19}F chemical shift difference of the *p*- and *m*-F atoms of the borate anions in **3**/**A** is found to be 4.1 ppm, which implies a very weak interaction with the cationic entity (tight ion pairs, ca. 5.4 ppm; none, 2.7 ppm).[15]

In conclusion, half-sandwich complexes $(C_5Me_5)Ln[(AlMe_3)$-$\{B(NDippCH)_2\}]_2$ can be accessed in high yields via addition of $[(Me_2Al)\{B(NDippCH)_2\}]_2$ to $[(C_5Me_5)LnMe_2]_3$ (Ln = Y, Lu; Dipp = $C_6H_3iPr_2$-2,6). The bulky boryl ligand $[B(NDippCH)_2]$ favors an unsymmetrical peripheral coordination (=terminal at aluminum), which markedly affects the fluxional behavior of the metal-bonded methyl groups. With respect to isoprene polymerization, the implementation of heteroaluminate ligands does not affect the cationization reaction with borate activators but bears on the microstructure of polyisoprene (switch from *cis*-1,4 to 3,4).

■ ASSOCIATED CONTENT

Supporting Information

Text, figures, tables, and a CIF file giving experimental details for the syntheses and characterization of complexes **2** and **3** as well as of the polymerization study, NMR spectra, and crystallographic data for **2**. This material is available free of charge via the Internet at http://pubs.acs.org.

■ AUTHOR INFORMATION

Corresponding Author

*E-mail for R.A.: reiner.anwander@uni-tuebingen.de.

Notes

The authors declare no competing financial interest.

■ ACKNOWLEDGMENTS

We thank the German science foundation for funding (Grant AN 238/14-2) and Jürgen Koch (THASS GmbH) for kindly providing the DSC measurements.

■ REFERENCES

(1) (a) Arndt, S.; Okuda, J. *Chem. Rev.* **2002**, *102*, 1953. (b) Fischbach, A.; Anwander, R. *Adv. Polym. Sci.* **2006**, *204*, 155. (c) Hou, Z. *Bull. Chem. Soc. Jpn.* **2003**, *76*, 2253. (d) Okuda, J. *Dalton Trans.* **2003**, 2367. (e) Zimmermann, M.; Anwander, R. *Chem. Rev.* **2010**, *110*, 6194. (f) Nishiura, M.; Hou, Z. *Nat. Chem.* **2010**, *2*, 257.

(2) (a) Evans, W. J.; Boyle, T. J.; Ziller, J. W. *J. Organomet. Chem.* **1993**, *462*, 141. (b) Fischbach, A.; Herdtweck, E.; Anwander, R. *Inorg. Chim. Acta* **2006**, *359*, 4855.

(3) (a) Anwander, R.; Klimpel, M. G.; Dietrich, H. M.; Shorokhov, D. J.; Scherer, W. *Chem. Commun.* **2003**, 1008. (b) Dietrich, H. M.; Zapilko, C.; Herdtweck, E.; Anwander, R. *Organometallics* **2005**, *24*, 5767. (c) Le Roux, E.; Nief, F.; Jaroschik, F.; Törnroos, K. W.; Anwander, R. *Dalton Trans.* **2007**, 4866. (d) Zimmermann, M.; Törnroos, K. W.; Anwander, R. *Angew. Chem., Int. Ed.* **2008**, *47*, 775. (e) Zimmermann, M.; Törnroos, K. W.; Sitzmann, H.; Anwander, R. *Chem. Eur. J.* **2008**, *14*, 7266. (f) Robert, D.; Spaniol, T. P.; Okuda, J. *Eur. J. Inorg. Chem.* **2008**, 2801. (g) Dietrich, H. M.; Törnroos, K. W.; Herdtweck, E.; Anwander, R. *Organometallics* **2009**, *28*, 6739. (h) Zimmermann, M.; Volbeda, J.; Törnroos, K. W.; Anwander, R. *Compt. Rend. Chim.* **2010**, *13*, 651. (i) Litlabø, R.; Enders, M.; Törnroos, K. W.; Anwander, R. *Organometallics* **2010**, *29*, 2588. (j) Jende, L. N.; Maichle-Mössmer, C.; Anwander, R. *Chem. Eur. J.* **2013**, *19*, 16321.

(4) For Ln(III) examples, see: (a) Evans, W. J.; Boyle, T. J.; Ziller, J. W. *J. Am. Chem. Soc.* **1993**, *115*, 5084. (b) Biagini, P.; Lugli, G.; Abis, L.; Millini, R. *J. Organomet. Chem.* **1994**, *474*, C16. (c) Giesbrecht, G. R.; Gordon, J. C.; Brady, J. T.; Clark, D. L.; Keogh, D. W.; Michalczyk, R.; Scott, B. L.; Watkin, J. G. *Eur. J. Inorg. Chem.* **2002**, 723. (d) Gordon, J. C.; Giesbrecht, G. R.; Brady, J. T.; Clark, D. L.; Keogh, D. W.; Scott, B. L.; Watkin, J. G. *Organometallics* **2002**, *21*, 127. (e) Fischbach, A.; Herdtweck, E.; Anwander, R.; Eickerling, G.; Scherer, W. *Organometallics* **2003**, *22*, 499. (f) Fischbach, A.; Klimpel, M. G.; Widenmeyer, M.; Herdtweck, E.; Scherer, W.; Anwander, R. *Angew. Chem., Int. Ed.* **2004**, *43*, 2234. (g) Fischbach, A.; Eickerling, G.; Scherer, W.; Herdtweck, E.; Anwander, R. *Z. Naturforsch., B* **2004**, *59b*, 1353. (h) Fischbach, A.; Meermann, C.; Eickerling, G.; Scherer, W.; Anwander, R. *Macromolecules* **2006**, *39*, 6811. (i) Occhipinti, G.; Meermann, C.; Dietrich, H. M.; Litlabø, R.; Auras, F.; Törnroos, K. W.; Maichle-Mössmer, C.; Jensen, V. R.; Anwander, R. *J. Am. Chem. Soc.* **2011**, *133*, 6323.

(5) For Ln(III) examples, see: (a) Evans, W. J.; Anwander, R.; Doedens, R. J.; Ziller, J. W. *Angew. Chem., Int. Ed.* **1994**, *33*, 1641. (b) Evans, W. J.; Anwander, R.; Ziller, J. W. *Inorg. Chem.* **1995**, *34*, 5927. (c) Evans, W. J.; Ansari, M. A.; Ziller, J. W.; Khan, S. I. *Inorg. Chem.* **1996**, *35*, 5435. (d) Gordon, J. C.; Giesbrecht, G. R.; Clark, D. L.; Hay, P. J.; Keogh, D. W.; Poli, R.; Scott, B. L.; Watkin, J. G. *Organometallics* **2002**, *21*, 4726. (e) Zimmermann, M.; Törnroos, K. W.; Anwander, R. *Organometallics* **2006**, *25*, 3644. (f) Zimmermann, M.; Estler, F.; Herdtweck, E.; Törnroos, K. W.; Anwander, R. *Organometallics* **2007**, *26*, 6029.

(6) (a) Evans, W. J.; Champagne, T. M.; Giarikos, D. G.; Ziller, J. W. *Organometallics* **2005**, *24*, 570. (b) Evans, W. J.; Champagne, T. M.; Ziller, J. W. *Organometallics* **2005**, *24*, 4882.

(7) Schädle, C.; Schädle, D.; Eichele, K.; Anwander, R. *Angew. Chem., Int. Ed.* **2013**, *52*, 13238.

(8) Nieland, A.; Mix, A.; Neumann, B.; Stammler, H.-G.; Mitzel, N. W. *Chem. Eur. J.* **2013**, *19*, 8268.

(9) Klimpel, M. G.; Eppinger, J.; Sirsch, P.; Scherer, W.; Anwander, R. *Organometallics* **2002**, *21*, 4021.

(10) Dettenrieder, N.; Dietrich, H. M.; Schädle, C.; Maichle-Mössmer, C.; Törnroos, K. W.; Anwander, R. *Angew. Chem., Int. Ed.* **2012**, *51*, 4461.

(11) (a) Segawa, Y.; Yamashita, M.; Nozaki, K. *Science* **2006**, *314*, 113. (b) Segawa, Y.; Suzuki, Y.; Yamashita, M.; Nozaki, K. *J. Am. Chem. Soc.* **2008**, *130*, 16069.

(12) The complexes $[(C_5Me_5)LnMe_2]_3$ can be obtained from the bis(tetramethylaluminates) $(C_5Me_5)Ln(AlMe_4)_2$[3b,g] via donor-induced cleavage with THF or diethyl ether: Dietrich, H. M.; Grove, H.; Törnroos, K. W.; Anwander, R. *J. Am. Chem. Soc.* **2006**, *128*, 1458.

(13) Crystal data for compound **2** ($C_{77}H_{126}Al_2B_2YN_4$, M_r = 1272.298): $P\bar{1}$, a = 13.5337 Å, b = 18.6533 Å, c = 33.0015 Å, α = 82.371°, β = 83.305°, γ = 78.392°. Because of the poor quality of the crystal, data were not deposited. Crystal data for compound **3** ($C_{77}H_{126}Al_2B_2LuN_4$, M_r= 1358.37): $P\bar{1}$, a = 13.4966(3) Å, b = 18.6094(5) Å, c = 32.8876(9) Å, α = 82.408(2)°, β = 83.663(1)°, γ = 79.017(2)°, V = 8006.9(4) Å^3, and d_{calcd} = 1.127 g cm^{-3} for Z = 4. CCDC 972153 contains supplementary crystallographic data for compound **3**. These data can be obtained free of charge from The Cambridge Crystallographic Data Centre via www.ccdc.cam.ac.uk/data_request/cif.

(14) Schaverien, C. J. *Organometallics* **1994**, *13*, 69.

(15) (a) Horton, A. D. *Organometallics* **1996**, *15*, 2675. (b) Horton, A. D.; de With, J.; van der Linden, A. J.; van de Weg, H. *Organometallics* **1996**, *15*, 2672.

Supporting Information

Half-Sandwich Rare-Earth Metal Alkylaluminate Complexes Bearing Peripheral Boryl Ligands

Nicole Dettenrieder, Christoph O. Hollfelder, Lars N. Jende, Cäcilia Maichle-Mössmer, and Reiner Anwander

Institut für Anorganische Chemie, Universität Tübingen, Auf der Morgenstelle 18, D-72076 Tübingen, (Germany)

Table of Contents:

S2 Experimental data including NMR spectra

S17 Crystallographic data

S18 References

General Considerations. All operations were performed with rigorous exclusion of air and water, using standard Schlenk, high-vacuum, and glovebox techniques (MBraun 200B; <0.1 ppm O_2, <0.1 ppm H_2O). *n*-Hexane and toluene were purified by using Grubbs columns (MBraun SPS-800, solvent purification system) and stored in a glovebox. Benzene-*d*6 (99.5 %) was received from Deutero GmbH, toluene-*d*8 (99.5%) from euriso-top. Both NMR solvents were dried over NaK for a minimum of 48 h, and filtered through a filter pipette (Whatman) before use. $[(C_5Me_5)YMe_2]_3$ was synthesized from $(C_5Me_5)Y(AlMe_4)_2$,[1] which was made according to the literature (route a).[2] $[(C_5Me_5)LuMe_2]_3$ was obtained from $(C_5Me_5)Lu(AlMe_4)_2$.[3] $(C_5Me_5)Lu(AlMe_4)_2$ was synthesized slightly modified to the literature synthesis,[3] with 4 equiv. of HC_5Me_5 and 6 days reaction time at 35 °C. $[Me_2Al\{B(NDippCH)_2\}]_2$ was also synthesized according to the literature.[4] NMR spectra were recorded by using *J. Young* valve NMR tubes and obtained on a Bruker AVII+400 (^{1}H: 400.11 MHz, ^{13}C: 100.61 MHz) and on a Bruker AVII+500 spectrometer (^{1}H: 500.13 MHz, ^{13}C: 125.76 MHz, ^{11}B: 160.46 MHz, ^{19}F: 376.43 MHz , ^{89}Y: 24.51 MHz). ^{1}H and ^{13}C shifts are referenced to internal solvent resonances and reported in parts per million relative to TMS. IR spectra were recorded on a NICOLET Impact 410 FTIR spectrometer using a DRIFT chamber with dry KBr/sample mixtures and KBr windows. For the latter the collected data were converted using the Kubelka-Munk refinement. Elemental analyses were performed on an Elementar Vario MICRO cube.
The molar masses (M_w and M_n) of the polymers were determined by size-exclusion chromatography (SEC). Sample solutions (1.0 mg polymer per mL THF) were filtered through a 0.45 mm syringe filter prior to injection. SEC was performed with a GPCmax VE2001 pump (Viscotek) by employing ViscoGEL columns. Signals were detected by using a triple detection array (TDA 305) and calibrated against polystyrene standards (M_w/M_n<1.15). The flow rate was set to 1.0 mL min^{-1}. The microstructure of the polyisoprenes was examined by ^{1}H NMR and ^{13}C NMR spectroscopy on an AV400 spectrometer in $CDCl_3$ at ambient temperature. The DSC measurement was performed applying a X-DSC 7000 by Hitachi attached with an electric cooling unit. The sample of 12.8 mg of the investigated polymer was measured within a temperature range from -80°C to 140°C applying a heating rate of 10 K min^{-1}.

The abbreviation Dipp denotes 2,6-di*iso*propylphenyl.

$(C_5Me_5)Y[(AlMe_3)\{B(NDippCH)_2\}]_2$ (2)

To a suspension of $[(C_5Me_5)YMe_2]_3$ (48 mg, 0.063 mmol) was added dropwise a solution of $[Me_2Al\{B(NDippCH)_2\}]_2$ (168 mg, 0.189 mmol) in a mixture of *n*-hexane/toluene. The resulting, nearly clear solution was stirred for 1 h at ambient temperature and dried in vacuo. To the resulting sticky, white residue, *n*-hexane was added, the mixture filtered through a filter pipette, its volume reduced and recrystallized at -40 °C to yield 150 mg (69%) of pure product. ^{1}H NMR (C_6D_6, 500.13 MHz, 26 °C): δ = 7.28 (4 H, *p*-C_6H_3-*i*Pr_2, unresolved t from AB_2 spin system, ^3J = 7.8 Hz), 7.23 (8 H, *m*-C_6H_3-*i*Pr_2, unresolved d from AB_2 spin system, ^3J = 7.8 Hz), 6.36 (s, 4 H, NC*H*), 3.40 (sep, 8 H, ^3J = 6.9 Hz, C*H*Me_2), 1.54 (s, 15 H, C_5Me_5), 1.36 (d, 24 H, ^3J = 6.9 Hz, CH*Me*$_2$), 1.25 (d, 24 H, ^3J = 6.8 Hz, CH*Me*$_2$), -0.63 (d, ^1J (Y-H) = 2.6 Hz, 18 H, $AlMe_3$) ppm. ^{13}C {^{1}H} NMR (C_6D_6, 125.77 MHz, 26 °C): δ = 146.6 (*o*-C_6H_3-*i*Pr_2), 142.6 (*i*-C_6H_3-*i*Pr_2), 127.4 (*p*-C_6H_3-*i*Pr_2), 123.4 (*m*-C_6H_3-*i*Pr_2), 121.9 (or 121.8) (N*C*H), 121.8(or 121.9) (*C*$_5$Me$_5$), 28.6 (*C*HMe_2), 26.5 (CH*Me*$_2$), 23.6 (CH*Me*$_2$), 12.0 (C_5Me_5) ppm. For the C atoms of the $AlMe_3$ groups, no signal could be detected at 26 °C. However, when lowering the temperature to -55 °C in toluene-*d*$_8$, two coupling signals for the bridging methyl groups could be located at 6.6 and 8.7 ppm, respectively, in the HSQC NMR spectrum. ^{11}B {^{1}H} NMR (C_6D_6, 160.46 MHz, 26 °C): δ = 31.4 ppm. ^{89}Y−^{1}H HSQC (C_6D_6, 24.51 MHz, 26 °C): δ (^{89}Y) = 144.5 ppm. IR (DRIFT, cm^{-1}): 3061 (w), 3023 (w), 2958 (vs), 2925 (s), 2862 (s),

2782 (w), 1456 (vs), 1442 (s), 1379 (s), 1323 (m), 1264 (m), 1255 (m), 1236 (m), 1206 (w), 1175 (w), 1150 (w), 1117 (m), 1058 (m), 936 (w), 894 (w), 803 (m), 761 (vs), 695 (vs), 615 (s), 552 (m), 512 (w), 459 (w). Elemental analysis (%) calcd. for $C_{68}H_{105}Al_2B_2N_4Y$ (1143.040 g mol^{-1}): C 71.45; H 9.26; N 4.90; found: C 72.19; H 8.91; N 4.53. Although these results are outside the range viewed as establishing analytical purity, they are provided to illustrate the best values obtained to date.

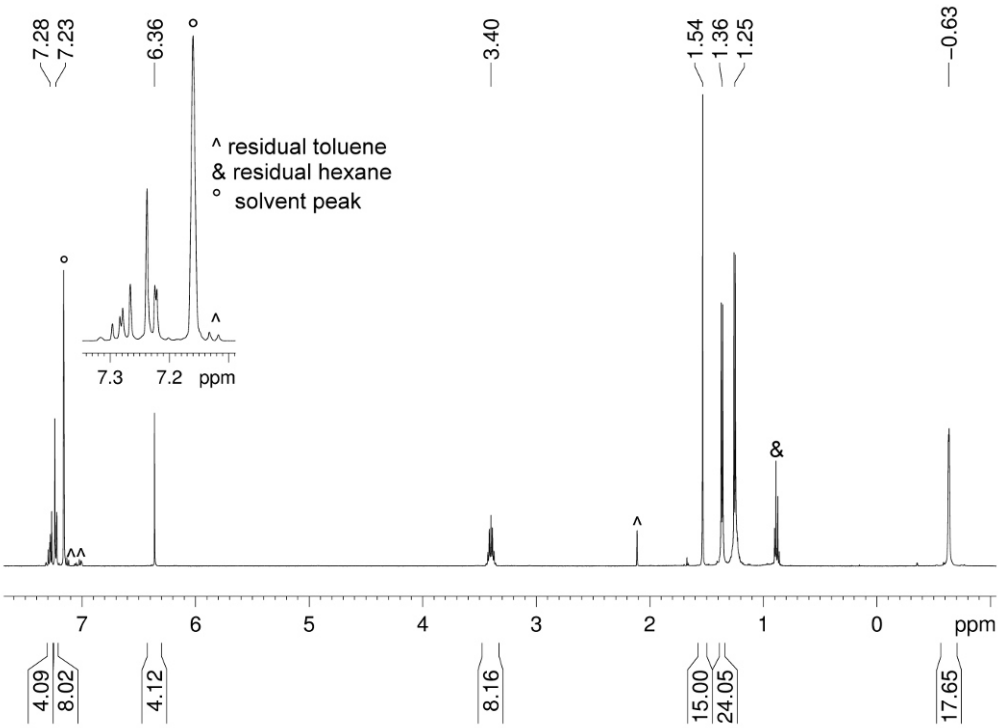

Figure S1. ^{1}H NMR spectrum of $(C_5Me_5)Y[(AlMe_3)\{B(NDippCH)_2\}]_2$ (**2**) in C_6D_6 at 26 °C.

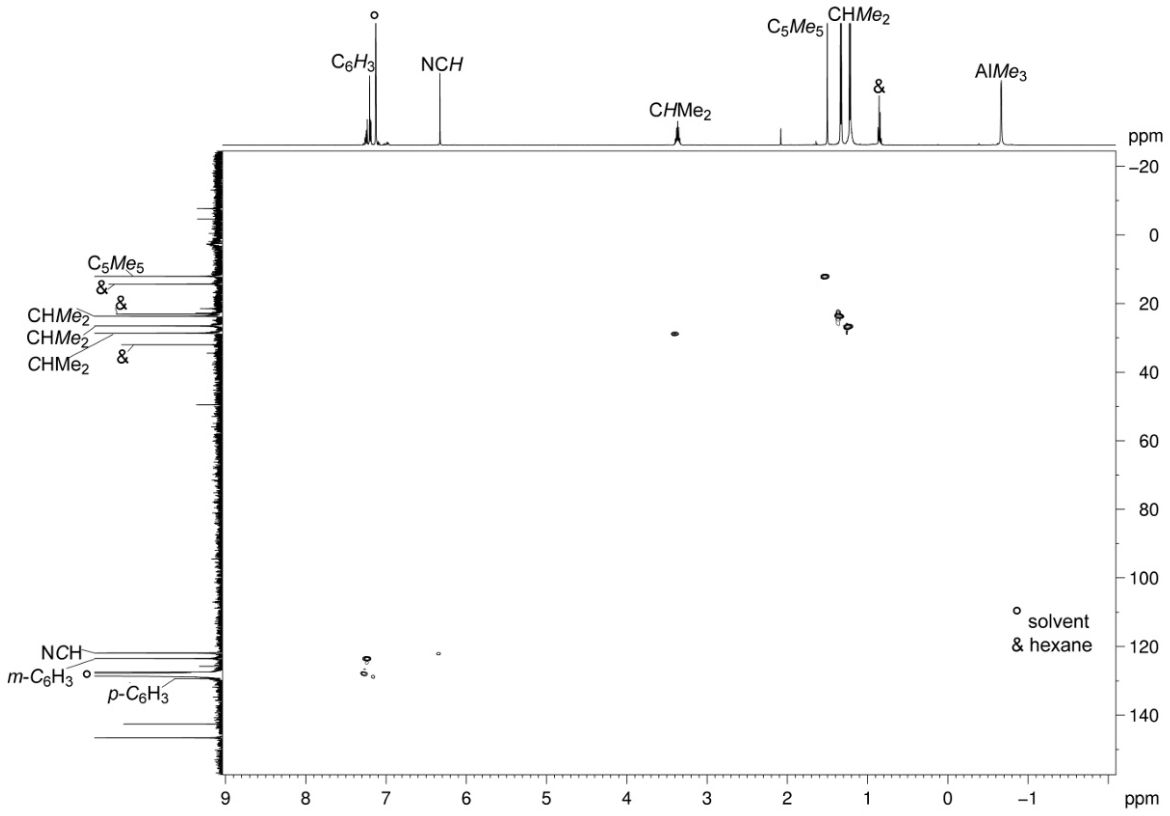

Figure S2. $^{1}H-^{13}C$-HSQC NMR spectrum of **2** in C_6D_6 at 26 °C.

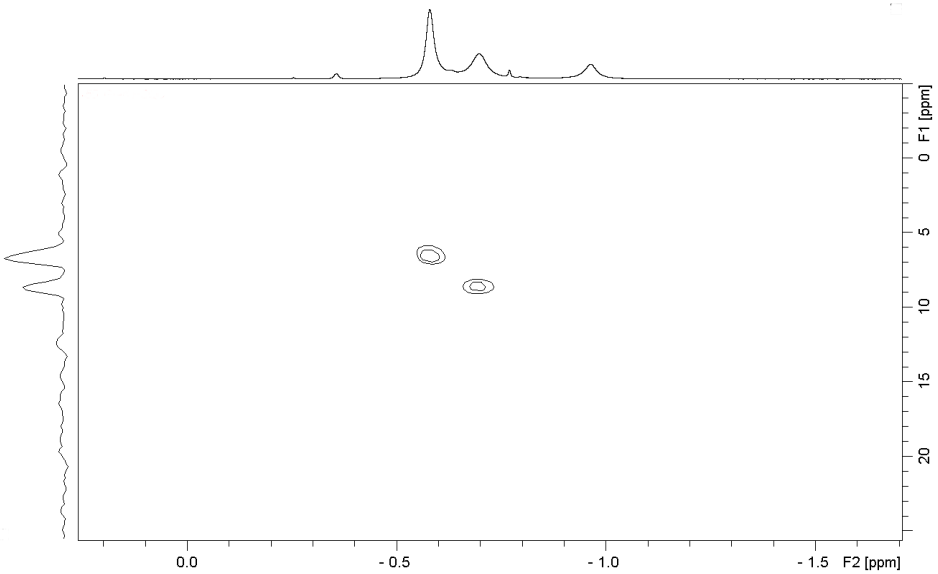

Figure S3. Cutout from a $^{1}H-^{13}C$-HSQC NMR spectrum of **2** at -55 °C in toluene-d_8 to detect the ^{13}C signals of the $AlMe_3$ units.

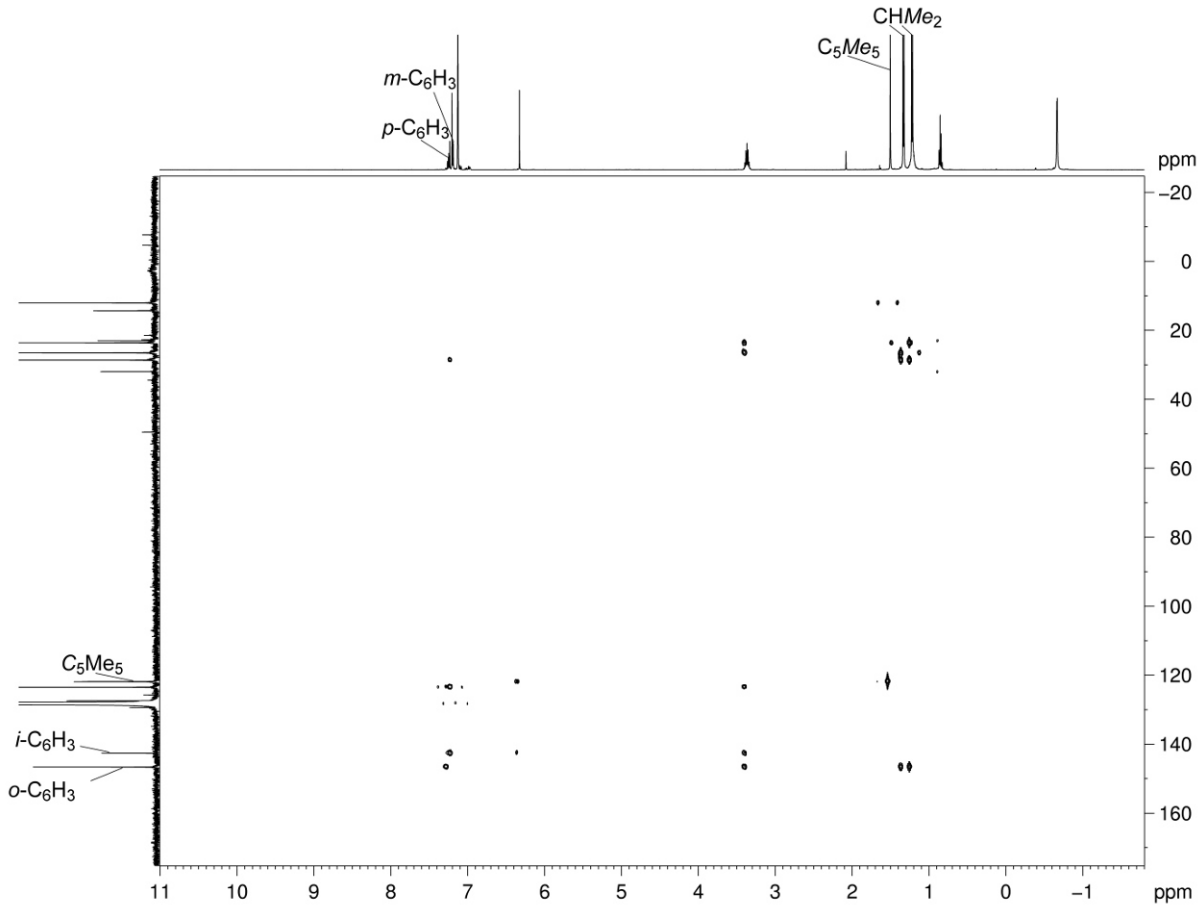

Figure S4. ^{1}H-^{13}C-HMBC NMR spectrum of **2** in C_6D_6 at 26 °C to detect quaternary C atoms.

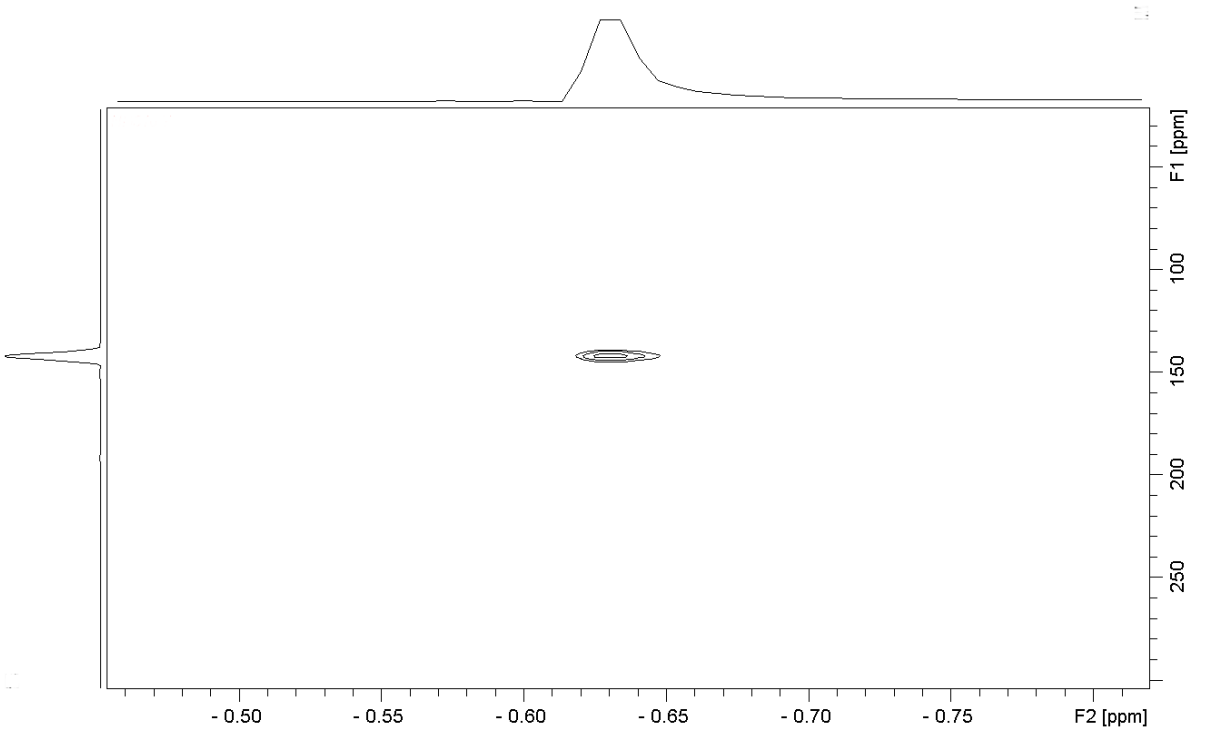

Figure S5. $^{1}H-^{89}Y$-HSQC NMR spectrum of **2** in C_6D_6 at 26 °C.

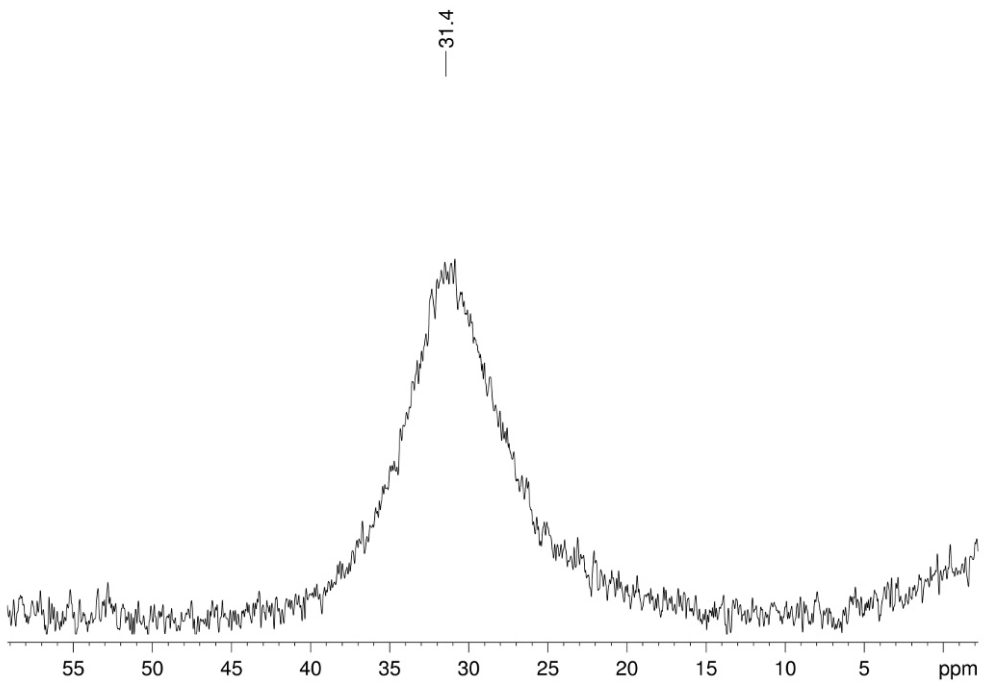

Figure S6. $^{11}B\{^1H\}$ NMR spectrum of **2** in C_6D_6 at 26 °C.

$(C_5Me_5)Lu[(AlMe_3)\{B(NDippCH)_2\}]_2$ (3)

To a solution of $\{Me_2Al[B(NDippCH)_2]\}_2$ (163 mg, 0.183 mmol) in 3 mL of *n*-hexane, $[(C_5Me_5)LuMe_2]_3$ (62 mg, 0.061 mmol) was added together with some drops of toluene. The resulting yellow suspension was stirred at +35 °C for one hour. The solvents were removed in vacuo and the sticky residue was recrystallized from *n*-hexane to yield colorless crystals with a yield of 148 mg (67%). ^1H NMR (C_6D_6, 400.11 MHz, 26 °C): $\delta = 7.26$ (4 H, *p*-C_6H_3-*i*Pr_2, m, A part of AB_2 spin system, ^3J = 7.9 Hz), 7.23 (8 H, *m*-C_6H_3-*i*Pr_2, m, B_2 part of AB_2 spin system, ^3J = 7.9 Hz), 6.36 (s, 4 H, NC*H*), 3.40 (sep, 8 H, ^3J = 6.8 Hz, C*H*Me_2), 1.56 (s, 15 H, (C_5Me_5)), 1.37 (d, 24 H, ^3J = 6.9 Hz, CH*Me*$_2$), 1.25 (d, 24 H, ^3J = 6.8 Hz, CH*Me*$_2$), -0.41 (s, 18 H, $AlMe_3$) ppm. $^{13}C\{^1H\}$ NMR (C_6D_6, 100.62 MHz, 26 °C): $\delta = 146.6$ (*o*-C_6H_3-*i*Pr_2), 142.5 (*i*-C_6H_3-*i*Pr_2), 127.4 (*p*-C_6H_3-*i*Pr_2), 123.4 (*m*-C_6H_3-*i*Pr_2), 121.9 (N*C*H), 120.4 (C_5Me_5), 28.6 (*C*HMe_2), 26.6 (CH*Me*$_2$), 23.6 (CH*Me*$_2$), 12.0 (C_5Me_5) ppm. For the C atoms of the $AlMe_3$ groups, no signal could be detected at 26 °C. However, when lowering the temperature to -40 °C in toluene-d_8, two C signals for the bridging methyl groups were located at 10.2 and 8.4 ppm, respectively. $^{11}B\{^1H\}$ NMR (C_6D_6, 160.46 MHz, 26 °C): $\delta = 31.0$ ppm. IR (DRIFT, cm^{-1}): 3065 (w), 3026 (w), 2958 (vs), 2937 (s), 2887 (m), 2866 (s), 1461 (s), 1442 (s), 1370 (vs), 1323 (m), 1267 (m), 1255 (m), 1239 (m), 1217 (w), 1182 (w), 1053 (w), 1112 (w), 939 (w), 897 (w), 803 (s), 761 (vs), 697 (s), 618 (m), 548 (w), 456 (w). Elemental analysis (%) calcd. for $C_{68}H_{105}Al_2B_2N_4Lu$ (1229.101 g mol^{-1}): C 66.45; H 8.61; N 4.56; found: C 65.87; H 8.62; N. 3.96. Although these results are outside the range viewed as establishing analytical purity, they are provided to illustrate the best values obtained to date.

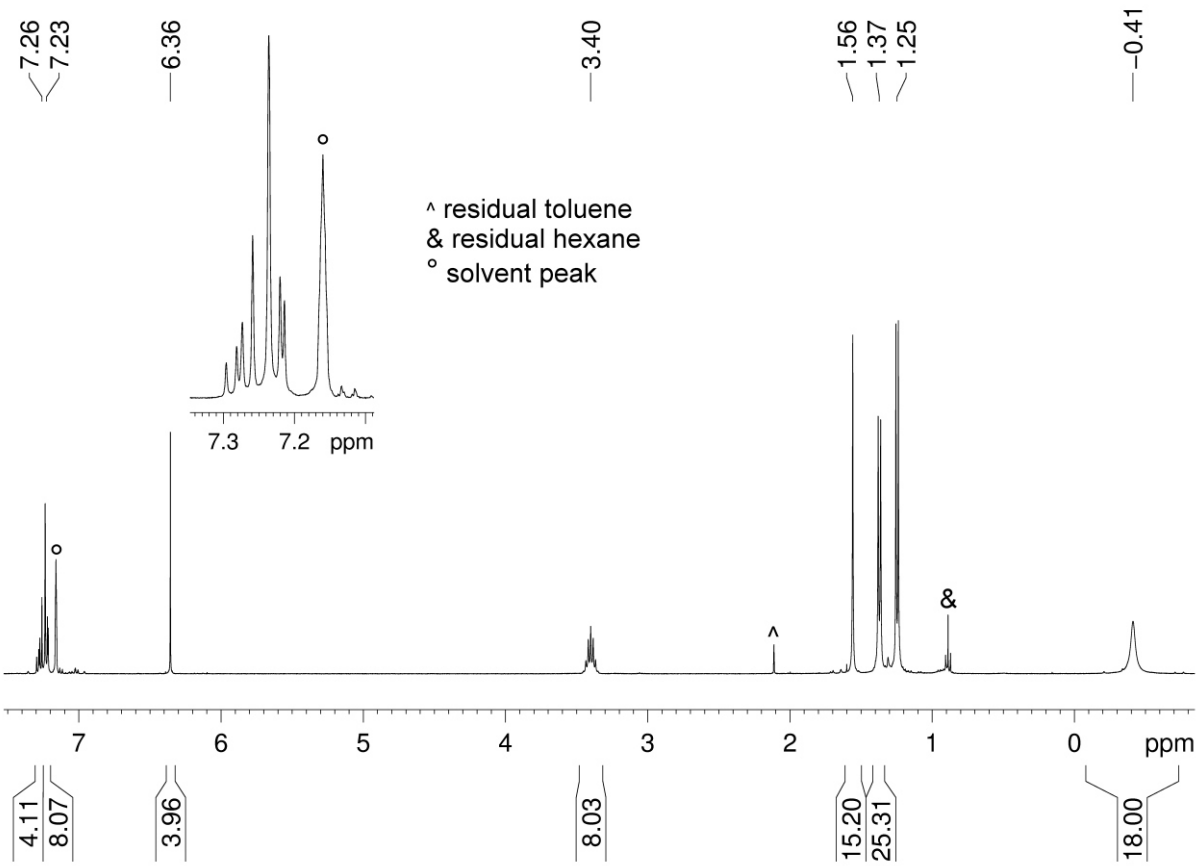

Figure S7. ^{1}H NMR spectrum of $(C_5Me_5)Lu[(AlMe_3)\{B(NDippCH)_2\}]_2$ (**3**) in C_6D_6 at 26 °C.

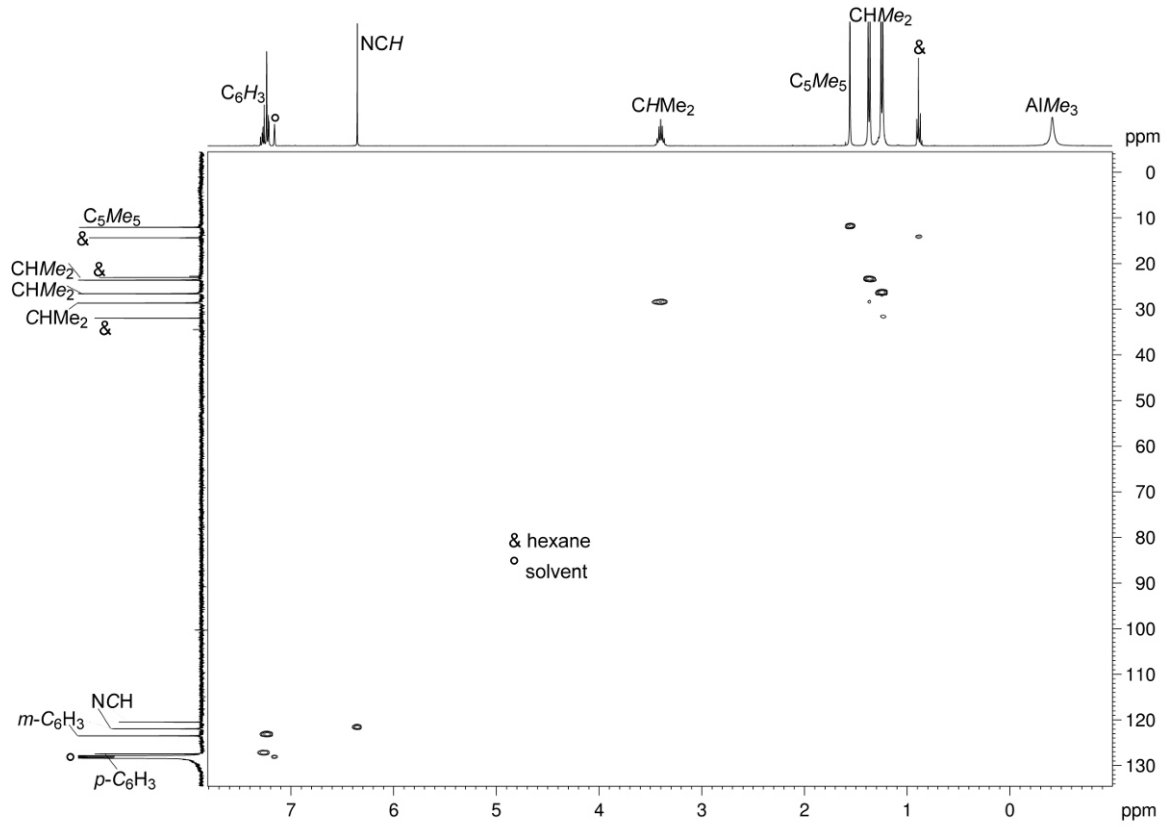

Figure S8. ^{1}H−^{13}C-HSQC NMR spectrum of **3** in C_6D_6 at 26 °C.

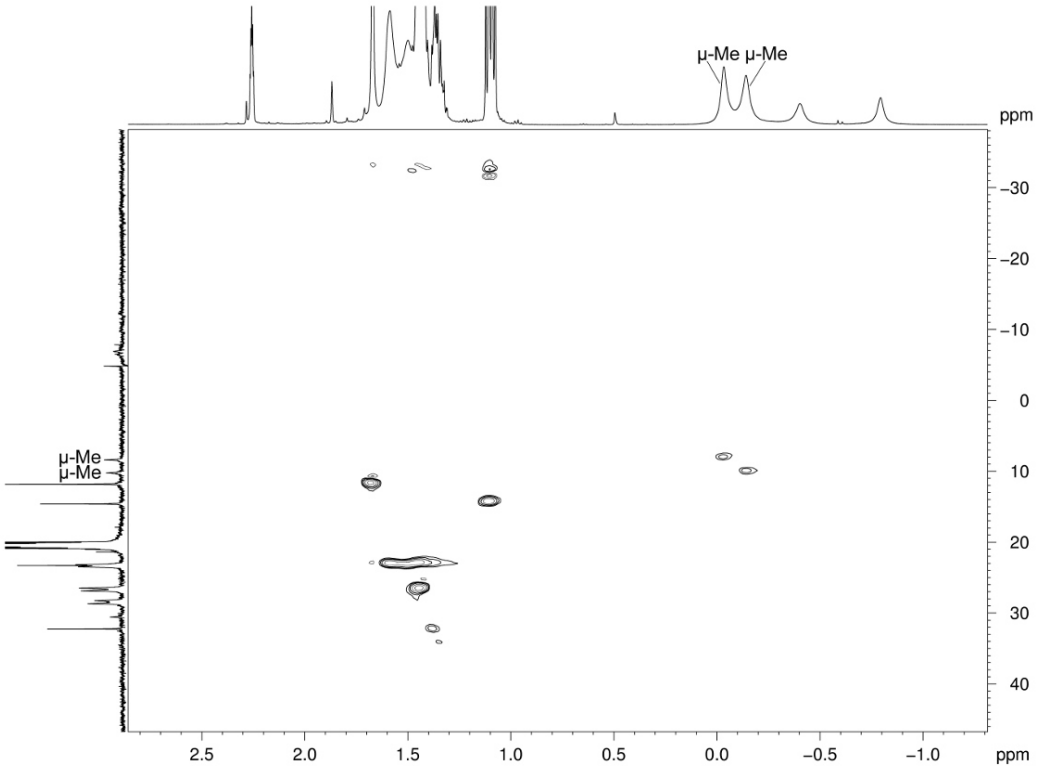

Figure S9. Cutout from a $^{1}H-^{13}C$-HSQC NMR spectrum of **3** at -40 °C in toluene-d_8 to detect ^{13}C signals of the $AlMe_3$ units.

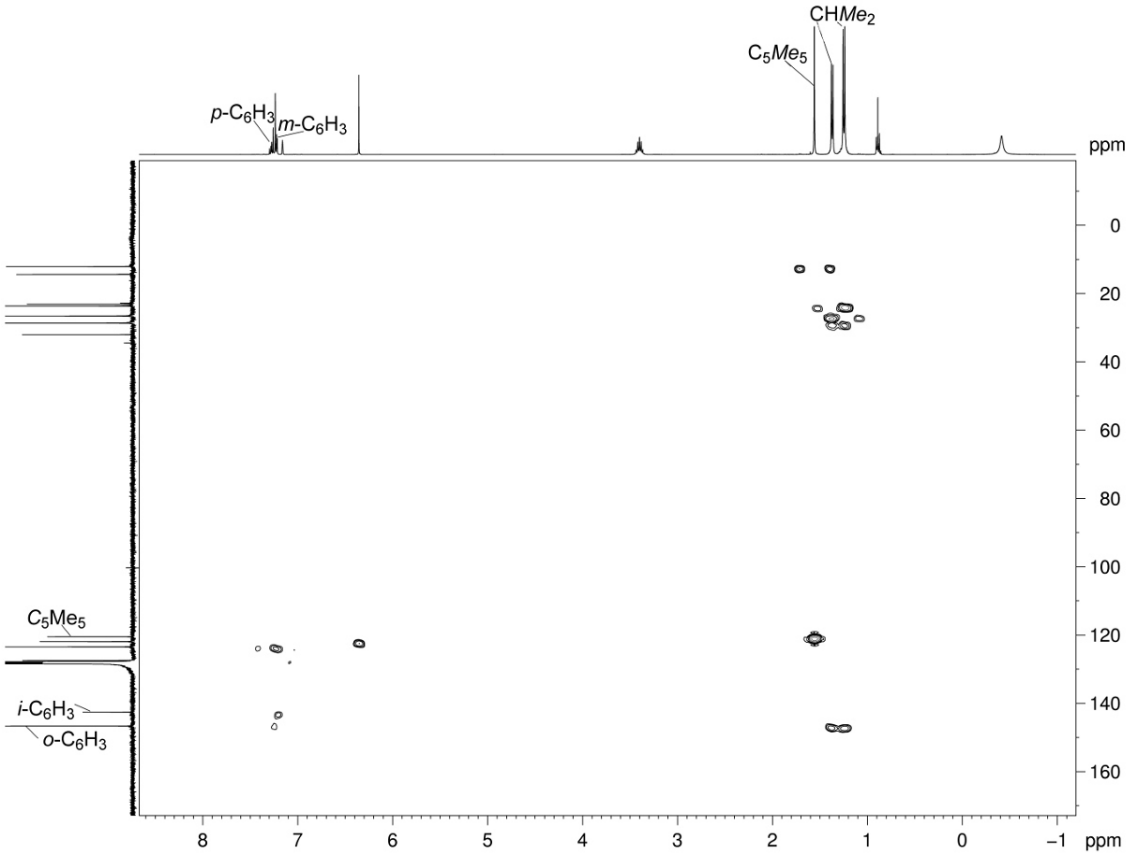

Figure S10. $^{1}H-^{13}C$-HMBC NMR spectrum of **3** in C_6D_6 at 26 °C to detect quaternary C atoms.

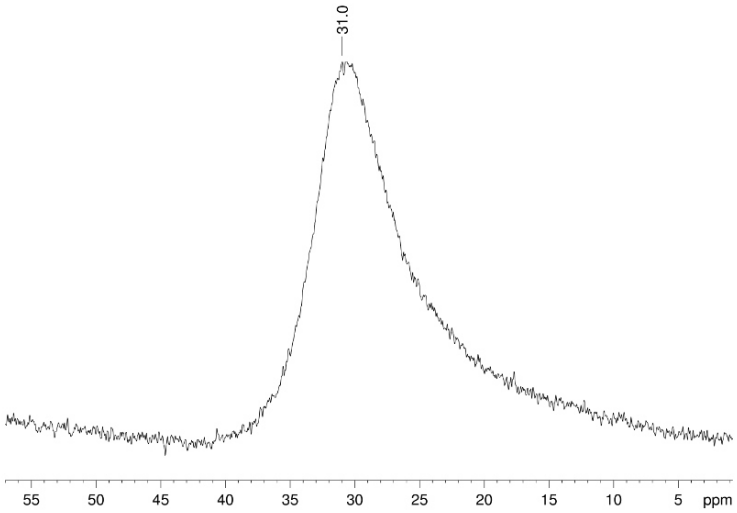

Figure S11. $^{11}B\{^{1}H\}$ NMR spectrum of **3** in C_6D_6 at 26 °C.

NMR reaction of $(C_5Me_5)Y[(AlMe_3)\{B(NDippCH)_2\}]_2$ (2) with two equivalents of THF

For the reaction, a stock solution of THF in C_6D_6 was prepared. Therefore, 6.5 mg (0.09 mmol) of THF were dissolved in 2.5 mL of C_6D_6. In a J. Young-valved NMR tube, 0.5 mL of the stock solution were added to 10.5 mg ($9.2 \cdot 10^{-3}$ mmol) of **2**. The reaction was monitored as shown in Figure S12.

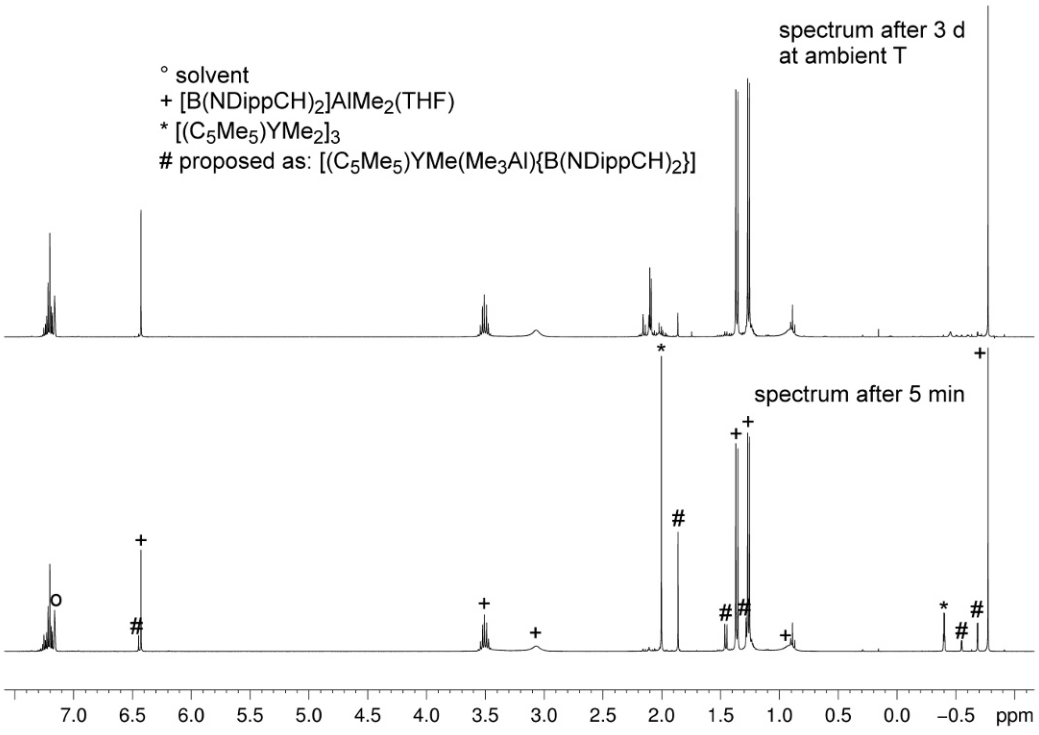

Figure S12. Reaction of $(C_5Me_5)Y[(AlMe_3)\{B(NDippCH)_2\}]_2$ (**2**) with 2 equiv of THF. C_6D_6 was used as a solvent. A cutout from the NMR spectrum is shown in Figure S13.

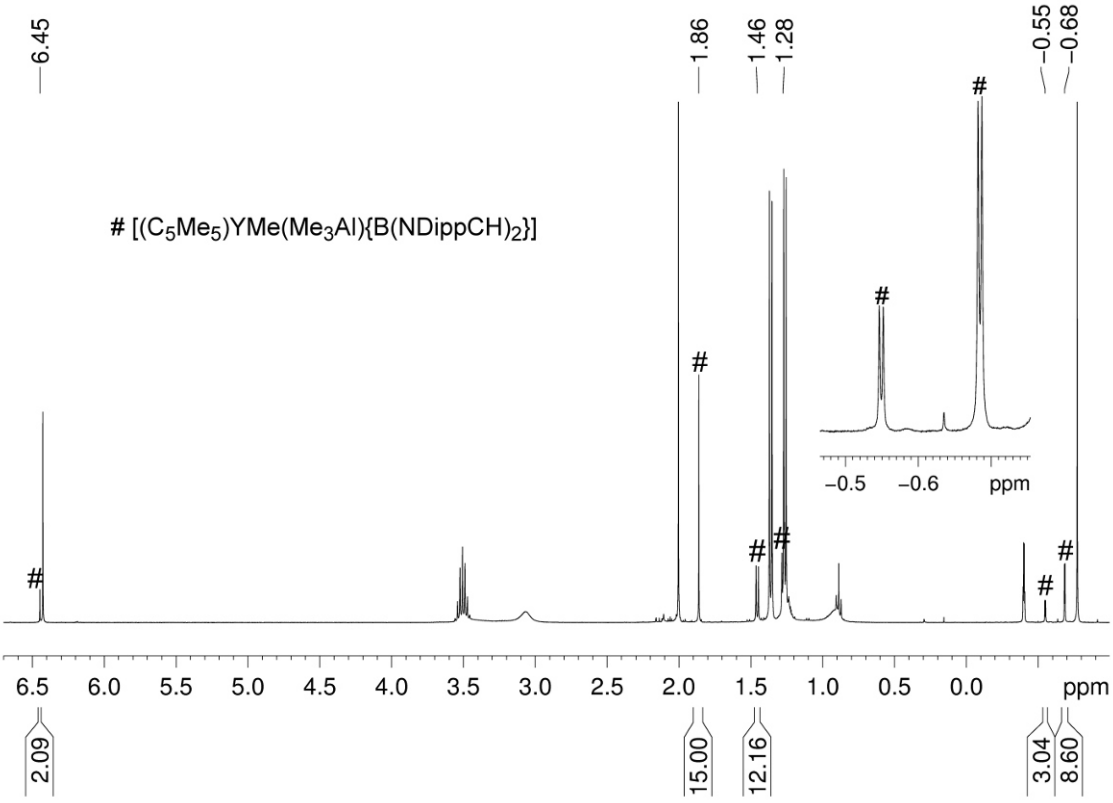

Figure S13. Cutout from Figure S12. The integrated and marked ^{1}H resonances belong to a species that is proposed to be [$(C_5Me_5)YMe(Me_3Al)\{B(NDippCH)_2\}$] (**4**) by NMR.

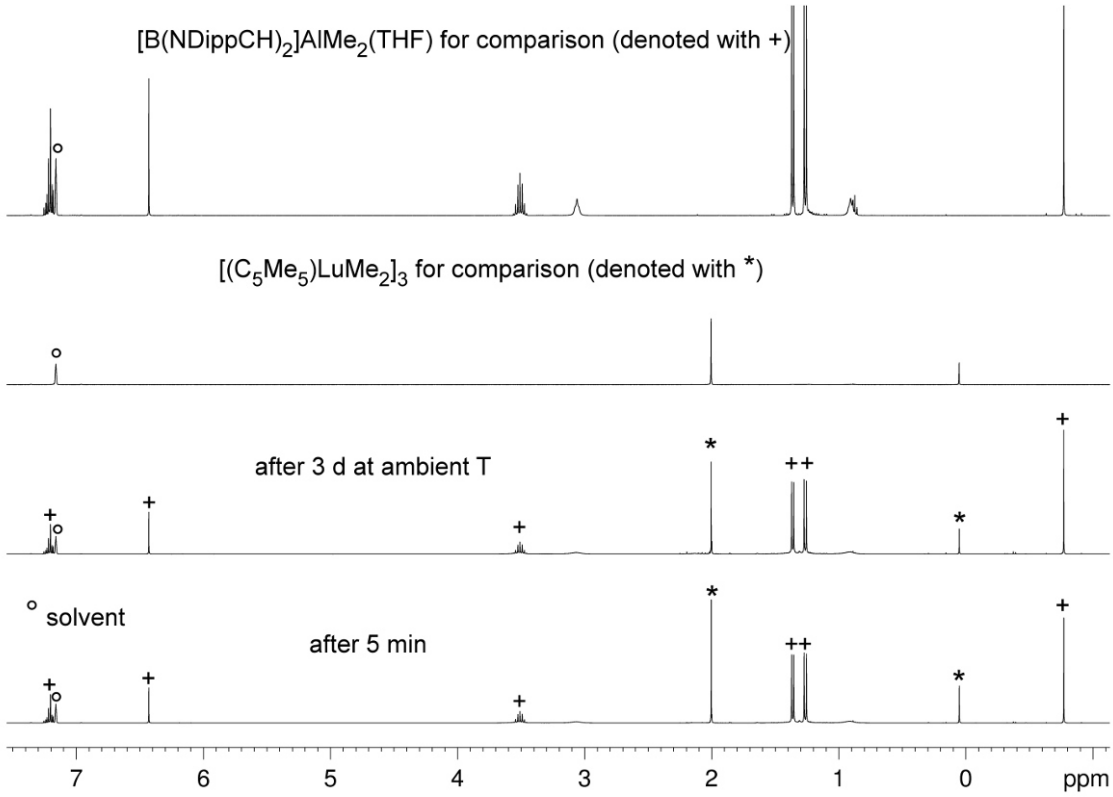

Figure S14. NMR-monitored reaction of $(C_5Me_5)Lu[(AlMe_3)\{B(NDippCH)_2\}]_2$ (**3**) with THF to form 2 $(THF)Me_2Al[B(NDippCH)_2]$ and 1/3 $[(C_5Me_5)LuMe_2]_3$. C_6D_6 was used as a solvent.

Polymerization of isoprene

A detailed polymerization procedure (run 5, Table 1 in the main publication) is described as a typical example. $[Ph_3C][B(C_6F_5)_4]$ (**A**, 18 mg, 0.02 mmol, 1 equiv) was added to a solution of compound **3** (24 mg, 0.02 mmol) in toluene (7 mL) and the mixture was aged under ambient temperature for 30 min. After the addition of isoprene (1.36 g, 20 mmol), the polymerization reaction was carried out at ambient temperature for 1 h. The reaction was terminated by pouring the polymerization mixture into methanol (200 mL) that contained 2,6-di-*tert*-butyl-4-methylphenol (0.1%, w/w) as a stabilizer and stirred for several minutes. The polymer was washed with methanol and dried under vacuum at ambient temperature to constant weight.

Table S1. Selected Examples of Isoprene Polymerization at ambient temperature.

entry[a]	precatalyst	cocatalyst[b]	t (h)	yield (%)	*cis*-1,4[c]	*trans*-1,4[c]	3,4[c]	M_n[d] (x 10^4)	M_w/M_n[d]	ref.
12	**2**	**C**	1	traces	---[e]	---[e]	---[e]	---[e]	---[e]	
13	**2**	**C**	24	71.8	1,9	84,1	11.2	5.4	2.02	
14	**3**	**C**	1	traces	---[e]	---[e]	---[e]	---[e]	---[e]	
15	**3**	**C**	24	34.1	21.2	68.4	10.4	3.0	1.97	
16	**3**	**C**	48	65.9	38.3	52.6	9.1	3.2	2.07	
17[f]	$Cp^*Y(AlMe_4)_2$	**C**	24	>99	1.9	93.6	4.5	9.0	1.78	5
18[f]	$Cp^*Lu(AlMe_4)_2$	**C**	0.5	26	74.6	20.7	4.7	11.0	1.39	

[a]Conditions: 0.02 mmol precatalyst, [Ln]/[cocat] = 1:1, 7 mL toluene, 20 mmol isoprene, r.t.. [b]Co-catalyst: **C** = $B(C_6F_5)_3$; [c]Determined by ^1H and ^{13}C NMR spectroscopy in $CDCl_3$. [d]Determined by means of size-exclusion chromatography (SEC) against polystyrene standards. [e]Not determined due to low yield. [f]Polymerizations at 40°C.

NMR-spectroscopic investigation on the active species

In order to investigate the active species of the polymerization run 5 of Table 1, 0.007 mmol (9 mg) of **3** were dissolved in 0.6 mL of toluene-d_8 and an equimolar amount of $[Ph_3C][B(C_6F_5)_4]$ (6.7 mg) was added as a solution in 0.3 mL of toluene-d_8. ^1H-NMR-Spectra were taken after 7, 10, 15, 20, 25 and 30 min. As no difference in the spectra was detected, only the first ^1H NMR spectrum is depicted (Figure S15). After 30 min, ^{19}F, ^{11}B, and ^{13}C NMR spectra were taken, as well as the 2D NMR spectra ^1H-^1H-COSY, ^{13}C-^1H-HSQC, and ^{13}C-^1H-HMBC.

The formation of three species is assumed: $[\{B(NDippCH)_2\}AlMe_2]_2$ (in the following denoted with the symbol &), $[\{B(NDippCH)_2\}(AlMe_3)Lu(C_5Me_5)]^+$ $[B(C_6F_5)_4]^-$ (in the following denoted with the symbol §), and Ph_3CMe (denoted as "t" in the spectra).

^1H NMR (toluene-*d*8, 500 MHz, 26 °C): δ = 7.70 (t, 1 H, ^3J = 7.7 Hz, *p*-$C_6H_3(i\text{Pr})_2$, §), 6.28 (s, 2 H, NC*H*, &), 6.22 (two overlapping doublets, 2 H, NC*H*, §), 3.21 (sep, ^3J = 6.9 Hz, 4 H, C*H*Me_2, &), 2.91 (sep, 2 H, ^3J = 7.0 Hz, C*H*Me_2, §), 2.83 (sep, 2 H, ^3J = 6.9 Hz, C*H*Me_2, §), 2.00 (s, 3 H, Ph_3CMe), 1.61 (s, 15 H, C_5Me_5), 1.21 (d, 12 H, CH*Me*$_2$, &), 1.15 (d, 12 H, CH*Me*$_2$, §), 1.12 (d, 12 H, CH*Me*$_2$, &), 0.95 (d, 6 H, CH*Me*$_2$, §), 0.87 (d, 6 H, CH*Me*$_2$, §), -0.25 (s, 6 H, μ-$AlMe_2$, §), -0.60 (s, 6 H, Al*Me*$_2$, &), -1.21 (s, 3 H, Al*Me*, §) ppm.

^{13}C {^1H} NMR (toluene-*d*8, 126 MHz, 26 °C) (incomplete and partly assigned on the basis of HSQC (see Figure S17) and HMBC spectra (see Figure S18)): δ = 158 (*o*-C_6H_3, §), 149 (*i*-$(C_6H_5)_3C$Me), 123 (C_5Me_5, §), 52 (Ph_3CMe), 28.6 (*C*HMe_2, &), 22.9 (μ-$AlMe_2$, §), 17.6 (CH*Me*$_2$, §), 11.4 (C_5Me_5, §) ppm.

^{11}B{^1H} NMR (toluene-*d*8, 160 MHz, 26 °C): δ = 16.0 ppm.

^{19}F{^1H} NMR (toluene-*d*8, 376 MHz, 26 °C): δ = -131.7 (br s, 2 F, *o*- C_6F_5), -162.5 (t, 1 F, ^3J = 20 Hz, *p*-C_6F_5), -166.4 (br s, 2 F, *m*- C_6F_5) ppm.

a)

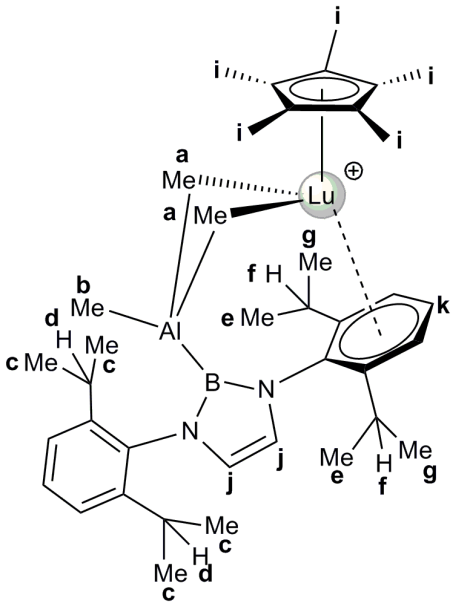

$[B(C_6F_5)_4]^-$

4

b)

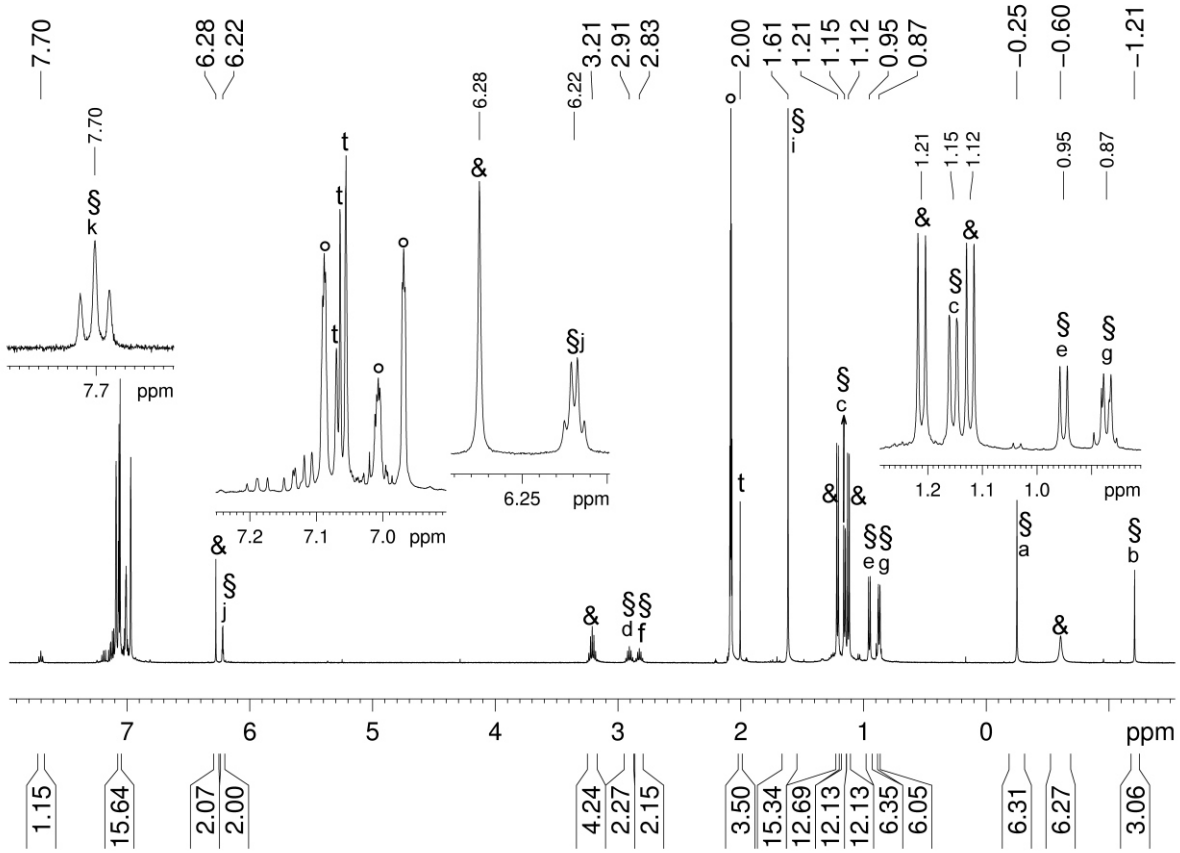

& $[\{B(NDippCH)_2\}AlMe_2]_2$ § $[\{B(NDippCH)_2\}(AlMe_3)Lu(C_5Me_5)]^+$ t $(CPh_3)Me$ ° solvent

Figure S15. a) Suggested active species **4**; b) ^{1}H NMR spectrum (toluene-*d*8) of the equimolar reaction of $(C_5Me_5)Lu[(Me_3Al)\{B(NDippCH)_2\}]_2$ (**3**) and $[Ph_3C][B(C_6F_5)_4]$ measured 7 min after addition of the compounds.

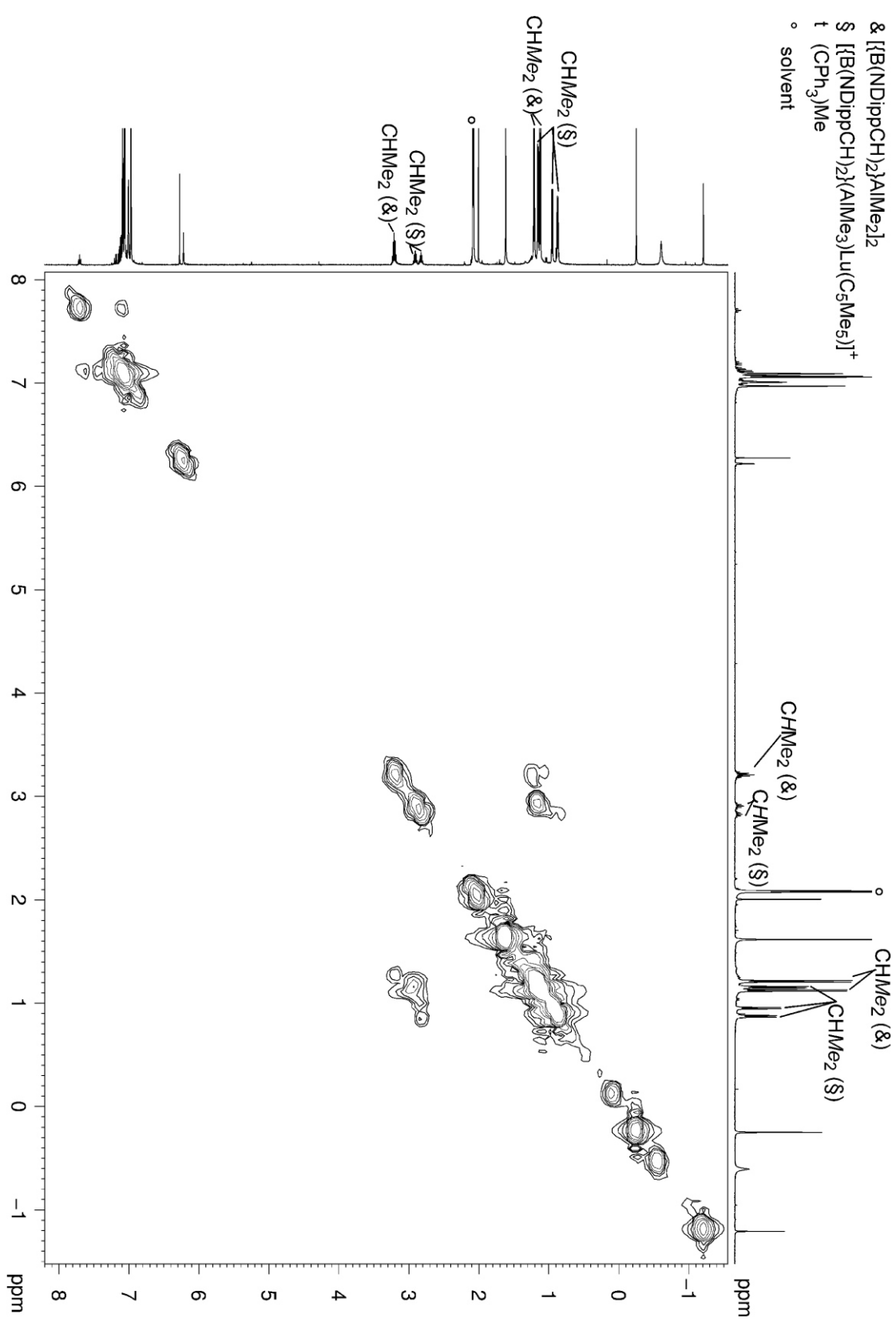

Figure S16. ^{1}H-^{1}H COSY NMR spectrum (toluene-*d*8) of the equimolar reaction of $(C_5Me_5)Lu[(Me_3Al)\{B(NDippCH)_2\}]_2$ (**3**) and $[Ph_3C][B(C_6F_5)_4]$. The cross-coupling peaks help for the assignment of the methyl signals of the isopropyl groups to the septet of the corresponding methine proton.

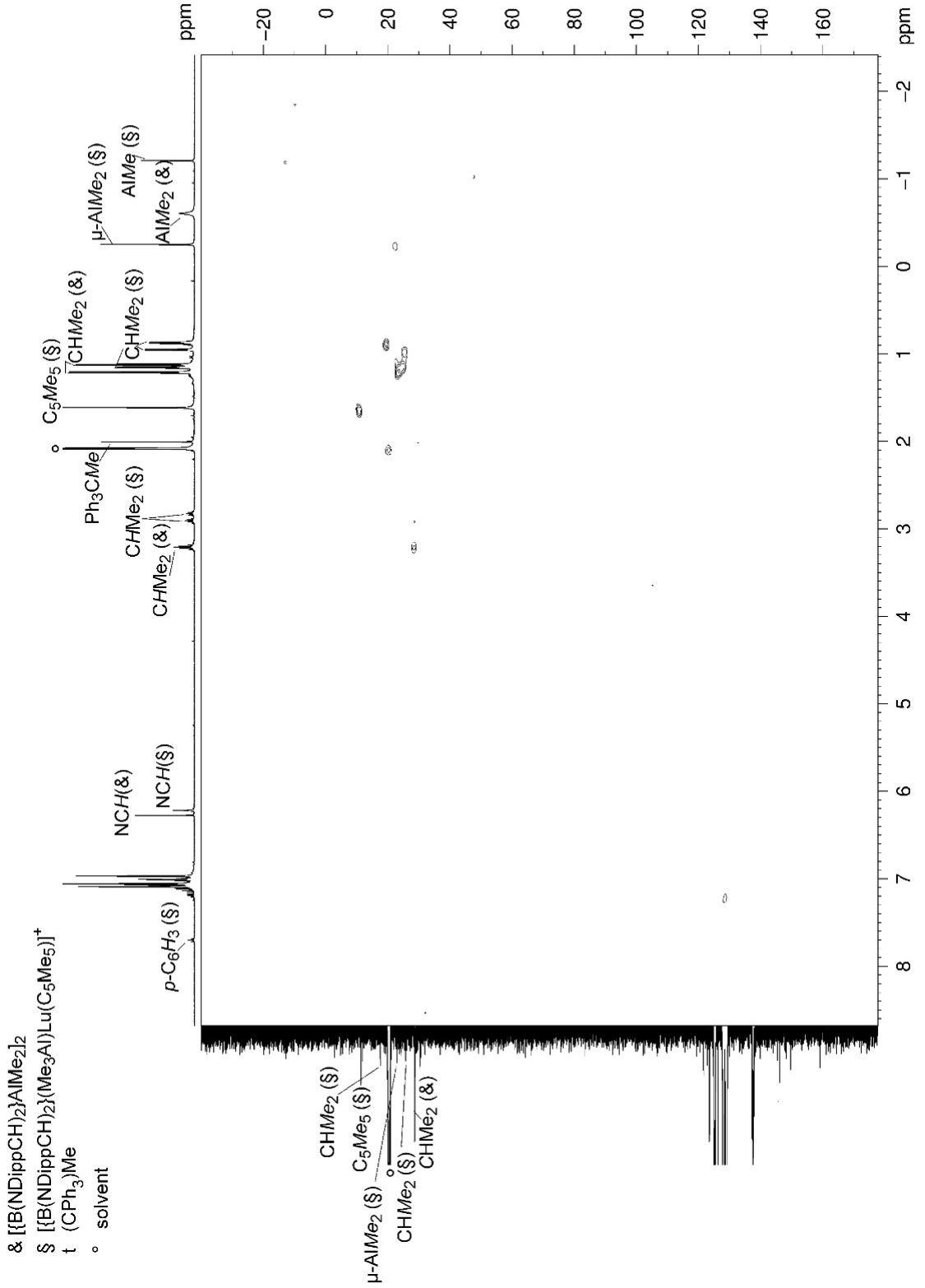

Figure S17. ^{1}H-^{13}C HSQC NMR spectrum (toluene-*d*8) of the equimolar reaction of $(C_5Me_5)Lu[(Me_3Al)\{B(NDippCH)_2\}]_2$ (**3**) and $[Ph_3C][B(C_6F_5)_4]$.

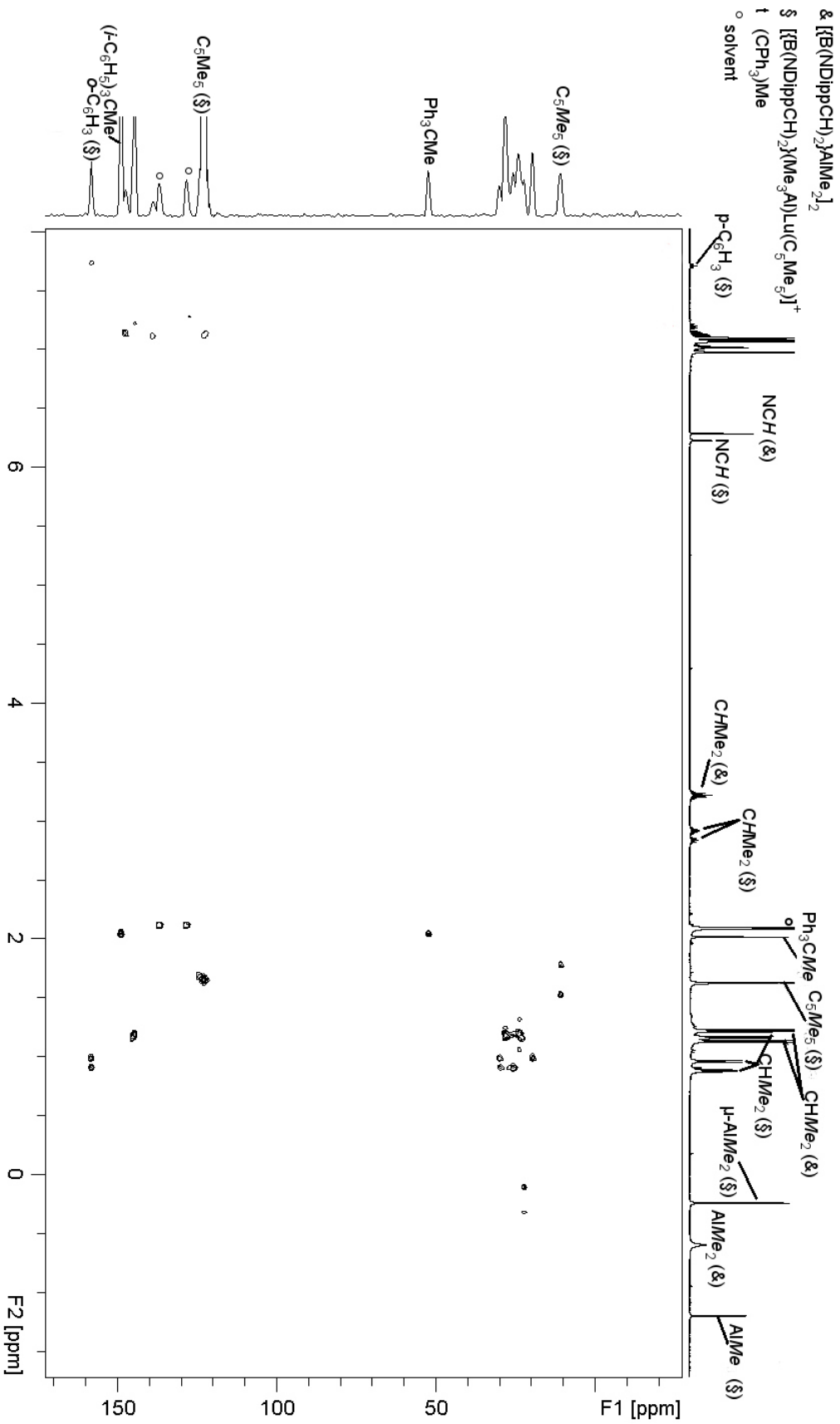

Figure S18. . ^{1}H-^{13}C HMBC spectrum (toluene-*d*8) of the equimolar reaction of $(C_5Me_5)Lu[(Me_3Al)\{B(NDippCH)_2\}]_2$ (**3**) and $[Ph_3C][B(C_6F_5)_4]$.

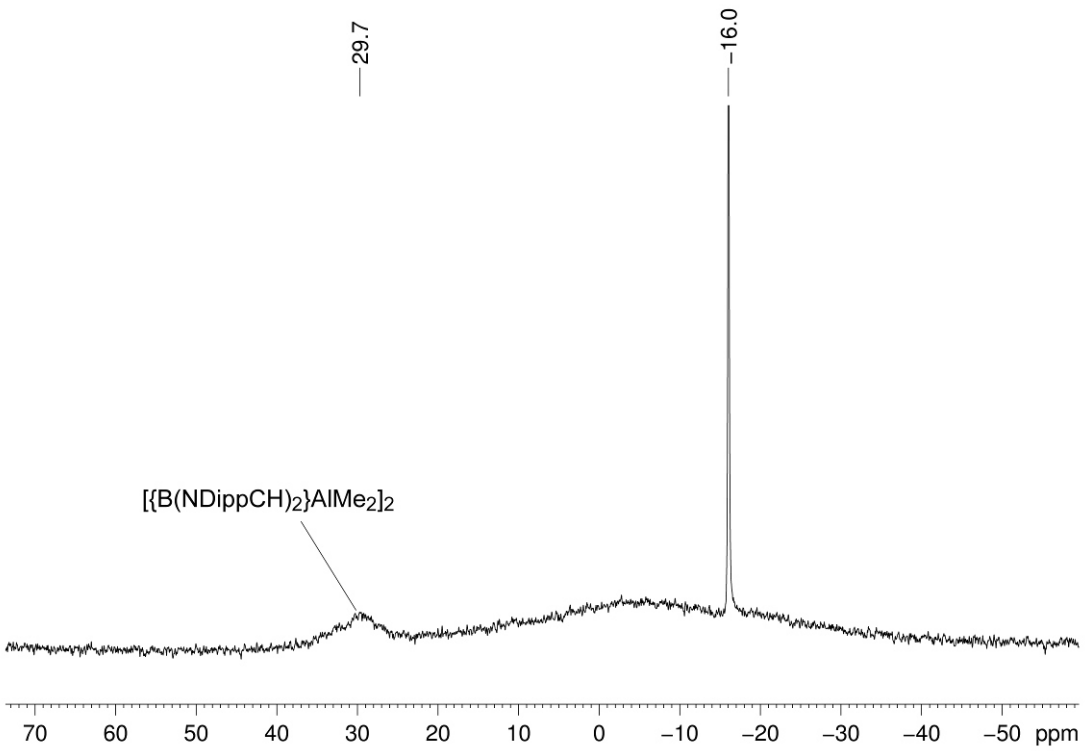

Figure S19. $^{11}B\{^{1}H\}$ NMR spectrum (toluene-*d*8) of the equimolar reaction of $(C_5Me_5)Lu[(Me_3Al)\{B(NDippCH)_2\}]_2$ (**3**) and $[Ph_3C][B(C_6F_5)_4]$.

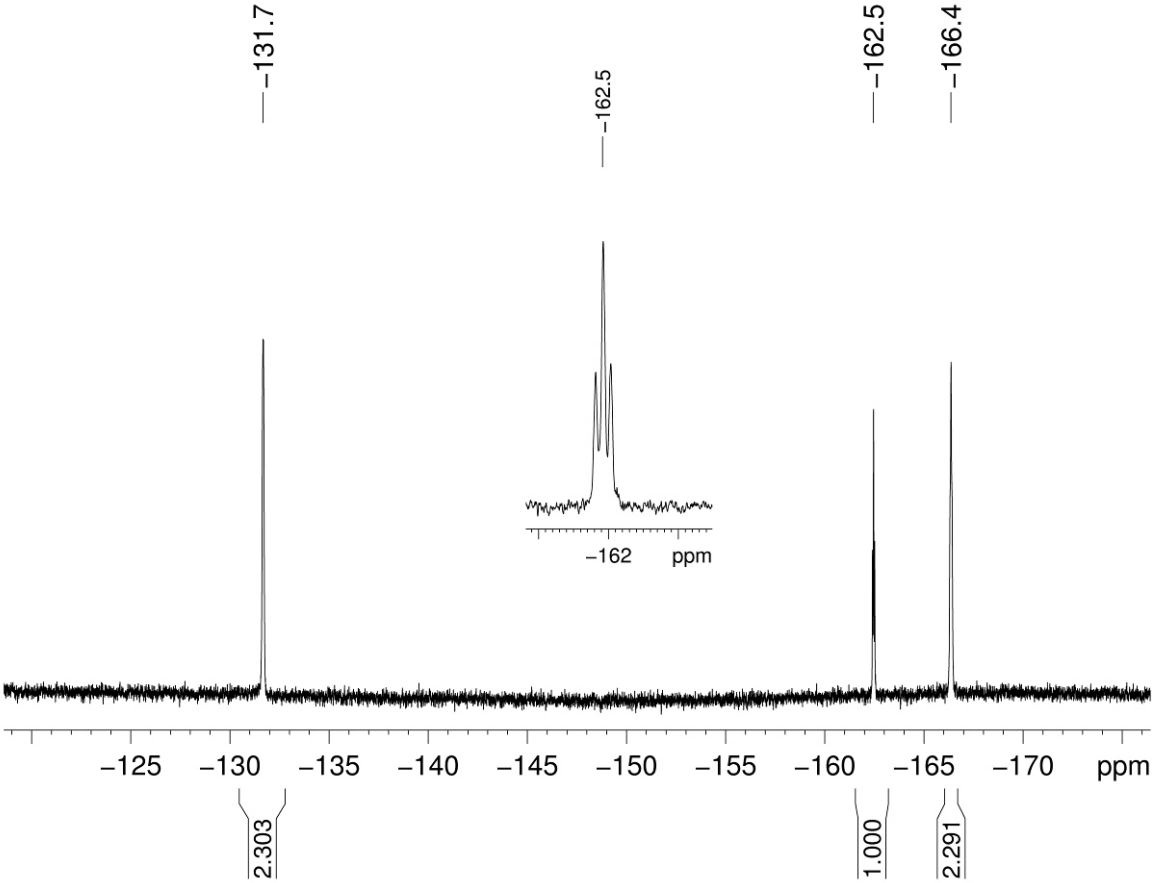

Figure S20. $^{19}F\{^{1}H\}$ NMR spectrum (toluene-*d*8) of the equimolar reaction of $(C_5Me_5)Lu[(AlMe_3)\{B(NDippCH)_2\}]_2$ (**3**) and $[Ph_3C][B(C_6F_5)_4]$.

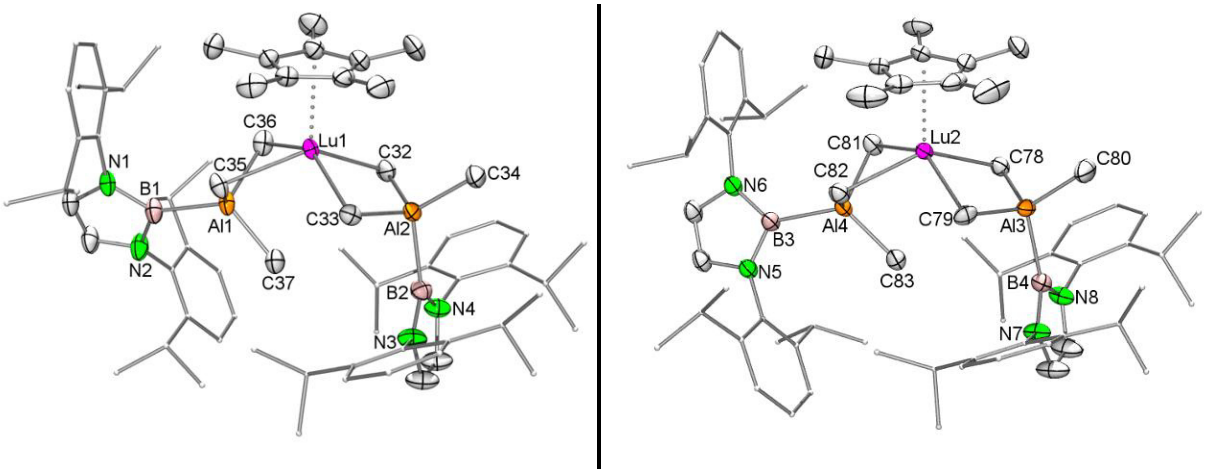

Figure S21. Solid-state structure of the two molecules in the asymmetric unit of $(C_5Me_5)Lu[(AlMe_3)\{B(NDippCH)_2\}]_2$ (**3**) with atomic displacement parameters set at the 50% level. The carbon atoms of the aromatic parts are shown with reduced radii. Hydrogen atoms and co-crystallized *n*-hexane have been omitted for clarity. Disorder in the aromatic parts has been removed. Selected bond lengths and angles are listed below in Table1.

Table S2. Relevant distances [Å] and angles [°] for the two molecules in the asymmetric unit of **3**.

Lu1−C32	2.506(4)	Lu2−C78	2.507(4)
Lu1−C33	2.504(3)	Lu2−C79	2.509(4)
Lu1−C35	2.605(4)	Lu2−C81	2.622(4)
Lu1−C36	2.590(4)	Lu2−C82	2.591(4)
Lu1···C37	3.381(4)	Lu2···C83	3.351(4)
Lu1···Al1	2.917(2)	Lu2···Al3	3.062(2)
Lu1···Al2	3.059(2)	Lu2···Al4	2.913(2)
Al1−C35	2.067(4)	Al4−C82	2.067(4)
Al1−C36	2.068(4)	Al4−C81	2.073(4)
Al1−C37	1.989(4)	Al4−C83	1.986(4)
Al2−C32	2.077(4)	Al3−C78	2.086(4)
Al2−C33	2.088(4)	Al3−C79	2.087(4)
Al2−C34	1.987(4)	Al3−C80	1.982(4)
B1−Al1	2.137(5)	B3−Al4	2.137(4)
B2−Al2	2.135(5)	B4−Al3	2.137(4)
C32Lu1C33−C32Al2C33	13.7	C78CLu2C79−C78Al3C79	13.1
C35Lu1C36−C35Al1C36	51.2	C81Lu2C82−C81Al4C82	51.6

Table S3. Crystallographic data information for **3**.

	3
Formula	$C_{77}H_{126}Al_2B_2LuN_4$
Fw	1358.37
temp (K)	100(2)
cryst syst	triclinic
space group	P-1
a (Å)	13.4966(3)
b (Å)	18.6094(5)
c (Å)	32.8876(9)
α (deg)	82.408(2)
β (deg)	83.6630(10)
γ (deg)	79.017(2)
vol (Å^3)	8006.9(4)
Z	4
ρ_{calcd} (mg/mm^3)	1.127
μ (mm^{-1})	1.295
R1[a] ($I > 2.0\sigma(I)$)	0.0423
wR2[b] (all data)	0.1148
diffractometer system	APEX II DUO

[a] $R1 = \Sigma(||F_o|-|F_c||)/\Sigma|F_o|$. [b] $wR2 = \{\Sigma[w(F_o^2-F_c^2)^2/\Sigma[w(F_o^2)^2]\}^{1/2}$

Because of poor crystal quality, data collection for complex **2** was not completed and hence not deposited. Due to the nearly identical cell parameters (a = 13.5337; b = 18.6533; c = 33.0015; α = 82.371; β = 83.305; γ = 78.392), crystals of complex **2** are assumed to be isomorphous to the ones of **3**. Crystals of compounds **2** and **3** are colorless and were crystallized from a mixture of toluene/ *n*-hexane at -40 °C. Data for **2** and **3** were collected on a Bruker APEX DUO instrument by using QUAZAR optics and MoK_α radiation (λ = 0.71073 Å), with ω and ϕ scans. The raw data was processed by using APEX2[6] and SAINT software;[7] structure solution and final model refinement were performed by using SHELXTL.[8] Corrections for absorption effects were applied by using SADABS.[9] All graphics were produced by using ORTEP-3[10] and POV-Ray.[11]

References

(1) Dietrich, H. M.; Grove, H.; Törnroos, K. W.; Anwander, R. *J. Am. Chem. Soc.* **2006**, *128*, 1458.
(2) Dietrich, H. M.; Törnroos, K. W.; Herdtweck, E.; Anwander, R. *Organometallics* **2009**, *28*, 6739.
(3) Dietrich, H. M; Zapilko, C.; Herdtweck, E.; Anwander, R. Organometallics **2005**, *24*, 5767.
(4) Dettenrieder, N.; Dietrich, H. M.; Schädle, C.; Maichle-Mössmer, C.; Törnroos, K. W.; Anwander, R. *Angew. Chem., Int. Ed.* **2012**, *51*, 4461.
(5) Zimmermann, M.; Törnroos, K. W.; Sitzmann, H.; Anwander, R. *Chem. Eur. J.* **2008**, *14*, 7266.
(6) APEX v. 2012.10_0 Madison, WI, **2010**.
(7) Saint v. 7.99A Madison, WI, **2010**.
(8) Sheldrick, G. M., SHELXTL v. 2012.10_2, Madison, WI, **2012**.
(9) Sheldrick, G. M., SADABS v. 2012/1, Madison, WI, **2012**.
(10) L. J. Farrugia *J. Appl. Crystallogr.* **1997**, 565.
(11) POV-Ray v. 3.6 Williamstown, Victoria, Australia, **2004**, (http://www.povray.org).